ARMY RESEARCH LABORATORY

Workshop on Numerical Analysis of Human and Surrogate Response to Accelerative Loading: Final Report

by Christopher P. R. Hoppel, Scott Kukuck, Ravi Thyagarajan, Michael Tegtmeyer, Dan Nicolella, Sikhanda Satapathy, Wayne Chen, Mat Philippens, Barry Shender, Spyros Masouros, Sarah Hug, Tusit Weerasooriya, Joel Stitzel, and William Errico III

ARL-SR-287 **May 2014**

NOTICES

Disclaimers

The findings in this report are not to be construed as an official Department of the Army position unless so designated by other authorized documents.

Citation of manufacturer's or trade names does not constitute an official endorsement or approval of the use thereof.

Destroy this report when it is no longer needed. Do not return it to the originator.

Army Research Laboratory
Aberdeen Proving Ground, MD 21005-5069

ARL-SR-287 **May 2014**

Workshop on Numerical Analysis of Human and Surrogate Response to Accelerative Loading: Final Report

Christopher P. R. Hoppel, Scott Kukuck, Michael Tegtmeyer, Sikhanda Satapathy, Sarah Hug, Tusit Weerasooriya, and William Errico III
Weapons and Materials Research Directorate, ARL

Ravi Thyagarajan
U.S. Army Tank Automotive Research, Development and Engineering Center

Dan Nicolella
Southwest Research Institute

Wayne Chen
Purdue University

Mat Philippens
TNO Defence

Barry Shender
Naval Air Systems Command

Spyros Masouros
Imperial College

Joel Stitzel
Wake Forest University

REPORT DOCUMENTATION PAGE	Form Approved OMB No. 0704-0188

1. REPORT DATE *(DD-MM-YYYY)*	2. REPORT TYPE	3. DATES COVERED (From - To)
May 2014	Final	1–31 January 2014

4. TITLE AND SUBTITLE
Workshop on Numerical Analysis of Human and Surrogate Response to Accelerative Loading: Final Report

5a. CONTRACT NUMBER

5b. GRANT NUMBER

5c. PROGRAM ELEMENT NUMBER

6. AUTHOR(S)
Christopher P. R. Hoppel, Scott Kukuck, Ravi Thyagarajan, Michael Tegtmeyer, Dan Nicolella, Sikhanda Satapathy, Wayne Chen, Mat Philippens, Barry Shender, Spyros Masouros, Sarah Hug, Tusit Weerasooriya, Joel Stitzel, and William Errico III

5d. PROJECT NUMBER

5e. TASK NUMBER

5f. WORK UNIT NUMBER

7. PERFORMING ORGANIZATION NAME(S) AND ADDRESS(ES)
U.S. Army Research Laboratory
ATTN: RDRL-WMP-B
Aberdeen Proving Ground, MD 21005-5069

8. PERFORMING ORGANIZATION REPORT NUMBER
ARL-SR-287

9. SPONSORING/MONITORING AGENCY NAME(S) AND ADDRESS(ES)

10. SPONSOR/MONITOR'S ACRONYM(S)

11. SPONSOR/MONITOR'S REPORT NUMBER(S)

12. DISTRIBUTION/AVAILABILITY STATEMENT
Approved for public release; distribution is unlimited.

13. SUPPLEMENTARY NOTES

14. ABSTRACT
The Warrior Injury Assessment Manikin (WIAMan) Project Management Office in conjunction with the Blast Protection for Platforms and Personnel Institute hosted the Workshop on Numerical Analysis of Human and Surrogate Response to Accelerative Loading on January 7–9, 2014, at the U.S. Army Research Laboratory. This workshop addressed the numerical analysis tools available to simulate and investigate human and human surrogate response to accelerative loading induced to vehicle occupants from blast, with emphasis on underbody blast. The workshop discussion focused on evaluating the maturity of current modeling and associated experimental efforts, establishing what can be done with current tools, and what additional research is needed to advance our understanding of predicting injuries under blast loading environment. There were two keynote presentations: Dr. Scott Wagner of the Walter Reed Spine Research Laboratory gave a presentation titled "A Clinical Overview of Wartime Spinal Injuries," and Mr. Michael Tegtmeyer and Dr. Warren Hardy gave a presentation titled "Experimental Simulation of the Under-body Blast Environment." Dr. Wagner's presentation provided insight into current efforts to repair Soldier spine injuries from accelerative loading events in Iraq and Afghanistan. Tegtmeyer and Hardy presented the research they have led under the WIAMan program to induce accelerative loading conditions to Hybrid 3 anthropomorphic test devices as well as cadaveric specimens. The following report documents the materials presented at the workshop, summarizes the discussion and major findings, and offers some recommendations that are suitable for guiding the future of research in this area.

15. SUBJECT TERMS
accelerative loading injuries, numerical modeling, blast, human response, underbody blast

16. SECURITY CLASSIFICATION OF:			17. LIMITATION OF ABSTRACT	18. NUMBER OF PAGES	19a. NAME OF RESPONSIBLE PERSON
a. REPORT	b. ABSTRACT	c. THIS PAGE			Christopher P. R. Hoppel
Unclassified	Unclassified	Unclassified	UU	574	19b. TELEPHONE NUMBER (*Include area code*) (410) 278-8878

Contents

List of Figures

INTENTIONALLY LEFT BLANK.

Executive Summary

The Warrior Injury Assessment Manikin (WIAMan) Project Management Office in conjunction with the Blast Protection for Platforms and Personnel Institute hosted the Workshop on Numerical Analysis of Human and Surrogate Response to Accelerative Loading on January 7–9, 2014, at the U.S. Army Research Laboratory. This workshop addressed the numerical analysis tools available to simulate and investigate human and human surrogate response to accelerative loading induced to vehicle occupants from blast, with emphasis on underbody blast. The workshop discussion focused on evaluating the maturity of current modeling and associated experimental efforts, establishing what can be done with current tools, and what additional research is needed to advance our understanding of predicting injuries under blast loading environment. There were two keynote presentations: Dr. Scott Wagner of the Walter Reed Spine Research Laboratory gave a presentation titled "A Clinical Overview of Wartime Spinal Injuries," and Mr. Michael Tegtmeyer and Dr. Warren Hardy gave a presentation titled "Experimental Simulation of the Under-body Blast Environment." Dr. Wagner's presentation provided insight into current efforts to repair Soldier spine injuries from accelerative loading events in Iraq and Afghanistan. Tegtmeyer and Hardy presented the research they have led under the WIAMan program to induce accelerative loading conditions to Hybrid 3 anthropomorphic test devices as well as cadaveric specimens. The following report documents the materials presented at the workshop, summarizes the discussion and major findings, and offers some recommendations that are suitable for guiding the future of research in this area.

INTENTIONALLY LEFT BLANK.

1. Introduction

Injuries from accelerative loading are a major concern to the Department of Defense. Blast weapons used against vehicles and dismounted personnel have caused significant injuries and fatalities during recent operations. Even in well-protected vehicles, Soldiers have sustained life-changing injuries to the spine or lower extremities as a result of the rapid acceleration of the body during a blast event. To reduce the potential for these injuries, the Army has invested in the development of a new anthropomorphic test device (ATD) specifically focused on accelerative loading injuries for vehicle occupants (the Warrior Injury Assessment Manikin, or WIAMan, project), as well as the development of numerical analysis tools to model the effects of blast on vehicles (the Blast Protection for Platforms and Personnel Institute, or BP3I, program).

Numerical modeling of the human subject to these accelerative loads offers tremendous potential to enhance the understanding of accelerative loading injuries and to subsequently reduce their occurrence. When the strengths and limitations of numerical models are well understood, the models can be used to provide insight into experimental efforts, thus providing data beyond what is measured. Models can also be used to study variations in experimental parameters, investigate effects of biodiversity, and investigate potential protective systems. Currently there are several ongoing efforts within the Department of Defense to model accelerative loading injuries in the human. The National Highway Traffic Safety Administration and the automotive industry also sponsor significant research in modeling the human response to automotive crashes. Therefore, this workshop was designed to bring together expertise from government and academia to discuss the state of the art in numerical modeling.

The workshop was organized into six sessions. Each session featured a series of 25-min presentations, followed by a 30-min discussion moderated by the session chairs. Section 2 of this report consists of the individual reports by the respective session chairs. The session chairs were asked to focus on drawing out the key technical challenges for numerical modeling of accelerative loading of humans and ATDs. It should be noted that there were common themes in the six sections, and these are reemphasized in the individual reports. Section 3 of the report draws conclusions based on the workshop, and section 4 offers recommendations that were derived from the insights gained from the workshop. The appendices of this report contain the workshop agenda (Appendix A), the abstracts (Appendix B), the slides from the original presentations (Appendix C), the session chair summary presentations (Appendix D), and the attendee list (Appendix E).

2. Summary of Technical Research Areas

2.1 Session 1: Numerical Analysis Techniques for Anthropomorphic Test Devices (ATDs) to Simulate Human Response to Accelerative Loading

Session 1 of the workshop included the following presentations:

- "A Preliminary Evaluation of Human & Dummy Finite Element Models under Blast-Induced Accelerative Loading Conditions" by Costin Untaroiu, Jacob Putnam, and Warren Hardy, presented by Costin Untaroiu, Virginia Polytechnic Institute and State University
- "Approaches for Predicting Human Anatomical Variations Using Anthropometric and Demo-Graphic Data" by Catherine Carneal, Yoshito Otake, Dean Kleissas, Andrew Merkle, Mehran Armand, Manuel Uy, Gaurav Thwait, John Carrino, Brian Corner, Marina Carboni, Barry DeCristofano, and Michael Maffeo, presented by Catherine Carneal, Johns Hopkins University Applied Physics Laboratory
- "Numerical Approach for Modeling Human Joints in Anthropomorphic Test Devices (ATDs)" by Renuka Jagadish and Hyunsok Pang, presented by Renuka Jagadish, Humanetics Corporation

In "A Preliminary Evaluation of Human & Dummy Finite Element Models under Blast-Induced Accelerative Loading Conditions," Costin Untaroiu discussed the challenges of modeling lower extremities and lumbar spine in human and dummies. Human finite-element (FE) models (Global Human Body Model Consortium [GHBMC] and Total HUman Model for Safety [THUMS] models) and dummy FE models (Hybrid III–Livermore Software Technology Corporation version and THOR-k -VT/NASA version) frequently used in automotive crash simulations were evaluated in this study. Kinematic responses predicted by these models were compared to published data recorded under various vertical impact conditions. In addition, dummy injury assessment reference values and human stress/strain data were calculated to evaluate the risk of injury predicted by the dummy and human models, respectively. This study emphasized the modeling challenges of lower extremities and lumbar spine and provided recommendations for improving current human and dummy FE models.

The second presentation, "Approaches for Predicting Human Anatomical Variations Using Anthropometric and Demo-Graphic Data," was presented by Catherine Carneal of the Johns Hopkins University Applied Physics Laboratory. Ms. Carneal described an approach that has been developed to create a statistical shape atlas of the human lung using medical image datasets and used to evaluate how variations in subject stature and demographics relate to changes in internal organ size. This method could be expanded for additional anatomical regions and tissue structures (both soft organs and skeletal) to provide a basis for developing computational human models appropriate for a range of human subjects.

The third presentation, “Numerical Approach for Modeling Human Joints in Anthropomorphic Test Devices (ATDs),” was given by Renuka Jagadish of Humanetics Corporation. Ms. Jagadish emphasized that the ATD neck has to be modeled as closely as possible to represent the kinematic response of the ATD hardware. This includes assigning the right contact and material properties to capture the response and get a good correlation with respect to the test curves. The “nodding” block is a small piece of rubber placed between the neck disc and the lower load cell. The nodding block rubber is prestressed during assembly; this initial compression force/prestress at the interface has a significant effect on the results.

In the discussions at the end of each paper and in the final session wrap-up, the following major challenges facing the community emerged:

1. End user-focus
    - Model needs to reflect its intended use.
    - The models should enable testing focused on important mechanisms.
    - Regulation needs standardization.
2. Proliferation of different ATD models
    - Which model should the end-user choose?
    - Geometry does not always reflect physical article used.
    - Scientific advances have not been broadly disseminated.
    - Scaling techniques need to be developed for ATD models.
    - Contact functions are needed for the models.
    - Material properties should be published and disseminated.
    - Improved numerical meshes are needed.
    - Full reporting of the model details will reduce duplication of efforts.
3. Common understanding of definition and accepted methods of conducting validation
    - Results and input from model validation available for peer review.
    - Caveats and limitations known and disseminated.
4. Data generally accepted as appropriate for validation of underbody blast (UBB) experiments
    - The modeling community needs data for both ATD and human models.

- Modeling community integrated early in the experimental process to ensure the right measurements and boundary conditions are recorded.

5. Scalability: Full-scale, system-level testing is needed

The following challenges were identified as not being fully addressed by the research community at the present time:

1. Posture, posture, posture
   - Vehicle refresh lag: We will have our current vehicles for a long time.
   - Validated models need to be useful for near- and medium-term occupant postures.
   - Articulation of ATD and human models into military-relevant postures is required.
2. A common understanding of the UBB loading environment
   - Definition of the loading rates appropriate for biological material in an UBB event.
   - Loading is not uniform.
3. Common anthropometry definition (e.g., WIAMan? Zygote?)
4. Are we sensitive in the right places? (Testing [and by extension, modeling] is intended to enhance protection systems.)
5. Kinetics and kinematics
   - How to address the interaction of the occupant with the vehicle structure.
   - How to model the belts and safety systems.
6. Bridge between accurate ATD and human response. (Regulation is ATD. Occupant protection is human.)

2.2 Session 2: Multi-Scale Modeling Techniques for Human Tissue Response

Session 2 of the workshop included the following presentations:

- "Effect of Loading Rate and Orientation on the Compressive Response of Human Cortical Bone" by Brett Sanborn, C. Allen Gunnarsson, Mark Foster, Paul Moy, and Tusit Weerasooriya, presented by Brett Sanborn, U.S. Army Research Laboratory (ARL)
- "Experimental and Finite Element Analysis of Brain Tissue under High Strain Rates" by Lakiesha N. Williams, Mark Horstemeyer, Jun Liao, and Rajkumar Prabhu, presented by Lakiesha N. Williams, Mississippi State University
- "Hierarchical Development of Biomedically Validated Human Computational Models" by Robert Armiger, Alexis Wickwire, Kyle Ott, Alex Iwaskiw, Tim Harrigan, Liming Voo,

- JiangYue Zhang, Catherine Carneal, Jack Roberts, and Andrew Merkle, presented by Robert Armiger, Johns Hopkins University Applied Physics Laboratory
- "Material Properties of the Human Heel Fat Pad Across Loading Rates" by Grigoris Grigoriadis, Nic Newell, Spyros Masouros, and Anthony Bull, presented by Spyros Masouros, Imperial College London
- "High Rate Experimental BioMechanics: Investigations to Quantify the Effect of Loading Rate and Micro/Sub-structural Details on the Fracture Response of Human Cortical Bones" by Tusit Weerasooriya, ARL
- "Recent Developments in a Computational Shock Physics Tool for Modeling Fluid-Structure Interaction" by Shane Schumacher, Sandia National Laboratories (SNL)
- "Human Body Models and Computational Tools for Human Response to Blast and Accelerative Loadings" by Dr. Andrzej Przekwas and Dr. X. G. Tan, presented by Dr. Andrzej Przekwas, Computational Medicine and Biology Div., CFD Research Corp.

This session consisted of talks in two important areas: tissue constitutive characterization and computational modeling methods. Unlike most conventional engineering materials, biological materials possess a great degree of anisotropy, inhomogeneity, nonlinear inelastic behavior, and time dependence. In addition, because of a hierarchical structure, there is a need to develop histology-informed constitutive models and bridge the scales from cellular mechanics to tissue-, organ-, and system-level phenomena.

The goal of multiscale modeling of humans is to minimize testing requirements for improved personal protective equipment (PPE) and vehicle design in the long term, and help design better-instrumented surrogates, such as WIAMan in the near term. To attain this objective, three critical challenges need to be addressed: development of biofidelic models, constitutive description of hard and soft tissues, and robust numerical methods to solve the initial boundary value problems.

2.2.1 Hierarchical Biofidelic Models

Accurate representation of the geometry of organs and important details of components, subcomponents, and how they interact are crucial to successful modeling of human system. The presentation by Robert Armiger emphasized this approach in their modeling of the head, neck, and lumbar spine system. A model validation hierarchy is depicted in figure 1, where experiments and modeling at multiple scales are envisaged. One of the challenges in developing a biofidelic computational model is accurate discretization of various complex geometries at different scales. First, the important anatomical features must be preserved, and second, an appropriate FE discretization must be realized. The complex anatomy often encourages the use of lower-order elements with reduced integration points, leading to computational inaccuracy.

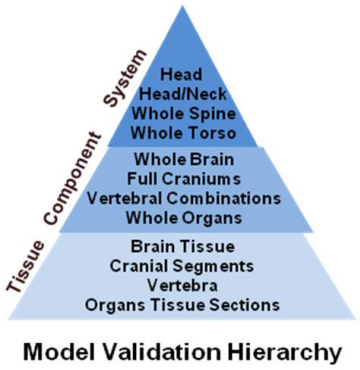

Figure 1. Model validation hierarchy
for head-neck system.

2.2.2 Constitutive Tissue Models

Accurately describing the constitutive response of tissues is critical to developing computational models of human systems. This has been the subject of extensive study over several decades for quasi-static loading conditions. For high-rate loading scenarios, such as an underbody loading event, relevant research has been pursued only more recently. At this initial phase of high-rate tissue studies, mostly conventional techniques have been used. There is a need to explore new experimental methods and novel analysis techniques to extract constitutive properties of biological tissues at the appropriate loading rates.

2.2.2.1 Soft Tissues

One of the main issues in measuring soft tissue response is that inertia effects dominate conventional high-strain-rate measurement techniques. For example, the highly nonlinear response reported by Williams, shown in figure 2, shows an “apparent” hardening and softening behavior of porcine brain. However, this is likely attributable to lateral inertial effects and a lack of stress equilibrium in the sample and not a material response. Therefore, either novel experimental techniques need to be developed or an inverse numerical method is required to extract the constitutive data. An example of a novel experimental technique was reported by Johns Hopkins University’s Applied Physics Laboratory group, where they modified the conventional Split Hopkinson Pressure Bar (SHPB) technique to apply shear loading to soft tissue. Other novel techniques such as plate impact experiments, where lateral strain is zero, need to be explored. Masouros et al. presented an inverse FE methodology to extract the constitutive response of the heal-pad from static and dynamic experiments. Such methods need to be further explored in interpreting experimental data.

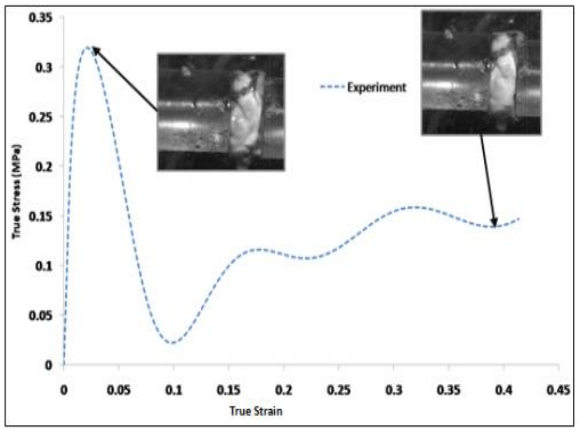

Figure 2. Highly "apparent" nonlinear hardening/ softening behavior of soft tissue measured in SHPB is attributable to inertial effects.

2.2.2.2 Hard Tissues

Bone, on the other hand, presents a high level of anisotropy due to the presence of osteons and other microstructural features. Bone properties are highly location dependent because of disparate cortical and trabecular compositions and differences in microstructure. Sanborn et al. showed that strain in bone specimens as measured by digital image correlation differs from the strain gage measurements in SHPB experiments. Their results captured strain rate effects, anisotropy, and spatial variation of human cortical femur bone tissue. Their results on property variation between different species (human, bovine, equine, etc.) bring up an important point on correlating dynamic bone properties to intrinsic properties, such as density, mineral content, etc. Dynamic fracture property measurement, reported by Weerasooriya et al., also indicated a similar need based on the variability of properties on location and age. Another important question that needs to be addressed is the property distribution as a function of population distribution. The inherent need to test large sample sizes renders this study expensive and time consuming, albeit necessary.

2.2.3 Robust Numerical Methods

FE methods have long been developed and used for solving continuum mechanics initial-boundary value problems and are being extensively applied for modeling human systems. For blast and ballistic applications, both Lagrangian and Eulerian techniques are essential to capture various fluid-structural interactions at multiple scales. Shumacher, from SNL, presented a repertoire of current capabilities in CTH, and the capabilities of the multiphysics code CoBi were discussed by Przekwas from CFD Research Corporation (e.g., figure 3). Biomechanical models are multiscale and multiphysics in nature, requiring use of massively parallel solvers. Micromechanics-based models are necessary at lower length scales, possibly containing multiple representative volume elements, whereas higher length scale models need to be biofidelic and multiphysics. Computational strategies must be developed to bridge these two length scales, as a

single computation is not likely to produce high-fidelity results for the whole human system. An important aspect of human modeling is incorporating the stochastic nature of input conditions and variability in anatomic structure and tissue constitution. Stochastic and probabilistic models are not commonly employed in computational models of engineering systems but appear to be essential for modeling human systems. While deformation-related phenomena are expected to be represented by mean value distributions, failure and post-failure behavior are expected to be manifested by extreme value distributions.

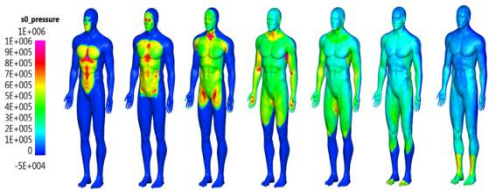

Figure 3. Human biomechanics models require fluid-structure interaction tools and accurate biofidelic models.

Another major need for human modeling is the hierarchical validation of computational models. Experimental data need to be generated at multiple scales, and quantitative metrics are needed for model validation. Current data collection is limited to a few integrated force/acceleration measurements, which are extrapolated into a spatial distribution of stress and strain through models which have been calibrated to limited data. As measurement methods improve, in situ measurement of stress-strain, fracture, and deformation would help validate numerical models.

2.2.4 Recommendations

Based on the information presented in this session and subsequent discussions, we've provided the following recommendations:

1. Material data for different tissues in relevant loading rate regimes are needed. These data need to contain failure and post-failure behavior and low and high strain rates. Current high-rate methods appear to be inadequate, and hence investment should be made to (a) develop new experimental techniques to measure dynamic properties of biological tissues and (b) develop inverse methods to extract constitutive data from experimental measurements.

2. Since injury biomechanics is heavily reliant upon animal and cadaveric data, similarity and differences between live, fixed, and cadaveric tissues need to be established to develop transfer functions between different models.

3. Model validation strategies/metrics need to be developed. This would include (a) carefully designed benchmark experiments, (b) high-fidelity characterization of postmortem human subjects (PMHS), and (c) adjudicated model validation data sets for the community.

4. Multiscale and multiphysics computational strategies also need to be developed. Algorithms to bridge multiple length scales going from tissue-level physics to whole human dynamics require development of new computational methodologies. New meshing techniques are needed to produce accurate biofidelic FE discretization using robust elements.

5. A concerted effort is needed to integrate measurement of different tissue structures and constitutive behavior, sensitivity analysis based on anthropometric differences, development of biofidelic FE models, multiscale computational techniques capable of representing stochastic data, and benchmark experiments for model validation.

2.3 Session 3: Numerical Methods to Simulate the Response of Human Tissue and Bone to High-Rate Loading

Session 3 of the workshop included the following presentations:

- "Comparing the Use of Dynamic Response Index (DRI) and Lumbar Load as Relevant Spinal Injury Metrics" by Ravi Thyagarajan, Kumar Kulkarni, and Jaisankar Ramalingam, and presented by Ravi Thyagarajan from the U.S. Army Tank Automotive Research, Development and Engineering Center (TARDEC)

- "Developing an Empirical Model to Estimate Tibia Injury" by Brian Benesch, Joseph Collins, and Joseph O'Bruba, presented by Joseph O'Bruba (ARL)

- "Towards A Micromechanics-Based Simulation of Calcaneus Fracture and Fragmentation Due to Impact Loading" by Rebecca A. Fielding, Wesley S. Teerlink, Michael V. Robinson, Christopher D. Kozuch, Hannah V. Putnam, Timothy M. Ryan, and Reuben H. Kraft, and presented by Reuben H. Kraft of the Pennsylvania State University

- "Pelvis Response Effects on Whole Body Under-Body Blast Simulations" by Adam Golman, Kyle Ott, Robert Armiger, Tim Harrigan, Catherine Carneal, Andrew Merkle, and presented by Adam Golman of the Johns Hopkins University Applied Physics Laboratory

- "Numerical Methods for Large-Scale Simulation of Tissue and Tissue Simulant Response to Blast, Model Validation and Limitations" by Raul Radovitzky of the Massachusetts Institute of Technology (MIT)

A main conclusion of the first presentation, "Comparing the Use of Dynamic Response Index (DRI) and Lumbar Load as Relevant Spinal Injury Metrics," was that the DRI is not a relevant injury metric. The poor correlation to injury for loading scenarios other than the aircraft-specific ejection seat has been proven in numerous publications since DRI was developed. Hence, there is a need to develop new injury metrics (initial recommendation was to the Compressive Lumbar Force measured in ATDs) that address the injuries to lumbar and thoracic spine for UBB load conditions. These metrics should include the following features:

- Provide a probability for multiple severities (not 0 or 1) resulting in an injury assessment tool.
- Display an injury severity similar to abbreviated injury scales but more understandable and quantitative, preferably related to short-term return to duty and long-term quality of life.
- Account for different failure modes (e.g., disc burst versus wedge failure) and based on observed dynamic injury mechanisms at different scales.
- Address effects of loading rate, duration, and load conditions, which include PPE and restraint systems.
- Apply to various sizes of occupants.

In the second presentation, "Developing and Empirical Model to Estimate Tibia Injury," the mechanical response of the vehicle at the location of the feet was correlated statistically to the injuries sustained. This was done for only a vertical lower leg position. Variations in lower limb orientations or footwear were not included. For empirical injury model development, a worst-case scenario needs to be identified, although the subsequently designed vehicle or protective gears may be overdesigned for most cases. This method will not be useful for predicting injury risk in a general way. Besides overpredicting the injury risk, it does not count for nonvertical tibia positions and consequently induced bending load. This method is also heavily relying on available injury data that need to be accompanied by detailed adequate data on the vehicle and threats.

In the third presentation, "Towards A Micromechanics-Based Simulation of Calcaneus Fracture and Fragmentation Due to Impact Loading," Dr. Kraft discussed that a primary challenge is that failure criteria at micromechanics scales or mesoscales are needed to identify injury or failure initiation and early-stage propagation of failure in bones. One example is that numerical techniques are needed to evaluate the effects of viscous fluid passing through permeable cell walls at high loading rates. The following issues need to be addressed in future development:

- Surrogates' response to blast loading needs to be validated by cadaver response; this should include a definition of biofidelity.
- Modes of failure need to be addressed (e.g., will failure include puncture of the cadaver skin?).
- Can the degrees of freedom at ATD joints mimic human joints?
- Effects of boots in shock isolation, and PPE effects in general.
- Effects of preexisting damage.
- A fundamental challenge is the highly scattered data for tissue response to high-rate loading.

- Need high-fidelity characterization methods to generate input data and validation cases.

This method is being applied for shock-induced calcaneus fractures. This increases the knowledge on fracture/failure mechanisms on a micro scale, which will be helpful in the design of footwear of shock-mitigating materials. However, the actual approach in vehicle design aims at shock mitigation provided by the vehicle structure to prevent any shock load directly applied to the occupant. Acceleration-induced inertial loading is more relevant for the UBB loading mechanisms leading to the occupant injuries. Consequently, the acceleration and blunt impact loading mechanisms causing injury are more relevant than shock mechanisms. The degree of required biofidelity at this component level will make it challenging to produce an effective biofidelic response at a higher system level.

The presentation "Pelvis Response Effects on Whole Body Under-Body Blast Simulations" shows the influence of the pelvis and material properties on the ATD response. The Vertical Acceleration Load Transfer System is valuable in generating realistic loading scenarios simulating UBB scenarios. The test showed that the design of the pelvis and pelvic flesh of the Hybrid III ATD is not optimized for vertical loading. In addition to the lack of biofidelic reference for vertical loads, the flesh is not durable. The FE modeling is a useful tool in analyzing and understanding the physics. The observation that the vertical motion of the lower limbs decreases the compression load in the lumbar spine is correct; however, this is most likely not realistic, as human lower limbs will fracture at these loading conditions. A challenge for future research is to identify significant short comings of the ATD with respect to the actual human occupant. Analysis of FE ATD model responses compared to PMHS and human body models appears to be promising to identify and quantify essential responses for the UBB ATD to be developed. However, the biofidelity and sensitivity of the models, as well as the ATD, should be optimized for the protective vehicle designs. Occupant load data for these designs are limited, as the first generation of these optimized vehicles and protection solutions are just starting to become available.

Raul Radovitzky (MIT) gave the final presentation, "Numerical Methods for Large-Scale Simulation of Tissue and Tissue Simulant Response to Blast, Model Validation and Limitations." Dr. Radovitzky discussed that numerical simulations are capable of capturing the functions of protective gears. For example, the use of a face shield attached to the helmet can significantly reduce the impact load to the brain under blast. Rate-dependent material models embedded to the simulation codes show the capability to capture the main features of material impact responses from dynamic experiments. However, the scatter in available experimental results is too high.

There is a need for improved communications between the modeling and simulation community and the experimental community to optimize the availability of experimental data to validate models. These communities need to focus on the actual sustained injuries in theatre to be most relevant. The vehicle designer and modeler need to be included in this process, as it is most likely that the first level of protection is most effective by integrating the shock mitigation in the

vehicle design. In general, add-on protection seems to be less effective than protection integral to the vehicle design. These communities need to develop and specify methods to assess the biofidelity and procedures and criteria to validate the models. These efforts should leverage current methods available in the automotive and aircraft crash communities with respect to biofidelity.

Microscale models are needed to help understand the details of the load-bearing capacities of the human body. These models could provide insight into the variations in biological mechanical response. These models could also be useful to optimize second and third generation vehicles. At this time, a large scale (full body) model of an ATD and a human body will be most effective to generate the first generation underbody blast ATD.

2.4 Session 4: Methodologies to Simulate Blast Loading Conditions

Session 4 of the workshop included the following presentations:

- "Current Trauma in Operations Iraqi and Enduring Freedom and rhBMP-2, The Walter Reed Experience" by Scott Wagner and Ronald Lehman, presened by Scott Wagner, Walter Reed National Medical Center
- "Development and Validation of the WSU Human Body Model" by Alan Goertz and David Viano, presented by Alan Goertz, Wayne State University
- "Adapting Automotive-Based Finite Element Models of Lower Extremity for High-Rate Impact Simulation of Occupants Subject to Under-Vehicle Blasts" by Matthew Panzer and Robert Salzar, presented by Robert Salzar, University of Virginia
- "Current Research and Development Activities of the Full Body Model Center of Expertise of the Global Human Body Models Consortium Project" by Scott Gayzik and Joel Stitzel, presented by Scott Gayzik, Wake Forest University
- "Modeling the Human" by Courtney Cox, Brian Bigler, Jason Luck, and Cameron R. Dale Bass, presented by Cameron R. Dale Bass, Duke University
- "Human Body Model Injury Analysis in Real-World Crash Simulations" by Kerry A. Danelson, James P. Gaewsky, Caitlin M. Weaver, and Joel D. Stitzel, presented by Kerry Danelson, Wake Forest University
- "Numerical Modelling Undertaken at Dstl (UK) Concerning Vehicle Floor Plate Impact of Surrogates and Anatomical Human Entities Due to Under-Body Mine Loading" by Dan Pope, Chris Taggart, Joe Cordell, and Ian Softley, presented by Daniel Pope, UK Defense Science and Technology Laboratory

- "Optimal Design of a Novel Energy Absorbing Material to Mitigate the Blast Effect on the Lower Extremities" by Feng Zhu and King H. Yang, presented by King Yang, Wayne State University

The first presentation of the session was a keynote address provided by LT Scott Wagner of the Walter Reed National Military Medical Center. The presentation was a clinical overview that showed injury examples observed during recent operations and treatments provided for these injuries. In addition to illustrating the trauma severity and complex procedures required to stabilize fractured skeletal sections, the presentation also revealed promising, novel, and cutting-edge treatments being investigated to aid in patient recovery. Yet-to-be-resolved issues with these treatment options were discussed. The presentation was well received by those in attendance. During the discussion time following the presentation, it was emphasized that the biomechanics research community should maintain a connection to the clinicians who are presented with the injuries and responsible for treatment. This connection serves to maintain focus on areas of deficiency and can guide the work needed to be done to establish useful injury prediction tools.

As originally envisioned, the technical content of session 4 was intended to revolve around methods of simulating the loads applied to humans and human surrogates that would represent what would be observed during blast events. Based upon the received submissions, the content evolved to include how to simulate the responses of full-body humans and human surrogates to loads generated during blast events. The session contained eight presentations, including one of the two workshop keynote addresses. All abstracts and presentations are included in the appendices of this report.

For simulating the response of the human to possibly injurious loading, three Human Body Models (HBMs) were discussed during the technical presentations: the Wayne State University Human Body Model (WSUHMB), the GHBMC, and the THUMS. All of the presented models are being developed for use with the LS-DYNA nonlinear transient dynamic FE computer program with limited support for other computational solvers. The development of these models has been driven, at least initially, by support from automobile manufacturing companies. Each model possesses different levels of computational fidelity and also has different restrictions on use/licensing (THUMS, for example, is prohibited for use in military applications).

Beyond HBMs, there were other topics covered in the technical presentations of session 4. An application was presented of FE methods to help understand how materials currently used to mitigate lower-extremity loading behave and how to potentially optimize these materials. An overview of topics of interest and current efforts being conducted by the United Kingdom's Defence Science and Technology Laboratory was provided. Both of these presentations highlighted how modeling and simulation of the human body can be used to assist protection technology developers in better enabling their technology to protect vehicle occupants.

The presentation that arguably generated the most conversation—and drove much of the post-session discussion—was given by Dr. Cameron Bass from the Duke Biomedical Engineering group. The presentation was modified, in near real time, to incorporate topics and thoughts relevant to presentations and discussions from the previous three sessions of the workshop. These topics served to center and reorient workshop attendees on items that are relevant to simulations involving human body model representations. The topics included anthropometry, validation, muscle activation and pretensioning, constitutive relations and material response, population variance, and distribution.

The following lists do not summarize the presentation material. Rather, they summarize the discussions that followed the talks and the major issues that need consideration by the program and scientific community.

The Verification/Validation Controversy

- There is considerable variability in defining validation.
- Ideally, validation should be quantitative, not merely visually comparing curves to see if they match. Computing a correlation metric, r^2 and p value, is not sufficient.
- Validation must be accompanied by an explanation of how it was performed and what limitations/caveats exist. Validation metrics and methods should be identified. It is important to identify where the model is both valid and invalid.
- Models should be developed using a hierarchical approach; determine the correct material models developed under the operationally relevant loading conditions at the component and subsystem levels. If the underlying component structure is verified and valid, then the system should behave predictably without the need for tweaking. Validation and verification occur during model development—not solely after the model is "complete."
- Ultimately, a human occupant/surrogate must interact with the environment, so models must also be developed for vehicle, seating, restraints, and PPE with material properties determined under relevant dynamic conditions.
- The attendees discussed whether a standard for validation could be developed. Papers that were referenced for quantitative validation as well as the hierarchical approach can be found in the references list (Francis, et al. 2012; Nicolella et al. 2006; Henninger, et al. 2010; Oreskes et al. 1994; Anderson et al. 2007; AR 5-11 in 2005; and ASME guides in 2006 and 2009).

What Constitutes Valid Scaling?

- Methodology to translate animal response to human; there are a number of techniques to do this, but they must account for realistically scaled loading conditions.

How Should Models Account for Variability?

- Account for input unknowns: physiology, loading, geometry, sex, age, etc.
- Muscle response is a source of variability that cannot be achieved through ATD or PMHS testing—how to account for muscle activation timing and magnitude and muscle wrapping in complex structures (e.g., neck).
- Material property models must account for variability—develop a statistical distribution.
- How do we deal with post-failure material behavior? Requires basic research.
- Automotive models may be a good starting point but require modification for use in blast environment.

What's Important To Model and What Is Not?

- Identify what parts of the model require high biofidelity and which parts do not based on operational needs—this will help to address practical computation needs (e.g., run time).
- Conduct a sensitivity analysis and focus on what's important based on requirements for what the ultimate use of the model is, not on including everything to the last detail.
- Focus on 50th percentile male of some existing models is problematic—50th percentile of what? No one is 50th percentile for all aspects. What about the rest of the population, including females and very large males?
- Program management must specify injury mechanisms from the trauma database to develop appropriate validation experimentation; this is not up to the experimentalists.

Relationship Between Testing and Model

- Use model requirements to inform testing requirements (loading, postures, instrumentation) before testing begins; this results in fewer, more comprehensive tests, better models, and cost savings.
- Validation experiments: There needs to be a compromise between funding and the desired number of data points, so ensure that there are sufficient data to account for the variability in the input parameters (geometry, posture, loading, sex).

What Are the Ultimate Goals of the Program?

- What do we want from the modeling? If, for example, it's a design tool, then it needs to be driven by operational requirements (focus on persistent, common injuries, not on nonsurvivable injuries).
- Ultimately, we want to develop modes of mitigation (technology or behavior).
- Prioritize investments based on the goal.

- The goal is to provide protection for a human occupant.
- A design toolbox based on human injury tolerance and achievable mitigation is a step towards that goal.

2.5 Session 5: Numerical Analysis Methodologies for Human Body Subject to High-Rate Loading

Session 5 of the workshop included the following presentations:

- "Constitutive Model and Parameter Sensitivity in Predicting Lower Leg Response for Underbody Blast Events" by Megan Lynch and Adam Sokolow, presented by Megan Lynch of ARL
- "Coupled Eulerian and Lagrangian Approaches for Dynamic Injury Analysis" by Timothy P. Harrigan, Robert Armiger, Catherine Carneal, JiangYue Zhang, and Andrew Merkle, presented by Timothy P. Harrigan of the Johns Hopkins University Applied Physics Laboratory
- "Crew Response in Full System HFCP" by Allen Shirley of CORVID Technologies
- "Evaluating the Effectiveness of Various Blast Loading Descriptors as Occupant Injury Predictors for Underbody Blast Events" by Kumar B. Kulkarni, Jaisankar Ramalingam, and Ravi Thyagarajan, presented by Jaisankar Ramalingam of TARDEC
- "Neck Response of a Finite Element Human Body Model During a Simulated Rotary-Wing Aircraft Impact" by Nicholas A. White, Kerry A. Danelson, F. Scott Gayzik, and Joel D. Stitzel, presented by Joel Stitzel of Wake Forest University

Three main topics were discussed during this session: (1) material models and parameters for biological tissues, (2) numerical analysis methodologies and levels of complexity, and (3) the numerous disparate efforts to model the human body, especially the lower leg. These areas and recommendations will be discussed in this section. For additional details on the five presentations within this session, please refer to the appendices for the abstracts and presentation slides.

A clear consensus showed that one of the main research challenges for numerical models of the human body in underbody blast is in the area of material models, and the required material parameters, of biological tissues. It was shown (in this session and previous sessions) that numerical models of functional units that work well in automotive conditions are likely not predictive in UBB conditions, and that knowledge of the strain-rate dependency of specific tissues is critical in order to improve the predictive ability of the models. In addition to the strain-rate dependency, the variability of biological tissues and the importance (or irrelevance) of various material parameters is not well understood for biological tissues. The first briefing,

"Constitutive Model and Parameter Sensitivity in Predicting Lower Leg Response for Underbody Blast Events," began to explore the variability of select material parameters within their developed lower-extremity model.

Another area of discussion in this session and other sessions was the methodology used for modeling the human body in highly dynamic events for the purpose of predicting injury. Harrigan, Shirley, and Ramalingam presented their research discussing numerical modeling methodologies of varying degrees of complexity for predicting injury to the vehicle occupant when subjected to an underbody blast event. The second briefing, "Coupled Eulerian and Lagrangian Approaches for Dynamic Injury Analysis," covered multiple numerical approaches for modeling the human body/organs in dynamic events. The research showed the value of using Eulerian and arbitrary Lagrangian-Eulerian computational techniques for modeling injury to human organs and questioned if these techniques are necessary for modeling injury during dynamic events.

In contrast to the above research area, Jaisankar Ramalingam of TARDEC presented "Evaluating the Effectiveness of Various Blast Loading Descriptors as Occupant Injury Predictors for Underbody Blast Events" to create and demonstrate an "easy-to-use injury estimator tool" to provide vehicle developers a quick and easy tool to estimate injury risk during the vehicle design process.

The discussions and talks surrounded the numerical modeling techniques, and subsequent complexity, that are required to adequately predict injury for the overall objective of the problem. The levels of complexity in the different numerical models offer unique benefits (and pitfalls) that may be "objective-specific."

Much of the discussion revolved around the disparate effort for a numerical model of the human in UBB. Specifically for the lower extremity, there are several organizations and institutions that are devoting resources to model the human lower extremity in UBB and little to no coordination between the efforts. It was also clear that there is no major funding effort to develop such a model or to pull together the various international efforts. As such, it was recommended by the group to address this lack of coordination and communication for the lower extremity and to potentially have a singular program to unify the efforts.

2.6 Session 6: Numerical Methods for Analysis of ATD Materials (Including Soft Materials) Undergoing High-Rate Loading

Session 6 of the workshop included the following presentations:

- "A Finite Element Model of the Military Lower Extremity Surrogate (MIL-Lx) With Combat Boot Validated for High Loading-Rate Inputs" by Nicolas Newell and Spyros D. Masouros, presented by Spyros D. Masouros, Imperial College

- "Rubber Material Modeling Methodology for FE Dummy Development" by Hyunsok Pang, Humanetics Innovative Solutions, Inc.
- "Effect of Strain Rates on the Compressive Response of ATD Neck and Foot Rubber Under Different Loading Sequences" by Brett Sanborn and Tusit Weerasooriya, presented by Brett Sanborn, ARL
- "Inertial Effects in Compression and Torsional Kolsky Bar Tests on Soft and Nearly Incompressible Materials" by Adam Sokolow, Mike Scheidler, and John Fitzpatrick, presented by Adam Sokolow, ARL

At the end of this session, there was a spirited discussion on current state of the art in high-rate experimental techniques and the need for computational methods to extract material models from those measurable data. A summary of the discussion is as follows:

- The community agreed that there is a critical need to develop and execute iterative computational methods to extract approximate mathematical representations of the material constitutive response of materials such as foams, very soft polymers, skull, calcaneus, connective tissues (tendons, ligaments), brain tissue, and other anisotropic soft tissues, etc., especially for high loading rates.
- There are several shortcomings in using current experimental techniques and data from these experiments. For example, when traditional test techniques are used to characterize soft biological tissues, the high strain-rate response is often confounded by inertial effects. In some cases these effects can be accounted for and corrected. However, novel test techniques will likely be required before further advances can be made.
- Another experimental shortcoming is that material scientists regularly use only dynamic mechanical analysis (DMA) data to obtain viscoelastic response models. However, DMA data alone are not sufficient to represent the material response of viscoelastic materials, as the data are obtained from experiments where the material is cyclically loaded with small amplitude loading. Thus, the responses at the larger realistic amplitudes are not represented. Relaxation or cyclic data alone do not represent the viscoelastic stress-strain material response for loading rates relevant to blast loading rates.
- Another issue that needs to be addressed in modeling includes material anisotropy. Typically, tissues exhibit anisotropic and inhomogeneous material properties. For a given physical problem, the role and relative importance of the anisotropy are not always clear. Therefore, we need to start thinking about designing, characterizing, and modeling methods for new surrogate materials that actually mimic hard, connective, and soft tissues to capture real human material response.
- It is almost impossible to extract specimens (uniform and in required sizes) from all the components of the human for experimental characterization. We need to think differently

by developing novel inverse methods with the following objective in mind: How do we extract approximate material response models from these small, nonuniform structures using, for example, a combined hybrid computational/experimental approach?

- It is almost impossible to tune any of the existing material model concepts (including current state-of-the-art models in literature) to all possible experimental data types (DMA, relaxation, compression, tension, shear, and combined loading experiments at different strain rates), so focus on the application-specific material behavior experiments.
- There is strong evidence that response of the ATD changes with repeated use and also with time because of the degradation of the polymeric material. Therefore, we need to understand the change in ATD material response (and hence the change in constitutive response) for repeated loading.
- Fracture of bones: future ATDs may need replaceable components to capture actual fracture response of bones.
- Experiments should have enough tissue samples to extract variability. Future material response models should have that variability built in to them, perhaps factored into the material model constants.

3. Conclusions

Researchers are currently making significant efforts to model the human and ATD response to accelerative loading injuries. For automotive crash applications, these include the WSUHMB, the GHBMC, and the THUMS for humans and the Hybrid III and THOR-k models for anthropomorphic test devices. For blast-induced accelerative loading, the Near-Term Underbody Blast and the Underbody Blast Methodology programs are developing models for the Hybrid 3 ATD. The High-Performance Computing Software Applications Institute for BP3I is funding modeling of ATD and an exploratory effort to identify challenges in modeling the human. There are efforts to model accelerative loading effects on specific human body regions funded by ARL (leg and spine), TARDEC (leg), and the Navy (spine). These efforts provide a foundation for the development of validated human models for blast-induced accelerative loading injuries. Additional research is needed to mature these efforts to the state where they can be effectively used by the Department of Defense to prevent accelerative loading injuries and assess Soldier protection technologies. The three primary research areas that were identified from the discussions in the six workshop sessions were model maturity and validation, material characterization, and biodiversity.

To address model maturity and provide a common understanding of model limitations, there is a clear need for the accelerative loading numerical analysis community to adapt standards similar to those of the American Society of Mechanical Engineers (ASME). In the current state-of-the-art models, the appropriate level of detail and the robustness of the results are not well understood. This imposes severe limitations on the models' validity that are often neglected. There was significant discussion at the workshop on the need for increased communication as well as standards for model validation. The term "validated" was often used in lieu of "calibrated" or "tuned." As described in ASME V&V 10-2006, model validation is "the process of determining the degree to which a model is an accurate representation of the real world from the perspective of the intended uses of the model." By this standard, the validation process describes not only the ability of the model to represent an event, but also, just as importantly, the intended uses of the model, thus also indicating areas where the model was not intended to be used or validated. Furthermore, a calibrated or tuned model is not a validated model. Several speakers used the word "validated" to describe their modeling results without any caveats on its limitations.

A second critical area is the characterization of material properties at the appropriate loading conditions. The materials that need to be studied include those from humans, animal surrogates, and ATDs. Currently the material properties for both cadaveric tissues and ATD materials are insufficient, inaccurate, or otherwise unavailable for accelerative loading at ballistic rates. The primary reason for the lack of data is that most of the high-rate experimental techniques were developed for stiffer and stronger materials and cannot be directly translated to soft materials. At best, the experimental data available now develops a wide corridor even for the simplest constitutive models and is inadequate for model predictive capabilities. Therefore, new experimental techniques are needed to measure the dynamic properties of soft materials, including both biological tissues as well as surrogate materials. Only with improved experimental techniques can we attempt to characterize the rich anisotropic, nonlinear viscoelastic behavior exhibited by these soft materials.

Biodiversity needs to be addressed and accounted for in modeling efforts. The term "biodiversity" applies range from structural variations, such as anthropometric differences between humans or their posture at the time of insult, to material response variations from subject to subject and from organ to organ. The significance of the structural and material differences between human responses to applied loading is not well understood. Carneal et al. demonstrated that the lung size and shape could not be accurately represented by simply scaling the size and the shape of the human. They developed an atlas of the lung, a reduced-order mathematical representation of the organ across genders, races, and age. Applying this approach to the full body could be extremely useful to extend modeling capability away from a one-subject, one-model approach (e.g., the commonly criticized 50th percentile male model). More complex approaches, like the one outlined by Carneal et al., will be necessary for the Department of Defense as it works to apply a survivability assessment to a broad range of Soldiers. An

approach that addressed biological variability in a constitutive model response was based on the development of probabilistic models (as described in Francis, 2012; Nicolella, 2006; and Thacker, 2007). These types of techniques provide insight into the range and probability of potential responses to blast loading while still modeling at the continuum scale and may be the most applicable approach to modeling current experimental data.

Also addressed in the workshop was the consideration of the sensitivity of the result (e.g., injury prediction) on the (potentially unknown) input parameters (e.g., loading or material response). Long-term solutions to capturing biological variability will require developing and enhanced understanding of the multiscale nature of the biological response. The continuum-level properties of tissues and bones, which vary by location both within a tissue and from organ to organ, are controlled by the lower-level structure of these materials. Important microstructural details may include multicellular, cellular, or subcellular properties (e.g., supracellular structures, cell-cell adhesion, and cytoskeletal structure). In-depth experimental efforts are needed to understand the relationship between the microlevel material properties and the continuum-scale behavior of biological materials as well as computational methodologies to bridge multiple length scales extending from tissue-level physics to whole human dynamics.

Finally, this workshop revealed that most members of the modeling and simulation community are currently working in their own specialty domains. They have not been challenged as a community to integrate and apply their latest research in a holistic fashion to create a major advance in the ability of the Department of Defense to address a particular problem, such as the effects of a known accelerative loading injury mechanism. The progress and potential shown during this workshop justify giving serious consideration to presenting such a challenge to this community.

4. Recommendations

The Department of Defense uses numerical modeling in both the development and the assessment of Soldier protection technologies. Errors and uncertainties in numerical modeling approaches therefore result in increased risks to programs, which will result in poorly designed protective systems as well as increased costs for acquisition programs. The following recommendations are made to develop a human body modeling capability to effectively develop protection systems and assessment methodologies for vehicles subject to blast loading conditions:

- An assessment of the current state of numerical modeling tools as well as uniform standards for model validation is needed by the research community. This could be developed through a round-robin exercise with data from the WIAMan project office. For example, an evaluation of current analysis tools for modeling lower leg response to

accelerative loading would be a good starting point. This would become the starting point for an investigation of model validation, material properties, and biodiversity and provide the community with a highly relevant challenge that will create opportunities to integrate the latest research findings in material models, human models, and medical research findings. The results of this assessment could lead to a near-term capability to mitigate injuries to the lower leg from underbody blast.

- Material data for different tissues in relevant regimes are needed. A concerted effort is needed to measure different tissue structure and constitutive behavior. These data need to contain failure and post-failure behavior for low and high strain rates. Current high-rate methods are inadequate; hence, investment should be made to (a) develop new experimental techniques to measure dynamic properties of biological tissues, (b) develop inverse methods to extract constitutive data from multiple sets of experimental measurements, and (c) apply statistical analyses, including model validations and characterization of its predictive limitations.
- Injury biomechanics heavily relies upon animal and cadaveric data as well results on ATDs. For this to be successful, investment should be made to (a) establish similarities and differences between live, fixed, and cadaveric tissues and (b) develop transfer functions between different models, i.e., between animals and humans, cadavers and humans, and ATDs (including the WIAMan) and humans.
- Computational injury prediction for a biodiverse population is needed to properly design and assess protection for a diverse Soldier population. This challenge is both multiscale and multiphysics. New strategies need to be developed, including (a) algorithms to bridge multiple length and time scales, i.e., from tissue-level physics to whole human dynamics, (b) new meshing techniques for rapid and accurate biofidelic FE discretization, and (c) methods to capture anthropomorphic or microstructural variability.

5. References

Anderson, A. E.; Ellis, B. J.; Weiss, J. A.; Verification, Validation and Sensitivity Studies in Computational Biomechanics. *Computer Methods in Biomechanics and Biomedical Engineering* **2007,** *10,* 171–184.

AR 5-11. *Management of Army Models and Simulations;* Headquarters, Department of the Army: Washington, DC, 1 March 2005. http://www.apd.army.mil/pdffiles/r5_11.pdf 1 (accessed April 2014).

ASME V&V 10-2006. *Guide for Verification and Validation in Computational Solid Mechanics;* The American Society for Mechanical Engineers: New York, 2006. http://cstools.asme.org /csconnect/pdf/CommitteeFiles/24816.pdf (accessed April 2014).

ASME V&V 20-2009. *Standard for Verification and Validation in Computational Fluid Dynamics and Heat Transfer;* The American Society for Mechanical Engineers: New York, 2009. ftp://ftp.demec.ufpr.br/disciplinas/TM777/Apostila_2010_3 /Extrato_norma_ASME_VeV_20-2009.pdf (accessed April 2014).

Francis, W. L.; Eliason, T. D.; Thacker, B. H.; Paskoff, G. R.; Shender, B. S.; Nicolella, D. P. Implementation & Validation of Probablistic Models of the Anterior Longitudinal Ligament and Posterior Longitudinal Ligament of the Cervical Spine. *Computer Methods in Biomechanics and Biomedical Engineering* **2012,** *17* (8), 905–916.

Henninger, H. B; Reese, S. P.; Anderson, A. E.; Weiss, J. A. Validation of Computational Models in Biomechanics. *Proc IMechE Part H: J Engineering in Medicine* **2010,** *224,* 801–812.

Nicolella, D. P.; Francis, W. L.; Bonivtch, A. R.; Thacker, B. H.; Paskoff, G. R.; Shender, B. S. Development, Verification and Validation of a Parametric Cervical Spine Injury Prediction Model. *Proceedings to the 47th AIAA/ASME/ASCE/AHS/ASC Structures, Structural Dynamics, and Materials Conference,* 2006; pp 3977–3985,

Oreskes, N.; Shrader-Frechette, K.; Belitz, K. Verification, Validation and Confirmation of Numerical Models in Eart Sciences. *Science* **1994,** *263,* 641–646.

Thacker, B. H.; Francis, W. L.; Nicolella, D. P. Model Validation and Uncertainty Quantification Applied to Cervical Spine Injury Assessment. *Computational Uncertainty in Military Vehicle Design;* NATO Research and Technology Organisation: Neuilly-sur-Seine Cedex, France, 2007; pp. 22-1–26-30.

INTENTIONALLY LEFT BLANK.

Appendix A. Workshop Agenda

This appendix appears in its original form, without editorial change.

AGENDA

Workshop on Numerical Analysis of Human and Surrogate Response to Accelerative Loading

January 7, 2014

0800	Registration	
0830	Opening Remarks, Dr. Christopher Hoppel, ARL	
0845	WIAMAN Program Overview, Mr. Randy Coates, ARL	
0915	Blast Protection for Platforms and Personnel Institute Overview, Dr. Scott Kukuck, ARL	
0935	Importance of Accelerative Loading Research, Mr. Richard Sayre, DOT&E	

BREAK

Session 1

Numerical analysis techniques for anthropomorphic test devices (ATDs) to simulate human response to accelerative loading

Chairs: Ravi Thyagarajan (TARDEC) and Mike Tegtmeyer (ARL)

1000	A Preliminary Evaluation of Human & Dummy Finite Element Models under Blast-Induced Accelerative Loading Conditions	Costin D. Untaroiu
1030	Approaches for Predicting Human Anatomical Variations Using Anthropometric and Demographic Data	Catherine Carneal
1055	Numerical Approach for Modeling Human Joints in Anthropomorphic Test Devices (ATDs)	Renuka Jagadish
1120	Discussion	

LUNCH

Session 2

Multi-scale modeling techniques for human tissue response

Chairs: Dan Nicolella (SWRI) and Sikhanda Satapathy (ARL)

1300	Effect of Loading Rate and Orientation on the Compressive Response of Human Cortical Bone	Brett Sanborn
1330	Experimental and Finite Element Analysis of Brain Tissue under High Strain Rates	Lakiesha N. Williams
1355	Hierarchical Development of Biomedically Validated Human Computational Models	Robert Armiger
1420	Material Properties of the Human Heel Fat Pad Across Loading Rates	Spyros Masouros

BREAK

1515	Effect of Loading Rate on the Fracture Behavior and Mode Mixity for Crack Initiation of Human Femoral Cortical Bone	Tusit Weerasooriya
1540	Recent Developments in a Computational Shock Physics Tool for Modeling Fluid-Structure Interaction	Shane Schumacher
1605	Multiscale Modeling of Human Body and Vital Organ Responses to Blast and Accelerative Loadings	Andrzej Przekwas
1630	Discussion	

ADJOURN

AGENDA

Workshop on Numerical Analysis of Human and Surrogate Response to Accelerative Loading

January 8, 2014

0800	Registration	
0815	Opening Remarks, Dr. Christopher Hoppel, ARL	
0830	Keynote: "Experimental Simulation of the Under-Body Blast Environment", Dr. Warren Hardy and Mr. Michael Tegtmeyer	

BREAK

Session 3

Numerical methods to simulate the response of human tissue and bone to high-rate loading

Chairs: Wayne Chen (Purdue) and Mat Philippens (TNO)

0915	Comparing the Use of Dynamic Response Index (DRI) and Lumbar Load as Relevant Spinal Injury Metrics	Ravi Thyagarajan
0940	Developing and Empirical Model to Estimate Tibia Injury	Brian Benesch
1005	Towards A Micromechanics-Based Simulation of Calcaneus Fracture and Fragmentation Due to Impact loading	Reuben H. Kraft

BREAK

1045	Pelvis Response Effects on Whole Body Under-Body Blast Simulations	Adam Golman
1110	Numerical Methods for Large-Scale Simulation of Tissue and Tissue Simulant Response to Blast, Model Validation and Limitations	Raul Radovitzky
1135	Discussion	

LUNCH

Session 4

Methodologies to Simulate Blast Loading Conditions

Chairs: Barry Shender (NAVAIR) and Scott Kukuck (ARL)

1310	A Clinical Overview of Wartime Spinal Injuries	Scott Wagner
1335	Development and Validation of the WSU Human Body Model	Alan Goertz
1400	Adapting Automotive-Based Finite Element Models of Lower Extremity for High-Rate Impact Simulation of Occupants Subject to Under-Vehicle Blasts	Matt Panzer
1425	Current Research and Development Activities of the Full Body Model Center of Expertise of the Global Human Body Models Consortium Project	Scott Gayzik
1450	Modeling the Human Head and Neck: Sensitivity and Response	Dale Bass

BREAK

1545	Human Body Model Injury Analysis in Real-World Crash Simulations	Kerry Danelson
1610	Numerical Modelling Undertaken at Dstl (UK) Concerning Vehicle Floor Plate Impact of Surrogates and Anatomical Human Entities Due to Under-Body Mine Loading	Daniel Pope
1635	Optimal Design of a Novel Energy Absorbing Material to Mitigate the Blast Effect on the Lower Extremities	King Yang
1700	Discussion	

ADJOURN

AGENDA

Workshop on Numerical Analysis of Human and Surrogate Response to Accelerative Loading

January 9, 2014

0815	Opening Remarks, Dr. Christopher Hoppel, ARL	

Session 5

Numerical analysis methodologies for human body subject to high rate loading

Chairs: Spyros Masouros (Imperial College) and Sarah Hug (ARL)

0830	Constitutive Model and Parameter Sensitivity in Predicting Lower Leg Response for Underbody Blast Events	Megan Lynch
0855	Coupled Eulerian and Lagrangian Approaches for Dynamic Injury Analysis	Timothy P. Harrigan
0920	Crew Response in Full System HFCP	Allen Shirley
0945	Evaluating the Effectiveness of Various Blast Loading Descriptors as Occupant Injury Predictors for Underbody Blast Events	Jai Ramalingam
1010	Neck Response of a Finite Element Human Body Model During a Simulated Rotary-Wing Aircraft Impact	Joel Stitzel
1035	Discussion	

LUNCH

Session 6

Numerical methods for analysis of ATD materials (including soft materials) undergoing high-rate loading

Chairs: Tusit Weerasooriya (ARL) and Joel Stitzel (Wake Forest)

1230	A Finite Element Model of the Military Lower Extremity Surrogate (MIL-Lx) with Combat Boot Validated for High Loading-Rate Inputs	Spyros Masouros
1255	Rubber Material Modeling Methodology for FE Dummy Development	Hyunsok Pang
1320	Effect of Strain Rates on the Compressive Response of ATD Neck and Foot Rubber under Different Loading Sequences	Brett Sanborn
1345	Inertial Effects in Compression and Torsional Kolsky Bar Tests on Soft and Nearly Incompressible Materials	Adam Sokolow

BREAK

1430	Panel Discussion: Chairs of Individual Sessions	

ADJOURN

Appendix B. Workshop Abstracts

This appendix appears in its original form, without editorial change.

ABSTRACTS

Workshop on Numerical Analysis of Human and Surrogate Response to Accelerative Loading

January 7, 2013
Session 1

Preliminary Evaluation of Human and Dummy Finite Element Models under Blast-Induced Accelerative Loading Conditions

Costin D. Untaroiu (costin@vt.edu), Jacob B. Putnam (jacobp@vt.edu), Warren N. Hardy (whardy@vt.edu),
Virginia Tech: Center for Injury Biomechanics
2280 Kraft Drive, Blacksburg, Virginia 24061, Tel: (540) 231-8997

Introduction: Lower extremity and spinal injuries have been the majority of non-fatal US troop injuries recorded in recent conflicts (Iraq and Afghanistan). Most commonly, these injuries were recorded in enclosed environments, such as in vehicles, and were caused by improvised explosive devices (IED). An explosion under a vehicle causes rapid local deformation of the floor and upward acceleration of the seat which transfers high-rate loading to the occupant's lower extremities. The injury mechanisms and appropriate vehicle design strategies to enhance the occupant protection remain unclear. As a compliment to dummy/PMHS testing, numerical simulations could provide efficient means to better understand human injury mechanisms, assess vehicle safety throughout the design process, and lead to further improvements to the design of physical dummies.

Methods: In this study, the challenges of modeling lower extremities and lumbar spine in human and dummies are discussed. Human FE models (GHBMC model -v.4.1.1- [1] and THUMS model -v.4)) and dummy FE models: (Hybrid III -LSTC version and THOR-k -VT/NASA version [2]) frequently used in automotive crash simulations were evaluated in this study. Kinematic responses predicted by these models were compared to published data recorded under various vertical impact conditions. In addition, dummy injury criteria and human stress/strain data were calculated to evaluate the risk of injury predicted by the dummy and human models, respectively.

Results: Preliminary results show some correlations between the responses of FE models and their physical counterparts. In addition, predicted dummy injury criteria and human model stress/strain values are shown to positively relate. Softer responses were observed in soft tissue models (e.g. pelvic region), which could be caused by the lack of material characterization of these parts within the range of high-rate compression loading. Kinematic comparison between human and dummy models indicates promising biofidelic response, although a slightly stiffer response is observed within the dummy.

Conclusion: This study emphasizes the modeling challenges of lower extremities and lumbar spine and provides recommendations for improving current human and dummy finite element models. Future improvements include better material characterization of dummy and human parts as well as the implementation of inherent variability in geometry and material properties in human FE models.

References:

1. Untaroiu, C.D., Shin, J., Yue, N., Kim Y-H, Kim J-E, Eberhardt (2012) A Finite Element Model of the Pelvis and Lower Limb for Automotive Impact Applications, 12th Int. LS-Dyna Conference, Dearborn, MI
2. Putnam J.B., Somers J.T., Untaroiu C.D. (2013) Evaluation of Human and Dummy Finite Element Models under Spaceflight Loading Conditions, 41st International Workshop on Human Subjects for Biomechanical Research, Orlando, Florida.

Approaches for Predicting Human Anatomical Variations Using Anthropometric and Demographic Data

Carneal Catherine[1], Yoshito Otake[2,3], Dean Kleissas[1], Andrew Merkle[1], Mehran Armand[1,2], Manuel Uy[1], Gaurav Thawait[4], John Carrino[4], Brian Corner[5], Marina Carboni[5], Barry DeCristofano[5], Michael Maffeo[5]

[1]*Applied Physics Laboratory, The Johns Hopkins University, Laurel, MD, USA*
[2] *Department of Computer Science, The Johns Hopkins University, Baltimore, MD, USA*
[3] *Department of Mechanical Engineering, The Johns Hopkins University, Baltimore, MD, USA*
[4]*Department of Radiology, The Johns Hopkins Hospital, Baltimore, MD, USA*
[5] *U.S. Army Natick Soldier Research Development and Engineering Center, Natick, MA USA*

Computational models of the human body for injury prediction are frequently based on 50th-percentile male anatomies. These models may have limited applicability for the range of subject sizes and demographics for which protection systems are needed. Therefore it is necessary to understand how anatomy, and subsequent biomechanical response during impact events, vary across a wide variety of patient demographics (multiple genders, age, race, sizes). An approach has been developed to create a statistical shape atlas of the human lung using medical image datasets, and used to evaluate how variations in subject stature and demographics relate to changes in internal organ size. This method could be expanded for additional anatomical regions and tissue structures (both soft organs and skeletal) to provide a basis for developing computational human models appropriate for a range of human subjects.

The lung atlas was generated using existing radiological CT scans of the chest region collected from 124 patients in the Johns Hopkins Hospital radiology archives. A statistical shape atlas was created by manually segmenting a single template image to generate a lung volume mesh, applying deformable registration methods to map each individual subject CT to the template CT image, and applying the resulting deformation fields to the template mesh to create volumetric mesh representations of each particular subject. External anthropometry collected included patient height, weight, and chest dimensions (height, width, depth). Patient height and weight was readily available from the existing radiological archives. However, external chest anthropometry was manually approximated from skeletal landmarks on the subject CT images. This patient anthropometric data was compared to relevant Army Anthropometric Survey metrics to ensure good representation of a military population.

Statistical analysis was performed to determine how the subject's external variables scaled with overall lung dimensions (height, width, depth). The data indicates that chest height, rather than total body height, is the most important single predictor of overall lung geometry. Furthermore, lung dimensions scaled with external chest anthropometry measurements in the same plane (e.g., internal lung depth scales with external chest depth). Interestingly, neither body weight nor height were found to be a significant predictor of internal lung size (i.e. volume), although these parameters are traditionally applied for human scaling laws. Gender was found significant for overall lung depth and width, while race was only found significant for a minor number of variables.

This initial work has been expanded to implement a novel statistical approach to predict individual subject-specific lung anatomy with good accuracy (<1cm error) using the atlas. Methods to enable automated multi-organ atlases have also been recently developed, and demonstrated for the lung and liver. These methods will enable the study of not only how an individual organ changes within patient populations, but the relationships of organs to one another. Ultimately, elucidations of the relationships of internal organ size to external anthropometric data will advance the scaling fidelity and accuracy of human computational models for a broad range of subject populations.

Numerical Approach for Modeling Human Joints in Anthropomorphic Test Devices (ATDs)

Renuka Jagadish, Hyunsok Pang, Fuchun Zhu

Humanetics Innovative Solutions, Inc.
47460 Galleon Drive
Plymouth MI, 48170

The neck is a sensitive part of the human body and usually vulnerable to a number of injuries be it a crash or an under body blast event. A criterion Nij (Normalized Neck Injury Criteria) is used to determine the amount of load the neck can sustain before undergoing a severe injury.

In FE dummy development, the neck has to be modeled as closely as possible to represent the hardware and should be assigned with the right contact and material properties to capture the kinematics and get a good correlation with respect to the test curves. The nodding block is a small piece of rubber placed between the neck disc and the lower load cell and performs the function of the OC joint in humans. The gravitational weight of the head assembly falls on the loadcell which in turn compresses the nodding block rubber. This initial compression force/ pre stress at the interface has a significant effect on the results.

In LS-DYNA, to take into account the pre stress a card *INITIAL_FOAM_ REFERENCE _GEOMETRY is included in the input deck. In this card, both the initial nodes and the deformed nodes are included and at the beginning of the simulation, first timestep the solver will calculate the pre stress induced in the rubber blocks. MAT_77_O (Ogden Rubber) is used to define the nodding block material properties. The deformed nodes are obtained by pre-simulation. The loadcell is pushed down on to the nodding blocks by a displacement boundary condition. Then, the initial and deformed nodes are included along with the card in the neck component extension and flexion certification validation case. It is observed that including the nodding block with pre simulation improved neck injury curve validation and kinematics. This similar numerical approach will be used for accounting the pre stress of the neck buffer for the WIAMan dummy.

January 7, 2013
Session 2

Effect of Loading Rate and Orientation on the Compressive Response of Human Cortical Bone

B. Sanborn, C.A. Gunnarsson, M. Foster, P. Moy, T. Weerasooriya

Army Research Laboratory
Aberdeen, MD 21005

Under extreme environments such as a blast or impact event the human body is subjected to high rate loading which results in torn tissues and broken bones. The ability to numerically simulate these high rate events would improve protective gear by iterating on different protective configurations. Computer codes require input of accurate rate dependent material models representing the deformation and failure (or injury) to properly predict the response during simulation. Therefore, the high-rate material response must be measured for simulation of high rate events like blast. In this study, cortical bone compression specimens were extracted from the longitudinal and transverse directions relative to the long axis of the femur from three donors of ages 36, 43, and 50. The compressive behavior of the cortical bone was studied at quasi-static (0.001/s), intermediate (1/s), and dynamic (2000/s) strain rates using a split-Hopkinson pressure bar to determine the strain rate dependency on the strength of bone. Experimental results indicate that the cortical bone material is anisotropic; the cortical bone was stronger in the longitudinal direction compared to the transverse direction. The human cortical bone was also rate dependent in both directions. No distinct relationship was found between donor age and compressive strength most likely due to the small sample and age range of the donors.

Experimental and Finite Element Analysis of Brain Tissue under High Strain Rates

R. Prabhu[1,2], M.F. Horstemeyer[1,2],W.R. Whittington[1], M. T. Tucker[3], E.B. Marin[1], J.L. Bouvard[1], J.A. Sherburn[4], R. King[1], J. Liao[1,5], L. N. Williams[1,5]

1 Center for Advanced Vehicular Systems, Mississippi State University, MS 39759.
2Mechanical Engineering Department, Mississippi State University, MS 39762.
3Group MST-8, Structure/Property Relations, MS G755, Los Alamos National Laboratory, Los Alamos, NM 87545.
4U.S. Army Engineer Research and Development Center, Vicksburg, MS 39180.
5Agricultural & Biological Engineering Department, Mississippi State University, MS 39762.

This paper presents a coupled experimental/modeling study of the mechanical response of porcine brain under high strain rate loading conditions. Essentially, the stress wave propagation through the brain tissue is quantified. A Split-Hopkinson Pressure Bar (SPHB) apparatus, using a polycarbonate (viscoelastic) striker bar was employed for inducing compression waves for strain rates ranging from 50 – 750 s^{-1}. The experimental responses along with high speed video showed that the brain tissue's response was nonlinear and inelastic. Also, Finite Element Analysis (FEA) of the SHPB tests revealed that the tissue underwent a non-uniform stress state during testing when glue is used to secure the specimen with the test fixture. This result renders erroneous the assumption of uniaxial loading. In this study, the uniaxial volume averaged stress-strain behavior was extracted from the FEA to help calibrate inelastic constitutive equations.

Hierarchical Development of Biomedically Validated Human Computational Models

Robert Armiger, Alexis Wickwire, Kyle Ott, Alex Iwaskiw, Tim Harrigan, Liming Voo, Jiangyue Zhang, Catherine Carneal, Jack Roberts, Andrew Merkle

The Johns Hopkins University Applied Physics Laboratory, Laurel, MD

Developing human computational models for high-rate injury prediction capable of simulating response over a range of inputs requires a robust model development process and validation at multiple levels. Biofidelic response and injury mechanisms should be defined at the tissue, component, and system levels in order to ensure the model's appropriateness for multiple loading regimes. We have successfully demonstrated a collaborative approach resulting in a framework for model development that applies this hierarchical approach for blast loading applications. Here we present the application of this hierarchical model development and validation framework for the human head and neck system. This high-fidelity head-neck model is intended to predict response to blast loading, including both blast overpressures and vertical loading.

At the tissue level, an experimental protocol was established to characterize the mechanical properties of key anatomical structures at high rates. Bulk and shear properties of human brain tissue (with a post mortem interval of < 48 hours) were measured using a modified Split Hopkinson Pressure Bar. Additionally, the falx cerebri and tentorium cerebelli were characterized at the tissue level using dynamic material analysis. Additional material properties were identified from the literature where appropriate and applicable. At the component level, falx material properties were validated against experimental response of the falx in-situ. Skull flexural properties were also investigated at the component level to assess brain response during dynamic head loading. Finally, at a system level, cadaveric head-neck complexes were exposed to blast overpressure using a shock tube coupled with a high-speed x-ray. Four columns of radio-opaque neutral density markers were inserted into the brain of the perfused specimen. Response was characterized using three primary metrics: head kinematic response, intracranial pressure response, and brain displacement relative to the skull.

At the system level, the dynamic overpressure experimental results were used to validate the computational model predictions. For a mild loading condition (700 kPa driver pressure), complex head kinematics were generated. Sagittal head rotation exhibited an initial flexion of the head at a small peak angle (<5 degrees) in the first 20 m/s and a larger flexion (-41.2 deg) at 150 msec. Data from multiple specimens were used to generate response corridors and the computational model response fell within the experimental corridor for the same loading severity. For brain model validation data, the tissue displacement generated from the tracked brain markers showed a similar spatial response with a maximum excursion (6.3 mm) located near the posterior-superior aspect of the skull. Due to shape variation across the specimens, parametric scaling and affine registration was applied to the computational model to compare the model's nodal displacement to experimental markers.

The hierarchical modelling approach employed in the development of the head-neck model involved deriving high-rate material properties from tissues being modeled. Isolated component tests were used to characterize in-situ response of anatomical structures, and then system level validation was used with a matched experimental model. The system level model and experiments were then used to validate that the tissue and component level models addressed the relevant ranges for the conditions being addressed. Parametric scaling of the model allows direct error analysis compared to the experimental results at the system level, and the hierarchical approach allowed parallel development efforts to be integrated into a final validated system. The resulting model, verified at several structural levels, is intended to be used in a predictive manner to design injury countermeasures with a high degree of confidence.

Material properties of the Human Heel Fat Pad Across Loading Rates

Grigoris Grigoriadis, Nicolas Newell, Spyros D Masouros, Anthony MJ Bull

The Royal British Legion Centre for Blast Injury Studies, Imperial College London, UK

In modern warfare and military operations, anti-vehicular (AV) landmines and improvised explosive devices (IEDs) are common causes of casualties with lower extremities injuries accounting for more than half of the skeletal injuries. In the case of an explosion under a vehicle, the rapid deformation of the floor causes intra-articular calcaneal fractures with high rates of amputation and poor outcome [1].The first body part in contact with the loading boundary is the heel fat pad whose material behaviour and load-attenuating capacity at high loading rates are ill-understood. The complexity of this material behaviour stems from its unique microstructure; it consists of septral walls that surround and retain adipose tissue, similar to a honeycomb. The aim of this project was to quantify the material behaviour of the human fat pad across loading rates.

Due to the complex tissue microstructure, extracting small samples might disturb material continuity and result in unrepresentative material properties; therefore an inverse finite element (FE) method was utilised. A cadaveric human foot was dissected leaving the calcaneus intact, with the fat pad attached to it. Quasi-static compressive (displacement rates of 0.01-1 mm/s) and drop (mass of 7 kg, velocities at impact of 0.4-3.5 m/s) tests were performed. An FE model of the cadaveric foot was developed in MSC.Marc (MSC.Software, Santa Ana, CA, USA). The geometry was acquired from MRI and CT scans. A material formulation combining the hyper-viscoelasticity and the strain-rate dependency of the tissue was developed and implemented. The constants of this formulation were obtained through a non-linear optimisation algorithm until numerical and experimental response matched to minimum error.

The best fit for the quasi-static hyperelastic behaviour of the material was achieved with an exponential formulation, resulting in a coefficient of determination value (R2) greater than 0.99 and an average error of 5%. Similarly, the strain-rate dependency was derived using a Cowper-Symonds formulation; this has been used elsewhere to model the strain-rate dependency of the human kidney capsule [2].

In conclusion, the material properties of the human heel fat pad for a cadaveric specimen were obtained through an inverse FE method. These properties will be implemented in a subject specific FE model of the foot for under-body blast. In addition, this procedure will be repeated for another six cadaveric specimens in order to obtain an average material behaviour for the fat pad.

References

[1] Ramasamy A, Hill AM, Phillip R, Gibb I, Bull AMJ, Clasper JC. 2011. The modern 'deck-slap' injury - calcaneal blast fractures from vehicle explosions. *The Journal of Trauma* 71: 1694-1698.

[2] Snedeker JG, Niederer P, Schmidlin FR, Farshad M, Demetropoulos CK, Lee JB, Yang KH. 2005. Strain-rate dependent material properties of the porcine and human kidney capsule. *Journal of Biomechanics* 38: 1011-1021.

Effect of Loading Rate on the Fracture Behavior and Mode Mixity for Crack Initiation of Human Femoral Cortical Bone

Tusit Weerasooriya, C. Allan Gunnarsson, Brett Sanborn, Mark Foster, Paul Moy

During injury causing events such as impact, blunt trauma, penetration or blast, the human body is subjected to high loading rates. These events will deform and damage human tissue, frequently causing tearing in soft tissues and cracking/fracture in hard tissue (bone), due to its inherent brittleness. For the development of accurate material models for computer simulation of bone fracture during these events, it is necessary to investigate the failure behavior (fracture) of hard tissue at different loading rates, including high loading rates found in blast and impact events. In this study, the Mode I fracture behavior of human femoral cortical bone is directly investigated as a function of loading rate. In addition, the displacement fields generated around the crack tip are measured using optical techniques allowing for the determination of the Mode I, II, and mode mixity fracture parameters. Human cortical bone fracture specimens were extracted from the longitudinal direction (long axis) of the femur from three male donors of ages 36, 43, and 50. The fracture behavior of the cortical bone was studied at quasi-static (0.005 kN/s), intermediate (0.5 kN/s), and dynamic (1000 kN/s) loading rates using a modified split-Hopkinson pressure bar with integrated quartz load cells. During these fracture experiments, the crack-tip displacement and strain field was measured using ultra high speed (500K fps) DIC (digital image correlation) to understand the fracture initiation behavior and to allow for development of crack growth criteria. Macro-level observations of the fracture surfaces from the fractured bone specimens provide insight on the influence of the underlying bone microstructure on the failure behavior. The fracture toughness of human bone increased as the loading rate increased from quasi-static to intermediate, but then decreased as rate again increased to the dynamic region. This behavior is similar to other fracture research on animal cortical bone. Using the measured crack-tip full-field displacement tensor evolution, a method is developed to obtain the Mode I and Mode II fracture parameters for the anisotropic bone material. With this method, K_I and K_{II} evolution is obtained as a function of loading rate, and as a function of time during each individual experiment. Using these K temporal evolution plots, the critical K_I and K_{II} values for crack initiation can be obtained for anisotropic human cortical bones as a function of loading rate. In this presentation, preliminary results from this study are presented.

Recent Developments in a Computational Shock Physics Tool for Modeling Fluid-Structure Interaction

Shane C. Schumacher, PhD PMP

Sandia National Laboratories[a]
PO Box 5800 MS---0836
Albuquerque, NM 87123---0836
505-284-0610
scschum@sandia.gov

A large challenge for modeling the human body and surrogates to various loadings has been to accurately computing the fluid--structure interactions. Over the past four years Sandia National Labs in collaboration with Los Alamos National Laboratories and the Department of Defense have been developing Lagrangian and Multifield numerical techniques for use in an Eulerian production based computational shock physics code. A benefit of modeling the response of the human to various loading in an Eulerian computation tool is the ability to perform solid object insertion and field interactions. These new numerical techniques provide a coupled fluid-interaction that may be used for modeling human and human surrogates subjected to accelerative or terminal ballistic loading conditions.

This is accomplished by adding numerical methods for Lagrangian field behavior, separate velocity fields for each field to model multiple field interactions, Multifield, and for addressing time scales from shock to late time structure responses using Implicit Continuous Eulerian (ICE) techniques. The Lagrangian Material Point Method (MPM) and one of its derivatives (Convective Particle Domain Interpolation, CPDI) have been implemented into CTH for modeling fields (materials) in a purely Lagrangian sense. The MPM provides a Lagrangian basis for proper integration of the deformation gradient tensor for modeling nonlinear elastic materials in shock, advection error elimination, and a mechanism for modeling large deformations with strength. The Multifield numerical method provides separate velocity fields for each field within a simulation. The separate velocity fields are remapped separately and require mass, energy and momentum exchanges to define the multiple field interactions. The interactions are models such as drag, and sticktion that define how a field interacts with another field not requiring surface or node contact definitions for computing the field interactions. The ICE methods addresses time scales of a simulation by regulating the time step bound by the velocity and shock courant time step limitations. Currently, most shock simulations are fixed to the shock currant time step, but with ICE, the simulation numerics sense a reduction of the shock waves and progress to a velocity courant time step. These techniques are currently under development and progress on the three tasks will be discussed along with scheduled release dates.

[a]Sandia National Laboratories is a multi-program laboratory managed and operated by Sandia Corporation, a wholly owned subsidiary of Lockheed Martin Corporation, for the U.S. Department of Energy's National Nuclear Security Administration under contract DE-AC04-
94AL85000.

Multiscale Modeling of Human Body and Vital Organ Responses to Blast and Accelerative Loadings

A.J. Przekwas and X.G. Tan

Computational Medicine and Biology Div.
CFD Research Corp., Huntsville AL

In the last few years anatomical/geometric models of a human body and computational biomechanics tools have progressed substantially toward accurately predicting injury biomechanics. However, because the multiple scales, in both time and space, involved in modeling human body biodynamic and injury biomechanics direct simulation of primary injury biomechanics is not possible yet.

In the last few years, in collaboration with DoD teams, CFDRC has developed anatomically accurate, articulated virtual human body models and multi-scale computational tools, CoBi, for simulations of blast and acceleration induced injury. This multi-physics, multiscale modeling tool has been adapted for the analysis of human body biodynamic response to blast, kinetic and accelerative loading. The loads are used for modeling biomechanics of primary injury mechanisms and to provide inputs for secondary physiology-neurobiology events. We present the approach and framework to generate anatomical and geometrical models of the whole human body and vital organs, including brain and vascular system, for coupled biomechanical and physiological simulations.

The human biodynamic, biomechanics and the vascular hemo-elasto-dynamics models have been validated against experimental human physical surrogates and *in vivo* animal models. Direct comparison between the experimental and computational data for test problems demonstrates very good predictive capability of the model. The implications of these results suggest that computational models could be used to predict the biomechanical response in the blast TBI event, and help design the protection against blast TBI. We will present numerical modeling details, current model capabilities and limitations. CoBi tools and human body models are being developed as a DoD Open Source form.

ABSTRACTS

Workshop on Numerical Analysis of Human and Surrogate Response to Accelerative Loading

January 8, 2013
Session 3

Comparing the use of Dynamic Response Index (DRI) and Lumbar Load as Relevant Spinal Injury Metrics

Ravi Thyagarajan and Jaisankar Ramalingam,
US Army TARDEC, Warren, MI 48397
Kumar B Kulkarni,
ESI-US Inc., Troy, MI 48084

Motivation/Objective:
It is well-known that the high vertical accelerative loads arising from vehicle underbody blasts result in debilitating spinal injuries to occupants, often resulting in severities ranging from non-return to duty for extended periods of time to life-long loss of mobility. The survivability community quickly realized that in order to design vehicles, seats, restraints and other mitigation features to combat the deleterious effects of underbody blasts, performance criteria that serve as representative metrics of spinal injuries, or lack thereof, were necessary. Initially, these criteria were based on "indirect" validation against potential injury during qualification testing. For example, in the late 1990s, MIL-STD-1290 stipulated an impact velocity change parameter based on operational mishap data. In the past 20 years, these criteria have become more "direct" in varying degrees. For example, the two most commonly used today for Spinal injuries are Dynamic Response Index (DRI) related to structural accelerations, usually of the seat pan, or even more directly, lumbar force measurements taken within the Hybrid-III anthropomorphic test device (ATD) as the evaluation criterion.

With respect to continued use of these two criteria for spinal injuries, this paper will examine the following aspects in detail:

1) Any existing correlation between Peak Lumbar loads and DRI for un-encumbered occupants, in the whole blast loading regime or at least within different loading regimes
2) Re-evaluate (1) for encumbered occupants, that is, with –additional mass on upper torsos
3) Potential changes to DRI calculations and Injury Assessment Reference Value thresholds for encumbered occupants
4) General discussion on continued use of DRI as a design criterion for spinal injuries given the availability of the more direct Lumbar load from fully encumbered ATDs in underbody blast testing.

Approach:
A dynamic simulation model of a vertical blast loading simulator was used, which contains a seated 50th percentile Hybrid-III ATD. Two different versions of the ATD, namely, the LS-DYNA finite-element model from Humanetics and the MADYMO rigid multi-body model from TASS were used. A parametric study was conducted on these setups by varying the peak accelerations, and durations of the pulse so as to result in a range of Δv (change in velocity). A rigid seat, with and without an energy-absorbing member, were used in the study. Best-fit analysis was also performed and overlaid against the data samples. Similar trend analyses were also performed for data from physical tests.

Developing an Empirical Model to Estimate Tibia Injury

Brian Benesch

Under-body blast (UBB) attacks against ground vehicles may result in lower leg injuries to mounted occupants. The Test and Evaluation (T&E) community currently lacks reduced-order (RO) tools that are capable of accurately and efficiently estimating these injuries. As part of an ongoing effort to develop RO under-body blast methodology, the Army Research Laboratory (ARL) and its partners are investigating empirical correlations of vehicle response and lower leg injury.

Live-fire testing is conducted to exploit vehicle and occupant protection from UBB threats and the resulting data offers a key source for empirical model development. Instrumentation from live-fire includes both anthropomorphic test devices (ATDs) and accelerometers mounted on the vehicle structure. While ATD's are the most common method of evaluating occupant injury, it is important to also interpret the structural response of the vehicle in terms of injury-causing potential. In doing so, vehicle designers can better understand the underlying causes for injuries and then more effectively design survivability improvements.

ARL compiled results from hundreds of live-fire UBB events in order to investigate a correlation between data from floor-mounted accelerometers and ATD lower-leg responses. The immediate focus of the effort was on ATD's seated in a nominal position (90 degree angle at the hips and 90 degree angle at the knees) with feet flat on the floor. Data measured from floor-mounted accelerometers near the ATD feet were characterized into a number of different metrics and correlated to the lower tibia compressive force as well as the lower revised tibia index (RTI).

Empirical models were developed to estimate lower tibia compressive force and RTI injuries as a function of floor accelerometers' peak velocity and local displacement. Two sets of models were developed for each injury type (compressive force and RTI); one set to estimate the specific force or RTI, and the second set to estimate a probability of exceeding the current injury threshold. These models serve as a preliminary approach for estimating injury given a floor response.

The empirical approach offers the rapid capability to estimate tibia injury using a known or estimated response at the vehicle floor. In terms of numerical modeling, this would minimize the need for a computationally-intense finite element representation of the ATD. However, a trade-off between accuracy and speed must be considered within the context of the desired use of the results. Additionally, the empirical model is restricted by the limitations of the underlying live-fire tests.

Towards A Micromechanics-based Simulation of Calcaneus Fracture and Fragmentation Due to Impact Loading

Rebecca A. Fielding[1], Wesley S. Teerlink[1], Michael V. Robinson[1], Christopher D. Kozuch[1], Hannah V. Putnam[1], Timothy M. Ryan[2] and Reuben H. Kraft[1]

[1]Computational Biomechanics Group
Pennsylvania State University,
Department of Mechanical and Nuclear Engineering,
University Park, PA 16802

[2]Center for Quantitative Imaging
Pennsylvania State University,
Anthropology and Information Sciences and Technology,
University Park, PA 16802

Within a hierarchical modeling framework adopted for biological systems, the components and sub-assemblies are critical to the system-level response. As full (system-level) human body finite element models become more widely used in the military design process, the need for region-specific constitutive models and robust fracture modeling methods at the component and sub-assembly level will increase. This presentation discusses early efforts at creating a high-resolution computational model of the human calcaneus, with primary focus on modeling the fracture network through the complex microstructure of the bone and creating micromechanically-based constitutive models that can be used within full human body models. Our ultimate goal is to develop a micromechanics-based simulation of calcaneus fracture and fragmentation due to impact loading. This presentation will focus on model development.

Scans of male and female cadaveric calcanei were scanned to a resolution of 55 microns using an industrial computed tomography (CT) scanner. The scans were post-processed and will ultimately be used to generate finite element meshes of calcanei. The microstructure of the calcaneus is extremely complex with intricate anisotropic trabecular patterns, which can be organized as compressive and tensile trabeculae. In these early efforts, we have been working to characterize the length scales associated with the cortical bone, the anisotropic structure of the trabecular bone and the region-specific porosity. Results and statistics will be presented.

Segmentation and finite element mesh creation is a challenge when dealing with the complex microstructure of the calcaneus. Part of our ongoing research is establishing the best processing algorithms on the raw image data (see Figure 1). In our current approach, first, all slices of each calcaneus were opened in Avizo Fire and resampled to decrease the size of the data. A median filter was then applied, and a label field was created to delineate the bone. The label field was used to generate a surface, which was then exported to a finite element meshing software. Finally, the meshed calcaneus was imported to a finite element solver. Current investigations are focused on re-ordering or eliminating the resampling step to help maintain the true topology of the trabecular bone.

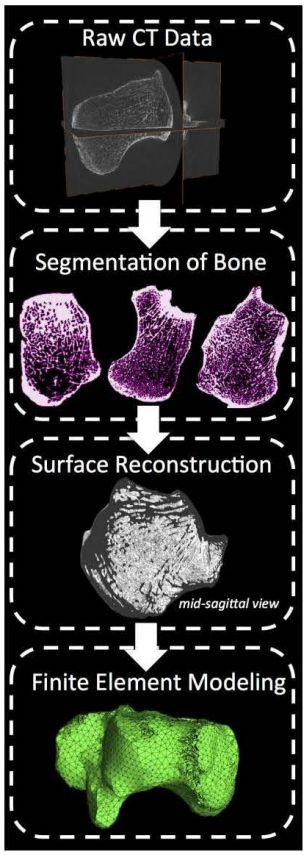

Figure 1. Imaging processing steps.

Pelvis Response Effects on Whole Body Under-Body Blast Simulations

Adam Golman, Kyle Ott, Robert Armiger, Tim Harrigan, Catherine Carneal, Andrew Merkle

The Johns Hopkins University Applied Physics Laboratory, Laurel, MD

Pelvic response is critical in determining the response of seated occupants exposed to under-body blast (UBB). This relationship has been demonstrated in both the analysis of human surrogate data and in finite element model (FEM) simulations. The pelvis response is dependent upon the compliance, structure, and mechanical linkage to the legs and lumbar spine. The Hybrid III (HIII) pelvis is not designed for, and therefore not durable, when loaded in the vertical direction. As a result, damage to the pelvis foam and skin can significantly affect the measured response in the pelvis and influence the whole body response. The objective of this study was to determine the effect of a range of pelvis foam material properties and exposure conditions on whole body response during simulated UBB loading.

Prior to UBB simulation, a HIII FEM was placed into a rigid seat and floor platform configuration identical to the JHU/APL's Vertically Accelerating Load Transfer System (VALTS) and then positioned by applying a gravity load and belt pretensioning. The pelvis foam material properties were varied and resulting effect on response assessed. Three nominal UBB loading scenarios were simulated using a Hybrid III FEM in a configuration modeling the VALTS. The simulated UBB loading scenarios were Case 1: Floor Vz = 3 m/s, duration = 9.3 ms; Seat Vz = 3 m/s, duration = 12.5 ms; Case 2: Floor Vz = 10 m/s, duration = 7.3 ms; Seat Vz = 5 m/s, duration = 19.6 ms; and Case 3: Floor Vz = 10 m/s, duration = 7.3 ms; Seat Vz = 3 m/s, duration = 32.3 ms. Biomechanical responses and relevant injury prediction were used to assess the whole body response. These responses included lumbar forces and moments, pelvis vertical acceleration, and tibia axial force.

Decreases in pelvis foam stiffness resulted in increases in pelvis acceleration and lumbar load. Upon closer inspection, these increases were due to the pelvis foam being fully compressed, thus allowing the rigid portions of the pelvic model to come in contact with the rigid seat. This bottoming out effect resulted in large stress concentrations (>300 MPa) on the bottom of the pelvis foam near the ischium, which are indicative of the pelvis foam and skin material failure seen experimentally in VALTS test results. Increasing UBB severity (Case 1 vs. Case 2) caused all injury metrics to significantly increase. After decreasing the seat velocity in the severe event (Case 2) to simulate a longer loading duration (i.e., an energy absorbing seat, Case 3), the vertical pelvis acceleration and vertical lumbar load decreased from 104 g to 46 g and 13.3 kN to 4.5 kN, respectively for the nominal pelvis foam material properties. Interestingly, the decreased seat velocity in Case 3 allowed the floor to push up on the legs at a higher velocity than the torso, causing the legs to pull the pelvis forward, rotate the pelvis around the belt and pull the torso downward. These kinematics resulted in an increased lumbar moment, but decreased lumbar axial force. This effect could ultimately lead to decreased loads transferred up the spine and possibly a decrease in incidence of roof impact, thus lowering the risk of head and neck injury.

This study demonstrates the use of finite element models to inform the whole body response in UBB loading. The results from this study suggest the significant influence the pelvic response has on the whole body response, which should be considered in future ATD development. These techniques for model setup and areas of special consideration including the pelvis can be extended to human FEMs in the future.

January 8, 2013
Session 4

Development & Validation of the WSU Human Body Model

Alan Goertz

The Wayne State University finite element Human Body Model (WSUHBM) has been under development for approximately twenty years. The model has been validated and utilized for a variety of automotive safety research functions such as restraint system development and injury mechanism analysis. These automotive applications have relied on loading primarily in the horizontal plane representing frontal and side impact collisions. Recently the model has been adapted to handle large vertical loading forces consistent with those experienced by occupants of vehicles in under body blast events (UBB) with focus on lower extremity and spine loading.

Various parts of the WSUHBM have been extensively validated for automotive crash loading conditions. Typical validation metrics are contact forces, accelerations or deflections or a combination thereof. The upper torso, shoulder and abdomen have been validated using blunt impacts representing contact with vehicle interior components such as door panels, arm rests, steering wheel, seat belts and airbags. Aortic rupture injuries have been investigated by determining dynamic aortic stress and haemostatic pressures. The lower leg has been validated for knee-instrument panel contact and axial compression of foot and lower leg resulting from toe pan deformation during frontal collisions.

The high incidence of UBB related injuries in Theater has renewed interest towards research in human response under vertical loading. Wayne State has recently published a validation of the lower leg under vertical blast loading conditions based on tibia axial forces and acceleration. ARL is currently working with the WSUHBM towards validating the model under vertical loading conditions and utilizing the model for preliminary evaluation of lower leg and spine injury mitigation concepts. Some success has been achieved in duplicating inertial spine loading and accelerations seen in physical tests.

Until a suitable physical surrogate is developed, numerical models such as the WSUHBM are poised to provide our maximum capabilities for determining body loading and injury prediction parameters that are necessary for developing and improving injury mitigation concepts.

Adapting automotive-based finite element models of lower extremity for high-rate impact simulation of occupants subject to under-vehicle blasts

MB Panzer, PhD and RS Salzar, PhD

Center for Applied Biomechanics,
Department of Mechanical and Aerospace Engineering,
University of Virginia,
4040 Lewis and Clark Dr.,
Charlottesville VA, 22911

One of the major concerns in automotive safety is the large number of severe injuries to the foot and ankle complex caused by axial loading to the lower leg, which is associated with an intruding foot-pan during frontal vehicular crashes (Crandall, 1994). Research on foot and ankle injury mechanisms for these impacts have led to the development of advanced, injury-predictive finite element (FE) models of the lower extremities (e.g., Shin et al., 2013). One of the major concerns in military safety is severe fractures to the foot-ankle-lower leg in occupants of armored vehicles that were exposed to a blast. These injuries account for over 80% of all skeletal injuries found in underbody blast (UBB) events (Ramasamy, 2011). Battlefield epidemiology suggests that these injuries are caused by axial loading to the lower extremities from contact between the deforming vehicle body and the occupant's feet. Thus, we can draw parallels between automotive and military lower extremity injuries, and potentially leverage our experiences with FE models intended for automotive impact loading to develop computational models for injury prediction from the high-rate dynamics caused by UBB.

This study focuses on predicting the mechanical response and injury outcome from high-rate axial impacts to the lower leg using FE models of the Hybrid III dummy (originally developed by LSTC) and the 50th percentile male (originally developed by UVa for Phase I of the Global Human Body Model Consortium). Both models have been previously validated for a multitude of loading conditions typically associated with automotive impacts. The current study extends the capabilities of both FE models for use with UBB loading. The lower leg FE models were compared to drop tower impact tests performed on 18 post-mortem human surrogate (PMHS) lower legs (Henderson et al., 2013), and 18 Hybrid III lower legs. For these tests, the proximal ends of the lower legs were mounted at the bottom of a drop tower equipped with an impactor capable of producing axial loading on the foot up to 600 g's acceleration over 1.5 ms duration.

Using the unmodified versions of the FE models, the force-time histories measured in the proximal load cells were a poor representation of the experimental data; compared to the experimental data, the FE model force magnitudes were much lower (by more than 50% in most cases), and the phase-delay and duration of the force pulse were nearly twice as long. Both models were modified to better reflect the loading conditions produced in the experiments, including the implementation of high-rate properties for the constitutive models of the soft materials in the feet of the human model and the dummy model. These changes greatly improved the fidelity in both models. Force amplitudes and phasing measured using the modified FE models were very similar to those in the experimental tests. The force-time history for the modified Hybrid III model was nearly identical to those measured in the experiment. The modified human model response had an average correlation coefficient with the experimental data of 0.85 over the entire time-history. Similar fracture patterns were seen in the calcaneus for both the FE model and the experiment. Many of the differences seen between the FE model and the experimental data may be attributed to not including the variations in geometry and age for the PMHS tested in the experiment.

This study demonstrates that military-spec FE models of dummies or humans can leverage prior modeling experiences with FE models developed for automotive safety to create tools for evaluating future systems designed to mitigate injury in UBB events.

Current Research and Development Activities of the Full Body Model Center of Expertise of the Global Human Body Models Consortium Project

Gayzik, F. S., Vavalle, N.V., Moreno, D.P., Stitzel, J.D.

Wake Forest University School of Medicine
Virginia Tech - Wake Forest University Center for Injury Biomechanics

Introduction: The Center for Injury Biomechanics at Wake Forest University is the Full Body Models Center of Expertise (FBM COE) for the Global Human Body Models Consortium (GHBMC) project. The GHBMC is a consortium of automotive manufacturers and suppliers who, along with a sponsoring federal agency (NHTSA), have consolidated individual research and development activities to advance the state of the art of computational human body modeling. This abstract reviews the activities of the FBM COE, including the development of the average male occupant model (M50) as well as current actives that aim to expand the scope of the project.

Development: The M50 model was developed using scans from multiple medical imaging modalities and extensive anthropometry data acquired from a living adult male volunteer (height 174.9 cm, weight 78.6 ± 0.77 kg, age = 26y). The individual matched the 50th percentile value of 15 external anthropometry measurements with an average deviation of 3%. Posture-specific CAD data was developed and served as the foundation for mesh generation. The geometry of the model has been verified against various literature sources, including the mass of body segments, thickness of cortical bone, volumes of organs, and diameters of major vessels.

Results and Current Version: Version 4.1.1 of the M50 model contains 2.2 million elements, 1.3 million nodes and weighs of 76.8 kg. Extensive anatomical detail is modeled: the brain with 22 subcomponents, neck musculature with 52 individual muscles, and major organs and vessels of the thoraco-abdominal cavity. Pre-programmed 'sensors' are included that provide output data analogous to ATDs such as head acceleration, Nij, chest acceleration, chest compression, pelvic and femur loads.

FBM Validation Summary: The FBM COE has conducted 13 trials including 9 validation, 2 repositioning, and 2 robustness simulations (frontal and lateral NCAP simulations) with the current version of the M50 model. Simulations were run using LS-Dyna R6.1.1. on a Linux cluster with 48 CPUs. Validation simulations included six hub-type impacts (frontal chest, lateral shoulder, frontal abdominal bar, oblique abdominal, lateral pelvis, and a lateral plate). The remaining three validation simulations were frontal and lateral sled tests. CORrelation and Analysis objective rating software (CORA, v. 3.5) was used to assess model agreement within experimental data. Along with validation at the full body level, body region specific validations of the head, neck, thorax, abdomen, pelvis and lower extremities were conducted by six collaborating universities. The M50 model matches experimental data well. In the six validation simulations with enough experimental data for a complete CORA comparison (including Magnitude, Phase, Shape and Corridor ratings), the average combined score was 0.75 (max of 1). For the subgroup of only hub-type impacts, the average was 0.83.

Current and Future Work: The FBM COE is currently working on Phase II of the GHBMC project. One focus is on continuous improvement and enhancement of the M50 model, but several new parallel modeling initiatives are underway. Detailed models of the 5th percentile female (F05) and 95th percentile male (M95) occupants are being developed, either through a similar process as described above (in the case of F05) or through scaling (in the case of M95). Simplified versions of the models are being generated for rapid kinematic assessment and stochastic modeling studies. Models will be developed in the pedestrian posture as well. The FBM COE at Wake Forest University, in conjunction with the GHBMC and its partners, is positioned to create a suite of models to advance the state of human body modeling in trauma research.

Modeling the Human Head and Neck: Sensitivity and Response

Courtney Cox, Brian Bigler, Jason Luck, Cameron R. ' Dale' Bass

Duke University

Computational modeling provides an effective means for capturing the response of complex systems. The data gleaned from such models is often difficult or impractical to capture experimentally. Using finite element analysis, one can determine the entire 3D mechanical response of biological systems subject to high-rate accelerative loading conditions. Such models allow for assessment of the effects of input variables such as posture, muscle activation, nonlinear and/or inhomogeneous material properties, and boundary conditions, including the assessment of variance on the response.

The Duke head/neck model consists of an osteoligamentous cervical spine (C1/C2, C3 to T1) and head modeled as rigid bodies coupled by six degree of freedom non-linear viscoelastic beam intervertebral joints (Occiput-C2, C2-C3, to C7-T1). The model includes 22 primary cervical spine muscles, which are split into 81 muscle strands to span their broad origins and insertions. Each muscle strand is modeled with viscoelastic beam elements to capture the active and passive muscle behaviors. This allows a computationally efficient model, while still obtaining parameters of interest (primarily kinematics and kinetics). By integrating other models, such as the MADYMO human model, underbody blast end conditions for C7/T1 can be determined and applied to the Duke head/neck model. Integration with Duke brain slice models can provide insight to brain injury during high-rate loading. In addition, the influence of personal protective equipment (PPE) on head and neck response can be quickly analyzed to assess ability to reduce injury.

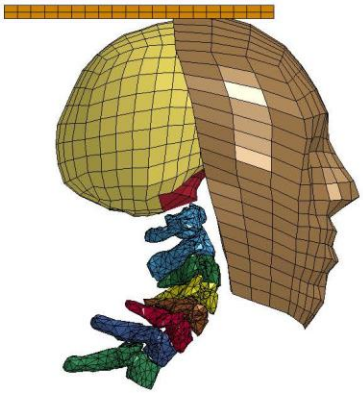

Figure 1. Duke head and neck model exhibiting buckling behavior during high-rate impact with a rigid plate. Musculature removed for visualization.

Inverse finite element analysis can match model parameters to experimental data to improve model biofidelity. By iteratively determining material properties that optimize the model response, the Duke head and neck model is capable of recreating experimental conditions *in silico* with a high degree of accuracy and predictive capability.

Sensitivity analyses allow for the determination of key factors affecting head and neck response including the effect of statistical variance. Variables such as head center of gravity and neck posture can be analyzed without numerous experimental tests. Capturing specimen variation through these methods allows for corridor response prediction that can be used to improve the effectiveness of costly cadaveric testing.

Human Body Model Injury Analysis in Real-World Crash Simulations

Kerry A. Danelson, 1, 2 James P. Gaewsky, 1, 2 Caitlin M. Weaver, 1, 2 and Joel D. Stitzel1, 2

1. VT/WFU School of Biomedical Engineering and Sciences
2. Wake Forest University School of Medicine

Real-world crash simulation with human body models is a useful technique to assess vehicle performance and injury mechanisms. A limiting factor in these simulations is the paucity of full vehicle models available for researchers. To address this limitation, an adjustable reduced vehicle model was created to simulate any vehicle in crash reconstruction simulations. Frontal crash cases with minimal intrusion and Event Data Recorder (EDR) data were the first crash type investigated. The reduced vehicle was based on the National Crash Analysis Center (NCAC) Ford Taurus full vehicle model. The surrounding structure was removed until the only parts remaining were the driver seat, dash panel assembly, and steering column assembly. A simplified flat floor replaced the existing floor pan. The reduced vehicle was tuned using a variation study that minimized error between the occupant response from a National Highway Traffic Safety Administration crash test and the simulation. The occupant was a Hybrid III Anthropomorphic Test Device (ATD). The position of the seat, steering wheel, knee bolster, and floor was adjusted to match the target crash test measurements. The tuned vehicle parameters were: the steering column shear bolt force, steering column stroke resistance, frontal airbag properties, knee bolster airbag properties, and seatbelt properties. The final vehicle configuration will be used with the Total HUman Model for Safety (THUMS) to simulate a CIREN case in a crash configuration similar to the crash test. To better relate the THUMS response during a motor vehicle crash simulation to risk of injury, our group has developed several injury risk metrics. These metrics are intended to mirror current measurement capabilities of Anthropometric Test Devices (ATDs) and leverage the anatomic detail of the model to supplement these standard measurements with additional injury risk data. The results of this work have demonstrated the ability of these enhanced metrics to more fully describe the occupant response during an impact event. Specifically, strain metrics within the bones and organs provide more detail on the potential location of injury through matching the finite element model results to actual patient radiology from the simulated cases. Ultimately, the techniques described in this study will be applied to multiple real world cases with both injured and non-injured occupants to begin to establish the metric thresholds of interest to predict real world injuries.

Numerical modelling undertaken at Dstl (UK) concerning vehicle floor plate impact of surrogates and anatomical human entities due to under-body mine loading

Dan Pope, Chris Taggart, Joe Cordell and Ian Softley

The Defence Science and Technology Laboratory (UK) has a strong interest in the numerical simulation of human and surrogate entities under dynamic loading. Over the past few years, the Structural Dynamics Capability within the organisation has developed numerical models of the Hybrid III and Mil-Lx physical leg dummies with the intention of faithfully predicting their response when impacted by the floor plates of military vehicles as a consequence of under-body mine blast loading. The research has now been extended to consider the simulation of anatomically-representative human legs under similar conditions. After providing a general description of the Structural Dynamics Capability in the field of human injury, this presentation details the approaches adopted in generating geometrically-faithful spatial representations and the steps taken to ensure the inclusion of faithful material models for the constituent components. The majority of simulation activity has been undertaken using Lagrange related functionality within the LS-DYNA finite element code, produced by LSTC. In generating these models emphasis has been placed on justifying the selection of element types and solvers; the use of appropriate contact logic to ensure proper component interaction; the extraction of meaningful response parameters from the models and the measures taken to ensure numerical stability. Focus has also been placed on the verification and validation of the various simulations, including the development of "mine-simulating" test rigs and the use of cadaveric specimens by our University research partners. The incorporation of Digital Image Correlation and other precision diagnostic techniques within our experiments when validating the response of hybrid entities within idealised vehicle rigs is also presented. In addition to describing these modelling initiatives, suggestions are also made concerning how Dstl could collaborate, with mutual benefit, with other agencies working in this field.

Optimal Design of a Novel Energy Absorbing Material to Mitigate the Blast Effect on the Lower Extremities

Feng Zhu and King H. Yang

Wayne State University Bioengineering Center
818 W. Hancock, Detroit, MI 48201

Abstract

Anti-vehicular (AV) landmine explosion may cause catastrophic structural failures of military vehicles and injuries/fatalities of the crew. When an AV charge is detonated under a vehicle, a shock wave with intensive energy is generated. It is transmitted to the vehicular floor rapidly and then results in large acceleration and deflection of the floor plate, which in turn applies high loads to the lower extremities of the occupants to induce injury. Such blast effect on the lower extremities has been experimentally investigated by employing physical dummy and cadaveric surrogates. However, existing dummy legs have limited biofidelity in high loading rate regime while the cadaveric test data are highly scattered. With these limitations, the use numerical human body model is a good intermittent step while a biofidlic military dummy is being developed. Recently, Wayne State University (WSU) Bioengineering Center developed a comprehensive numerical human model (WSU Human Model, or WSUHM) to simulate the
lower extremity injury due to blast. The model has been validated against the experimental data in terms of bone fracture pattern and bending moment/axial force responses (Dong et al. 2013). To lower the blast effect on lower extremities, the kinetic energy and pressure transferred to the feet must be reduced. This can be achieved by applying energy absorbing materials as the foot mat in the vehicle. Such materials are usually made of low density porous media with a large number of microstructures. During the crushing process, the microstructures undergo large deformation at a nearly constant stress level, and thus absorbing a large amount of kinetic energy before collapsing into a more stable configuration. Recently, a novel lightweight energy absorber, namely the SKYDEX® pad was developed and applied as the vehicular floor matting material (SKYDEX Technologies, CO). A SKYDEX® pad consists of double layers of periodic microstructures made of thermoplastic. During crushing, the two microstructures compress against each other and deform layer by layer to dissipate energy and reduce the pressure transfer. Combined experimental and numerical studies on the mechanical properties of SKYDEX® material at high loading rates have been conducted at WSU, and its compressive stress-strain response exhibits a strong strain softening behavior, which limits the energy dissipating capability (Zhu et al. 2012; Jiang et al. 2013). To maximize its energy absorption, a series of computational optimization have been performed (Zhu et al. 2013). In that study, the shape and size of the microstructure were described by a number of key geometric parameters. The relationship between the structural responses (e.g. pressure transfer and energy absorption) and these key parameters was established through numerical modeling, which was then validated against experimental data. Adjusting these parameters, the topology of the microstructure can be controlled and the overall response can be tailored to obtain the best protective function. Integrating the optimized energy absorber to the WSUHM further demonstrated that lower limb injury risk can be greatly mitigated through these processes.

References

Dong L, Zhu F. Jin X, Suresh M, Jiang B, Sevagan G, Cai Y, Li G and Yang KH. Blast effect on the lower extremities and its mitigation: a computational study. Journal of the Mechanical Behavior of Biomedical Materials, 2013; Vol. 28: 111-124.

Jiang B, Zhu F, Jin X, Cao L and Yang KH. Computational modeling of the crushing behavior of SKYDEX® material using homogenized material laws. Composite Structures, 2013; 106: 306-316.

Zhu F, Jiang B, Yang KH et al. Crushing behaviour of SKYDEX® material, Key Engineering Materials, 2013; 535-536:121-124.

Zhu F, Dong L, Ma H, Chou CC and Yang KH. Parameterized optimal design of a novel cellular energy absorber. International Journal of Mechanical Sciences, 2013, in press.

ABSTRACTS

Workshop on Numerical Analysis of Human and Surrogate Response to Accelerative Loading

January 9, 2013
Session 5

Constitutive Model and Parameter Sensitivity in Predicting Lower Leg Response for Underbody Blast Events

Megan Lynch[1] and Adam Sokolow[2]

[1] U.S. Army Research Laboratory, Aberdeen Proving Ground, MD 21005
[2] Oak Ridge Institute for Science and Education, Aberdeen, MD

In an underbody blast event, local deformation of a vehicle's floor plate can cause severe injuries to the lower extremities of vehicle occupants. Such injuries include soft tissue rupture and comminuted bone fracture, which can lead to permanent disability, limb amputation, or death. In an effort to understand, predict, and prevent such injuries, finite element models of the lower extremities are used to study the human response to such an event. Though injury mechanisms are rooted in biological microstructure, for numerical simulation purposes, they are often correlated to the state variables on the continuum-level (e.g. peak stress and peak strain). These state variables, however, are highly dependent upon the constitutive models and material parameters selected for an analysis. Despite large biological variability in the human population, and large variability in the material properties within an individual, typically only a small subset of material models and parameters are used in the simulation literature for modeling the human body in underbody blast events. The importance or irrelevance of the underlying physics for calibrated constitutive models as it directly relates to predicting the failure of tissues is not well understood. A similar lack of understanding exists for the sensitivity of tissue failure as it relates to material parameters. The intent of our research is to begin the process of exploring the extraordinarily large phase space of material parameters, constitutive models, and failure criteria. Such a study will help develop a data corridor within which experimental cadaveric data is expected to fall as we move towards a validated numerical model of the human body. This type of study can also reveal parameter or model sensitivities relevant to tissue failure. In this talk we will introduce our biofidelic model of the leg and foot, provide an overview of the constitutive models and material parameters considered, as well as report on the current progress of this project.

Coupled Eulerian and Lagrangian Approaches for Dynamic Injury Analysis

Timothy P. Harrigan, Robert Armiger, Catherine Carneal, JiangYue Zhang, Andrew Merkle

The Johns Hopkins University Applied Physics Laboratory, Laurel, MD

Injury prediction in computational human finite element models (FEMs) can be achieved by implementing a number of mechanical failure criteria to calculate damage incurred to specific body regions. These include *tissue level* failure criteria, which calculate cumulative pressures or strains in specific tissue types that exceed a failure threshold, as well as *structural* failure criteria, where overall forces or moments applied to specific anatomical structures (e.g., vertebral body compression force) are calculated and related to available injury predictors. While standard structural Lagrangian numerical models techniques can be readily applied for both injury predictors, these techniques are often ill-suited to accurately model the large pressure and deformation that occurs within human interstitium under high-rate dynamic loads. Eulerian modeling methods, while better suited to model high levels of deformation, have limited ability for injury analyses which require cumulative tracking of tissue damage or structural failure criteria.

In order to address these challenges, a coupled Lagrangian-Eulerian approach was investigated which could allow for a detailed (Lagrangian) method for assessing damage in the important structures (such as bones and major organs) while modeling the essential character (pressure and strain transmission) of interstitial tissues using an Eulerian mesh. In this study, pressure and deformation propagation was modeled for dynamic loading relevant to the torso, the major organs consisted of Lagrangian FEMs and the surrounding interstitial tissue consisted of Eulerian meshes. This approach differentiated regions of high interest for damage (major organ systems) from regions of interstitial tissue. The tissue stress propagation and overall numerical stability was tracked to confirm the modeling approach's suitability for dynamic injury prediction.

The Lagrangian meshes of each major organ (heart, liver, lung, stomach, kidneys) were generated using hexahedral elements. The Eulerian meshes were rectilinear, and coupling between the Eulerian and Lagrangian meshes was achieved through constraints in LS-Dyna such that the Lagrangian organ displaced the interstitial flesh. High-frequency pressure and lower-frequency shear loading was applied to the models to test the propagation of pressure through the coupled meshes. As a validation case, shear and compressive properties were matched between the Lagrangian organs and the Eulerian interstitial tissue for pressure wave propagation tests.

The coupled Lagranian-Eulerian model was successfully able to accurately represent organ pressure transmission predicted in the uniform Lagranian mesh. Although minor pressure artifacts (<15 kPa) did occur in the mixed-mesh approach, these were largely confined to surface elements and nodal averaging of pressures in the FEM decreased these artifacts to less than 5 kPa. Checkerboard instabilities in pressure predictions within the Eulerian mesh were observable but small (<10kPa), and they did not scale up with the magnitude of imposed pressure. Leakage at the organ-interstitium interface was controlled using a contact penalty method. Observations of these artifacts indicated appropriate numerical procedures for modeling dynamic loading of human tissue, and showed that mesh refinement will decrease their magnitude.

The current study results indicate that utilization of a coupled Lagrangian-Eularian approach in human computational models for dynamic injury analysis is promising. Challenges unique to this modeling method for numerical stability and organ interfaces were successfully addressed using standard LS-Dyna capabilities. The numerical tests for simulated dynamic loading for the torso organs indicated that this method can successfully enable a calculation of pressure and strain distributions for injury prediction. Ultimately, this mixed-model approach will enable a broader variety of modeling capabilities and injury scoring for the study of both dynamic (blast-related) and static (postural) large strain effects. Additionally, this approach simplifies mesh development and refinement to enable more versatile human models.

Crew Response in Full System HFCP

Allen Shirley

CORVID Technologies

Over the past four years, Corvid Technologies has been developing and applying high fidelity computation physics (HFCP) technology and methods to address USMC PEO LS survivability analysis needs related to accelerative loading based crew injury across multiple platforms supporting DT and LFT&E. Extensive solver and methodology development has been carried out in effort to capture the complex physics of a buried IED threat and the full vehicle-level structural response including local deformation and failure. Corvid subsequently leveraged these capabilities to develop and integrate a corresponding high fidelity Hybrid III 50th percentile male anthropomorphic test device (ATD) model capable of resolving the level of ATD structural damage experienced in DT events, which cannot be captured in currently available ATD models due to the use of rigid components and coarse mesh representation.

The key emphasis in Corvid's physically-based modeling approach is to limit the set of simplifying assumptions through enhanced mesh and constitutive model fidelity. In order to accomplish this for ATD modeling, Corvid characterized visco-elastic/plastic materials in the ATD as well as the sole of the boot used in LFT&E across the full range of loading rates applicable to this type of impulsive event. With these data, constitutive model fits have been developed through optimization routines, and the baseline model has undergone verification and validation testing based on limited available data sets. Additionally, the high resolution finite element (FE) mesh model was developed from CAD data provided by Humanetics who also has received the material characterization data to aid the development of future ATD systems. These data are also available to the broader community through USMC PEO LS, a co-sponsor of this effort.

Initial validation was conducted against CSBES test data collected by ARL researchers, and results to these loading conditions will be discussed. To further validate the Velodyne ATD model, Corvid has recently begun working with PMO WIAMAN to model the 4.2 test bed setup. Test results including relevant ATD configurations are being used to support efforts within PEO LS to expand the validation set for the Velodyne model. The initial results of this effort will be presented. Additionally, current and future efforts focused on human modeling will be discussed.

These technologies have enabled accelerated development of significant survivability upgrade kits for M-ATV and MaxxPro vehicle platforms to current overmatch levels through predictive pre-test assessment of design performance and relative performance comparisons leading to successful DT demonstrators at reduced development cost. Future capabilities will further enhance the utility of these tools for the acquisition community to achieve compressed development schedules and reduce system cost within the IED survivability key performance parameter trade space.

Evaluating the Effectiveness of Various Blast Loading Descriptors as Occupant Injury Predictors for Underbody Blast Events

Kumar B. Kulkarni[1], Jaisankar Ramalingam[2] and Ravi Thyagarajan[2]

[1]ESI-US Inc., Troy, MI 48084
[2]US Army TARDEC, Warren, MI 48397

Motivation/Objective:
It is of considerable interest to developers of military vehicles, in early phases of the concept design process, to quickly assess occupant injury risk due to under body blast loading. The most common occupant injuries in these extremely short duration events arise out of the very high vertical acceleration of vehicle due to its close proximity to hot high pressure gases from the blast. A typical blast vertical acceleration pulse is predominantly triangular shaped in nature. In the past, several blast loading parameters have been proposed, alone or in combination, to serve as indicators or predictors of occupant injuries. Some examples of these are (i) magnitude of the peak acceleration, G in g's, (ii) time duration of pulse, T in ms, (iii) rate of onset of acceleration, in g/ms, (iv) change in velocity, Δv in m/s, (v) effective-g (slope of the velocity profile) in g's, (vi) specific power (G*Δv) in g-m/s. Of these, the design community has mostly used change in velocity Δv, or to a lesser extent, peak acceleration G, to determine the severity of, and classify any given blast pulse. The primary objectives of this paper are to conduct an extensive parametric study in a systematic manner so as (1) to determine if a single blast loading parameter is sufficient to adequately characterize the occupant injury, at least for the duration of typical blast events (0-20ms) and (2) to create look-up tables that decision-makers can use to quickly estimate the different injury responses for both stroking and non-stroking seat systems in terms of such a parameter.

Approach:
A dynamic simulation model of a vertical blast loading simulator was used, which contains a seated 50th percentile Hybrid-III Anthropomorphic Test Dummy (ATD). A parametric study was conducted on this setup by varying the peak acceleration from 10g - 1200g, and duration of the pulse from 2.5ms to 60ms such that Δv was limited to below 15 m/s. In addition to considering a non-energy absorbing rigid seat, two generic energy-absorbing (EA) blast mine seats of different ratings (EA1, EA2) were used in the study. Ten different upper body injuries were tracked for a sample size for each of the three seating variants consisting of 230 MADYMO simulations each, for a total of 6900 data points. Each of these ten injury responses were compared against three leading blast loading indicators, namely, Effective-g, Specific Power and Δv. Linear and quadratic best fit analysis was also performed and overlaid against the data samples. Similar trend analyses were also performed for physical vertical sled/drop tower tests.

Conclusions:
- No single blast loading parameter from an input pulse can be used to fully determine the occupant injury risk over the entire wide range of pulse durations (0-60ms).
- Among the different blast pulse parameters considered in this study, Δv is the best single indicator for estimating injury criteria, for typical blast pulse duration ranges (0-20 ms), independent of seat type.
- For a given Δv and T, the shape of the pulse and its peak value has no significant effect on the injury criteria, again for typical blast pulse duration ranges, an important finding for design of test setups.
- Occupant injury trends observed in this study strongly agree with physical test data.
- An easy-to-use injury estimator tool was constructed in Microsoft Excel as a function of duration T, and Δv, from the occupant injury regression trends obtained from this parametric study. This tool will enable decision makers arrive at informed decisions during early concept design stages, Analysis of Alternatives (AoA) studies, etc.

Neck Response of a Finite Element Human Body Model during a Simulated Rotary-Wing Aircraft Impact

Nicholas A. White1, 2, Kerry A. Danelson1, 3, F. Scott Gayzik1, 3, and Joel D. Stitzel1, 3,*
1. VT/WFU School of Biomedical Engineering and Sciences
2. Virginia Tech
3. Wake Forest University School of Medicine

***Presenting author**

A finite element simulation of a 30-deg, pitch-down rotary-wing aircraft impact was validated against an experimental sled test reported in the literature. This 7.62 m/s delta-V impact was simulated using a Hybrid III Anthropomorphic Test Device (ATD) with 1.8 kg of head-supported mass. The simulation was then repeated with the Global Human Body Models Consortium (GHBMC) 50th percentile seated male model to further investigate the neck response during such an impact. A more biofidelic neck response was produced with the human body model, including realistic changes in neck curvature. Unlike the ATD, neck load cells data was not readily available in the human body model. A methodology was developed to measure forces and moments at different levels of the GHBMC neck using a series of cross sections. A local coordinate system (LCS) was rigidly attached to each cervical vertebra, with the local origin defined at the vertebral center of gravity. The local x-axis was defined as the vector from the local origin to the midpoint of the anterior vertebral body, in the midsagittal plane. The local z-axis was defined as a vector directed inferiorly from the local origin along the midsagittal plane, orthogonal to the local x-axis. Transverse cross sections were then defined at each cervical level, coplanar with each local xy-plane. These cross sections measured the force and moment contributions of the bones, ligaments, muscles, and soft tissue during the course of the simulation, with values reported in their respective LCSs. Cross sections were also implemented to measure forces transmitted though the intervertebral discs and cervical facets. The measured neck forces and moments were compared to existing injury threshold values and used to calculate injury criteria, including the Nij and Beam Criterion. This cross-sectional methodology to measure neck loading during a rotary-wing aircraft impact can be readily applied to investigate loading in the human body model from under-body blast.

January 9, 2013
Session 6

A finite element model of the military lower extremity surrogate (MIL-Lx) with combat boot validated for high loading-rate inputs

Nicolas Newell and Spyros D Masouros
The Royal British Legion Centre for Blast Injury Studies,
Imperial College London, UK

Abstract
The improvised explosive device (IED), capable of causing multiple severely injured casualties in a single incident, has been the most prevalent single threat to Coalition Troops in recent conflicts [1]. Occupants of vehicles are particularly susceptible to lower extremity injury [2]. Mitigation systems have been shown to reduce the force transmitted to the lower extremity [3], however, experimental analysis of these technologies is expensive and time consuming. The MIL-Lx anthropometric test device was developed in 2009 to mimic to some extent the behaviour of the human leg in an under-vehicle blast scenario and presents the most biofidelic surrogate for under-vehicle blast to date [4].

The aim of this study was to develop a validated fast-running numerical model of the MIL-Lx fitted with a combat boot, which can be used as a tool to assess mitigation systems.

Axi-symmetric, implicit finite element models of the MIL-Lx and combat boot (Meindl Desert Fox Combat Boot) were developed using MSC Marc (MSC Software, USA) and validated separately against experimental data. The geometry of the combat boot model was obtained through analysis of the dimensions of the individual layers as captured on a micro-CT scan. The geometry of the MIL-Lx was reverse engineered. The properties of the materials of both combat boot and MIL-Lx were obtained experimentally using quasi-static and dynamic uniaxial compression tests.

The model of the combat boot was validated against drop-tower tests [5]. The MIL-Lx model was validated against traces of upper tibia axial force and compliant element compression obtained through experiments conducted on a traumatic injury simulator at a range of severities [6]. In order to gain further confidence in the FE model, boundary conditions and respective tibial axial loads were obtained from 5 MIL-Lx experiments conducted independently on University of Virginia's ODYSSEY rig [7]. The difference in peak axial force in lower and upper tibia load cells of the MIL-Lx were 9% (range 1-17%) and 13% (range 9-19%), respectively.

In conclusion, a validated numerical model of the MiL-Lx with combat boot has been developed which can now be used as a tool for preliminary assessments of the efficacy of mitigation systems without the need for expensive experimentation.

References
[1] Ramasamy A, Harrisson SE, Clasper JC, Stewart MPM. 2008. Injuries from roadside improvised explosive devices. *The Journal of Trauma* 65: 910-914.
[2] Ramasamy A, Hill AM, Masouros S, Gibb I, Bull AMJ, Clasper JC. 2011. Blast-related fracture patterns: a forensic biomechanical approach. *Journal of The Royal Society Interface* 8: 689-698.
[3] Quenneville CE, Dunning CE. 2011. Evaluation of energy-attenuating floor mats for protection of lower limbs from anti-vehicular landmines. *Journal of Battlefield Technology* 14: 1-4.
[4] McKay BJ. 2010. Development of lower extremity injury criteria and biomechanical surrogate to evaluate military vehicle occupant injury during an explosive blast event. PhD Thesis, Wayne State University, Detroit, MI, USA.
[5] Newell N, Masouros SD, Pullen AD, Bull AMJ. 2012. The comparative behaviour of two combat boots under impact. *Injury Prevention* 18: 109-112.
[6] Newell N, Masouros SD, Ramasamy A, Bonner TJ, Hill AM, Clasper JC, Bull AM. 2012. Use of cadavers and anthropometric test devices (ATDs) for assessing lower limb injury outcome from under-vehicle explosions. *Proceedings of the International Research Council on the Biomechanics of Injury conference*, 40: 296-303.
[7] Bailey A, Christopher J, Henderson K, Brozoski F, Salzar R. 2013. Comparison of Hybrid-III and PMHS response to simulated underbody blast loading conditions. *Proceedings of the International Research Council on the Biomechanics of Injury conference*, 41: 158-170.

Rubber Material Modeling Methodology for FE Dummy Development

Hyunsok Pang
Humanetics Innovative Solutions, Inc.
47460 Galleon Drive
Plymouth MI, 48170

This abstract describes rubber material modeling in FE dummy development. Material modeling is very important in FE models to match real hardware test data. In particular, the purpose of FE dummy model developments is to predict the injury responses of ATD dummies in crash testing events as close as possible. The ATD dummies currently being used in any fields consist of rubber, foam, metal, damping, plastic and few other materials. Among them, rubber is the most widely used and important material because it is being used in the critical injury body parts such as neck, lumbar and skins. Also, the dummy from WIAMan project will have many rubber materials which will undergo large strain and high strain rates. Therefore, in this paper, an material modeling method for rubber is investigated with the MAT_77_O (Ogden Rubber) in LS-DYNA. And this modeling method will be applied to the WIAMan project.

First, the uniaxial tension and compression test curves are curve-fitted to Ogden strain energy-based and stress-based equations. Curve-fittings are conducted with MATLAB Genetic algorithm. Two set of Ogden parameters from curve-fittings are evaluated through both Ogden strain energy-based and stress-based equations and are proved to be almost identical when Poisson ratio is 0.499. In addition, planar tension and biaxial tension test data are considered together with uniaxial tension and compression test data for curve fittings. Then, the Ogden parameters from uniaxial tension & compression, planar tension and biaxial tension modes are evaluated and compared with the Ogden parameters from the uniaxial tension & compression mode only. Two sets of parameters are proved to produce very similar curves close to test data.

Second, the short term compression relaxation tests are conducted to obtain the Prony Series parameters which are required to be inputted in the MAT_77_O (Ogden Rubber) card. The short term relaxation tests have both ramp-up and relaxation regions to consider strain rate effect and unloading characteristics. Curve-fitting is conducted against the relaxation test using Matlab Genetic algorithm to obtain Prony Series parameters.

Coupon simulations are conducted with Ogden parameters and Prony Series parameters. For quasi-static tests (0.01 /s), only Ogden parameters are used. For strain rate tests over 0.01 /s, Prony Series parameters are inputted with Ogden parameters in the MAT_077_O card to consider strain rate effect. Coupon simulation results were close to the test data, proving that the applied method is very effective and fast in rubber material modeling for FE dummy model development.

Effect of Strain Rates on the Compressive Response of ATD Neck and Foot Rubber under Different Loading Sequences

B. Sanborn and T. Weerasooriya
Army Research Laboratory

Anthropomorphic Test Dummies (ATDs) are used to understand the response of humans exposed to different possible extreme loading scenarios encountered as occupants of automotives, aircrafts, and military vehicles. The WIAMan (Warrior Injury Assessment Manikin) program has been established by the Army to create a higher fidelity ATD that will be used to assess severity of injury to humans in blast and high accelerative loading situations, where loading rates could be higher than during the standard automotive crash tests. Simulation of these extreme events to extract the accurate response of ATDs requires incorporation of the constitutive response of the materials used in the ATDs under different loading rates. To build constitutive models for numerical codes for WIAMan, the materials used in ATDs must be investigated to discover how the materials behave at various loading rates. In this study, the rate dependent behavior of neck and foot rubber used in the Hybrid III, an automotive ATD, was investigated over quasi-static (0.001 s^{-1}), intermediate (1 s^{-1}), and high (500 s^{-1}, 1300 s^{-1}, 2300 s^{-1}) strain rates. The stress relaxation behavior at quasi-static and intermediate rates was also studied. In addition, storage and loss moduli of the rubbers were also obtained as a function of frequency and temperature. These various types of loading under different rates were used to evaluate the various representations of constitutive models in literature. The Bergstrom-Boyce (BB) model was identified as the model that best represents the experimental data.

Inertial Effects in Compression and Torsional Kolsky Bar Tests on Soft and Nearly Incompressible Materials

Adam Sokolow, Mike Scheidler and John Fitzpatrick

Understanding the high strain-rate response of soft biological tissues such brain, liver, and lung tissue as well as the response of tissue surrogates such as ballistic gelatin is critical for the development and calibration of computational models that estimate injury. In particular, the viscoelastic response of brain tissue is used to model wave propagation in the brain in an effort to predict traumatic brain injury. Brain tissue, along with the other tissues listed above, is soft and nearly incompressible.

Traditional *compression* Kolsky bar methods, which successfully characterize the rate-dependence of metals and stiff polymers, are plagued by radial inertia effects when used on soft, nearly incompressible materials. Consequently, the conventional data analysis techniques are no longer valid for compression tests on these soft materials. In an effort to bypass these difficulties, researchers at Purdue University have more recently modified the traditional *torsional* Kolsky bar test so that it can be used for specimens as soft as brain tissue.

For *compression* Kolsky bar tests, we have developed theoretical estimates for the full, non-uniform, stress state in soft materials that depend only on data that can actually be measured in this test. Since these estimates are based on radial momentum balance in the specimen, they are referred to as "inertial corrections". However, they rely on various simplifying assumptions (e.g., an approximately uniform strain state), so their range of validity needs to be determined. There does not seem to be any way to do this experimentally since only the mean value of axial stress on either face of the specimen can be inferred. Consequently, we have utilized numerical simulations of compression Kolsky bar tests as these provide the full stress and strain states at each point in the specimen against which the theoretical inertial corrections can be compared. The results of this part of the study provide new guidelines for the use of compression Kolsky bar tests on soft tissues and tissue surrogates.

We also investigated whether inertial effects are present in this new *torsional* Kolsky bar test when the specimens are soft and nearly incompressible. The results are relevant for any soft material with a shear modulus on the order of 1—1000 kPa and density on the order of water. We have conducted one and three dimensional analyses and numerical simulations to understand the stress and strain states that exist in these materials in quasi-static and dynamic torsion tests. We demonstrate that the short loading pulses typically used for high strain-rate (e.g., 700/s) tests do not allow the softer specimens to "ring-up" to uniform stress and strain states, and that consequently the shear stress vs. shear strain data reported in the literature is erroneous. We also show that normal stress components, which are present even in quasi-static tests, can be amplified by the inertial effects in dynamic torsion tests on soft materials. We provide strict requirements for the successful application of torsional Kolsky bar tests to the characterization of soft tissues.

In this talk, we will provide an overview of the Kolsky bar test configurations for both compression and torsion. For both cases we will discuss the key features of how specimen inertia confounds traditional Kolsky bar data and propose possible future directions in the problem of understanding the high strain-rate response of soft biological tissues.

INTENTIONALLY LEFT BLANK.

Appendix C. Workshop Slides

This appendix appears in its original form, without editorial change.

Preliminary Evaluation of Human and Dummy Finite Element Models under Blast-Induced Accelerative Loading Conditions

Costin D. Untaroiu, Jacob B. Putnam, Warren N. Hardy
Center for Injury Biomechanics

VirginiaTech *Invent the Future*

Overview

- Introduction: Underbody-blast vs. Automotive/Aerospace
- Human / Dummy FE Models: ***THUMS vs. GHBMC; HIII vs. THOR-k***
- GHBMC Lower Limb Model: ***Development & Validation & Applications***
- Model Calibration & Validation: ***Methodology (example THOR head-neck)***
- Evaluation of Human/Dummy FE under High Impact Loadings
- Future work

Under-body blast impact loading

(Youtube.com)

The improvised explosive devices (IED) – the leading cause of injury and death for service members (more than **50,000 coalition forces** injured or killed)

(Champion et al. 2009,Belmont et al. 2010)

Vehicle Occupant injury mechanisms

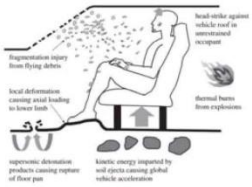

(Ramasamy et al. 2010)

Time sequence of Events during an Anti-Vehicular Mine Detonation

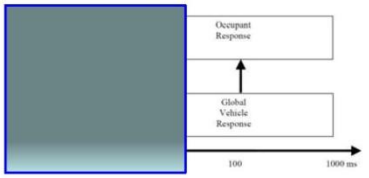

(NATO 2007 Report)

Injury Distribution per body region

- U.K. Army (2006-2008)
- 63 service personnel injured from under-body IED explosion
- 26 ± 5.7 years
- Lower limb: the most severely injured body region
- 89 foot/ankle injuries

(Ramasamy et al. 2013)

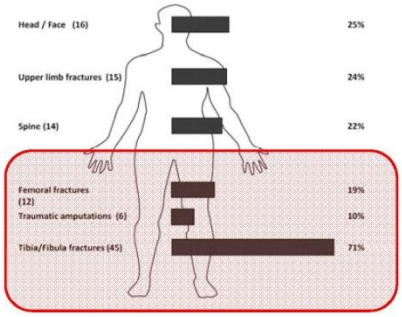

Impact loading in Aerospace & Automotive

Helicopter Crash (Aerospace)

Multipurpose Crewed Vehicle (MPCV) - Water Landing

Automobile Crash (Automotive)

Floor Intrusion during an Offset Crash

Human vs. Dummy / Testing vs. Modeling

ATD

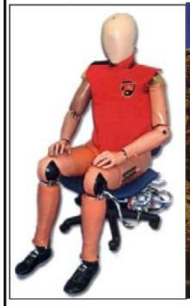

Dummy FE Model Human FE Model

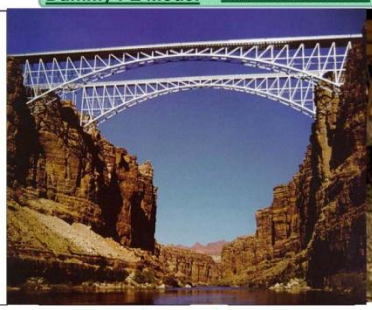

Durable
Expensive
Biofidelity?

Inexpensive
Unlimited Testing
Accurate?

Biofidelic
Testing Limitations
FEHIS Issues

Improved Safety Standards & Vehicle Design

Full-Body Finite Element Models Available

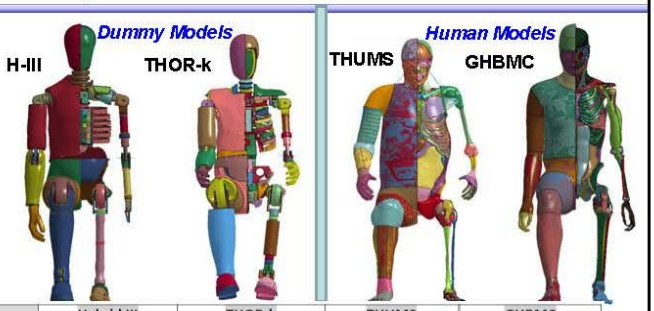

FE Model	Hybrid III	THOR-k	THUMS	GHBMC
Sponsor	LSTC	(NHTSA- VT/NASA)	Toyota	GHBMC - WFU
Part #	367	428	1,273	981
Node #	276k	239k	630k	1,255k
Elem. (Def.) #	452k (438k)	525k (211k)	1,755k (1,750k)	2,185k (2,103k)
Time step (with Mass Scaling)	0.18 μs (0.2 μs)	0.63 μs (0.7μs)	0.39 μs (0.44 μs)	0.3 μs (0.33μs)
Valid. Comp.	Calib. Tests	Calib. & Biom. Tests	Body parts	Body parts
Valid. Full	-	Horiz./Vert./Lat.	Horiz./Lat.	Horiz./Lat.

Human Lower Limbs FE Models

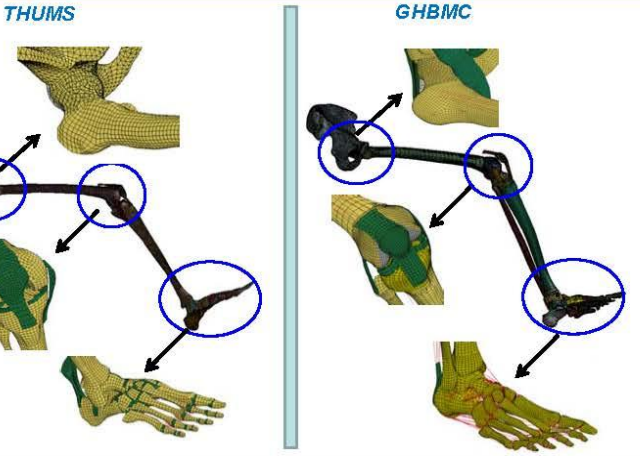

Dummy Lower Limbs FE Models

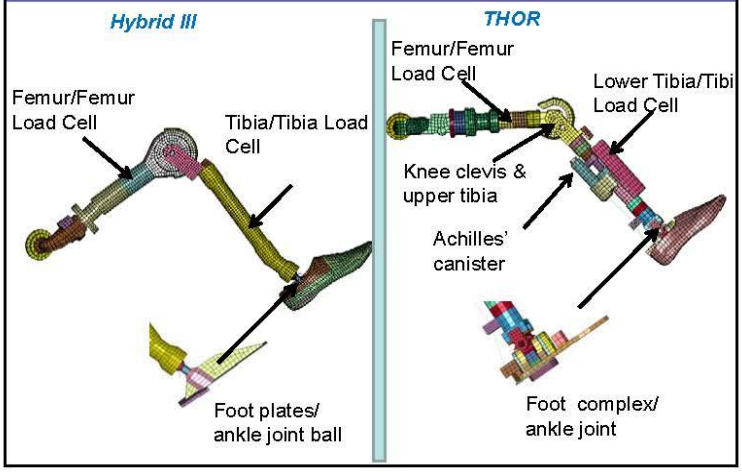

GHBMC Validations & CII Summary

Frontal Impact Validations

- **Lower Limb (7)**
  - FO-1 Knee Impact (Rupp et al. 2002/2003)
  - FO-2 Mid-shaft femoral bending (Funk et al. 2004)
  - FO-3 Mid-shaft femoral axial & bending (Ivarsson et al. 2009)
  - FO-4 Proximal femur compression (Keyak et al. 1998)
  - FO-5 Distal femur compression (Rupp et al. 2003)
  - FO-6 Knee - PCL impact (Balasubramanian et al. 2004)
  - FO-7 Mid-leg axial & bending (Untaroiu et al. 2008)
- **Foot (5)**
  - FO-8 Axial rotation (Chen et al. 1988)
  - FO-9 Inversion/eversion loading (Funk et al. 2002)
  - FO-10 Axial Impact (Funk et al. 2000)
  - FO-11 Dorxiflexion Loading (Rudd et al 2004)
  - FO-12 Hindfoot compression (Funk et al. 2000)

GHBMC Validations & CII Summary

Lateral Impact Validations

- Pelvis (3)
  - SO-1 Pubic symphysis lateral compress.(Dakin et al. 2003)
  - SO-2 Lateral compression (Guillemot et al. 1997/1998)
  - SO-3 Lateral compression (Beason et al. 2003)
- Lower Limb (1)
  - SO-7 Femoral head lateral compression (Keyak et al 1998)
- Foot (1)
  - SO-10 Xversion Impact (Jaffredo et al. 2000)

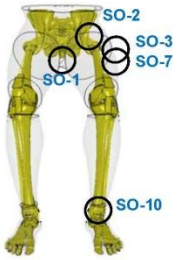

Other Impact Validations

Foot (2)

- O-1 Forefoot Impact (Wheeler et al. 2000)
- O-2 Ankle Lig. Impact (Funk et al. 2000)

References

1) Shin et al. 2012
2) Untaroiu et al. 2013
3) Shin & Untaroiu 2013
4) Kim et al. 2014
5) Yue & Untaroiu 2014

Validation: Femoral Shaft

Femur shaft three-point bending

CII: Mid-shaft femur bending fracture

Input: Impactor prescribed disp.

Output: Impactor force time history

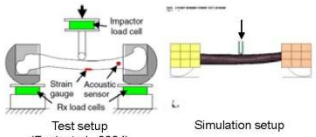

Test setup (Funk et al., 2004)

Simulation setup

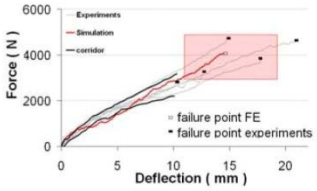

Femur shaft combined loading

CII: Mid-shaft femur combined loading fracture

Input:

- Ramp-increased axial comp. force
- Dynamic transversely impact w/ velocity of 1.5 m/s

Output: Impactor force time history

Test setup (Ivarsson et al., 2009)

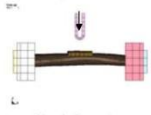

Simulation setup

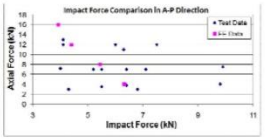

Validation: Foot-Ankle Complex

Axial loading validation

CII: Hindfoot bony fracture
Input: Displacement time history of impactor
Output: Force time history of distal tibia

Funk et al., 2000

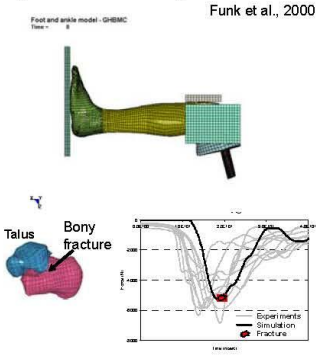

Dorsiflexion loading validation

CII: Ankle bony fracture / ligament failure
Input: Velocity time history of pedal impactor
Output: Moment – angle response of ankle

Rudd et al., 2004

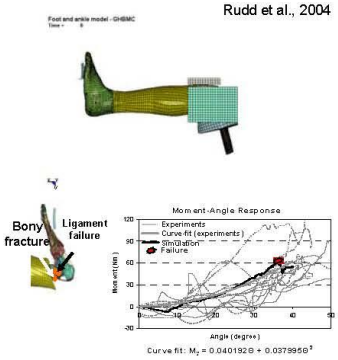

Applications: Injury Criteria

Tibia Index

$$TI = \frac{F}{F_c} + \frac{M}{M_c}$$

Tibia ~~- Straight beam~~ !

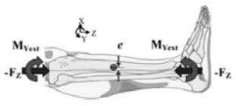

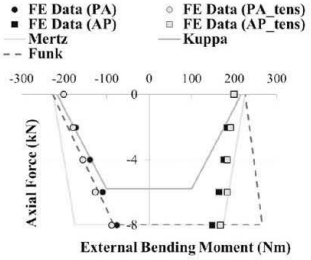

Initial configuration

Under PA loading

Most common fracture sites

Under AP loading

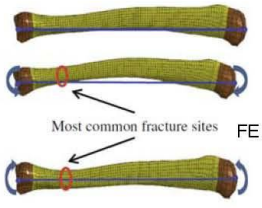

FE model ⇒ **More biofidelic injury criteria**

(Untaroiu et al. 2013)

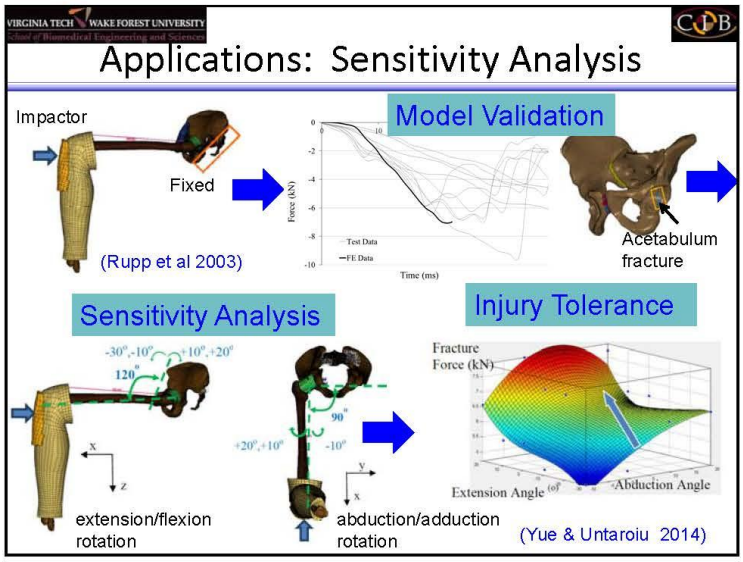
Applications: Sensitivity Analysis
Impactor
Fixed
(Rupp et al 2003)
Model Validation
Test Data
FE Data
Force (kN)
Time (ms)
Acetabulum fracture
Sensitivity Analysis
Injury Tolerance
-30°,-10°,+10°,+20°
120°
90°
+20°,+10°
-10°
extension/flexion rotation
abduction/adduction rotation
Fracture Force (kN)
Extension Angle (o)
Abduction Angle
(Yue & Untaroiu 2014)

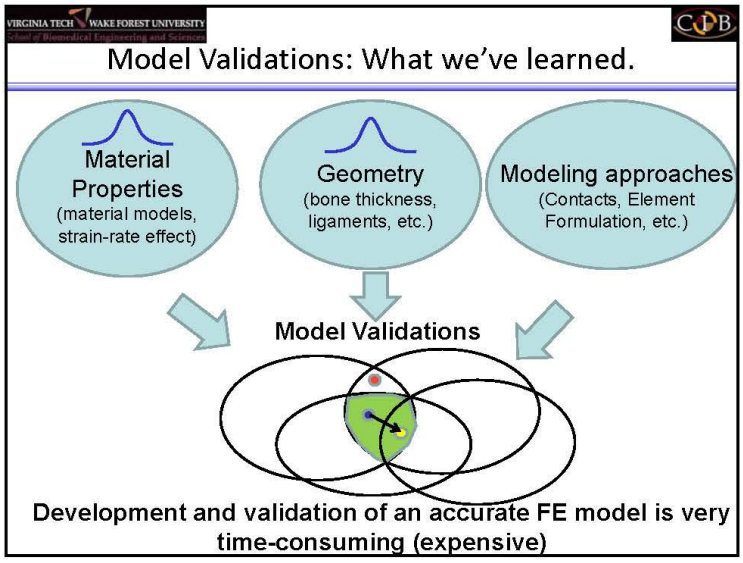
Model Validations: What we've learned.
Material Properties
(material models, strain-rate effect)
Geometry
(bone thickness, ligaments, etc.)
Modeling approaches
(Contacts, Element Formulation, etc.)
Model Validations
Development and validation of an accurate FE model is very time-consuming (expensive)

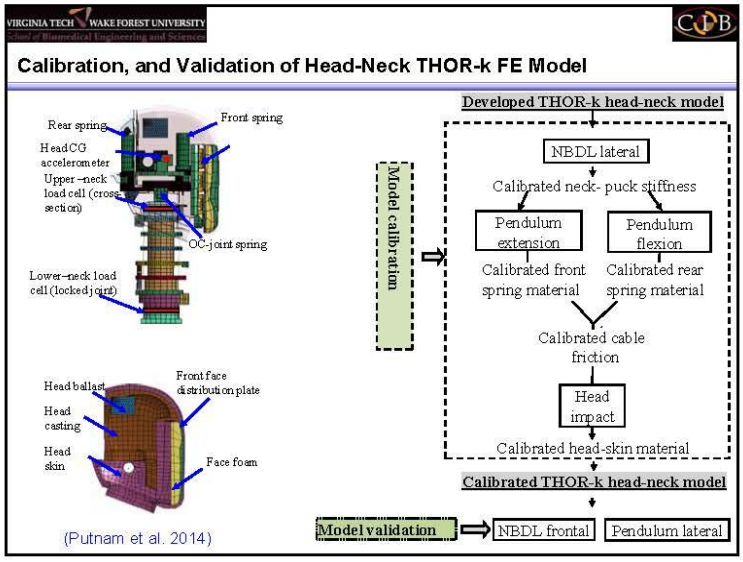
VIRGINIA TECH WAKE FOREST UNIVERSITY
School of Biomedical Engineering and Sciences
CIB
Calibration, and Validation of Head-Neck THOR-k FE Model
Rear spring
Front spring
Head CG accelerometer
Upper –neck load cell (cross-section)
OC-joint spring
Lower–neck load cell (locked joint)
Head ballast
Front face distribution plate
Head casting
Head skin
Face foam
(Putnam et al. 2014)
Developed THOR-k head-neck model
NBDL lateral
Calibrated neck- puck stiffness
Pendulum extension
Pendulum flexion
Calibrated front spring material
Calibrated rear spring material
Calibrated cable friction
Head impact
Calibrated head-skin material
Model calibration
Calibrated THOR-k head-neck model
Model validation
NBDL frontal
Pendulum lateral

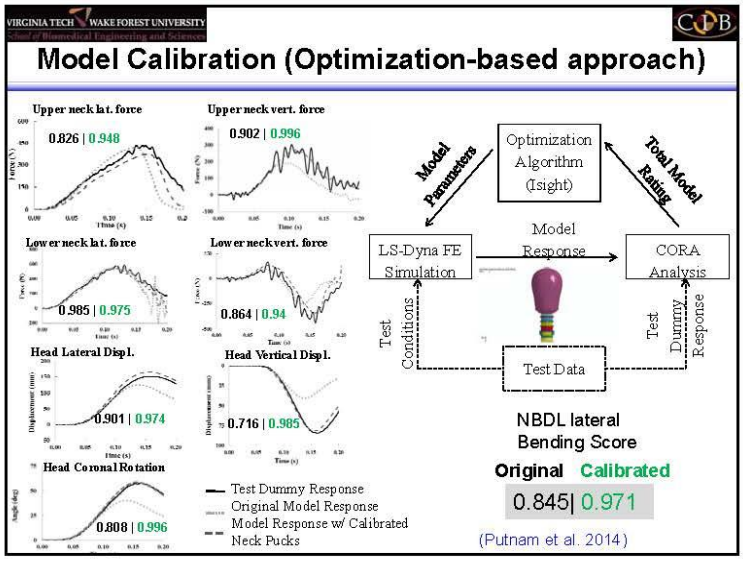
VIRGINIA TECH WAKE FOREST UNIVERSITY
School of Biomedical Engineering and Sciences
CIB
Model Calibration (Optimization-based approach)
Upper neck lat. force
0.826 | 0.948
Upper neck vert. force
0.902 | 0.996
Lower neck lat. force
0.985 | 0.975
Lower neck vert. force
0.864 | 0.94
Head Lateral Displ.
0.901 | 0.974
Head Vertical Displ.
0.716 | 0.985
Head Coronal Rotation
0.808 | 0.996
Test Dummy Response
Original Model Response
Model Response w/ Calibrated Neck Pucks
Model Parameters
Optimization Algorithm (Isight)
Total Model Rating
LS-Dyna FE Simulation
Model Response
CORA Analysis
Test Conditions
Test Dummy Response
Test Data
NBDL lateral Bending Score
Original Calibrated
0.845| 0.971
(Putnam et al. 2014)

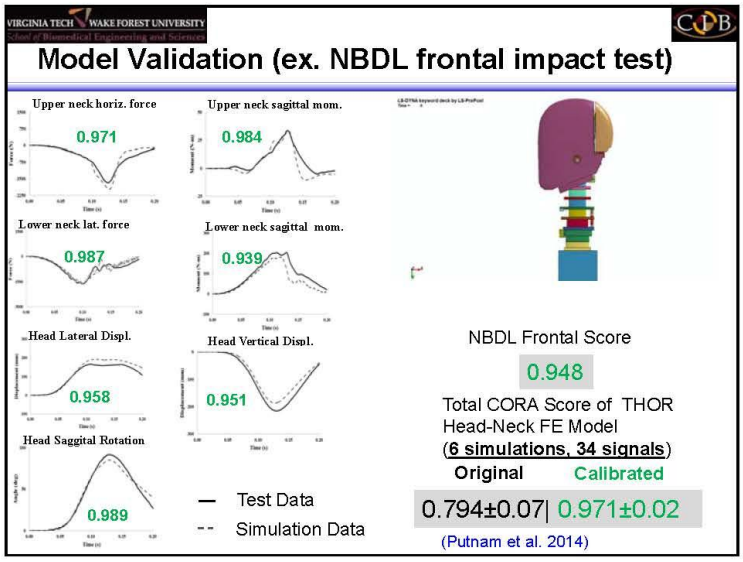
VIRGINIA TECH WAKE FOREST UNIVERSITY
School of Biomedical Engineering and Sciences
CIB
Model Validation (ex. NBDL frontal impact test)
Upper neck horiz. force
0.971
Upper neck sagittal mom.
0.984
Lower neck lat. force
0.987
Lower neck sagittal mom.
0.939
Head Lateral Displ.
0.958
Head Vertical Displ.
0.951
Head Saggital Rotation
0.989
Test Data
Simulation Data
NBDL Frontal Score
0.948
Total CORA Score of THOR Head-Neck FE Model
(6 simulations, 34 signals)
Original
Calibrated
0.794±0.07| 0.971±0.02
(Putnam et al. 2014)

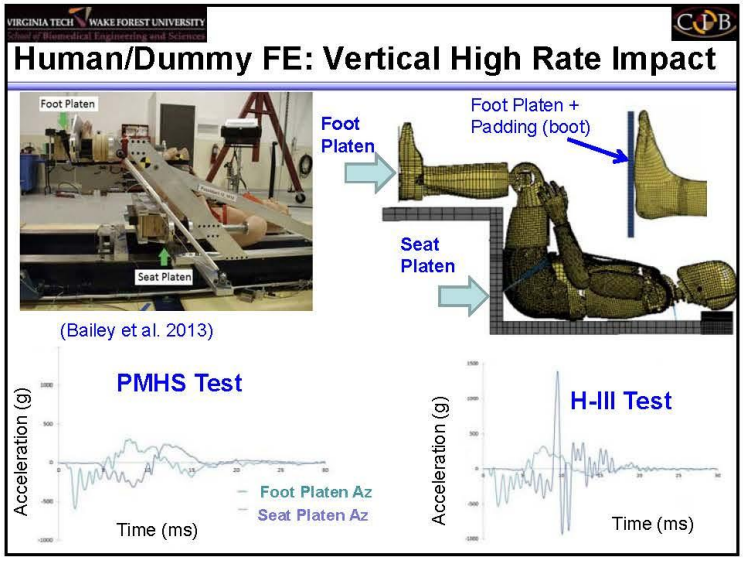
VIRGINIA TECH WAKE FOREST UNIVERSITY
School of Biomedical Engineering and Sciences
CIB
Human/Dummy FE: Vertical High Rate Impact
Foot Platen
Seat Platen
(Bailey et al. 2013)
Foot Platen
Foot Platen + Padding (boot)
Seat Platen
PMHS Test
Acceleration (g)
Time (ms)
Foot Platen Az
Seat Platen Az
H-III Test
Acceleration (g)
Time (ms)

Dummy/Human positioning

1. Dummy FE Model

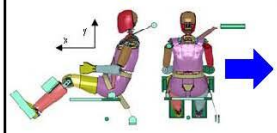

Positioning tree for aerospace/ military FE simulations

Neck pitch change mechanism

Lower thoracic spine pitch change mechanism

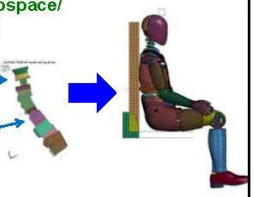

2. Human FE Model

Rotational Joints
- Shoulder
- Elbow
- Hip
- Knee
- Ankle

GHBMC FE model vs. THUMS FE model

THUMS

GHBMC

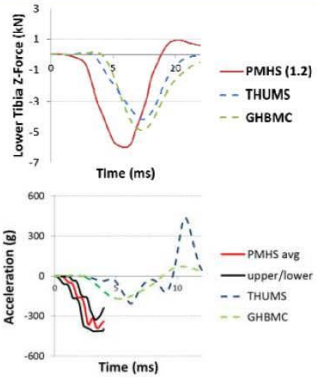

Several preliminary observations:

*Both models were stable during the simulation
*A delay (3-4 ms) between the test vs simulation
*The levels of max. tibia force & acceleration

Possible causes/Future work

- Improve the setup model /add boot models
- Improve the human models (material properties, contacts , etc.)

H-III FE model vs. THOR FE model

H-III THOR

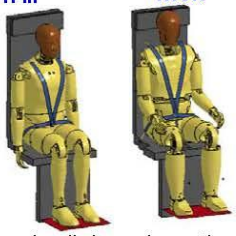

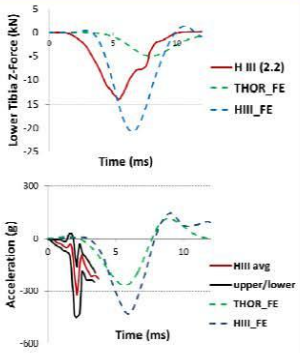

Several preliminary observations:

*Both models were relatively stable, but the foot/shoe shows higher def. than human models
*A delay (3-4 ms) between the test vs simulation
* For H-III, both max force and acceleration were higher than average response

Possible causes/Future work

- Improve the setup model /add boot models
- Improve both dummy models (material properties, contacts, etc.)

Future/possible improvements: Material Properties

Uni-axial tests (high strain rates)

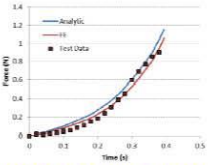

(Lu et al 2013, Untaroiu & Lu 2013)

Bi-axial tests (high strain rates)

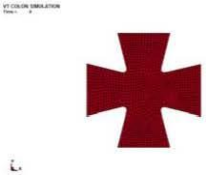

(Howes & Hardy 2013)

Future/possible improvements: Statistical FE Models

VirginiaTech Invent the Future

Statistical Shape Analysis

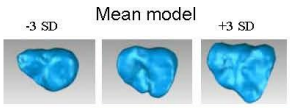

Stochastic Material Models

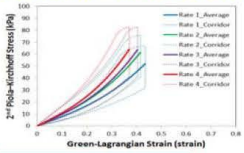

Size and Shape Variation

Material Property Variation

(Lu et al. 2013)

Probabilistic Inputs → Statistical FE Human Model → Distributions of Outputs

Acknowledgements

- Wake Forest University
  - Provided the latest version of GHBMC model
- Toyota
  - Provided the latest version of THUMS model
- Simulia
  - Provided Isight
- Sponsors (GHBMC, NASA, NHTSA, etc.)

VIRGINIA TECH WAKE FOREST UNIVERSITY
School of Biomedical Engineering and Sciences

CCIB

Thank you for your attention !

Questions?

Workshop on Numerical Analysis of Human and Surrogate Response to Accelerative Loading
Aberdeen Proving Ground, MD
January 7-9, 2014

Approaches for Predicting Human Anatomical Variations Using Anthropometric & Demographic Data

Catherine Carneal [1], Yoshito Otake[2], Dean Kleissas[1], Andrew Merkle[1], Mehran Armand[1,2], Manuel Uy[1], Gaurav Thawait[3], John Carrino[3], Brian Corner[4], Marina Carboni[4], Barry DeCristofano[4], Michael Maffeo[4]

[1] *The Johns Hopkins University Applied Physics Laboratory, Laurel, MD 20723, USA*
[2] *The Johns Hopkins University Department of Computer Science, Baltimore, MD, USA*
[3] *The Johns Hopkins Medical Institute Department of Radiology, Baltimore, MD, USA*
[4] *U.S. Army Natick Soldier Research Development and Engineering Center, Natick, MA USA*

BIOMECHANICS AND INJURY MITIGATION SYSTEMS

APL
The Johns Hopkins University
APPLIED PHYSICS LABORATORY
11100 Johns Hopkins Road
Laurel, MD 20723-6099

Motivation

- **Human models based on a single anatomy may have limited applicability for range of subject populations**
- **Biomechanical response and injury predictions are often scaled for subject height and weight**
  - However, limited available data on scaling of internal organ geometries
- ***Understanding allometry (scaling law) critical for accurate human models***

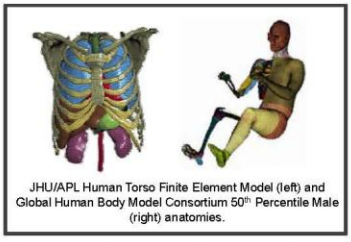

JHU/APL Human Torso Finite Element Model (left) and Global Human Body Model Consortium 50th Percentile Male (right) anatomies.

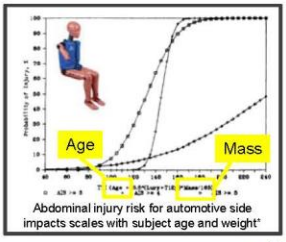

Abdominal injury risk for automotive side impacts scales with subject age and weight*

*Eppinger et al, "Development of Dummy and Injury Index for NHTSA's Thoracic Side Impact Protection Research Program, 1994

APL

Motivation

- **Statistical shape atlases provide a method for determining these allometric relationships**
- **Atlases currently exist for a variety of applications**
  - Medical studies for clinical diagnoses, orthopedics
  - Impact biomechanics for select body regions (boney structures, select organs)

Image intensity atlas of brain from 25 subjects*

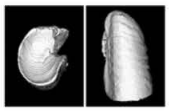

Statistical lung atlas from 6 subjects for lung feature characterization**

Liver mean shape and statistical boundary models from 15 seated human adults for automotive impact studies.***

Existing Gaps

- Robust dataset representative of military population
- Correlation to relevant external anthropometrics
- Multi-organ relationships

*Rueckert, et al, "Automatic Construction of 3D Statistical Deformation Models of Brain Using Nonrigid Registration," IEEE Trans Med Imaging 2003
**Li et al, "Establishing a Normative Atlas of the Human Lung: Intersubject Warping and Registration of Volumetric CT Images," Acad Radio 2003
***Lu et al, "Statistical Modeling of Human Liver Incorporating Variations in Shape, Size, and Material Properties," Stapp 2013

APL

Session 1, Presentation 2
1/7/2014

Objectives

- **<u>Overall</u>: Determine whether external subject parameters (demographics, anthropometry) can accurately predict internal lung geometry, and the associated implications for injury assessment**
- **<u>Tasks</u>:**

- Collect subject dataset (demographics, anthropometry, and lung geometry) representative of military population

- Create statistical shape atlas of the lung

- Employ statistical approaches to investigate anatomical differences in patient populations

APL

Session 1, Presentation 2
1/7/2014

Collection of Subject Data

APL

Data Collection
Medical Images

Session 1

- **Goal: Collect medical image dataset of the lung as a basis for establishing allometric laws and organ models**
  - Greater # images provides better atlases
  - Target: 200 datasets with balanced gender, race/ethnicity, & age
- **Source: Johns Hopkins Hospital Radiology Information Systems**

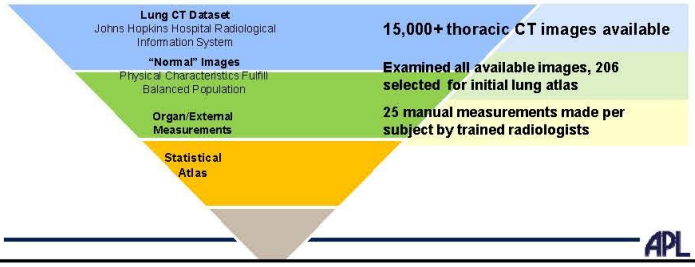

APL

Data Collection
Medical Image Examples

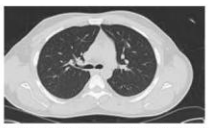
Axial View of Lower Lung Slice

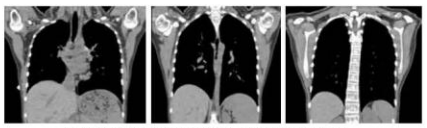
Coronal View (anterior, mid, posterior)

Normal Images

Abnormal Images

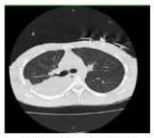
Pleural Effusion


Metal Artifacts


Collapsed Lung

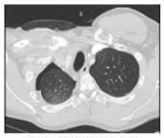
Pneumothorax

Data Collection
Medical Images

- **Population bins primarily based on Army Anthropometric Survey (ANSUR88)**
- **Good gender, race, and age balance established in dataset**

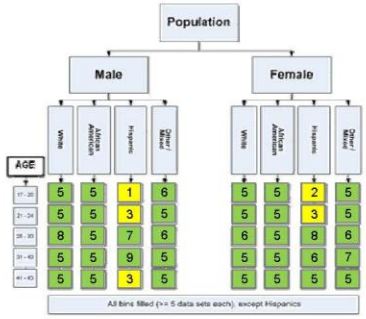

Data Collection
Medical Images

- Population bins primarily based on Army Anthropometric Survey (ANSUR88)
- Good gender, race, and age balance established in dataset
- APL dataset generally representative of military height & weight

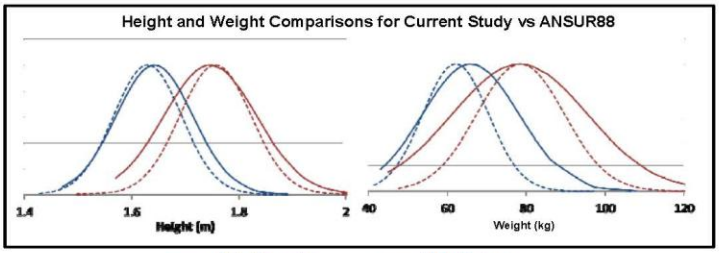

Data Collection
Anthropometric Measurements

- Limited anthropometric data available for medical subjects
- Radiologists manually approximated external skin and skeletal based metrics from lung CT scans

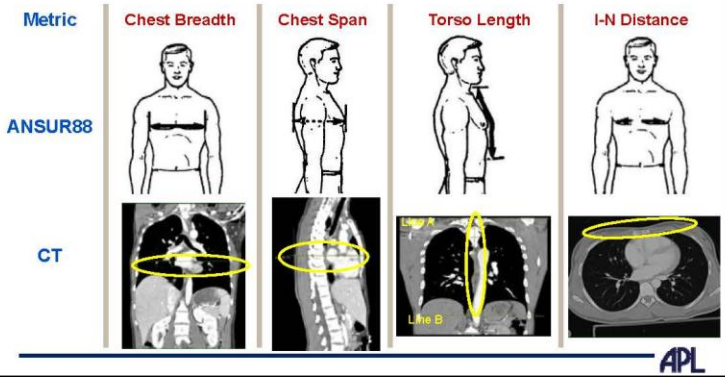

C20

Statistical Atlas Creation

APL

Statistical Atlas Creation

Overview

- **Goal:** Create a statistical shape atlas of the lung to study potential shape variations among patient populations
- **Approach:**

(1) Prepare Template

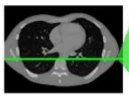

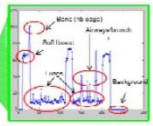

Template Mesh

APL

Statistical Atlas Creation
Overview

- **Goal:** Create a statistical shape atlas of the lung to study potential shape variations among patient populations
- **Approach:**

(1) Prepare Template

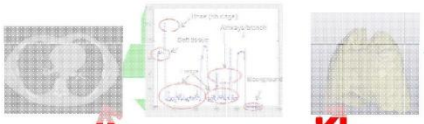

(2) Mesh Individuals

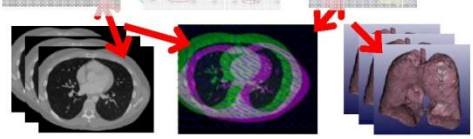

APL

Statistical Atlas Creation
Overview

- **Goal:** Create a statistical shape atlas of the lung to study potential shape variations among patient populations
- **Approach:**

(1) Prepare Template

Template Mesh

(2) Mesh Individuals

Individual Meshes

(3) Create Atlas

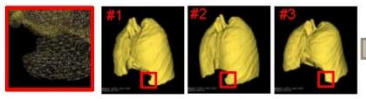

Grand Mean

$$\bar{X} = \frac{1}{N}\sum_{j=1}^{N} X_j$$

i-th vertex in jth sample: $(x_{j,i}, y_{j,i}, z_{j,i})$

$$X_j = (x_{j,0}\ y_{j,0}\ z_{j,0}\ x_{j,1}\ y_{j,1}\ z_{j,1}\ x_{j,2}\ y_{j,2}\ x_{j,2}, \ldots\ x_{j,n}\ x_{j,n}\ x_{j,n})^T$$

APL

Statistical Atlas Creation

Subject Specific Geometries

- **Subject-specific lung shapes with consistent mesh topology**

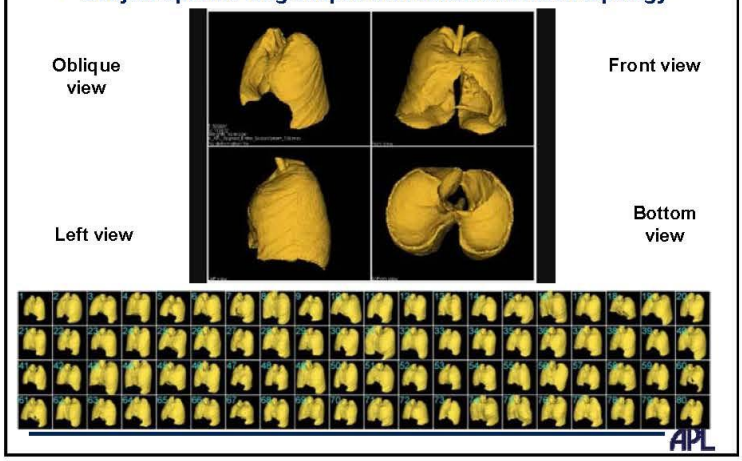

Statistical Atlas Creation

Statistical Analysis

- **Mean shape calculations**

Grand Mean

$$\bar{X} = \frac{1}{N}\sum_{j=1}^{N} X_j$$

Population Means

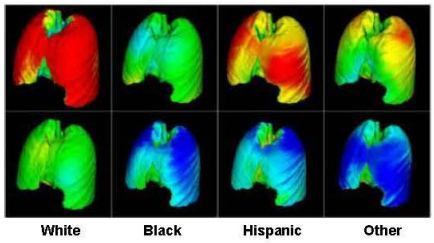

Difference from Mean Shape

APL

Statistical Atlas Creation

Statistical Analysis

- **Principal Component Analysis (PCA) captures the shape variations in the lung dataset**
  - i) Decreasing variance captured as mode # increases

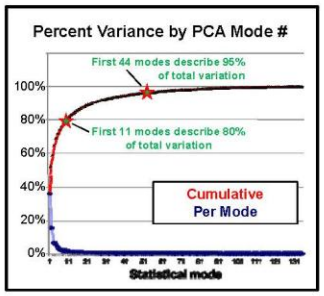

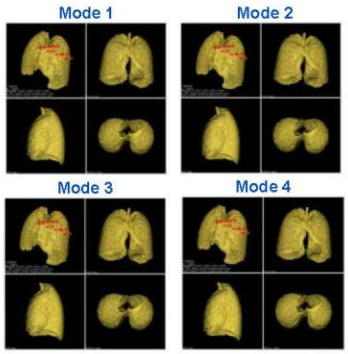

Statistical Atlas Creation

Statistical Analysis

- **Principal Component Analysis (PCA) captures the shape variations in the lung dataset**
  - i) Decreasing variance captured as mode # increases
- **Each subject expressible by summation of modes**

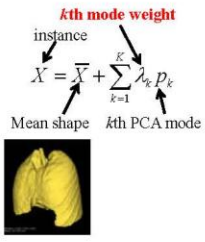

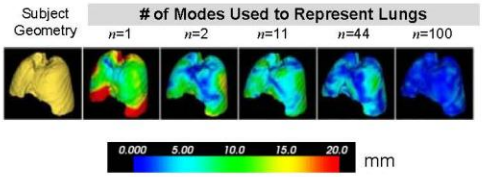

Differences in Patient Populations

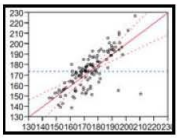

APL

Statistical Analysis
Overview

- **Goal: Determine how lung size and shape relate to various patient demographics**
- **2 logistic regression analyses approaches used:**
  - **Overall Lung Shape** → Trends for lung scaling with anthropometry
  - **PCA Mode Weights** → Prediction of subject specific anatomy
- **Effects Model Regression used to determine correlating trends and statistical significance**
  - Fits a line to actual data by the Least Squares Method

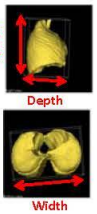

$$y_{ij} = \mu + \Sigma\beta_i x_i + \Sigma\varepsilon_{ij}$$

- y_{ij}: Dependent Variables — *Lung Size, Mode Weights*
- μ: Grand Mean of All Data
- $\Sigma\beta_i$: Factorial Coefficients
- x_i: Independent Variable — *Anthropometry, Demographics*
- $\Sigma\varepsilon_{ij}$: Error

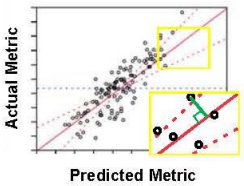

APL

C25

Statistical Analysis
Overall Lung Dimensions

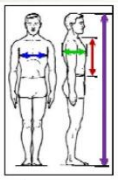

Height, weight, & age not prominent factors, but are basis for most scaling laws

Chest span important for most measurements

Gender and Race/Ethnicity mattered only for select metrics

Lung dimensions significant in same plane as external dimension

Metric	Gender	Race / Ethnicity	Age	Height	Weight	Chest Height	Chest Depth	Chest Width	IC Distance
Lung Width (cm)	↓				↑	↑		↑	
Lung Depth (cm)	↓		↓				↑		
Lung Height (cm)		↓				↑	↑		
Lung Volume (cm^3)						↑	↑	↑	

Base-lined against Male Gender & White Ethnicity

APL

Statistical Analysis
Recreation of Individual Lung Geometry

- **Coefficient of the computed regression functions for each Mode Weight**

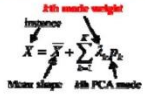

$$\lambda_1 = A_1 + B_{1,1}X_1 + B_{1,2}X_2 + 6 + B_{1,n}X_n$$
$$\lambda_2 = A_2 + B_{2,1}X_1 + B_{2,2}X_2 + 6 + B_{2,n}X_n$$
$$\lambda_K = A_K + B_{K,1}X_1 + B_{K,2}X_2 + 6 + B_{K,n}X_n$$

λ_K: mode weights
X_n: measurements (external & demographic)

- **Predicted mode weights to recreate individual lung geometries**
  - Average error for all subjects/vertices 10.48 ± 5.48 mm

Example Subject
- Female, "Other" Ethnicity
- 43 y.o.
- Weight: 48.53 kg
- Height: 152 cm

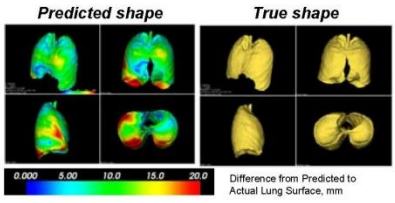

Lung Geometry Predicted Solely from Demographic and Anthropometric Features

APL

Summary & Limitations

- **Multi-disciplinary team of engineers, anthropologists, computer scientists, & radiologist successfully collaborated to:**
  - Create a lung statistical shape atlas
  - Investigate allometric scaling laws
  - Predict internal organ shape from external features
- **Computational pipeline established and ready to deploy for human model development**
- **Limitations**
  - Increased # subjects for improved statistical significance
  - Single posture only
  - External metrics not optimized for predicting internal anatomy
  - Current study applied for single organ geometry only

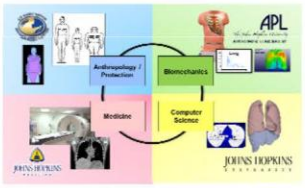

Future Applications

- **Implementation into accurately scaled human computational models**
- **Expansion to additional organ systems or imaging modalities**
- **Understanding injury implications**
- **Personalized medicine**

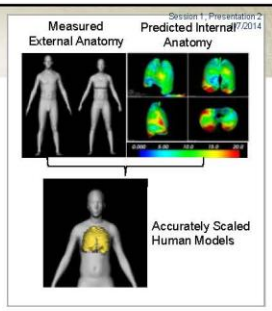

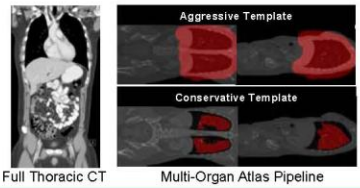

Full Thoracic CT | Multi-Organ Atlas Pipeline | Lung & Liver Geometries | Human FEMs

Workshop on Numerical Analysis of Human and Surrogate Response to Accelerative Loading
Aberdeen Proving Ground, MD
January 7-9, 2014

Approaches for Predicting Human Anatomical Variations Using Anthropometric & Demographic Data

Catherine Carneal [1], Yoshito Otake[2], Dean Kleissas[1], Andrew Merkle[1], Mehran Armand[1,2], Manuel Uy[1], Gaurav Thawait[3], John Carrino[3], Brian Corner[4], Marina Carboni[4], Barry DeCristofano[4], Michael Maffeo[4]

[1] *The Johns Hopkins University Applied Physics Laboratory, Laurel, MD 20723, USA*
[2] *The Johns Hopkins University Department of Computer Science, Baltimore, MD, USA*
[3] *The Johns Hopkins Medical Institute Department of Radiology, Baltimore, MD, USA*
[4] *U.S. Army Natick Soldier Research Development and Engineering Center, Natick, MA USA*

BOMS
BIOMECHANICS AND INJURY MITIGATION SYSTEMS

APL
The Johns Hopkins University
APPLIED PHYSICS LABORATORY
11100 Johns Hopkins Road
Laurel, MD 20723-6099

CT Image Details

- **Indications**
  - Trauma
  - Infection
  - To find blood clots in veins
  - Chest Pain
  - Find cancer or spread of cancer
- **Method: Inspiration, Single breath hold**
- **Parameters:**
  - 0.75mm slice thickness acquisition
  - 3mm reconstruction
  - 512x512 matrix
  - Isotropic voxels
  - Excellent reconstruction in other planes
  - 120 kV, 300 eff. mAs, pitch 0.65

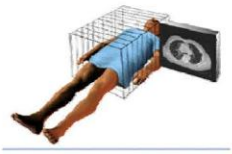

www.mayoclinic.com/health/medical/IM03614

APL

C28

External Measurements
Chest Breadth

Session 1, Presentation 2
1/7/2014

Comparable ANSUR	CT Measurement
• Maximum horizontal breadth of chest at level of the right bustpoint/thelion landmark.	• At carina • Proper position at the level of nipples confirmed on another view (axial plane)

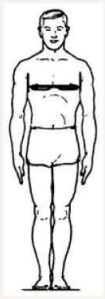

APL

External Measurements
Chest Depth

Session 1, Presentation 2
1/7/2014

Comparable ANSUR	CT Measurement
• Horizontal distance between the chest and back, at the level of the right bustpoint on women or the nipple on men	• At level of vertebral bodies and sternum • Proper position at level of nipples confirmed on another view (axial plane)

APL

C29

External Measurements

Chest Span (Cranio-Caudal)

Comparable ANSUR	CT Measurement
• Distance between landmark at the front of the neck and anterior waist landmark (natural indentation)	• Coronal section where posterior part of 1st rib is visible • Vertical distance between highest level of first rib to the lower costophrenic angle

APL

External Measurements

Internipple distance

Comparable ANSUR	CT Measurement
• Distance between right and left bustpoint on women and the center of nipples on men.	• Axial view. • Slide with both nipples visible.

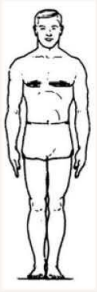

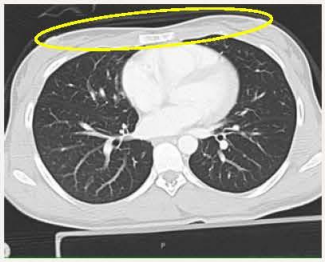

APL

15

Data Collection
Comparison with Military Population

- **Subject weight and height have similar means**
  - More variance in APL population (males especially)
- **Overall chest proportions also similar**
  - Chest span discrepancy likely due to CT-based measurement method

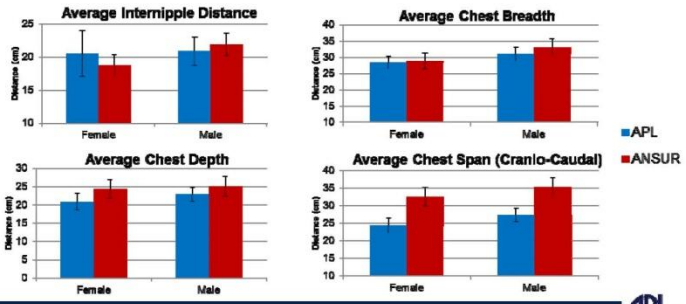

Lung Atlas for Subject-Specific Models
Approach

Session 1, Presentation 2
1/7/2014

- **Can we predict an individual's lung shape solely on external variables?**

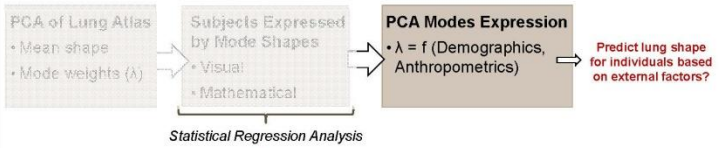

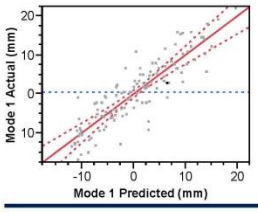

Mode 1 = -84.0 – 1.25*Gender [F] + 0.66 * Chest Breadth
+ 0.53 * Chest Depth + 1.3 * Chest Span
+ 0.0*Age -1.04*Race [B] – 0.86*Race [H] – 0.35 * Race [0]
+ 0.04*Weight + 8.05*Height + 0.13*IN distance

Green Indicates Significance ($p < 0.05$)

C31

Predicting Lung Bounding Box Depth
Single Factorial

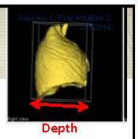

- **Lung Depth is significantly predicted by 3 of 9 external factors:**
  - Increases with Chest Depth
  - Decreases if "Other" demographic
  - Decreases if Female Gender

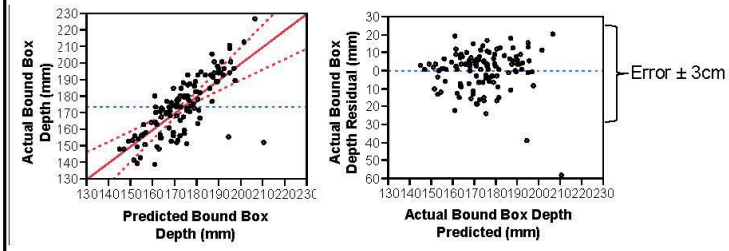

Lung Depth = 58.92 + Chest Depth*3 + Race[O] * -4.37 + Gender[F]*-2.91 + …..

APL

Internal Lung Measurements

Session 1, Presentation 2
1/7/2014

- **Atlas-made measurements (30 landmark points, 17 measurements)**
  - Lung Breadth
  - Right Lung Height
  - Left Lung Height
  - Right Lung Transverse width (3-Branch View)
  - Right Lung Anterior-Posterior depth (3-Branch View)
  - Left Lung Transverse width (3-Branch View)
  - Left Lung Anterior-Posterior depth (3-Branch View)
  - Right Lung Transverse width (Diaphragmatic Peak View)
  - Right Lung Anterior-Posterior depth (Diaphragmatic Peak View)
  - Left Lung Transverse width (Diaphragmatic Peak View)
  - Left Lung Anterior-Posterior depth (Diaphragmatic Peak View)
  - Transverse width of Trachea
  - Anterior-Posterior depth of Trachea

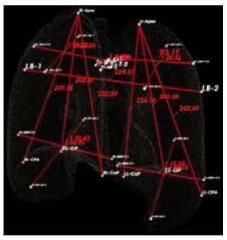

APL

17

C32

Lung Atlas for Subject-Specific Models

Session 1, Presentation 2
1/7/2014

Results

- **Prediction accuracy of each mode & geometry validated by performing PCA & regression analysis with a subject "leave out" test**
  - All subjects were left out and validated one at a time
- **Average error for all subjects/vertices : 10.48 ± 5.48 mm**

Plot shows avg displ error (mm) for all 112,602 lung vertices
(box plot: 25-75%, whisker plot: max and min, dot: median).

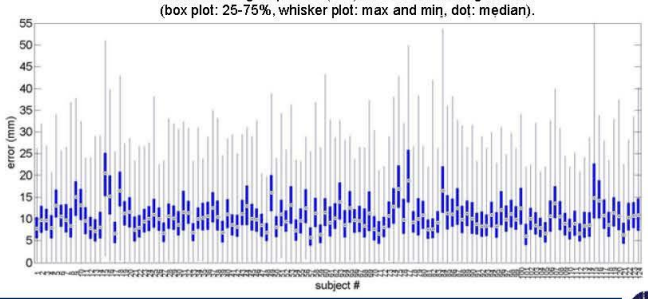

APL

HUMANETICS
Innovative Solutions

Numerical Approach for Modeling Joint Stops in Anthropomorphic Test Devices(ATDs)

Humanetics Innovative Solutions Inc.
Renuka Jagadish
Hyunsok Pang

Agenda

- Introduction
  - ATD Joints
  - Joint Stops
  - Nodding Block
- Modeling approach for Nodding Block
  - Nodding Block Hardware
  - Nodding Block FE
  - Nodding Block Presimulation
  - Neck Pendulum Test
  - Results
- WIAMan Application - Neck Model
- Conclusions

 01.07.2014

1

Introduction - ATD Joints

- In FE dummies a spherical joint is used when the physical joint is a ball joint (e.g. hip and ankle joints) and revolute joint is used when the physical joint acts as a hinge (e.g. the wrist to hand joint)
- In FE development, LS-DYNA *CONSTRAINED_JOINT_REVOLUTE/ *CONSTRAINED_JOINT_SPHERICAL/* CONSTRAINED_JOINT_TRANSLATIONAL is used to define the joint between two parts

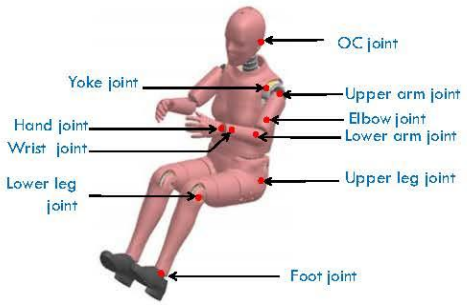

5th Percentile Model

Introduction - Joint Stops

- The articulating joint motion is stopped by the material compression of joint stops
- Modeling the physical bumpers in recent FE development
- Replaces the moment curves/stop angles which had been defined previously
- Provide better physical response and reduces/eliminates noise seen in stiffness curve approach

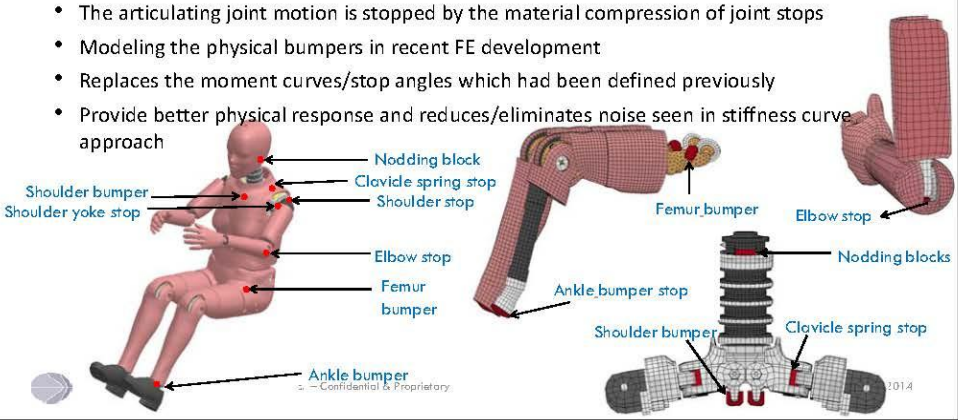

Introduction - Nodding Block

- Nodding block is a small block of rubber placed between the neck bracket and the upper neck load cell and performs the function of the occipital condyle joint in humans
- Movement of the head along the coronal plane (Y-Z plane) is stopped by the nodding blocks
- In the physical hardware, the nodding block pin bends and is pressed into the circular slot on the nodding block bracket

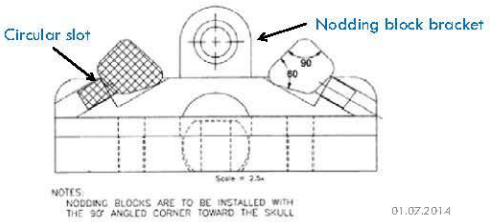

01.07.2014

Modeling Approach - Nodding Block Hardware

- Next step is to assembly the head and neck together
- Place the head over the neck assembly and push down the upper loadcell into the nodding block bracket where the holes coincide (OC joint) and insert the transducer pin
- Bottom surface of the loadcell and top surface of the nodding block are in contact in the assembled head-neck hardware
- Nodding block rubber compresses and is in pre stressed state

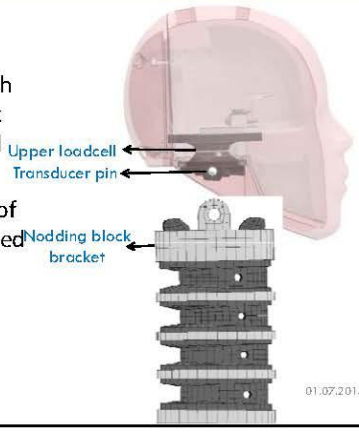

01.07.2014

Modeling Approach - Nodding Block FE Model

- CAD drawing has the undeformed geometry information
- FE mesh follows the undeformed geometry profile
- Penetration at the interface of the loadcell and nodding block
- Pre simulation is performed to account for compression of rubber and pre stress

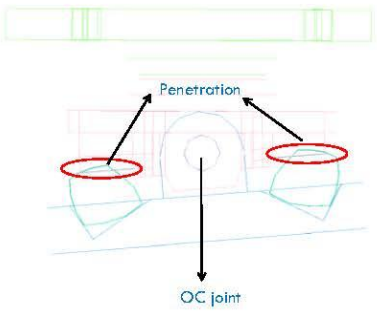

Nodding Block Presimulation: Step 1

- Solver: LS-DYNA
- Nodding Block Material: MAT_77_O (Ogden Rubber)
- Pre simulation is done by pushing down the loadcell with a boundary displacement condition
- Surface contact is defined at the interface of the nodding block and the loadcell
- General contact is defined to take care of edge to edge intersections
- Deformed shape of nodding block

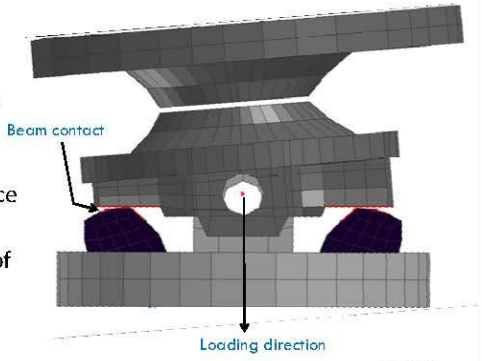

Nodding Block Presimulation: Step 1

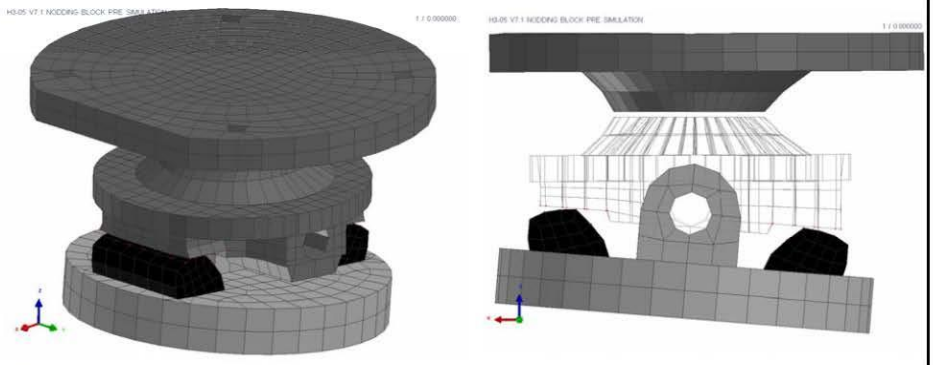

Nodding Block Presimulation: Step 2

- Deformed nodes are output and defined in the step 1 input deck under *NODE card
- Initial nodes are defined in *INITIAL_FOAM_REFERENCE _GEOMETRY card
- In the *MAT_77_O card, switch REF parameter to 1 from 0 to use reference geometry to initialize the stress tensor
- Sanity run is done to check if there are instabilities and an equilibrium state is attained
- Pre stress is induced at 0 ms of the simulation

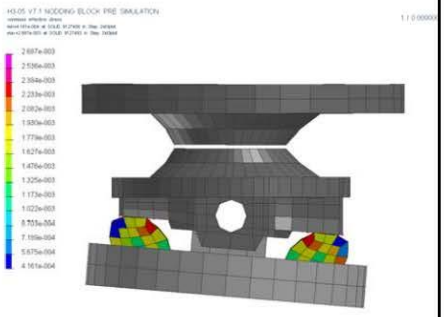

Neck Pendulum Test

- In FE dummy development, neck has to be modeled as close as possible to the hardware
  - Capture the kinematics
  - Good correlation with respect to certification test results
- Certification Speed
  - Flexion - 7.01 m/s
  - Extension - 6.31 m/s

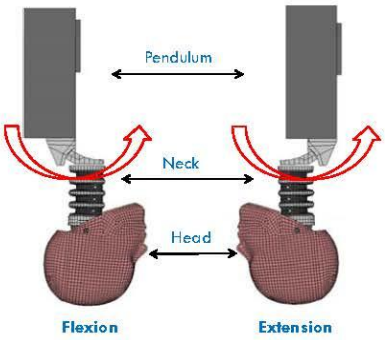

Results - Flexion

- Certification Speed - 7.01 m/s

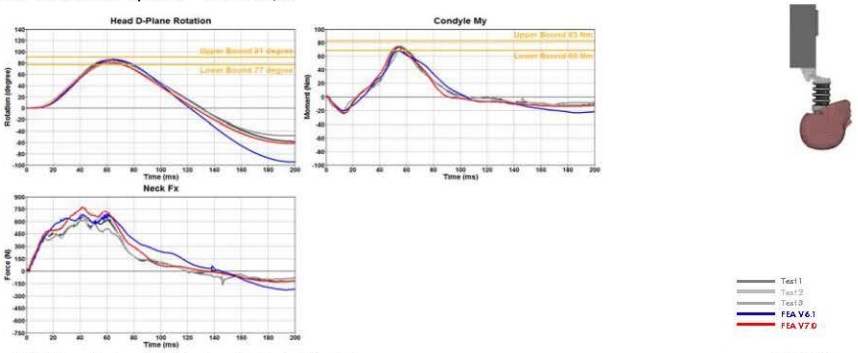

Results - Flexion

Nodding Block v7.0

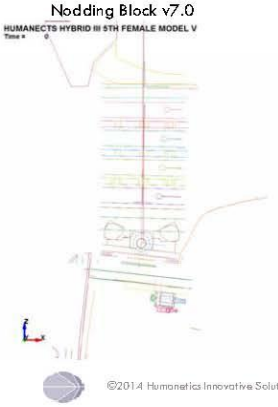

Joint Stiffness Curve v6.1

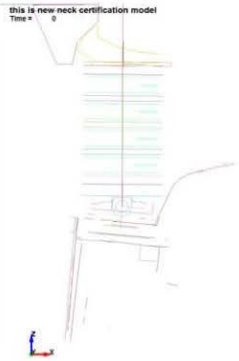

Results – Flexion - Nodding Block

Nodding Block - With Pre Stress

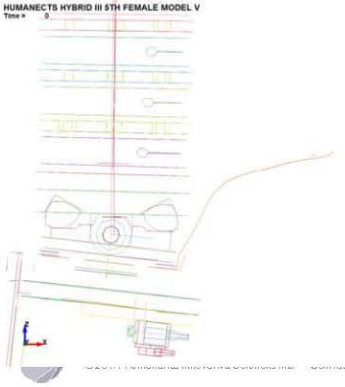

Nodding Block - Without Pre Stress

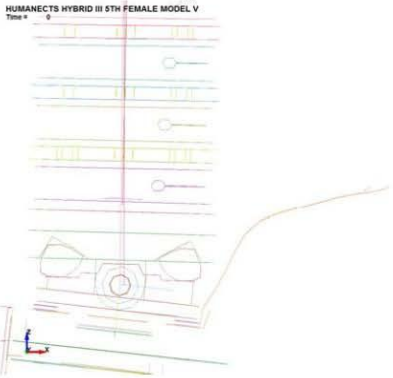

7

Results - Extension

- Certification Speed - 6.31 m/s

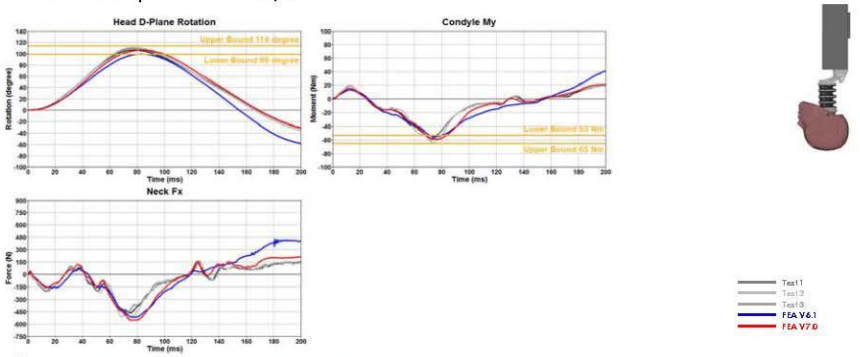

Results - Extension

Nodding Block v7.0

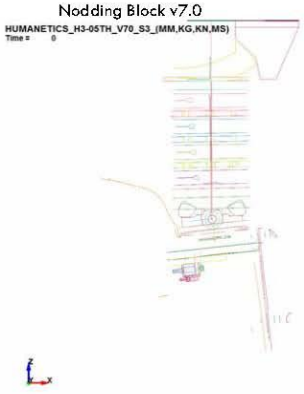

Joint Stiffness Curve v6.1

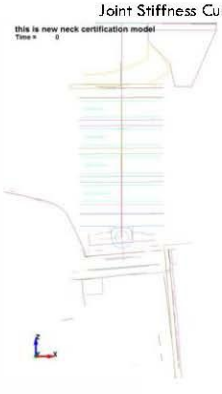

WIAMan Application – Neck Model

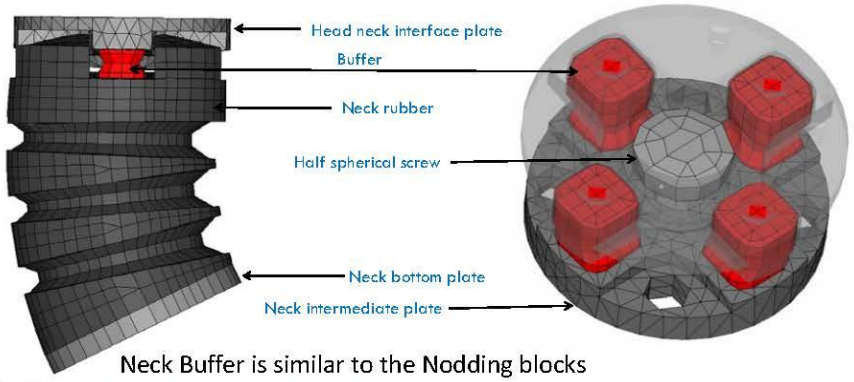

Neck Buffer is similar to the Nodding blocks

Conclusions

- Modeling the physical geometry of the nodding block is a better representative of the hardware
- Results are better, captures the moment peak and the D - Plane rotation
- Force signals are smoother, but further investigation has to be done in the future to improve the correlation
- Based on our experience, a similar pre simulation approach will be followed in the WIAMan neck model for the neck buffer

Thank You

Questions?

HUMANETICS

Numerical Approach for Modeling Joint Stops in Anthropomorphic Test Devices(ATDs)

Humanetics Innovative Solutions Inc.
Renuka Jagadish
Hyunsok Pang

PUBLIC RELEASE-DISTRIBUTION UNLIMITED

US ARMY RDECOM U.S. Army Research, Development and Engineering Command

Effect of Loading Rate and Orientation on the Compressive Response of Human Cortical Bone

ARL

TECHNOLOGY DRIVEN. WARFIGHTER FOCUSED.

B. Sanborn, C.A. Gunnarsson, M. Foster, P. Moy, T. Weerasooriya

Workshop on Numerical Analysis of Human and Surrogate Response to Accelerative Loading

January 2013

PUBLIC RELEASE-DISTRIBUTION UNLIMITED

PUBLIC RELEASE-DISTRIBUTION UNLIMITED

US ARMY RDECOM

Structure of Bone

ARL

- Bone is a organized on multiple length scales
- Smallest elements are collagen fibrils and hydroxyapatite crystals
- Long bones have Haversian structure with osteons that run along the vertical axis of the bone
- Osteon structure leads to anisotropy

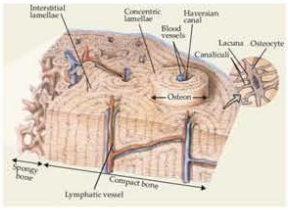

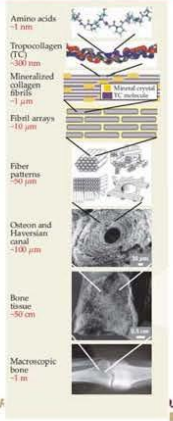

R.O. Ritchie, M.J. Buehler, P. Hansma. Plasticity and Toughness in Bone. Physics Today June 2009

TECHNOLOGY DR

PUBLIC RELEASE-DISTRIBUTION UNLIMITED

Initial Studies on Human Bone

- Studies of rate dependence conducted in 1966 on embalmed human bone
- Embalming affects stiffness and strength
  - Embalming degrades collagen fibers in the bone microstructure
- Formalin concentration level and length of time of embalming process affect mechanical properties
- Despite embalming, the bone was rate dependent

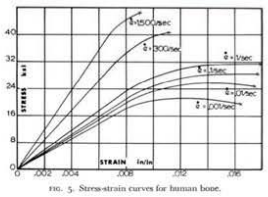

FIG. 5. Stress-strain curves for human bone.

FIG. 1. Miniature bone specimen, strain gage, and load cell.

J.H McElhaney. Dynamic response of bone and muscle tissue. J. Appl. Physiol 21: 1231-1236. 1966

Animal Studies - Bovine

- Kolsky bar technique applied to bone as early as 1970 in dynamic compression [1]
- Expanded to compression, tension, torsion, and compression/torsion later (1975) [2]
- Bovine bone studied again in 2006 (along with fracture properties) [3] [4] [5]
- All studies show that the failure strength increases with increasing strain rate

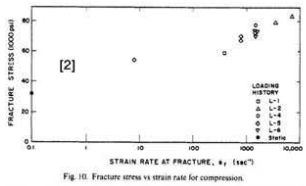

Fig. 10. Fracture stress vs strain rate for compression.

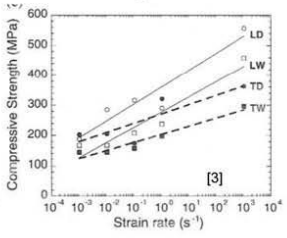

[1] Tennyson, R.C., Ewert, R. Applicatoin of the split-Hopkinson bar to determine the dynamic response of bone. Proc 3rd Can. Med. and Bio. Eng. Conf. Sept 1970

[2] Lewis, J.L., Goldsmith, W. The dynamic fracture and prefracture response of compact bone by SHPB. 1975 J. Biomechanics 8:27-40.

[3] R. R. Adharpurapu, F. Jiang, K.S. Vecchio. Dynamic fracture of bovine bone. 2006 Materials Science and Engineering C 26. 1325-1332.

[4] Ferreira, M. A. Vaz, J.A Simoes, Mechanical properties of bovine cortical bone at high strain rate. Materials Characterization, 57, 71-79.

[5] O.S. Lee, J.S. Park. Dynamic deformation of bovine femur using SHPB. 2011 Journal of Mechanical Science and Technology 25(9). 2211-2215.

Animal Studies - Equine

- Equine results at high rate are similar to bovine results
- Anisotropic
- Increase in strength and stiffness with increasing strain rate
- Magnitude of strength found in animal studies is higher than other preliminary human results (even embalmed human specimens)
- Studies that use SHPB bar signals to determine failure strain are inaccurate

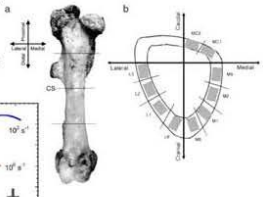

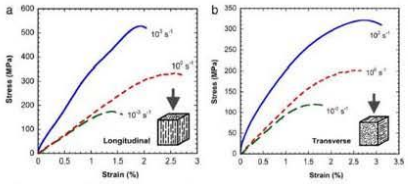

R. M. Kulin, F. Jiang, K.S. Vecchio. Effects of age and loading rate on equine bone failure. 2011. Journal of the Mechanical Behavior of Biomedical Materials 4: 57-75.

Experimental Setup

- Quasi-static and intermediate rate experiments: Hydraulic Load frame (Instron)
- High rate experiments: split Hopkinson pressure bar (SHPB)
- Standard compression setup
- High-speed camera at 1M frames per second to measure surface strains using DIC

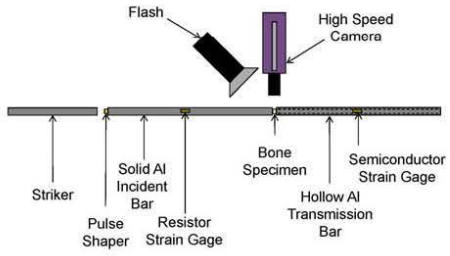

Materials

- Cortical bone samples extracted from three male cadavers along femur diaphysis
- Ages 36, 43, 50
- Extracted from medial, lateral, anterior, and posterior sides
- Cubes of bone were nominally 3 x 3.25 x 4 mm
- Specimens were oriented transverse and longitudinal to the axis of the bone
- Total of 71 experiments conducted

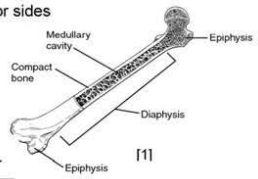

[1]

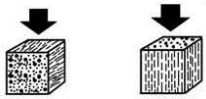

	Transverse Direction	Longitudinal Direction
Quasi-static Rate (~0.001/s)	12	12
Intermediate Rate (~1/s)	11	11
High Rate (~1000/s)	14	11

[1] Dorland's Illustrated Medical Dictionary, 29th ed. 2000. Saunders. St. Louis Mo.

TECHNOLOGY DRIVEN. WARFIGHTER FOCUSED.

Experimental Results

- Triangular shaped incident pulse – used for more brittle materials
- Specimen in dynamic equilibrium
- Attained constant strain rate
- After specimen beings to fail, around 90 us, the strain rate increases

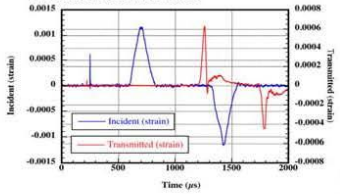

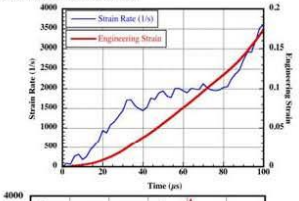

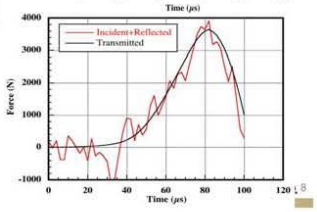

DIC Results

- Digital Image Correlation (DIC) used to make strain and strain rate measurements
- Studies that use SHPB bar signals to determine failure strain are inaccurate
- Speckle pattern is applied to the surface of the specimen
- Pixel gray level values are tracked throughout experiment by software
- Increase in strain rate once specimen reaches max load (failure) is seen on DIC

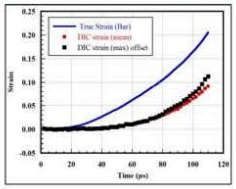

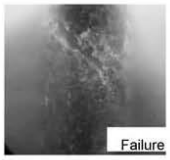

Stress-Strain Response

- Stress-strain results show anisotropic behavior of human femoral cortical bone
- High amount of scatter as expected in bio materials
  - Natural variability
  - Different mineral content
  - Microstructural flaws
  - Variation in osteon size
- Failure strength increases with strain rate (both directions)

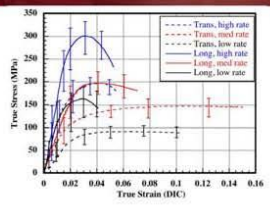

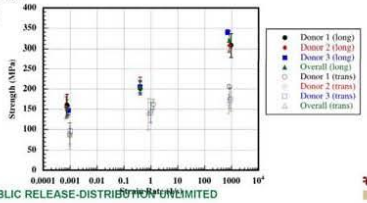

PUBLIC RELEASE-DISTRIBUTION UNLIMITED

Modulus Results

- Stiffness is higher in longitudinal direction
- This is due to the orientation of specimens WRT the osteon axis
- Stiffness was lower compared to other studies
  - Typically 15-18 GPa for femur
- Failure strain was higher for transverse specimens (cylindrical osteons crushed in transverse direction)
- At high rate the failure strains were nearly identical

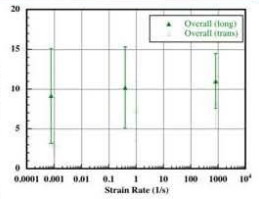

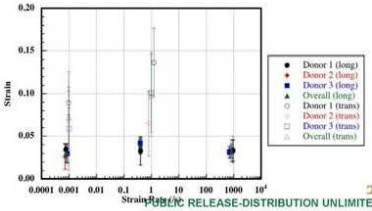

TECHNOLOGY DRIVEN. WARFIGHTER FOCUSED.11

PUBLIC RELEASE-DISTRIBUTION UNLIMITED

PUBLIC RELEASE-DISTRIBUTION UNLIMITED

Comparison with Animal Studies

- Qualitatively the results agree with other studies on animal bone (shape of S-S)
- Compressive strength results fall in line with results of others
- Results of animal studies poorly represent the response of human bone
- Constitutive models should employ results obtained from human experiments only for accurate results

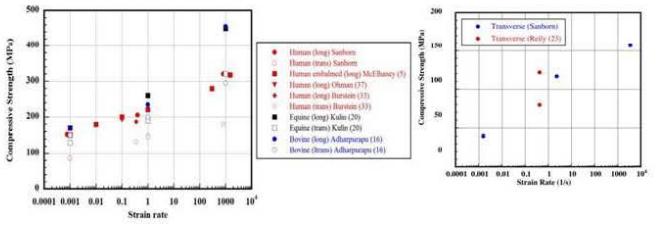

TECHNOLOGY DRIVEN. WARFIGHTER FOCUSED.12

PUBLIC RELEASE-DISTRIBUTION UNLIMITED

Comparison to Tibia

- Longitudinal compression results fall in the same range as other studies
- Strength and stiffness obtained from femur should not be used as typical values for cortical bone found in other areas of the body
- For instance, the stiffness of the tibia can be twice that of femur
- Statistically significant regional variations in stiffness have been found in human femur – different levels of anisotropy were found along femur shaft – high anisotropy at ends

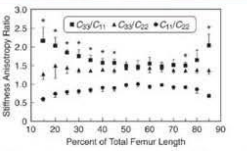

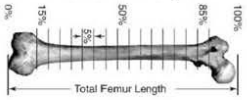

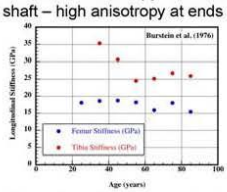

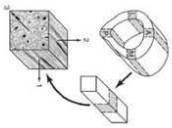

A A. Espinoza Orias, J.M. Deuerling, M. D. Landrigan, J.E. Renaud, R.K. Roeder. Anatomic variation in the elastic anisotropy of cortical bone tissue in human femur. 2009. Journal of the Biomechanical Behavior of Biomedical Materials.

Summary

- Human femoral cortical bone samples from longitudinal and transverse directions
- Compressive failure strength as a function of strain rate was studied up to high rates
- Utilized DIC methods for strain measurements, achieved constant strain rate and dynamic equilibrium – not evident in other SHPB bone work
- The bone was shown to be anisotropic in the two directions
- Failure strengths in the two directions compared well with other studies
- Young's modulus was lower than other studies on human femur
- Recorded failure strengths lower than comparable animal studies
- Strengths and stiffness found from femur results should not be applied to other bones in the body for numerical modeling purposes. Regional variations in stiffness within a given bone exist

Experimental and Finite Element Analysis of Brain Tissue under High Strain Rates

Lakiesha N. Williams, PhD, Mark F. Horstemeyer, PhD,
Jun Liao, PhD,and Rajkumar Prabhu, PhD

Workshop on Numerical Analysis of Human and Surrogate Response to Accelerative Loading
January 7-9, 2014

Prabhu, R., Horstemeyer, M., Marin, E., Bouvard, J-L., Tucker, M., Sherburn, J., Liao, J., Williams, L.N.,
"Coupled Experiment / Finite Element Analysis on the Mechanical Response of Porcine Brain under High Strain Rates,"
Journal of Mechanical Behavior of Biological Materials, 4(7), 2011: 1067-1080 doi:10.1016/j.jmbbm.2011.03.015, 2011

Motivation: Curious Case of John Grimsley*

John Grimsley, a retired NFL linebacker; who accidently shot himself in the chest while cleaning a gun.

Brain Sagittal Section

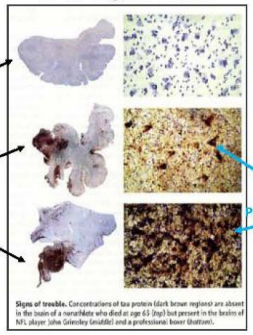

Histology of John Grimsley's brain (*middle*). Brain sagittal section in the top (*left*) is healthy, while Grimsley's (*left middle*) and a professional boxer's sagittal section (*left bottom*) show presence of high concentrations of tau protein

*Miller, G., (2009), "A late hit for Pro Football Player, Science, August 7, 325, pp. 670-672

Motivation: Owen Thomas

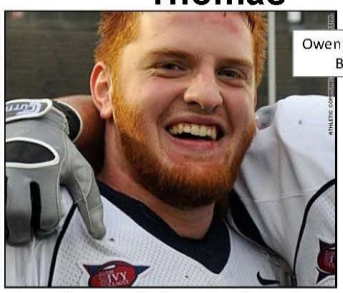

Owen Thomas, a junior at the University of Pennsylvania, had symptoms of chronic traumatic encephalopathy.

*http://www.cnn.com/2010/HEALTH/09/14/thomas.football.brain/index.html?hpt=C2

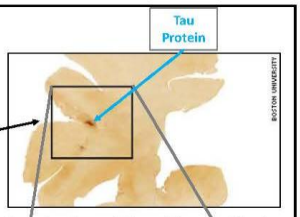

Examination of Owen Thomas' brain sections showing dense tau protein in multiple areas.

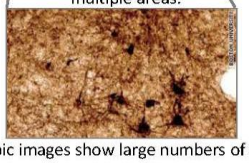

Microscopic images show large numbers of tau (dark brown spots) in the areas of damage. In healthy brain tissue, there would be no such protein tangles.

Objective

- Understand the mechanical behavior of the porcine brain under high strain rate loading conditions.
- Analyze the stress state using FEA with a specific material model (MSU TP Ver.1) that captures the physics of tissue deformation, under high strain rate loading conditions.

Experimental Background

- Hopkinson, (1914):
  - First to conduct high rate compression tests.
  - Hopkinson studied the impact at various rates (213.36, 377.95 and 609.6 m/s) to quantify the pressure experienced by specimens.
- Kolsky, (1949):
  - Implemented the split-Hopkinson pressure bar technique.
  - Polythene, rubber, polymethyl-methacrylate, copper and lead were studied to analyze dynamic properties in the range 100 – 10,000 s^{-1}.
- Fallenstein *et al.*, (1969):
  - Performed a series of dynamic shear tests (9-10 s^{-1}) on the human brain.
- Donnelly and Medige, (1997):
  - Conducted the most extensive shear tests on the human brain (125 samples), in the range 0.1-80 s^{-1}.
- Gary et al., (1995); Zhao et al., (1996, 1997):
  - Implemented polycarbonate bars for high strain rate testing.
  - Used viscoelastic dispersion for the stress waves.

MISSISSIPPI STATE UNIVERSITY | JAMES WORTH BAGLEY COLLEGE OF ENGINEERING MISSISSIPPI STATE UNIVERSITY | CAVS CENTER FOR ADVANCED VEHICULAR SYSTEMS 5

Experimental Background

- Bain and Meaney, (2000); Geddes *et al.*, (2001); Pfister *et al.*, (2003); Bayly *et al.*, (2006):
  - Conducted in-vivo studies on rat brain specimens and in-vitro studies on brain cell culture.
  - Traumatic Brain Injury (TBI) on at strains > 0.2, and strain rates > 40 s^{-1}.
- Gray and Blumenthal (2001):
  - Specimen aspect ratio (L/D) for soft materials < 0.5.
- Prange and Margulies, (2002); Nicole *et al.*, (2004):
  - Noted that there was no significant difference existed between the compressive mechanical properties of the human and porcine brain tissue.
- Tamura *et al.*, (2007):
  - Conducted compression tests in the range 1-50 s^{-1}. Also showed that orientation and location effects were negligible.
- Song *et al.*, (2007):
  - Attributed the initial hardening trend of the mechanical response of soft biological materials to inertial effects, and asserted that the usage of annular specimens (donut specimens) negates the inertial effects.
- Pervin and Chen (2009):
  - Conducted compression tests on the bovine brain in the range 1000-3000 s^{-1}.

MISSISSIPPI STATE UNIVERSITY | JAMES WORTH BAGLEY COLLEGE OF ENGINEERING MISSISSIPPI STATE UNIVERSITY | CAVS CENTER FOR ADVANCED VEHICULAR SYSTEMS 6

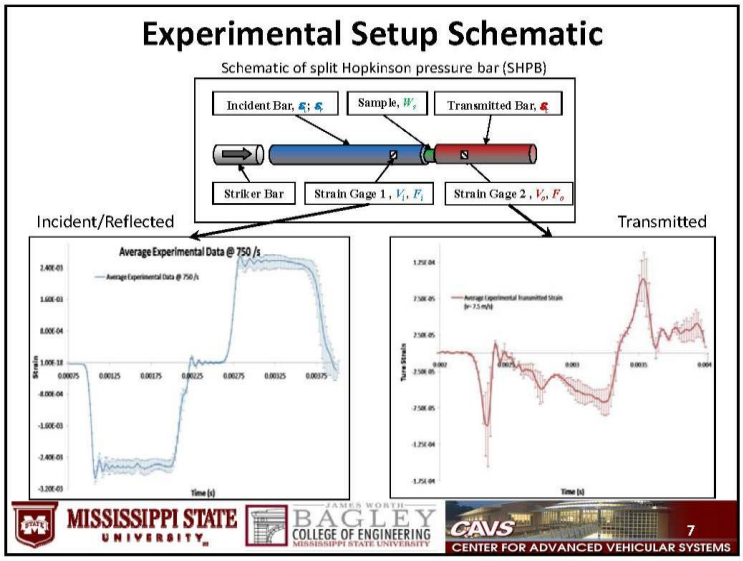
Experimental Setup Schematic
Schematic of split Hopkinson pressure bar (SHPB)
Incident Bar, E_i; A_i
Sample, W_s
Transmitted Bar, E_t
Striker Bar
Strain Gage 1 , V_1, F_1
Strain Gage 2 , V_2, F_2
Incident/Reflected
Transmitted
Average Experimental Data @ 750 /s
MISSISSIPPI STATE UNIVERSITY
BAGLEY COLLEGE OF ENGINEERING
CAVS
CENTER FOR ADVANCED VEHICULAR SYSTEMS
7

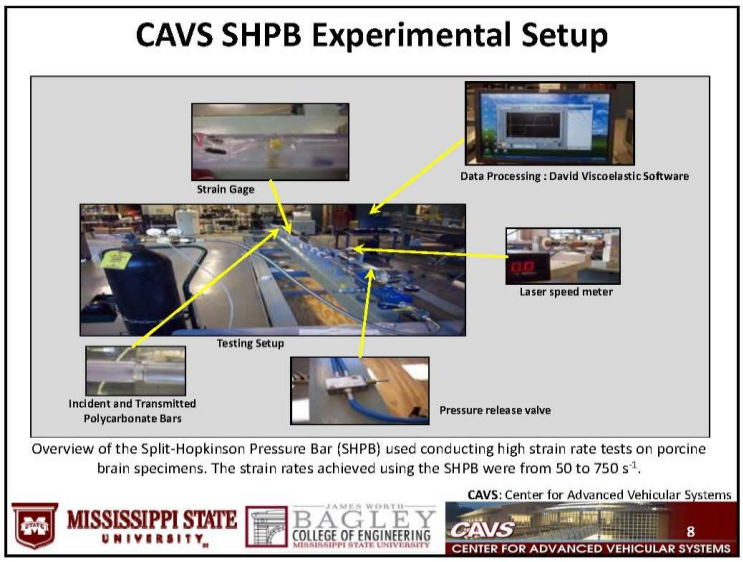
CAVS SHPB Experimental Setup
Strain Gage
Data Processing : David Viscoelastic Software
Laser speed meter
Testing Setup
Incident and Transmitted Polycarbonate Bars
Pressure release valve
Overview of the Split-Hopkinson Pressure Bar (SHPB) used conducting high strain rate tests on porcine brain specimens. The strain rates achieved using the SHPB were from 50 to 750 s^{-1}.
CAVS: Center for Advanced Vehicular Systems
MISSISSIPPI STATE UNIVERSITY
BAGLEY COLLEGE OF ENGINEERING
CAVS
CENTER FOR ADVANCED VEHICULAR SYSTEMS
8

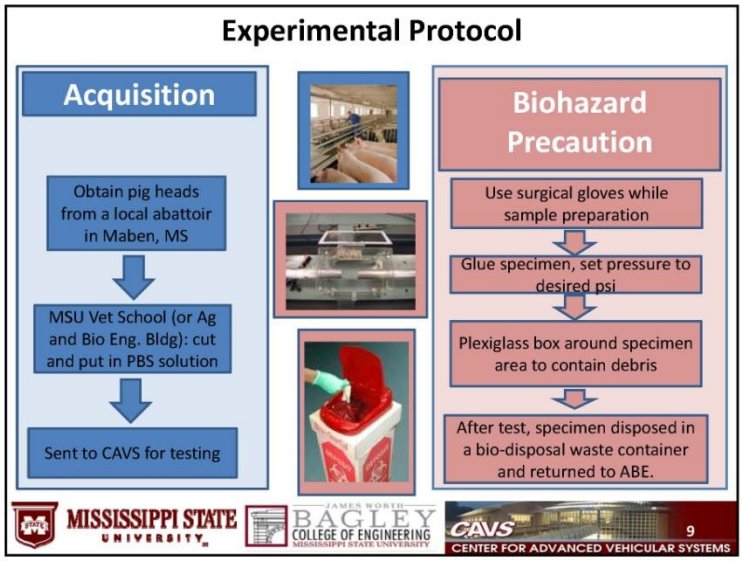
Experimental Protocol
Acquisition
Obtain pig heads from a local abattoir in Maben, MS
MSU Vet School (or Ag and Bio Eng. Bldg): cut and put in PBS solution
Sent to CAVS for testing
Biohazard Precaution
Use surgical gloves while sample preparation
Glue specimen, set pressure to desired psi
Plexiglass box around specimen area to contain debris
After test, specimen disposed in a bio-disposal waste container and returned to ABE.
MISSISSIPPI STATE UNIVERSITY
JAMES WORTH BAGLEY COLLEGE OF ENGINEERING MISSISSIPPI STATE UNIVERSITY
CAVS CENTER FOR ADVANCED VEHICULAR SYSTEMS
9

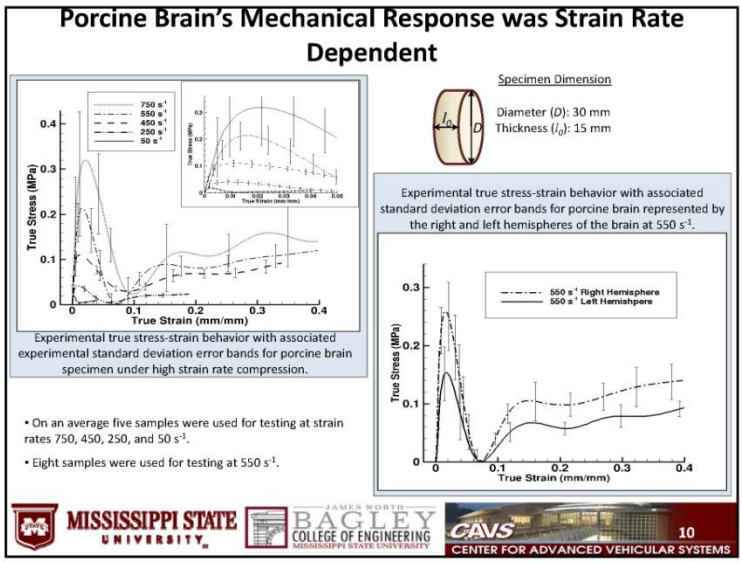
Porcine Brain's Mechanical Response was Strain Rate Dependent
750 s-1
550 s-1
450 s-1
250 s-1
50 s-1
True Stress (MPa)
True Strain (mm/mm)
Experimental true stress-strain behavior with associated experimental standard deviation error bands for porcine brain specimen under high strain rate compression.
Specimen Dimension
Diameter (D): 30 mm
Thickness (l0): 15 mm
Experimental true stress-strain behavior with associated standard deviation error bands for porcine brain represented by the right and left hemispheres of the brain at 550 s-1.
550 s-1 Right Hemisphere
550 s-1 Left Hemisphere
• On an average five samples were used for testing at strain rates 750, 450, 250, and 50 s-1.
• Eight samples were used for testing at 550 s-1.
MISSISSIPPI STATE UNIVERSITY
JAMES WORTH BAGLEY COLLEGE OF ENGINEERING MISSISSIPPI STATE UNIVERSITY
CAVS CENTER FOR ADVANCED VEHICULAR SYSTEMS
10

Porcine Brain's Mechanical Response was Highly Non-Linear

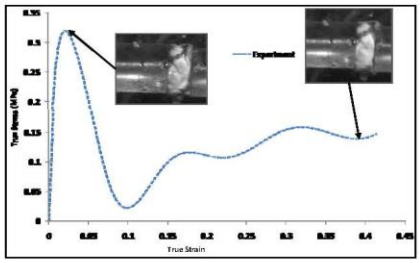

True Stress-Strain plot for porcine brain at a of strain rate 750 s^{-1}, with snapshots from the experiment.

Salient Features of the Brain's Mechanical Response:

- The response is marked by initial hardening effect, followed by a softening trend, and then strain hardening at larger strains.
- Since 65-80%† of cellular structures in the brain are comprised of water, part of this initial yielding can be attributed to the water content.
- Resistance from rapid deformation by cellular structures also contributed to the initial hardening.

†Neeb *et al.*, (2010)

MISSISSIPPI STATE UNIVERSITY | JAMES WORTH BAGLEY COLLEGE OF ENGINEERING MISSISSIPPI STATE UNIVERSITY | CAVS CENTER FOR ADVANCED VEHICULAR SYSTEMS | 11

FE Simulation Overview

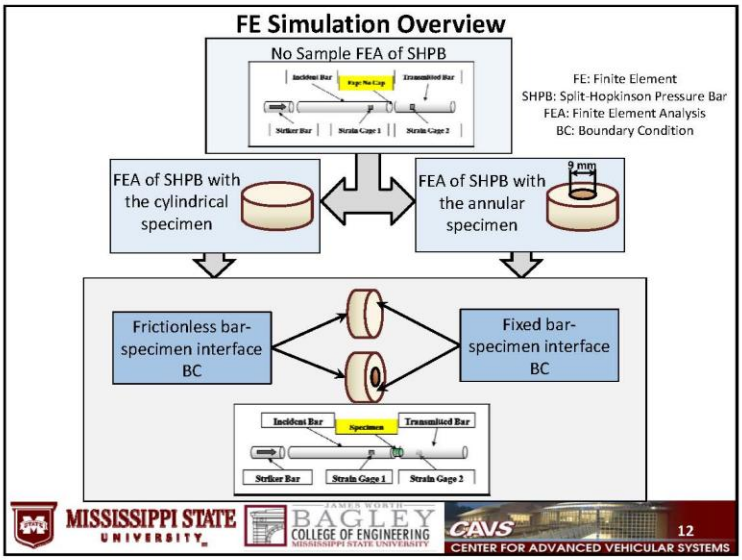

MISSISSIPPI STATE UNIVERSITY | JAMES WORTH BAGLEY COLLEGE OF ENGINEERING MISSISSIPPI STATE UNIVERSITY | CAVS CENTER FOR ADVANCED VEHICULAR SYSTEMS | 12

No Sample Experiment and FE Model Overview

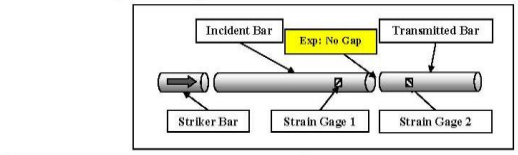

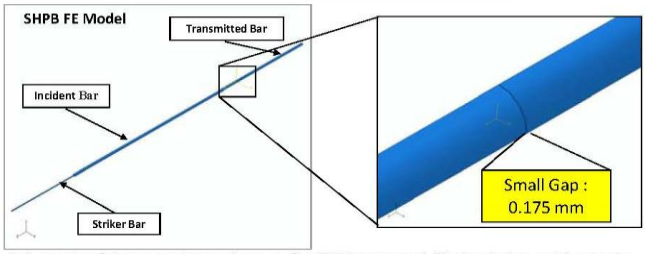

Schematic of the experimental set up for SHPB tests and FE simulation, without any sample. α_R and β_R for the simulations were maintained at 3.0 and 1.2.

No Sample Experiment and FE Simulation Correlated Well

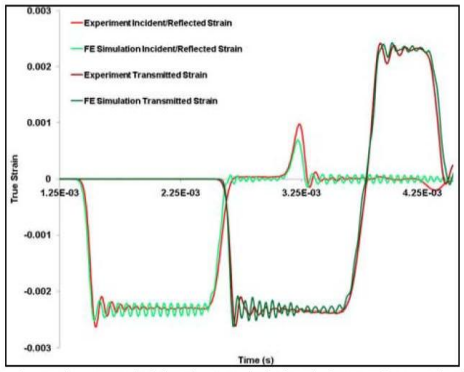

Comparison of experiment and Finite Element (FE) simulation σ_{33} for porcine brain sample compression, at 6.5 ms^{-1}. FE simulation σ_{33} were calculated by post processing the strain measurements from FE simulation through DAVID Viscoelastic software.

Cylindrical Sample FE Model Overview

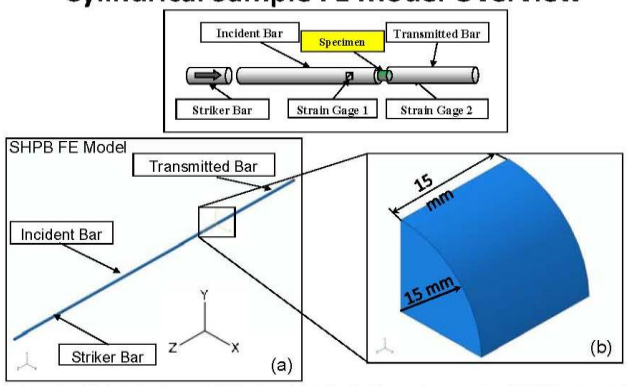

Schematic of (a) Finite Element (FE) set up for Split-Hopkinson Pressure Bar (SHPB) tests and (b) FE simulation sample dimensions, with a sample. α_R and β_R for the simulations were maintained at 3.0 and 1.2.

MISSISSIPPI STATE UNIVERSITY | JAMES WORTH BAGLEY COLLEGE OF ENGINEERING | CAVS CENTER FOR ADVANCED VEHICULAR SYSTEMS 15

FE Material Model Calibration Procedure

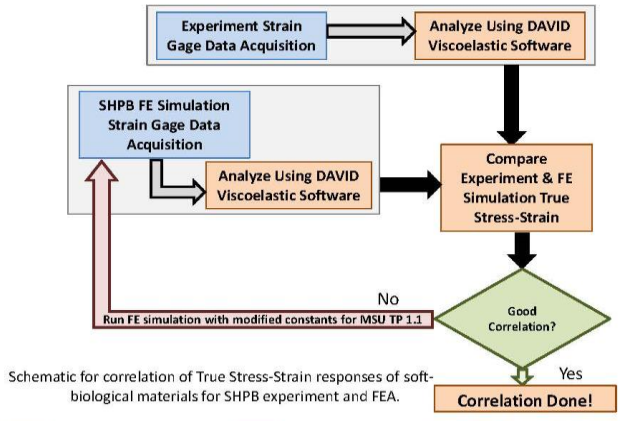

Schematic for correlation of True Stress-Strain responses of soft-biological materials for SHPB experiment and FEA.

MISSISSIPPI STATE UNIVERSITY | JAMES WORTH BAGLEY COLLEGE OF ENGINEERING | CAVS CENTER FOR ADVANCED VEHICULAR SYSTEMS 16

Good Correlation Between Experiment and FE Model

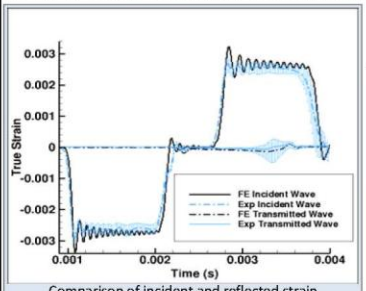

Comparison of incident and reflected strain measurements in a Split-Hopkinson Pressure Bar (SHPB), for experiment and Finite Element Analysis (FEA). The error bands in the experimental incident/reflected waves represented uncertainty.

Comparison of experiment and Finite Element (FE) simulation σ_{33} for porcine brain sample compression at 750 s^{-1}. FE simulation σ_{33} were calculated by post processing the strain measurements from FE simulation through DAVID Viscoelastic software.

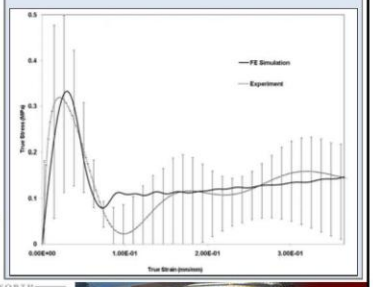

MISSISSIPPI STATE UNIVERSITY | JAMES WORTH BAGLEY COLLEGE OF ENGINEERING MISSISSIPPI STATE UNIVERSITY | CAVS CENTER FOR ADVANCED VEHICULAR SYSTEMS | 17

FE Material Model: Calibration

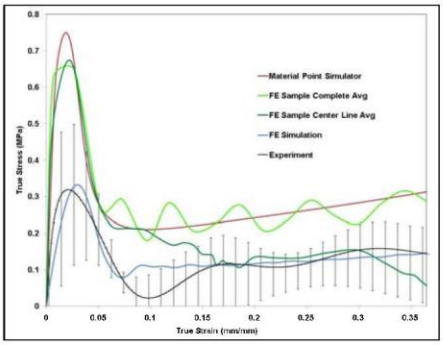

Comparison of σ_{33} for experiment, MATLAB Fitting Routine (material point simulator), FE specimen average data and FE strain measures through DAVID Viscoelastic, at 750 s^{-1}.

(Strain Rate, /s)	750
V (Striker speed, m/s)	7.72
μ	25
K	12492
γ_{∞}	100000
m	1
γ_o	8.2
σ_p	0
λ_L	5
μ_R	0.0493197
R_{v1}	1.4
h_o	47.2095
ξ^o_{v1}	0.75
$\xi^*_{v\,sat}$	0.01
$\xi^*_{v\,o}$	1.2
g_o	0.3
Ck_1	0.4
h_1	0
ε^o_{v2}	0
ε^{sat}_{v2}	0.4
Ck_2	0

MISSISSIPPI STATE UNIVERSITY | JAMES WORTH BAGLEY COLLEGE OF ENGINEERING MISSISSIPPI STATE UNIVERSITY | CAVS CENTER FOR ADVANCED VEHICULAR SYSTEMS | 18

FE Simulation σ_{33} Showed Non-Uniform Stress State

Cylindrical Sample

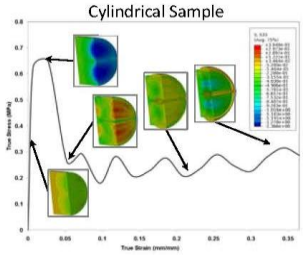

Annular Sample

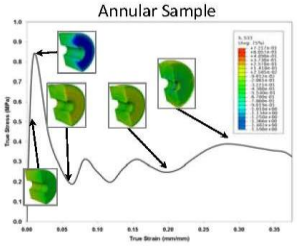

Contour plots of the loading direction stress (σ_{33}) at different stages of the true stress-stress curve at a compressive strain rate of 750 s^{-1}. Compressive σ_{33} in the plot ordinate is treated as positive, while the contour level compressive σ_{33} are negative.

FE Simulation σ_{Mises} Revealed Multiaxial Stress State

Cylindrical Sample

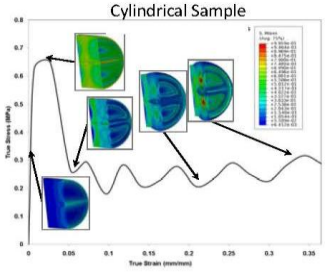

Annular Sample

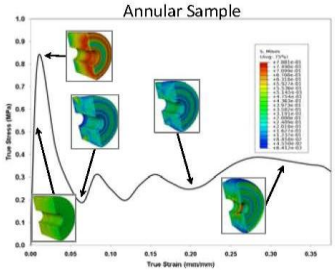

Contour plots of σ_{Mises} at different stages of the true stress-stress plot at a strain rate of 750 s^{-1}. Compressive σ_{33} in the plot ordinate is treated as positive.

FE Simulation 1st Invariant of Stress Exposed Concentrated Regions of Stress

Cylindrical Sample

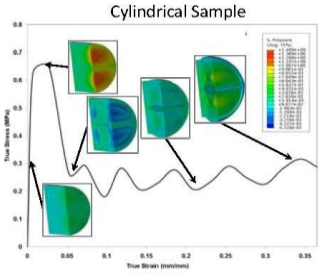

Annular Sample

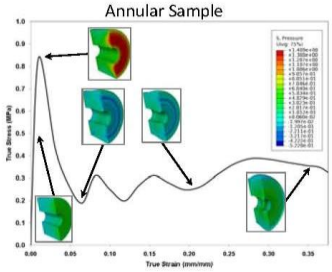

Contour plots of the first invariant of stress (Pressure) at different stages of the true stress-stress plot at a strain rate of 750 s^{-1}. Compression in the plot ordinate is treated as positive, while the contour level compressive σ_{33} are negative.

FE Simulation Stress Tensor Revealed Multiaxial Stress State

Cylindrical Sample

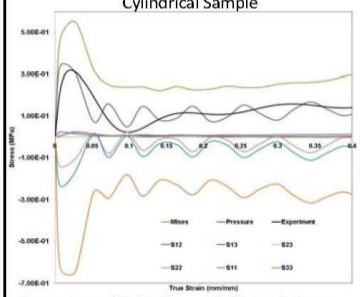

Annular Sample

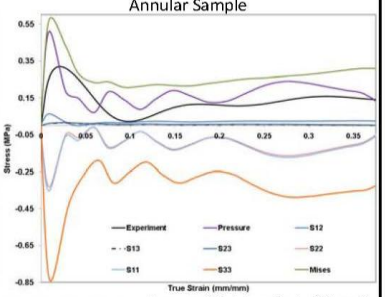

Comparison of Finite Element (FE) simulation σ_{Mises}, σ_{11}, σ_{22}, σ_{33}, σ_{12} σ_{23}, Pressure (First Invariant of Stress) and σ_{13} and experiment during deformation for cylindrical sample, at 750 s^{-1}. Here compressive stresses are negative.

Frictionless Bar-Sample BC Lowered Sample Stress State

Cylindrical Sample

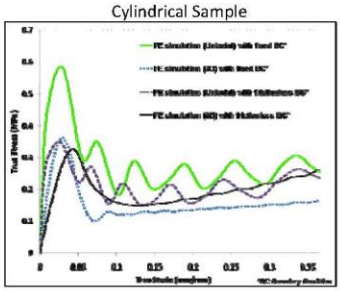

Annular Sample

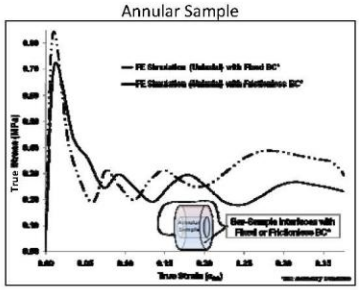

Comparison of uniaxial and 3-Dimensional true stress-strain plots for FE simulation with fixed BC and with frictionless BC on a cylindrical sample, at 750 s^{-1}.

BC: Boundary Condition

Experiment and FE Simulation Animation

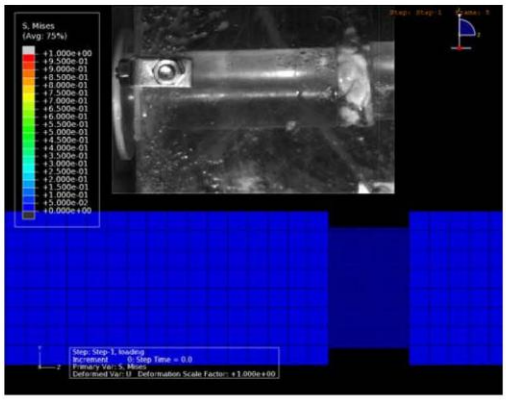

SHPB FE animation of the Von Mises Stress in SHPB test. Upper movie insert is actual experiment and lower animation is FE simulation of test, at 550 s^{-1}.

Conclusions

- High strain tests conducted using a SHPB apparatus show that the porcine brain is strain rate dependent. The material response is marked by an initial (hardening) effect, followed by a softening trend and then strain hardening at larger strains.
- Simulations of SHPB test show that axial stress, σ_{33}, is primarily concentrated in the central region of the specimen during the initial (hardening) effect, thus uniaxial stress state is not maintained.
- Annular specimens also have the initial hardening trend; implying certain quantity of the initial hardening trend may be intrinsic to the material behavior. Additionally, a frictionless bar-sample boundary condition gives the correct uniaxial stress (σ_{33}).

Thank you for your attention

Questions?

Workshop on Numerical Analysis of Human and Surrogate Response to Accelerative Loading
Aberdeen Proving Ground, MD
January 7-9, 2014

Hierarchical Development of Biomedically Validated Human Computational Models

Robert Armiger, Alexis Wickwire, Kyle Ott, Alex Iwaskiw, Tim Harrigan, Liming Voo, JiangYue Zhang, Catherine Carneal, Jack Roberts, Andrew Merkle

BOMS
BIOMECHANICS AND INJURY MITIGATION SYSTEMS

APL
The Johns Hopkins University
APPLIED PHYSICS LABORATORY

Human Computational Modeling

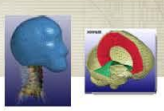

- APL is developing human models for understanding blast, ballistic, and accelerative loading environments
- Focused on end-to-end approach for model development and hierarchical validation
- Collaborative investigations:
  - ATD Modeling
  - Vasculature Modeling
  - Parametric Probabilistic Approaches
- Validate and apply models in relevant loading environments

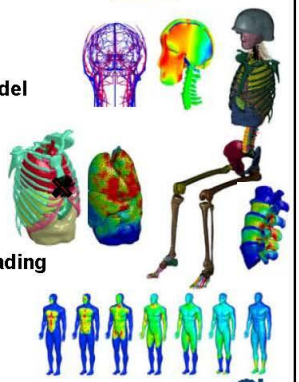

2

APL

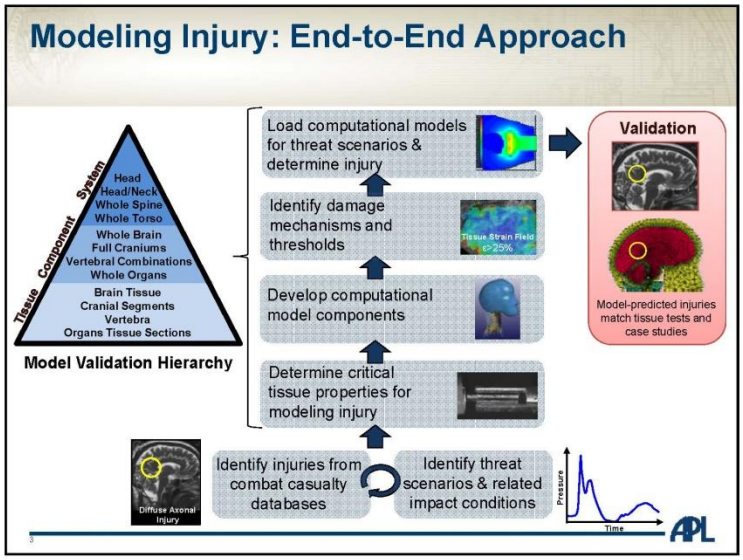
Modeling Injury: End-to-End Approach
System
Component
Tissue
Head
Head/Neck
Whole Spine
Whole Torso
Whole Brain
Full Craniums
Vertebral Combinations
Whole Organs
Brain Tissue
Cranial Segments
Vertebra
Organs Tissue Sections
Model Validation Hierarchy
Load computational models for threat scenarios & determine injury
Identify damage mechanisms and thresholds
Tissue Strain Field e>25%
Develop computational model components
Determine critical tissue properties for modeling injury
Validation
Model-predicted injuries match tissue tests and case studies
Diffuse Axonal Injury
Identify injuries from combat casualty databases
Identify threat scenarios & related impact conditions
Pressure
Time
APL

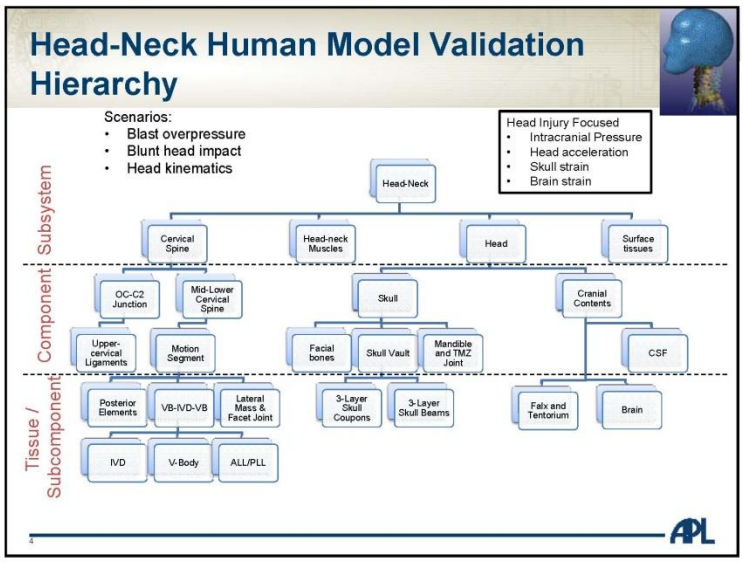
Head-Neck Human Model Validation Hierarchy
Scenarios:
• Blast overpressure
• Blunt head impact
• Head kinematics
Head Injury Focused
• Intracranial Pressure
• Head acceleration
• Skull strain
• Brain strain
Subsystem
Component
Tissue / Subcomponent
Head-Neck
Cervical Spine
Head-neck Muscles
Head
Surface tissues
OC-C2 Junction
Mid-Lower Cervical Spine
Skull
Cranial Contents
Upper-cervical Ligaments
Motion Segment
Facial bones
Skull Vault
Mandible and TMZ Joint
CSF
Posterior Elements
VB-IVD-VB
Lateral Mass & Facet Joint
3-Layer Skull Coupons
3-Layer Skull Beams
Falx and Tentorium
Brain
IVD
V-Body
ALL/PLL
APL

Model Validation Hierarchy Example:

Head and Neck Tissue Characterization

APL

High Rate Tissue Characterization

Modified Split Hopkinson Bar Test Technique

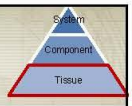

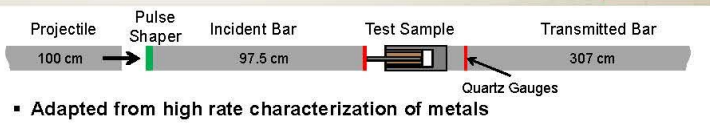

- Adapted from high rate characterization of metals
- Measure bar displacement (line laser) and force (quartz gauge)
- Keys to well-characterized soft tissue response:
  - Pulse shaping
  - High signal to noise ratio of quartz force transducers
  - Known and uniform tissue geometry

Before Impact 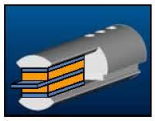 During Impact 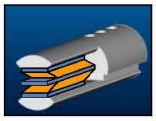

*Tresler, M. M., et al. "Verification and implementation of a modified split Hopkinson pressure bar technique for characterizing biological tissue and soft biosimulant materials under dynamic shear loading." *Journal of the mechanical behavior of biomedical materials* 48 (2011): 1920-1928.
Ott, Kyle A., et al. "Determination of Simple Shear Material Properties of the Brain at High Strain Rates." *Dynamic Behavior of Materials, Volume 1*. Springer New York, 2013. 139-147.

6

APL

Brain mSHPB Shear Testing

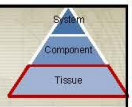

Developed Protocol for never frozen (fresh), unfixed human brain tissue:

Specimen ID	Cause of Death	Age	Race	Sex	PMI (hrs)	Brain Region	# of Samples
HB01	Myocardial Infarction	37	Caucasian	Male	34	Anterior Cerebral Cortex	29
HB02	Cardiac arrhythmia associated with Cardiomegaly	45	African American	Male	25	Parietal Cerebral Cortex	31
HB03	Carbon monoxide poisoning	59	Caucasian	Male	25	Posterior Cerebral Cortex	19
HB04	Pulmonary Embolism	29	African American	Male	24	Cerebellum	15

7

Fresh Human Brain Shear Sample

Specimen Preparation Procedure

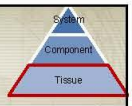

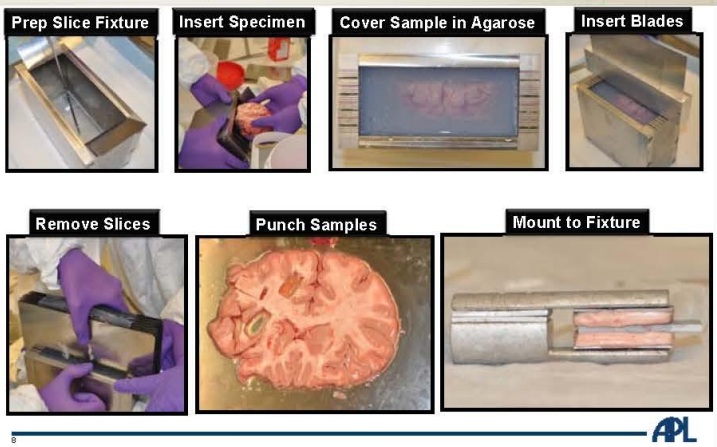

8

Brain mSHPB Shear Test Results

Shear Modulus – Strain Rate

- Compared results versus calculated moduli (assuming incompressibility)
- Only directly measured shear modulus determination at 100 strain/s
- Average Shear Modulus 16.9 kPa ± 9.6

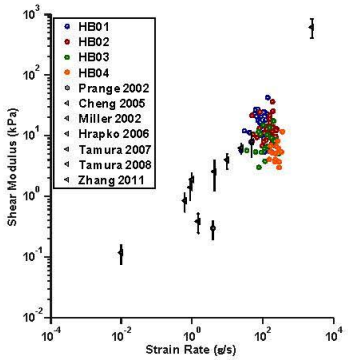

APL

Falx Cerebri Tissue Characterization

- Specimen preparation
  - Die cut dogbone coupons
    - ASTM D638
  - Multiple fiber orientations
  - 94 samples from 6 specimen
- Testing protocol
  - Uniaxial tensile loading
    - TA Instruments: RSA-G2
  - 3 loading rates
    - 0.01, 10, 100 mm/s (fail)
  - Output: elastic modulus

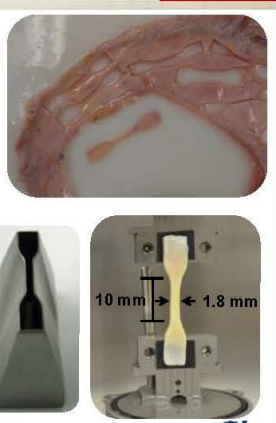

APL

Falx / Tentorium Tissue Response

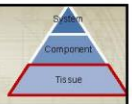

- No difference between falx / tentorium (p=0.95)
  - Combined tension tests
- Rate dependency (p<0.001)
- Specimen difference (p<0.001)
- Orientation effects (p<0.001)

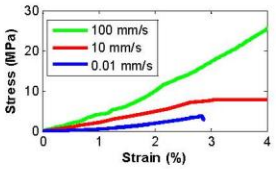

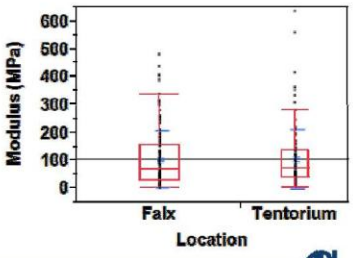

Model Validation Hierarchy Example:

Head and Neck Component Validation

Component Level: Skull Table Bending

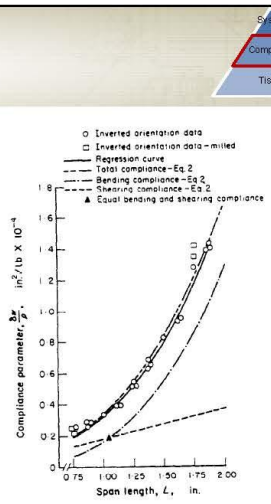

- **Prior literature skull bending characterization (Hubbard 1971)**
  - 3-Point Bending with Cylinder Contact
  - Loaded span 0.75 to 2.0 inch in 0.25 inch increments
  - Varied FEM skull thickness and element composition
- **Output**
  - Skull Compliance Parameter

13

Component Using Average Experimental Dimensions

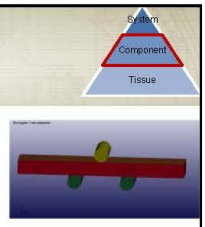

- **Solid element diploe, shell elements for outer/inner tables**
- **Overall Thickness 6.5 mm (including shell thickness)**
- **Table thickness 1.5 mm, E=11.9 GPa, v=0.3**
- **Diploe E=700 MPa, v=0**

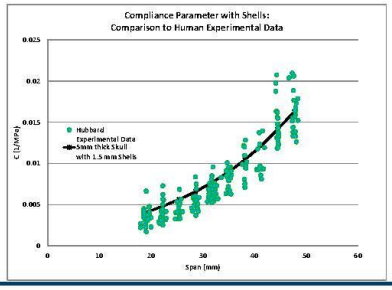

14

Component Level – Falx Cerebri

In-Situ Indentation Tests

- **Specimen preparation**
  - Maintained attachment to skull
  - Mark 1x1 cm grid onto falx
    - Digitize point location
  - 4 specimen (23-46 points)
- **Testing protocol**
  - Fixed skull within Instron (8821S)
    - 2527 Series Dynacell
  - Load control 0-3 N
    - Sub failure loads

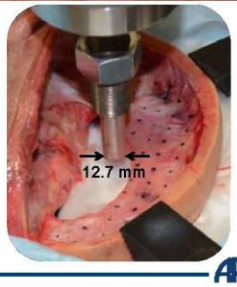

15

Component Level – Results

In-Situ Indentation Tests

- **Regional stiffness variation**
  - Stiff near skull
  - Compliant near inner edge

Deflection at 3N Loading

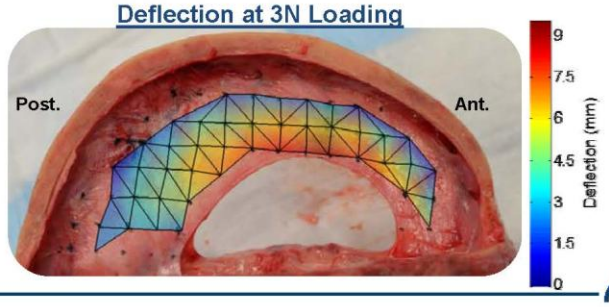

16

C71

Model Response Versus Experimental Corridor

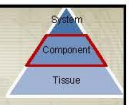

Hierarchical Approach:
E=36 MPa, t=0.41 mm, ε=0.3%

Prior literature values:
E=31.5 MPa, t = 1.0mm ε=0.0%

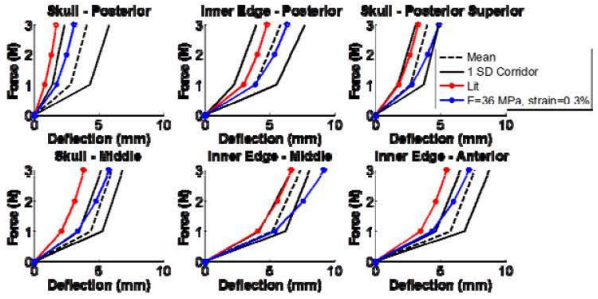

17

Model Validation Hierarchy Example:

Head and Neck System Validation

Head and Neck System Validation

System
Component
Tissue

- Shock Tube simulated primary blast overpressure
- Head-neck system inverted and placed 15 cm in front of tube opening
- High-speed camera positioned at X-ray output

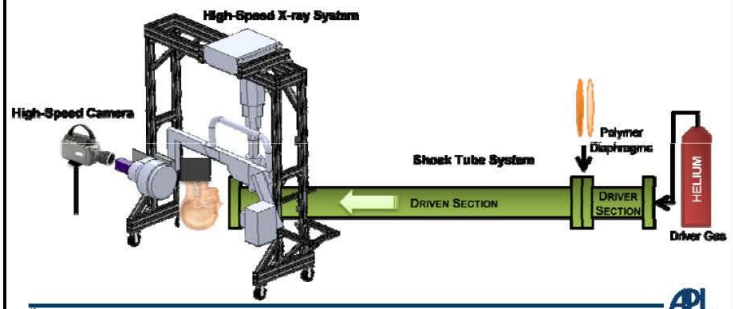

19

APL

Head and Neck Specimen

System
Component
Tissue

- **Response Metrics**
  - Head Kinematics
  - Internal Pressure Response
  - Relative Brain Motion
- **Instrumentation techniques**
  - Radio-opaque brain markers used to track brain motion
  - Stereotactic computer assisted surgical approach for registering, localizing and inserting brain markers
  - Perfused specimen

20

APL

Brain displacement tracking

System
Component
Tissue

- High speed X-ray images dewarped using calibration phantom
- Skull reference frame established using image based co-registration
- Background removal filters applied to highlight marker locations
- Radial symmetry filter applied to segment and track brain markers

21

APL

Head Kinematic Response

System
Component
Tissue

- Global head kinematics
  - Loading pressure was consistent
  - Peaks increased with dose
  - Frequency increased with dose

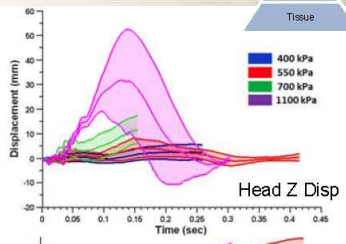

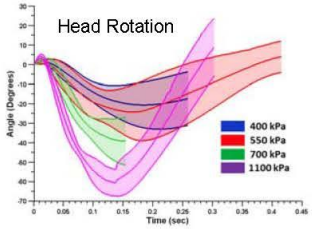

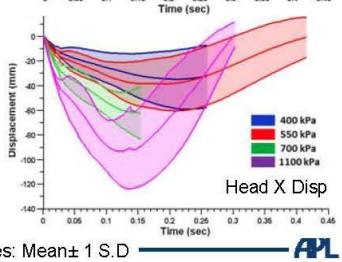

22

Front Exposures: Mean± 1 S.D

APL

Shock Tube FEM Results Comparison

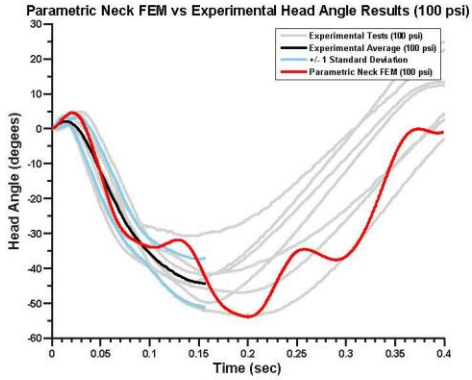

23

Subject specific scaling to validate brain motion response

- Segmentation and marker localization from CT
- Affine co-registration of FEM
- Nearest neighbor correlation of nodal points

	x	y	z
12-1208	161	143	87
HHFEM – Original	163	136	86
Scaling Factor	0.989	1.054	1.003

24

C75

Preliminary Brain Motion Response using FEM

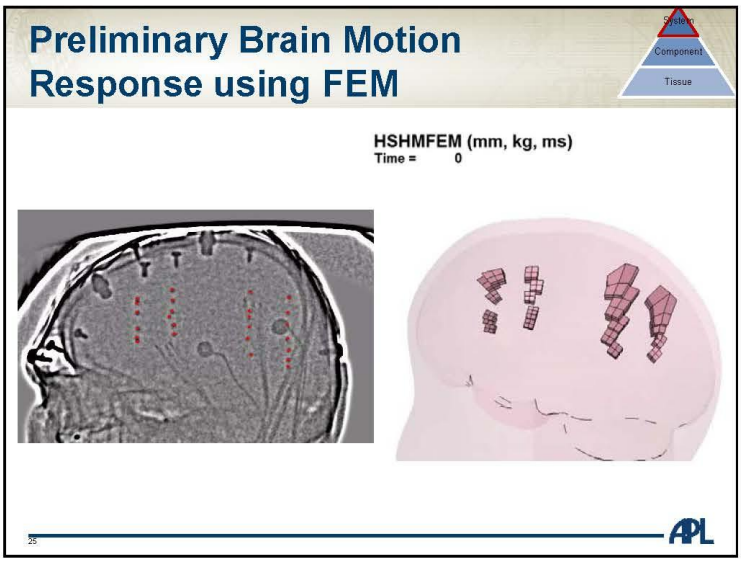

Lumbar Spine

Lumbar Spine Model Validation Hierarchy

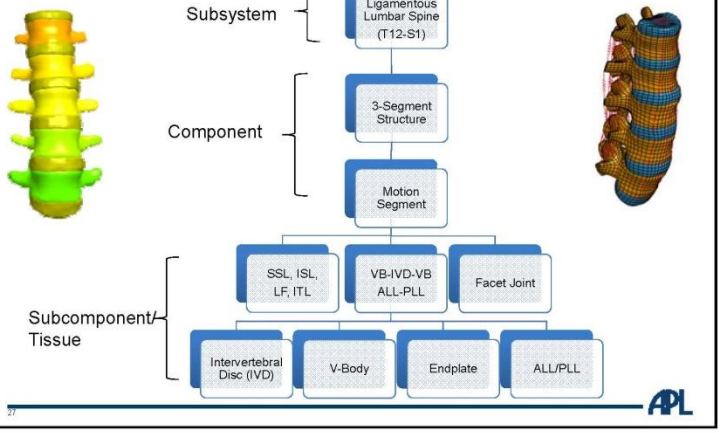

Integrated sitting lumbar/pelvis model

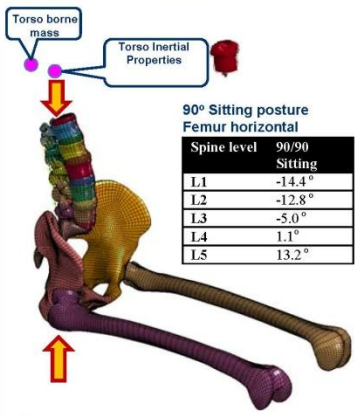

90° Sitting posture
Femur horizontal

Spine level	90/90 Sitting
L1	-14.4°
L2	-12.8°
L3	-5.0°
L4	1.1°
L5	13.2°

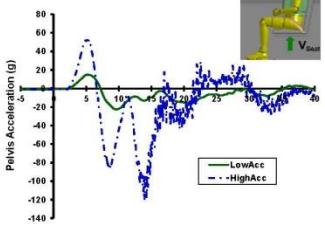

Pelvis acceleration	Without Torso-borne mass	With Torso-borne mass
Low Acc	Case 1	Case 3
High Acc	Case 2	Case 4

BBM: 28 kg, 10 cm posterior to torso CG

APL

Von-Mises stress distribution

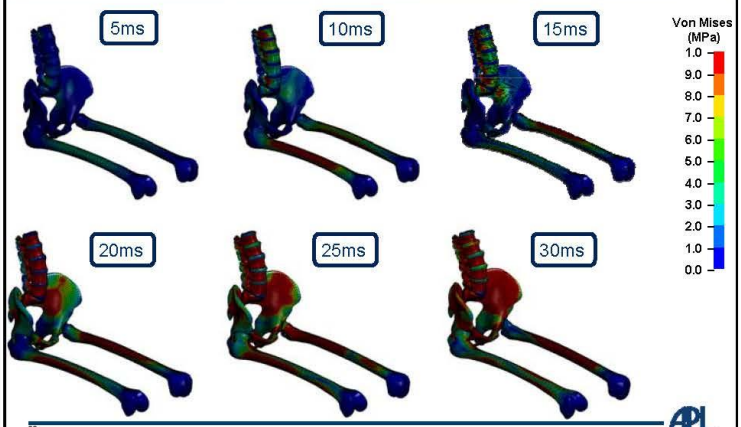

29

APL

Summary

- **Developing Validated Human Models for blast exposure, ballistic impact, and accelerative loading requires an end-to-end approach**
  - Understand threat and injury outcomes
  - Translate scenario to model boundary and loading conditions
  - Develop and validate using data produced under similar loading conditions
- **APL using models to investigate dynamic loading**
  - Focus on multi-level hierarchical validation
    - High rate tissue characterization
    - Component level response validated at injurious rates
    - Subject-specific scaling and system-level response characterization
- **Research and Development still required for injury mechanisms, integration, and system level validation**

30

APL

Acknowledgements

The U.S. Army Medical Research Acquisition Activity,
820 Chandler Street, Fort Detrick MD 21702-5014
is the awarding and administering acquisition office.

The content included in this work does not necessarily reflect the position or policy of the U.S. government.

31

APL

Workshop on Numerical Analysis of Human and Surrogate Response to Accelerative Loading
Aberdeen Proving Ground, MD
January 7-9, 2014

Hierarchical Development of Biomedically Validated Human Computational Models

Robert Armiger, Alexis Wickwire, Kyle Ott, Alex Iwaskiw, Tim Harrigan, Liming Voo, JiangYue Zhang, Catherine Carneal, Jack Roberts, Andrew Merkle

BIOMECHANICS AND INJURY MITIGATION SYSTEMS

The Johns Hopkins University
APPLIED PHYSICS LABORATORY

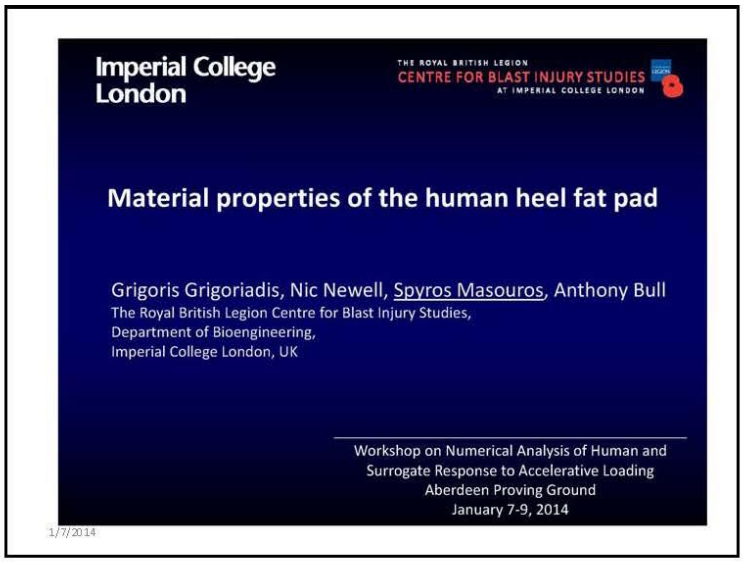
Imperial College London
THE ROYAL BRITISH LEGION
CENTRE FOR BLAST INJURY STUDIES
AT IMPERIAL COLLEGE LONDON
Material properties of the human heel fat pad
Grigoris Grigoriadis, Nic Newell, Spyros Masouros, Anthony Bull
The Royal British Legion Centre for Blast Injury Studies,
Department of Bioengineering,
Imperial College London, UK
Workshop on Numerical Analysis of Human and Surrogate Response to Accelerative Loading
Aberdeen Proving Ground
January 7-9, 2014
1/7/2014

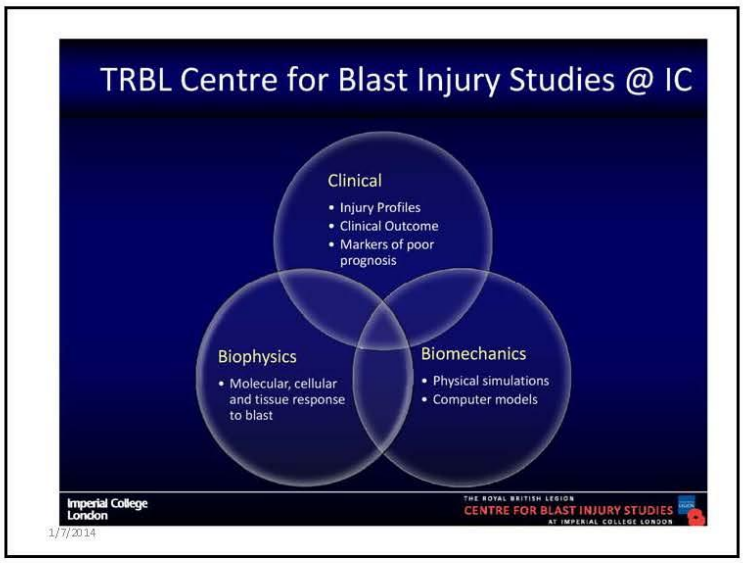
TRBL Centre for Blast Injury Studies @ IC
Clinical
• Injury Profiles
• Clinical Outcome
• Markers of poor prognosis
Biophysics
• Molecular, cellular and tissue response to blast
Biomechanics
• Physical simulations
• Computer models
Imperial College London
THE ROYAL BRITISH LEGION
CENTRE FOR BLAST INJURY STUDIES
AT IMPERIAL COLLEGE LONDON
1/7/2014

The problem – vehicle occupant injury

Imperial College London

THE ROYAL BRITISH LEGION CENTRE FOR BLAST INJURY STUDIES AT IMPERIAL COLLEGE LONDON

1/7/2014

The solution – injury prediction

Prediction of injury risk for every occupant in every deployed vehicle

Imperial College London

THE ROYAL BRITISH LEGION CENTRE FOR BLAST INJURY STUDIES AT IMPERIAL COLLEGE LONDON

1/7/2014

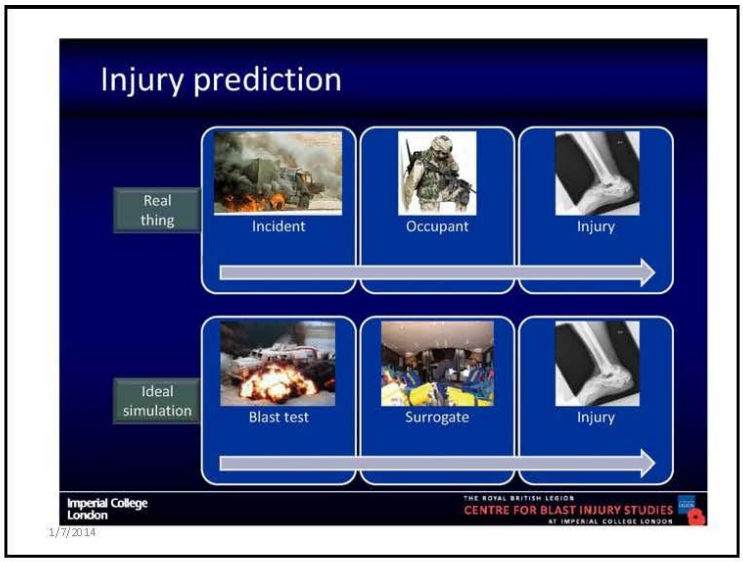
Injury prediction
Real thing
Incident
Occupant
Injury
Ideal simulation
Blast test
Surrogate
Injury
Imperial College London
THE ROYAL BRITISH LEGION
CENTRE FOR BLAST INJURY STUDIES
AT IMPERIAL COLLEGE LONDON
1/7/2014

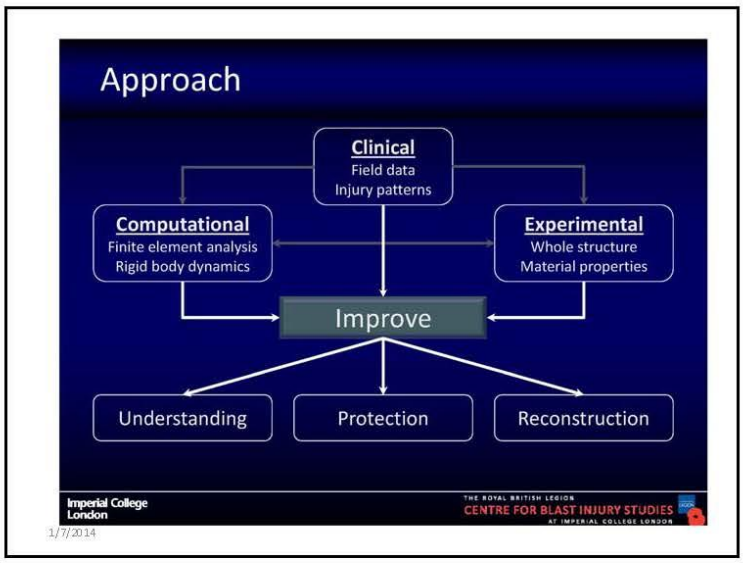
Approach
Clinical
Field data
Injury patterns
Computational
Finite element analysis
Rigid body dynamics
Experimental
Whole structure
Material properties
Improve
Understanding
Protection
Reconstruction
Imperial College London
THE ROYAL BRITISH LEGION
CENTRE FOR BLAST INJURY STUDIES
AT IMPERIAL COLLEGE LONDON
1/7/2014

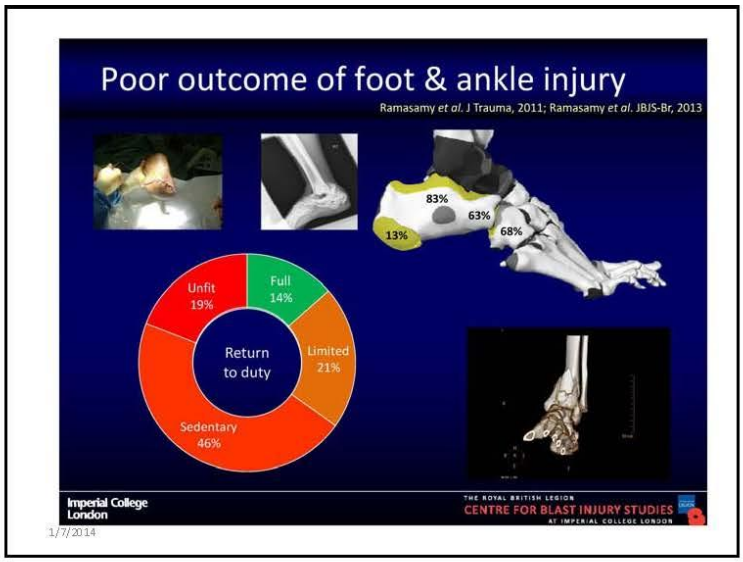
Poor outcome of foot & ankle injury
Ramasamy et al. J Trauma, 2011; Ramasamy et al. JBJS-Br, 2013
83%
63%
68%
13%
Unfit 19%
Full 14%
Limited 21%
Sedentary 46%
Return to duty
Imperial College London
THE ROYAL BRITISH LEGION
CENTRE FOR BLAST INJURY STUDIES
AT IMPERIAL COLLEGE LONDON
1/7/2014

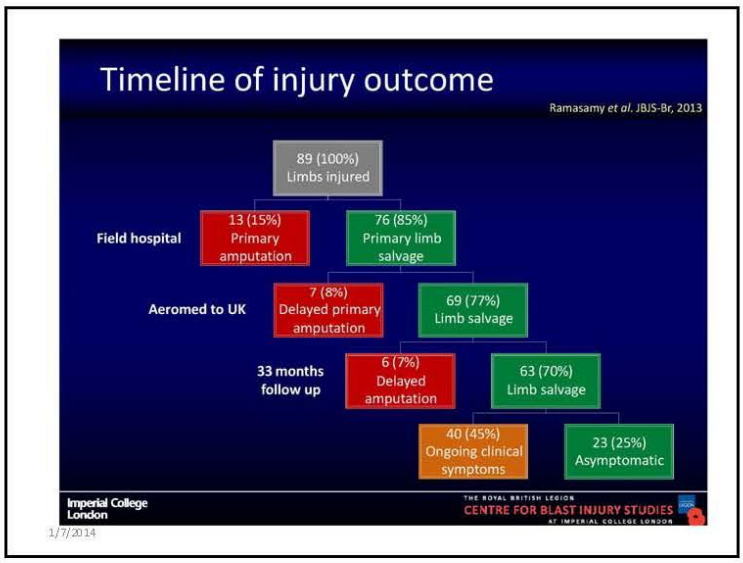
Timeline of injury outcome
Ramasamy et al. JBJS-Br, 2013
89 (100%) Limbs injured
Field hospital
13 (15%) Primary amputation
76 (85%) Primary limb salvage
Aeromed to UK
7 (8%) Delayed primary amputation
69 (77%) Limb salvage
33 months follow up
6 (7%) Delayed amputation
63 (70%) Limb salvage
40 (45%) Ongoing clinical symptoms
23 (25%) Asymptomatic
Imperial College London
THE ROYAL BRITISH LEGION
CENTRE FOR BLAST INJURY STUDIES
AT IMPERIAL COLLEGE LONDON
1/7/2014

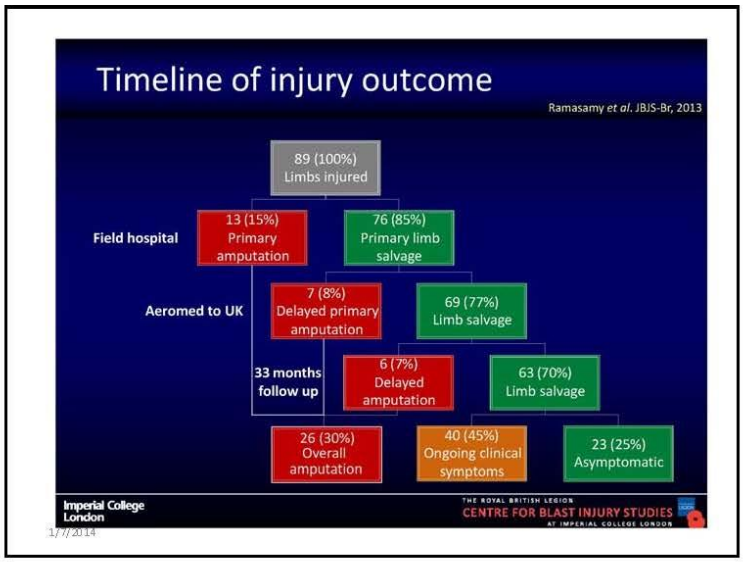
Timeline of injury outcome
Ramasamy et al. JBJS-Br, 2013
89 (100%)
Limbs injured
Field hospital
13 (15%)
Primary
amputation
76 (85%)
Primary limb
salvage
Aeromed to UK
7 (8%)
Delayed primary
amputation
69 (77%)
Limb salvage
33 months
follow up
6 (7%)
Delayed
amputation
63 (70%)
Limb salvage
26 (30%)
Overall
amputation
40 (45%)
Ongoing clinical
symptoms
23 (25%)
Asymptomatic
Imperial College
London
THE ROYAL BRITISH LEGION
CENTRE FOR BLAST INJURY STUDIES
AT IMPERIAL COLLEGE LONDON
1/7/2014

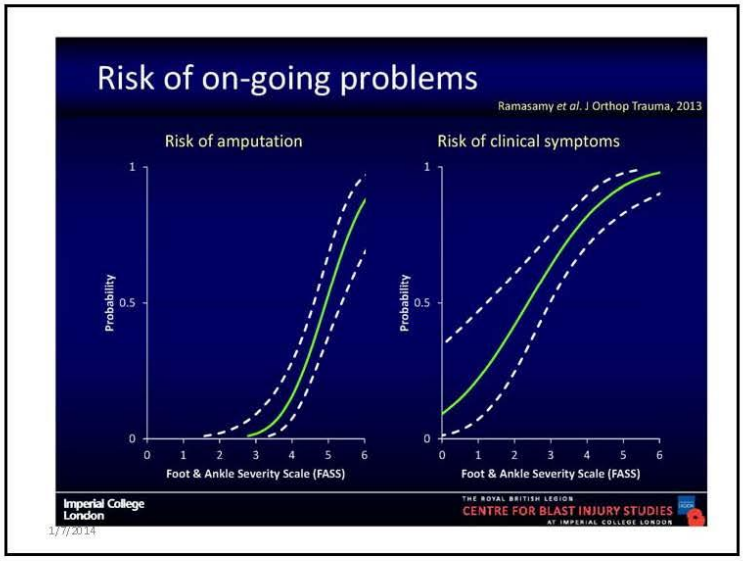
Risk of on-going problems
Ramasamy et al. J Orthop Trauma, 2013
Risk of amputation
Risk of clinical symptoms
Probability
1
0.5
0
0 1 2 3 4 5 6
Foot & Ankle Severity Scale (FASS)
Imperial College
London
THE ROYAL BRITISH LEGION
CENTRE FOR BLAST INJURY STUDIES
AT IMPERIAL COLLEGE LONDON
1/7/2014

5

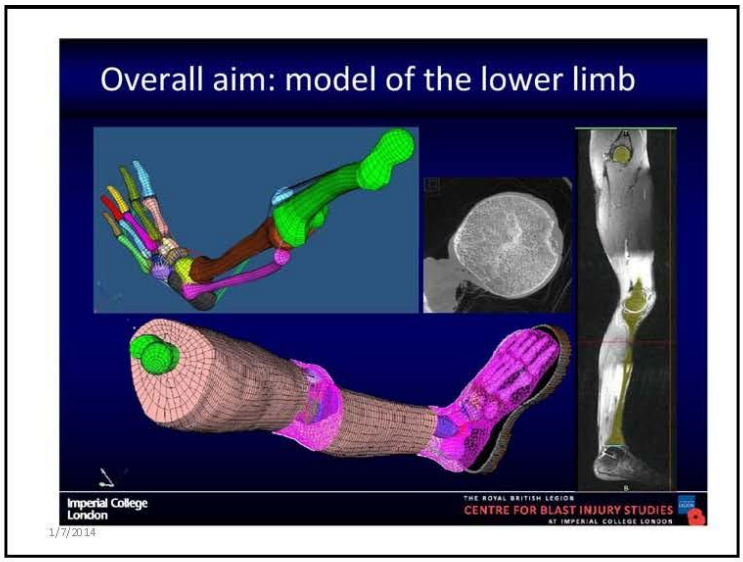
Overall aim: model of the lower limb
Imperial College London
THE ROYAL BRITISH LEGION
CENTRE FOR BLAST INJURY STUDIES
AT IMPERIAL COLLEGE LONDON
1/7/2014

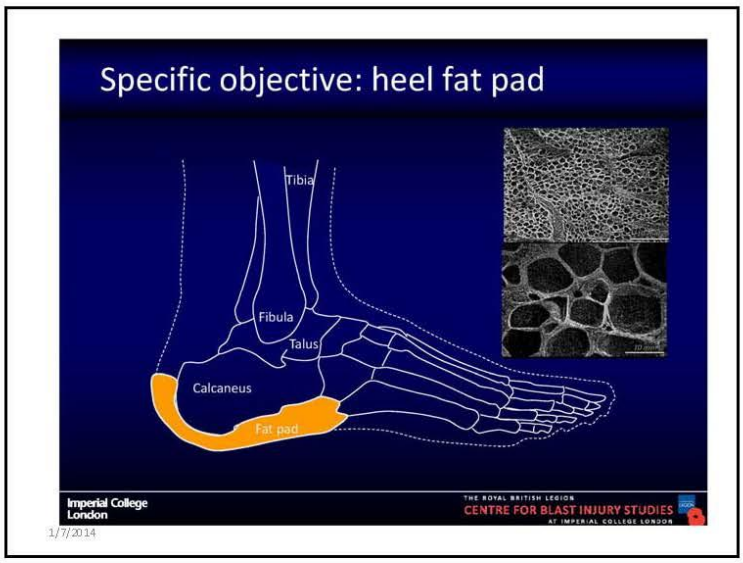
Specific objective: heel fat pad
Tibia
Fibula
Talus
Calcaneus
Fat pad
Imperial College London
THE ROYAL BRITISH LEGION
CENTRE FOR BLAST INJURY STUDIES
AT IMPERIAL COLLEGE LONDON
1/7/2014

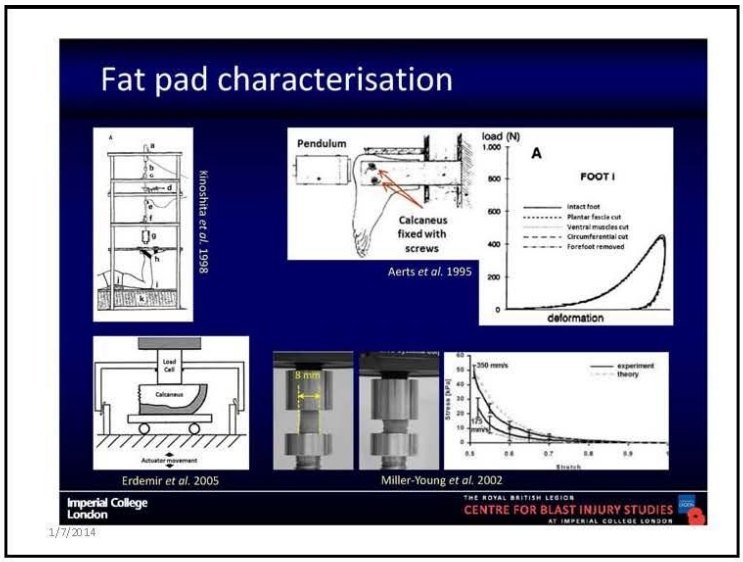
Fat pad characterisation
Kinoshita et al. 1998
Pendulum
Calcaneus fixed with screws
Aerts et al. 1995
load (N)
A
FOOT I
deformation
Erdemir et al. 2005
8 mm
Miller-Young et al. 2002
Imperial College London
THE ROYAL BRITISH LEGION
CENTRE FOR BLAST INJURY STUDIES
AT IMPERIAL COLLEGE LONDON
1/7/2014

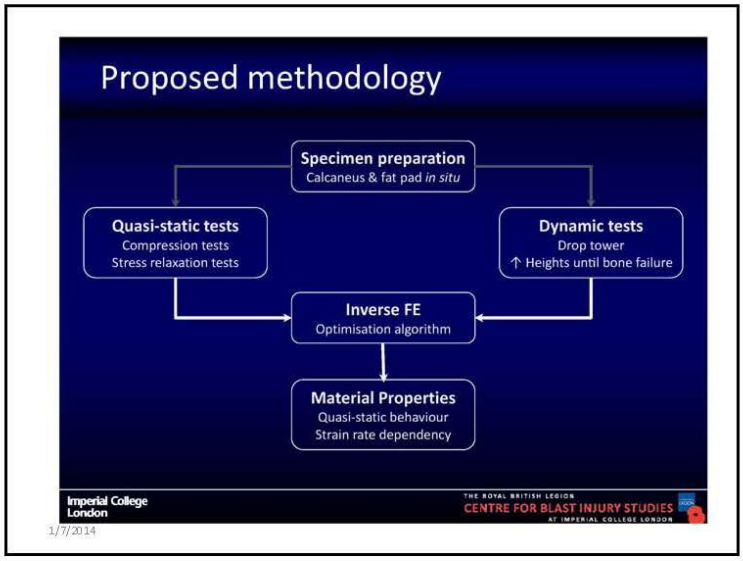
Proposed methodology
Specimen preparation
Calcaneus & fat pad in situ
Quasi-static tests
Compression tests
Stress relaxation tests
Dynamic tests
Drop tower
↑ Heights until bone failure
Inverse FE
Optimisation algorithm
Material Properties
Quasi-static behaviour
Strain rate dependency
Imperial College London
THE ROYAL BRITISH LEGION
CENTRE FOR BLAST INJURY STUDIES
AT IMPERIAL COLLEGE LONDON
1/7/2014

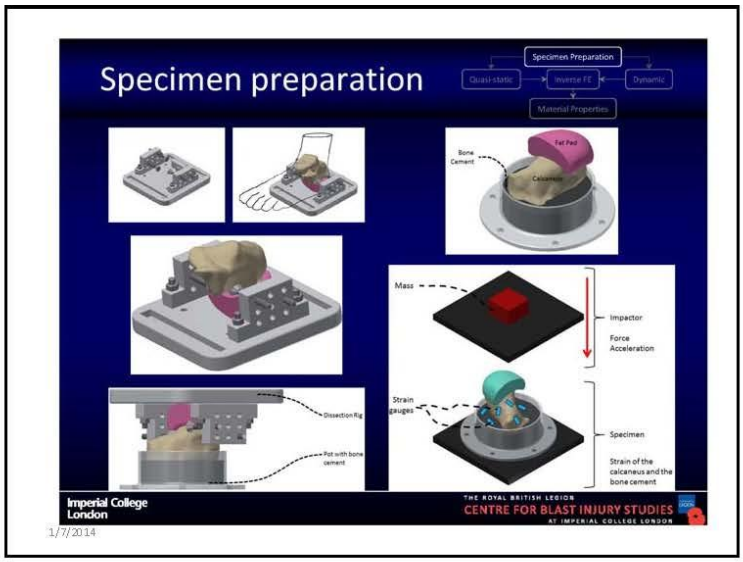
Specimen preparation
Specimen Preparation
Quasi-static
Inverse FE
Dynamic
Material Properties
Bone Cement
Fat Pad
Calcaneus
Mass
Impactor
Force
Acceleration
Strain gauges
Specimen
Strain of the calcaneus and the bone cement
Dissection Rig
Pot with bone cement
Imperial College London
THE ROYAL BRITISH LEGION
CENTRE FOR BLAST INJURY STUDIES
AT IMPERIAL COLLEGE LONDON
1/7/2014


Specimen preparation
Specimen Preparation
Quasi-static
Inverse FE
Dynamic
Material Properties
Imperial College London
THE ROYAL BRITISH LEGION
CENTRE FOR BLAST INJURY STUDIES
AT IMPERIAL COLLEGE LONDON
1/7/2014

Quasi-static uniaxial

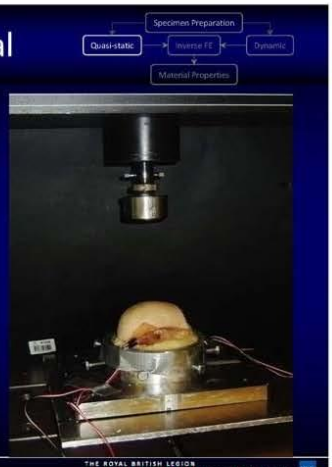

- 3 precycles to 1.5 N
- target strains 35 and 50%
- strain rates 0.0005, 0.05, 0.3/s
- 10 mins between tests + hydration
- stress relaxation
  - 0.3/s to max strain
  - 35 and 50%
- 2 specimens

Imperial College London

THE ROYAL BRITISH LEGION CENTRE FOR BLAST INJURY STUDIES AT IMPERIAL COLLEGE LONDON

1/7/2014

Quasi-static uniaxial

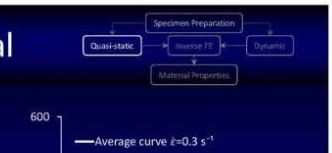

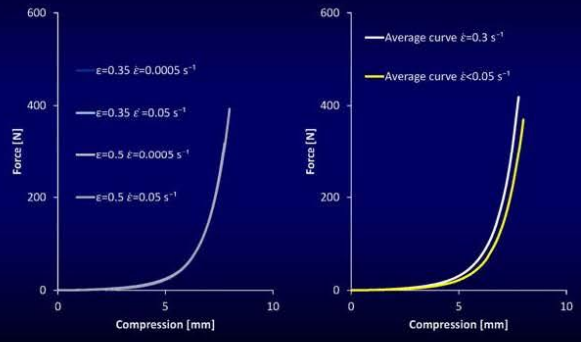

Imperial College London

THE ROYAL BRITISH LEGION CENTRE FOR BLAST INJURY STUDIES AT IMPERIAL COLLEGE LONDON

1/7/2014

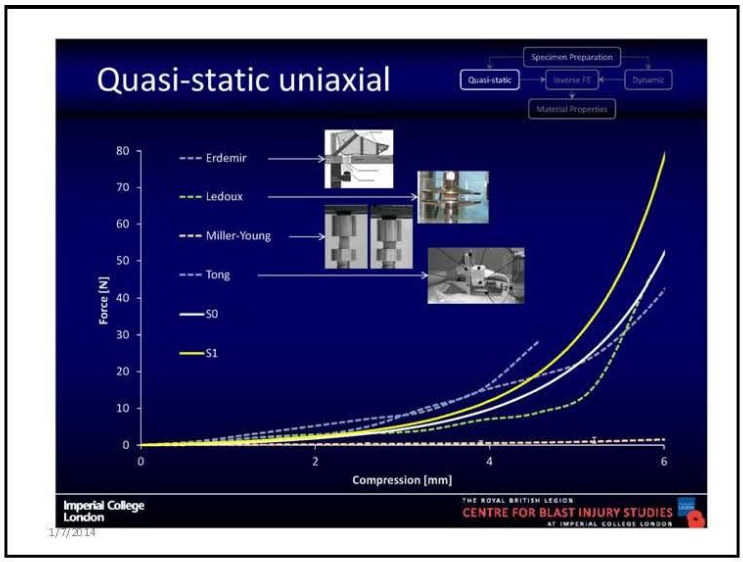
Quasi-static uniaxial
Specimen Preparation
Quasi-static
Inverse FE
Dynamic
Material Properties
Erdemir
Ledoux
Miller-Young
Tong
S0
S1
Force [N]
Compression [mm]
Imperial College London
THE ROYAL BRITISH LEGION
CENTRE FOR BLAST INJURY STUDIES
AT IMPERIAL COLLEGE LONDON
1/7/2014

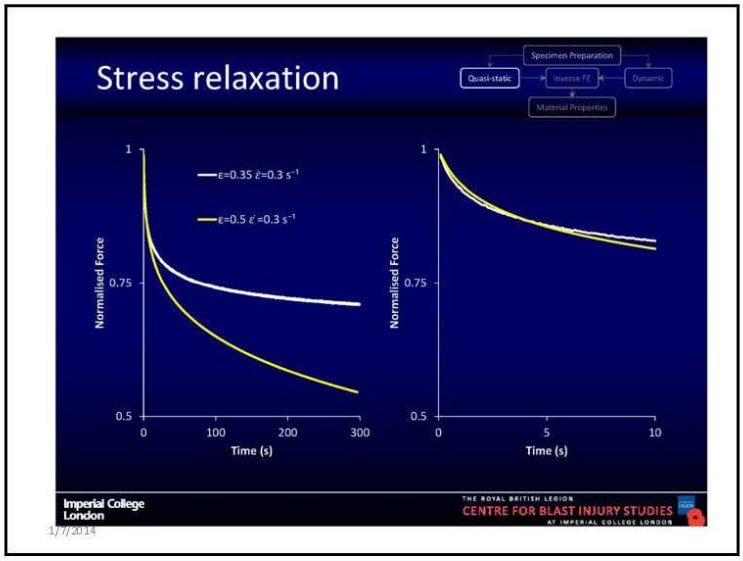
Stress relaxation
Specimen Preparation
Quasi-static
Inverse FE
Dynamic
Material Properties
ε=0.35 ε̇=0.3 s⁻¹
ε=0.5 ε̇=0.3 s⁻¹
Normalised Force
Time (s)
Imperial College London
THE ROYAL BRITISH LEGION
CENTRE FOR BLAST INJURY STUDIES
AT IMPERIAL COLLEGE LONDON
1/7/2014

Drop tests

Specimen Preparation
Quasi-static → Inverse FE ← Dynamic
Material Properties

- Impactor mass = 7 kg
- Heights = 2, 4, 8, 16, 32, 64 cm
- Drop from 2 cm after each test
- 10 mins between drops + hydration

- Velocities = 0.4, 0.9, 1.25, 1.8, 2.5, 3.5 m/s
- Estimated $\dot{\varepsilon}_{max}$ = 30, 53, 73, 100, 147, 205 /s

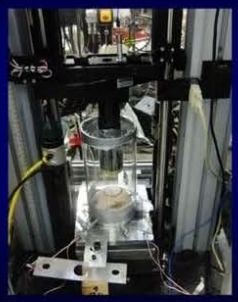

Imperial College London
THE ROYAL BRITISH LEGION CENTRE FOR BLAST INJURY STUDIES AT IMPERIAL COLLEGE LONDON
1/7/2014

Drop tests

Specimen Preparation
Quasi-static → Inverse FE ← Dynamic
Material Properties

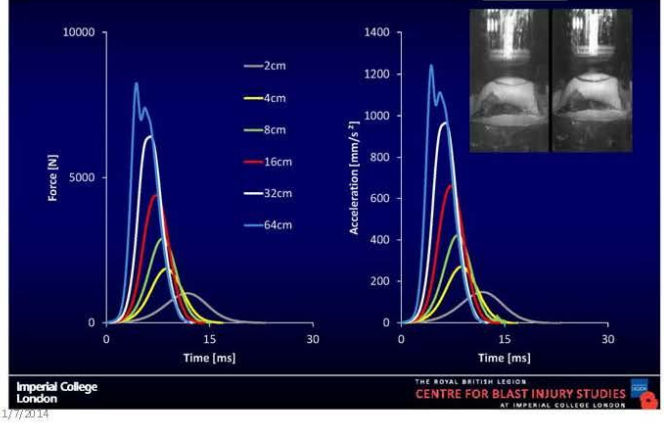

Imperial College London
THE ROYAL BRITISH LEGION CENTRE FOR BLAST INJURY STUDIES AT IMPERIAL COLLEGE LONDON
1/7/2014

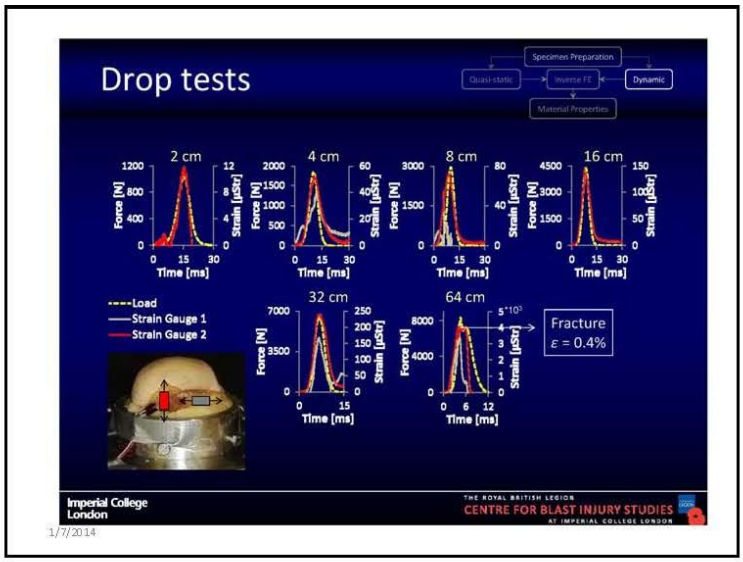
Drop tests
Specimen Preparation
Quasi-static
Inverse FE
Dynamic
Material Properties
2 cm
4 cm
8 cm
16 cm
32 cm
64 cm
Force [N]
Strain [μStr]
Time [ms]
Load
Strain Gauge 1
Strain Gauge 2
Fracture
ε = 0.4%
Imperial College London
THE ROYAL BRITISH LEGION
CENTRE FOR BLAST INJURY STUDIES
AT IMPERIAL COLLEGE LONDON
1/7/2014

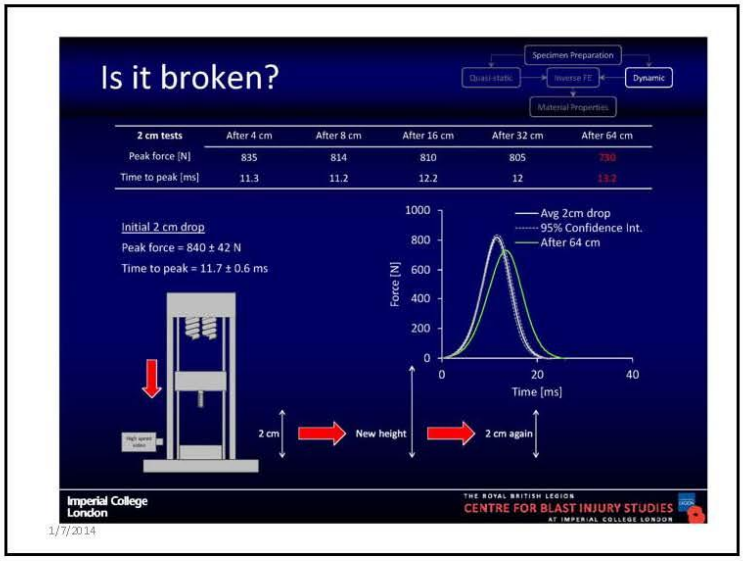
Is it broken?
Specimen Preparation
Quasi-static
Inverse FE
Dynamic
Material Properties
2 cm tests | After 4 cm | After 8 cm | After 16 cm | After 32 cm | After 64 cm
Peak force [N] | 835 | 814 | 810 | 805 | 730
Time to peak [ms] | 11.3 | 11.2 | 12.2 | 12 | 13.2
Initial 2 cm drop
Peak force = 840 ± 42 N
Time to peak = 11.7 ± 0.6 ms
Avg 2cm drop
95% Confidence Int.
After 64 cm
Force [N]
Time [ms]
2 cm
New height
2 cm again
Imperial College London
THE ROYAL BRITISH LEGION
CENTRE FOR BLAST INJURY STUDIES
AT IMPERIAL COLLEGE LONDON
1/7/2014

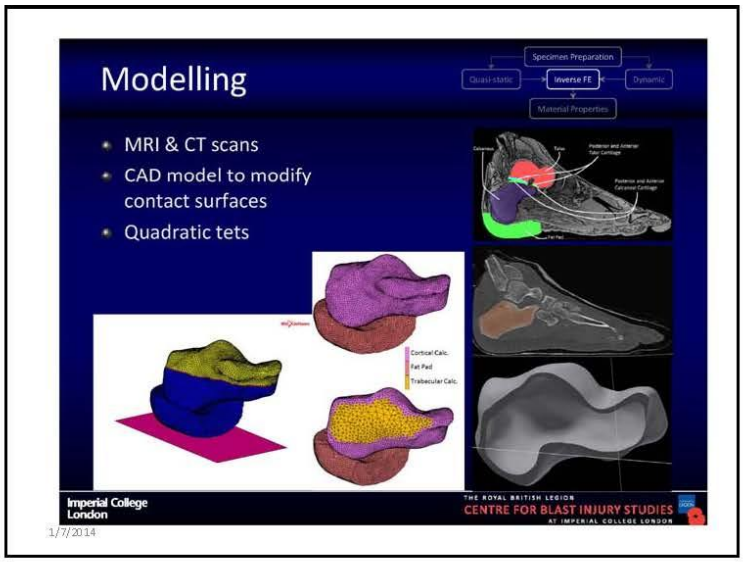
Modelling
Specimen Preparation
Quasi-static
Inverse FE
Dynamic
Material Properties
MRI & CT scans
CAD model to modify contact surfaces
Quadratic tets
Cortical Calc.
Fat Pad
Trabecular Calc.
Imperial College London
THE ROYAL BRITISH LEGION
CENTRE FOR BLAST INJURY STUDIES
AT IMPERIAL COLLEGE LONDON
1/7/2014

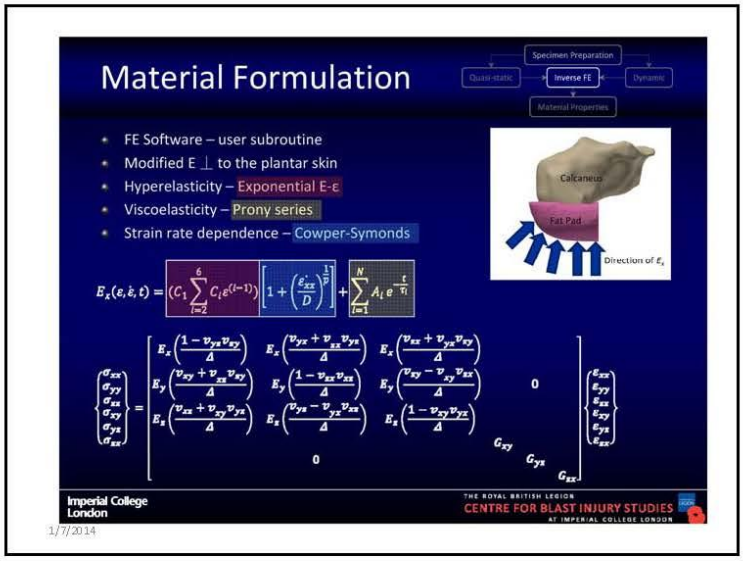
Material Formulation
Specimen Preparation
Quasi-static
Inverse FE
Dynamic
Material Properties
FE Software – user subroutine
Modified E ⊥ to the plantar skin
Hyperelasticity – Exponential E-ε
Viscoelasticity – Prony series
Strain rate dependence – Cowper-Symonds
Calcaneus
Fat Pad
Direction of ε_x
$E_x(\varepsilon,\dot{\varepsilon},t) = \left(C_1 \sum_{i=2}^{6} C_i \varepsilon^{(i-1)}\right)\left[1+\left(\frac{\dot{\varepsilon}_{xx}}{D}\right)^{\frac{1}{p}}\right] + \left[\sum_{i=1}^{N} A_i e^{-\frac{t}{\tau_i}}\right]$
$\begin{Bmatrix}\sigma_{xx}\\ \sigma_{yy}\\ \sigma_{zz}\\ \sigma_{xy}\\ \sigma_{yz}\\ \sigma_{zx}\end{Bmatrix} = \begin{bmatrix} E_x\left(\frac{1-\nu_{yz}\nu_{zy}}{\Delta}\right) & E_x\left(\frac{\nu_{yx}+\nu_{zx}\nu_{yz}}{\Delta}\right) & E_x\left(\frac{\nu_{zx}+\nu_{yx}\nu_{zy}}{\Delta}\right) & & & \\ E_y\left(\frac{\nu_{xy}+\nu_{xz}\nu_{zy}}{\Delta}\right) & E_y\left(\frac{1-\nu_{zx}\nu_{xz}}{\Delta}\right) & E_y\left(\frac{\nu_{zy}-\nu_{xy}\nu_{zx}}{\Delta}\right) & & 0 & \\ E_z\left(\frac{\nu_{xz}+\nu_{xy}\nu_{yz}}{\Delta}\right) & E_z\left(\frac{\nu_{yz}-\nu_{yx}\nu_{xz}}{\Delta}\right) & E_z\left(\frac{1-\nu_{xy}\nu_{yz}}{\Delta}\right) & & & \\ & & & G_{xy} & & \\ & 0 & & & G_{yz} & \\ & & & & & G_{zx} \end{bmatrix} \begin{Bmatrix}\varepsilon_{xx}\\ \varepsilon_{yy}\\ \varepsilon_{zz}\\ \varepsilon_{xy}\\ \varepsilon_{yz}\\ \varepsilon_{zx}\end{Bmatrix}$
Imperial College London
THE ROYAL BRITISH LEGION
CENTRE FOR BLAST INJURY STUDIES
AT IMPERIAL COLLEGE LONDON
1/7/2014

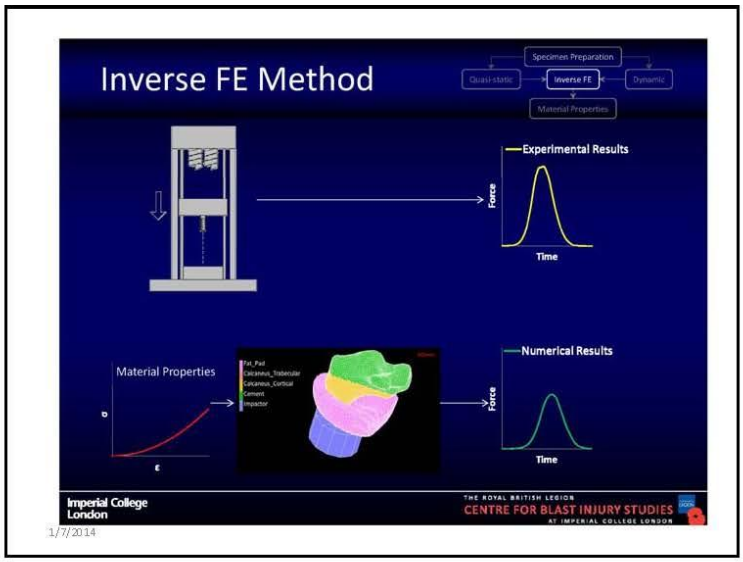
Inverse FE Method
Specimen Preparation
Quasi-static
Inverse FE
Dynamic
Material Properties
Experimental Results
Force
Time
Material Properties
Numerical Results
Force
Time
Imperial College London
THE ROYAL BRITISH LEGION
CENTRE FOR BLAST INJURY STUDIES
AT IMPERIAL COLLEGE LONDON
1/7/2014

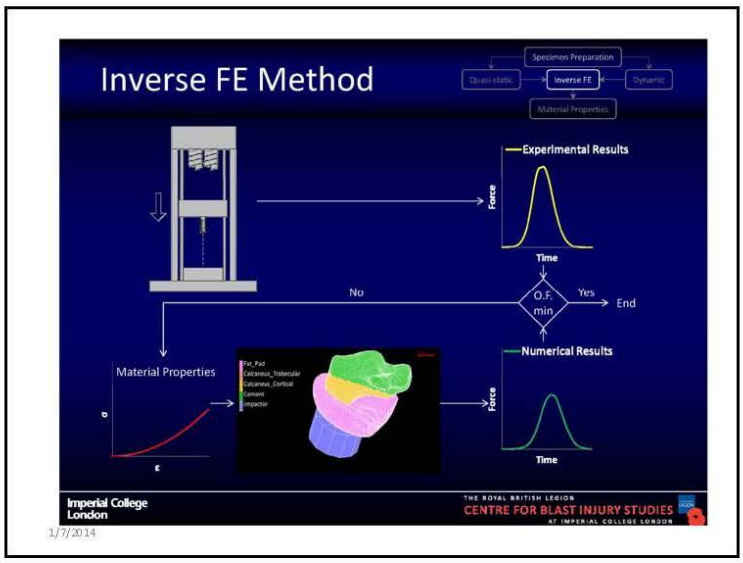
Inverse FE Method
Specimen Preparation
Quasi-static
Inverse FE
Dynamic
Material Properties
Experimental Results
Force
Time
No
O.F. min
Yes
End
Material Properties
Numerical Results
Force
Time
Imperial College London
THE ROYAL BRITISH LEGION
CENTRE FOR BLAST INJURY STUDIES
AT IMPERIAL COLLEGE LONDON
1/7/2014

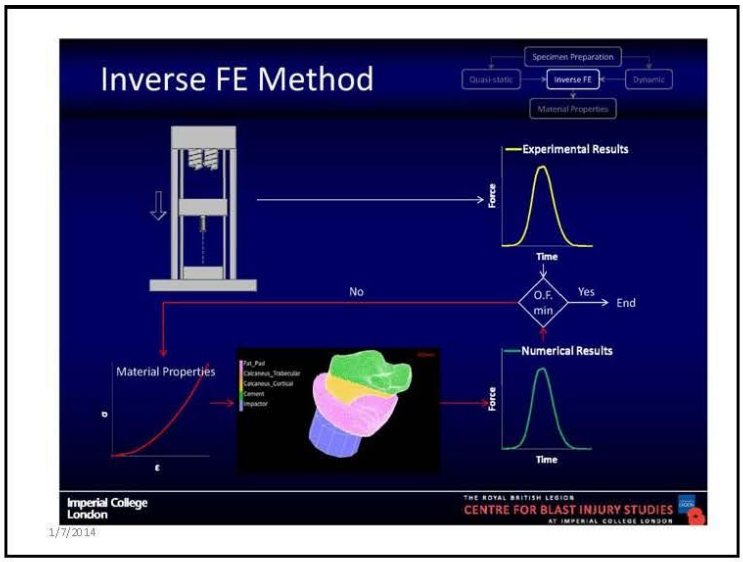
Inverse FE Method
Specimen Preparation
Quasi-static
Inverse FE
Dynamic
Material Properties
Experimental Results
Force
Time
No
O.F. min
Yes
End
Material Properties
Numerical Results
Force
Time
Imperial College London
THE ROYAL BRITISH LEGION
CENTRE FOR BLAST INJURY STUDIES
AT IMPERIAL COLLEGE LONDON
1/7/2014

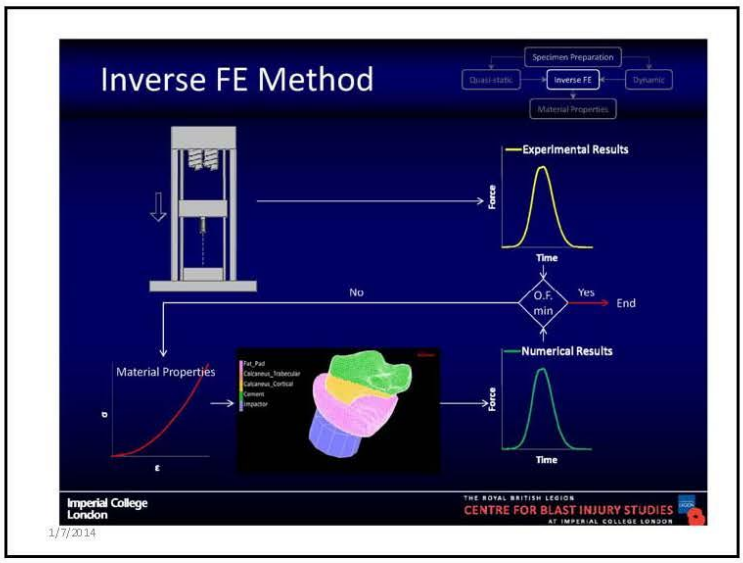
Inverse FE Method
Specimen Preparation
Quasi-static
Inverse FE
Dynamic
Material Properties
Experimental Results
Force
Time
No
O.F. min
Yes
End
Material Properties
Numerical Results
Force
Time
Imperial College London
THE ROYAL BRITISH LEGION
CENTRE FOR BLAST INJURY STUDIES
AT IMPERIAL COLLEGE LONDON
1/7/2014

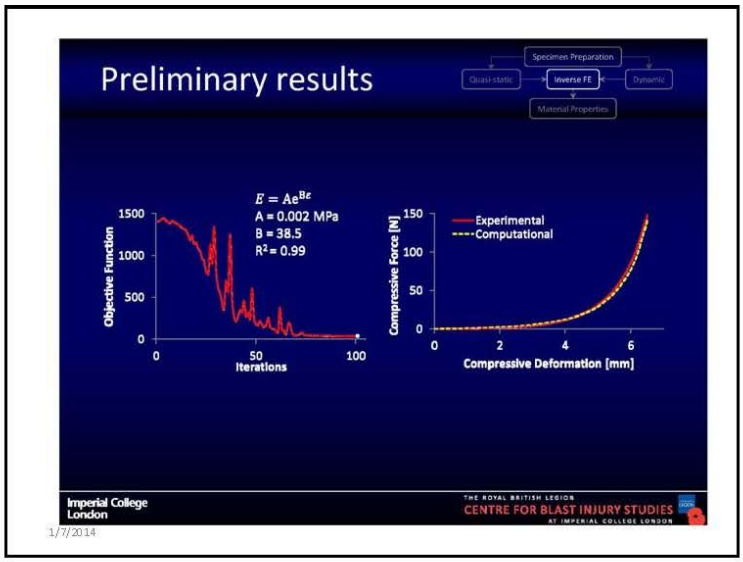
Preliminary results
Specimen Preparation
Quasi-static
Inverse FE
Dynamic
Material Properties
$E = Ae^{B\varepsilon}$
A = 0.002 MPa
B = 38.5
R^2 = 0.99
Objective Function
Iterations
Compressive Force [N]
Experimental
Computational
Compressive Deformation [mm]
Imperial College London
THE ROYAL BRITISH LEGION
CENTRE FOR BLAST INJURY STUDIES
AT IMPERIAL COLLEGE LONDON
1/7/2014

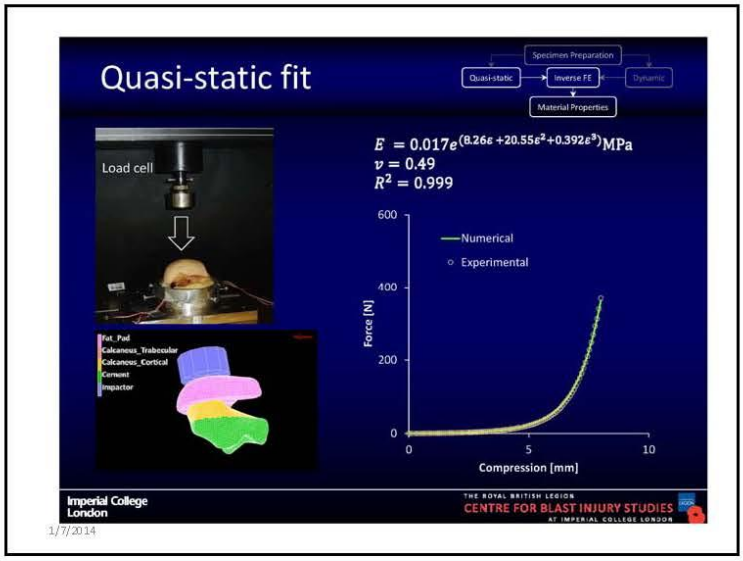
Quasi-static fit
Specimen Preparation
Quasi-static
Inverse FE
Dynamic
Material Properties
Load cell
Fat_Pad
Calcaneus_Trabecular
Calcaneus_Cortical
Cement
Impactor
$E = 0.017e^{(8.26\varepsilon + 20.55\varepsilon^2 + 0.392\varepsilon^3)}$MPa
$\nu = 0.49$
$R^2 = 0.999$
Numerical
Experimental
Force [N]
Compression [mm]
Imperial College London
THE ROYAL BRITISH LEGION
CENTRE FOR BLAST INJURY STUDIES
AT IMPERIAL COLLEGE LONDON
1/7/2014

C95

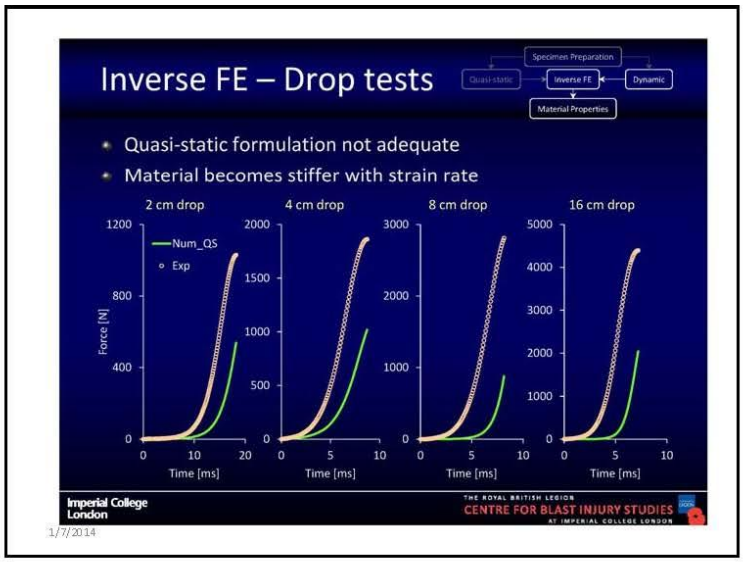
Inverse FE – Drop tests
Specimen Preparation
Quasi-static
Inverse FE
Dynamic
Material Properties
Quasi-static formulation not adequate
Material becomes stiffer with strain rate
2 cm drop
4 cm drop
8 cm drop
16 cm drop
Num_QS
Exp
Force [N]
Time [ms]
Imperial College London
THE ROYAL BRITISH LEGION
CENTRE FOR BLAST INJURY STUDIES
AT IMPERIAL COLLEGE LONDON
1/7/2014

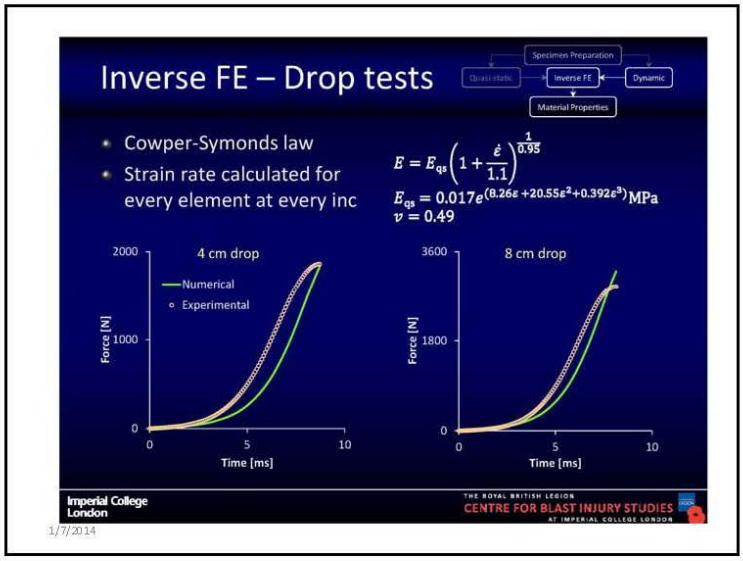
Inverse FE – Drop tests
Specimen Preparation
Quasi-static
Inverse FE
Dynamic
Material Properties
Cowper-Symonds law
Strain rate calculated for every element at every inc
$E = E_{qs}\left(1 + \frac{\dot{\varepsilon}}{1.1}\right)^{\frac{1}{0.95}}$
$E_{qs} = 0.017e^{(8.26\varepsilon + 20.55\varepsilon^2 + 0.392\varepsilon^3)}$ MPa
$\nu = 0.49$
4 cm drop
8 cm drop
Numerical
Experimental
Force [N]
Time [ms]
Imperial College London
THE ROYAL BRITISH LEGION
CENTRE FOR BLAST INJURY STUDIES
AT IMPERIAL COLLEGE LONDON
1/7/2014

Next steps

- Finalize strain-rate dependence law
- Introduce viscoelasticity (if necessary)
- More specimens
- Sensitivity analysis to identify the crucial coeffs
- Implement in FE model of lower limb

Imperial College London

THE ROYAL BRITISH LEGION CENTRE FOR BLAST INJURY STUDIES AT IMPERIAL COLLEGE LONDON

1/7/2014

Imperial College London

THE ROYAL BRITISH LEGION CENTRE FOR BLAST INJURY STUDIES AT IMPERIAL COLLEGE LONDON

Material properties of the human heel fat pad

Grigoris Grigoriadis, Nic Newell, Spyros Masouros, Anthony Bull
The Royal British Legion Centre for Blast Injury Studies,
Department of Bioengineering,
Imperial College London, UK

s.masouros@imperial.ac.uk
www.imperial.ac.uk/traumabiomechanics
www.imperial.ac.uk/blastinjurystudies

1/7/2014

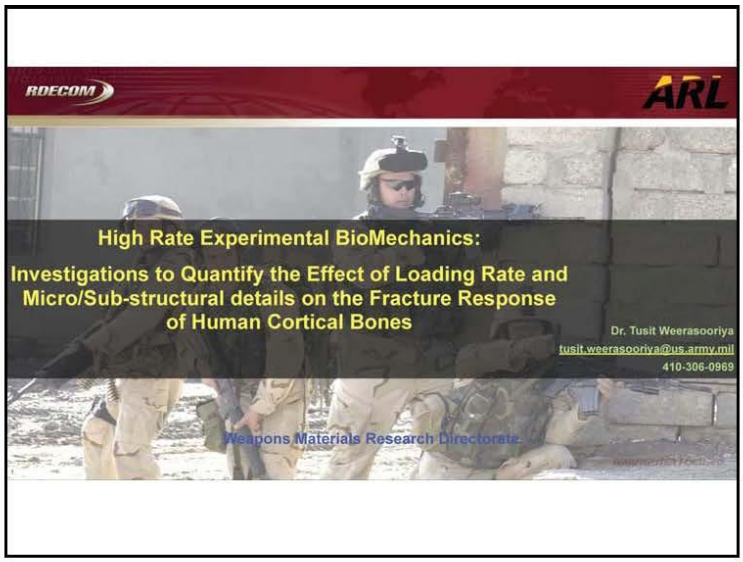
RDECOM
ARL
High Rate Experimental BioMechanics:
Investigations to Quantify the Effect of Loading Rate and Micro/Sub-structural details on the Fracture Response of Human Cortical Bones
Dr. Tusit Weerasooriya
tusit.weerasooriya@us.army.mil
410-306-0969
Weapons Materials Research Directorate

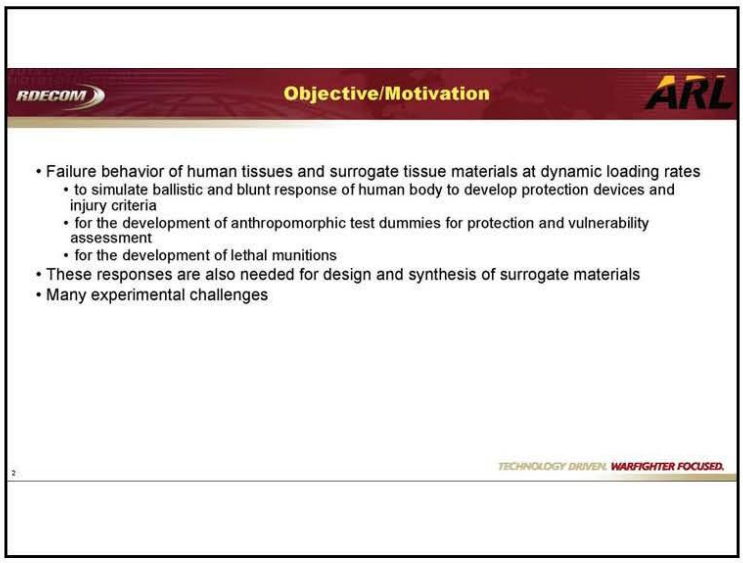
RDECOM
Objective/Motivation
ARL
• Failure behavior of human tissues and surrogate tissue materials at dynamic loading rates
• to simulate ballistic and blunt response of human body to develop protection devices and injury criteria
• for the development of anthropomorphic test dummies for protection and vulnerability assessment
• for the development of lethal munitions
• These responses are also needed for design and synthesis of surrogate materials
• Many experimental challenges
2
TECHNOLOGY DRIVEN. WARFIGHTER FOCUSED.

C98

Background

- Relevant Bone Literature - many investigations on various aspects of bones
- Mechanical behavior
  - Deformation behavior
    - Anisotropic elastic constants (great work at Notre Dame)
    - Age related studies (great work by Rob Ritchie et al at Berkley)
      - Extending to micro-length-scale
    - High Rate - a recent study to obtain compression response longt and transv to osteon axis (by Veccio et al on horse femur Sanborn et al human femur)
      - Rate sensitive, longitudinal deformation response is stronger
  - Fracture behavior
    - Age related studies (work by Rob Ritchie et al at Berkley)
      - Extending to micro-length-scales
    - High Rate - recent studies (by Gunnarson et al on Human and Veccio et al on Bovine and Horse) femur
      - In general high rate fracture response lower than low rate behavior, but lot of variability
- Collagen fibril level multi-scale simulation and x-ray microscopy etc
  - Mechanical properties by Markus Buehler, Rob Ritchie et al
    - Effect of cross-linking of tropocollagen on stress-strain and effect of aging

TECHNOLOGY DRIVEN. WARFIGHTER FOCUSED.

3

Bone (Background)

- By shape
  - Long (humerus)
  - Short (carpals)
  - Flat (cranial vault)
  - Irregular (vertebra)
- Bone tissue:
  - Cortical/compact: hard, brittle that makes up surface and structure of bones
  - Cancellous/trabecular/spongy: soft, spongy, where marrow and blood are produced
- Chemical composition
  - Organic matrix (35%)
    - Stretching & twisting, flexibility, tensile strength, structure
      - Cells
      - Osteon
  - Inorganic mineral (65%)
    - Hydroxyapatite (Ca, P, S, Mg, Cu)
- Bone structure remodeling with time
  - Almost 100% in first year to less than 10% per year in adults
  - Cells associated with remodeling process
    - Osteoclasts - removal of old bones
    - Osteoblasts - formation of new bones

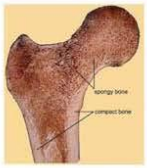

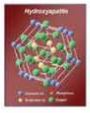

TECHNOLOGY DRIVEN. WARFIGHTER FOCUSED.

4

Hierarchical Structure of Bone

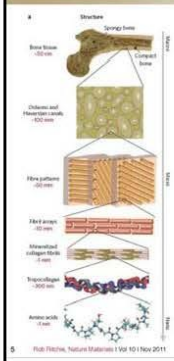

- Understanding of bone mechanical behavior needs investigations at multiple length scales
  - Molecular:amino acids (~1nm) ->
    - Tropocollagen-I triple-helix: (300nm) nano ->
      - Mineralized-collagen fibrils: Periodic arrays (~1um) sub-micro ->
        - aligned fibril lamella (3-7um) micro ->
          - osteon (~100um) micro ->
            - bone mat (cm) macro-structure
- Size of constituents: ~1 nm (amino acids) to ~100 μm (osteon diameter)
- Each level of the hierarchical structure influences the response at the next level

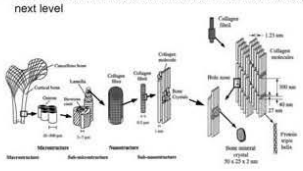

Rho et al. Medical Eng and Physics (1998)

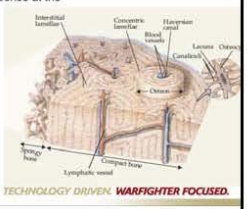

TECHNOLOGY DRIVEN. WARFIGHTER FOCUSED.

Mechanical Response of Biological Tissues at Extreme High Rate Loading & Relate to micro/sub-structure

- Mechanical Response of Tissues at Extreme Loading (high-rate)
- Relate to micro & sub-structure of the tissues
- Focus
  - Hard Tissues
  - Human Tissues

- Fracture & Deformation of Bones
  - *Loading Rate Dependance*
  - Subjects
    - Human (at ARL)
    - Porcine (past work with Purdue)
  - Bone Morphology
    - Cortical (hard)
    - Cancellous (spongy)
  - Type of Bones
    - Leg
      - Femur
      - Tibia
      - Fibula
    - Head
      - Skull (next step)

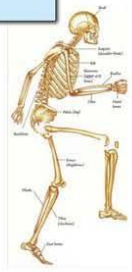

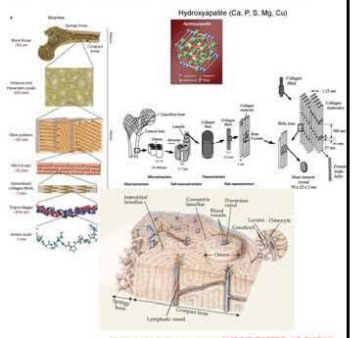

TECHNOLOGY DRIVEN. WARFIGHTER FOCUSED.

Cadeveric Bone Specimens

- Six cadaveric specimens (from legs) were used from three donors
  - D1: Donor 12-111: 36 y.o., male, 5'10" ~180lb
  - D2: Donor 12-114: 50 y.o., male, 5'10" ~210lb
  - D3: Donor 12-184: 43 y.o., male, 6'0" ~170lb
- Cadaveric Specimens
  - Extract femur from thigh
    - Disarticulate distal femur
    - Dissect away soft tissues to isolate femur
    - Sand to remove most of soft tissues attached to femur

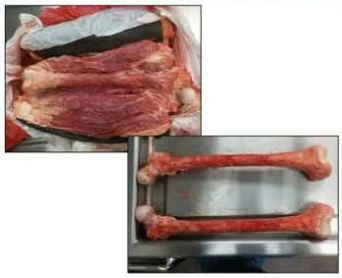

TECHNOLOGY DRIVEN. WARFIGHTER FOCUSED.

Mechanical Response of Biological Tissues at Extreme High Rate Loading

- Unique High Rate Experimental Capabilities
  - micro-Second time scale
- Relate Response to micro and sub-structural details by in-situ & post test analysis at
  - sub-mm scale using
    - micro-CT, nano-CT and eSEM analysis
    - Histological analysis

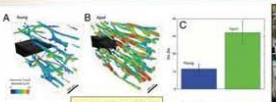

Unique High Rate Fracture Methods are used in these Studies

Relative Scale of Contributions to Fracture Resistance from each Micro-mechanism

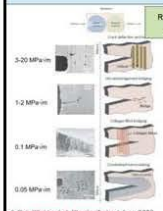

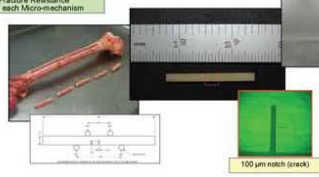

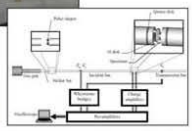

100 µm notch (crack)

TECHNOLOGY DRIVEN. WARFIGHTER FOCUSED.

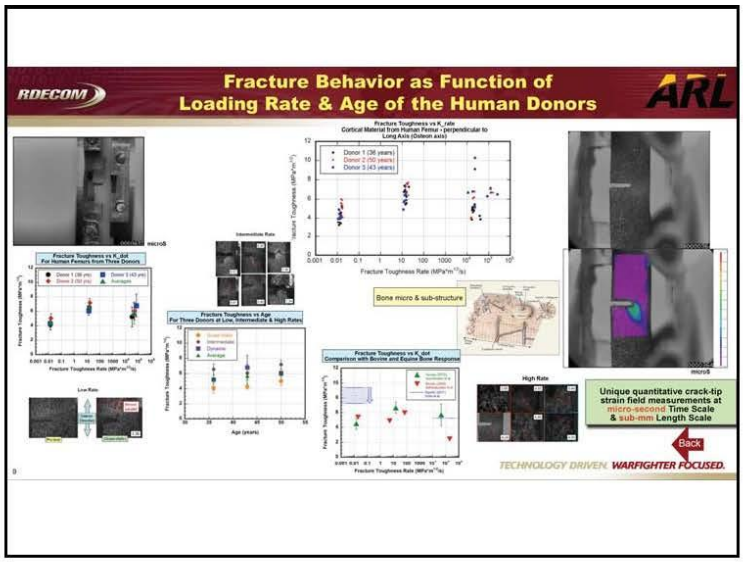
RDECOM
Fracture Behavior as Function of
Loading Rate & Age of the Human Donors
ARL
Bone micro & sub-structure
Unique quantitative crack-tip strain field measurements at micro-second Time Scale & sub-mm Length Scale
Back
TECHNOLOGY DRIVEN. WARFIGHTER FOCUSED.

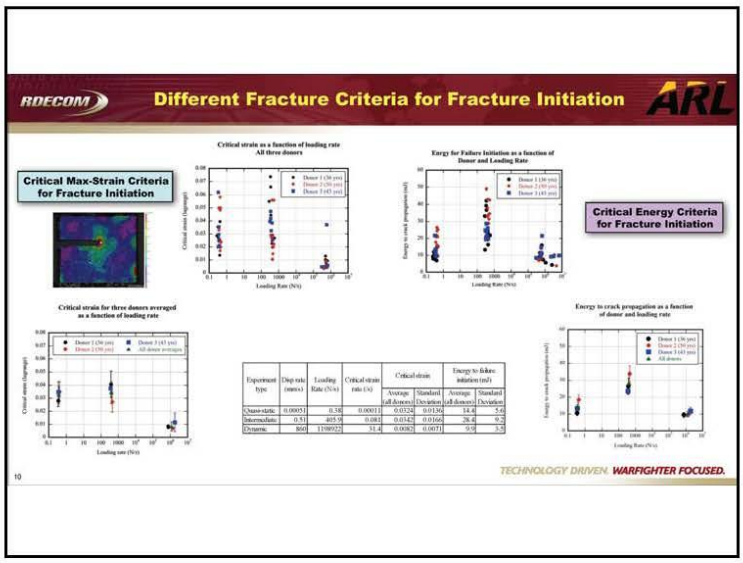
RDECOM
Different Fracture Criteria for Fracture Initiation
ARL
Critical Max-Strain Criteria for Fracture Initiation
Critical Energy Criteria for Fracture Initiation
TECHNOLOGY DRIVEN. WARFIGHTER FOCUSED.

C102

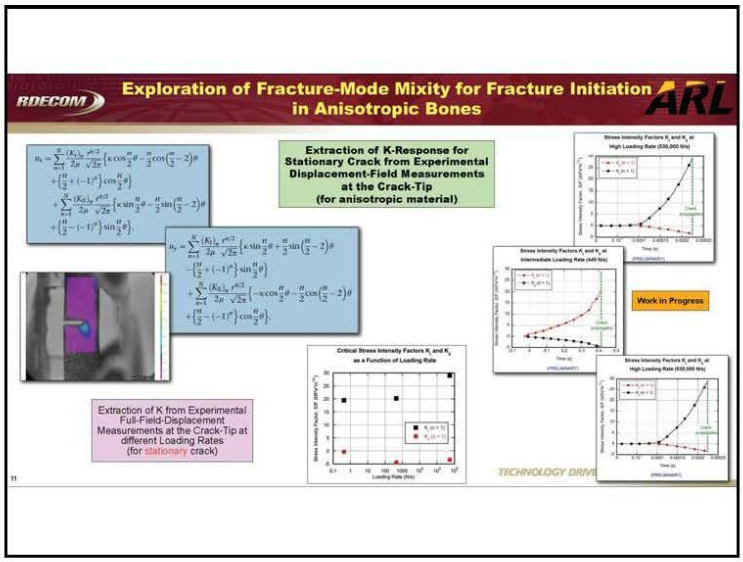
RDECOM
Exploration of Fracture-Mode Mixity for Fracture Initiation in Anisotropic Bones
ARL
Extraction of K-Response for Stationary Crack from Experimental Displacement-Field Measurements at the Crack-Tip (for anisotropic material)
Work in Progress
Extraction of K from Experimental Full-Field-Displacement Measurements at the Crack-Tip at different Loading Rates (for stationary crack)
TECHNOLOGY DRIV

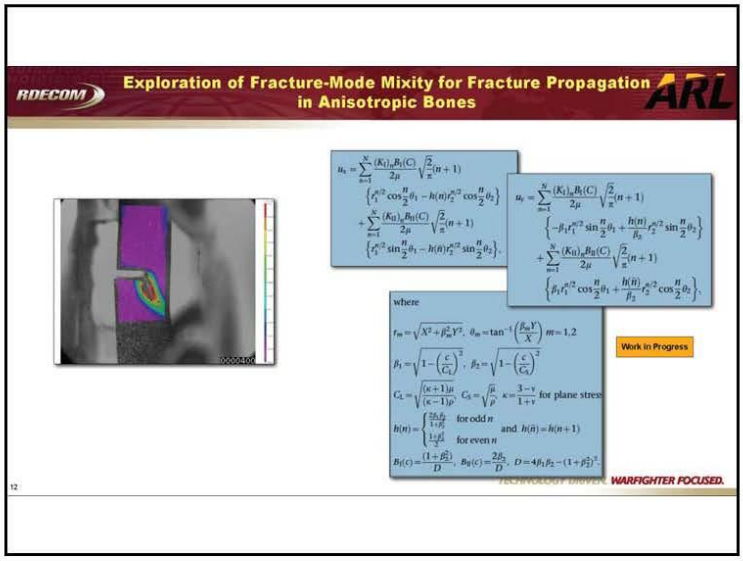
RDECOM
Exploration of Fracture-Mode Mixity for Fracture Propagation in Anisotropic Bones
ARL
where
Work in Progress
TECHNOLOGY DRIVEN
WARFIGHTER FOCUSED.

C103

Qunatification of Cortical Bone Micro/Sub-structural Details

- Mechanical Response Relate to micro & sub-structure of the tissues
- Focus
  - Hard Human Tissues
- Bone Mechanical Response
  - Age - not a good criterion
  - Bone Elemental Content
    - Tissue Mineral Density (TMD)
  - Bone quality
    - Bone architecture, remodeling, mineralization, bone volume (porosity)

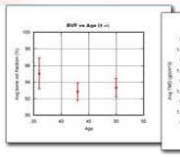

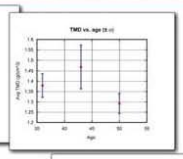

- Measurement via micro-CT or Bone-histology
  - Cortical Bone Volume Fraction (BVF) or Porosity (BPF)
    - Haversian canals
    - less contribution: Lacunae, Volkman's canals, canaliculi channels
  - Tissue Mineral Density (TMD of CaHA)
  - Osteon density (Haversian vs. Interstitial)
  - Cementline length quantification
  - Quantifying pre micro-cracks (?)

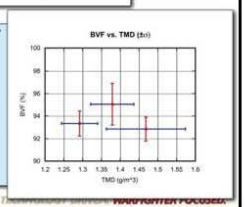

Microstructure of the osteonal cortical bone according to Martin and Burr (1989) and Fung (1993). Canals and osteons are not to scale.

13

Fracture Response as a function of Quantified Microstructural Details

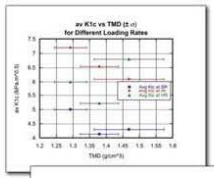

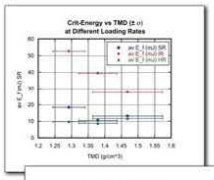

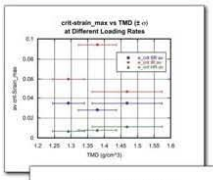

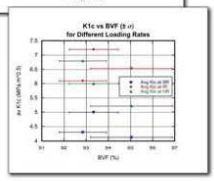

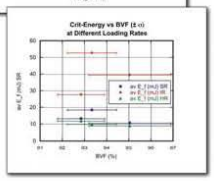

14

RDECOM ARL

Thank You
Questions?

Back

15

TECHNOLOGY DRIVEN. WARFIGHTER FOCUSED.

RDECOM

Age Related Changes in Bone Fracture Mechanisms at Small-Length Scales

ARL

- Primary mechanisms related to loss of bone toughness:
  - More cross linking of collagen molecules during aging suppresses plasticity at nanoscale level by restricting fibril sliding mechanism thus stiffening them and reducing toughness
  - Aging increases cross links reducing the strain carrying capability of tropocollagen making them stiffer, which leads to increase in micro-cracking and macro-scale fracture
  - Increased osteonal density limits potency of crack bridging at micro-scale to suppress crack growth; also availability of more weak hyper mineralized cementlines for fracture path and fracture initiation sites
  - Reduction in bone remodeling and hence reduction in micro-crack repair
  - With age decrease in osteocyte lacunar density with blockage due to hyper-mineralization cause deteriorations in the canalicular fluid flow and reduce the detection of micro-damage for repair - making bone fragile
- Bone Mineral Density (BMD) alone is not a good predictor of fracture risk

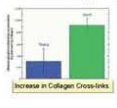

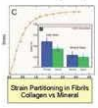

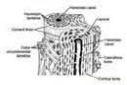

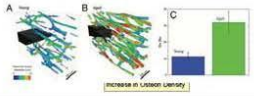

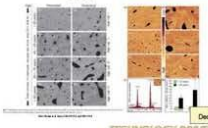

Decrease in Osteocytes

Back

16

TECHNOLOGY DRIVEN. WARFIGHTER FOCUSED.

Recent Developments in a Computational Shock Physics Tool for Modeling Fluid-Structure Interaction

Shane Schumacher
Sandia National Laboratories
scschum@sandia.gov

Sandia National Laboratories is a multi-program laboratory operated by Sandia Corporation, a wholly owned subsidiary of Lockheed Martin company, for the U.S. Department of Energy's National Nuclear Security Administration under contract DE-AC04-94AL85000.

NNSA

Sandia National Laboratories

Project Summary

- Capitalize on the strengths of Eulerian and Lagrangian numerical methods
  - Model fluids Eulerian
  - Model strength bearing material Lagrangian
- Mixed frame computations
  - Mixed Lagrangian and Eulerian numerical methods
  - Numerical method types
- Massively parallel computations for system analysis
  - 1000's, 100,000's of cores
- Interface existing constitutive models
  - Equation of state (shock mechanics)
  - Strength
  - Failure
- Verification and validation
  - Comparison to experiments

Sandia National Laboratories

Project Path

- Research and information from Sandia, LANL and DoD
- SNL-LANL Cross laboratory collaborations
- Implement marker methods into CTH for Lagrangian material behavior
  - Lagrangian marker method
    - Nonlinear elasticity
    - Advanced mechanics of materials
  - CFDLib formulation
    - Interpolation algorithms and schemes
- Multifield interaction of n materials
  - Tensor of interactions between materials
  - Constraints on interactions based on physics
  - Separate material velocities (mixed cell computations)
- Implicit Continuous-fluid Eulerian methods to address time scale

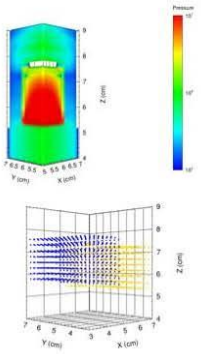

Sandia National Laboratories

CTH

CTH is a massively-parallel shock-physics code.

- Eulerian shock wave physics computer code solving conservation equations of mass, momentum, and energy for up to 98 simultaneous materials including gases, fluids, solids, and reactive materials
  - Analytic & Tabular Equation-of-State models
  - Advanced Strength & Fracture models
  - Adaptive Mesh Refinement
- Widely used for the simulation of complex high strain rate, large deformation and strong shock mechanics
- Applications (partial list):
  - Armor, Anti-Armor, Munitions Design, Blast Effects
  - Planetary Science, Asteroid Impact & Planetary Defense
- CTH license
  - 800+ users

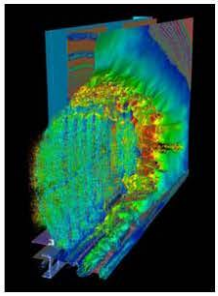

32,000 processor Cielo calculation showing nearby blast on aluminum and steel structure

Sandia National Laboratories

Lagrangian Marker Methods

- 1D, 2D and 3D
- Solid object insertion of Marker fields
  - No meshing needed, directly from primitive object, CAD, geometric scans, etc.
- Numerical techniques
  - FLuid Implicit Particle
    - Brackbill, J.U. and Ruppel, H.M.
  - Material Point Method
    - Sulsky, Deborah, Chen Z., and Schreyer, Howard L.
  - Integration of Convective Particle Domain Interpolation (CPDI)
    - University of Utah collaboration (Rebecca Brannon)
- Equation of State, strength and failure
- Massively parallel Marker capability with/without AMR
  - Vertex communication
  - Combining and splitting
- Plate and shell-type theories on Marker

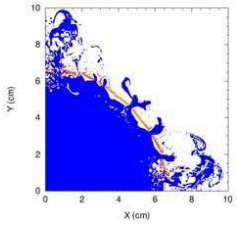

Sandia National Laboratories

Multifield

- Second order accurate finite volume numerical method
- N number of fields with separate velocities
- Field interactions
  - No surface designation needed
  - Simple and easy to use interface
  - Describe (n x n - n)/2 interactions (similar to contact)
- Material interaction models (mass, momentum and/or energy)
  - Slip
  - Welded
  - Friction models ("gripping" rebar in concrete, etc.)
  - Turbulence models (particle in gas or fluid)
  - Viscous models (fluid-solid, fluid-fluid, etc.)
- Hydrodynamics
  - Vertex pressure acceleration with TVD limiting
  - Vertex momentum exchange
  - Cell centered velocity, energy, density and pressure
- Remapping
  - Unsplit 1st and 2nd order remapping techniques with TVD limiting

Sandia National Laboratories

Implicit Continuous Eulerian

- High demand from users
- Address time scales in CTH
  - Adds capability to have simulation time out to seconds
  - Accuracy vs. cycles
- ICE methods
  - Frank Harlow, LANL
  - Routinely used in shock and non-shock physics codes
- Time step modification
  - Bound by shock and velocity courant time steps
- Adaptive
  - Scales time step by "sensing" when simulation
- Numerical Method
  - Semi-implicit
  - Implicit

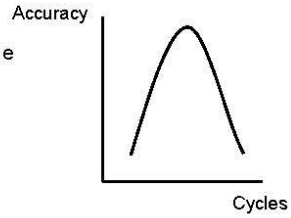

Sandia National Laboratories

SOD 1D, Single Field

- 1D Reimann problem
- 2000 cells used
- Tests hydrodynamics with analytical
- Compares well with standard CTH solution
  - Wave speeds and interactions correct

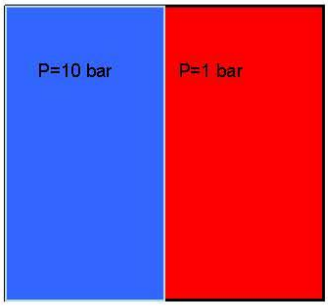

Sod, G. A. (1978). "A Survey of Several Finite Difference Methods for Systems of Nonlinear Hyperbolic Conservation Laws". *J. Comput. Phys.* **27**: 1–31.

Sandia National Laboratories

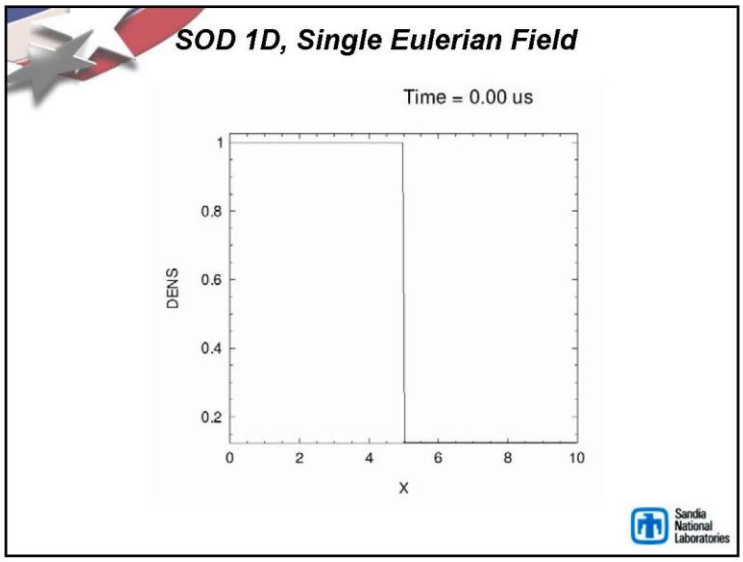
SOD 1D, Single Eulerian Field
Time = 0.00 us
DENS
X
Sandia National Laboratories

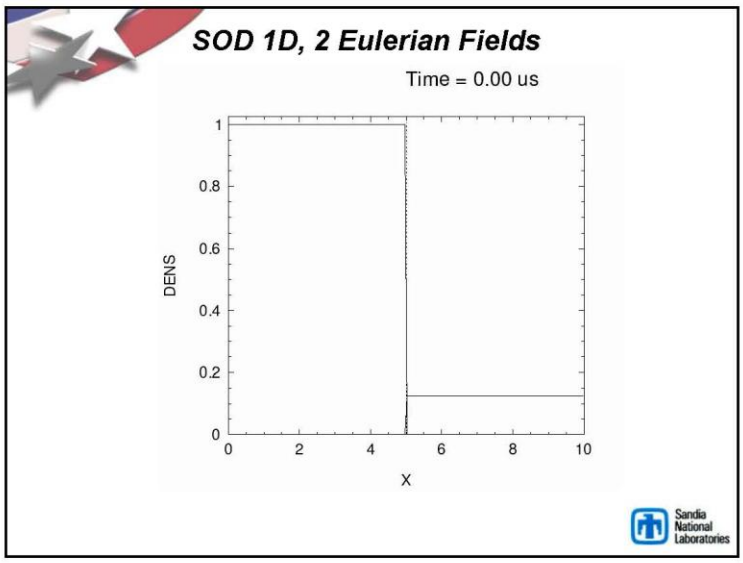
SOD 1D, 2 Eulerian Fields
Time = 0.00 us
DENS
X
Sandia National Laboratories

C110

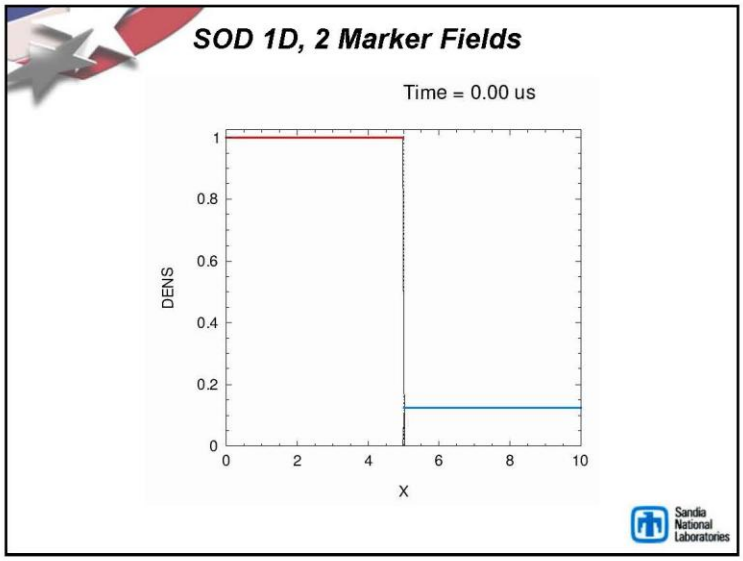
SOD 1D, 2 Marker Fields
Time = 0.00 us
DENS
X
0
0.2
0.4
0.6
0.8
1
0
2
4
6
8
10
Sandia National Laboratories

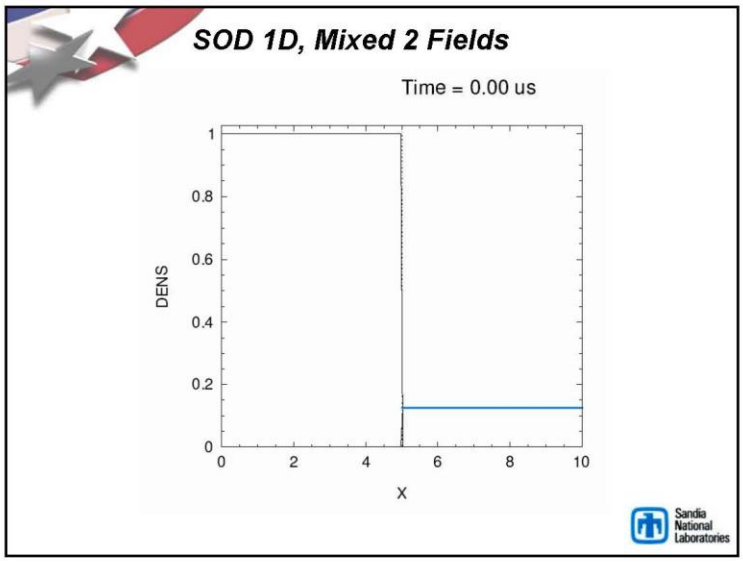
SOD 1D, Mixed 2 Fields
Time = 0.00 us
DENS
X
0
0.2
0.4
0.6
0.8
1
0
2
4
6
8
10
Sandia National Laboratories

6

Bullet Interactions

- 45 ACP bullet
  - 260 m/s (850 ft/s)
- Ballistic Gellatin
  - EOS - water
  - Mooney-Rivlin strength
  - Strain to failure
- ~500,000 Markers
  - ~200 MB memory
- 16,000 cells
  - ~27 MB memory
- Typical runtime ~25 min.

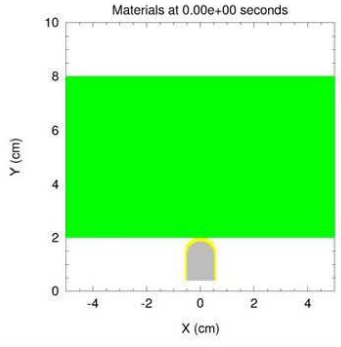

Sandia National Laboratories

CTH with Lagrangian Markers

- 45 ACP bullet
  - 260 m/s (850 ft/s)
- Ballistic Gellatin
  - EOS - water
  - Mooney-Rivlin strength
  - Strain to failure

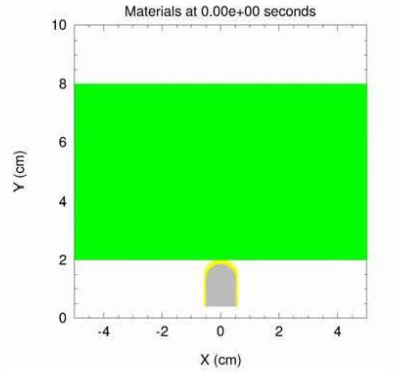

Sandia National Laboratories

CTH with Lagrangian Markers

- 45 ACP bullet
  - 260 m/s (850 ft/s)
- Ballistic Gellatin
  - EOS - water
  - Mooney-Rivlin strength
  - Strain to failure

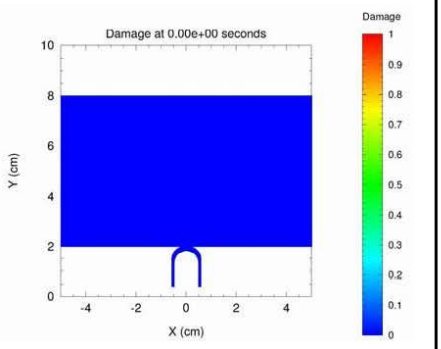

Sandia National Laboratories

Lagrangian Markers

- 45 ACP bullet
  - 260 m/s (850 ft/s)
- Ballistic Gellatin
  - Mooney-Rivlin strength
  - Strain to failure
- No EOS

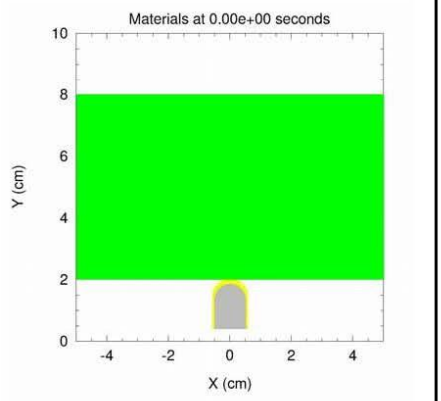

Sandia National Laboratories

Lagrangian Markers

- 45 ACP bullet
  - 260 m/s (850 ft/s)
- Ballistic Gellatin
  - Mooney-Rivlin strength
  - Strain to failure
- No EOS

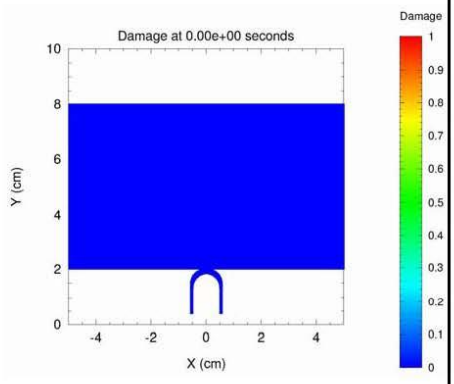

Sandia National Laboratories

Multifield with Lagrangian Markers

- 45 ACP bullet
  - 260 m/s (850 ft/s)
- Ballistic Gellatin
  - EOS - water
  - Mooney-Rivlin strength
  - Strain to failure

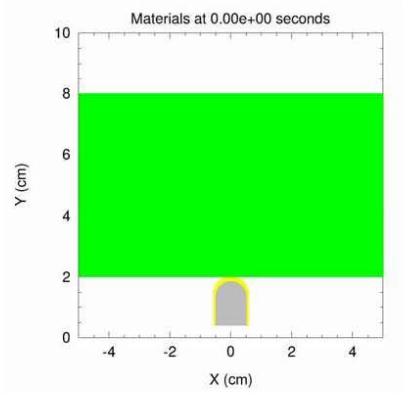

Sandia National Laboratories

Multifield with Lagrangian Markers

- 45 ACP bullet
  - 260 m/s (850 ft/s)
- Ballistic Gellatin
  - EOS - water
  - Mooney-Rivlin strength
  - Strain to failure

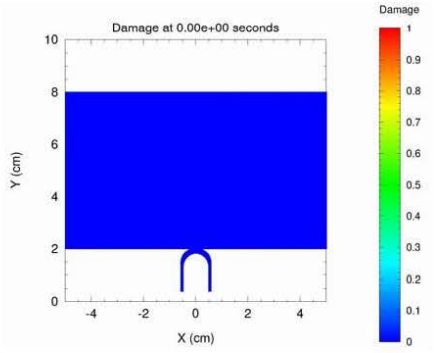

Sandia National Laboratories

Multiple Material Interactions

- Rod penetrating two plates
- Bimetallic plates
  - No bonding
- ~220,000 Markers
  - ~95 MB memory
- 30,000 cells
  - ~76 MB memory
- Typical runtime ~20 min.

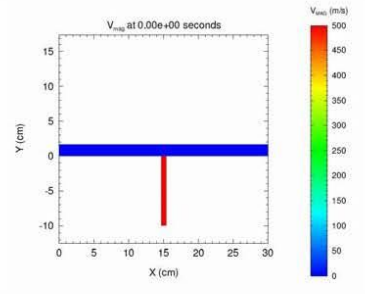

Sandia National Laboratories

Multifield with Lagrangian Markers

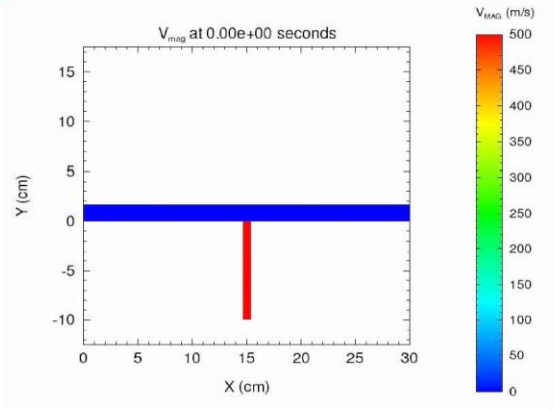

Sandia National Laboratories

Necking example

- Copper
- 4 markers per cell
- CPDI used
- 100 m/s block
- 2DR

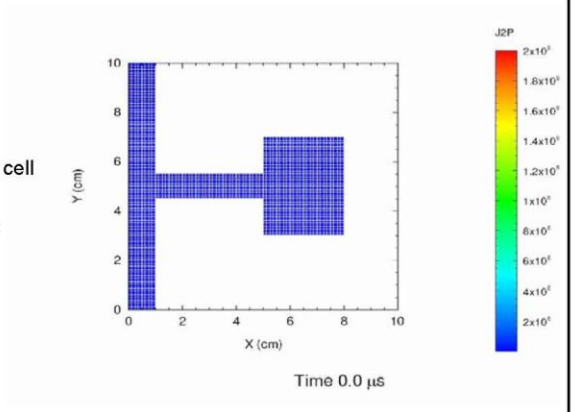

Sandia National Laboratories

Current Directions

- Parallelization of Multifield
- Advection (Euler)
  - Investigate and implement methods to reduce diffusion at material interfaces/contact surfaces
  - Anti-diffusion method
- Thin structure mechanics
  - Shock support method for membranes/shells
- Implicit Continuous Eulerian (ICE++)
- Marker insertion
  - Techniques to "randomize" insertion
- New material models
  - Fracture and failure
  - Non-linear elasticity in shock
    - Rate dependent, anisotropic, etc.
  - Stochastic fields

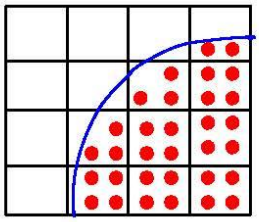

Sandia National Laboratories

Conclusion

- New tool will provide a means to accurately predict strategic structural response to terminal ballistics and/or blast
  - Utilizing the correct mathematics and physics to meet project goals
  - Enhanced strength and fracture capabilities
    - Damage and failure evolution
  - Integrated (tight) coupling for enhanced fluid/structure capabilities
  - Immersed boundary method utilizing the strengths of Lagrangian and Eulerian numerical techniques
- Solid object insertion
- Field based interactions
- Development in progress
  - Marker beta release January 2014
- Training added as part of CTH regular CTH class

Sandia National Laboratories

CFD Research Corporation

215 Wynn Dr. , Huntsville, AL 35805 (256) 726-4800 FAX: (256) 726-4806 www.cfdrc.com

Human Body Models and Computational Tools for Human Response to Blast and Accelerative Loadings

Andrzej Przekwas, X.G. Tan and Alex Zhou
Computational Medicine and Biology Div.
CFD Research Corp., Huntsville AL

Workshop on Numerical Analysis of Human and Surrogate Response to Accelerative Loading
USAARL Aberdeen, MD, January 7-9, 2014

Our Goal and Outline

Goal

Develop multiscale simulation framework, CoBi, for modeling soldier performance, injury and protection.
Integrate: human body anatomy/geometry generator & models, material databases, exposure scenarios, GUI & post-processing

CoBi tools and Body Models are DoD Open Source

- CMB & CoBi Tools
- Human anatomy/geometry model generator
- Blast wave and loading model – human & vehicle
- Accelerative loading on seated occupants
- Human biodynamic response models
- Ongoing Work and Plans

2

C118

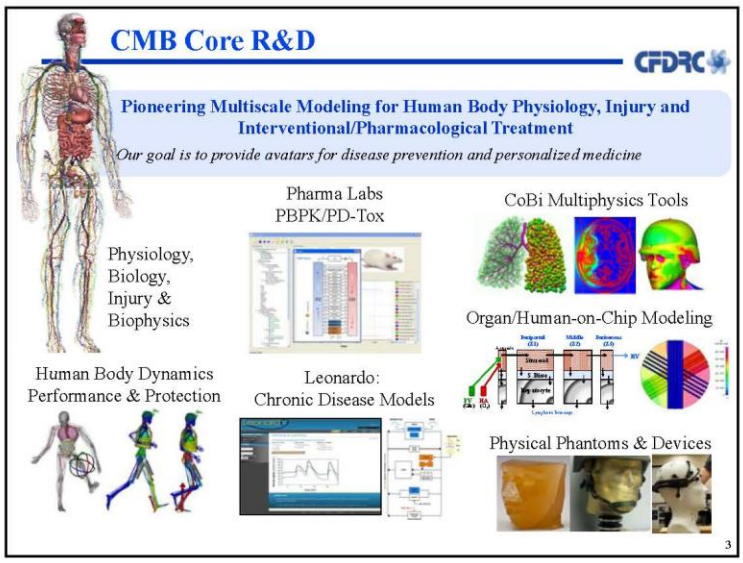
CMB Core R&D
CFDRC
Pioneering Multiscale Modeling for Human Body Physiology, Injury and Interventional/Pharmacological Treatment
Our goal is to provide avatars for disease prevention and personalized medicine
Physiology, Biology, Injury & Biophysics
Pharma Labs PBPK/PD-Tox
CoBi Multiphysics Tools
Organ/Human-on-Chip Modeling
Human Body Dynamics Performance & Protection
Leonardo: Chronic Disease Models
Physical Phantoms & Devices
3

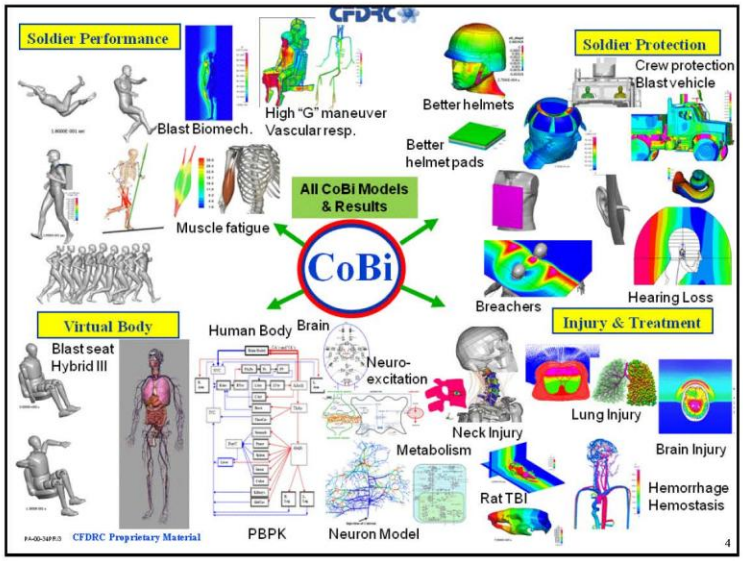
Soldier Performance
Blast Biomech.
High "G" maneuver Vascular resp.
Muscle fatigue
All CoBi Models & Results
CoBi
Soldier Protection
Crew protection Blast vehicle
Better helmets
Better helmet pads
Breachers
Hearing Loss
Virtual Body
Blast seat Hybrid III
Human Body
Brain
Neuro-excitation
Metabolism
PBPK
Neuron Model
Injury & Treatment
Neck Injury
Lung Injury
Brain Injury
Rat TBI
Hemorrhage Hemostasis
CFDRC Proprietary Material
4

2

C119

CoBi- Multiscale and Metaphysics Capabilisties

Multiscale:

- 3D/2D/1D/0D PDE Solvers – for all disciplines
- User Defined ODE Systems – for all disciplines
- Coupled PDEs-ODEs– for all disciplines

Parallel Computing:

- multicore clusters (implicit)
- GPU (explicit)

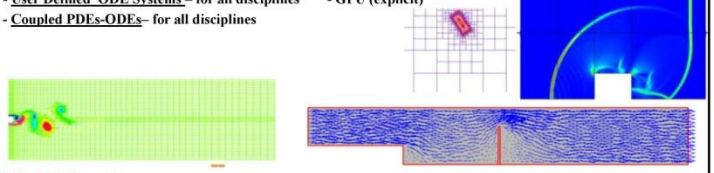

Multiphysics:

CFD Fluid Mechanics – compressible/incompressible flows, porous media, reactive flows, biomechanics, tight link to other disciplines: structures, electrochemistry, biology; physiology and immunology…

FEM Structure Mechanics – linear/nonlinear problems, user defined material models, tight link to other disciplines (flow, thermal, electrostatics, biochemistry, physiology, systems biology)

Thermal – convection, diffusion, sources, conjugate heat transfer, …

Chemistry – chemical kinetics in fluid/solid, surface chemistry, user defined models, biochemistry

Electrostatics– electric field and current continuity eq.

Electrochemistry – coupled chemistry + flow + thermal

Optimization, Inverse Problems, and Parameter Estimation

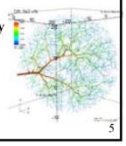

5

Human Body Anatomy/Geometry for Physiology & Physics Models

Anatomic Templates

Joint Manipulation Framework

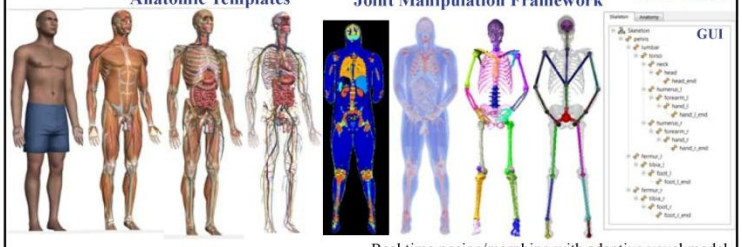

Real time posing/morphing with adaptive voxel model

Anatomic/Geometry and Morphing Tools

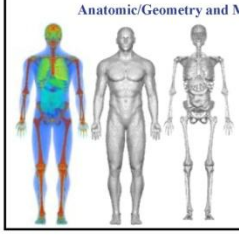

Postural and Anthropometric Body Variations

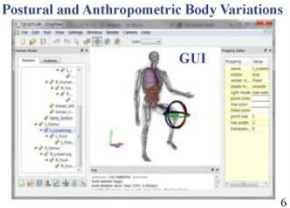

6

C120

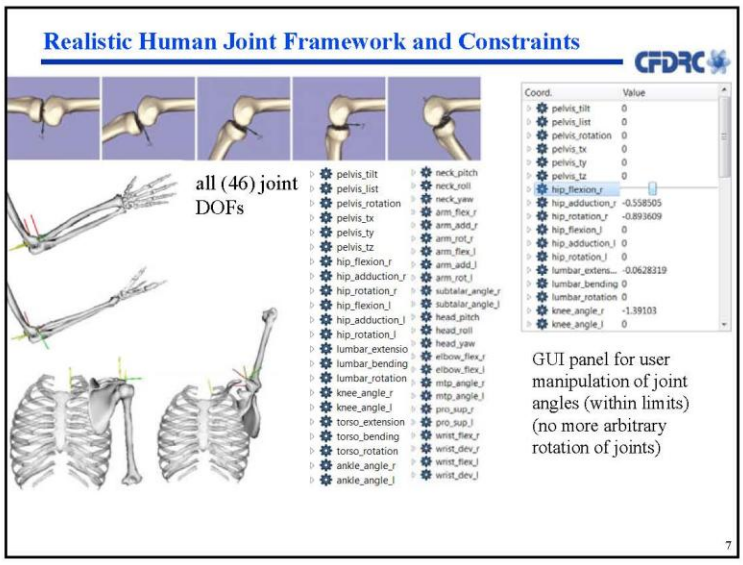
Realistic Human Joint Framework and Constraints
CFDRC
all (46) joint DOFs
pelvis_tilt
pelvis_list
pelvis_rotation
pelvis_tx
pelvis_ty
pelvis_tz
hip_flexion_r
hip_adduction_r
hip_rotation_r
hip_flexion_l
hip_adduction_l
hip_rotation_l
lumbar_extensio
lumbar_bending
lumbar_rotation
knee_angle_r
knee_angle_l
torso_extension
torso_bending
torso_rotation
ankle_angle_r
ankle_angle_l
neck_pitch
neck_roll
neck_yaw
arm_flex_r
arm_add_r
arm_rot_r
arm_flex_l
arm_add_l
arm_rot_l
subtalar_angle_r
subtalar_angle_l
head_pitch
head_roll
head_yaw
elbow_flex_r
elbow_flex_l
mtp_angle_r
mtp_angle_l
pro_sup_r
pro_sup_l
wrist_flex_r
wrist_dev_r
wrist_flex_l
wrist_dev_l
Coord.
Value
hip_adduction_r -0.558505
hip_rotation_r -0.893609
GUI panel for user manipulation of joint angles (within limits) (no more arbitrary rotation of joints)
7

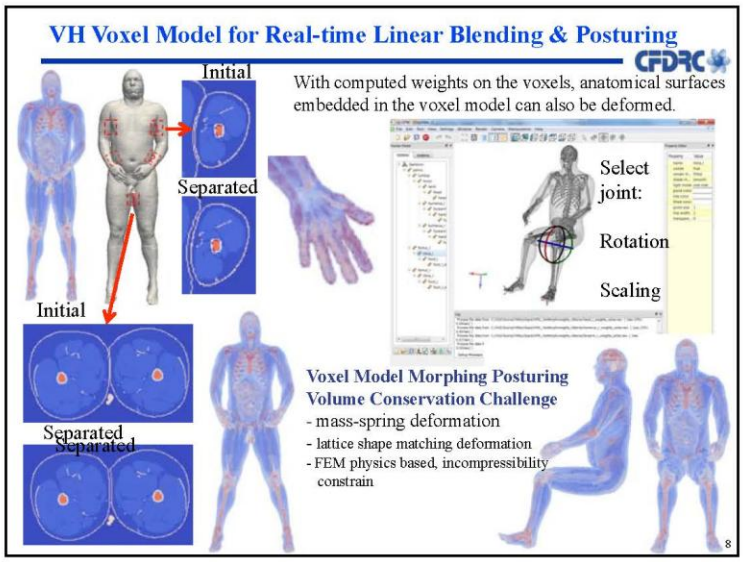
VH Voxel Model for Real-time Linear Blending & Posturing
CFDRC
Initial
Separated
Initial
Separated
Separated
With computed weights on the voxels, anatomical surfaces embedded in the voxel model can also be deformed.
Select joint:
Rotation
Scaling
Voxel Model Morphing Posturing
Volume Conservation Challenge
- mass-spring deformation
- lattice shape matching deformation
- FEM physics based, incompressibility constrain
8

4

C121

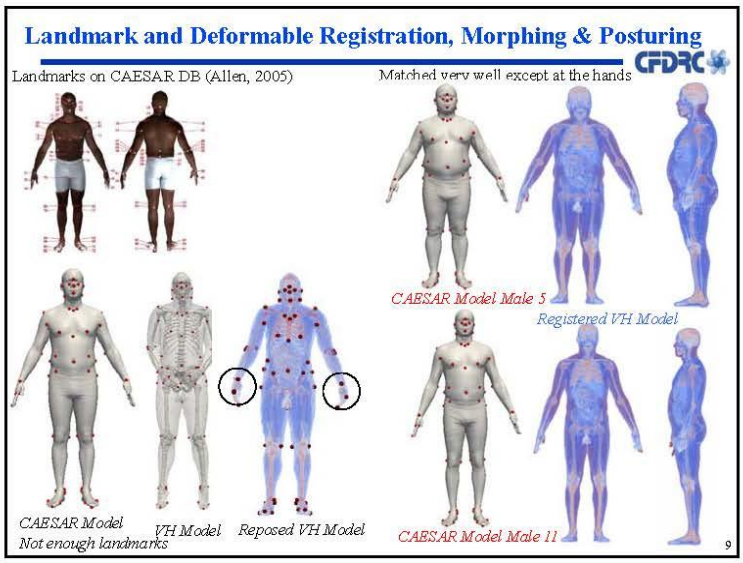
Landmark and Deformable Registration, Morphing & Posturing
Landmarks on CAESAR DB (Allen, 2005)
Matched very well except at the hands
CAESAR Model Male 5
Registered VH Model
CAESAR Model
Not enough landmarks
VH Model
Reposed VH Model
CAESAR Model Male 11
9

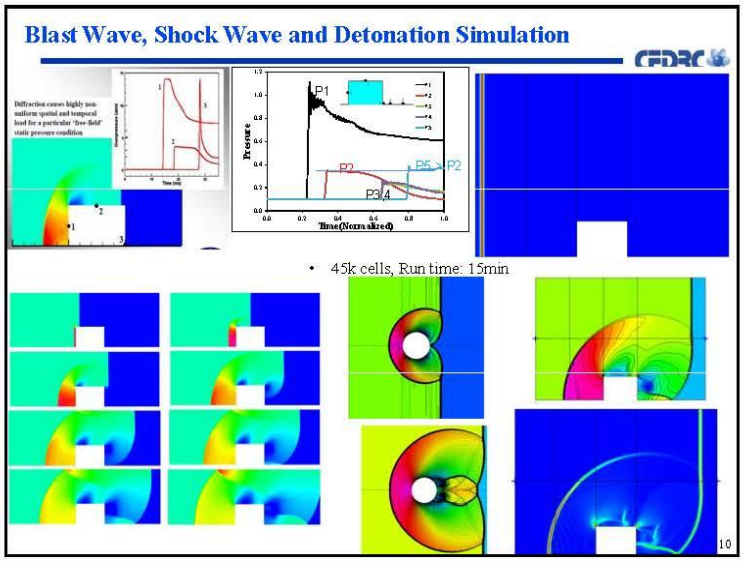
Blast Wave, Shock Wave and Detonation Simulation
P1
P2
P5
P2
P3,4
• 45k cells, Run time: 15min
10

5

C122

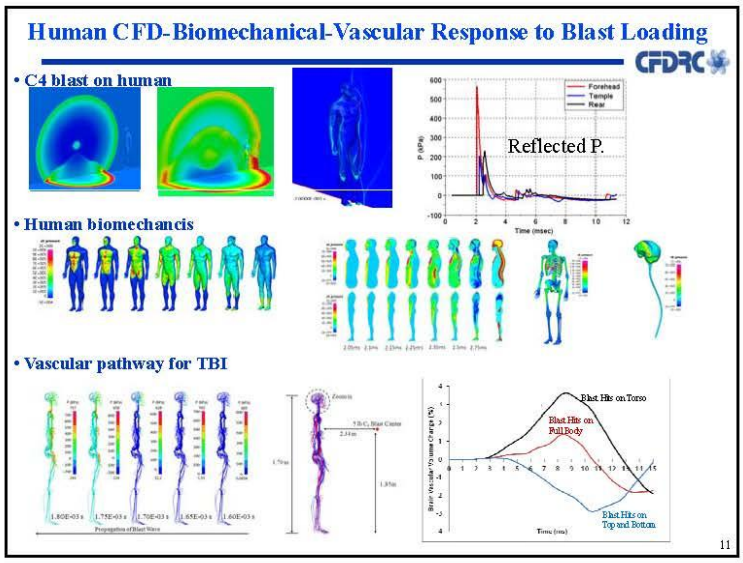
Human CFD-Biomechanical-Vascular Response to Blast Loading
CFDRC
• C4 blast on human
Reflected P.
Forehead
Temple
Rear
Time (msec)
• Human biomechancis
• Vascular pathway for TBI
Blast Hits on Torso
Blast Hits on Full Body
Blast Hits on Top and Bottom
11

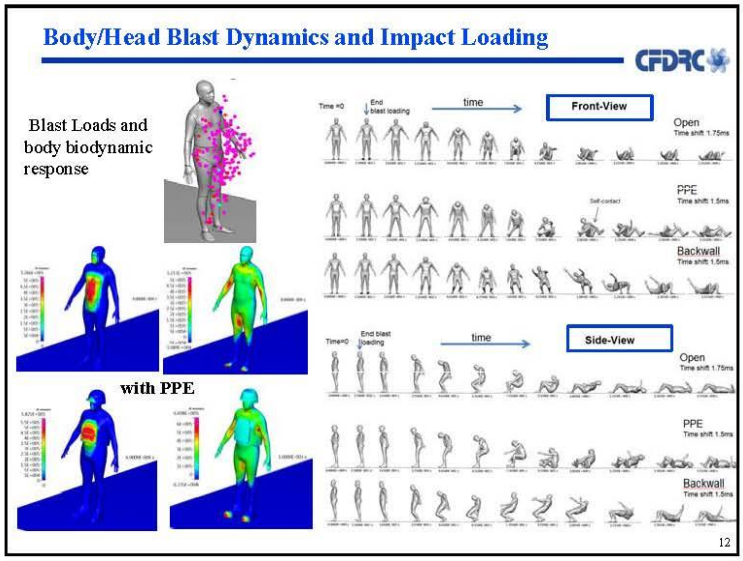
Body/Head Blast Dynamics and Impact Loading
CFDRC
Blast Loads and body biodynamic response
with PPE
time
Front-View
Open
PPE
Backwall
Side-View
12

C123

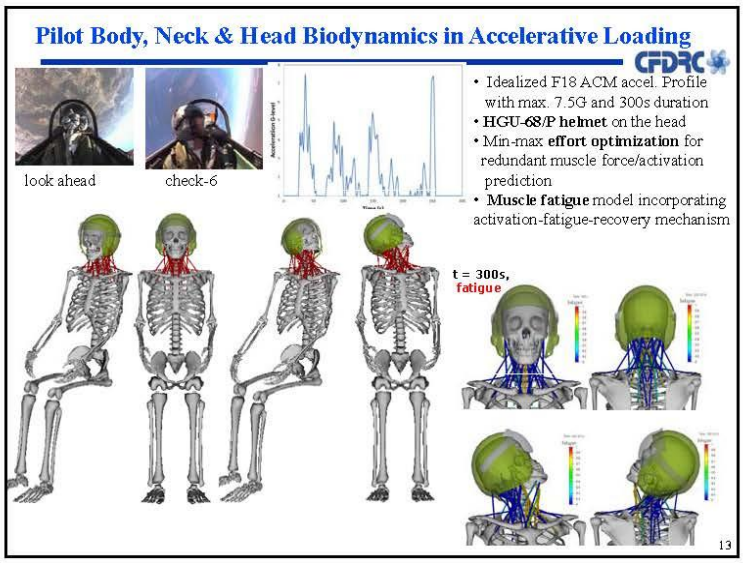
Pilot Body, Neck & Head Biodynamics in Accelerative Loading
look ahead
check-6
• Idealized F18 ACM accel. Profile with max. 7.5G and 300s duration
• HGU-68/P helmet on the head
• Min-max effort optimization for redundant muscle force/activation prediction
• Muscle fatigue model incorporating activation-fatigue-recovery mechanism
t = 300s, fatigue
13

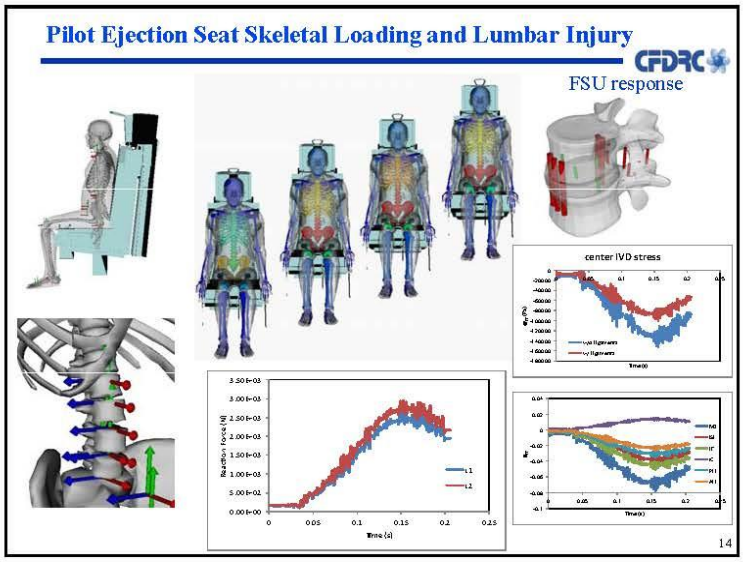
Pilot Ejection Seat Skeletal Loading and Lumbar Injury
FSU response
center IVD stress
14

C124

Validation: Bertholon's Sled Data For Rear Impact

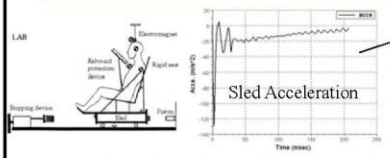

- Short impulse
- Max. acce. = 12G
- Max. Vel. < 3m/s
- Rigid seat

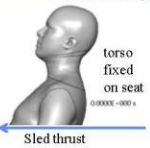

- Good fit with test data in terms of magnitude and timing
- Both acceleration and Angul. Acceler. peak around 0.17 sec.;

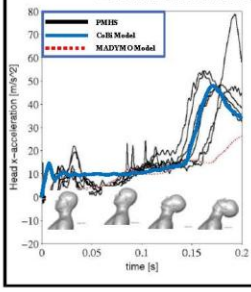

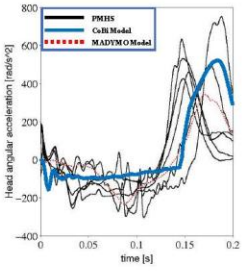

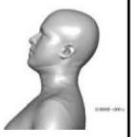

Ph.D. thesis by
Horst, van der Marike J., 2002

15

Blast Vehicle – Occupant Response Model

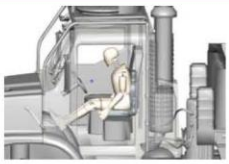

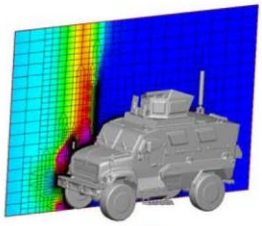

Body positioning And outfling w PPE

Ill fit

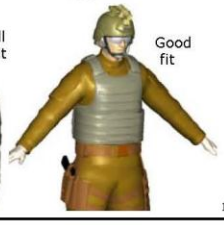

Good fit

16

Validation: Human Surrogate Head Under Shock Tube Loading

Simulate ARA 18" diameter shock tube:
94 in, about 5atm in 4" driver chamber

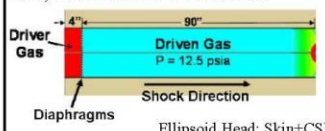

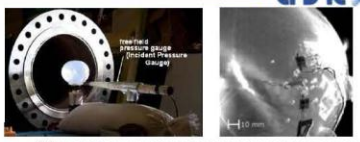

Ellipsoid Head: Skin+CSF+Gel

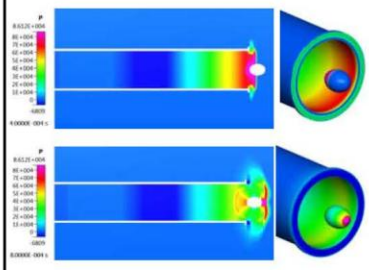

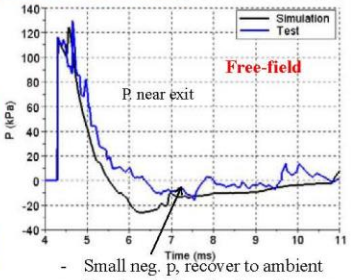

- Small neg. p, recover to ambient
- Exact probe location is not known
- Driver Rupture is not modeled

Shock tube apparatus and test *see : Goeller et al., 2012, J. Neurotrauma*

Investigation of Cavitation as a Possible Traumatic Brain Injury (TBI) Damage Mechanism from Blast 17

Validation: Human Surrogate Head FEM Model vs. Experiment

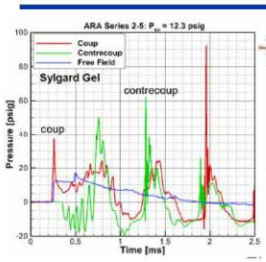

Experiments: Goeller et al., 2012, J. Neurotrauma

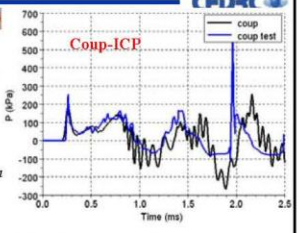

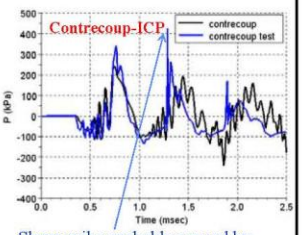

- Qualitative comparable
- Time delay of 0.1msec between coup and contrecoup
- Coup site:
  lower positive peak than contrecoup
- Contrecoup site:
  1) In tension first,
  2) Three positive peak in weakening,
  3) Three negative dip, 4) Cavitation does happen
- Justify one-way coupling for milliseconds event
- Similar observations in human model

Sharp spike probably caused by cavitation collapse

18

Ongoing Work and Plans

CFDRC

- Continuous improvements of numeric and Physics in CoBi
- Development of QtCoBi GUI tools
- Anatomic/Geometry of Human Body Models for: soldier performance (Army Natick), Bio-effects in RF Exposure (AFRL HEPA)
- Experiment/Modeling of helmet protection of TBI (USAARL)
- Experiment/Multiscale model of neuroaxnal injury (MRMC)
- Validation of primary/secondary TBI animal models (WRAIR)
- Spinal injury and chronic pain in naval aviators (NAVAIR)
- Physics/physiology based human body model of blast injury of mounted & dismounted soldier (MRMC)
- Physical surrogate and virtual human for non-lethal weapons (Navy)
- Neck and shoulder injury models, extra-skeletal support, …

19

U.S. ARMY TANK AUTOMOTIVE RESEARCH, DEVELOPMENT AND ENGINEERING CENTER (TARDEC)

Comparing the Use of Dynamic Response Index (DRI) and Lumbar Load as Relevant Spinal Injury Metrics

Ravi Thyagarajan
Jai Ramalingam
Kumar Kulkarni
TARDEC/Analytics

Workshop on Numerical Analysis of Human and Surrogate Response to Accelerative Loading
Army Research Laboratory (ARL)
Aberdeen, MD
Jan 7-9, 2014

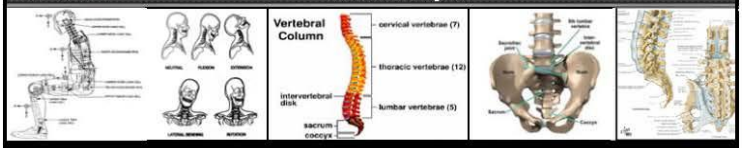

OUTLINE

- Mechanical and Injury Models for DRI
- Mechanical and Injury Models for Lumbar Load
- DRI and LL: Temporal Behavior
- M&S Model Descriptions
- Behavior of Peak Compressive LL vs. DRI Cross-plots
- Proposal for Mechanical Model for Encumbered DRI
- Known Issues with DRI
- Summary / Conclusions

Dynamic Response Index (DRI) – Mechanical Model

- Simple lumped mass parameter model (single spring-mass-damper) to simulate the biomechanical response of the human upper body/vertebral column/pelvis [2,3]
- Values of **m**, **k**, **c** (and thus ω_n, ζ) were derived by compressive strengths of individual vertebrae [1], and load-deflection curves [4]
- Values established for a representative population of Air Force pilots with a mean age of 27.9 years [3]

  m = 34.51 kg
  k = 9.66E04 N/m
  c = 818.1 Nsec/m
- ω_n = 52.9 rad/s, and $\zeta = 0.224$
- Lumbar Force = $k*\delta$
- Maximum Lumbar Force = $k*\delta_{max}$

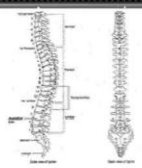

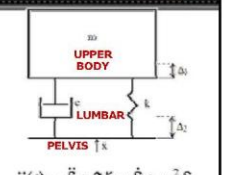

$$\ddot{x}(t) = \ddot{\delta} + 2\xi\omega_n\dot{\delta} + \omega_n^2\delta$$

- δ is the relative displacement between the upper body and pelvis $(\delta=\Delta_1-\Delta_2)$
- ζ is the damping coefficient[33] (0.224) $\zeta = c/(2*sqrt(m*k))$
- ω_n is the natural frequency[33] (52.9 rad/s) $\omega_n = sqrt(k/m)$
- **Normalized Lumbar Force** $= (k*\delta_{max}) / (mg) = \omega_n^2 * \delta_{max}/g$

$$DRI = \frac{\omega_n^2 \delta_{max}}{g}$$

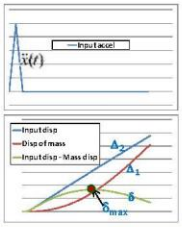

Maximum Lumbar Force, when normalized by the weight m*g, is called DRI

Dynamic Response Index (DRI) – Injury Risk Model

- During World War II, Geertz generated data on compressive vertebral strengths either with individual vertebrae or vertebral complexes of PMHS between 19 and 46 years old [1]
- Stech and Payne [3] used the above to relate the DRIz to an injury risk of 50% vs age, and for an average age of 27.9 of Air Force pilots, estimated a DRIz of 21.3 (7220N/1622 lbf). Brinkley used a normal distribution around this to set up the **laboratory data curve** [5]
- DRI value of 17.7 leads to a 10% risk of spinal injury (corresponds to 5992 N/1346 lbf)
- Injury model based on the laboratory data curve has the pelvis as point of initiation, so as far as possible, the pelvic acceleration rather than the seat acceleration should be used to calculate the DRI [13]

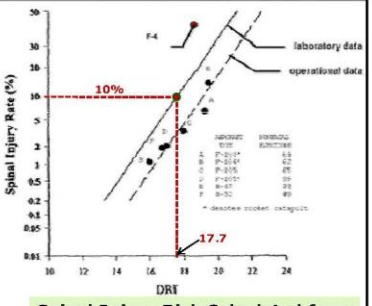

Spinal Injury Risk Calculated from Laboratory and Operational Data valid for AIS 2+ Injuries [3,5] .

- Quasi-static testing on PMHS specimens led to a 10% risk of spinal injury for DRI = 17.7
- Underlying principles for DRI model are based on lumbar load

Compressive Lumbar Load (LL) – Mechanical Model

- Development of anthropomorphic test devices (ATD) and subsequent addition of load transducers in them represents a revolutionary increase in capability [20]
- Curved lumbar spine is incorporated to replicate typical seated automotive occupant positions, also used in military vehicle applications
- Three-Axis Lumbar Spine Load Cell measures time-dependent forces/moment at desired sampling rates during blast/crash
- Lumbar load cell did not adversely affect measured accelerations and forces, nor modify the spinal flexural characteristics [17]
- ATDs capable of producing reproducible results in greater detail under controlled testing conditions
- Biofidelic enhancements to the Hybrid III design were made which support its use in predicting human injury during high-speed dynamic events [20]

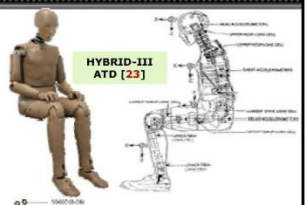

Part 572 Hybrid-III Lower Torso Assembly [23]

Lumbar Force measured here is a "direct" representation of lumbar response/injury

Compressive Lumbar Load (LL) – Injury Risk Model

Source	Chandler [7,10]	Tremblay [24], Ripple [25]	Mertz [18,21,22,12]
Approach	• Proposed for aircraft seats • Derived a compression force criterion by correlating the DRI and maximum compression force measured on a H-II lumbar load spine cell in 12 tests • 1500 lb / 6675 peak value corresponds to a DRI of ~19 • Adopted by FAA Regulations in Title 49/CFR 572	• Proposed by Tremblay based on Ripple and Mundie's paper, but that paper doesn't specify any tolerance values, so not clear on origin • NATO RTO-TR-HFM-090 suggests that these criteria arise from Mertz criteria [19] for a scaling factor of 3.4-3.8, which also does not match the paper. • Perhaps Tremblay meant to refer to Alem [8], who also refers to a factor 3.4 that was used on Mertz's neck data in estimating 6675 N for peak lumbar load	• Tolerance curves for compressive neck loading in high school football players and the adult populace using a H-III ATD outfitted with a football helmet impacted by a tackling block • Scaling factor from neck to lumbar based on waist and neck dimensions • Limiting force rationale (ratio applied to large-duration value); more conservative in mitigating lumbar spine injuries
ATD	H-II Straight Lumbar Spine	Unknown	H-III Curved Lumbar Spine
	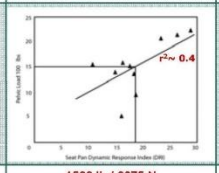	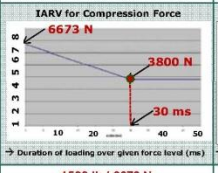	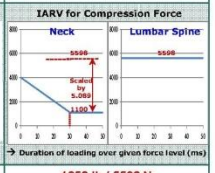
Peak LL Criterion (C)	1500 lb / 6675 N	1500 lb / 6673 N	1258 lb / 5598 N

Different approaches, but they lead to similar injury criteria for Compressive Lumbar Load

DRI and LL: Temporal Behavior

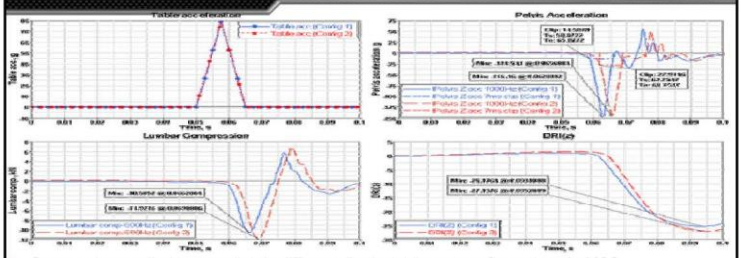

- Same pulse applied to two slightly different (both rigid) seat configurations in M&S
- Direct value of LL for C1 is 10.5 KN, indirect value (from DRI) is 8.5 KN; In addition, time of occurrence of the peak is quite different (8.7 ms after table peak for LL vs. 35.9 ms for DRI)
- The larger shift means that later changes in Pelvic accel will still affect DRI, but not peak LL
- Peak LL for C2 shifted by 2.8 ms vs. C1, and value higher by 13%
- Pelvic acceleration peak for C2 shifted by 2.8 ms, only 1% less, but wider (based on 7 ms clip)
- DRI for C2, calculated from pelvis acceleration, is shifted by 1.8 ms, value higher by only 8%

DRI does not track direct LL well in the time domain and can be affected by minor late data

M&S Model Description - MADYMO

MADYMO Dynamic simulation model including Q-version of AM50 H-III ATD

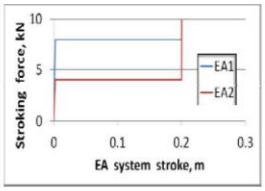

In addition to Rigid Seat, two other EA seats (4 and 8 KN limiting force) were also included

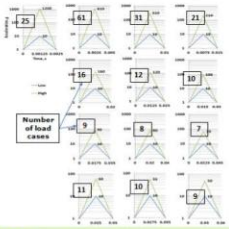

230 Triangular blast inputs were used for each of the 3 seats

- A triangular blast wave pulse was applied to the vertical drop tower/sled.
- For unencumbered occupant: A total of eleven duration levels are studied; from 2 ms to 60 ms. At each ΔT, peak deceleration was varied from 10g to 1200g in 10g increments up to the point when Δv reached ~15m/s, where Δv =0.5*Peak acceleration*ΔT (230 runs for each seat type)
- ~30 kg of encumbered PPE mass on the typical AM50 soldier was lumped on the upper torso, and 31 simulations were run covering Peak acceleration between 10-360g, **ΔT** between 5-15 ms (corresponding to a Δv between 1.5-12 m/s) for encumbered occupants

Systematic study was performed on MADYMO ATD setup for a large sample of input pulses

M&S Model Description - LSDYNA

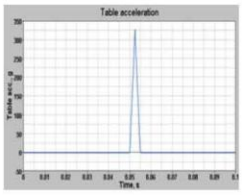

Un-Encumbered AM50 H-III Occupant | Encumbered AM50 H-III Occupant | Triangular pulse applied to table of magnitude Ap and time duration ΔT

- A triangular blast wave pulse was applied to the vertical drop tower/sled.
- Only rigid seats were used in the LS-DYNA simulations, and the Humanetics version [23] of the LS-DYNA ATD (military version) were used
- For encumbered occupant studies, the vest and helmet were modeled in FEA using finite elements. The remaining PPE mass on the upper body of a typical AM50 encumbered soldier (~30kg - mass of vest) was lumped on the vest
- 31 simulations were run covering Peak acceleration between 10-360g, **ΔT** between 5-15 ms (corresponding to a Δv between 1.5-12 m/s) for both unencumbered and encumbered occupants

A reduced set of simulations were performed on LS-DYNA ATD setup

Behavior of Peak Compressive LL vs. DRI

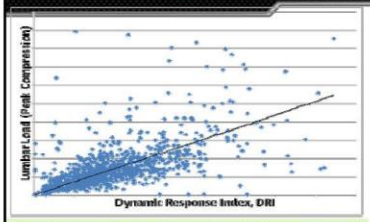

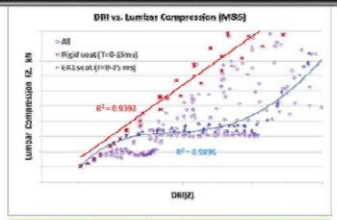

Data from underbody mine tests (~1200 samples) | Data from MADYMO M&S (~700 samples)

- DRI and LL test data have been obtained for restrained occupants (usually encumbered) from a multitude of vehicles of different sizes and weights subjected to underbody mines of different sizes, positioned in different seats in different vehicle positions and configurations.
- While amount of scatter is reduced for M&S data, it is clear that there is a lack of a general overall governing relationship between DRI and Peak LL.
- When some other factors are also included, for example, only data for a seat type and a reduced range of DT, some patterns can be discerned in the M&S data.
- One interesting observation is that based on previously described IARVs, for 94% of the samples in test and 89% in M&S, DRI and LL both predict the same outcome (incapacitation, or no incapacitation)

Mechanical Model for DRI of Encumbered Occupant (DRI')

M corresponds to the weight to be added to m in DRI calculator to account for encumbrance on upper body of occupant. It is usually only a fraction of the actual physical weight of the encumbrance.

Example: M=30.4 kg

	Unencum	Encum #1	Encum #2
m	m	m+M	m+M
k	k	k	k
c	c	c	c
ω^2_n	k/m	k/m	k/(m+M)
DRI	$\frac{\omega_n^2 \delta_{max}}{g} = \frac{(k*\delta_{max})}{mg}$	$\frac{\omega_n^2 \delta'_{max}}{g} = \frac{(k*\delta'_{max})}{mg}$	$\frac{\omega_n^2 \delta'_{max}}{g} = \frac{(k*\delta'_{max})}{(m+M)g}$
IARV	17.7	17.7	$\frac{17.7}{(1+M/m)}$
RI = DRI / IARV	$\frac{k*\delta_{max}}{17.7*mg}$	$\frac{k*\delta'_{max}}{17.7*mg}$	$\frac{k*\delta'_{max}}{17.7*mg}$

	Unencum	Encum #1	Encum #2
m, kg	34.51	64.91	64.91
k, N/m	9.66E4	9.66E4	9.66E4
c, Ns/m	818.1	818.1	818.1
ω^2_n	2799.2	2799.2	1488.2
DRI	285.34* δ_{max}	285.34* δ'_{max}	151.86* δ'_{max}
IARV	17.7	17.7	9.4
RI = DRI / IARV	16.1* δ_{max}	16.1* δ'_{max}	16.1* δ'_{max}

- The Mass quantity in the DRI SDOF calculator MUST be increased to compensate for the encumbrance (actual factor to be used (<1) on added mass is under review)
- Approach #1 is strongly preferred since the familiar IARV values (17.7) are still the same

Lumbar Load as Relevant Spinal Injury Metrics UNCLASSIFIED: Distribution Statement A. Approved for Public Release

DRI for Encumbered Occupants (DRI') - Example

Let's calculate DRI for unencumbered (m=34.51 kg) and encumbered (m=64.91 kg) occupants based on the SDOF system, i.e, assuming that an added mass of *30.4 kg* to the upper body *fully affects lumbar load and DRI*.

The analysis is being done for triangular pelvic accelerations all of fixed duration 5 ms, but the amplitude is allowed to vary from 25-300g

- From the max allowable lumbar load of 5992 N, it can be seen that a max pelvic acceleration of 188g and 131g can be withstood, for the unencumbered and encumbered occupants.
- Depending on the normalization constant used in determination of the encumbered DRI, the correct corresponding IARV must be used to get consistent and accurate results.
- Because the lumbar load (k*δ) is uniquely defined, it is a good idea to verify that DRI results are consistent with lumbar load.

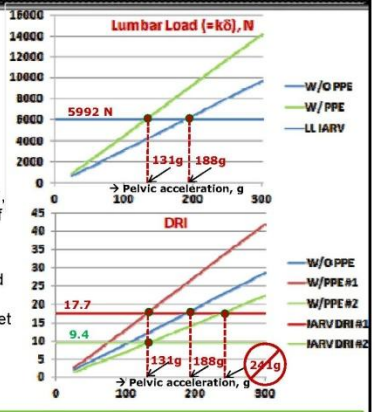

Depending on how the DRI calculator is coded and which normalization factor is used, the DRI value will be different and must be compared against the right IARV

Comparing the Use of Dynamic Response Index (DRI) and Lumbar Load as Relevant Spinal Injury Metrics UNCLASSIFIED: Distribution Statement A. Approved for Public Release [12

Behavior of Peak Compressive LL vs. DRI

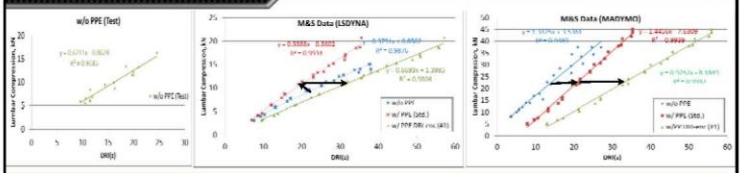

LL vs DRI behavior from drop tower tests (left), LSDYNA M&S (middle) and MADYMO (right) M&S

	Peak Acceleration,g	Duration, ms	ΔV, m/s
M&S	10 - 360	5 - 15	1.5 - 12
Test	3 - 285	5, 20	3 -7

- For a specific seat and limited ΔT range, DRI-LL relationship is linear in both tests and M&S
- For the LS-DYNA results, when the pelvic accels from increased upper body weights are run through the DRI calculator without changing the mass, the DRIs are seen to drop (red curve), which is not realistic, since the lumbar loads increased. Using DRI calculations as per #1, shifts to green curve, indicating higher DRIs as expected.
- For MADYMO results, because all the added weight affects pelvic accel, the DRI curve moves from blue to red, and increases even further as per #1. This indicates that a smaller factor (<1) needs to be applied to the physical added mass in order to accurately capture vest separation.

DRI (properly calculated) and LL both go up for encumbered occupants

Comparing the Use of Dynamic Response Index (DRI) and Lumbar Load as Relevant Spinal Injury Metrics UNCLASSIFIED: Distribution Statement A. Approved for Public Release 13

DRI - Applicability to Ejection Seats

- Stech and Payne also presented the injury risk for operationally experienced non-fatal spinal injuries in ejection seat tests, shown as **operational data curve [3, 5?]**
- F-4 operational data [5] does not match the injury trend. For the F-4 DRI value of ~19, the operational data curve yields 9% risk of injury, not the observed 34% in reality.
- DRI-Injury Rate Relationship is only valid for misalignments of the seat with respect to the catapult direction < 5 degrees, which was not true for the F-4 seat
- In a survey of 223 ejections by British aircraft pilots over 1968-83, Anton [8] found a poor agreement between the incidence of spinal fracture and the DRI for ejections from 5 out of 6 ejector seats and concluded that predictors such as DRI "**have no apparent practical utility**" [11]

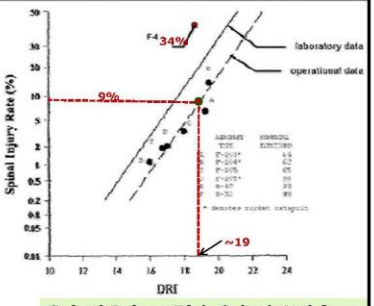

Spinal Injury Risk Calculated from Laboratory and Operational Data valid for AIS 2+ Injuries [3,5] .

Ejector Seat Data raises doubts as to suitability of the DRI as an injury measure [11]

Comparing the Use of Dynamic Response Index (DRI) and Lumbar Load as Relevant Spinal Injury Metrics UNCLASSIFIED: Distribution Statement A. Approved for Public Release 14

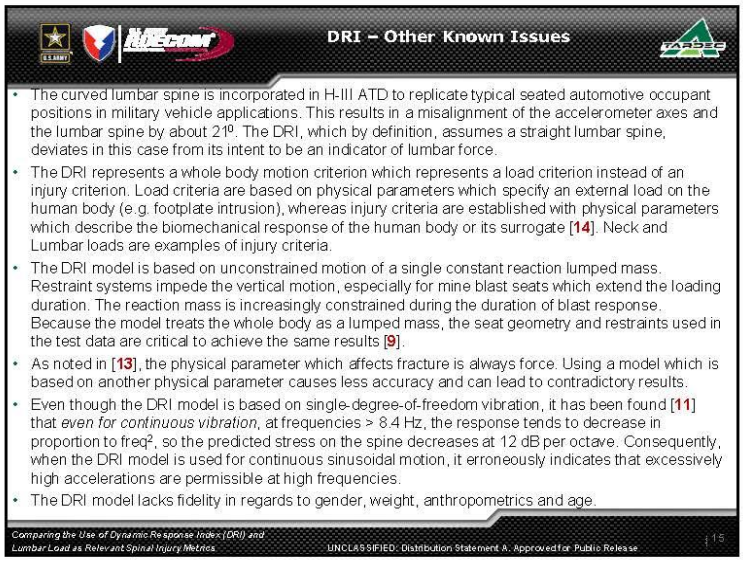
DRI – Other Known Issues
• The curved lumbar spine is incorporated in H-III ATD to replicate typical seated automotive occupant positions in military vehicle applications. This results in a misalignment of the accelerometer axes and the lumbar spine by about 21⁰. The DRI, which by definition, assumes a straight lumbar spine, deviates in this case from its intent to be an indicator of lumbar force.
• The DRI represents a whole body motion criterion which represents a load criterion instead of an injury criterion. Load criteria are based on physical parameters which specify an external load on the human body (e.g. footplate intrusion), whereas injury criteria are established with physical parameters which describe the biomechanical response of the human body or its surrogate [14]. Neck and Lumbar loads are examples of injury criteria.
• The DRI model is based on unconstrained motion of a single constant reaction lumped mass. Restraint systems impede the vertical motion, especially for mine blast seats which extend the loading duration. The reaction mass is increasingly constrained during the duration of blast response. Because the model treats the whole body as a lumped mass, the seat geometry and restraints used in the test data are critical to achieve the same results [9].
• As noted in [13], the physical parameter which affects fracture is always force. Using a model which is based on another physical parameter causes less accuracy and can lead to contradictory results.
• Even though the DRI model is based on single-degree-of-freedom vibration, it has been found [11] that *even for continuous vibration*, at frequencies > 8.4 Hz, the response tends to decrease in proportion to freq², so the predicted stress on the spine decreases at 12 dB per octave. Consequently, when the DRI model is used for continuous sinusoidal motion, it erroneously indicates that excessively high accelerations are permissible at high frequencies.
• The DRI model lacks fidelity in regards to gender, weight, anthropometrics and age.
Comparing the Use of Dynamic Response Index (DRI) and Lumbar Load as Relevant Spinal Injury Metrics
UNCLASSIFIED: Distribution Statement A. Approved for Public Release
15

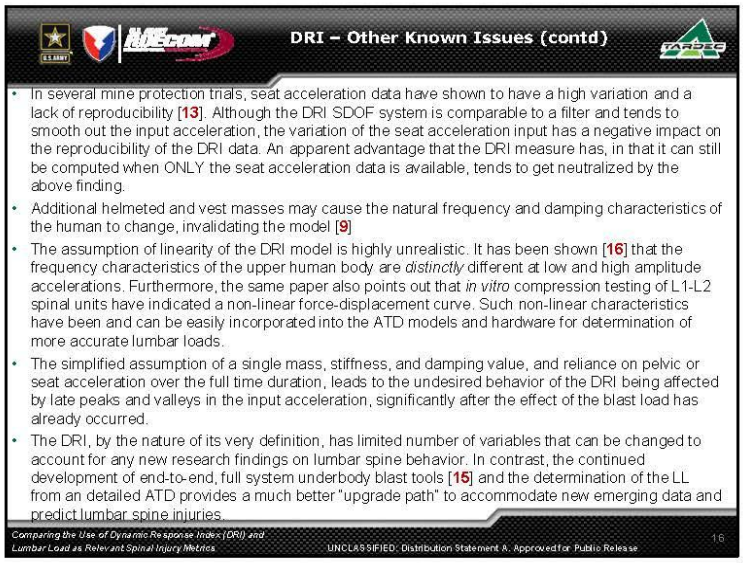
DRI – Other Known Issues (contd)
• In several mine protection trials, seat acceleration data have shown to have a high variation and a lack of reproducibility [13]. Although the DRI SDOF system is comparable to a filter and tends to smooth out the input acceleration, the variation of the seat acceleration input has a negative impact on the reproducibility of the DRI data. An apparent advantage that the DRI measure has, in that it can still be computed when ONLY the seat acceleration data is available, tends to get neutralized by the above finding.
• Additional helmeted and vest masses may cause the natural frequency and damping characteristics of the human to change, invalidating the model [9]
• The assumption of linearity of the DRI model is highly unrealistic. It has been shown [16] that the frequency characteristics of the upper human body are *distinctly* different at low and high amplitude accelerations. Furthermore, the same paper also points out that *in vitro* compression testing of L1-L2 spinal units have indicated a non-linear force-displacement curve. Such non-linear characteristics have been and can be easily incorporated into the ATD models and hardware for determination of more accurate lumbar loads.
• The simplified assumption of a single mass, stiffness, and damping value, and reliance on pelvic or seat acceleration over the full time duration, leads to the undesired behavior of the DRI being affected by late peaks and valleys in the input acceleration, significantly after the effect of the blast load has already occurred.
• The DRI, by the nature of its very definition, has limited number of variables that can be changed to account for any new research findings on lumbar spine behavior. In contrast, the continued development of end-to-end, full system underbody blast tools [15] and the determination of the LL from an detailed ATD provides a much better "upgrade path" to accommodate new emerging data and predict lumbar spine injuries.
Comparing the Use of Dynamic Response Index (DRI) and Lumbar Load as Relevant Spinal Injury Metrics
UNCLASSIFIED: Distribution Statement A. Approved for Public Release
16

Summary / Conclusions

- DRI has the attraction of being an apparently simple, tangible model which clearly had high utility before the advent of detailed ATDs that could produce reproducible results in controlled testing.
- While DRI can be calculated when only seat accelerations are available and indeed may be the only injury measure that can be calculated in such a case (like when an ATD is not used), the consistency and usefulness of such data is highly questionable due to the variability in the seat accelerations.
- Human responses are highly nonlinear, and to expect a simple linear model such as DRI to be capable of responding accurately to a wide range of shock amplitudes is highly unrealistic.
- DRI and LL responses are both dynamic, and the peak values may even be in the ball-park, but DRI lags far behind as to when the peak occurs due to the use of only one frequency characteristic. This can lead to unrealistic consequences where later changes in pelvic acceleration can affect the DRI.
- There is a lack of any kind of overall general correlation between DRI and LL.
- Requiring pelvic accelerations for accurate DRI calculations means ATD is required. In which case, the lumbar load can be directly measured and compared against its IARV.
- Calculating DRI for encumbered occupants can be tricky in that while it is clear that the increased mass increases the lumbar load, what factor to use on the actual physical mass is still not clear. Also, it is recommended that if DRI is used at all, that it be determined using the standard normalization constant so that the familiar DRI values are still preserved.
- The availability of force-based IARV injury criteria on direct measurements such as lumbar load, makes them highly attractive as candidates for incapacitation assessment for the lumbar region.

Too simple, Too many assumptions, Too many questions.... DRI had an important role 50 years ago in the evolutionary timeline, but has the since largely outlived its utility

..... Time to move to a more "direct" injury measure (Lumbar Load from detailed ATDs)

GLOSSARY / ACRONYMS

AIS	Abbreviated Injury Scale
AM50	American Male 50th Percentile
APG	Aberdeen Proving Grounds, Maryland
ARL	Army Research Laboratory
ATD	Anthropomorphic Test Device
ATEC	Army Test and Evaluation Center
COTS	Commercial-off-the-Shelf
DOF	Degree-of-Freedom
FEA/FEM	Finite Element Analysis/Method
g	acceleration due to gravity
H-II / H-III	Hybrid-II or Hybrid-III ATD
kg	kilogram, unit of mass; 1kg ~ 2.204 lb
lb/lbf	pounds, pounds of force; 1lbf ~ 4.45 N
IARV	Injury Assessment Reference Value
LL	Lumbar Load
LSDYNA	COTS structural dynamics software from LSTC, CA
LSTC	Livermore Software Technology Corporation, CA
ms	msec, milliseconds, unit of time (1 ms = 0.001 second)
M&S	Modeling & Simulation
MADYMO	MAthematical DYnamic MOdels (COTS software from TNO)
N	Newtons, unit of force, 1 N ~ 0.22472 lbf
OCP	Occupant-Centric Platform
PMHS	Post-mortem Human Specimens
R&D	Research & Development
RDECOM	Research, Development and Engineering Command
RI	Relative Injury Index = Injury Value / IARV
SimBRS	Simulation-Based Reliability and Safety
SDOF	Single Degree-of-Freedom
SLAD	Survivability and Lethality Analysis Directorate in ARL
TARDEC	Tank Automotive Research, Development and Engineering Center
T&E	Test & Evaluation
UBM	Underbody Blast Modeling/Methodology
WMRD	Weapons and Materials Research Directorate in ARL

ACKNOWLEDGMENTS / DISCLAIMER

ACKNOWLEDGMENTS

The authors would like to thank the Blast Protection for Platforms and Personnel Institute (BP3I) program managed by ARL/WMRD and the HPC Modernization Office, for the partially funding of this project. The authors also gratefully acknowledge physical test data provided by Mr Craig Barker/Mr Brian Benesch of ARL/SLAD, and Mr Ami Frydman of ARL/WMRD. We express our gratitude to Dr. Harold (Bud) Mertz for reviewing this material and providing valuable feedback.

This material is based on R&D work partially supported under Contract No. W56HZV-08-C-0236, through a subcontract with Mississippi State University (MSU), and was performed for the Simulation Based Reliability and Safety (SimBRS) research program. Any opinions, finding and conclusions or recommendations in this paper are those of the authors and do not necessarily reflect the views of the U.S. Army TACOM Life Cycle Command.

DISCLAIMER

Reference herein to any specific commercial company, product, process, or service by trade name, trademark, manufacturer, or otherwise does not necessarily constitute or imply its endorsement, recommendation, or favoring by the United States Government or the Dept. of the Army (DoA). The opinions of the authors expressed herein do not necessarily state or reflect those of the United States Government, the DoD, or U.S. Army TACOM Life Cycle Command and shall not be used for advertising or product endorsement purposes.

REFERENCES

1. Ruff, S., *Brief Acceleration: Less than One Second*, German Aviation Medicine in World War II, Vol. I, Chapter VI-C, Dept of the Air Force, 1950
2. Latham, F., *A Study in Body Ballistics, Seat Ejection*, Proceedings of the Royal Society of London, Series B – Biological Sciences, Vol. 147, pp. 121-139, 1957
3. Stech, E.L. and Payne, P.R., *Dynamic Models of the Human Body*, Aerospace Medical Research Laboratory, Wright Patterson Air Force Base, Ohio, USA, 1969
4. Yorra, A.J., *The Investigation of the Structural Behavior of the Intervertebral Discs*, Master Thesis, Massachusetts Institute of Technology, 1956
5. Brinkley, J.W. and Shaffer, J.T., *Dynamic Simulation Techniques for the Design of Escape Systems: Current Applications and Future Air Force Requirements*, Symposium on Biodynamic Models and their Applications, Report No. AMRL-TR-71-29, Aerospace Medical Research Laboratory, Wright-Patterson Air Force Base, Ohio, USA, 1970
6. Alem, N.M., *Acceleration Injuries: Assessment Methods and Criteria*, Protection of Wheeled Vehicle Occupants from Landmine Effects, WTP 1, KTA 1-29, Melbourne Australia, 1996

REFERENCES

7. Chandler, R.F., *Human Injury Criteria Relative to Civil Aircraft Seat and Restraint Systems*, 851847, Society of Automotive Engineers, PA, USA, 1988
8. Anton, D.J., *The incidence of spinal fracture on Royal Air Force ejections 1968-1983*, Report No. 529, Aircrew Equipment Group, Royal Air Force, Institute of Aviation Medicine, Farmborough, UK, 1986
9. Caldwell, E., Gernhardt, M., Somers, J.T., Younker, D., Newby, *Evidence Report: Risk of Injury due to Dynamic loads*, Human Reseach Program, Human Health and Countermeasures Element, NASA –Johnson,TX, 2012
10. Spink, R.J., *Injury Criteria for the Analysis of Soldier Survivability in Accelerative Events*, ARL-TR-6121, 2012
11. Griffin, M.J., *Handbook of Human Vibration*, Academic Press, London, ISBN 0-123030412, 1990
12. Sanders, D., Hanlon, E., Howard, H., Mertz, H., Wodzinski, C., *Enhanced Injury Assessment Reference Value Report (DRAFT)*, OCP-TECD Report, Feb 2013
13. Final Report of HFM-090 Task Group 25, *Test Methodology for Protection of Vehicle Occupants against Anti-Vehicular Landmine Effects*, NATO RTO TECHNICAL REPORT TR-HFM-090, April 2007

REFERENCES

14. Dosquet, F., Lammers, C., Soyka, D., Hennemann, M., *Hybrid III Thoraco-lumbar Spine Impact Response in Vehicular Protection Applications for Vertical Impacts*, PASS, 2010
15. Thyagarajan, R., *End-to-end System level M&S tool for Underbody Blast Events*, 27th Army Science Conference, Army Technology Showcase, Orlando, FL, Nov 29 – Dec 2. DTIC Report # ADA550921, 2000
16. Nicol, J.J., *Modeling the Dynamic Response of the Human Spine to Mechanical Shock and Vibration Using an Artificial Neural Network*, Ph. D. Thesis, Simon Fraser University, Aug 1996
17. Schoenbeck, A., Forster, E., Rapaport, M., Domzalski, L., *Impact Response of Hybrid III Lumbar Spine to +Gz Loads*, 981215, Society of Automotive Engineers, Warrendale, PA, USA, 1998
18. Mertz, H.J., Irwin, A. L., Prasad, P., *Biomechanical and Scaling Bases for Frontal and Side Impact Injury Assessment Reference Values*, Stapp Car Crash Journal, 2003-22-0009, Vol. 47, pp. 155-188, October 2003
19. Mertz, H.J., Jr. and Patrick, L.M., *Investigation of the Kinematics and Kinetics of Whiplash*, 670919, Society of Automotive Engineers, Warrendale, PA, USA, 1967

REFERENCES

20. Mertz, H.J., *Injury Assessment Values Used to Evaluate Hybrid III Response Measurements*, GM submission USG 2284 to NHTSA Docket 74-14/Notice 32, 1984. Later reprinted in *Hybrid III: The First Human-Like Crash Test Dummy*, SAE PT-44, SAE, Warrendale, PA,1994
21. Mertz, H.J., Jarrett, K., Moss, S., Salloum, M. and Zhao, A., *The Hybrid III 10-Year-Old Dummy*, Stapp Car Crash Journal, Vol. 45, Warrendale PA, 2001
22. Mertz, H.J., Hodgson, V.R., Thomas, L.M., Nyquist, G.W., *An Assessment of Compressive Neck Loads Under Injury-Producing Conditions*, The Physicial and Sports Medicine, pp. 95-106, November 1978
23. Humanetics Innovative Solutions, *Hybrid-III 50th Male Dummy, 78051-218-H, FMVSS208, 49CFR Part 572, Subpart E, Hybrid-III 50th Male Dummy Parts Catalog, Rev. 4*, July 2013
24. Tremblay, J., Bergeron, D.M., Gonzalez, R., *Protection of Soft-Skinned Vehicle Occupants from Landmine Effects*, The Technical Cooperation Program (TTCP), WPN/TP-1, KTA 1-29, August 1998
25. Ripple, G.R. and Mundie, T.G., Medical Evaluation of Nonfragment Injury Effects in Armored Vehicle Live Fire Tests", ADA233058, Walter Reed Army Institute of Research (WRAIR), D.C., USA, 1989

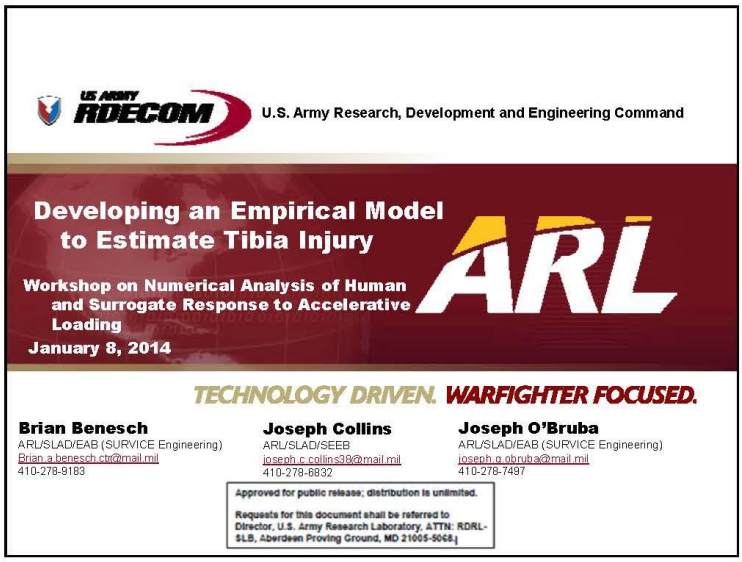
US ARMY RDECOM
U.S. Army Research, Development and Engineering Command
Developing an Empirical Model to Estimate Tibia Injury
Workshop on Numerical Analysis of Human and Surrogate Response to Accelerative Loading
January 8, 2014
ARL
TECHNOLOGY DRIVEN. WARFIGHTER FOCUSED.
Brian Benesch
ARL/SLAD/EAB (SURVICE Engineering)
Brian.a.benesch.ctr@mail.mil
410-278-9183
Joseph Collins
ARL/SLAD/SEEB
joseph.c.collins38@mail.mil
410-278-6832
Joseph O'Bruba
ARL/SLAD/EAB (SURVICE Engineering)
joseph.g.obruba@mail.mil
410-278-7497
Approved for public release; distribution is unlimited.
Requests for this document shall be referred to Director, U.S. Army Research Laboratory, ATTN: RDRL-SLB, Aberdeen Proving Ground, MD 21005-5068.


US ARMY RDECOM
Agenda
ARL
• Introduction
• Approach
• Results
• Discussion
• Caveats
• Conclusion
TECHNOLOGY DRIVEN. WARFIGHTER FOCUSED.
2

C140

Introduction

Issue/background

- Under-body blast (UBB) can induce lower extremity fractures to seated occupants.
- The test and evaluation community currently lacks reduced-order (RO) tools capable of accurately and efficiently estimating these injuries.
- Assessing occupant injury from data from anthropomorphic test devices (ATDs) in live-fire (LF) tests is the most common method of evaluating occupant injury.
- But it is also important to interpret the vehicle's structural response in terms of injury-causing potential.

Objective

Can empirical models be developed to estimate lower-leg injuries based on structural response data?

TECHNOLOGY DRIVEN. WARFIGHTER FOCUSED.

3

Approach: Test Data

Overall approach: Perform a correlation analysis between floor accelerometer data and lower-leg responses of associated ATDs from LF test events.

- Fifty-two predictor metrics were associated with two response metrics
- Focused on the cases with the most complete datasets: *accelerometer mounted on a floor panel within approximately six inches of one or more of an ATD's feet where the ATD is fitted with combat boots and seated with normal hip and knee angles.*
- Test data was taken from over two hundred UBB events against vehicles.

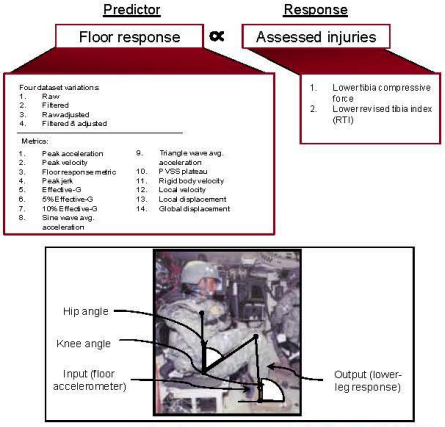

TECHNOLOGY DRIVEN. WARFIGHTER FOCUSED.

4

Approach: Correlation Analysis

- Simple linear regression analyses conducted for one- (linear) and two-predictor (quadratic) models as a function of each response
  - Coefficient of determination, R^2, was calculated for each model
  - Prediction intervals (PIs) calculated around the models using a student t-distribution of the data
  - Response plots (actual versus model) generated
- Logistic regression analyses performed to identify the probability of exceeding the injury threshold value (confidence intervals calculated as well).

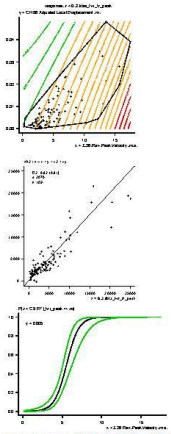

TECHNOLOGY DRIVEN. WARFIGHTER FOCUSED.

5

Results: Predicting Force and RTI

- Quadratic models with predictors, *raw peak velocity* and *adjusted local displacement*, were found to yield the best relationship with lower tibia compressive force and RTI.
- The model to estimate lower tibia force and RTI is described by:

$$z = \boldsymbol{v}^T \boldsymbol{b} \pm \gamma s \sqrt{1 + \boldsymbol{v}^T \boldsymbol{U} \boldsymbol{v}}$$

  - $\boldsymbol{v}$ is a vector of model terms (combination of x = raw peak velocity and y = local displacement)
  - $\boldsymbol{b}$ is a coefficient vector
  - $\boldsymbol{U}$ is a matrix of variance components
  - The form of the equation is consistent between the two injury types and the model terms, $\boldsymbol{v}$, are the same, but the values of $\boldsymbol{b}$ and $\boldsymbol{U}$ depend on the injury type (the specific values for each injury type are in the back-up)
  - The term following the +/- symbol represents the prediction interval where γ is the critical value for a *t*-distribution given the degrees of freedom equal to 104.

TECHNOLOGY DRIVEN. WARFIGHTER FOCUSED.

6

Results: Predicting Tibia Force

- The best two-predictor model for lower tibia compressive force resulted in an R^2 value of 0.82 on a set of 109 data points.
- The 90% PIs yield a variation in model results of about +/- 3500 N.

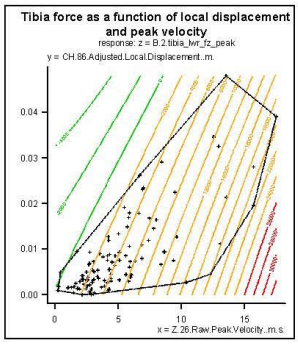

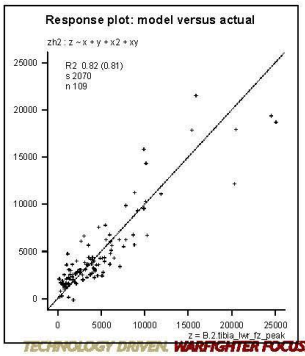

TECHNOLOGY DRIVEN. WARFIGHTER FOCUSED.

7

Results: Predicting Tibia RTI

- The best two-predictor model for lower tibia RTI resulted in an R^2 value of 0.81 on a set of 109 data points.
- The 90% PIs on this model yield a variation of about +/-0.54.

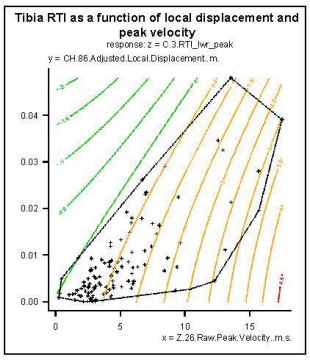

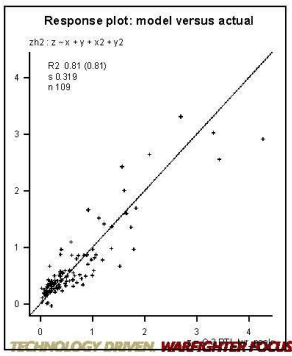

TECHNOLOGY DRIVEN. WARFIGHTER FOCUSED.

8

Results: Logistic Regression

- The logistic regression analysis for the best two predictors was performed based on the compressive force and RTI values relative to their appropriate injury threshold.
  - Tibia force: {no-injury < 7980 N ≤ injury}
  - Tibia RTI: {no-injury < 0.75 ≤ injury}
- The model to estimate the probability of exceeding the injury threshold is described by:

$$P(z > z_o) = \left(1 + e^{-\boldsymbol{v}^T \boldsymbol{b} \pm \gamma\sqrt{\boldsymbol{v}^T \boldsymbol{U} \boldsymbol{v}}}\right)^{-1}$$

  - $\boldsymbol{v}$ is a vector of model terms (combination of x = raw peak velocity and y = local displacement)
  - $\boldsymbol{B}$ is a coefficient vector
  - $\boldsymbol{U}$ is a matrix of variance components
  - The form of the equation is consistent between the two injury types and the model terms, $\boldsymbol{v}$, are the same, but the values of $\boldsymbol{b}$ and $\boldsymbol{U}$ depend on the injury type (the specific values for each injury type are in the back-up)
  - The term following the +/- symbol represents the prediction interval where γ is the critical value for a *t*-distribution given the degrees of freedom equal to 104.

TECHNOLOGY DRIVEN. WARFIGHTER FOCUSED.

9

Results: Predicting Probability of Tibia Force Injury

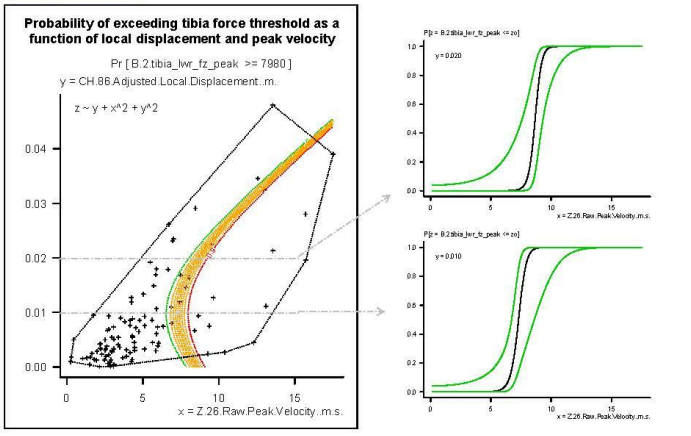

TECHNOLOGY DRIVEN. WARFIGHTER FOCUSED.

10

Results: Predicting Probability of Tibia RTI Injury

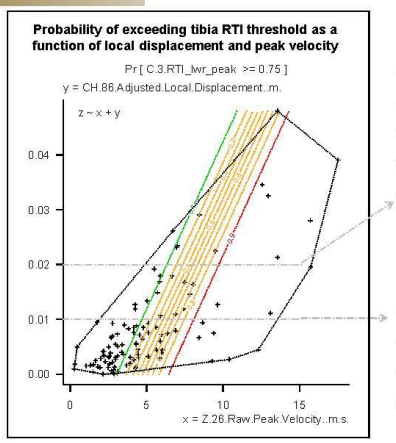

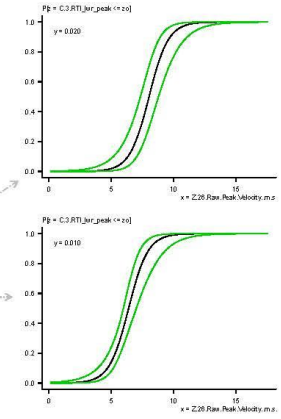

TECHNOLOGY DRIVEN. WARFIGHTER FOCUSED.

11

Discussion

- Models with greater than two predictors were not pursued because there is a diminishing return on R^2 relative to model complexity, the number of data points decreases, the domain of data becomes more sparse, and the quality of the model is hard to visually assess.
- Raw and filtered peak velocities were nearly identical; raw, filtered, and adjusted local displacements were nearly identical.
- Lower tibia compressive force and lower RTI are closely correlated with an R^2 value of 0.90.
- Force and RTI increases as velocity increases and local displacement decreases (i.e., a short duration velocity pulse is more severe than a longer duration velocity)

TECHNOLOGY DRIVEN. WARFIGHTER FOCUSED.

12

Caveats

- In order to utilize the empirical models, predictor data should be comparable to that obtained from floor-mounted accelerometers placed in armored ground vehicles subjected to an under-body blast.
  - The velocity and local displacement should lie within the dashed boundary lines shown in many of the earlier plots.
  - Using these models with predictor data different than this would be considered extrapolation.
- The results of these models provide estimates of lower leg injury responses for ATDs with booted feet placed flat on the same floor panel as the accelerometer, within about six inches of the accelerometer, and with the ATD hip and knee angles in normal positions.

Conclusion

- Empirical models were developed to estimate lower tibia compressive force and RTI injuries as a function of floor accelerometers' peak velocity and local displacement.
- These models can also serve as methods to assess severity of floor response from an under-body blast in terms of lower-leg injury potential and, at the very least, indicate the significance of peak velocity and local displacement to lower-leg injury assessed using ATDs.
- Future work will consist of performing controlled laboratory tests to further refine this correlation.

C146

Back-up: Variables for Empirical Models

Variables for Predicting Lower Tibia Compressive Force

$$\boldsymbol{b} = [137.64 \quad 771.25 \quad -127940 \quad 63.27 \quad -12767.2]$$

$$\boldsymbol{v} = \begin{bmatrix} 1 \\ x \\ y \\ x^2 \\ xy \end{bmatrix} \quad \boldsymbol{U} = \begin{bmatrix} 0.08677 & -0.0288 & 1.958 & 0.00176 & -0.203 \\ -0.0288 & 0.0157 & -3.485 & -0.00116 & 0.3382 \\ 1.958 & -3.484 & 1767.4 & 0.3125 & -165.07 \\ 0.00176 & -0.00116 & 0.3125 & 0.0001 & -0.0349 \\ -0.203 & 0.3382 & -165.07 & -0.0349 & 18.095 \end{bmatrix}$$

$$s = 2074.28 \quad d = 104$$

Variables for Predicting Lower Tibia RTI

$$\boldsymbol{b} = [0.0208 \quad 0.09719 \quad -17.961 \quad 0.00944 \quad -588.26]$$

$$\boldsymbol{v} = \begin{bmatrix} 1 \\ x \\ y \\ x^2 \\ y^2 \end{bmatrix} \quad \boldsymbol{U} = \begin{bmatrix} 0.0845 & -0.02542 & 0.3422 & 0.00139 & -6.852 \\ -0.02542 & 0.0118 & -1.957 & -0.000664 & 44.659 \\ 0.3422 & -1.957 & 1245.06 & 0.09033 & -28194.7 \\ 0.00139 & -0.000664 & 0.09033 & 0.000436 & -2.767 \\ -6.852 & 44.659 & -0.000282 & -2.767 & 808332.9 \end{bmatrix}$$

$$s = 0.318642 \quad d = 104$$

Variables for Probability of Lower Tibia Compressive Injury

$$\boldsymbol{b} = [-15.297 \quad 834.75 \quad 0.2119 \quad -0.00043]$$

$$\boldsymbol{v} = \begin{bmatrix} 1 \\ y \\ x^2 \\ y^2 \end{bmatrix} \quad \boldsymbol{U} = \begin{bmatrix} 49.57 & -0.00342 & -0.5736 & 151068 \\ -0.00342 & 296938 & 27.758 & -10677040 \\ -0.5736 & 27.758 & 0.00985 & -1857.5 \\ 151068 & -10677040 & -1857.5 & 492288236 \end{bmatrix}$$

Variables for Probability of Lower Tibia Compressive Injury

$$\boldsymbol{b} = [-6.1534 \quad 1.2949 \quad -212.03]$$

$$\boldsymbol{v} = \begin{bmatrix} 1 \\ x \\ y \end{bmatrix} \quad \boldsymbol{U} = \begin{bmatrix} 1.3389 & -0.302 & 49.076 \\ -0.302 & 0.08134 & -16.592 \\ 49.076 & -16.592 & 4787.09 \end{bmatrix}$$

TECHNOLOGY DRIVEN. WARFIGHTER FOCUSED.

15

PENNSTATE

Towards a Micromechanics-Based Simulation of Calcaneus Fracture and Fragmentation Due to Impact Loading

Reuben Kraft, PhD

Workshop on Numerical Analysis of Human and Surrogate Response to Accelerative Loading

Sponsored by the Warrior Injury Assessment Manikin Project Management Office and the Blast Protection for Platforms and Personnel Institute

Aberdeen Proving Ground, MD

January 7-9, 2014

Human body models will continue to offer great insight into military accelerative loading injuries…

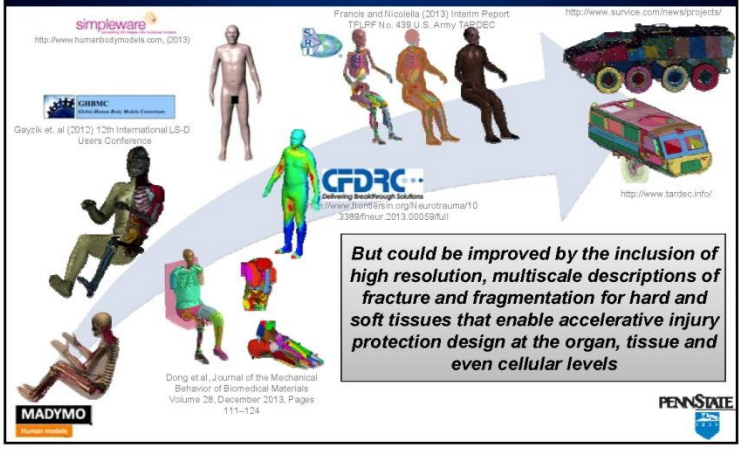

But could be improved by the inclusion of high resolution, multiscale descriptions of fracture and fragmentation for hard and soft tissues that enable accelerative injury protection design at the organ, tissue and even cellular levels

PENNSTATE

The calcaneus is a commonly fractured bone for both military and civilian populations.

Military

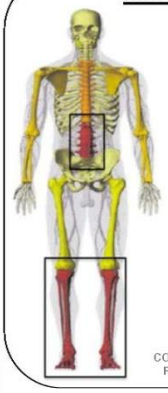

Head – 4%
Neck (hyoid) – <1%
Face – 8%

Hand – 2%
Upper Extremity – 10%

Spine
Cervical – 5%
Thoracic – 12%
Lumbar – 18%

Ribs/Sternum – 5%
Pelvis – 5%

Femur – 7%
Tibia/Fibula – 18%
Foot/Ankle – 26%

Of 456 WIA – 26% had Foot/Ankle Fractures

COL John Alvarez, NATO RTO HFM 207 (2011).

Civilian

Calcaneal fractures represent 60% of fractures involving the tarsal bones.

Badillo K et al. Radiographics 2011;31:81-92

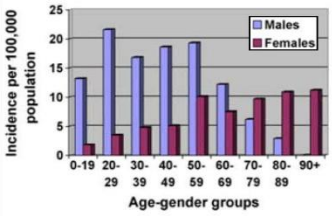

Mitchell, M. J., McKinley, J. C., & Robinson, C. M. (2009). The epidemiology of calcaneal fractures. The Foot, 19(4), 197-200.

The calcaneus is structurally and functionally unique.

External Features

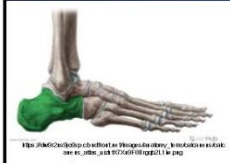

Kraft Lab
Penn State

3D Printed Calcaneus

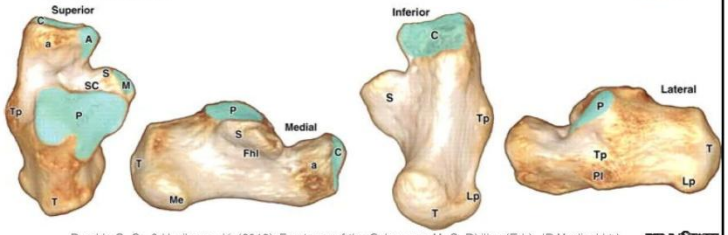

Parekh, S. G., & Hariharan, K. (2013). Fractures of the Calcaneus. M. S. Dhillon (Ed.). JP Medical Ltd.

PENNSTATE

The calcaneus is structurally and functionally unique.

Predominately cancellous in structure & enveloped in a shell of thin cortical bone

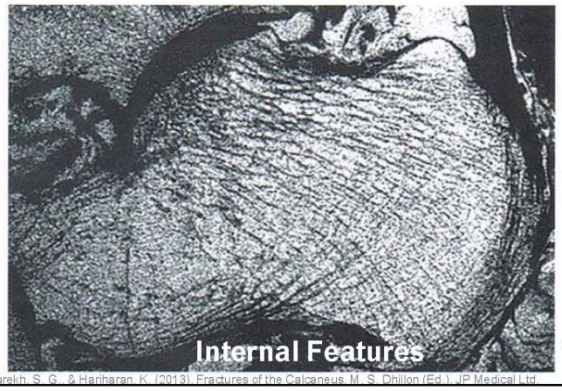

PENNSTATE

Parekh, S. G., & Hariharan, K. (2013). Fractures of the Calcaneus. M. S. Dhillon (Ed.). JP Medical Ltd.

The calcaneus is structurally and functionally unique.

Predominately cancellous in structure & enveloped in a shell of thin cortical bone

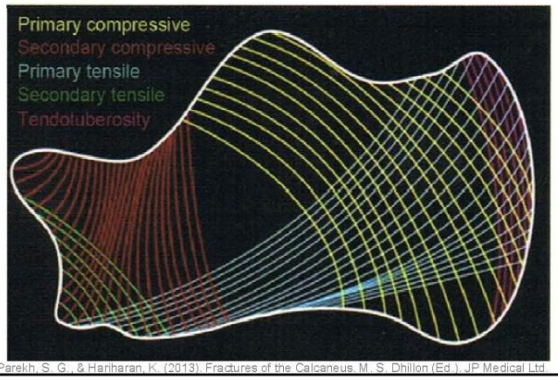

PENNSTATE

Parekh, S. G., & Hariharan, K. (2013). Fractures of the Calcaneus. M. S. Dhillon (Ed.). JP Medical Ltd.

Preliminary simulations (previously conducted) of lower extremity impact suggested calcaneus comminution.

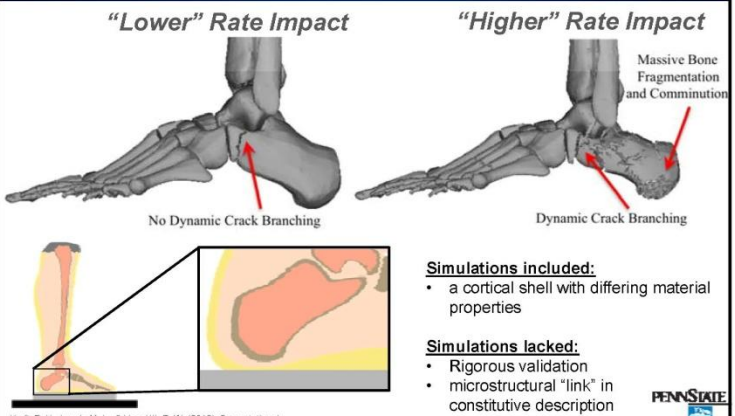

Simulations included:
- a cortical shell with differing material properties

Simulations lacked:
- Rigorous validation
- microstructural "link" in constitutive description

Kraft, P. H., Lynch, M. L., & Vogel III, E. W. (2012). Computational Failure Modeling of Lower Extremities (No. APL-PP-346).

The human bone models of Johnson, Socrate & Boyce (2010) worked to incorporate "microstructural features"

Cortical

$$\sigma(t) = E_0\varepsilon^{VE} + \eta_1\dot{\varepsilon}^{VE}\left(1 - e^{-\frac{E_1 t}{\eta_1}}\right) + \eta_e\dot{\varepsilon}^{VE}\left(1 - e^{-\frac{E_2 t}{\eta_2}}\right)$$

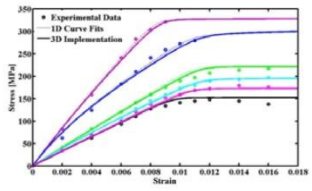

Trabecular

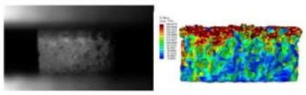

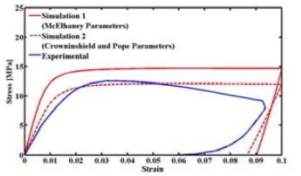

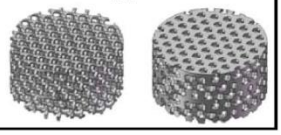

Did not include:
- Effect of material orientation
- Incorporation of material behavior that distinguishes between tensile and compressive loading modes
- Bone marrow

Johnson, T. P. M., Socrate, S., & Boyce, M. C. (2010). A viscoelastic, viscoplastic model of cortical bone valid at low and high strain rates. Acta biomaterialia, 6(10), 4073-4080.

Dynamic Fracture Studies of Pino & Radovitzky (2013)

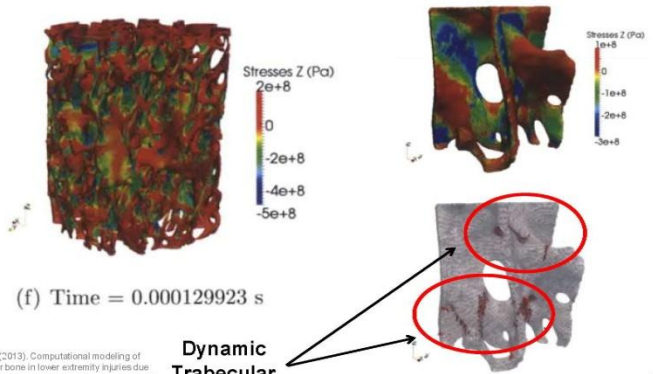

Pino, W. (2013). Computational modeling of trabecular bone in lower extremity injuries due to impact (Master's dissertation, Massachusetts Institute of Technology).

Dynamic Trabecular Fracture

PENNSTATE

Definitions of Various Microstructural Indices Should be Included in Damage Models

Microstructural Measure	Definition
Bone mineral density (MD)	2-D derivation of mineral density (g/cm2) as derived by DEXA
Bone volume fraction (BV/TV)	Relative percentage of bone within 3-D Region of Interest (ROI)
Connectivity density (ConnD)	Quantification of relative connectedness of one trabeculae to the next
Structural model index (SMI)	Quantification of relative shape of trabeculae from rod-like to plate-like
Trabecular number (TbN)	Quantification of relative number of individual trabeculae within 3-D ROI
Trabecular thickness (TbTh)	Quantification of relative thickness of individual trabeculae within 3-D ROI
Trabecular separation (TbSp)	Quantification of relative spacing between individual trabeculae within 3-D ROI
Mean intercept length (MIL)	Quantification of the three-dimensional anisotropy of a 3-D ROI. These numbers provides eigenvectors based on the fabric tensor that defines the principal direction of the ROI
Degree of anisotropy (DA)	Ratio of the largest to the smallest MIL value. It provides another way to quantify the relative anisotropy of the ROI

Two cadaveric calcanei were scanned with a industrial micro-CT

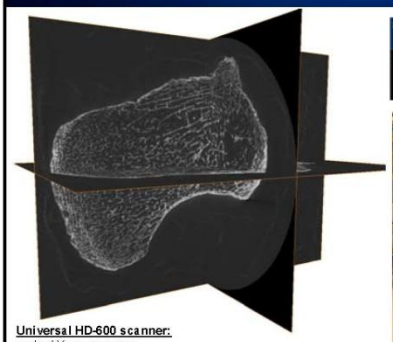

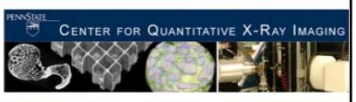

Universal HD-600 scanner:

- dual X-ray sources
- 1024 x 1024-pixel area detector with image intensifier
- continuously tiltable gantry for horizontal or vertical sample orientation
- The micro-focus source is an X-tek 225 kV, 225 watt tube with a minimum focal spot size of about 5 microns at 8 watts.
- The higher-power source is a Pantak 1600 watt sealed x-ray tube capable of 320 kV with the minimum focal spot of about 100 microns.
- capable of continuously variable magnification with pixel sizes approximately 1/1000 of the sample diameter.

PENNSTATE

Our measured cortical shell measurements are smaller then what is reported in literature

Coronal Plane @ slide 255
(Avg. Shell size .408mm)

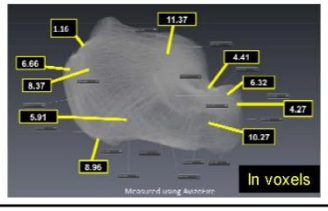

Distribution of Width Measurements

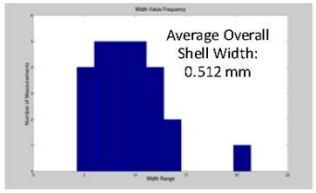

Cortical Thickness Measurements On the Calcaneus
(in millimeters)

	Male	Female	Total
Anterior Surface	2.2 + 0.3	2.1 + 0.2	2.15 + 0.1
Posterior Surface	3.6 + 0.1	3.0 + 0.3	3.3 + 0.2
Medial Surface	2.4 + 0.6	2.2 + 0.4	2.3 + 0.3
Lateral Surface	3.1 + 0.2	2.8 + 0.1	2.95 + 0.1

Average measured thickness: 2.675 mm

Sabry, Ebraheim, Mehalik, Rezcallah (2000)

PENNSTATE

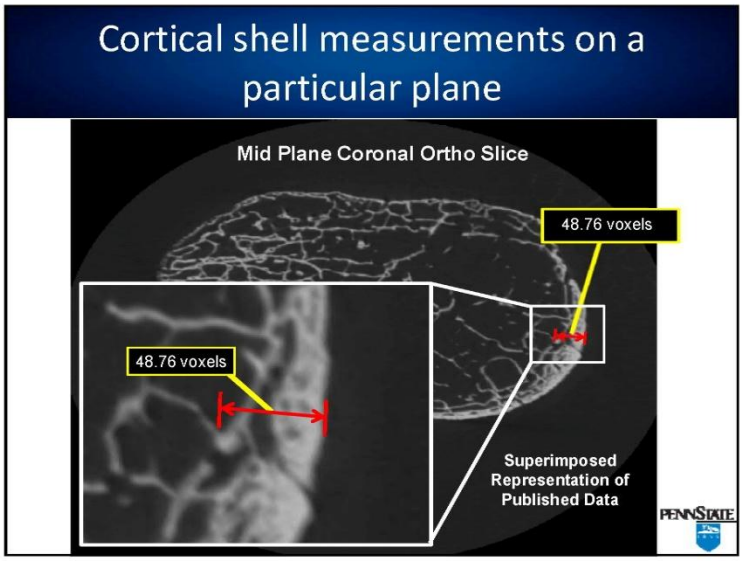
Cortical shell measurements on a particular plane
Mid Plane Coronal Ortho Slice
48.76 voxels
48.76 voxels
Superimposed Representation of Published Data
PENNSTATE

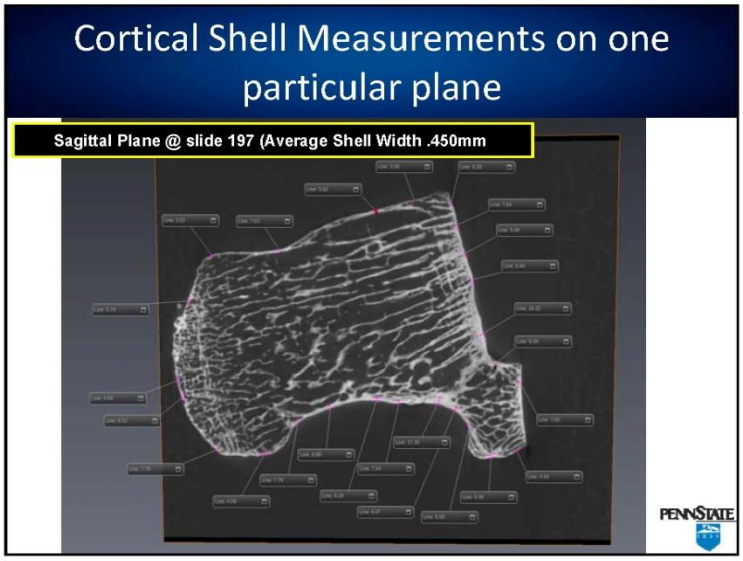
Cortical Shell Measurements on one particular plane
Sagittal Plane @ slide 197 (Average Shell Width .450mm
PENNSTATE

Segmentation was performed to obtain a surface mesh of the calcaneus

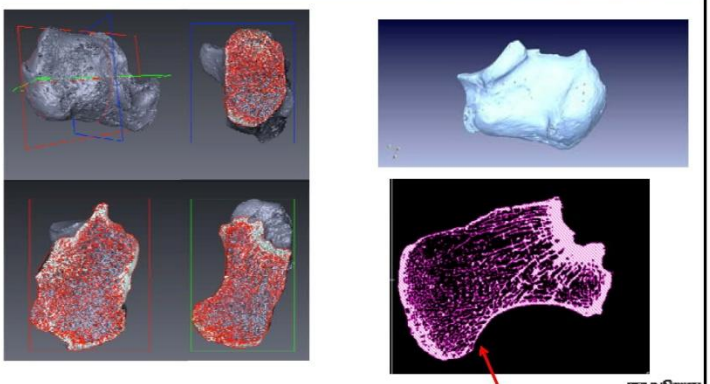

This looks like what Sabry et al. measured

PENNSTATE

The influence of bone marrow on dynamic loading of bone is unclear

- Bone marrow mechanical environment can be completely defined by quantifying and characterizing the hydrostatic pressure, fluid flow induced shear and viscosity in natural and altered conditions.

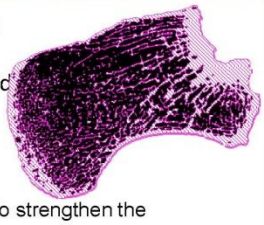

Gurkan and Akkus. (2008). *"The Mechanical Environment of Bone Marrow: A Review"*. Annals of Biomedical Engineering, Vol. 36, No. 12

- Three ways in which the marrow could function to strengthen the bone:
  - By pressing on the walls of the bone the marrow could prevent the bone from buckling.
  - By acting as a column in compression the marrow could support part of the load.
  - By viscous interaction with the trabeculae, the marrow could strengthen the trabecular bone.

Bryant, J. D. "The effect of impact on the marrow pressure of long bones *in vitro*." Journal of biomechanics 16.8 (1983): 659-665.

PENNSTATE

The 3D model is difficult to obtain, so in the mean time we examined a 2D model

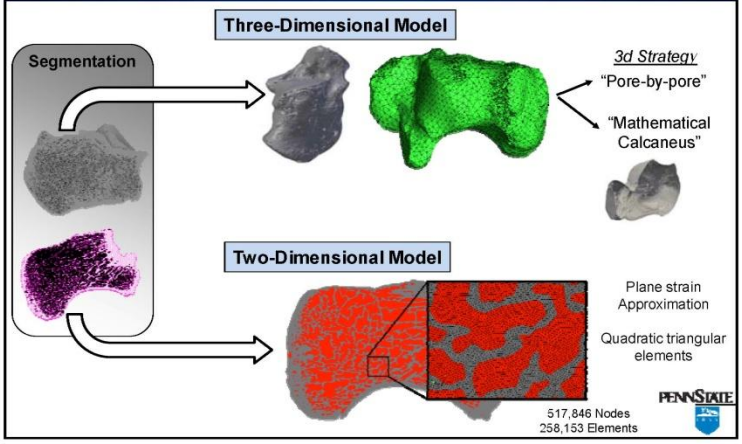

Our ultimate goal is to model fracture so we must consider important length and time scales

Time scales

Average longitudinal wave speed $c_{avg} \approx 3000$ m/s

Duration for wave to propagate across calcaneus ≈ 15 μs

Viscoelastic and viscoplastic time scales > 3.2 μs

Length scales

$$l_{cal} = 3.5 \text{ cm}$$

$$l_{trab} = 1 \text{ mm}$$

$$l_{cort} = 0.5 - 2 \text{ mm}$$

$$l_z = \frac{9\pi}{32} \frac{E}{(1-\nu^2)} \frac{G_c}{\sigma_c^2} = 2.21 \text{ mm}$$

$$l_{mesh} = l_z/5 = 0.44 \text{ mm}$$

To resolve physics associated with dynamics fracture Δt < 1ms and l_{mesh} < 0.44 mm, but this neglects microfractures that exist in bone:

$$l_{micro} = 50 - 100 \ \mu\text{m}$$

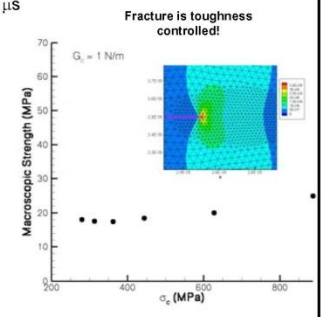

PENNSTATE

The mesh size required for toughness controlled fracture is achieved

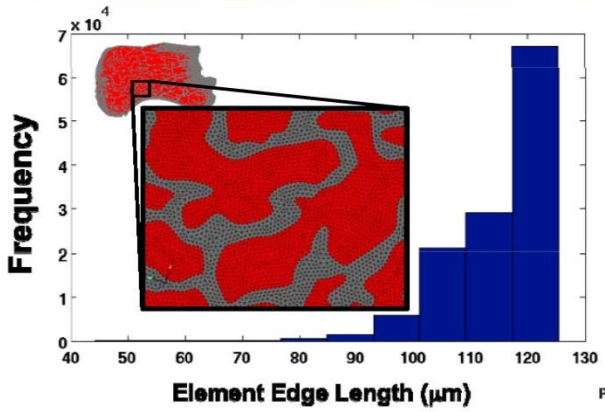

PENNSTATE

Our boundary conditions are very simple now, but we hope to introduce additional anatomy in the future

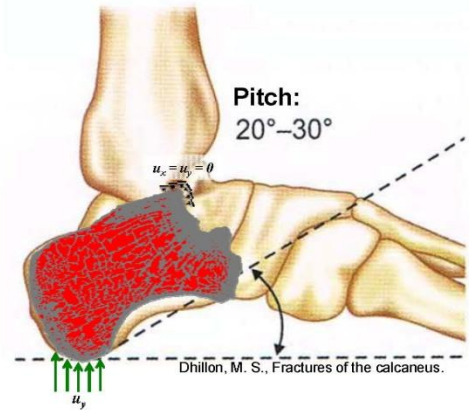

50 μm in 50 μs estimating the nominal strain rate of $\dot{\epsilon} = 28\ \mathrm{s}^{-1}$

PENNSTATE

So far we have examined three cases…

- Isotropic material, all with the same properties
- Heterogeneous material properties, but no cortical shel
- Heterogeneous material properties, with a cortical shell
  - Cortical bone
  - Trabecular bone
  - Bone Marrow

Cortical
ρ = 1810 kg/m^3
E = 15 GPa
ν = 0.4
σ_c = 100 MPa
K_{Ic} = 5 MPa m$^{1/2}$ [2]

Trabecular
ρ = 1400 kg/m^3
E = 200 MPa
ν = 0.45
σ_c = 10 MPa [4]
K_{Ic} = 0.5 MPa m$^{1/2}$ [1]

Marrow
Density = 1000 kg/m^3
K = 2.2 GPa [3]
ν = 0.49

[1] Cook, R. B., and P. Zioupos. "The fracture toughness of cancellous bone." Journal of biomechanics 42.13 (2009): 2054-2060.
[2] Ural, Ani, et al. "The effect of strain rate on fracture toughness of human cortical bone: A finite element study." Journal of the mechanical behavior of biomedical materials 4.7 (2011): 1021-1032.
[3] Gurkan, Umut Atakan, and Ozan Akkus. "The mechanical environment of bone marrow: a review." Annals of biomedical engineering 36.12 (2008): 1978-1991.
[4] Harrison, Noel M., et al. "Failure modelling of trabecular bone using a non-linear combined damage and fracture voxel finite element approach." Biomechanics and modeling in mechanobiology (2013): 1-17.

PENNSTATE

Including the Heterogeneous Structure Matters

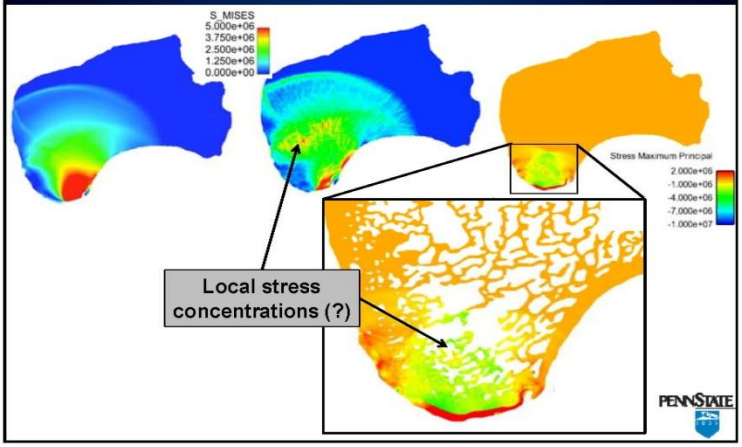

PENNSTATE

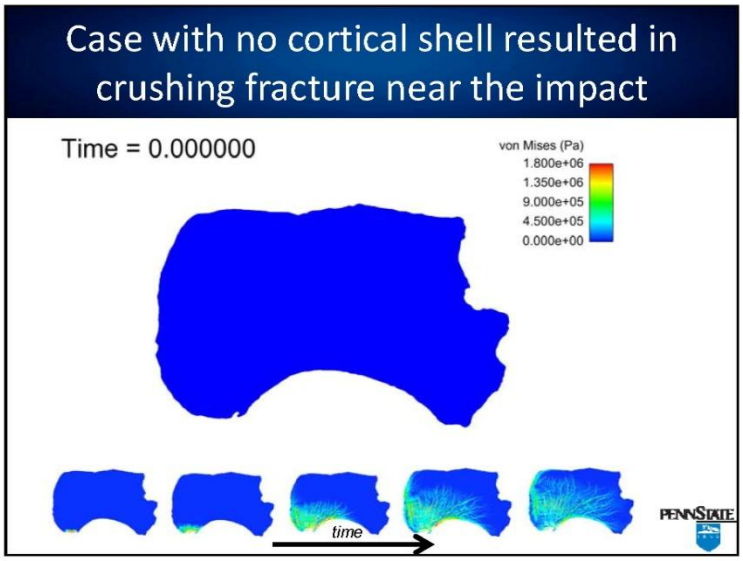
Case with no cortical shell resulted in crushing fracture near the impact
Time = 0.000000
von Mises (Pa)
1.800e+06
1.350e+06
9.000e+05
4.500e+05
0.000e+00
time
PENNSTATE

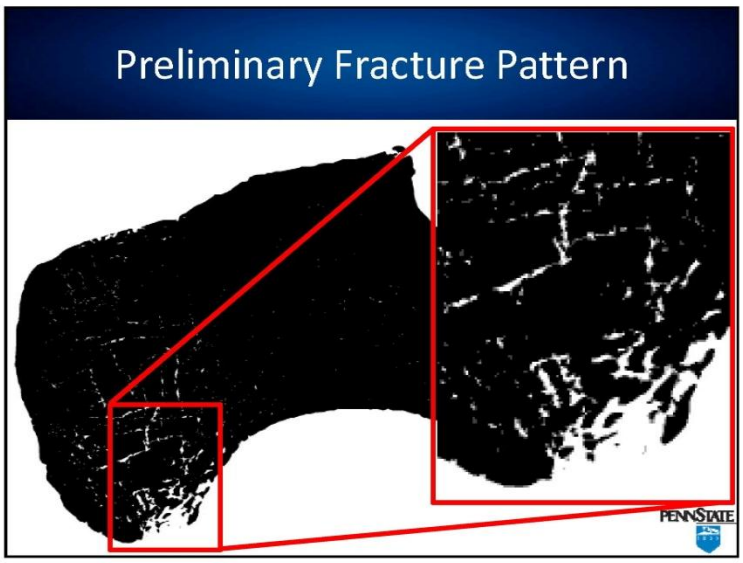
Preliminary Fracture Pattern
PENNSTATE

Including the cortical shell "shifts" stress diagonally to common fracture path

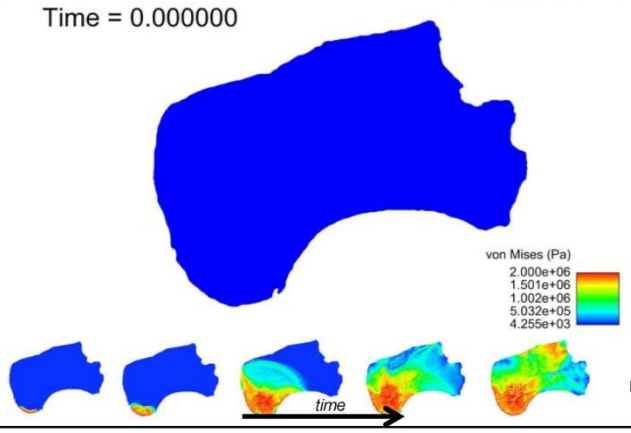

Including the cortical shell "shifts" stress diagonally to common fracture path

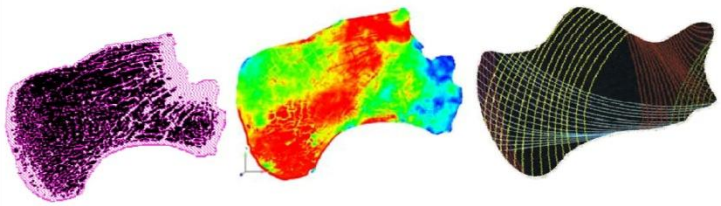

The weakest plane of resistance to stress is parallel to these organized trabeculae or through areas lacking trabeculae.
Sabry FF, Ebraheim NA, Mehalik JN, Rezcallah AT.

In the near future, we will focus on the following areas...

Continue to build 3D Model		two strategies: "pore-by-pore" and "mathematical calcaneus"
X-Ray Nanotomography		an anatomical study to examine critical calcaneal features
Anisotropic Measurements	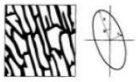	measure and integrate anisotropic descriptions
Additional Anatomy		include additional anatomy that will improve our boundary conditions
Fracture and Fragmentation Modeling	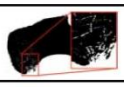	improve our fracture modeling approaches

First things last: what do we hope to learn?

Some of our research questions include:

- How does the inclusion of anisotropic properties influence calcaneus fracture and fragmentation? Is the most important microstructural feature to include?
- What is the influence/importance of bone marrow in modeling the dynamic fracture of the calcaneus?

Our technical objectives include:

- Develop a high resolution model of calcaneus that other models could use or benefit from
- Capture qualitative fracture surfaces for lower rates of impact
- Could be used for injury and non-injury
- Could be used to study foot and ankle positioning and resulting fracture
- Could be used to understand and improve accelerative impact calcaneal fracture reconstruction. For example, how does the fracture surfaces and predicted reconstruction interfere with maintaining Bohler's angle.

PENNSTATE

Acknowledgements


Rebecca Fielding
(graduate student)


Darnell Slaughter
(graduate student)


Wesley Teerlink
(graduate student)


Michael Robinson
(junior ME)


Christopher Kozuch
(sophomore ME)


Hao Yuan
(senior ME)


Mary McGoldrick
(junior Biology)


Hannah Putnam
(junior ME)


Timothy Ryan
(Assistant Prof.)


Timothy Stecko
(Research Tech.)

Anthropology

Thank You!

http://www.mne.psu.edu/compbio

PENNSTATE

Workshop on Numerical Analysis of Human and Surrogate Response to Accelerative Loading
Aberdeen Proving Ground, MD
January 7-9, 2014

Pelvis Response Effects on Whole Body Under-Body Blast Simulations

Adam Golman, Kyle Ott, Robert Armiger,
Tim Harrigan, Catherine Carneal, Andrew Merkle

BOMS
BIOMECHANICS AND INJURY MITIGATION SYSTEMS

APL
The Johns Hopkins University
APPLIED PHYSICS LABORATORY

Motivation

- **Investigation of whole body (WB) sensitivity to loading conditions**
  - Threat environment
  - Physical simulations
    - APL Vertically Accelerated Load Transfer System (VALTS)
  - Finite element model (FEM) simulations

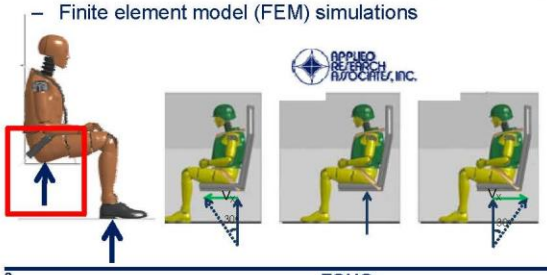


VALTS

2 FOUO APL

Motivation

- **Pelvic response, due to seat loading, significantly influences WB response**
  - Mechanical linkage to body
  - Compliance
  - Loading conditions

- **HIII pelvis not developed for nor durable in vertical loading**

- **Understanding effect of pelvis response important for ATD & human model development**

3

APL

Objectives

- **Use HIII FEM to characterize effects of pelvis-seat interaction on WB response**

  Inputs
  - Pelvis foam material properties
  - Floor & seat velocity pulses

  Outputs
  - Kinematics
  - Pelvis acceleration & lumbar force

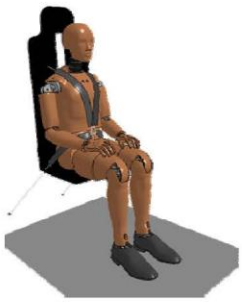

- **Identify areas for ATD pelvis design improvement**

4

APL

Methods
Model set up

- LSTC HIII FEM
- Rigid floor / seat
- 5 point belt (100 N preload)
- Varied pelvis material properties
  - Original LSTC HIII: *Mat_Viscous_Foam
  - Modification: *Mat_Low_Density_Foam
    - From LSTC ES-2re

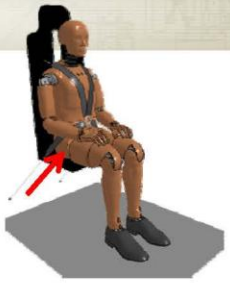

Foam Mat Props	Scaling Factor
Compliant	1/4
Nominal	1
Stiff	5

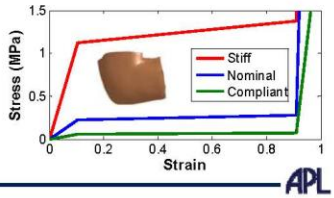

5 APL

Results
UBB relevant exposure conditions

Case 1: F-Lo, S-Lo

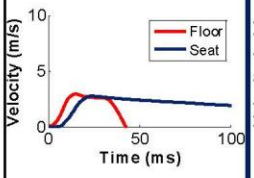

Case 2: F-Hi, S-Hi

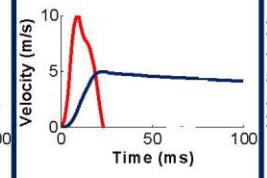

Case 3: F-Hi, S-Lo

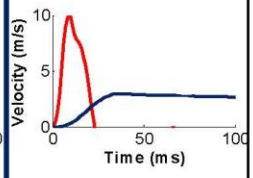

F = Floor
S = Seat

Case	Name	Floor Vz (m/s)	TTP (ms)	Seat Vz (m/s)	TTP (ms)
1	F-Lo, S-Lo	3	9	3	13
2	F-Hi, S-Hi	10	7	5	20
3	F-Hi, S-Lo	10	7	3	32

6 APL

Methods
Positioning and initialization

- **Positioned to reach target angles**
- **Simulation time = 500 ms**
  - KE reaches steady state

1. **Gravity load**
   - Vertical loading
   - Pre-compress pelvis foam & spine
2. **Belt pretension**
   - 100 N
   - Pretensions lumbar spine
3. **Raise floor**
   - Positions legs & avoids penetration

Angle (deg)	Target
Heel	90
Knee	80
Hip	80
Frankfort	20

7

APL

Methods
Positioning and initialization

- **Positioned to reach target angles**
- **Simulation time = 500 ms**
  - KE reaches steady state

1. **Gravity load**
   - Vertical loading
   - Pre-compress pelvis foam & spine
2. **Belt pretension**
   - 100 N
   - Pretensions lumbar spine
3. **Raise floor**
   - Positions legs & avoids penetration

Angle (deg)	Target	FEM	Diff
Heel	90	89	-1
Knee	80	80	0
Hip	80	82	2
Frankfort	20	16	-4

8

APL

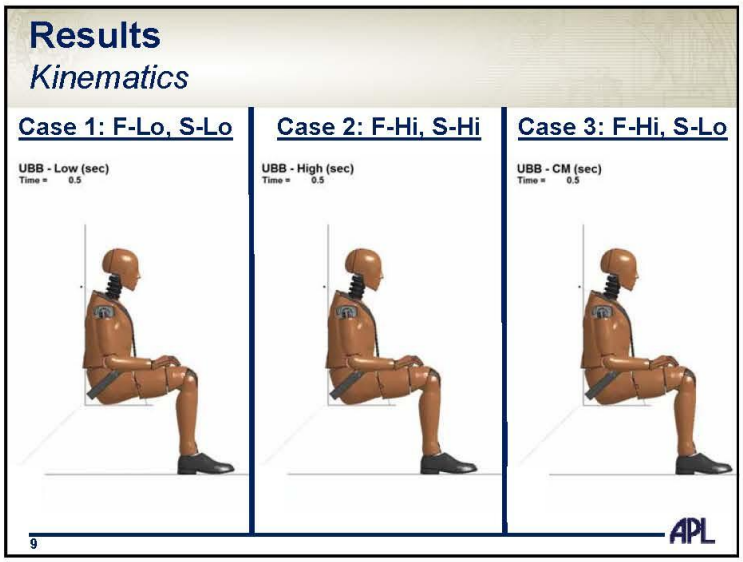
Results
Kinematics
Case 1: F-Lo, S-Lo
Case 2: F-Hi, S-Hi
Case 3: F-Hi, S-Lo
UBB - Low (sec)
Time = 0.5
UBB - High (sec)
Time = 0.5
UBB - CM (sec)
Time = 0.5
9
APL

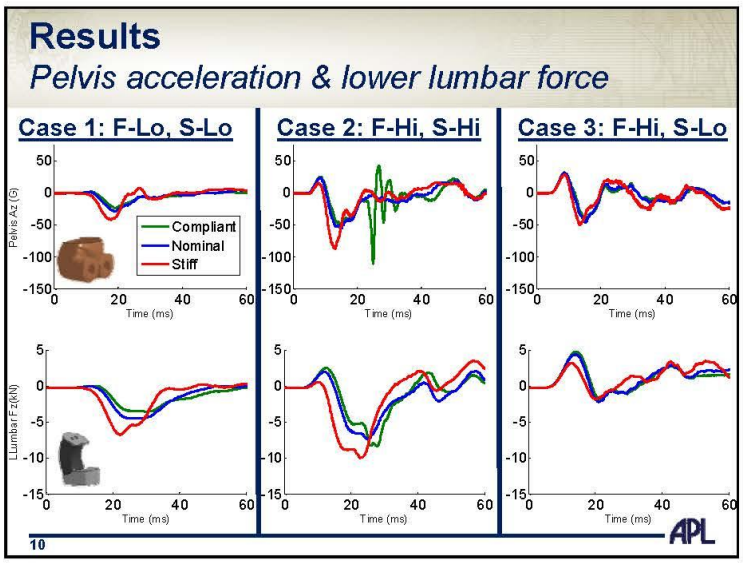
Results
Pelvis acceleration & lower lumbar force
Case 1: F-Lo, S-Lo
Case 2: F-Hi, S-Hi
Case 3: F-Hi, S-Lo
Pelvis Az (G)
Lumbar Fz(kN)
Compliant
Nominal
Stiff
Time (ms)
10
APL

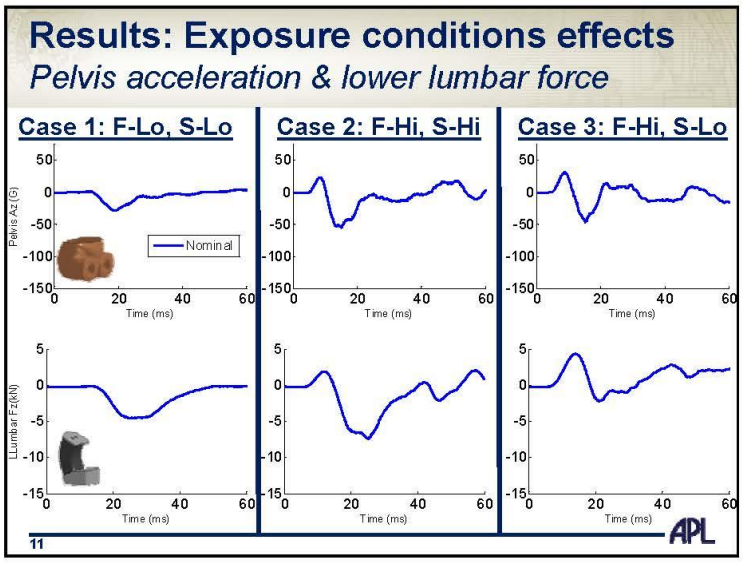
Results: Exposure conditions effects
Pelvis acceleration & lower lumbar force
Case 1: F-Lo, S-Lo
Case 2: F-Hi, S-Hi
Case 3: F-Hi, S-Lo
Pelvis Az (G)
LLumbar Fz(kN)
Nominal
Time (ms)
11
APL

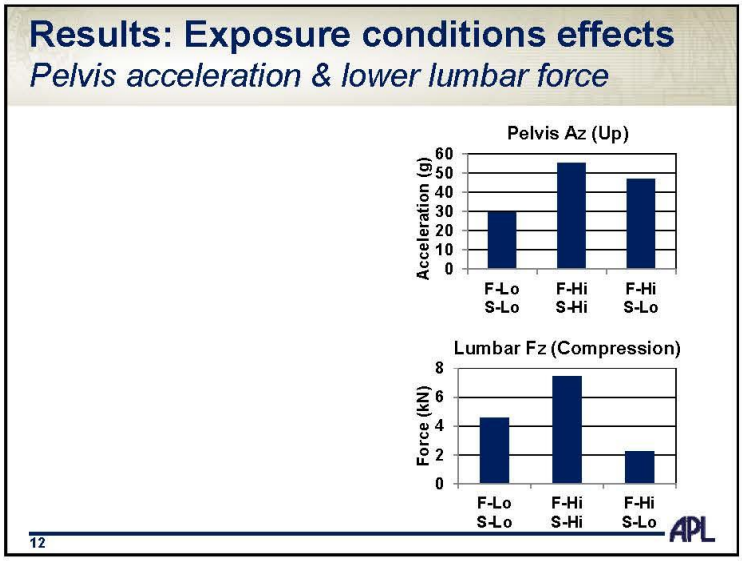
Results: Exposure conditions effects
Pelvis acceleration & lower lumbar force
Pelvis Az (Up)
Acceleration (g)
F-Lo S-Lo
F-Hi S-Hi
F-Hi S-Lo
Lumbar Fz (Compression)
Force (kN)
12
APL

Results: Exposure conditions effects
Pelvis acceleration & lower lumbar force

- **Increase seat & floor velocity**
  - ↑Pelvis acceleration
  - ↑Lumbar force

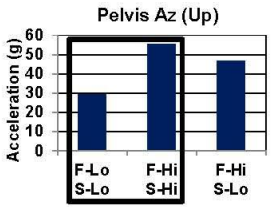

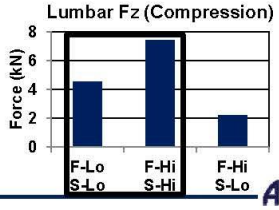

13

APL

Results: Exposure conditions effects
Pelvis acceleration & lower lumbar force

- **Increase seat & floor velocity**
  - ↑Pelvis acceleration
  - ↑Lumbar force
- **Decrease seat velocity**
  - ↓Pelvis acceleration
  - ↓Lumbar force

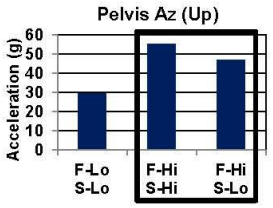

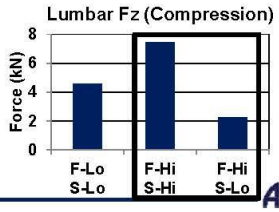

14

APL

Results: Exposure conditions effects
Pelvis acceleration & lower lumbar force

- **Increase seat & floor velocity**
  - ↑Pelvis acceleration
  - ↑Lumbar force
- **Decrease seat velocity**
  - ↓Pelvis acceleration
  - ↓Lumbar force
- **Increase floor velocity**
  - ↑Pelvis acceleration
  - ↓Lumbar force

?

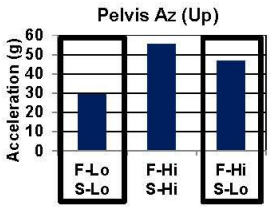

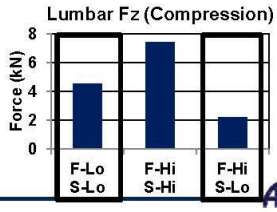

15

APL

Discussion: Exposure conditions effects
Forced posterior pelvis rotation

- **Early (relative to seat) & significant loading to lower extremity**
  1. Pulls pelvis down & forward
  2. Rotates the pelvis around belt
  3. Pulls the torso downward

Case 3: F-Hi, S-Lo overlay with Case 1: F-Lo, S-Lo

16

APL

Discussion: Exposure conditions effects

Forced posterior pelvis rotation

- **Early (relative to seat) & significant loading to lower extremity**
  1. Pulls pelvis down & forward
  2. Rotates the pelvis around belt
  3. Pulls the torso downward
- **↑ lumbar Fz tension**
- **↑ lumbar y-moment**
- **↓ lumbar Fz compression**

Could decrease spine loads & head-roof impact incidence

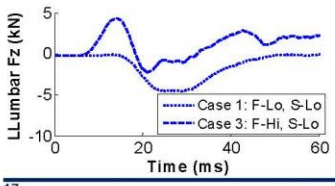

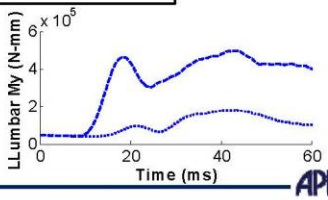

17

APL

Results: Exposure conditions effects

Pelvis acceleration & lower lumbar force

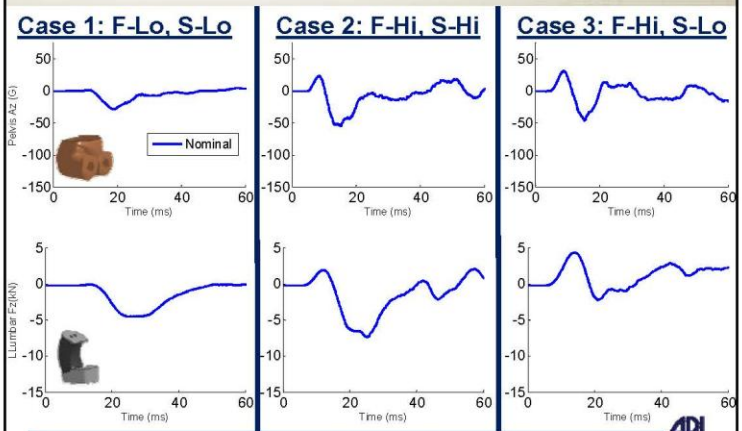

18

APL

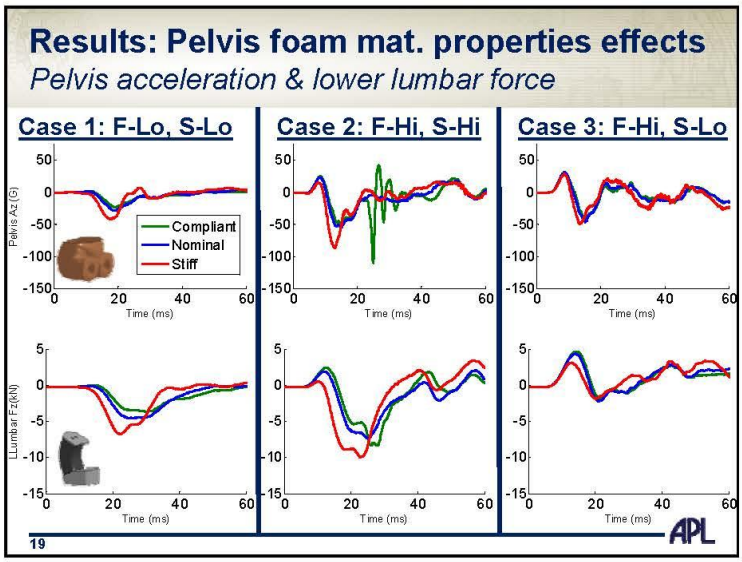
Results: Pelvis foam mat. properties effects
Pelvis acceleration & lower lumbar force
Case 1: F-Lo, S-Lo
Case 2: F-Hi, S-Hi
Case 3: F-Hi, S-Lo
Pelvis Az (G)
LLumbar Fz(kN)
Compliant
Nominal
Stiff
Time (ms)
19
APL

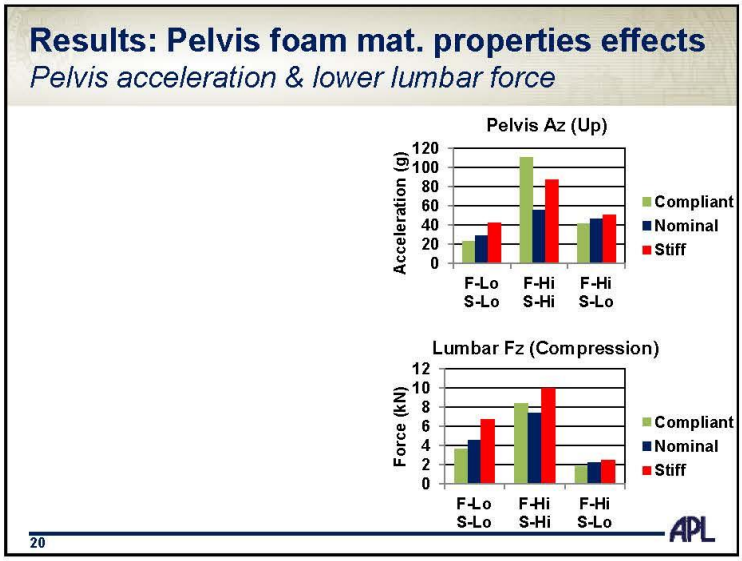
Results: Pelvis foam mat. properties effects
Pelvis acceleration & lower lumbar force
Pelvis Az (Up)
Acceleration (g)
Compliant
Nominal
Stiff
F-Lo S-Lo
F-Hi S-Hi
F-Hi S-Lo
Lumbar Fz (Compression)
Force (kN)
20
APL

Results: Pelvis foam mat. properties effects

Pelvis acceleration & lower lumbar force

- **Stiff vs nominal foam**
  - ↑Pelvis accel
  - ↑Lumbar force

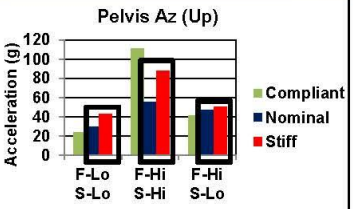

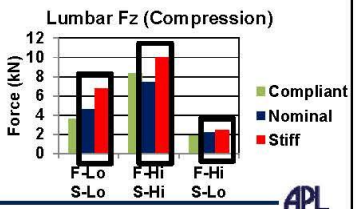

21

APL

Results: Pelvis foam mat. properties effects

Pelvis acceleration & lower lumbar force

- **Stiff vs nominal foam**
  - ↑Pelvis accel
  - ↑Lumbar force
- **Compliant vs nominal foam in high case**
  - ↑Pelvis accel
  - ↑Lumbar force

?

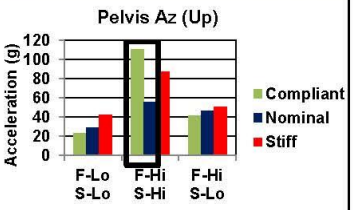

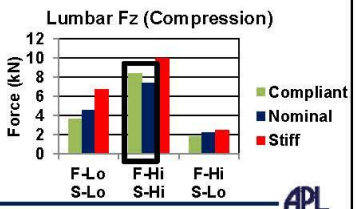

22

APL

Discussion: Pelvis foam mat. properties effects
Pelvis bottoming out

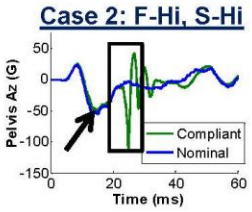

23

APL

Discussion: Pelvis foam mat. properties effects
Pelvis bottoming out

- Compliant foam w/ F-Hi, S-Hi causes bottoming out at pelvis accel mount

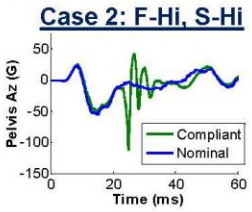

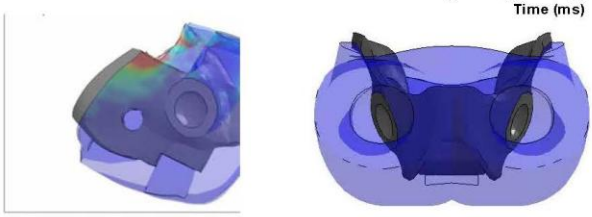

24

APL

Discussion: Pelvis foam mat. properties effects
Pelvis bottoming out

- **Compliant foam w/ F-Hi, S-Hi causes bottoming out at pelvis accel mount**
  - Shows another area for stress concentrations to occur

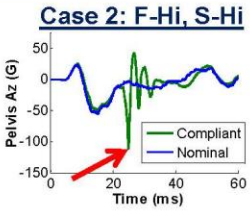

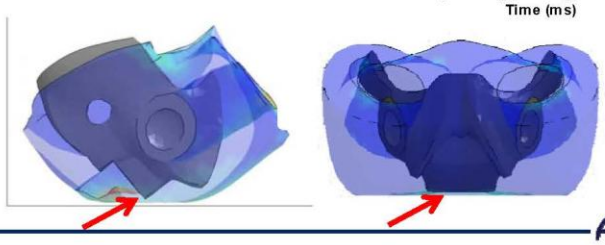

25

APL

Discussion: Pelvis foam mat. properties effects
Pelvis bottoming out

- **Compliant foam w/ F-Hi, S-Hi causes bottoming out at pelvis accel mount**
  - Shows another area for stress concentrations to occur
- **Ischium stress concentration**
  - When seat & floor velocities are similar
    - less pelvis rotation occurs

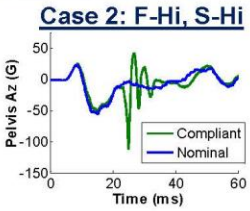

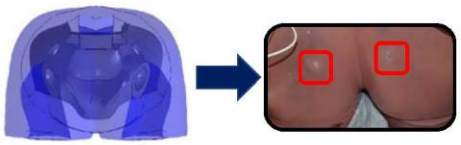

26

APL

Summary

- **FEM application to characterize kinematics & pelvis-seat interaction**
  - Response dependent on severity & timing
  - Pelvis accel & lumbar loads are sensitive to pelvis foam mat properties
- **HIII FEM has helped attribute non biofidelic response to design features**
  - Hip constraint influences WB response
  - Stress concentrations at ischium & accel mount

27 APL

Limitations & Next Steps

- **Trends only confirmed for these loading conditions**
- **Is forced posterior pelvis rotation biofidelic?**
  - Investigate hip constraint effects
    - FEM simulation
    - PMHS testing
- **Currently investigating these effects on lumbar & pelvis injury with human body model**

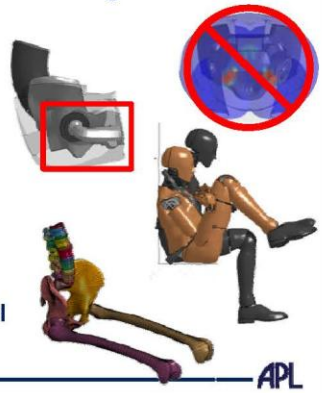

28 APL

Acknowledgement

The U.S. Army Medical Research Acquisition Activity,
820 Chandler Street, Fort Detrick MD 21702-5014
is the awarding and administering acquisition office.

The content included in this work does not necessarily
reflect the position or policy of the U.S. government.

29

APL

Workshop on Numerical Analysis of Human and Surrogate Response to Accelerative Loading
Aberdeen Proving Ground, MD
January 7-9, 2014

Pelvis Response Effects on Whole Body Under-Body Blast Simulations

Adam Golman, Kyle Ott, Robert Armiger,
Tim Harrigan, Catherine Carneal, Andrew Merkle

BIOMECHANICS AND INJURY MITIGATION SYSTEMS

APL
The Johns Hopkins University
APPLIED PHYSICS LABORATORY

BACK UP SLIDES

BIOMECHANICS AND INJURY MITIGATION SYSTEMS

The Johns Hopkins University
APPLIED PHYSICS LABORATORY

Exposure conditions effects

Forced posterior pelvis rotation

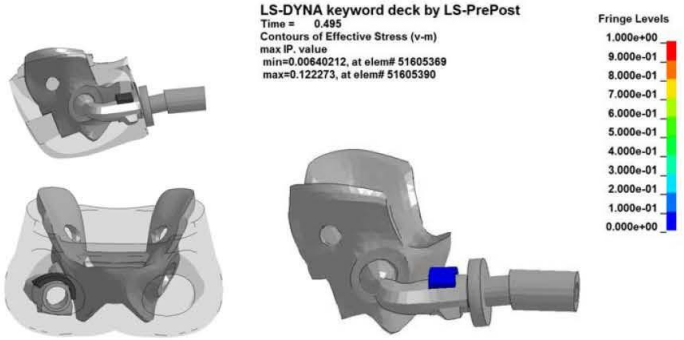

32

Pelvis foam MPs effects

Pelvis bottoming out

Two pelvis foam stress concentration locations

1. **Pelvis accel mount**
   - Difference in seat & floor velocity
     - Pelvis rotation

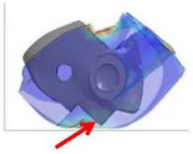

2. **Ischium**
   - Similar seat & floor velocity
     - Less pelvis rotation

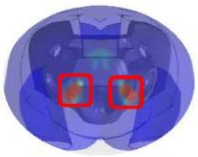

33

APL

LSTC ES-2RE Pelvis Validation

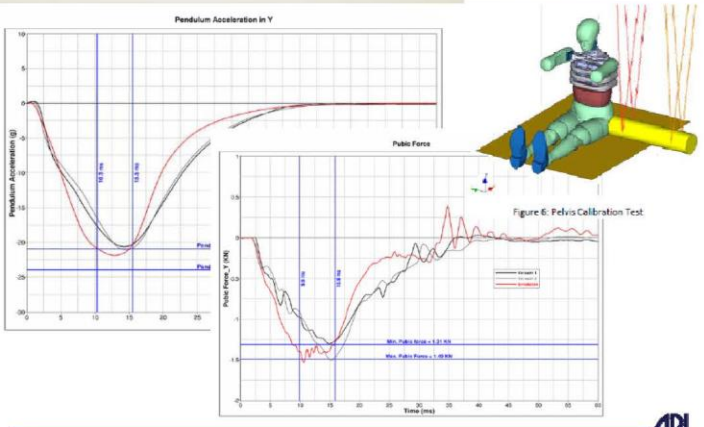

34

APL

Comparison to Experiments

Pelvis accel and lower lumbar force

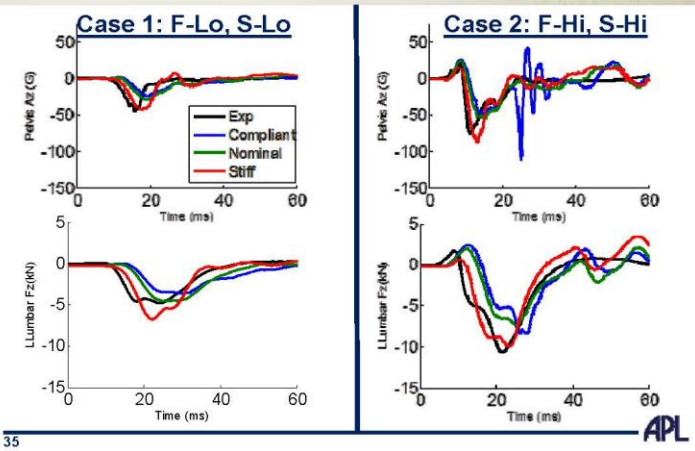

35

APL

Vertically Accelerated Load Transfer System

Underbody Blast Simulator

- **Unique laboratory device designed to be an UBB simulator**
  - Controlled accelerative impulse (simulate global rigid body motion), and deceleration impulse (simulate slam-down impact of the vehicle)
  - 50 inch x 60 inch high-strength aluminum table
    - Threaded inserts on a 4 inch grid pattern
- **High level impact energies achieved by propelling precision guided ballistic masses**
  - Programming materials produce the desired pulse duration
  - Pressure level controlling the impact speed

APL

18

C180

Vertically Accelerated Load Transfer System
Underbody Blast Simulator

- **Impact velocity range from 2 to 10 m/s with durations of 8 to 40 ms for the carriage**
  - 7 to 16 m/s with durations of 2 to 10 ms for the lower leg
- **Able to match loading profiles recorded during live fire testing**

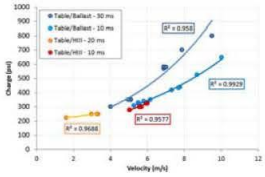

Charge □ Velocity

Elastomers□ Pulse Duration

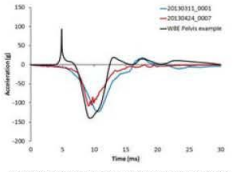

Hybrid III VALTs pelvis acceleration results from two different tests compared to nominal WBE pelvis response

AFL

Numerical methods for large-scale simulation of tissue and tissue simulant response to blast, model validation and limitations

Presenter: Raul Radovitzky
Collaborators: Aurelie Jean, Martin Hautefeuille (MIT)
Marina Carboni, Barry Decristofano, Michael Maffeo (NSRDEC)
James Zheng, Virginia Halls (PEO Soldier)
Phil Dudt, Alyssa Littlestone, Roshdy Barsoum (ONR)

Workshop on Numerical Analysis of Human and Surrogate Response to Accelerative Loading
Army Research Laboratory
January 7-9, 2014

Outline

- Previous and ongoing work using low (2^{nd}) order coupled Eulerian-Lagrangian methods for blast TBI analysis:
  - Hybrid III dummy blast tests (collaboration with NSRDEC)
  - ONR/Carderock manikin blast tests
  - Exploration of bTBI mitigation strategies (mask)
- Limitations:
  - Gel stiffness vs brain tissue
  - Numerical methods:
    - Wave dispersion for low-order methods
    - A solution: High-order discontinuous Galerkin methods

A simulation study to assist the development of a standard blast test for head protection equipment

C182

- NSRDEC collaborators: Marina Carboni, Barry Decristofano, Michael Maffeo
- Objective: use ISN simulation tools to:
  - Optimize sensor locations
  - Inform design of laboratory-scale blast test using shock tubes
- Status:
  - preliminary comparisons of simulation results with tests (no helmet)
  - CAVEATS!

Hybrid III: Headform and Mounting

- 9 surface pressure gauges, PCB 102B06
- 3 linear accelerometers Endevco 7270a 6kg
- 3 angular rate DTS 12k deg/sec

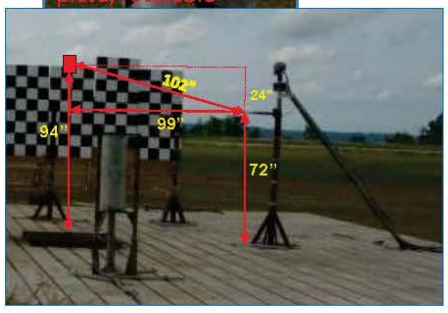

From CAD model to FE mesh

C183

- Hybrid III without "flesh"
- Collaboration with Navneet Sharma (Humanetics)

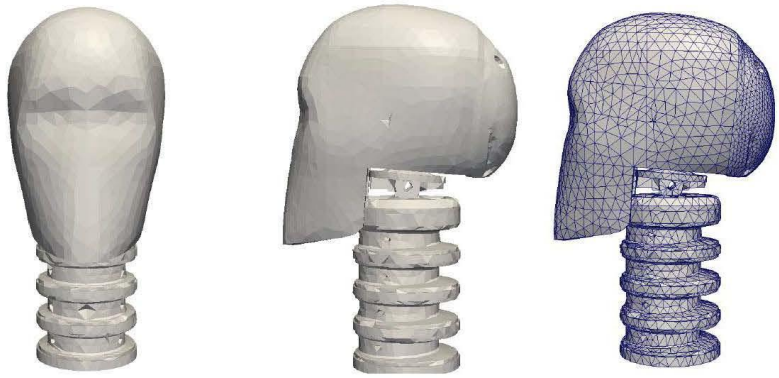

Blast Hybrid-III Manikin head interaction simulation

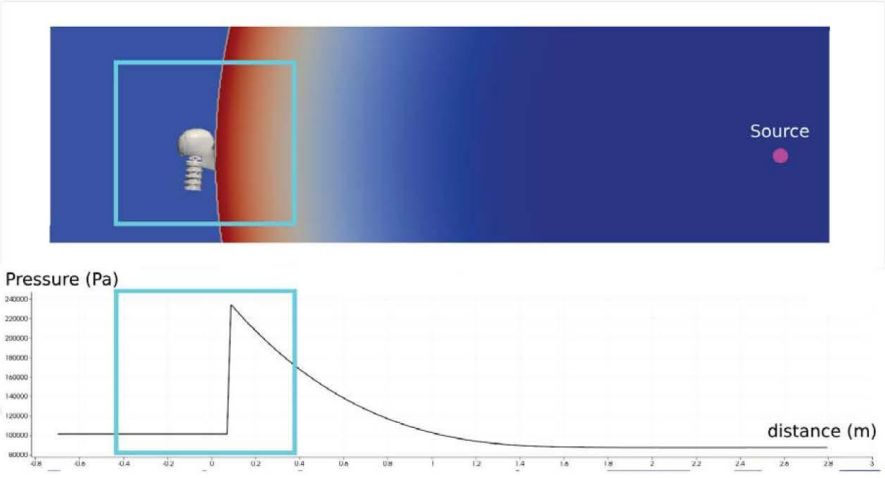

Blast Hybrid-III Manikin head interaction simulation

C184

- Front-facing blast with initial energy of 10 MJ at 2.3m standoff computed with ISN blast estimator and validated with CONWEP
- Free-field pressure comparison

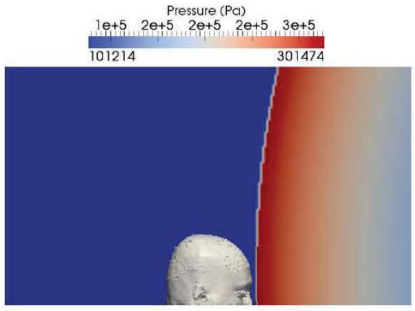

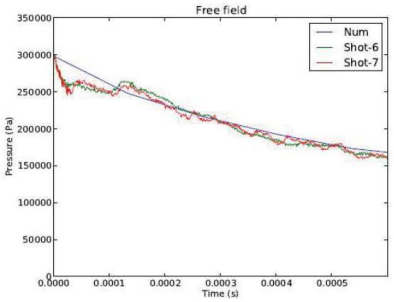

Sensor locations

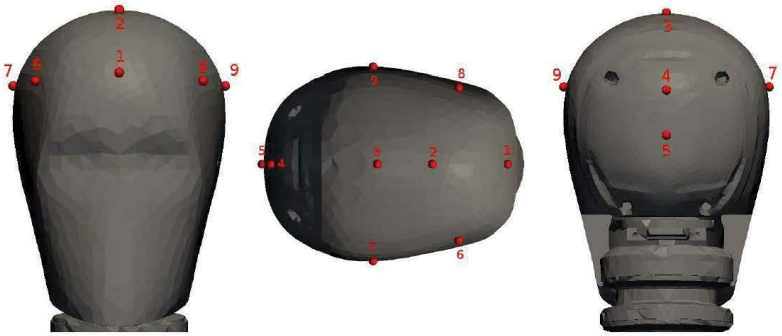

Comparison of test and simulation

C185

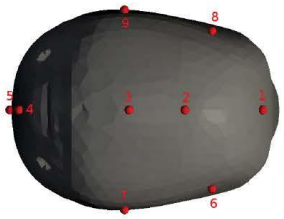

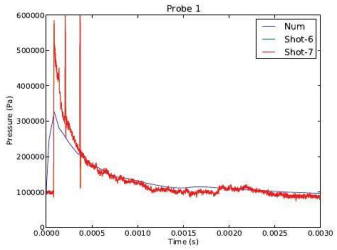

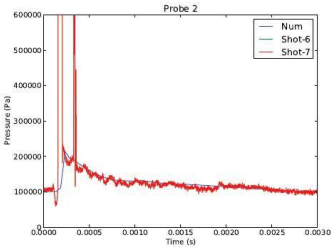

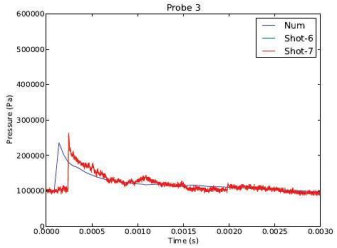

Comparison of test and simulation

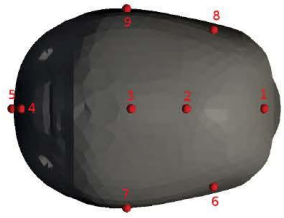

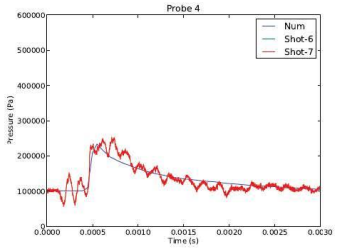

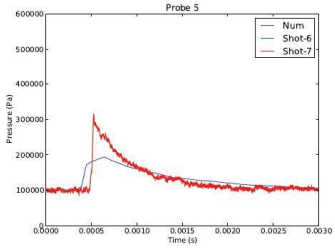

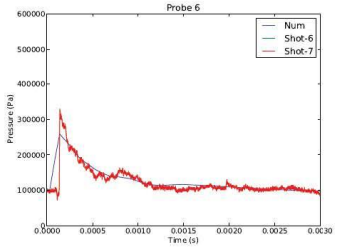

Comparison of test and simulation

C186

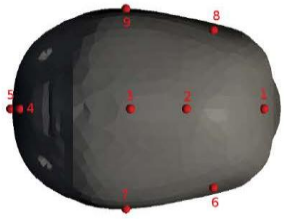

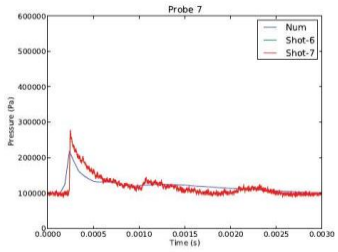

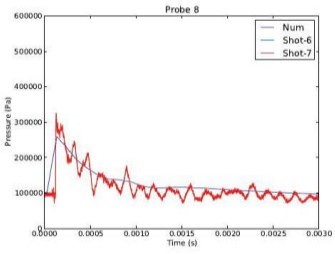

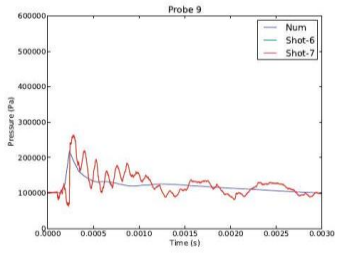

11

Model validation against Carderock Dummy Blast Tests (Barsoum, Dudt, Littlestone)

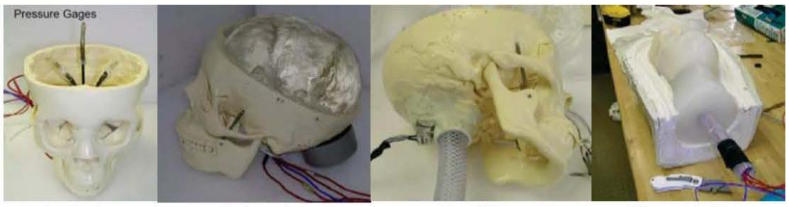

Polyethylene Skull with pressure gages and accelerometers

Sylgard Gel Brain

Flexible "Neck"

Silicon Polymer "Flesh"

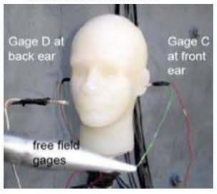

Bare head

Head + ACH

6

Pressure sensor locations

C187

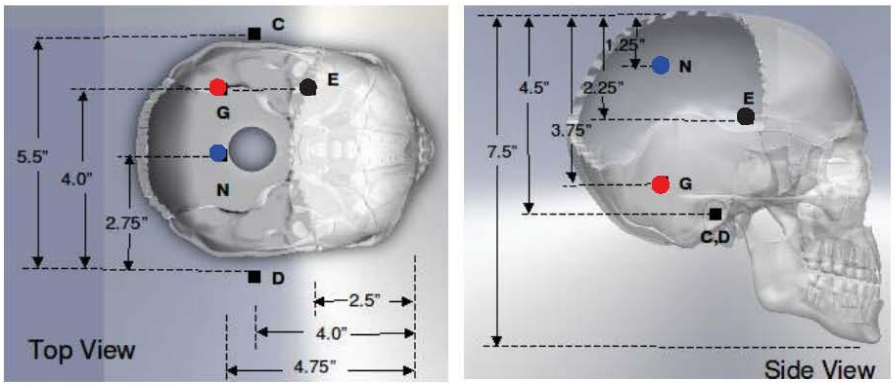

Experimental findings

- Side blast: 1/8 lb explosive, 3.5ft standoff

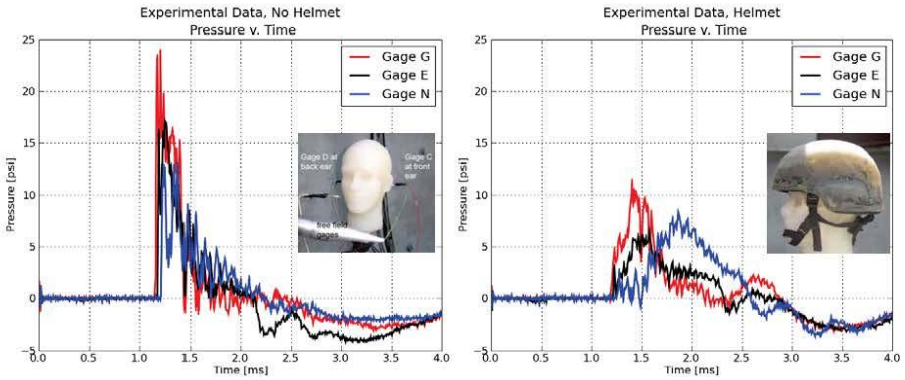

For side blast, the ACH noticeably reduces intracranial stresses

MIT/DVBIC Full Head Model with ACH

C188

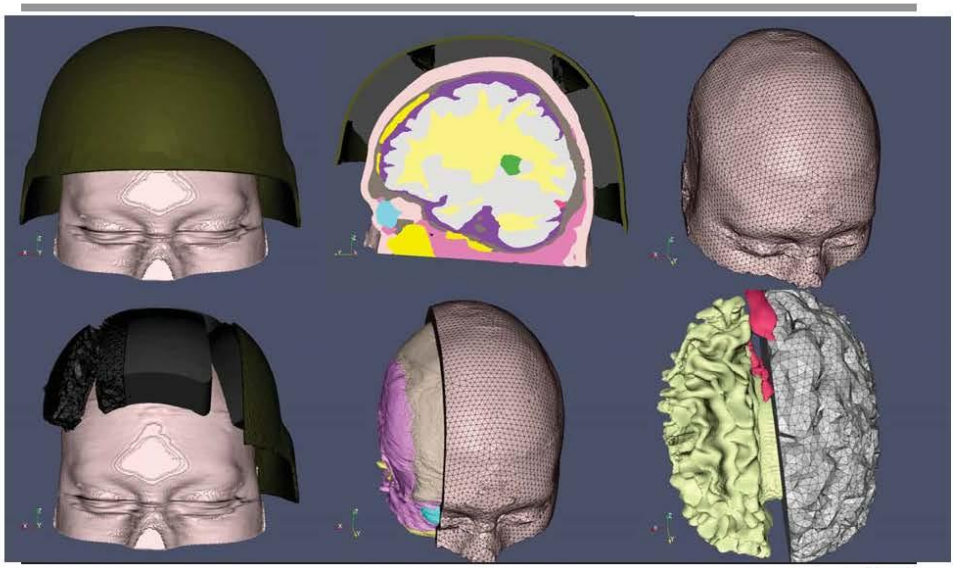

Model Modifications for validation tests:

- Replaced tissue with simulants:
  - CSF, eyes, venous cavities, ventricles, GM, WM, glia, and sinus cavities replaced with Sylgard gel
  - Skull replaced with PVC
  - Skin, fat, muscle replaced with DragonSkin
- Constitutive models for tissue simulants
  - Sylgard gel, DragonSkin: linear viscoelastic with Tait EOS
  - PVC: linear viscoelastic with Mie-Gruneisen EOS

Simulations of Carderock test: 3.5ft standoff

C189

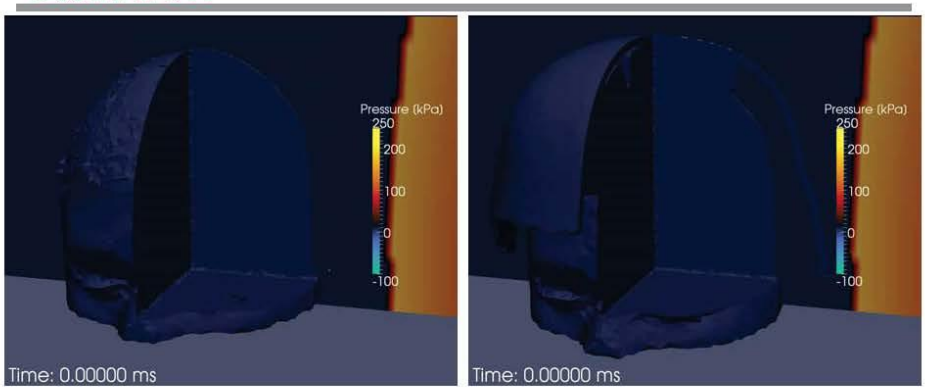

- Approximate geometry: MIT/DVBIC FHM different from Carderock dummies
- Approximate material properties for tissue simulants: Sylgard gel (brain tissue), PVC (skull bone)

Comparison: Free-field pressure histories for different stand-offs

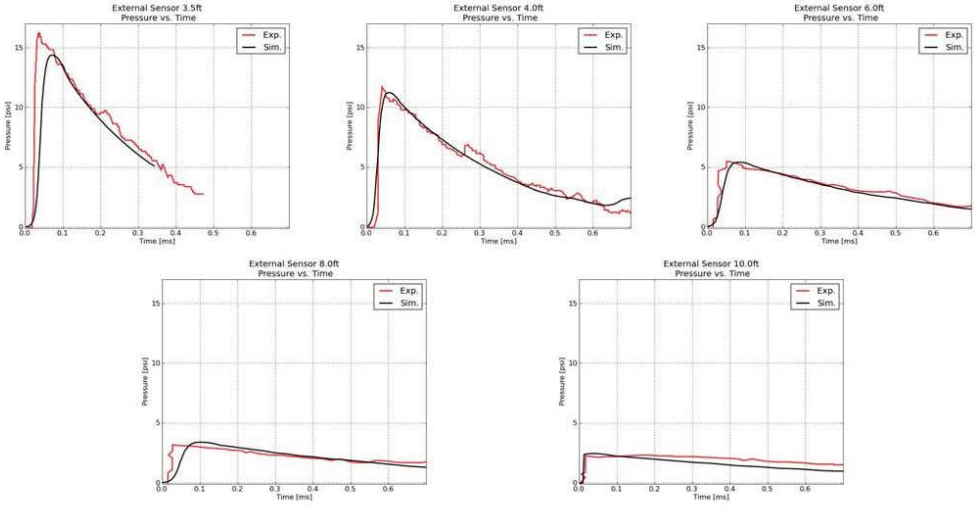

Comparison of simulation and experiment (3.5ft stand-off test)

C190

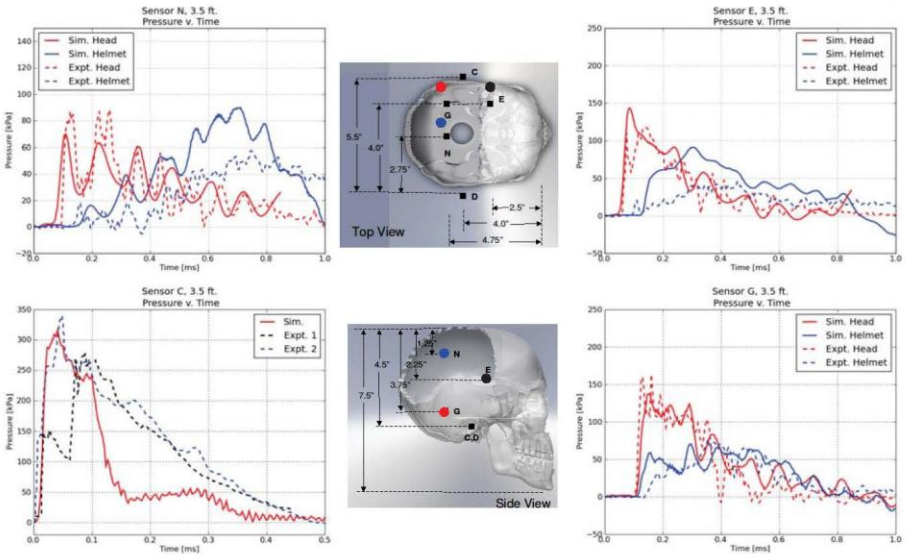

Limitations in geometry: Construction of actual manikin mesh

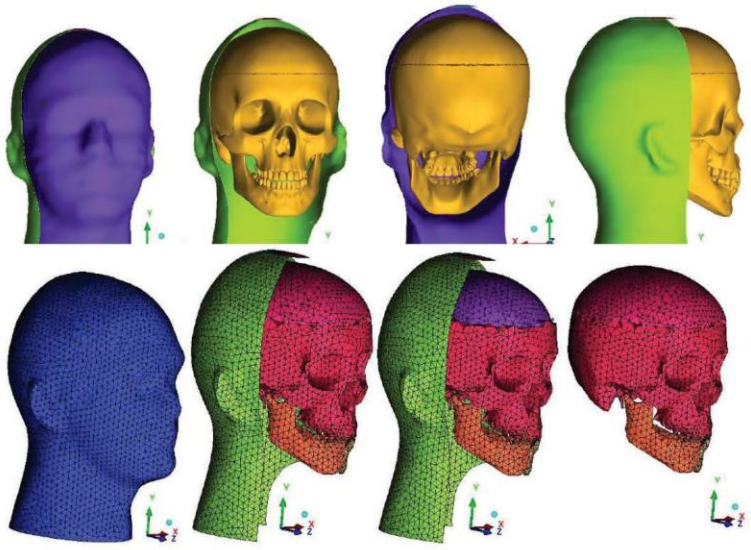

Limitation: Wave dispersion issues in low-order discretization methods:

High-order discontinuous Galerkin formulations for accurate wave propagation in solid mechanics

A. Rosolen, M. Hautefeuille, A. Jean, G. Becker
R. Radovitzky

High-order DG methods

- FE revisited:
  - New nodal positions
  - New discontinuous basis functions
  - New quadrature rules
  - ...

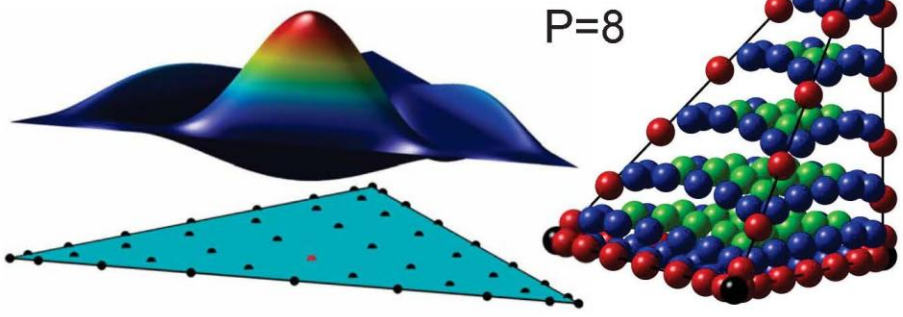

Basis functions and node positions

C192

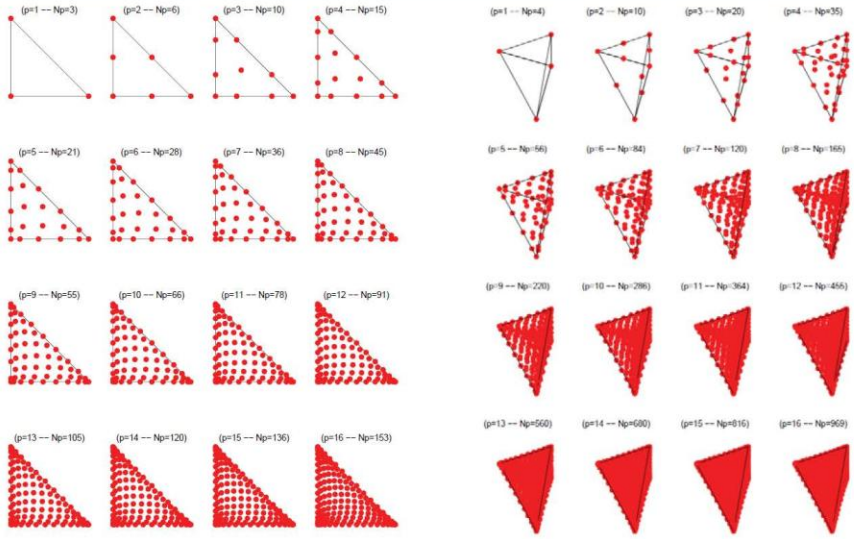

Wave dispersion: h vs p refinement

- Uniaxial stress and strain wave propagation in bi-material plate: PU, Kevlar

non-uniform h-refinement (p=2)

uniform p-refinement (p=9)

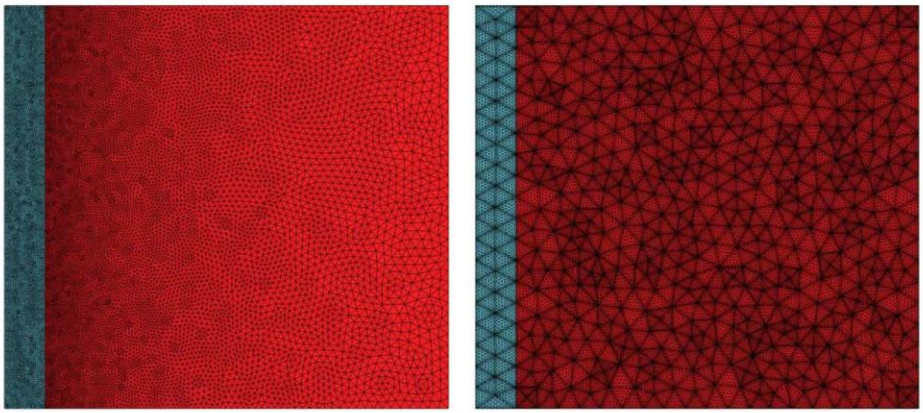

12

Relevance of dummy tests to human injury: biomimicry of tissue simulants

C193

- Explore differences of synthetic vs biological materials:
  - Sylgard gel vs brain tissue
  - PVC vs bone
- Use Brain tissue nonlinear visco-hyperelastic model (Prevost et al, 2011) calibrated for pig brain tissue test data (Chen)

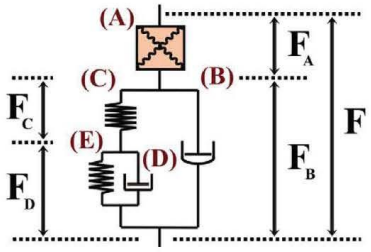

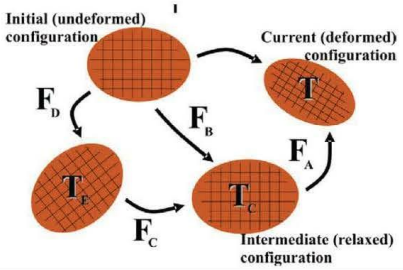

G_0 (Pa)	K (Pa)	n	σ_0 (Pa)	λ_L	μ_0 (Pa)	η (Pa·s)	G_∞ (Pa)	ρ (kg·m^{-3})
6.0×10^3	10^7	0.3	2.0×10^3	1.03	10^4	10^3	2.0×10^3	10^3

Sylgard gel stiffer than brain

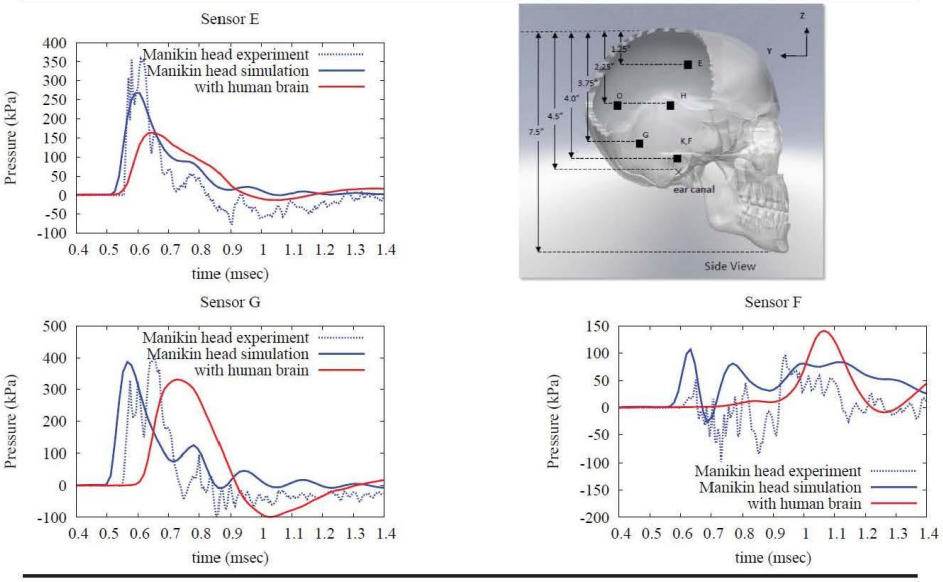

Mitigating brain tissue exposure levels with a face mask

C194

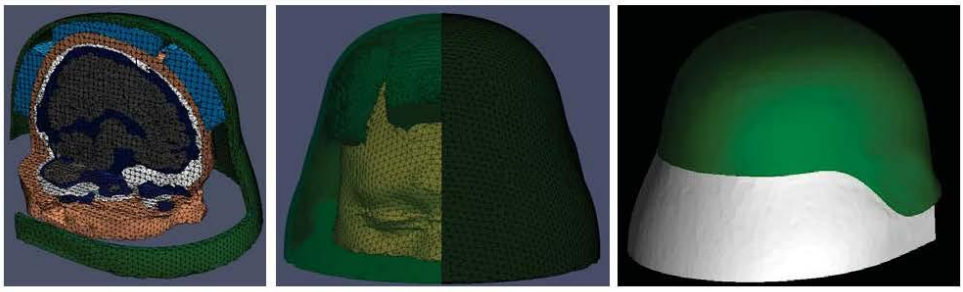

Human head response: unprotected, with ACH, with face shield

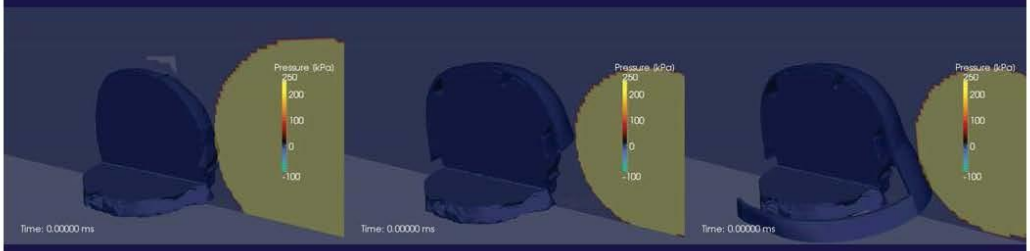

PNAS, 2010

AEROASTRO MIT

C195

Mitigation of Blast Induced Mild Traumatic Brain Injury

Helmet Face Shields

Final Presentation
December 8, 2011

Advisor: Raúl Radovitzky
Christian Valledor
Andrew Wimmer

AEROASTRO MIT

Completed Test Articles

- Two helmet configurations tested

Standard ACH

ACH with
MTek FAST G-Series

MIT AEROASTRO

Test Setup

C196

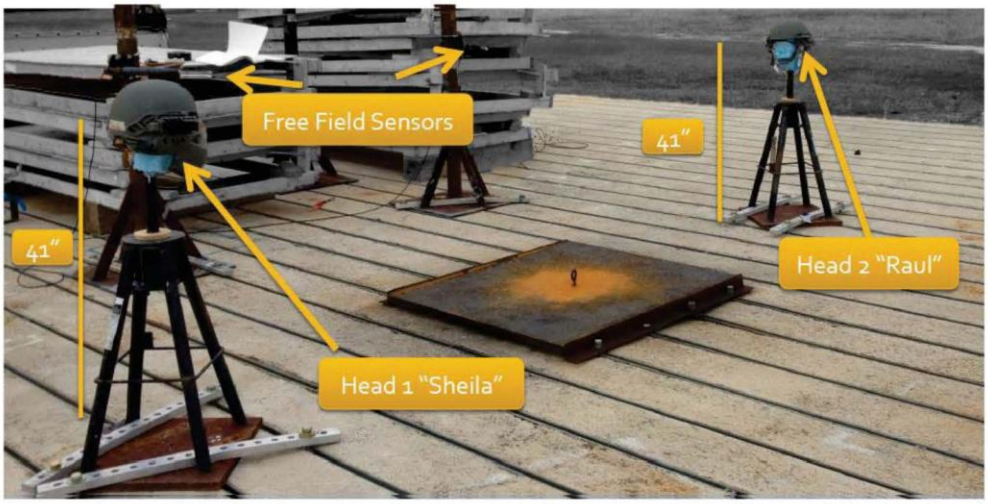

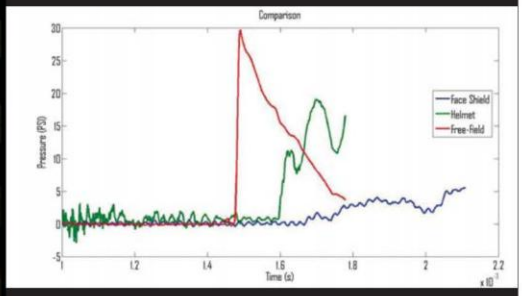

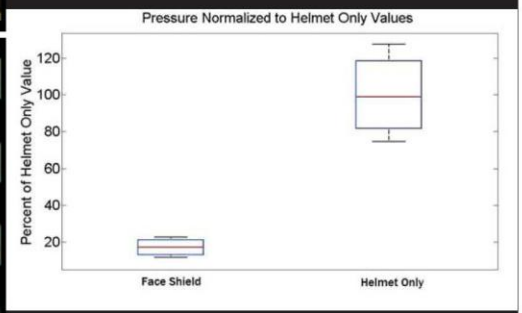

16

Thank you

Back-up slides

Current Trauma in Operations Iraqi and Enduring Freedom and rhBMP-2
The Walter Reed Experience

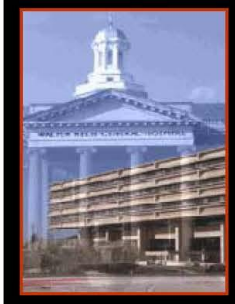

Scott C. Wagner, MD
LT, MC, USN
Ronald A. Lehman, Jr., MD
LTC, MC, USA
Director, Pediatric and Adult Spine
Associate Professor of Surgery
Walter Reed NMMC
Washington, D.C.

Multiple Injuries in Combat Wounded

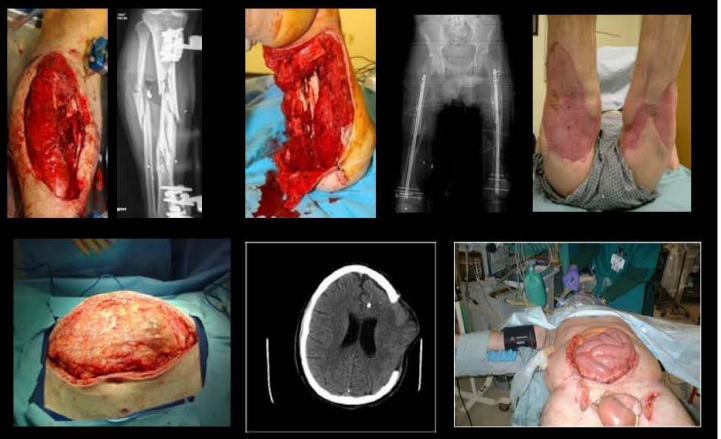

1

Fractures – Upper Extremity

	Closed	Open
• Clavicle	3	10
• Scapula	11	16
• Humerus	13	68
• Radius	19	59
• Ulna	11	69
• Hand	14	51


12 wks s/p skin graft – ROM ~ 60-120°

Wound Coverage

Lessons Learned Dictum!

- BMP (Bone Morphogenetic Protein)
  - Pros: Successful for segmental defects
    - Lower # of operations
    - Probable ↓ infection rate
  - Cons:
    - Excess bone formation (HO)
    - ? with VAC

Selected Cases

32 y.o. Special Forces Soldier

MOI: Fast-rope injury from 60 ft. in Iraq

Immediate back pain
BLE paresthesias
Evacuated to CSH

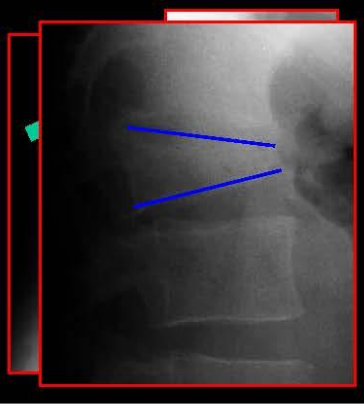

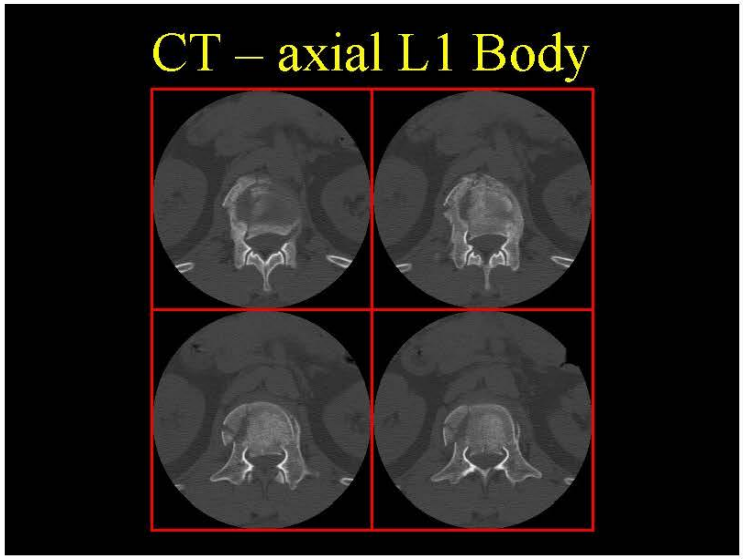
CT – axial L1 Body

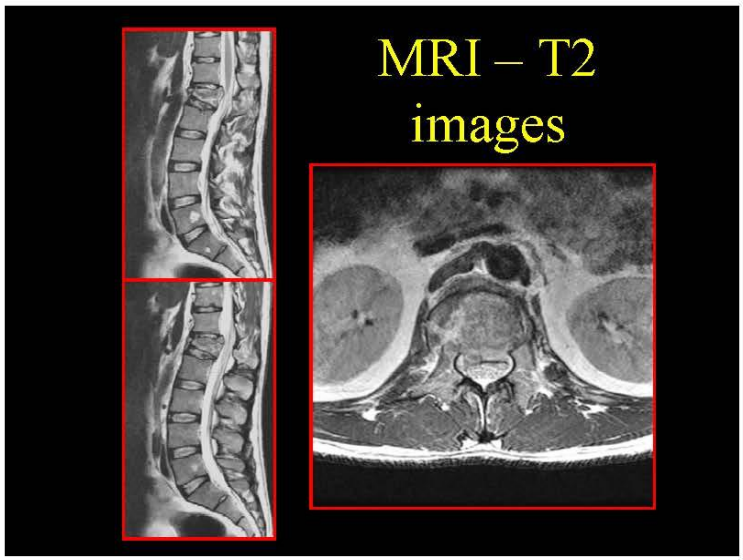
MRI – T2
images

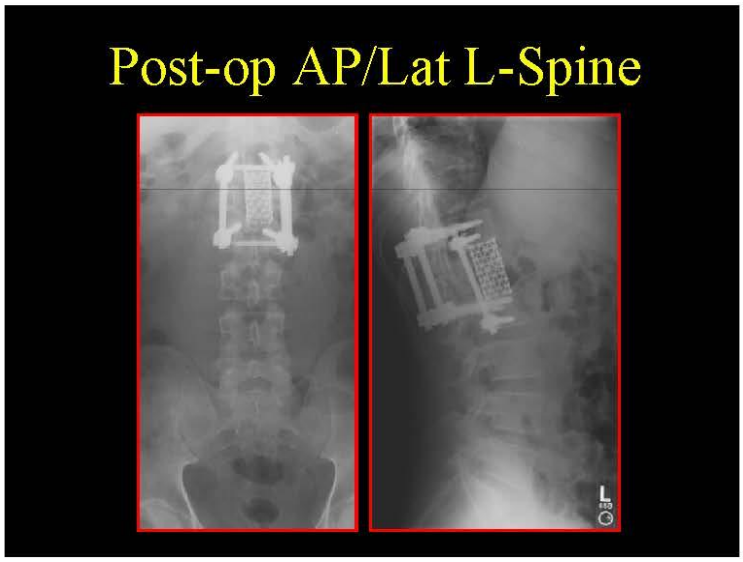
Post-op AP/Lat L-Spine

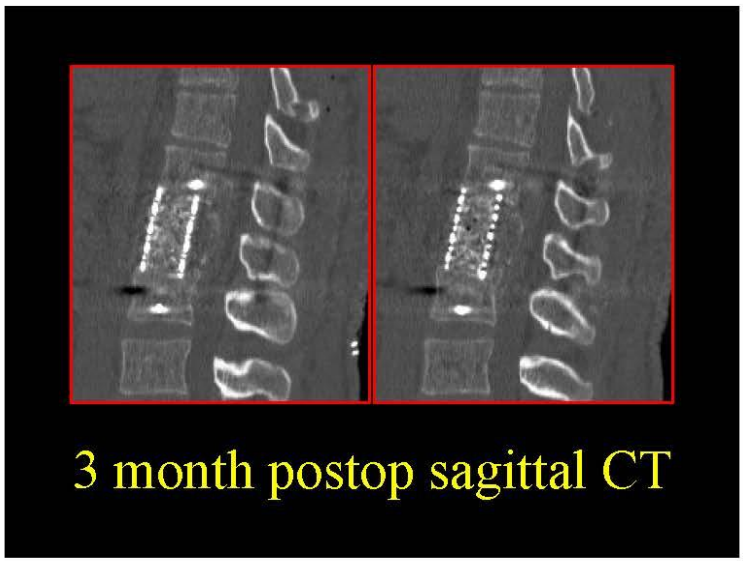
3 month postop sagittal CT

37 yo Apache pilot

MOI: helicopter crash - 900 feet

T2 burst fx
C6 teardrop fx
C7 vertebral body fx
C6,C7,T1,T3,T4 lamina fxs

NL neurologic exam!

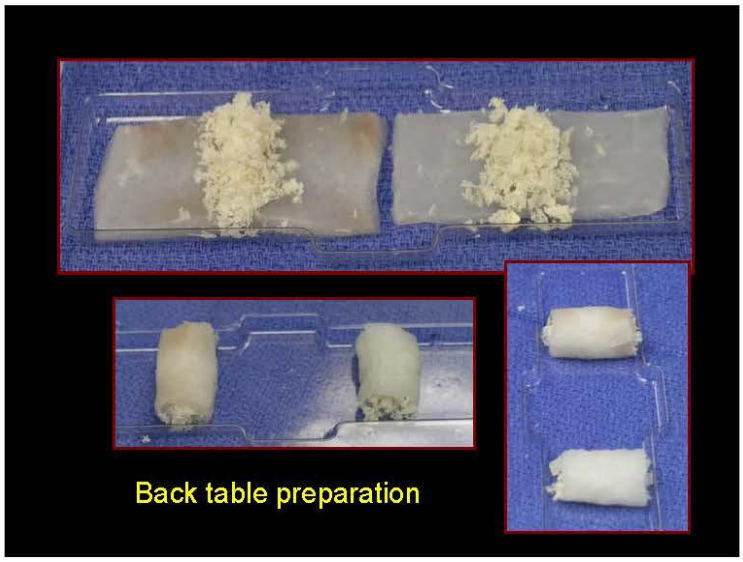
Back table preparation

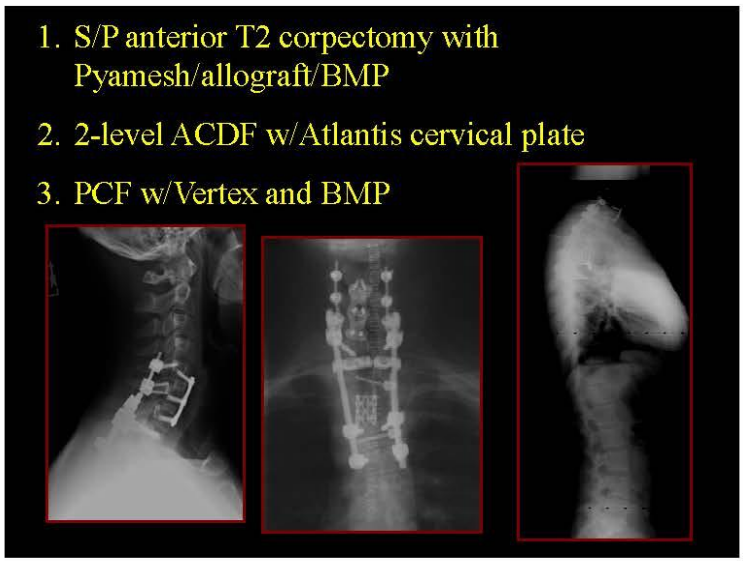
1. S/P anterior T2 corpectomy with Pyamesh/allograft/BMP
2. 2-level ACDF w/Atlantis cervical plate
3. PCF w/Vertex and BMP


HT - 42 y.o. male
MOI: GSW
GSW: L tib/fib fx w/
bone loss s/p exfix
R
R

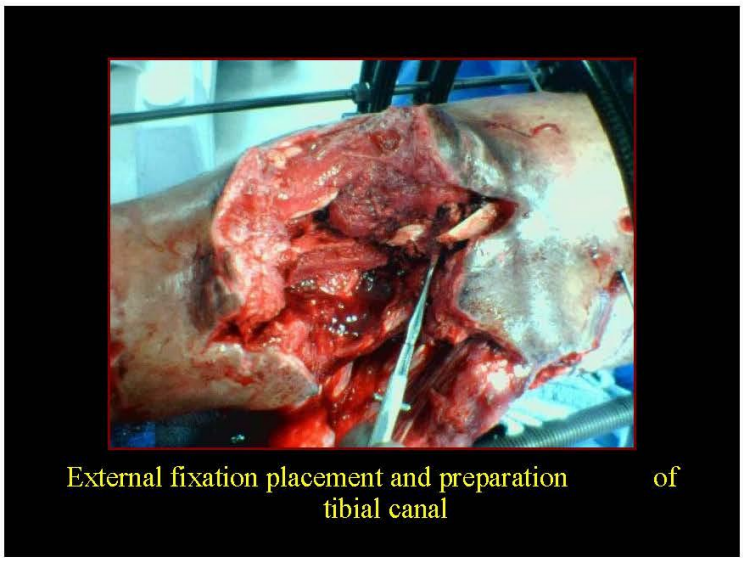
External fixation placement and preparation of
tibial canal

Bone Morphogenetic Protein (BMP)

- rhBMP-2
- Collagen matrix holds BMP
- Tubular configuration, with bone graft
- Decorticate endosteal surface w/burr
- Placed in segmental defect
- Soleus flap/STSG

Placement of BMP/Bone Graft

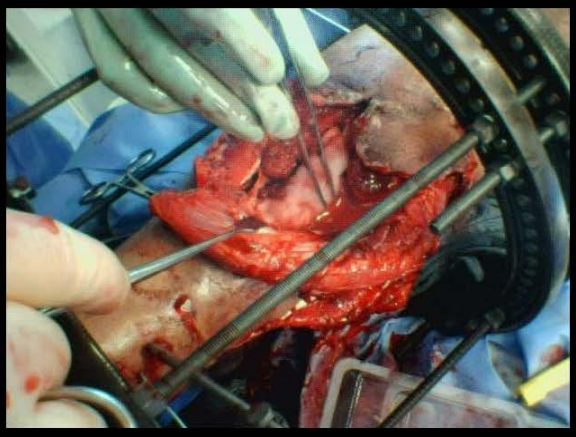

C210

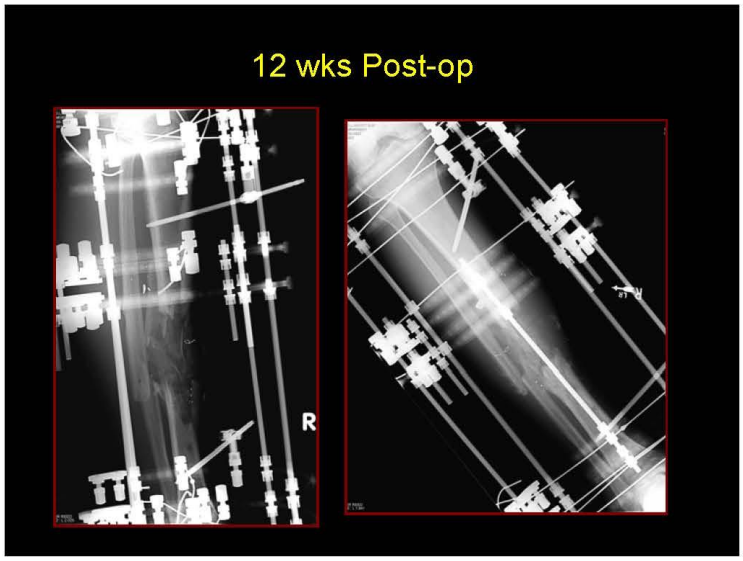

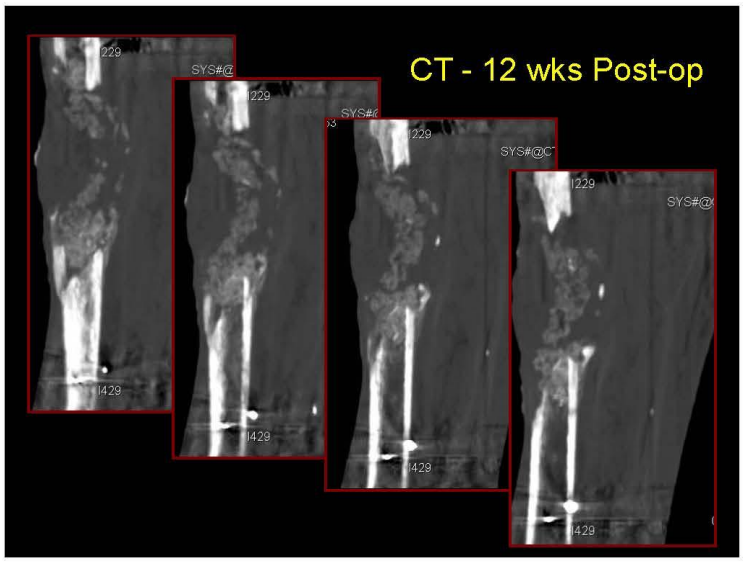

13


12 month follow-up

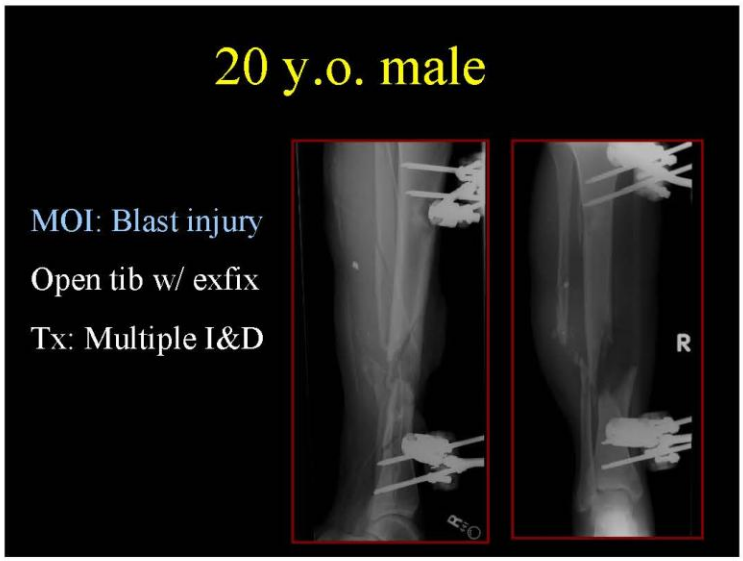
20 y.o. male
MOI: Blast injury
Open tib w/ exfix
Tx: Multiple I&D
R

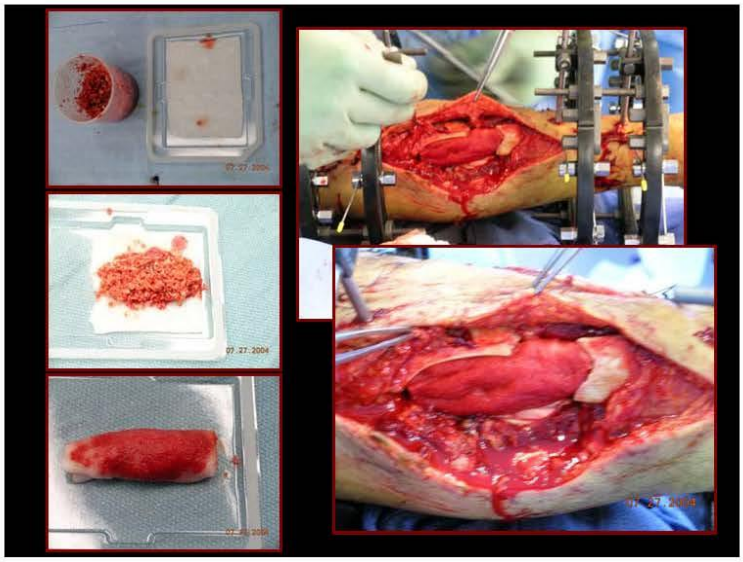

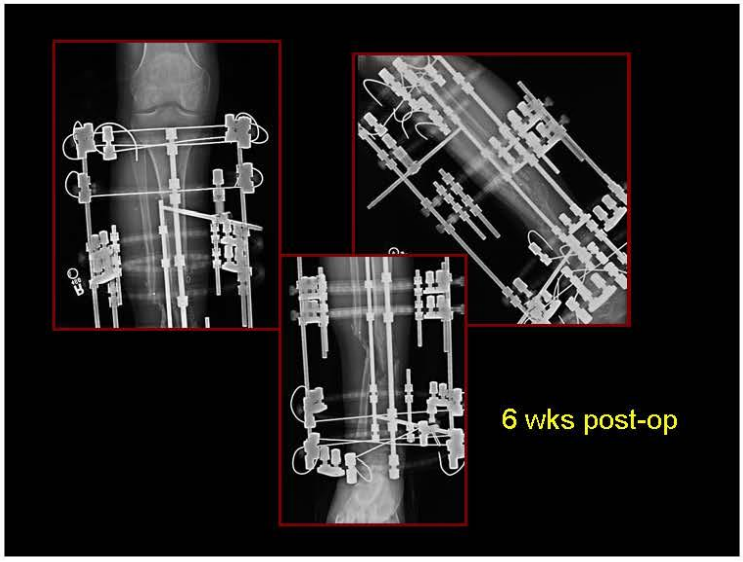
6 wks post-op

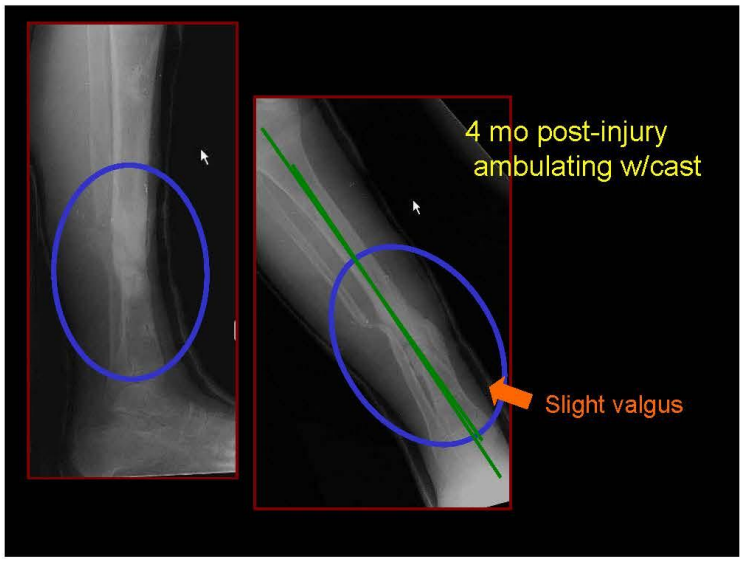
4 mo post-injury
ambulating w/cast
Slight valgus

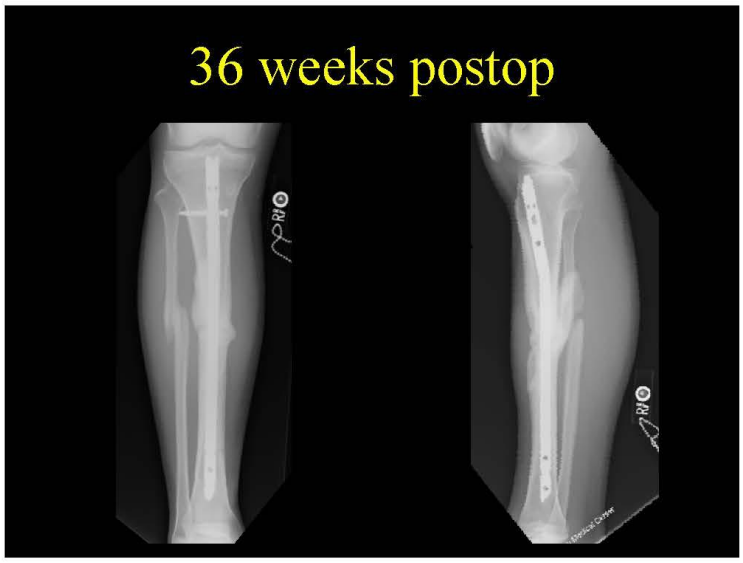
36 weeks postop

BUT…..

There were many clinical failures!

Adjacent Vertebral Body Osteolysis with Bone Morphogenetic Protein Use in Transforaminal Lumbar Interbody Fusion

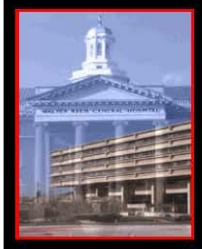

Ronald A. Lehman, Jr., MD
Melvin D. Helgeson, MD
Jeanne C. Patzkowski, MD
Michael K. Rosner, MD
Anton Dmitriev, PhD
Andrew W. Mack, MD

Walter Reed Army Medical Center
Washington, D.C.

Introduction

- Transforaminal lumbar interbody fusion (TLIF): Posterior-only approach
  - Harms and Jeszensky. Orthop Traumatol 1998.
- Bone morphogenetic protein (BMP)
  - gained popularity
  - widely utilized inside IBD in ALIFs
- Reports ~ osteolysis w/ BMP use in TLIFs
  - McClellan et al. J Spinal Disord Tech, 2006.
- No study has quantified the amount of osteolysis present at various time points and compared this to fusion rates

Introduction

- Resorption in 69% of levels
  No correlation with fusion
  - McClellan et al JSDT 2006.
- Avoid overpacking
  - Burkus et al. Spine J 2006.
- Stand-alone ALIFs/FRA w/ BMP
  56% nonunion vs 36% ICBG
  - Pradhan et al. Spine 2006.
- ALIFs/FRA w/ BMP and PSF
  Fusion rates 100% vs allograft
  - Slosar et al. Spine J 2007.

Objectives

1. To determine the incidence and resolution of osteolysis associated with the use of rhBMP-2 during transforaminal lumbar interbody fusions (TLIF) at various time points

2. Correlate the presence of osteolysis to fusion rates

Materials & Methods

- Retrospective analysis
- All patients at our facility who underwent a TLIF with rhBMP-2 from 2003-2006
  - Currently off-label use of the product
  - 6 mg/level on ACS
- Two Surgeon Experience
- Inclusion Criteria: CT scan
  - Within 48 hours of surgery
  - 3 to 6 months postoperatively
  - 1 to 2 years postoperatively

Results

- 224 TLIFs w/ BMP (2003-06)
- Qualifying Patients:
  23 (5 females; 18 males)
- Avg. age = 38.2 years at TOS (range 23-81)
- CT scans at all time periods *(ordered prior to visit)*
- 78 vertebral bodies/endplates assessed for osteolysis
- ~39 levels

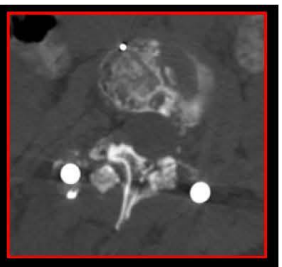

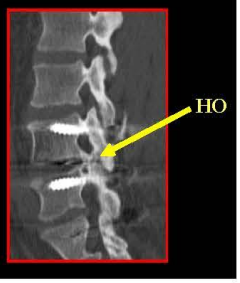

Results

- Osteolysis ~ 3-6 mos postop in adjacent vertebral bodies = 54%
- Incidence at 1 & 2 years = 41%
- 24% consolidation rate
- The mean volume of osteolysis:
  - < at 1-2 years (0.216 cm3) vs.
  - 3-6 mos (0.306 cm3) (p=0.082)
- The area/rate of osteolysis did NOT appear to sig. affect fusion rate
- Overall union rate ~ 83%

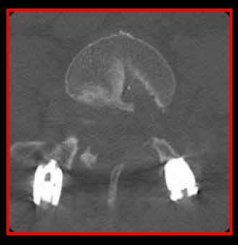

Conclusions

- The rate of osteolysis decreased at 1 year (41%) compared to 3-6 months (54%).
- Only 24% of the vertebral bodies with evidence of osteolysis at 3-6 months showed evidence of consolidation by one year.
- Ultimately: More research needed!

Thanks

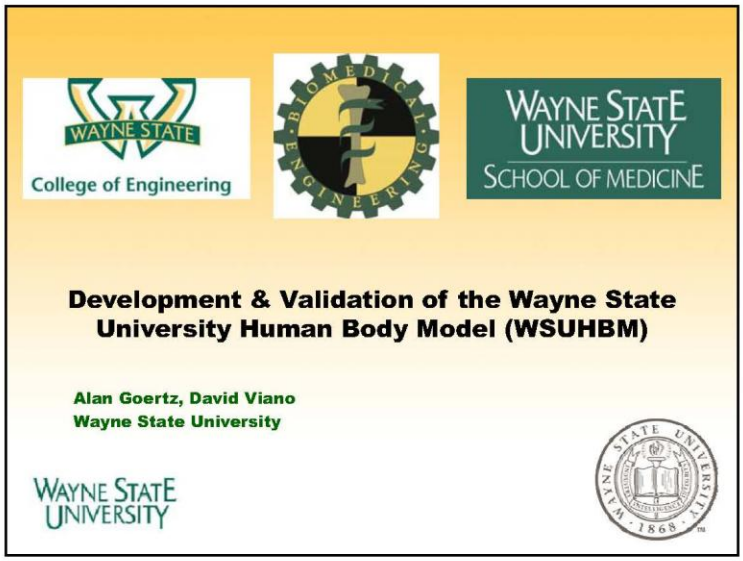

Overview

- Development & Validation (automotive)
- Model Overview
- Underbody Blast Application
- Flexion Injuries & Posture
- Conclusions

WAYNE STATE UNIVERSITY

C220

WSUHBM - Torso

Thorax - Wang, H, 1995 & Shah et al, 2001

- 1st version w/organs – lungs, heart and associated major arteries/veins (including aorta hemodynamic pressure effects)
- Anthropometry from Visual Human Project
- Validation – pendulum impacts : lateral & sternum (Krull, 1974 & Viano,1989)

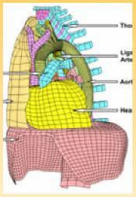

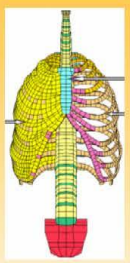

Shoulder - Iwamoto et al, 2000

- Anthropometry from Viewpoint Datalabs®
- Validation – Lateral impacts: pendulum (Bendjellal, 1984), sled (Cavanaugh, 1993), side airbag (WSU/TRW)

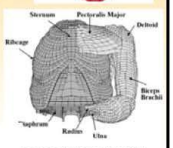

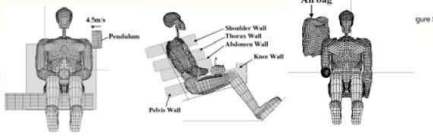

WAYNE STATE UNIVERSITY

/cont

/cont WSUHBM - Torso

Abdomen – Lee/Yang, 2001 & Lee, 2002

- Human Abdomen Model (WSUHAM)
- Anthropometry from Visual Human Project
- Validation – seat belt loading (Hardy, 2001) and impacts: pendulum (Viano, 1989), armrest (Walfisch, 1980), & bar (steering wheel) (Cavanaugh, 1986)

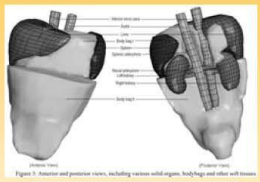

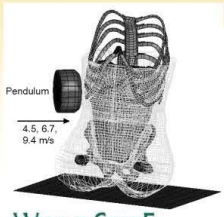

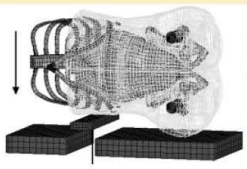

WAYNE STATE UNIVERSITY

/cont

/cont WSHM04-1 – Whole Body

Shah, 2002-2004, Integration of

- Shoulder (Iwamoto et al)
- Thorax (Shah et al)
- Abdomen (Lee and Yang)
- Modifications –
  - Improved mesh
  - Extended abdominal skin
  - Truncated arms to avoid validation contacts
  - Added "blood" to the aorta
- Validation – Impacts: pendulum oblique chest, oblique abdomen, and frontal chest, armrest, bar (steering wheel) and mid abdominal seatbelt and airbag

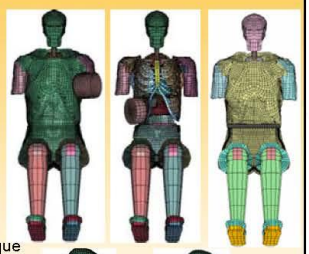

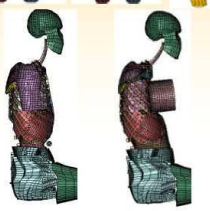

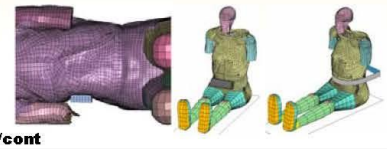

/cont

/cont WSHM06-1 – Aorta

Shah el al, 2005, Shah, 2007, Siegel el al, 2006, Siegel el al, 2010, Belwadi el al, 2011, Belwadi el al, 2012,

- Refined WSHM04-1 leg joints, respiratory & cardiovascular system & reintroduced ¾ arm
- Validation – Aortic stress, aortic arch haemostatic pressure, and average maximum principal strain (AMPS)
  - Vehicle-to-vehicle impacts into driver side door
  - Indy race car lateral impact (Begeman and Melvin, 2002 - MADYMO)

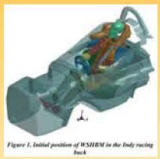

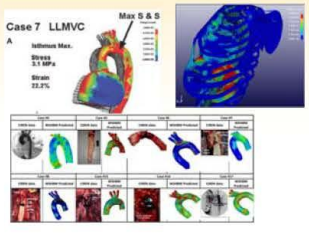

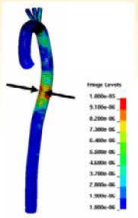

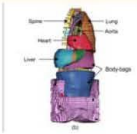

WSU LLMS-Lower Extremity

Beillas et al, 1999, 2001, 2004, 2007

- Lower Limb Model for Safety (LLMS) from CT & MRI of subject

Validation

Test Condition	Setup	Reference	Static or Dynamic
Tibia region:			
Axial compression	Present reanalysis		S
Foot & Tibia complex (new set-up only)			
Axial compression along the tibia	Present reanalysis		S
Femur-Knee-Tibia complex:			
Horizontal impact on patella	90° knee angle	Haut, R.C. et al. (1995)	D
Horizontal impact on patella	90°(+) knee angle	Hayashi et al. (1996)	D
Vertical impact on tibia	90° knee angle	Banglmaier et al. (1999)	D
A-P shear on tibia	90° knee angle	Viano et al. (1978)	D
Whole lower limb			
lateral-medial shear on proximal tibia	Standing position	Kajzer et al. (1990)	D
Knee bending (lateral-medial shear on distal tibia)	Standing position	Kajzer et al. (1993)	D
Whole Body			
Sled		Cheng et al. (1984)	D

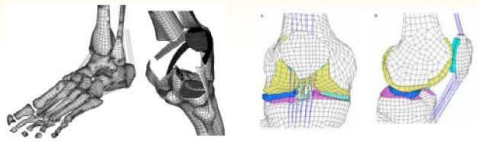

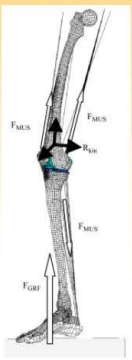

/cont

WSUHBM V3 - Lower Extremity

Suresh et al, 2012, "Finite element evaluation of human body response to vertical loading," WCCM 2012

- Re-meshed lower extremities in higher detail
- Whole body vertical drop test with varied lower leg flexion/extension
- 120g for 10msec
- Validation – n/a
- Comparison with Hybrid-III lower extremity response
  - **Femur** shear force and bending moment 500-1000N & 200-300N*m (ATD 2.6-6.7kN & 400-1000N*m)
  - **Upper tibia** axial force 2.3-3.4kN (ATD 8-10kN)
  - **Lower tibia** axial force 3.9-4.5kN (ATD 10-12kN)

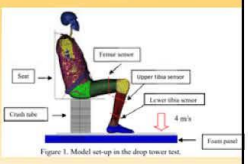

Figure 1. Model set-up in the drop tower test.

WAYNE STATE UNIVERSITY

Overview

- Development & Validation (automotive)
- Model Overview
- Underbody Blast Application
- Flexion Injuries & Posture
- Conclusions

WAYNE STATE UNIVERSITY

WSUHBM – Statistics

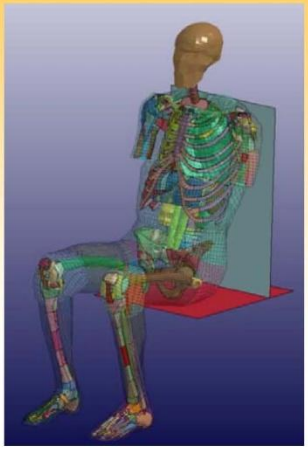

- LS-DYNA
- Whole Body
  - Part Count - 432
  - Nodes – 275,000
  - Shells – 110,000
  - Solids – 200,000

Upper – Lower Body Distribution

- Upper Body (to Distal Femur)
  - Nodes – 180,000
  - Shells – 70,000
  - Solids – 130,000
- Lower Extremities (from Distal Femur)
  - Nodes – 95,000
  - Shells – 40,000
  - Solids – 70,000

WSUHBM – Hierarchy

Model Numbering & Naming Protocol

ID	Body Region	Abbr
1*	Not used – fixture	n/a
2*	Whole Body	Wh
3*	Head, Face, & Neck	Hd
4	Thorax (diaphragm & above)	Tr
5	Abdomen (including pelvic region)	Ab
6	Spine	Sp
7	Upper Extremity	UE
8	Lower Extremity	LE
9	Unspecified (external to anatomy i.e. clothing)	Unsp

* - varies from AIS coding

ID	Structure	Abbr
1	Whole Area	Wh
2	Vessels	Vs
3	Nerves	Nv
4	Organs (incl muscle/tendon)	Or
5	Skeletal (incl cartilage)	Skl
6	Joint (incl ligaments)	Jnt
7	Instrumentation	Inst
8	Other	Oth
9	Skin (incl subcutaneous tissue)	Skn

ID	Aspect	Abbr
1	Right	R
2	Left/Cervical Spine	L/Cv
3	Bilateral	Bi
4	Central/Thoracic Spine	Ct/Th
5	Anterior/front/ventral	Ant
6	Posterior/back/dorsal/Lumbar Spine	Post/Lb
7	Superior/upper	Sup
8	Inferior/lower/Sacral Spine	Inf/Sc
9	Unknown/multiple regions	Unk
0	Whole region (including whole spinal cord)	Wh

- Based on Body Regions for AIS Coding
- Number Protocol – Nodes, Elements, Parts, Materials, ….
  - [**B**ody Region][**S**tructure][**A**spect][Sequential Numbering **#**] = **BSA#####**
- Name Protocol [Body Region]-[Structure]-[Aspect]-Description
- Examples:
  - Number: 85200021 Name: LE-Skl-L-Tibea
- Avoids ID conflicts when updating body regions

WAYNE STATE UNIVERSITY

/cont

WSUHBM – Hierarchy

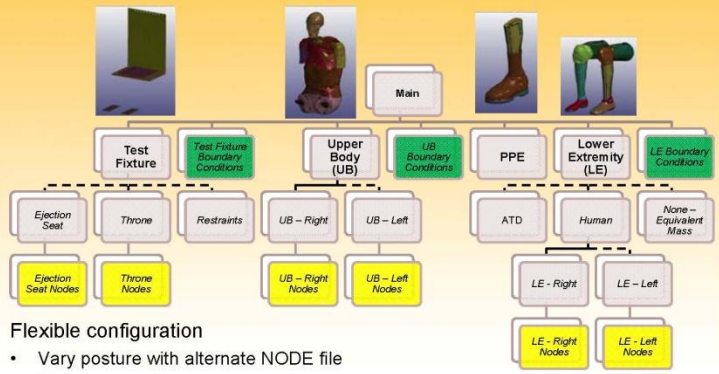

Flexible configuration

- Vary posture with alternate NODE file
- Utilize symmetry

WAYNE STATE UNIVERSITY

WSUHBM – Performance

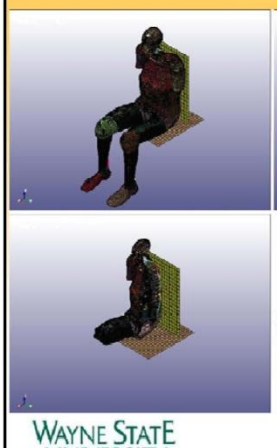

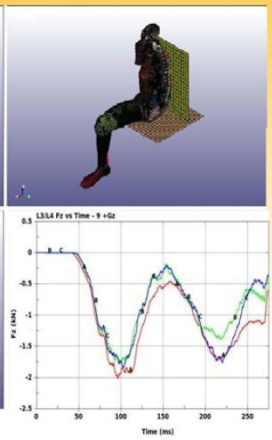

Optimization

- Full: 6-7 min/ms
  * 24-cores
  1x
- Half: 3-4 min/ms
  * 24-cores
  2x
- Quarter: 1-2 min/ms
  * 8-cores
  5x (8-cores)
  (3 x 8-cores)
  15x

* 24-core Opteron 61xx server, single precision

WAYNE STATE UNIVERSITY

Overview

- Development & Validation (automotive)
- Model Overview
- Underbody Blast Application
- Flexion Injuries & Posture
- Conclusions

WAYNE STATE UNIVERSITY

UBB Application – Lower Leg

Dong, Zhu et al, 2013, "Blast effect on the lower extremities and its mitigation: a computational study," Journal of the Mechanical Behavior of Biomedical Materials

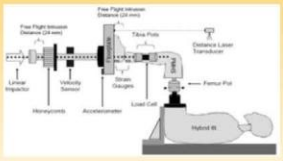

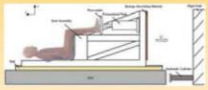

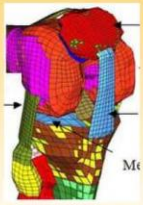

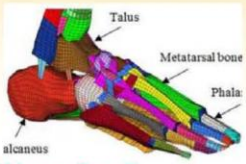

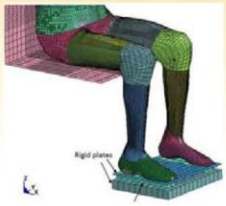

WAYNE STATE UNIVERSITY

/cont

/cont UBB Application – Lower Leg

- Validation – <u>tibia axial force and acceleration</u>
  - Impactor 7.2-11.6m/s, F = 5-7kN (McKay, 2009)
  - V_{foot} = 20m/s, Accel = 450g, w/fracture (Jin, 2013 submitted)

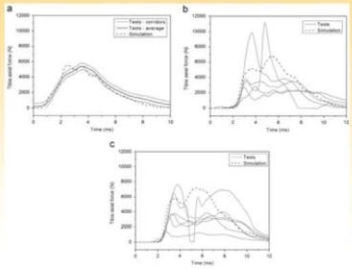

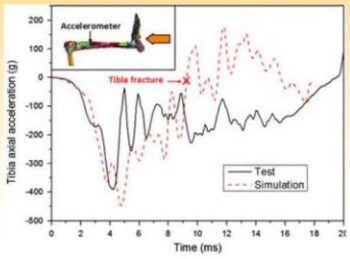

WAYNE STATE UNIVERSITY

/cont

UBB Application – Spine

WSUHBM spine validation target

- Axial load L3-L4, 9g vertical acceleration test (Prasad, 1974)

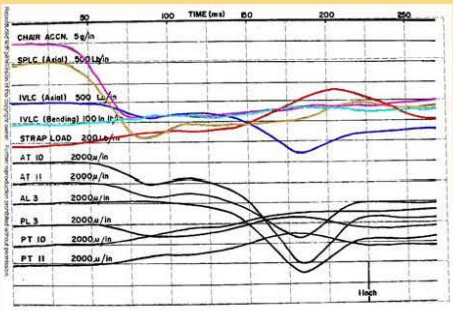

Prasad, P.,(1974),"The dynamic response of the spine during +Gz acceleration", Ph.D. Thesis, Wayne State University, Detroit.

King, A.I., Vulcan, P.,(1971),"Elastic deformation characteristics of the spine", J Biomechanics, (4), 413-29

WAYNE STATE UNIVERSITY

/cont UBB Application – Spine

Validation of WSUHBM under vertical acceleration – work-in-progress

- Target: PMHS spine loads from Prasad ejection seat tests (WSU,1973)

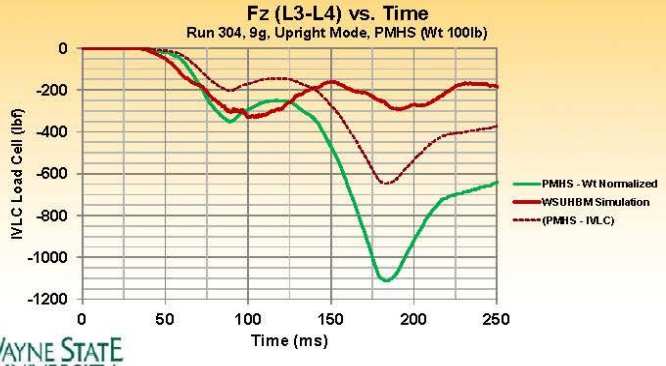

WAYNE STATE UNIVERSITY

Overview

- Development & Validation (automotive)
- Model Overview
- Underbody Blast Application
- Flexion Injuries & Posture
- Conclusions

WAYNE STATE UNIVERSITY

Posture Tolerance

Comparison of fracture tolerance with other postures under +Gz impact acceleration

Spinal Posture (seated)	Fracture G-level	N	Mean Age
Hyperextended	17.8 ±5.6	4	61.5
Upright (Normal)	10.4 ±3.8	5	61.0
Flexed	9.0 ±2.0	3	54.3

Ewing C.L., King, A.I., Prasad, P.,(1973),"Structural considerations of the human vertebral column under +Gz impact acceleration", ONR N00014-69-A-0235

WAYNE STATE UNIVERSITY

Flexion Injuries

Thoracolumbar spine fractures

- OEF Theater, NATO, Mounted, IED attacks, Jan-May(2008)

Fracture Type	Spine Posture	N	Distribution
Chance	Hyperflexion	5	42%
Compression	Flexion	5	42%
Burst	Upright	3	25%

Ragel, B.T., Allred, C.D., Brevard, S., Davis, R.T., Frank, E.H., 2009. Fractures of the thoracolumbar spine sustained by soldiers in vehicles attacked by improvised explosive devices. Spine 34, 2400-2405

WAYNE STATE UNIVERSITY

Flexion Injuries

Denis Three-column Spine

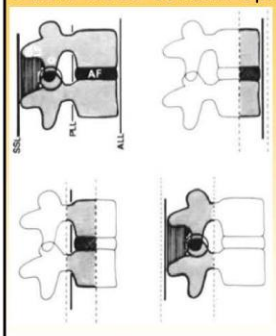

Denis, F., 1983. The three column spine and its significance in the classification of acute thoracolumbar spine injuries. Spine 8, 817-31

WAYNE STATE UNIVERSITY

Fracture loading (primary)

Compression Anterior

Chance Posterior

Burst Anterior & Middle

Flexion Injuries

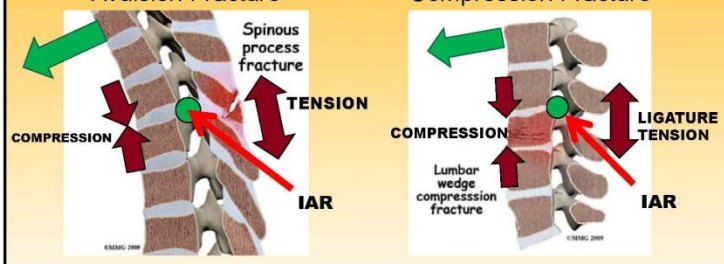

- $F_{Net\ Compression} = F_{"Nutcracker"} + F_{Inertial}$
- Failure Mode
  - Compression Fx – "nut cracked"
  - Avulsion(i.e. Chance) Fx – hinge fails

WAYNE STATE UNIVERSITY

Overview

- Development & Validation (automotive)
- Model Overview
- Underbody Blast Application
- Flexion Injuries & Posture
- Conclusions

WAYNE STATE UNIVERSITY

Conclusions

Observations and Conclusions

- Three-column spine characteristics are important to Theater injuries
  - High prevalence of flexion-related fractures
- Three-column ≠ Single-column spine
  - Flexion/"Nutcracker" force may increase spine compression beyond accelerative inertial loading
- Path forward, physical surrogate will be challenge
  - Numerical models best near term
  - WSUHBM single/double-column to three-column
    1. Flexion
    2. Extension

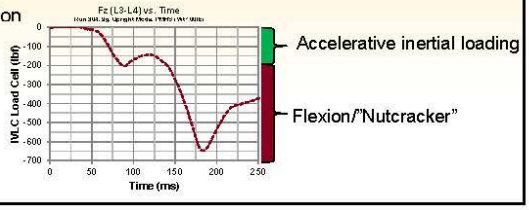

WAYNE STATE UNIVERSITY

The End

WAYNE STATE UNIVERSITY

- Human Anatomic Variability

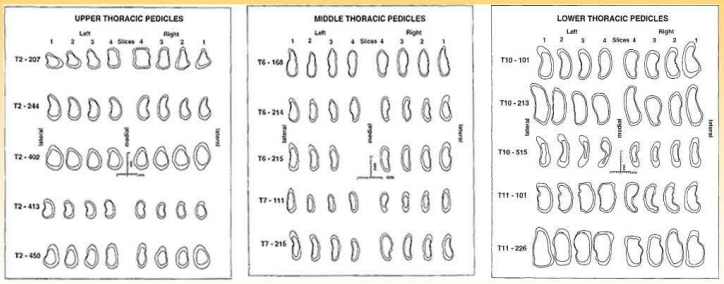

Panjabi et al., 1997

WAYNE STATE UNIVERSITY

- Human Anatomic Variability

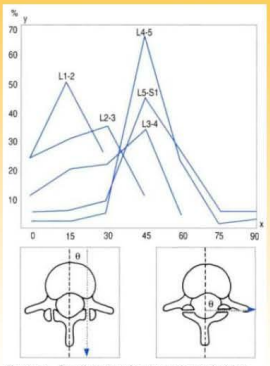

Figure 3.4 The orientation of lumbar zygapophysial joints with respect to the sagittal plane: incidence by level. (Based on Horwitz and Smith 1940[16]). x axis, orientation (degrees from sagittal plane), y axis, proportion of specimens showing particular orientation.

Bogduk, 1985

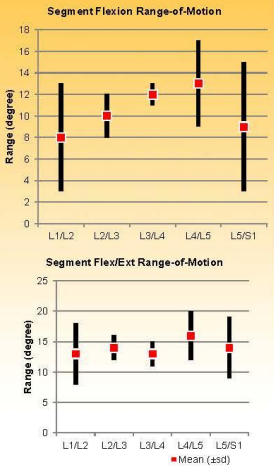

Pearcy, 1984

WAYNE STATE UNIVERSITY

MCW – PMHS vs. HIII

Pintar, F.A., Hallman, J.J., Yoganandan, N.,"Medical College of Wisconsin: Comments Baseline," WIAMan Briefing 06-DEC-2011

- Compare Sacrum, T1, & Head Accelerations
  - PMHS
  - Hybrid-III ATD (curved lumbar spine)
  - SID-HIII ATD (straight lumbar spine)

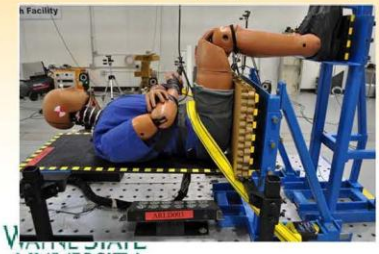

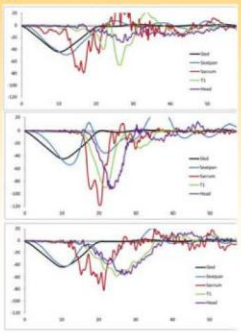

WAYNE STATE UNIVERSITY

/cont

/cont MCW – PMHS vs. HIII

MCW PMHS & HIII Physical Test Accelerations - **Seatpan**

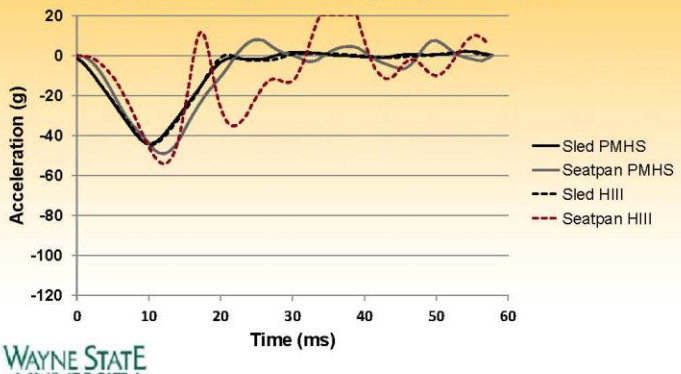

WAYNE STATE UNIVERSITY

/cont

MCW – PMHS vs. HIII

MCW PMHS & HIII Physical Test Accelerations

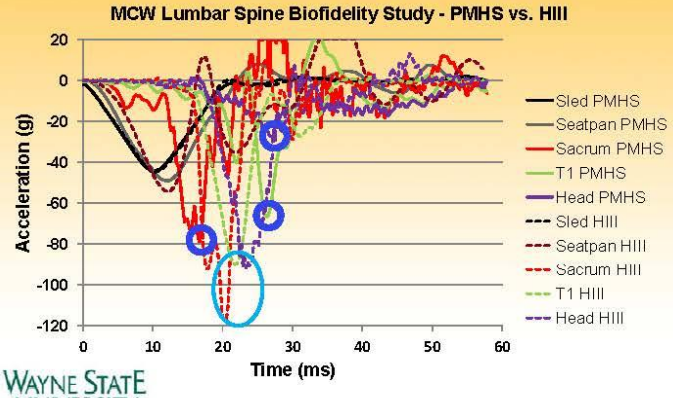

WAYNE STATE UNIVERSITY

/cont

Appendices

WAYNE STATE UNIVERSITY

WSUHBM - Thorax

Wang, H, 1995, "Development of a side impact finite element human thoracic model," Ph.D. thesis, Wayne State University, Detroit, MI

- 1st version w/organs – lungs, heart and associated major arteries/veins
- Anthropometry from Visual Human Project
- Validation – lateral pendulum impacts (Viano,1989)

Shah et al, 2001, "Development of a computer model to predict aortic rupture due to impact loading," Stapp Car Crash Journal Vol 45, SAE Paper No.: 2001-22-0007

- Modified aorta to include hemodynamic pressure effects
- Validation - **side impact**
  - Sternum pendulum impact (Kroell, 1974) : ~20kg @ 4-10m/s producing F = 5kN
  - Lateral pendulum impact (Viano, 1989) : 23.4kg producing F=3.5kN

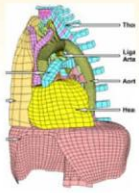

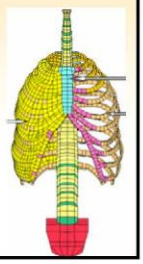

WAYNE STATE UNIVERSITY

WSUHBM - Shoulder

Iwamoto et al, 2000, "Development of a finite element model of the human shoulder," Stapp Car Crash Journal Vol. 44, SAE Paper No.: 2000-01-SC19

- Model scaled from CAD (Viewpoint Datalabs®)
- Integrated with Wang (1995) WSU thorax, WSU simple head & simple abdomen, WSU pelvis, and Hybrid III hands & lower extremities
- Validation - **side impact**
  - Pendulum impact: 23kg @ 4.5m/s producing F=3kN (Bendjellal, 1984)
  - Lateral impact: sled @ 6.2-8.6m/s producing F = 2-4kN (Cavanaugh, 1993)
  - Side airbag: 100-250g peak shoulder acceleration (WSU/TRW)

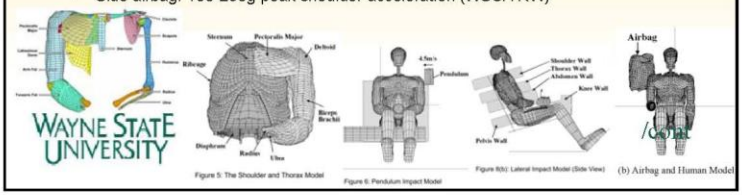

WAYNE STATE UNIVERSITY

WSUHAM - Abdomen

Lee/Yang, 2001, "Development of a finite element model of the human abdomen," Stapp Car Crash Journal Vol . 45, SAE Paper No.: 2001-22-0004

- Human Abdomen Model (WSUHAM)
- Derived from scaled Visible Human Male Project
- Validation - **side impact** & **narrow frontal impact (steerin**
  - 23.4kg pendulum 3" below sternum 5-10m/s producing F = 2-7kN (Viano, 1989)
  - 1 or 2m lateral freefall to armrest 4-9m/s producing 30-90g T12 peak acceleration (Walfisch, 1980)
  - Bar frontal impact @ T1 producing 2-15kN (steering wheel rim) (Cavanaugh, 1986)

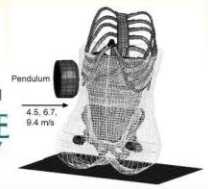

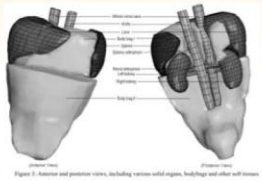

WAYNE STATE UNIVERSITY

/cont

/cont WSUHAM - Abdomen

Lee, 2002, "Development of a finite element model of the human abdomen," PhD Thesis, Wayne State University, Detroit

- Validation **side impact** & **narrow frontal impact (steering wheel/belt)**
  - As Lee/Yang (2001)
  - Seat belt loading – F = 4kN, Deflection = 3in. (Hardy, 2001)

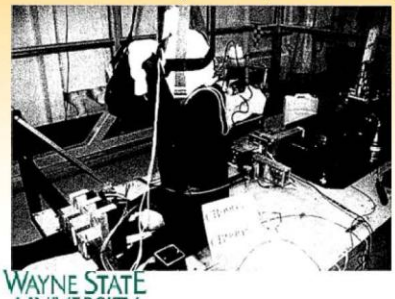

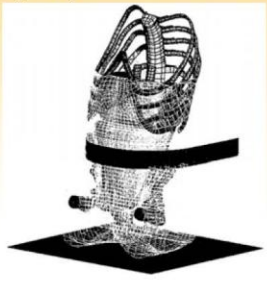

WAYNE STATE UNIVERSITY

WSHM02-1 – Whole Body

Wayne State Human Model Version 2002-1 (WSHM02-1)
Integration of

- Shoulder (Iwamoto et al, 2000) – PAM-CRASH
- Thorax (Shah et al, 2001) – LS-DYNA
- Abdomen (Lee and Yang, 2001) – PAM-CRASH

By Shah - A.K.A Wayne State Human Body Model (WSUHBM)
Validations – none (relied upon component level)

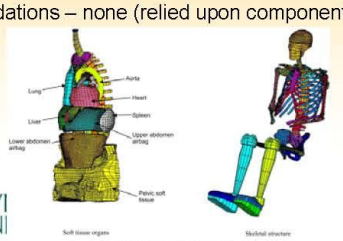

/cont

/cont WSHM04-1 – Whole Body

Shah, 2004, "A partially validated finite element whole-body human model for organ level injury prediction," Proceedings of IMECE04, 2004 ASME International Mechanical Engineering Congress

- Modified – version of WSHM02-1
  - Improved mesh
  - Extended abdominal skin
  - Truncated arms to avoid validation contacts
  - Added "blood" to the aorta
- Validation – **frontal (belt, airbag, steering wheel)**
  - Mid-abdominal seatbelt & airbag: 2-20msec, F = 3.5-4.5kN, Abdominal penetration = 3-4in, (Hardy, 2001)

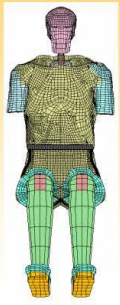

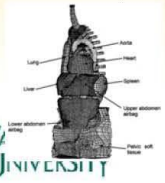

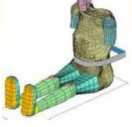

/cont

/cont WSHM04-1 – Whole Body

Shah, 2004, "User's manual whole-body human finite element model," Bioengineering Center, Wayne State University, Detroit, MI.

- Validation – **frontal/oblique** (pendulum impacts, loading 30-50msec)
  - Oblique chest: 23.4kg @ 6.5m/s, F = 5kN peak, 100mm deflection (Viano, 1989)
  - Frontal chest: 23.1kg @ 6.5m/s, F=4kN peak, 60mm deflection (Kroell, 1974)
  - Oblique abdomen: 23.4kg @ 6.5m/s, F=4kN, 75mm deflection (Viano, 1989)
- Validation – **abdomen (steering wheel, side arm rest)**
  - Abdomen bar impact: 32kg @ 6.1m/s, F=4kN,120mm deflection (Cavanaugh, 1986)
  - Whole body drop: 1m drop (4.4m/s), F=5kN (Walfisch, 1980 IRCOBI)

WAYNE STATE UNIVERSITY

/cont

/cont WSHM06-1 – Whole Body

Shah el al, 2005, "Analysis of a real-world crash using finite element modeling to examine traumatic rupture of the aorta", SAE Paper No.: 2005-01-1293

- Refined WSHM04-1 leg joints, respiratory & cardiovascular system
- Validation – **side impact (aortic stress)**
  - Vehicle-to-vehicle impact into driver side door
  - PDOF 240 degrees, Impact velocity 14mph
  - Metric: Aortic stress

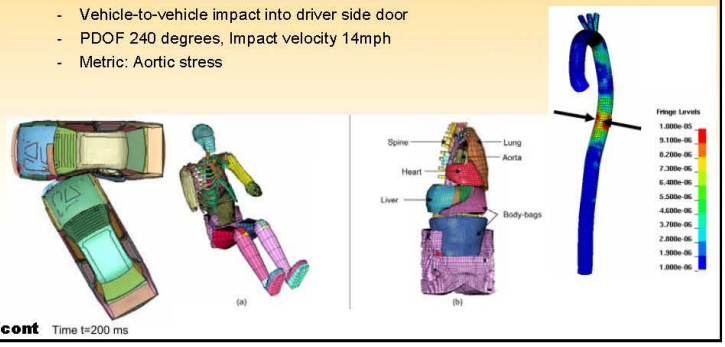

/cont Time t=200 ms

/cont WSHM06-1 – Whole Body

Shah, 2007, "Investigation of traumatic rupture of the aorta (TRA) by obtaining aorta material and failure properties and simulating real-world aortic injury crashes using the whole-body finite element (FE) human model," PhD. Thesis, Wayne State University, Detroit

- A.K.A. Wayne State Human Body Model-II (WSUHBM)
- Refined WSHM04-1 (Validation follows)
  - Aortic injury investigation
  - Reintroduced ¾ arm
  - refined abdomen, respiratory & cardiovascular system
  - Added kinematic joints for hip, knee, and ankle

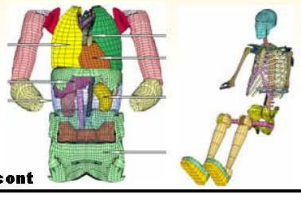

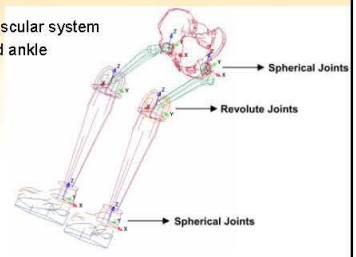

/cont

/cont WSHM06-1 – Whole Body

Siegel el al, 2006, "Computer simulation and validation of the Archimedes Lever hypothesis as mechanism for aortic isthmus disruption in a case of later impact motor vehicle crash: a Crash Injury Research Engineering Network (CIREN) study", J Trauma Injury, Infection, and Critical Care, 1072-82.

- Validation - **side impact (haemostatic pressure)**
  - Vehicle-to-vehicle impact into driver side door
  - PDOF 260 degrees, Delta-V 46kph
  - Metric: Aortic arch haemostatic pressure

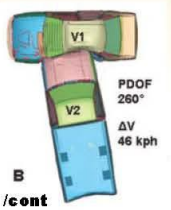

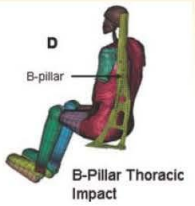

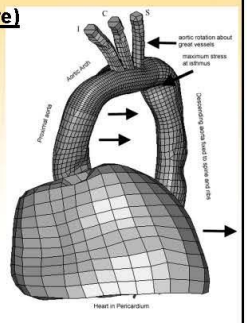

/cont

/cont WSHM06-1 – Whole Body

Siegel el al, 2010, "Analysis of the mechanism of lateral impact aortic isthmus disruption in real-life motor vehicle crashes using a computer-based finite element numeric model: with simulation of prevention strategies", J Trauma Injury, Infection, and Critical Care.

- Investigate efficacy of side impact mitigation schemes (i.e. airbag)
- Validation - **side impact (haemostatic pressure)**
  - Vehicle-to-vehicle crashes (CIREN)
  - Delta-V: 59 and 45kph (37 and 28mph)
  - Metric: Aortic arch haemostatic pressure

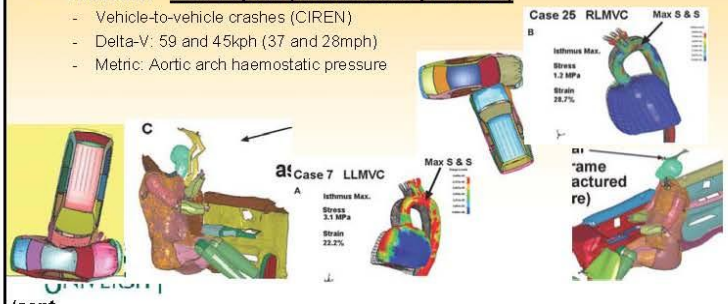

/cont

/cont WSHBM-II – Whole Body

Belwadi el al, 2011, "Finite element reconstruction of real world aortic injury in near-side lateral automotive crashes with conceptual countermeasures," PhD Thesis, Wayne State University, Detroit.

Belwadi el al, 2012, "Finite element aortic injury reconstruction of near side lateral impacts using real world crash data," J of Biomech Eng.

- Validation – **side impact (aortic pressure & strain)**
  - compared metrics to real-world crash outcomes
  - Average maximum principal strain (AMPS)
  - Maximum pressures in the aorta

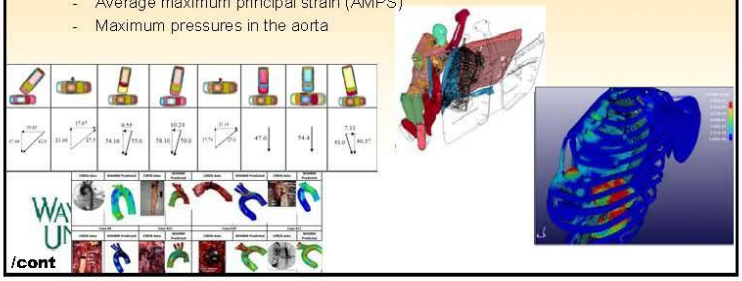

/cont

/cont WSHBM-II – Whole Body

Belwadi el al, 2012, "Aortic mechanics in high-speed racing crashes", SAE Paper No.: 2012-01-0101

- Evaluate 6-point harness and shoulder pad
- Validation – **side impact (aortic pressure , strain, & kinematics, thoracic deformation)**
  - Indy race car lateral impact (Begeman and Melvin, 2002 - MADYMO)
  - Delta-V 86.9-104.6kph (54-65mph)
  - Metric: Aortic haemostatic pressure, ave max principal strain (AMPS) (vs Belwadi, 2011), aortic motion and deformation of the thorax.

Figure 1. Initial position of WSHBM in the Indy racing buck

WSU LLMS-Lower Extremity

Lower Limb Model for Safety (LLMS) from CT & MRI of subject

Beillas et al, 1999, "Foot and ankle finite element modeling using CT-scan data," 43nd Stapp Car Crash Conference, SAE Paper No.: 99SC11 [affiliated with Wayne State University]

Beillas et al, 2001,"Lower limb: advanced FE model and new experimental data," 45th Stapp Car Crash Conference, SAE Paper No.: 2001-22-00022

Validation

Table 2: List of the set-up used for the validation of the model by anatomical region and loading type

Test Condition	Setup	Reference	Static or Dynamic
Tibia region:			
Axial compression	Present reanalysis		S
Foot & Tibia complex (new set-up only)			
Axial compression along the tibia	Present reanalysis		S
Femur-Knee-Tibia complex:			
Horizontal impact on patella	90° knee angle	Haut, R.C. et al. (1995)	D
Horizontal impact on patella	90°(+) knee angle	Hayashi et al. (1996)	D
Vertical impact on tibia	90° knee angle	Banglmaier et al. (1999)	D
A-P shear on tibia	90° knee angle	Viano et al. (1978)	D
Whole lower limb			
lateral-medial shear on proximal tibia	Standing position	Kajzer et al. (1990)	D
Knee bending (lateral-medial shear on distal tibia)	Standing position	Kajzer et al. (1993)	D
Whole Body			
Sled		Cheng et al. (1984)	D

/cont

/cont WSU LLMS-Lower Extremity

Beillas et al, 2004,"A new method to investigate in vivo knee behavior using a finite element model of the lower limb," 45th Stapp Car Crash Conference, J Biomech, 37, 1019-30

- Hopping on one leg, flexed knee
- Validation – **kinematics during hop**
  - Joint angle
  - Joint displacement

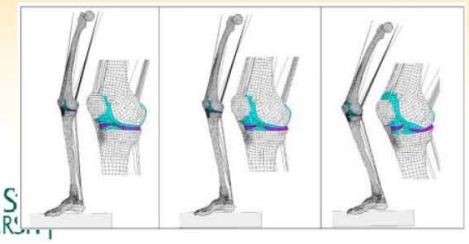

WAYNE S
UNIVER

/cont

/cont WSU LLMS-Lower Extremity

Beillas et al, 2007,"Sensitivity of the tibio-femoral response to finite element modeling parameters," Computer Methods in Biomechanics and Biomedical Engineering, 209-21

- Hopping on one leg, flexed knee
  - Prescribed femur motion
  - Prescribed ground motion – peak 2500N
- Simulated muscle forces
- Validation - **joint angles**

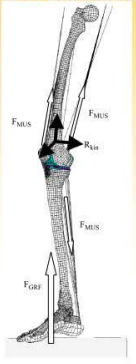

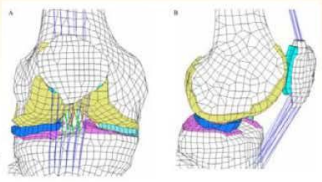

WAYNE STATE UNIVERSITY

Overview

- Development & Validation (automotive)
- Model Overview
- Underbody Blast Application
- Flexion Injuries & Posture
- Conclusions

WAYNE STATE UNIVERSITY

/cont MCW – Baseline Pulse

MCW PMHS Physical Test Accelerations

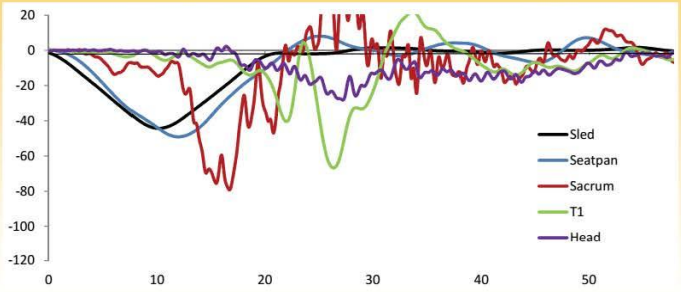

Note: Subject sustained a pelvic ring fracture

WAYNE STATE UNIVERSITY

C244

/cont **MCW – PMHS vs. HIII**

MCW PMHS & HIII Physical Test Accelerations - **Sled**

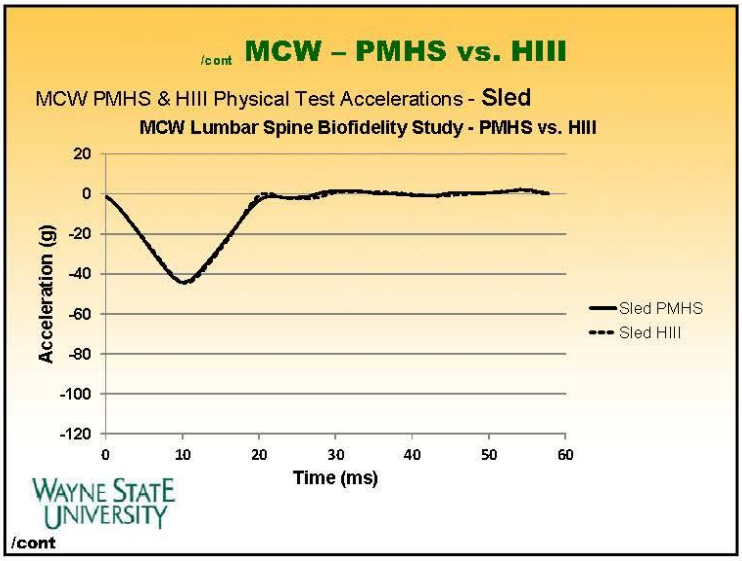

WAYNE STATE UNIVERSITY

/cont

/cont **MCW – PMHS vs. HIII**

MCW PMHS & HIII Physical Test Accelerations - **Seatpan**

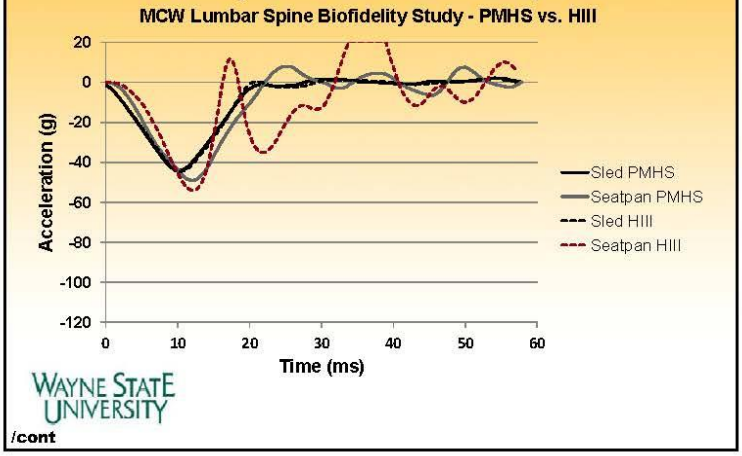

WAYNE STATE UNIVERSITY

/cont

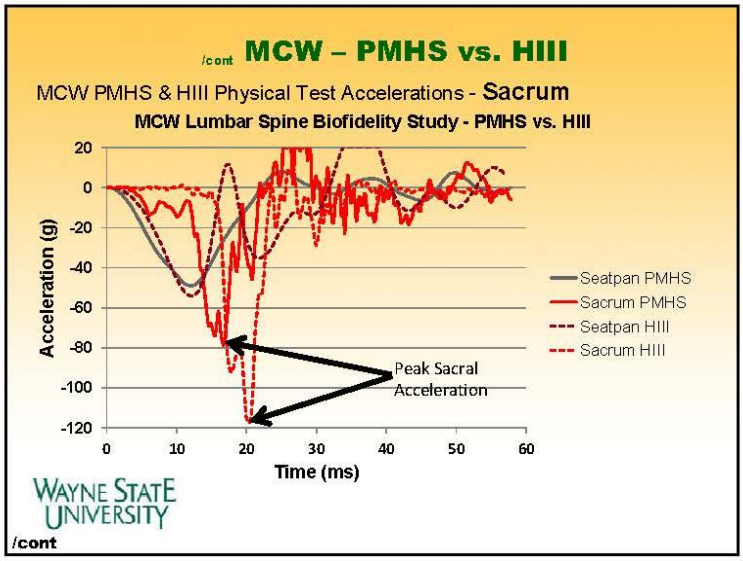
/cont MCW – PMHS vs. HIII
MCW PMHS & HIII Physical Test Accelerations - Sacrum
MCW Lumbar Spine Biofidelity Study - PMHS vs. HIII
Acceleration (g)
Time (ms)
Seatpan PMHS
Sacrum PMHS
Seatpan HIII
Sacrum HIII
Peak Sacral Acceleration
WAYNE STATE UNIVERSITY
/cont

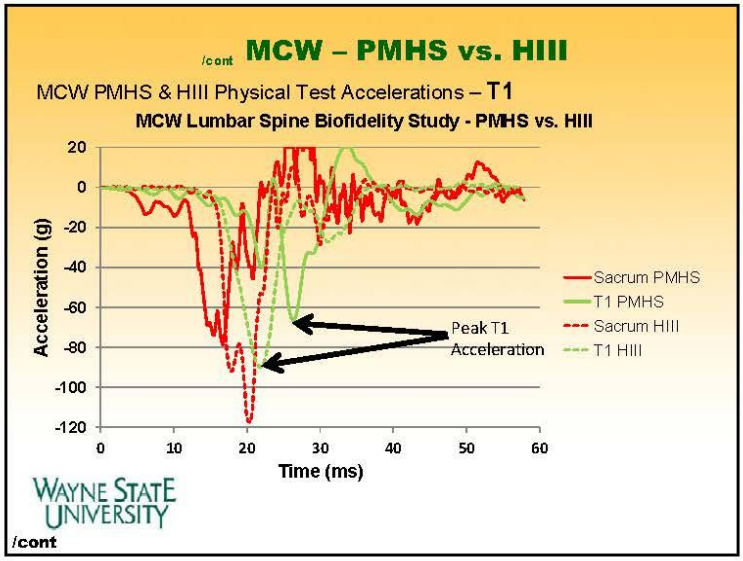
/cont MCW – PMHS vs. HIII
MCW PMHS & HIII Physical Test Accelerations – T1
MCW Lumbar Spine Biofidelity Study - PMHS vs. HIII
Acceleration (g)
Time (ms)
Sacrum PMHS
T1 PMHS
Sacrum HIII
T1 HIII
Peak T1 Acceleration
WAYNE STATE UNIVERSITY
/cont

/cont **MCW – PMHS vs. HIII**

MCW PMHS & HIII Physical Test Accelerations - **Head**

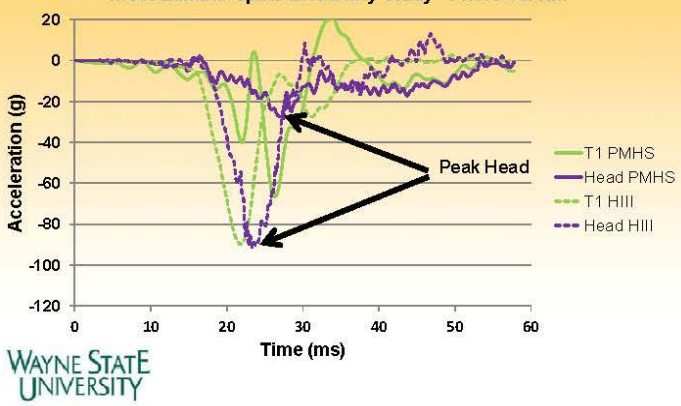

WAYNE STATE UNIVERSITY

WSUHBM - Simulations

WSUHBM Simulations – Two Postures

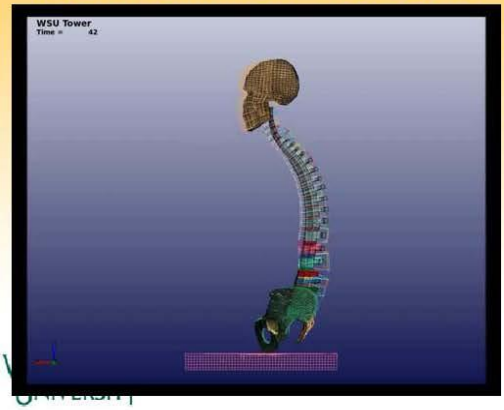

Solid - Posture_1
(Upright pelvis)

Wire - Posture_2
(Reclined pelvis)

/cont

C247

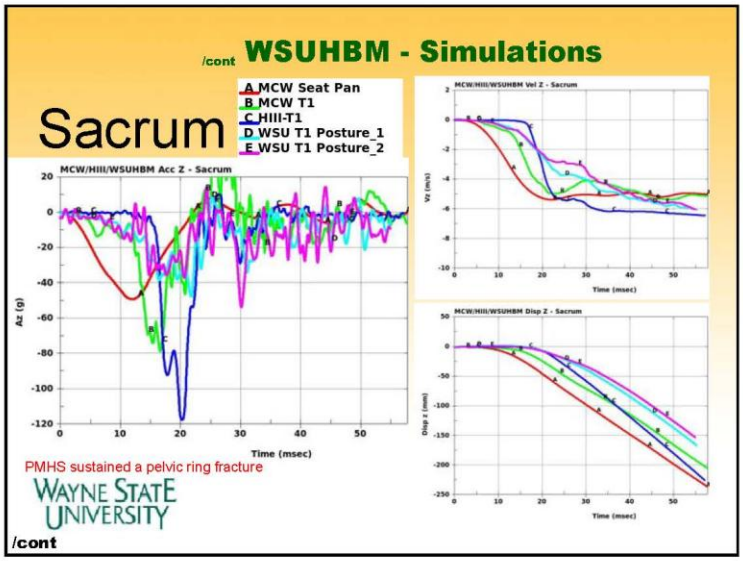
/cont
WSUHBM - Simulations
Sacrum
A MCW Seat Pan
B MCW T1
C HIII-T1
D WSU T1 Posture_1
E WSU T1 Posture_2
MCW/HIII/WSUHBM Acc Z - Sacrum
Az (g)
Time (msec)
MCW/HIII/WSUHBM Vel Z - Sacrum
Vz (m/s)
MCW/HIII/WSUHBM Disp Z - Sacrum
Disp z (mm)
PMHS sustained a pelvic ring fracture
WAYNE STATE UNIVERSITY
/cont

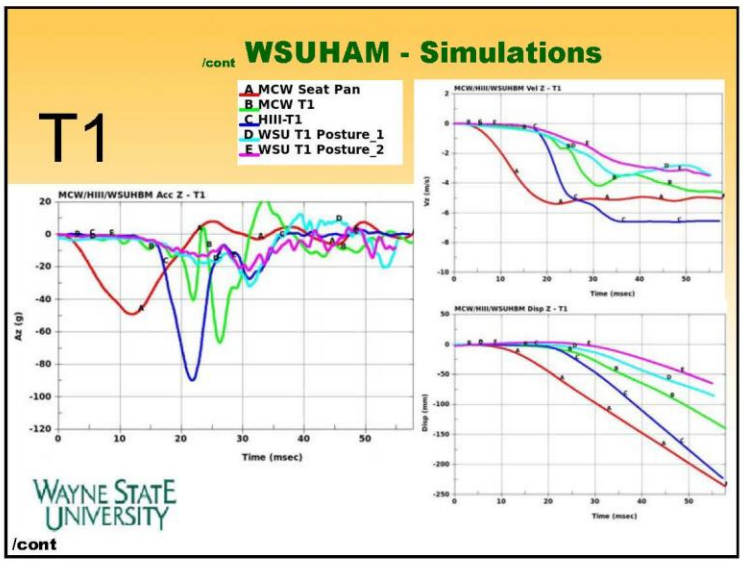
/cont
WSUHAM - Simulations
T1
A MCW Seat Pan
B MCW T1
C HIII-T1
D WSU T1 Posture_1
E WSU T1 Posture_2
MCW/HIII/WSUHBM Acc Z - T1
Az (g)
Time (msec)
MCW/HIII/WSUHBM Vel Z - T1
Vz (m/s)
MCW/HIII/WSUHBM Disp Z - T1
Disp (mm)
WAYNE STATE UNIVERSITY
/cont

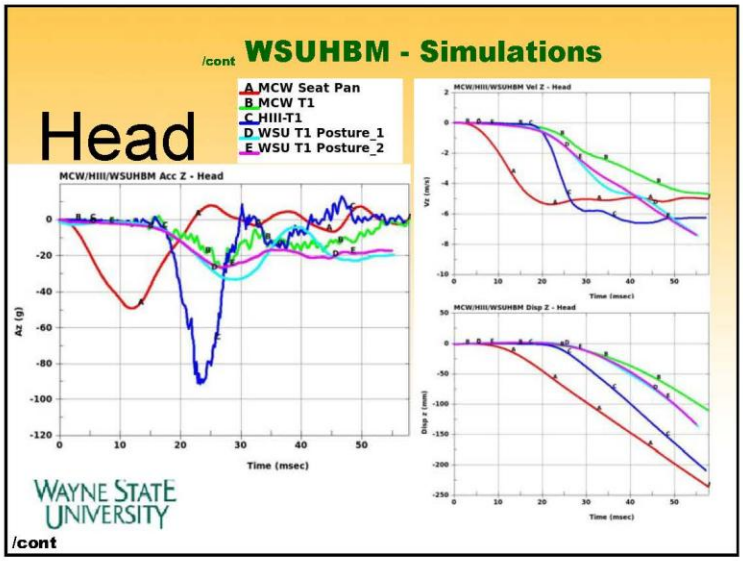
/cont
WSUHBM - Simulations
Head
A MCW Seat Pan
B MCW T1
C HIII-T1
D WSU T1 Posture_1
E WSU T1 Posture_2
MCW/HIII/WSUHBM Acc Z - Head
Az (g)
Time (msec)
MCW/HIII/WSUHBM Vel Z - Head
Vz (m/s)
Time (msec)
MCW/HIII/WSUHBM Disp Z - Head
Disp z (mm)
Time (msec)
WAYNE STATE UNIVERSITY
/cont

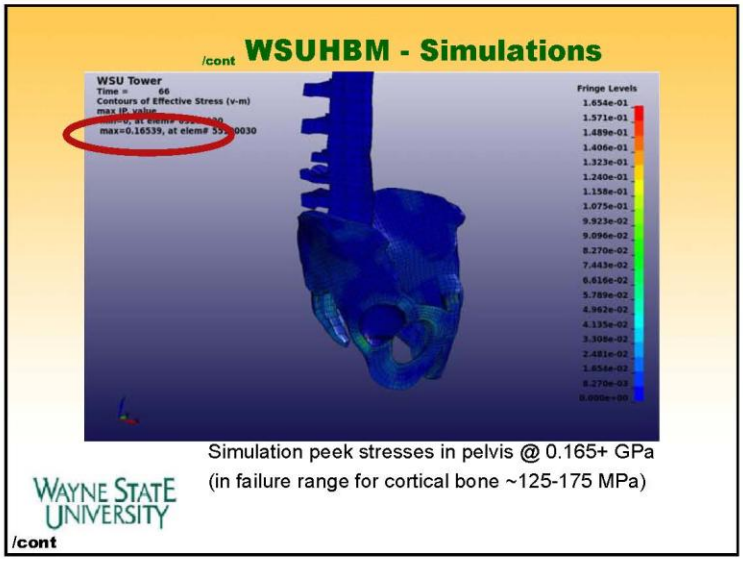
/cont
WSUHBM - Simulations
WSU Tower
Contours of Effective Stress (v-m)
max IP value
max=0.16539, at elem# 55
Fringe Levels
1.654e-01
1.571e-01
1.489e-01
1.406e-01
1.323e-01
1.240e-01
1.158e-01
1.075e-01
9.923e-02
9.096e-02
8.270e-02
7.443e-02
6.616e-02
5.789e-02
4.962e-02
4.135e-02
3.308e-02
2.481e-02
1.654e-02
8.270e-03
Simulation peek stresses in pelvis @ 0.165+ GPa
(in failure range for cortical bone ~125-175 MPa)
WAYNE STATE UNIVERSITY
/cont

C249

- WSUHBM Posterior Spine & Ligature
  - Human highly variable
  - Rigid beams/belts
  - Parametrically defined

Table 2. *Values for anthropometric calculated dimensions measured in the mid-sagittal plane*

Vertebra	n	α (deg.)	L	VBH	VBW
Cervical region					
C_3	150	10·7	51·3	17·60	13·95
C_4	141	14·4	45·2	14·30	15·20
C_5	141	12·1	45·3	13·65	17·65
C_6	141	9·1	48·9	13·25	17·80
C_7	140	3·8	56·2	13·45	16·30
C_7	126	7·3	63·3	16·75	16·35
Lumbar region					
L_1	154	−5·8	80·9	26·25	33·80
L_2	157	−3·6	84·6	27·10	34·55
L_3	157	−0·3	85·2	27·90	34·65
L_4	157	1·9	83·5	27·25	34·60
L_5	156	8·2	77·4	27·00	34·05

α, angular inclination of the spinous process of vertebra; *L*, overall length of vertebra; VBH, average vertebral body height; VBW, average vertebral body width; n, number of measurements.

Gilad & Nissan, 1985

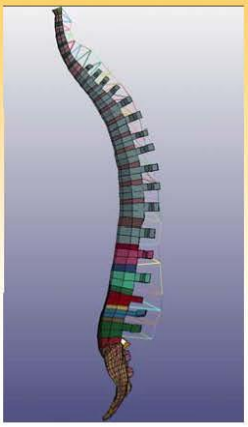

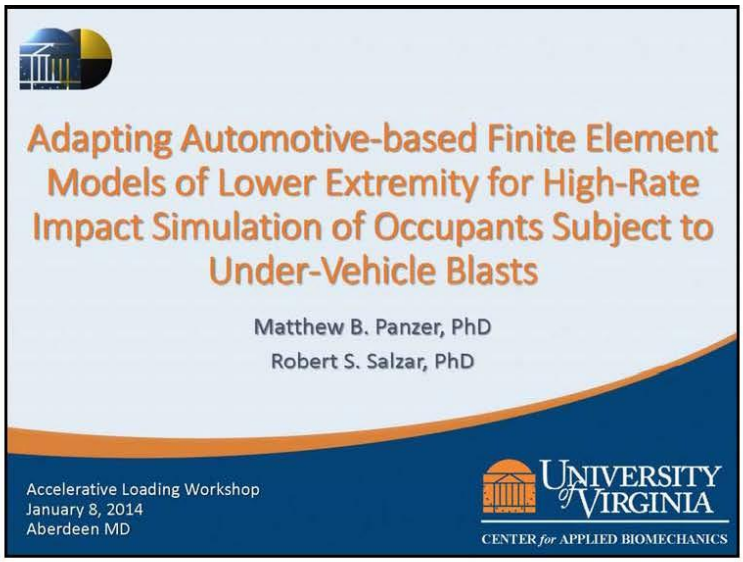
Adapting Automotive-based Finite Element Models of Lower Extremity for High-Rate Impact Simulation of Occupants Subject to Under-Vehicle Blasts
Matthew B. Panzer, PhD
Robert S. Salzar, PhD
Accelerative Loading Workshop
January 8, 2014
Aberdeen MD
UNIVERSITY of VIRGINIA
CENTER for APPLIED BIOMECHANICS

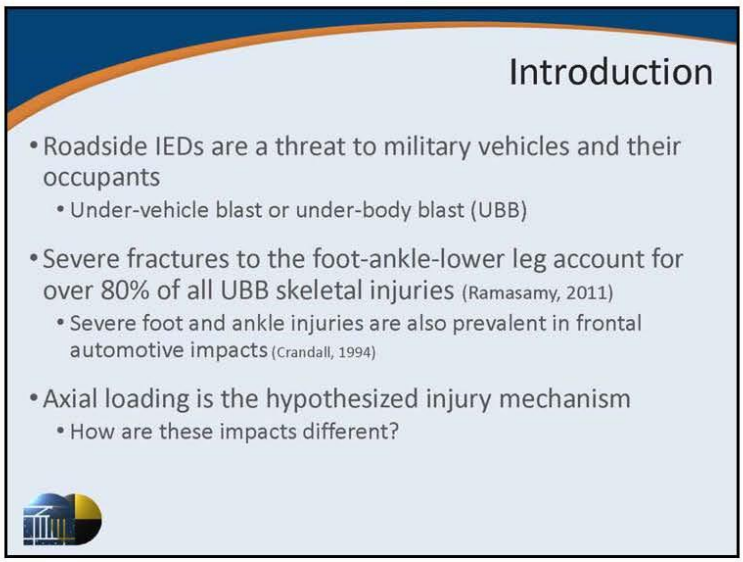
Introduction
• Roadside IEDs are a threat to military vehicles and their occupants
• Under-vehicle blast or under-body blast (UBB)
• Severe fractures to the foot-ankle-lower leg account for over 80% of all UBB skeletal injuries (Ramasamy, 2011)
• Severe foot and ankle injuries are also prevalent in frontal automotive impacts (Crandall, 1994)
• Axial loading is the hypothesized injury mechanism
• How are these impacts different?

Introduction

- Automotive occupant foot-ankle-leg loading in crash
  - Large stroke, moderate rate

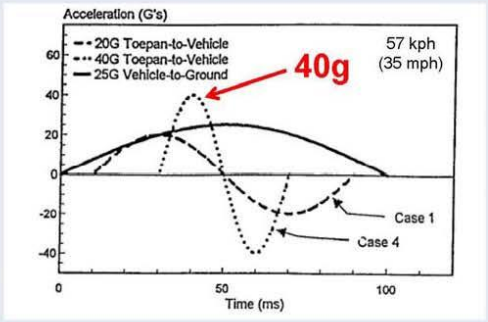

Crandall et al.,1995

Introduction

- Occupant foot-ankle-leg loading in UBB?
  - Short stroke, high rate

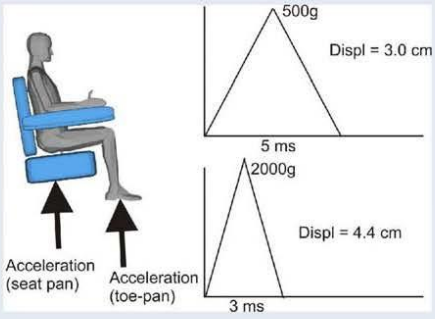

Salzar et al., 2013

Questions

- Can we use experience with automotive injury biomechanics to better understand military injuries?
  - Many human body models (HBM) developed for automotive injury biomechanics
- How well do automotive-based models perform in military environment?
  - Can these models be modified for a loading regime that they were not initially designed for?

Objectives

- Evaluation of existing automotive-based finite element (FE) models of the human and Hybrid-III lower leg for predicting the response and injury caused by UBB
- Modifications made to the model to improve their response for UBB loading
- Identification of areas of future research on model development and testing

FE Lower Leg Models

- Human model
  - Phase 1 GHBMC lower extremity FE model developed by UVa (UVA is Center of Expertise for the lower extremity and thorax)
  - 50th percentile male (175 cm, 77 kg) (Gayzik et al., 2009)
  - Shin et al., 2012. ABME
- Hybrid-III model
  - Hybrid-III (50th percentile male) lower extremity FE model developed by NCAC (GWU) and LSTC
  - Hybrid-III is a commonly used ATD in current UBB testing
  - Included with LS-Dyna license

FE Lower Leg Models

- Human model
  - Foot and ankle

Ligament modeling

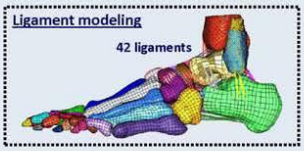

Foot modeling

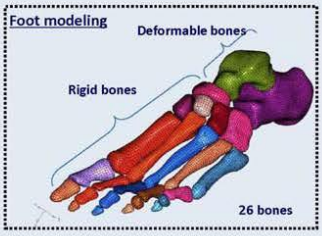

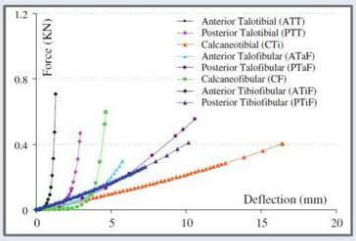

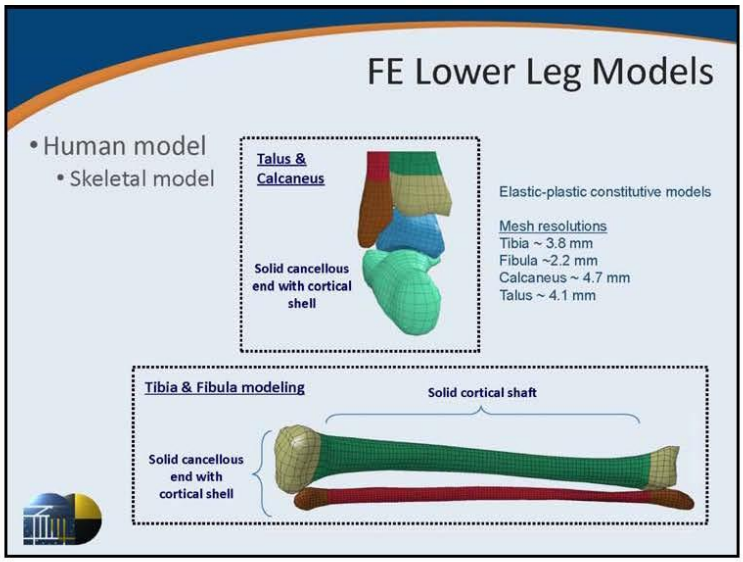
FE Lower Leg Models
• Human model
• Skeletal model
Talus & Calcaneus
Solid cancellous end with cortical shell
Elastic-plastic constitutive models
Mesh resolutions
Tibia ~ 3.8 mm
Fibula ~2.2 mm
Calcaneus ~ 4.7 mm
Talus ~ 4.1 mm
Tibia & Fibula modeling
Solid cortical shaft
Solid cancellous end with cortical shell

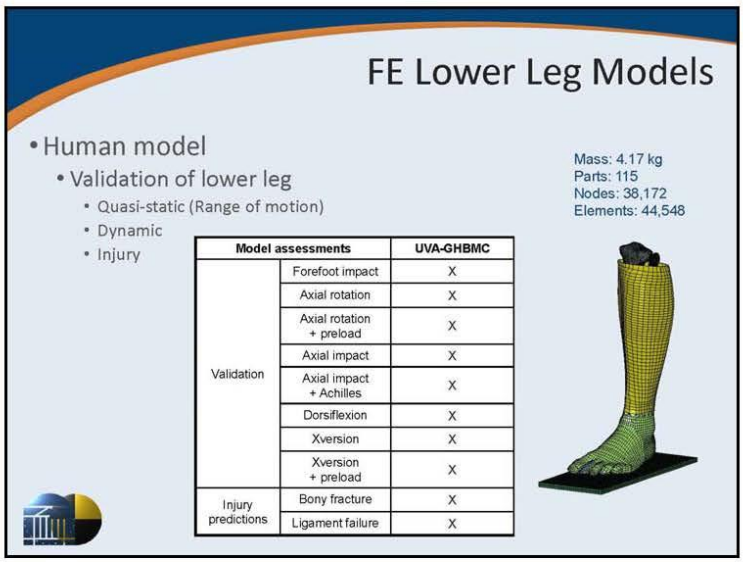
FE Lower Leg Models
• Human model
• Validation of lower leg
• Quasi-static (Range of motion)
• Dynamic
• Injury
Mass: 4.17 kg
Parts: 115
Nodes: 38,172
Elements: 44,548
Model assessments
UVA-GHBMC
Validation
Forefoot impact X
Axial rotation X
Axial rotation + preload X
Axial impact X
Axial impact + Achilles X
Dorsiflexion X
Xversion X
Xversion + preload X
Injury predictions
Bony fracture X
Ligament failure X

FE Lower Leg Models

- Hybrid-III model

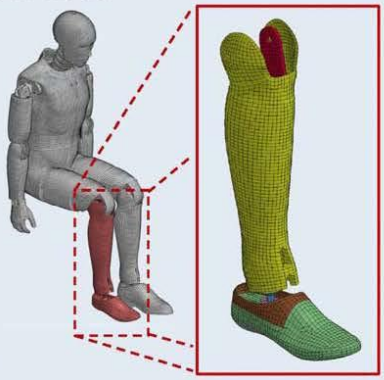

Mass: 5.02 kg
Parts: 15
Nodes: 17,293
Elements: 18,411

Structural members (steel components) are linear elastic.

Leg flesh and foot is modeled as a composite of foam and rubber (skin).

Spherical joint at ankle between foot and tibia.

Experimental UBB Injury Model

- UVa UBB lower leg injury model
  - Drop height
    - 1 to 2 m (4.4 to 5.9 m/s)
  - Impact hammer mass
    - 38.5 to 61.2 kg
  - Stroke limited, pulse shaper
    - 25 mm (1")
    - EPS and Al honeycomb
  - Up to 600 g impact
    - Less than 2 ms duration

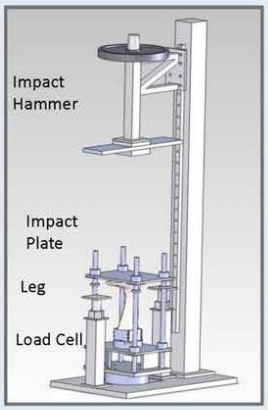

Experimental UBB Injury Model

- PMHS UBB testing
  - 18 fresh-frozen PMHS lower legs
    - Henderson et al., 2013. *IRCOBI.*

Age (years)	Height (cm)	Weight (kg)	Tibia Length (mm)
53.4 ± 6.9	181.7 ± 3.6	96.1 ± 20.6	387.3 ± 21.6

  - 18 tests with Hybrid-III 50th leg
    - Bailey et al., 2013. *IRCOBI.*
  - Proximal tibia potted with plantar surface facing up
  - Preloaded impact plate (10.2 kg)
  - Reaction mass (7.2 kg) at proximal tibia unconstrained in vertical

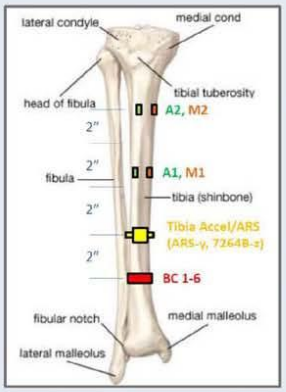

Experimental UBB Injury Model

- Example impact time-history
  - PMHS data

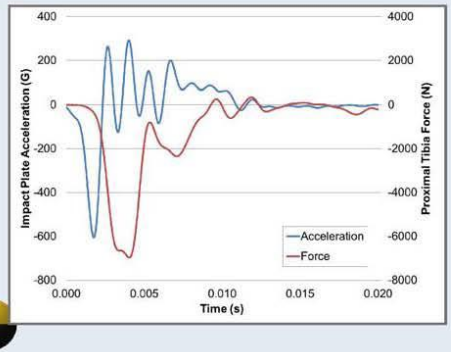

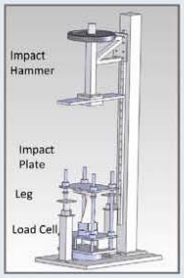

Simulation Setup

- FE Model setup
  - Preload 100 N
  - Impact plate prescribed test acceleration pulse
  - Simulation time:
    - 20 ms
  - Output focus:
    - Load cell force(s)
    - Distal tibia strain (PMHS)

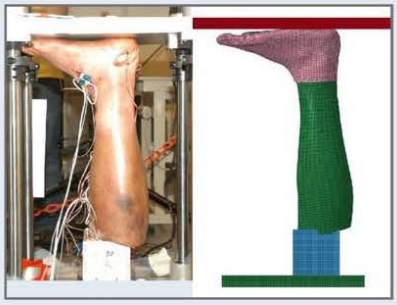

Results – Original Models

- Human lower leg model
  - Substantial under-estimation of force, loading rate

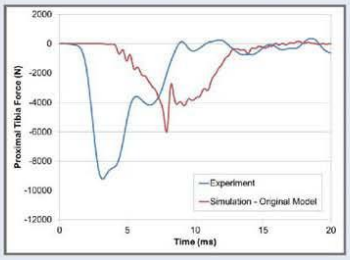

← 61 kg @ 5.4 m/s

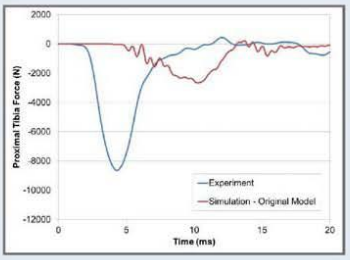

34 kg @ 4.7 m/s →

Results – Original Models

- Human lower leg model
  - Substantial under-estimation of anterior tibia strain

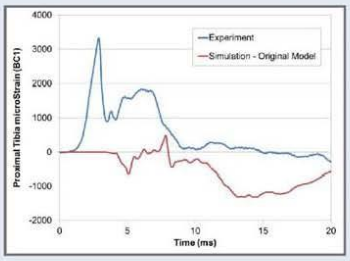

← 61 kg @ 5.4 m/s

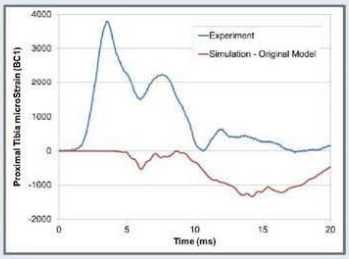

34 kg @ 4.7 m/s →

Results – Original Models

- Human lower leg model
  - Under-estimation of posterior tibia strain

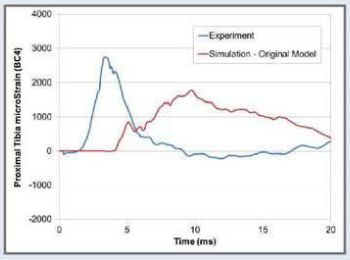

← 61 kg @ 5.4 m/s

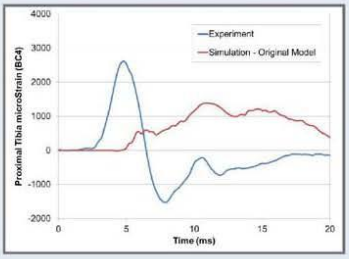

34 kg @ 4.7 m/s →

Results – Original Models

- Hybrid-III lower leg model
  - Under-estimation of tibia forces

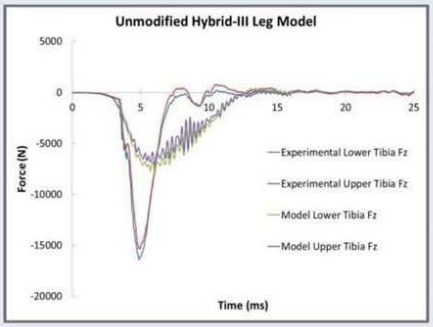

Results – Original Models

- Summary
  - Original lower legs models, developed for automotive applications, were not accurate for UBB loading
    - Slower loading rates, lower peak forces
- Key areas for improving model response
  - Material properties for the foot/heel
    - Both human and Hybrid-III models used non-rate sensitive material properties
  - Mesh refinement for bony tissues in human model
    - Fracture sensitivity, contact continuity issue for poorly meshed areas
    - Single-layer solid elements in tibia/fibula cortical bone affect bending
  - Geometry refinement in Hybrid-III foot model
    - Incorrect ankle

Modifications

- Human model
  - Increased mesh density
    - Tibia: 3.8 mm to 1.9 mm
    - Fibula: 2.2 mm to 1.1 mm
    - Calcaneus: 4.7 mm to 3.2 mm
    - Talus: 4.1 mm to 2.3 mm

Increased to 2 through-thickness elements in shaft

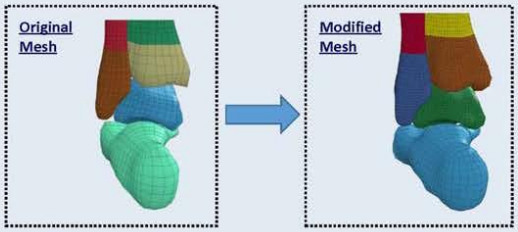

Modifications

- Human model
  - Incorporated a visco-hyperelastic model for dynamic heel-pad mechanics (Natali et al., 2010)

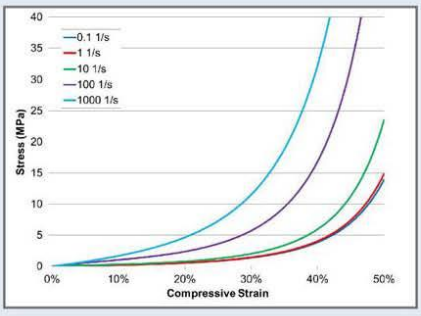

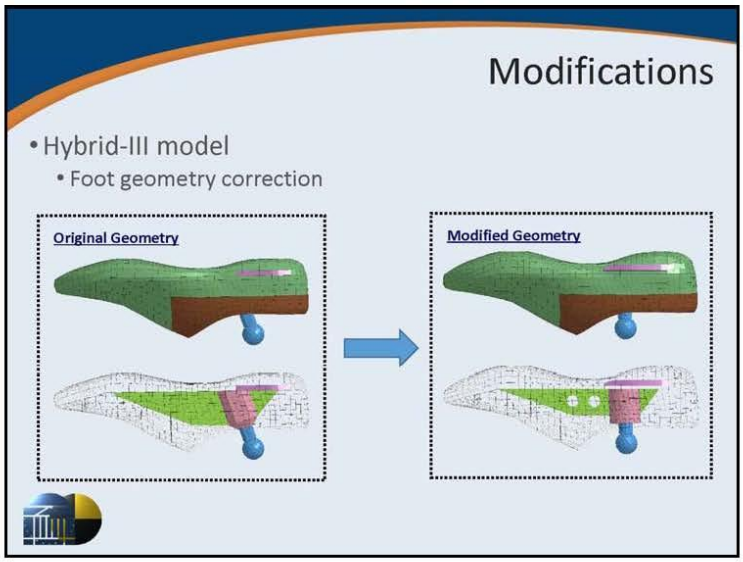
Modifications
• Hybrid-III model
• Foot geometry correction
Original Geometry
Modified Geometry

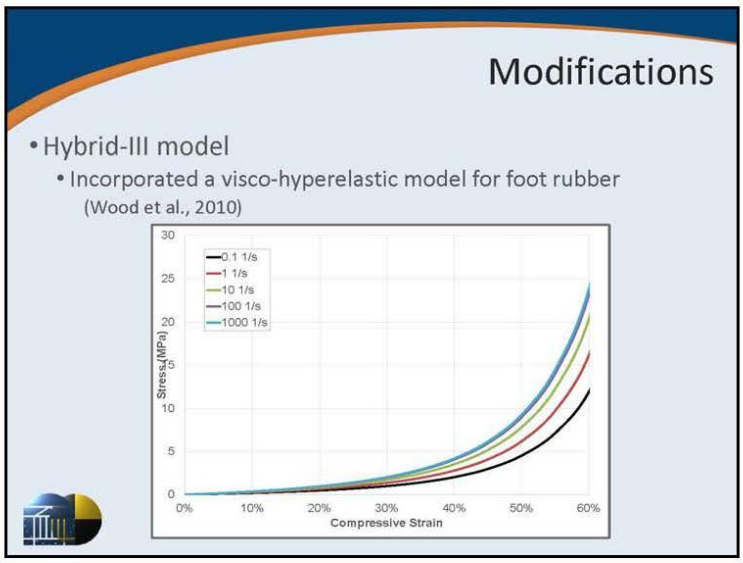
Modifications
• Hybrid-III model
• Incorporated a visco-hyperelastic model for foot rubber
(Wood et al., 2010)
0.1 1/s
1 1/s
10 1/s
100 1/s
1000 1/s
Stress (MPa)
Compressive Strain
0
5
10
15
20
25
30
0%
10%
20%
30%
40%
50%
60%

Results – Improved Models

- Human model
  - Improved loading rate, peak force, and phasing

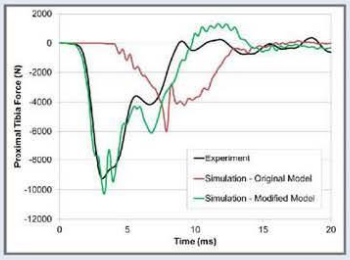

← 61 kg @ 5.4 m/s

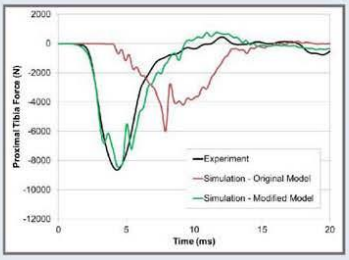

34 kg @ 4.7 m/s →

Results – Improved Models

- Human model
  - Under-estimation of peak anterior tibia strain persists

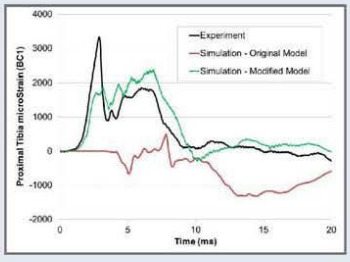

← 61 kg @ 5.4 m/s

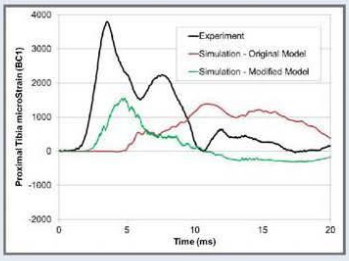

34 kg @ 4.7 m/s →

Results – Improved Models

- Human model
  - Under-estimation of peak posterior tibia strain persists

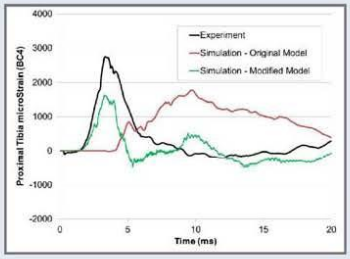

← 61 kg @ 5.4 m/s

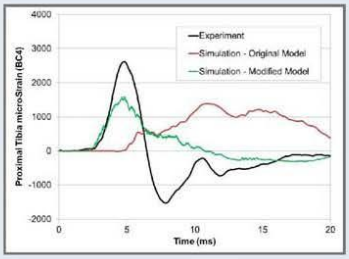

34 kg @ 4.7 m/s →

Results – Improved Models

- Human model
  - Summary of peak load cell force [mean R^2 = 0.85 for all traces]

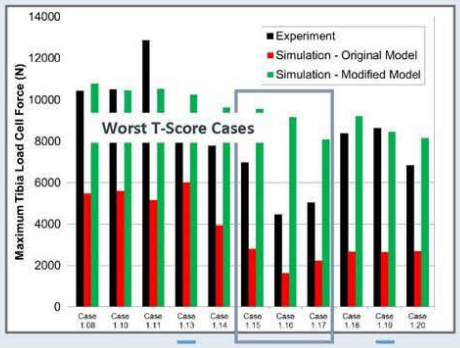

Case 1.13 and 1.19 were the example traces

Results – Improved Models

- Human model
  - Summary of peak anterior strain [mean R^2 = 0.44 for all traces]

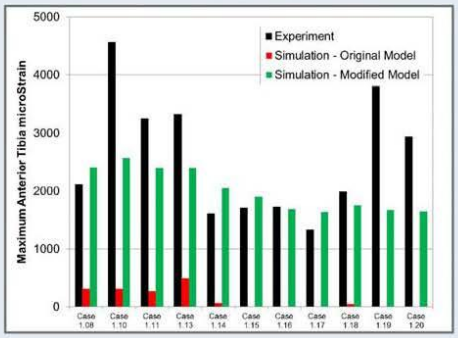

Case 1.13 and 1.19 were the example traces

Results – Improved Models

- Human model
  - Summary of peak posterior strain [mean R^2 = 0.52 for all traces]

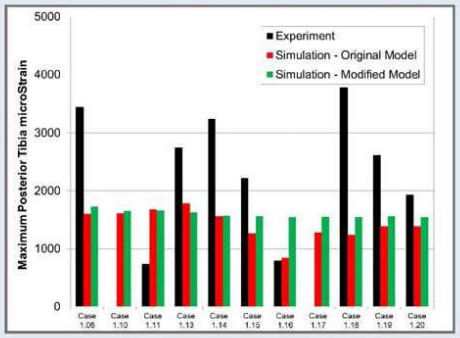

Case 1.13 and 1.19 were the example traces

Results – Improved Models

- Human model
  - Similar fracture patterns between experimental and model
    - Calcaneal fractures initiating at the subtalar joint

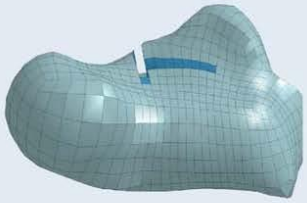

Case: 61 kg @ 5.4 m/s

Results – Improved Models

- Human model

Case	Hammer Mass (kg)	Velocity (m/s)	Injuries reported	Simulation Injury
1.08	61.2	5.73	Calcaneus: fx line into one joint surface	Calcaneus fx
1.10	61.2	4.09	Distal Tibia: fx, partial articular	Calcaneus fx
1.11	61.2	5.57	Talus: fx NFS Calcaneus: fx NFS	Calcaneus fx
1.13	61.2	5.35	Distal Tibia: fx, partial articular Calcaneus: fx, extra articular	Calcaneus fx
1.14	34.2	5.46	Calcaneus: fx line into one joint surface Talus: fx NFS	Calcaneus fx
1.15	34.2	5.46	Calcaneus: fx NFS	Calcaneus fx
1.16	34.2	4.98	Calcaneus: fx, extra articular	Calcaneus fx, shell only
1.17	34.2	4.44	Calcaneus: fx, extra articular	Calcaneus fx, shell only
1.18	34.2	4.93	None	Calcaneus fx, shell only
1.19	34.2	4.66	None	Calcaneus fx, shell only
1.20	34.2	4.70	None	Calcaneus fx, shell only

Results – Improved Models

- Hybrid-III model
  - Improved loading rate, peak force, and phase response
  - Good differentiation between upper and lower tibia forces

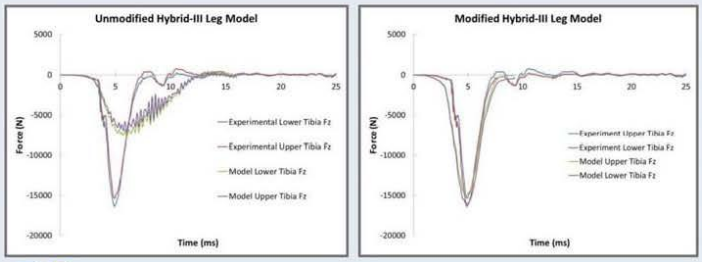

Summary

- Validating high-rate load transmission through a complex anatomical structure like the ankle is a challenge!
  - Results are encouraging
- External load response is representative for modified human and Hybrid-III lower leg models
- Internal load response in human needs improvement
- Very close to matching injury/no-injury in human model
- Model response is sensitive to soft material properties

Discussion

- Differences between human model and PMHS data
  - PMHS specific parameters (i.e., geometry, age, sex) were not accounted for in the model
    - Sensitivity of response to bone fracture thresholds
  - GHBMC ankle geometry may not be sufficient for UBB loading
    - No articular cartilage makes ankle lax, may alter kinematics

Ankle model tends to "roll" on impact, causing some tibia bending → experimental data suggests mainly axial tibia loading

Acknowledgements

- UVa Center for Applied Biomechanics
  - Founded in 1989, CAB is a joint venture between the University of Virginia Schools of Engineering and Medicine
  - State-of-the-art 30,000 sq ft facility north of Charlottesville VA
  - ~60 Researchers, staff, and students

Military Injury Biomechanics Group (Rob Salzar)
- 2 Mechanical Engineers
- 5 Graduate Students

Computational Biomechanics Group (Matt Panzer)
- 2 Research Scientists
- 2 Post-Docs
- 7 Graduate Students
- 2 Visiting Scholars


Thank you!

Current Research and Development Activities of the Full Body Model Center of Expertise of the Global Human Body Models Consortium Project

F. Scott Gayzik & Joel Stitzel
Co-PI's FBM COE
Wake Forest University
January 8th, 2014

Wake Forest School of Medicine

Virginia Tech COLLEGE of ENGINEERING

Global Human Body Models Consortium (GHBMC)

- An international consortium of automakers & suppliers working with research institutes and government agencies to advance human body modeling (HBM) technologies for crash simulations

- OBJECTIVE: To consolidate world-wide HBM R&D effort into a single global effort

- MISSION: To develop and maintain high fidelity FE human body models for crash simulations

GHBMC: A Research Project with Global Reach

Full Body Model Center of Expertise

Wake Forest School of Medicine

Medical Imaging

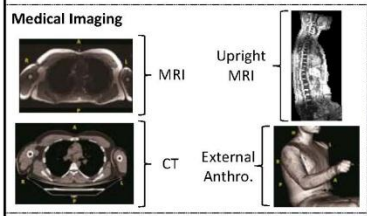

CAD Development

- NURBS (CAD), 400+ components, G1 continuous

Model integration

- Model integration at 5 intersections of body region models
- Examples:

Model Validation and robustness

- Key challenges
- Good agreement with data
- Robustness for a broad user base

Reference: Gayzik, F.S. et al., The development of full body geometrical data for finite element models: A multi-modality approach. 2011. *Annals of Biomedical Eng.*, Oct;39(10):2568-83. Epub 2011 Jul 23.

C271

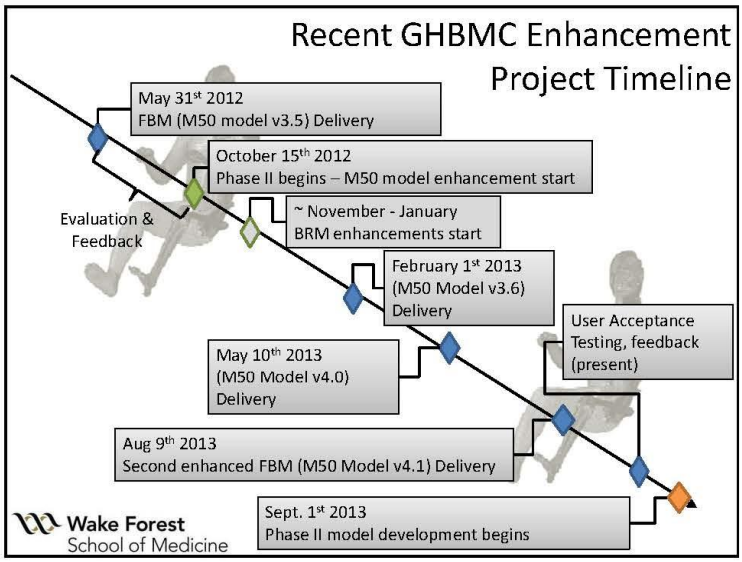
Recent GHBMC Enhancement Project Timeline
May 31st 2012
FBM (M50 model v3.5) Delivery
October 15th 2012
Phase II begins – M50 model enhancement start
~ November - January
BRM enhancements start
Evaluation & Feedback
February 1st 2013
(M50 Model v3.6)
Delivery
User Acceptance Testing, feedback (present)
May 10th 2013
(M50 Model v4.0)
Delivery
Aug 9th 2013
Second enhanced FBM (M50 Model v4.1) Delivery
Sept. 1st 2013
Phase II model development begins
Wake Forest
School of Medicine

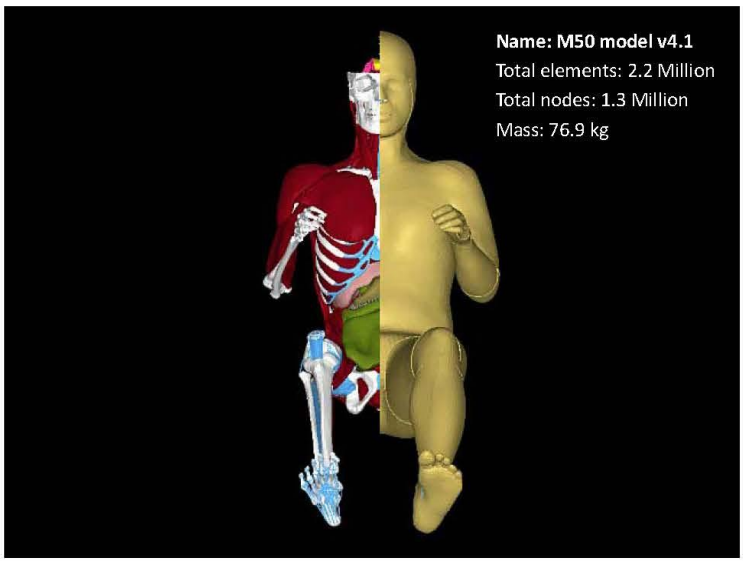
Name: M50 model v4.1
Total elements: 2.2 Million
Total nodes: 1.3 Million
Mass: 76.9 kg

3

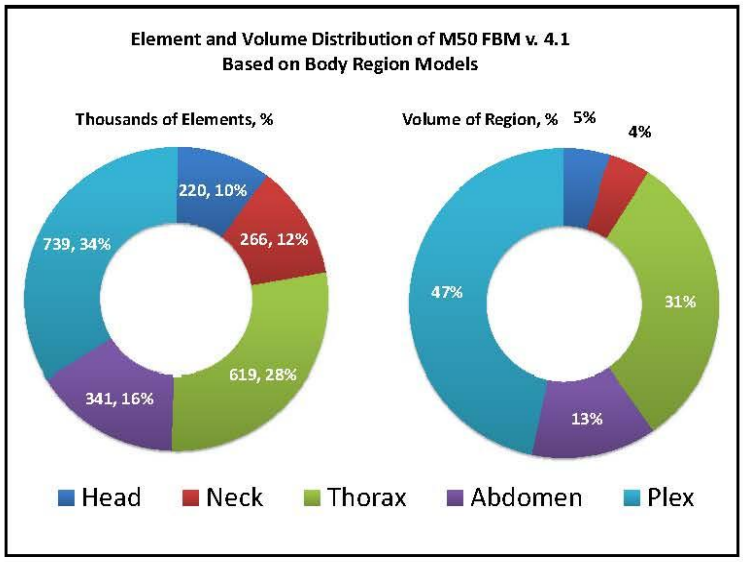
Element and Volume Distribution of M50 FBM v. 4.1
Based on Body Region Models
Thousands of Elements, %
220, 10%
266, 12%
619, 28%
341, 16%
739, 34%
Volume of Region, %
5%
4%
31%
13%
47%
Head
Neck
Thorax
Abdomen
Plex

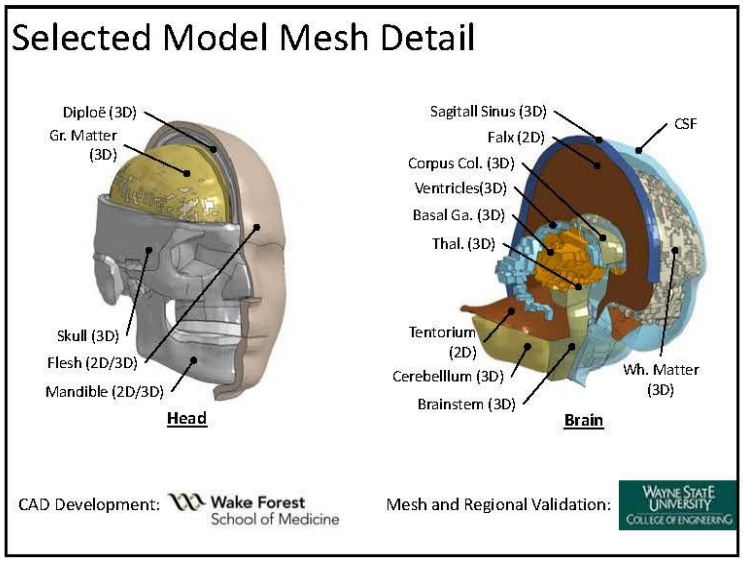
Selected Model Mesh Detail
Diploë (3D)
Gr. Matter (3D)
Skull (3D)
Flesh (2D/3D)
Mandible (2D/3D)
Head
Sagitall Sinus (3D)
Falx (2D)
Corpus Col. (3D)
Ventricles(3D)
Basal Ga. (3D)
Thal. (3D)
CSF
Tentorium (2D)
Cerebelllum (3D)
Brainstem (3D)
Wh. Matter (3D)
Brain
CAD Development:
Wake Forest School of Medicine
Mesh and Regional Validation:
Wayne State University College of Engineering

Selected Model Mesh Detail

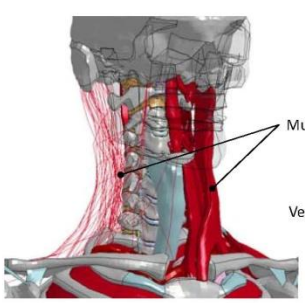

Neck

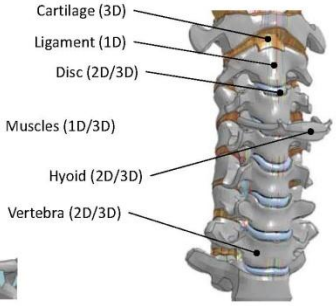

Cervical Vertebral Column

CAD Development: Wake Forest School of Medicine

Mesh and Regional Validation: University of Waterloo

Selected Model Mesh Detail

Back

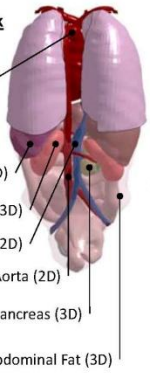

Front

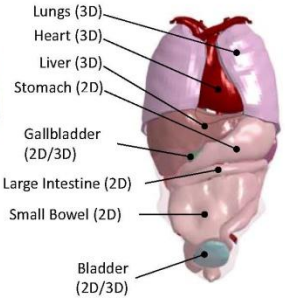

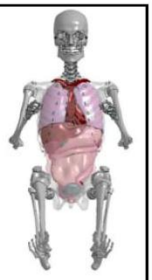

Mesh and Regional Validation:

University of Virginia Engineering

IFSTTAR

Virginia Tech College of Engineering

CAD Development: Wake Forest School of Medicine

Wake Forest School of Medicine

Selected Model Mesh Detail

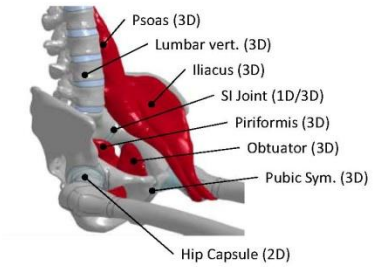

Pelvis

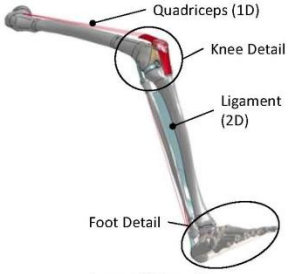

Lower Extremity

CAD Development: Wake Forest School of Medicine

Mesh and Regional Validation: UAB

Selected Model Mesh Detail

Wake Forest School of Medicine

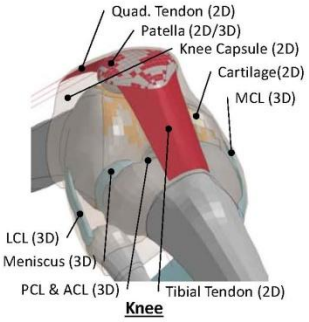

Knee

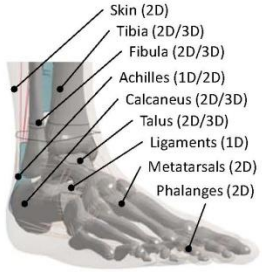

Foot

CAD Development: Wake Forest School of Medicine

Mesh and Regional Validation: UAB

Pre-programmed Dummy Location Outputs

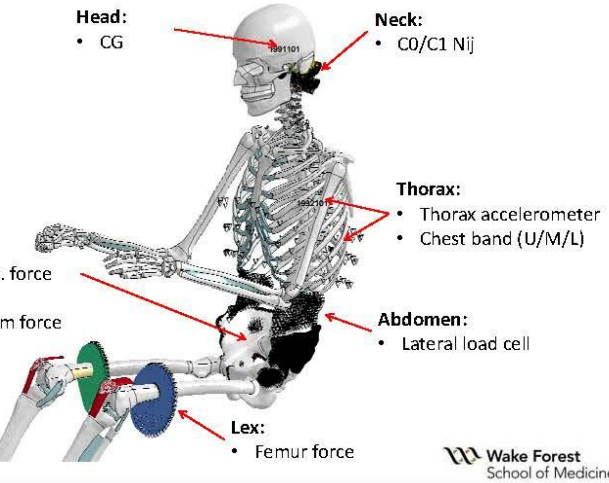

Wake Forest School of Medicine

FBM Hub-Impacts

Wake Forest School of Medicine

- Frontal Bar Abdominal Impact
  - Hardy et al. 2001, 6.0 m/s, 48 kg
- Frontal Chest Impact
  - Kroell, Neathery 1972, '74, 6.7 m/s, 23.4 kg
- Oblique Thoracoabdominal Impact
  - Viano et al. 1989, 6.7 m/s, 23.4 kg
- Lateral Block Pelvis Impact
  - Boquet et al. 1998, 10 m/s, 16 kg
- Lateral Shoulder Impact
  - Koh et al. 2005, 4.5 m/s, 23.4 kg
- Plate Impact
  - Kemper et al. 2009, 9 m/s, 2.34 kg

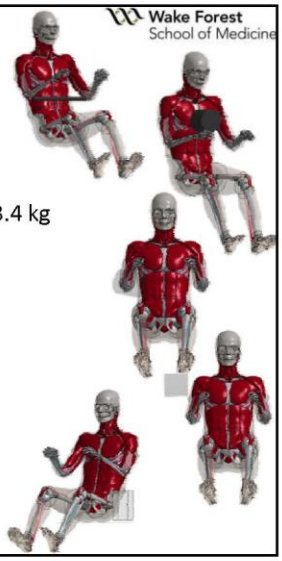

FBM Hub-Impacts

Wake Forest School of Medicine

- Frontal Bar Abdominal Impact
  - Hardy et al. 2001, 6.0 m/s, 48 kg
- Frontal Chest Impact
  - Kroell, Neathery 1972, '74, 6.7 m/s, 23.4 kg
- Oblique Thoracoabdominal Impact
  - Viano et al. 1989, 6.7 m/s, 23.4 kg
- Lateral Block Pelvis Impact
  - Boquet et al. 1998, 10 m/s, 16 kg
- Lateral Shoulder Impact
  - Koh et al. 2005, 4.5 m/s, 23.4 kg
- Plate Impact
  - Kemper et al. 2009, 12 m/s, 23.4 kg

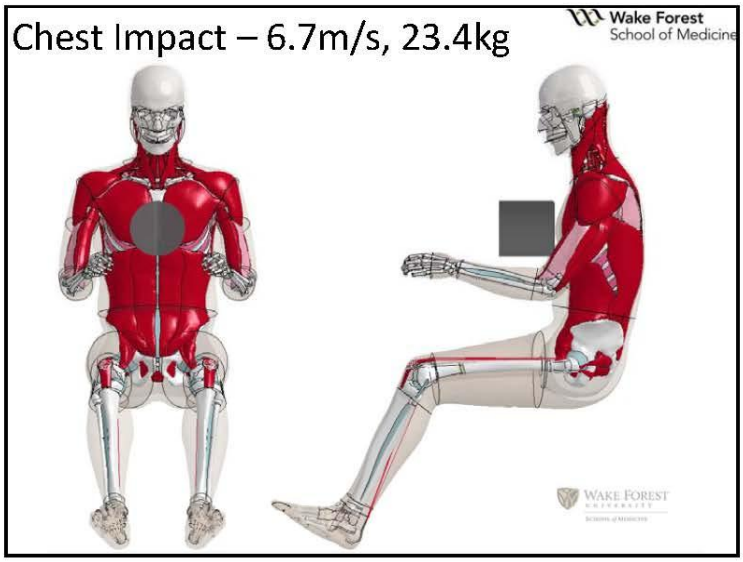

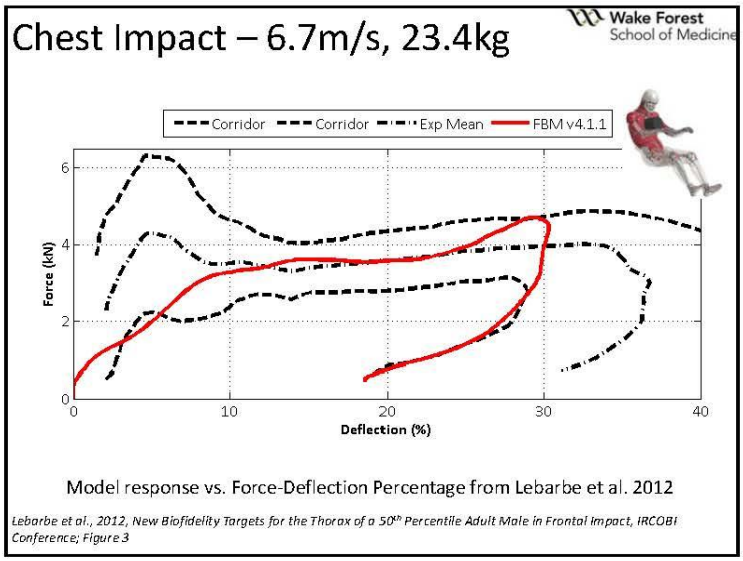

Model response vs. Force-Deflection Percentage from Lebarbe et al. 2012

Lebarbe et al., 2012, New Biofidelity Targets for the Thorax of a 50th Percentile Adult Male in Frontal Impact, IRCOBI Conference; Figure 3

Lateral Plate Impact (Kemper) – 12 m/s

Lateral Plate Impact (Kemper) – 12 m/s

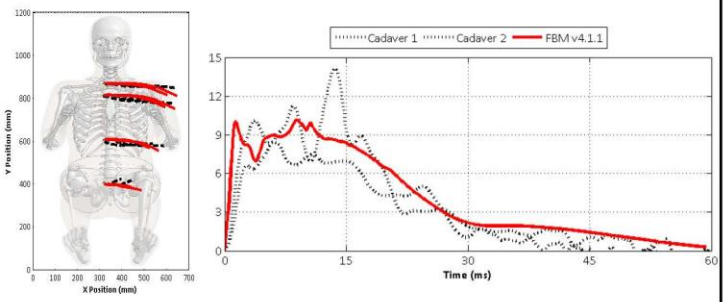

CORA Results: 1 (best), 0 (worst)

Data	Corridor	Correlation	Magnitude	Phase
Reaction Force	0.60	0.94	0.85	1.0
T4 Y	0.84	0.99	0.87	0.78
T4 Z	0.25	0.11	0.15	0.25

Kemper et al., 2008, The Influence of Arm Position on Thoracic Response in Side Impacts, Stapp Car Crash Conference

FBM Belted Simulations

Wake Forest School of Medicine

- Frontal Buck
  - Shaw 2009, 11.0 m/s
- Frontal NCAP
  - NCAP Test #7147, Driver
- Lateral NCAP
  - NCAP Test #3263, Driver
- Frontal Buck, Rear Seat
  - Forman et al., 2009 occupant

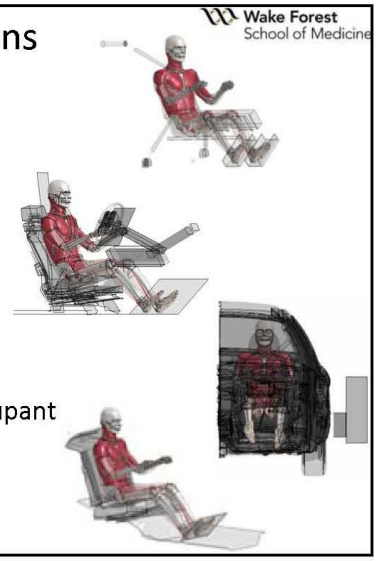

FBM Belted Simulations

Wake Forest School of Medicine

- Frontal Buck
  - Shaw 2009, 11.0 m/s
- Frontal NCAP
  - NCAP Test #7147, Driver
- Lateral NCAP
  - NCAP Test #3263, Driver
- Frontal Buck, Rear Seat
  - Forman et al., 2009 occupant

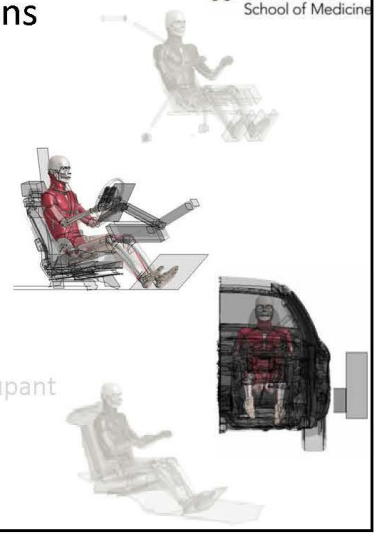

Frontal NCAP Robustness Check

Wake Forest School of Medicine

Gravity settle M50 model in vehicle, fit belt, apply pulse from NCAP test M50 v. 4.1

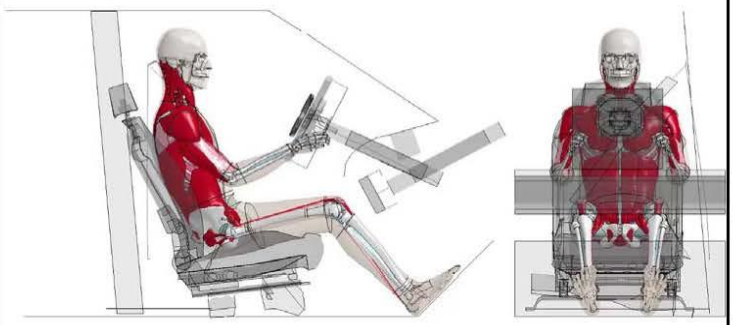

Lateral NCAP Robustness Check

Wake Forest School of Medicine

Gravity settle M50 model in vehicle, fit belt, apply pulse from NCAP test to vehicle model with M50 v. 4.1

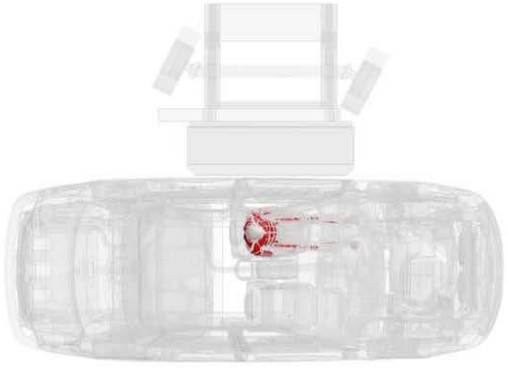

Overview of Phase II GHBMC Modeling Initiatives at WFU

- Outline of Phase II plan
- M50 Standing (pedestrian) cad model Development
- F05 occupant CAD development
- Simplified models
- Scaling existing models

Wake Forest
School of Medicine

GHBMC Phase II Plan

Performance Period: Sept. 1st 2013 to July 31st 2017	'13	2014				2015				2016				2017			
Tasks ↓, Project Quarters →	Q1	Q2	Q3	Q4	Q5	Q6	Q7	Q8	Q9	Q10	Q11	Q12	Q13	Q14	Q15	Q16	Q17
	SO	NDJ	FMA	MJJ	ASO	NDJ	FMA	MJJ	ASO	NDJ	FMA	MJJ	ASO	NDJ	FMA	MJJ	ASO
1.0 M50 Model Development Work																	
1.1.1 Enhanced detailed M50 occupant models - FBM COE																	
1.1.2. Enhanced detailed M50 occupant models - BRM COE																	
1.2. M50 pedestrian CAD models																	
1.3. Simplified M50 pedestrian models																	
1.4. Simplified M50 occupant models																	
1.5. Detailed M50 pedestrian models																	
2.0 F5 Model Development Work																	
2.1. F5 occupant & pedestrian CAD models																	
2.2. Detailed F5 occupant model - FBM COE																	
2.3. Detailed F5 occupant model - BRM COE																	
2.4. Simplified F5 pedestrian model (scaled from M50 model)																	
2.5. Simplified F5 occupant model																	
2.6. Detailed F5 pedestrian models																	
3.0 M95 Model Development Work																	
3.1. M95 occupant & pedestrian CAD models																	
3.2. Detailed M95 occupant model (scaled from M50) - FBM COE w/ refine... M95 CAD																	
3.3. Detailed M95 occupant model (scaled from M50) - BRM COE w/ re... using M95 CAD																	
3.4. Simplified M95 pedestrian model (scaled from M50 model)																	
3.5. Simplified M95 occupant model (scaled from M50 model)																	
3.6. Detailed M95 pedestrian model (scaled from M50 model including ... CAD as necessary)																	
4.0 6 yr-old Child Model Development Work																	
4.1. Simplified 6 yr-old child pedestrian model (scaled from M50 model)																	

- 5 year execution plan
- BRM – FBM design cycle for 5th female development
- 5 CAD figures, 12 models
- Enhancement of M50 occupant
- Models of 95th ptle. Male, 5th ptle. Female and 6 year old child (ped. only)
- Detailed and simplified
- Occupant and pedestrian
- Uses scaling approach to leverage Phase I data
- Model conversion from LS-Dyna to Pamcrash and Radioss solvers

GHBMC
Global Human Body Models Consortium

NHTSA

Phase II Activities Outline

Wake Forest School of Medicine

- ***Approximately 4 years***
- ***Leverage previous modeling work, know-how and data***
- ***Utilizing scaling to rapidly expand models available***

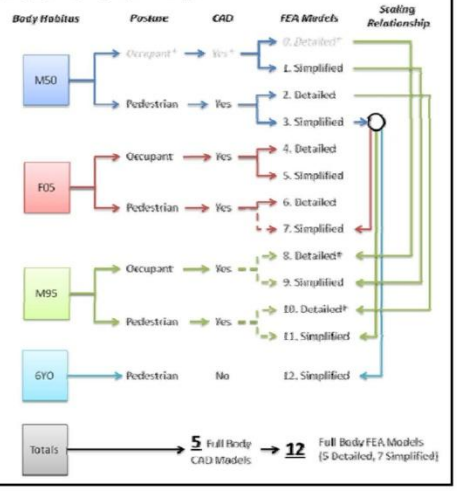

M50 Standing CAD

Wake Forest School of Medicine

- Assembled bony CAD from Occupant model CAD
- **These data were collected in Phase I**
- Confirmed bone locations with external landmarks and medical images in the standing posture
- Soft tissues developed from medical images in the standing posture
- **Target delivery to GHBMC: April 2014**

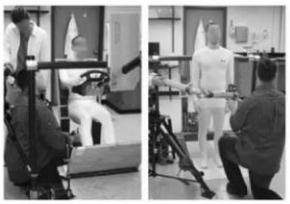

FIGURE 1. Data collection methodology in the seated (left) and standing (right) postures.

F05 CAD Development: Assembly

Wake Forest School of Medicine

Methods:

- **Phase I data**
- Segmented bones, fit to EA landmarks
- Verify alignment with seated scan data (MRI, CT)
- H-Point is at (0,0,0), SAE J211 CS
- Symmetrized

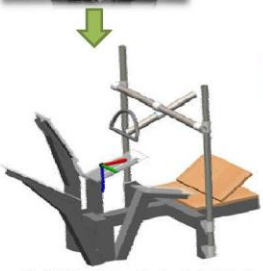

- Gayzik FS et al. External Landmark, Body Surface, and Volume Data of a Mid-Sized Male in Seated and Standing Postures. *Ann Biomed Eng*. September 2012;40(9):2019-2032.

Wake Forest School of Medicine

IRB #5705

F05 Occupant CAD: Assembly

Wake Forest School of Medicine

- Symmetrized NURBS Skeleton Complete
- Thoraco-abdominal organs NURBS underway, utilize posture specific geometry
- Target Delivery: CAD (July 2014), alpha model (mid-2015)

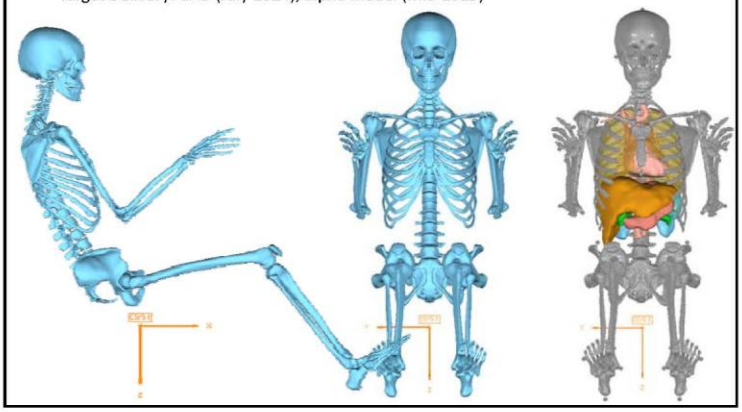

Simplified Occupant Model: Motivation

Wake Forest School of Medicine

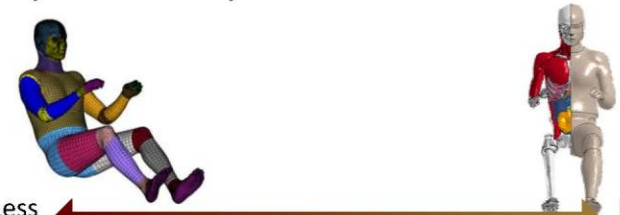

Less Detail ⟷ More Detail

- Rapid run time (**50x faster**)
- Rapid kinematic and kinetic assessment
- Modularity
- Ease of positioning
- Target Delivery M50 Occupant (mid 2014)

- Fine mesh
- Detailed evaluation
- Crash Induced Injury assessment
- Inputs from coarse model can be used to drive the detailed model

M95 Occupant Scaling

Wake Forest School of Medicine

- An M95 seated occupant model is being developed by scaling the M50 model
- Methods developed in this part of the project can be applied to scale to many other sizes
- Accelerate development
- Facilitate comparisons between the two

Scaling: Homologous Landmark Placement

Wake Forest School of Medicine

- Leverage existing Phase I data: External Anthropometry, medical images
- Landmarks were placed on the surface of M50 and transformed to the surface of M95
- This created homologous landmarks that could be used in the FE morph
- Target delivery, mid 2014

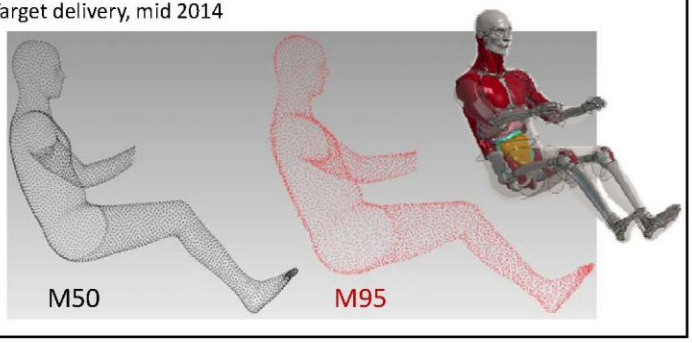

GHBMC FBM Study Team and Collaborators

Wake Forest School of Medicine

CIB

Virginia Tech
COLLEGE of ENGINEERING

Summary & Conclusions

- GHBMC Program is a global and consolidated human body modeling effort, initiated by automotive manufacturers
- FBM v. 4.1.1 delivered and undergoing user acceptance testing (UAT)
- Phase II of this project greatly expands scope to development models for pedestrian, female, scaled models and simplified

Wake Forest School of Medicine

CIB

Virginia Tech
COLLEGE of ENGINEERING

Acknowledgements

Funding: Global Human Body Models Consortium (GHBMC)

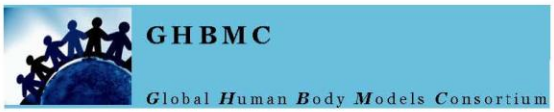

Chrysler LLC
General Motors Corp.
Honda R&D Co.

Hyundai Motor Co.
NHTSA
Nissan Motor Corp. Ltd

Renault s.a.s.
Takata Corp.
PSA Peugeot-Citroën

Data appearing in this document were prepared under the support of the Global Human Body Models Consortium by the FBM GHBMC Center of Expertise. Any opinions or recommendations expressed in this document are those of the authors and do not necessarily reflect the views of the Global Human Body Models Consortium.

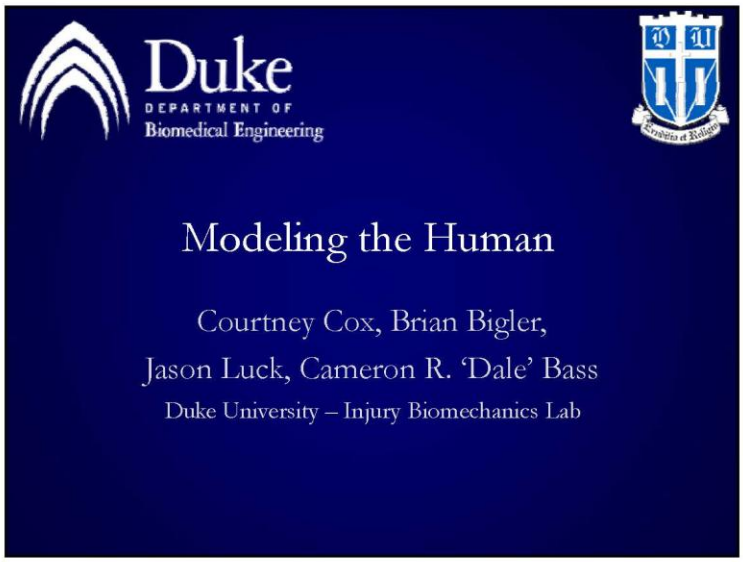
Duke
DEPARTMENT OF
Biomedical Engineering
Modeling the Human
Courtney Cox, Brian Bigler,
Jason Luck, Cameron R. 'Dale' Bass
Duke University – Injury Biomechanics Lab

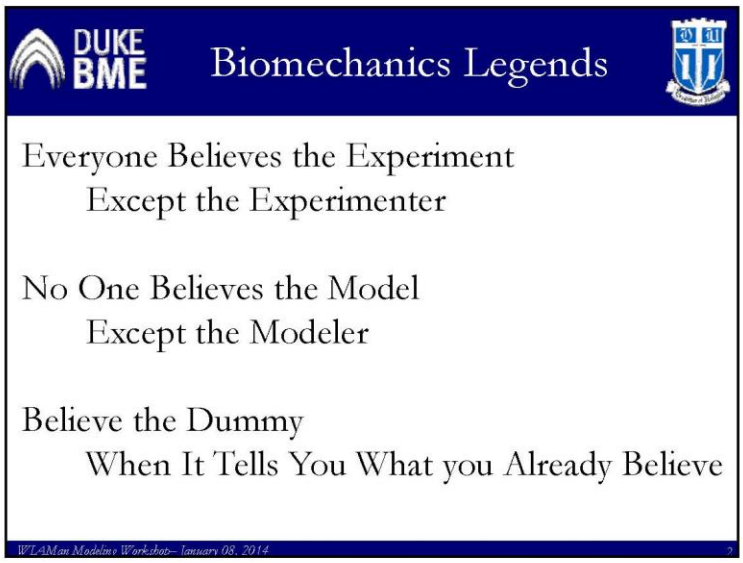
DUKE
BME
Biomechanics Legends
Everyone Believes the Experiment
Except the Experimenter
No One Believes the Model
Except the Modeler
Believe the Dummy
When It Tells You What you Already Believe
WLAMan Modeling Workshop– January 08, 2014

Some Human Modeling Issues

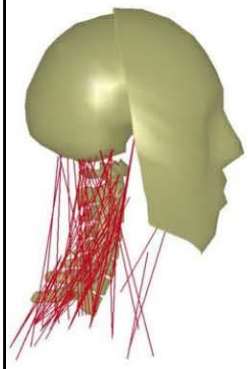

Dibb, 2012

- Anthropometry
- **Construction and Model Validation/Hierarchy**
- Physiology/Muscular Response
- **Material Models/Constitutive Relations**
- **Variance/Distributions**
- Special Issues for Blast
- …

Important!

Modeling is an Approximation.

Anthropometry

Yang, 2010

- With Current Automated Tools

  (and minor guidance)

  High School Students and

  Early Undergraduates

  Can Now Construct FE Models

  that 'Look' Humanlike

- ?

Anthropometry

Yang, 2010

- Let high school students take over all modeling (cheaper)?
- Nontrivial problems prevent this:
  - Grid refinement/element selection/element quality
  - Materials
  - Local detailed geometry
  - Anisotropy
  - Inhomogeneity
  - …

Blessing and a Curse?

Panzer, 2013

- Modern FE Models may have
  - Millions of elements
  - Tens or more different materials
  - Innumerable material/material interfaces
  - Different element type/interfaces
- An enormous number of degrees of freedom
- An enormous number of parameters to be used to 'calibrate' models

What About This Element Here?

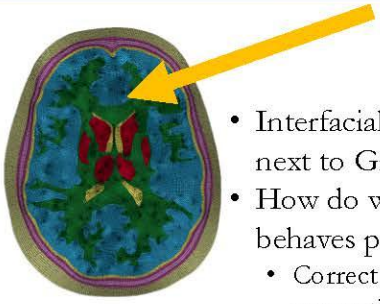

Panzer, 2013

- Interfacial Element – White Matter next to Gray Matter
- How do we make sure this element behaves properly?
  - Correct size? Correct material properties? Correct interfacial properties? Response is sensitive to this element if it 'should be'? Etc.

What About This Element Here?

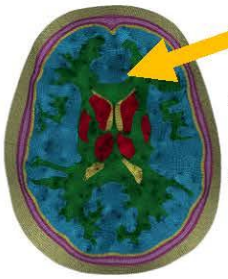

Panzer, 2013

- Interfacial Element – White Matter next to Gray Matter
- How do we make sure this element behaves properly?

1. We can't.

2. Hierarchical validation.

Hierarchical Validation

Construct Lowest Level Constitutive/Geometric Properties (e.g. Ligament, IVD, etc)

↓ Validate with low level data

Construct Subsystem (e.g. Functional Spinal Unit)

↓ Validate with subsystem data

Construct System (Head/Neck)

↓ Validate with system data

Validated

Hierarchical Validation

Two General Rules:

1. Cannot 'tweak' things at lower 'validated' level to 'validate' higher level

2. Needs some objective metric
   - ASME, several options in the literature, developing
   - Note: R^2 is not good enough

Validation

Random Example of a published 'validation' – head impact pressure

One Side of Head | The Other Side of Head

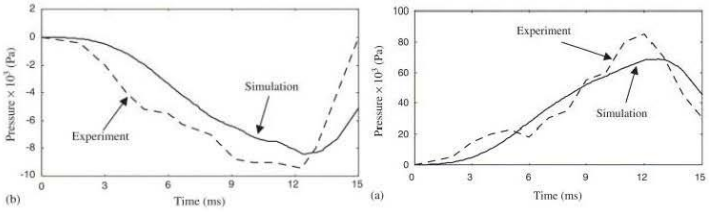

Quite often in the current literature: 'Validated' has no meaning

Caveat

This Approach Assumes that
The Macroscale (Large Stuff) is Composed of Microscale (Small Stuff)

Pretty good for bony/osteoligamentous, response etc.

Where is this Not True?

?

For Example: Muscles/Physiology

Seti I - Egypt

- Muscle activations in the Living
  - Positioning
  - Pretensioning
- Note:
  - Cadavers are not living humans
  - Cadavers are not relaxed humans
  - Cadavers are not comatose humans
- Value of Modeling for Use in Dummy Design/Development of Injury Criteria

Muscles/Physiology

- Muscles Activate in an Individual Pattern
  - At times systematically similar
  - But can be large differences between strategies
- Important: Activation can Use Large Percentage of Fracture Tolerance, e.g.
  - Effect of Achilles tendon loading on Tibial tolerance (Funk, 2002)
  - Effect of neck muscle tension on compressive tolerance (Cox, 2013)

Effect of Muscles on Neck Fracture Tolerance

Fully Tensed C6-C7 Axial Preloads as a Percentage of Neck Quasistatic Compressive Tolerance (Cox, 2013)

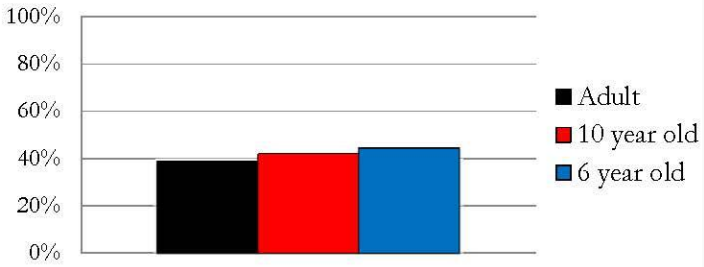

Effect of Muscles on Neck Fracture Tolerance

40% of Fracture Tolerance Axial Load by Neck Pretension (e.g. Pre-event Tension)

Constitutive Relations/ Material Response

- As Discussed Yesterday, Big Issue
- Anisotropy, Inhomogeneities, Micromechanics…
- Postfailure Behavior?
  - Not uncommon in biomechanics, initial failure influences course of subsequent failure.
- Troubling Example, Brains

Constitutive Relations/ Material Response

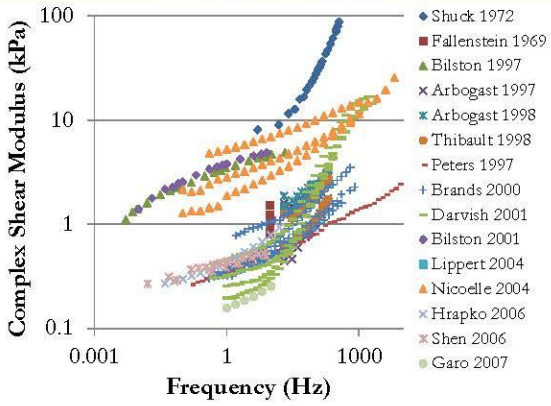

Constitutive Relations/ Material Response

One of the Biggest Problems Remaining

FE Modeling and Inverse FE Modeling May Play a Big Role in Clarifying Human Material Constitutive Relations

Variance/Distribution/ Population

All the World is Not a 50th Percentile Male

Variance/Distribution/ Population

Even Worse: A 50th Percentile Male is not a 50th Percentile Male

Variance/Distribution/ Population

What Do I Mean?

It is unlikely that any single individual will have 50th percentile values for every aspect of micro and macro anthropometry

Variance/Distribution/ Population

Even More Important:

Every aspect of an FE model is potentially governed by some statistical distribution.

- Anthropometry/measurements
- Grid/node location
- Material properties
- …

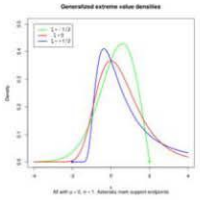

As emphasized yesterday, these distributions need not be Gaussian.

Variance/Distribution/ Population

So, ideally, these distributions/variances will be assessed/measured *and* incorporated into the FE model.

How?

Interacting Distributions/Sensitivity

Distribution graph

Variance/Distribution/ Population

How?

- Simplest common approach: A bunch of runs with different parameters (desire fast running tools)
  — Comprehensive info on interacting distributions?
- Other examples:
  - Nessus (SWRI)
  - Sample Distributions with Deterministic Equations for Material/Other Parameters
  - Evolution of Probability Density (Something like a Fokker-Planck approach for solid mechanics)

Duke Head and Neck Adult Model

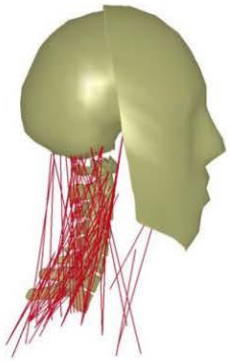

- Model structural components
  - Ligamentous spine
  - Muscular spine

- Camacho et al. 1997 (CDC/NHTSA)
- Van Ee et al. 2000 (NHTSA)
- Chancey et al. 2003 (NHTSA)
- Dibb 2010 (NHTSA)

Duke Model: Ligamentous Spine

- The ligamentous spine consists of:
  - Finite element head
    - Viscoelastic face
    - Rigid body
  - 7 rigid body vertebrae
    - C1/C2
    - C3, C4, C5, C6, C7
    - T1
  - 7 intervertebral joints
    - Base of skull (Occiput) – C2 (O-C2)
    - C2-C3, C3-C4, C4-C5, C6-C7
    - C7-T1

Duke Model: Muscular Spine

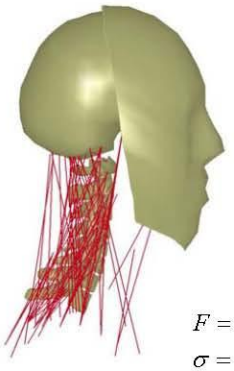

- The muscular spine consists of:
  - 22 muscles
  - 81 muscle strands
- Muscle model
  - Rate sensitive
  - Passive and active musculature
  - Generally curved paths

$$F = PCSA \times \sigma$$

$$\sigma = \sigma_{passive}(\varepsilon, \dot{\varepsilon}) + \sigma_{active}(\varepsilon, \dot{\varepsilon}, \alpha(t))$$

Duke Pediatric Models

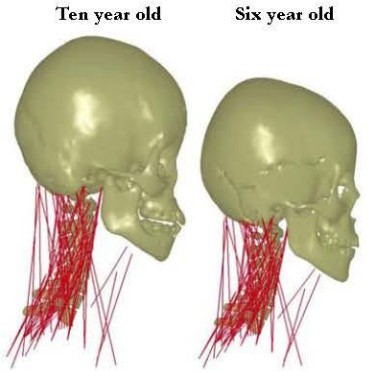

- Head (Loyd, 2010)
  - Inertial properties
  - Anthropometry
- Vertebrae
  - Inertial properties (Yu, unpub)
  - Anthropometry (Luck, 2012)
- Intervertebral Joints (Dibb, 2010)
- Cervical Muscles (Dibb, 2010)

Gratuitous Video - Duke Model for Underbody Blast

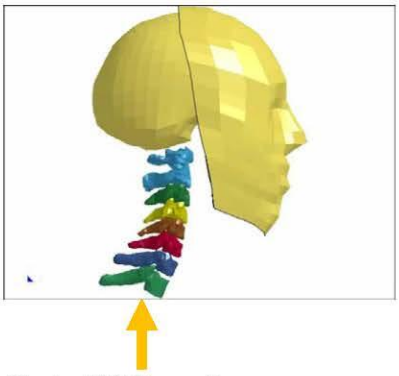

Typical T1 Ramp Input

Modeling Uncertainty

- Probabilistic vs. stochastic FEM
- Probabilistic FEM – run *N* deterministic FE simulations, where cases are determined by some sampling method, to determine response space
- Stochastic FEM – replace traditional PDE's with their stochastic counterparts and solve for the response uncertainty directly
  - Still an ongoing area of research

Modeling Uncertainty

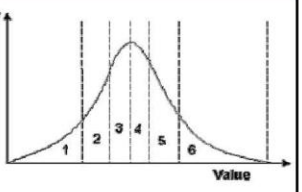

- Latin Hypercube Sampling
  - Parameters assigned an appropriate probability distribution
  - Distribution divided into *N* equal-area regions
  - *N* Cases sampled across all parameters of interest such that all cases have equal probability.

http://www.ems-i.com/gmshelp/Stochastic_Modeling/Parameter_Zonation.htm

Corridor Development through Uncertainty Analysis

Ten year old Six year old

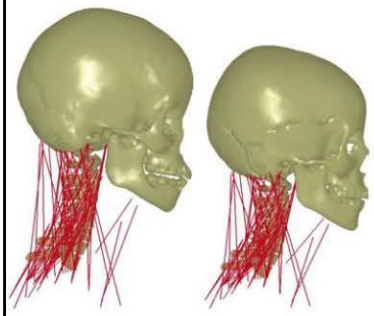

- Parameters varied (13 total):
  - Head:
    - Mass, inertia, size (x, y, z)
  - Vertebra:
    - Mass, inertia, size (x, y, z)
  - Upper and lower cervical spine joint stiffness
  - Muscle PCSA
- 50 simulations per parameter = 650 simulations total
- Assume distribution

WIAMan Modeling Workshop– January 08, 2014

Results: Pendulum Certification Test

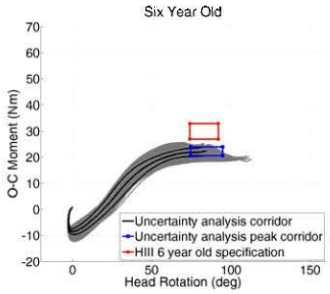

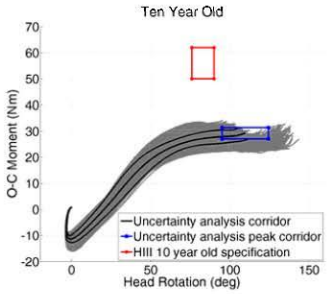

WIAMan Modeling Workshop– January 08, 2014

Optimization of Muscle Activation

- Activation schemes maintaining an upright, stable head for 22 muscle pairs were found using LS-OPT.
- Two activation schemes
  - relaxed state- unaware subject

$$\min f(\alpha) = \sum_{i=1}^{22} \left(\frac{F_i}{F_{max,i}}\right)^2 = \sum_{i=1}^{22} \alpha^2$$

  - tensed state- aware subject

$$\max f(\alpha) = \sum_{i=1}^{22} F_i$$

Optimization of Muscle Activation

- Constant Activation State
  - Relaxed
  - Tensed
- Optimized : varied activation level, initiation time, termination time
  - Pediatric and Adult

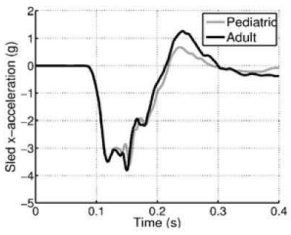

Low-speed Frontal Crash
(Arbogast et al. 2009)

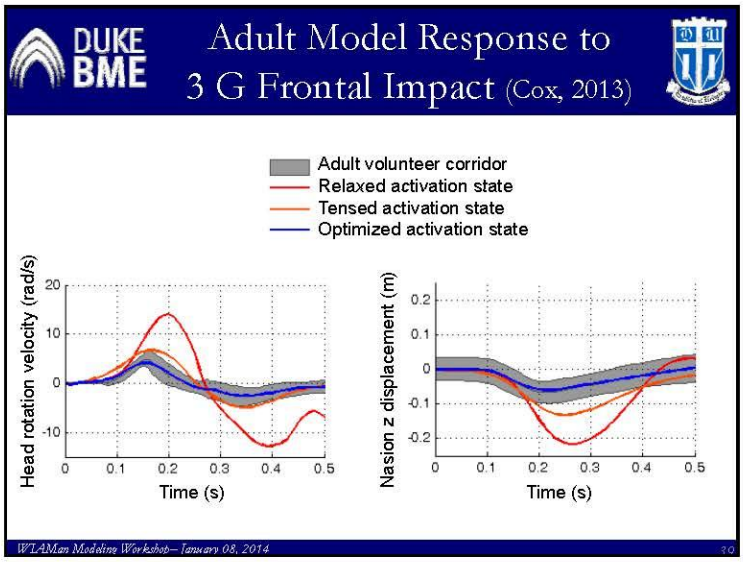
DUKE BME
Adult Model Response to 3 G Frontal Impact (Cox, 2013)
Adult volunteer corridor
Relaxed activation state
Tensed activation state
Optimized activation state
Head rotation velocity (rad/s)
Time (s)
Nasion z displacement (m)
Time (s)
WLAMan Modeling Workshop– January 08, 2014

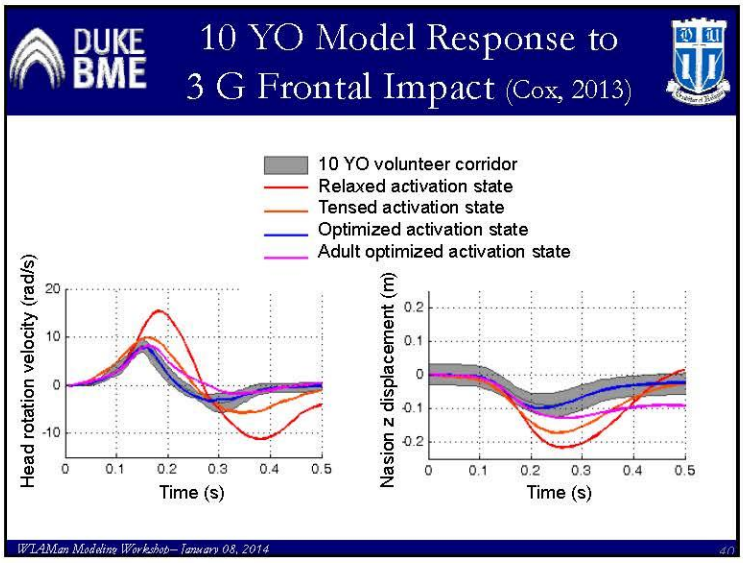
DUKE BME
10 YO Model Response to 3 G Frontal Impact (Cox, 2013)
10 YO volunteer corridor
Relaxed activation state
Tensed activation state
Optimized activation state
Adult optimized activation state
Head rotation velocity (rad/s)
Time (s)
Nasion z displacement (m)
Time (s)
WLAMan Modeling Workshop– January 08, 2014

Lesson?

- In Many Problems, Getting Correct Kinematics/Dynamics May Require Muscles

Bottom Lines

- Generally, Complexities Must Be Reduced for Tractable Problems
- However, Variance is not a 'Complexity' but an Intrinsic Part of the Problem.
- Validation Necessary, Global Validation Often Not Good Enough
- Material Properties Still A Known Sensitivity in Many Problems.
- Muscles May Be Necessary for Replicating Human Response!

[dstl]

20 January 2014

Ministry of Defence

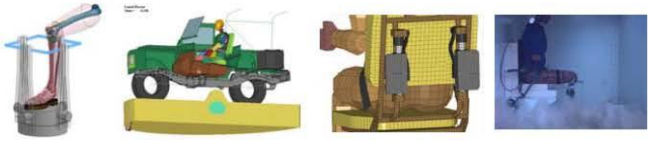

Numerical Modelling Undertaken at Dstl (UK) Concerning Vehicle Floor Plate Impact of Surrogates and Anatomical Human Entities Due to Under-Body Mine Loading

Accelerative Loading Workshop - ARL- 8th January 2014

Dan Pope, Chris Taggart, Joe Cordell, Ian Softley
Structural Dynamics Capability, Physical Protection Group (PSD)

Contents

- Numerical simulation of protection in Dstl
- Modelling and validation of blast loading of military vehicles and occupant injury
- Modelling of surrogate leg systems
- Modelling of anatomically-representative legs
- Other areas of interest
- Summary

Numerical simulation of Protection at Dstl

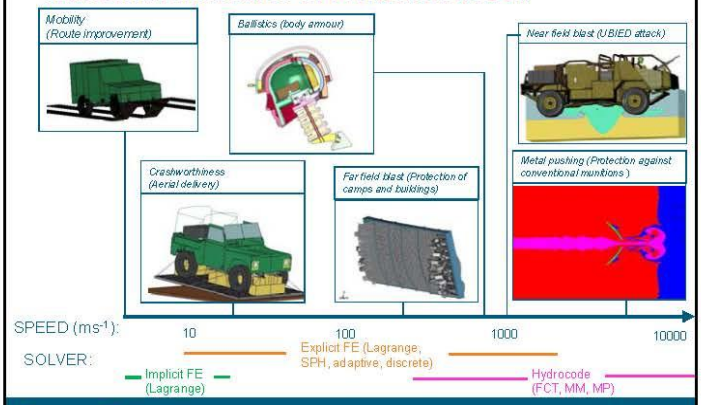

General modelling approach (vehicle protection)

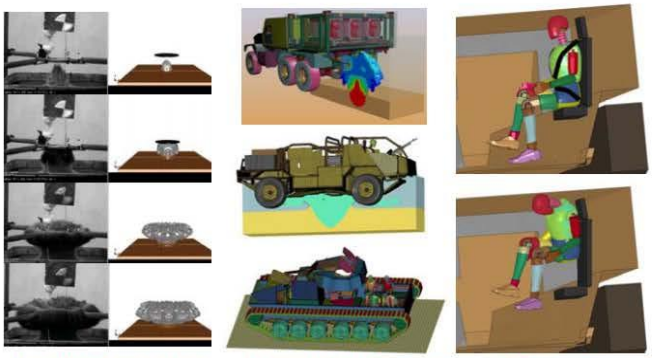

Validated mine-load prediction method | *FE database of key UK vehicles* | *Integration of ATDs for injury assessment*

Soil characterisation (Material model development)

EOS: Pressure/Volume response (Static)

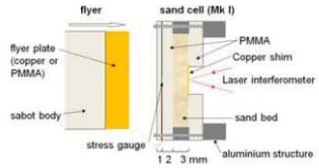

EOS: Shock loading aspects

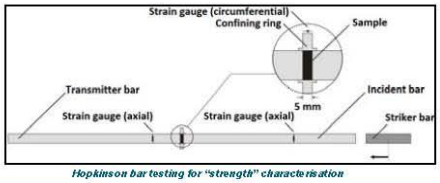

Hopkinson bar testing for "strength" characterisation

Soil characterisation (Macroscopic validation)

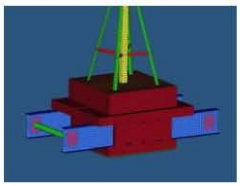

Mine rigs

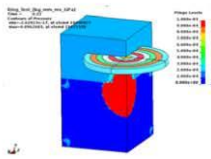

Momentum trap testing

Incorporation of seating

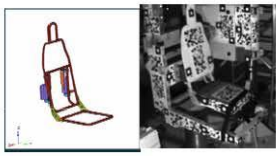

Seat deflection characterisation

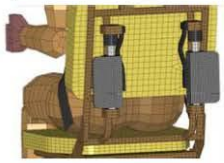

ArmorWorks ShockRideCrew Seat

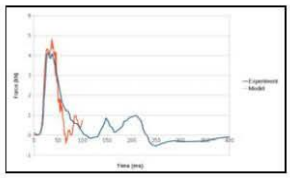

Output comparison

Numerical ATD Validation within "idealised" vehicles

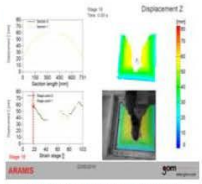

'Flanagatron' test rig

Digital Image Correlation (DIC)

[dstl] 30 January 2014 UNCLASSIFIED METROPOLITAN POLICE Ministry of Defence

Numerical ATD Evaluation

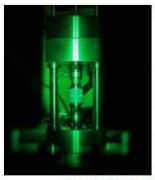

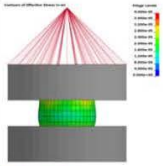

Low modulus materials test rig

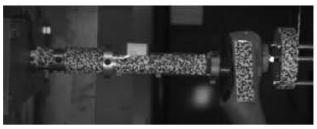

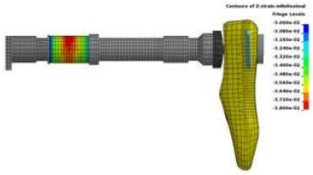

MiHLx model

[dstl] 30 January 2014 UNCLASSIFIED Imperial College London Ministry of Defence

Numerical ATD Evaluation (Material characterisation)

Imperial College ANUBIS rig

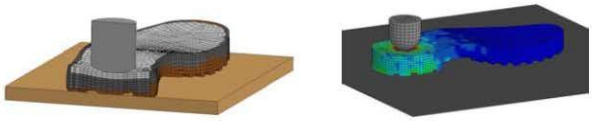

Drop rig testing on military footwear

Numerical anatomical leg model

Incorporation of leg model into ANUBIS rig

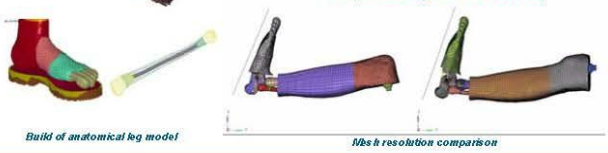

Build of anatomical leg model

Mesh resolution comparison

Quick running prediction methods

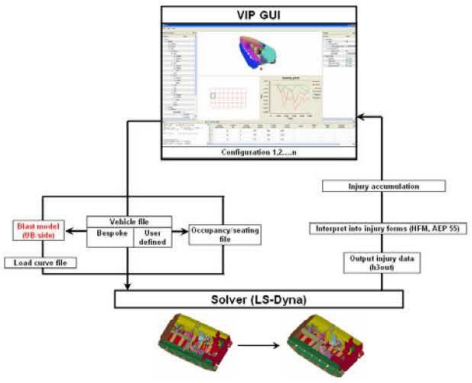

Other areas of interest

- Penetration injury

HIP Code:
Low fidelity: General survivability predictions

WTI:
Medium fidelity: Specific lethality assessments

FE Simulation:
High fidelity: Mechanistic assessments

Other areas of interest

- Penetration injury

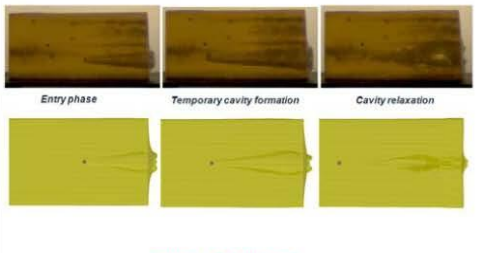

Penetration (High strain rate)

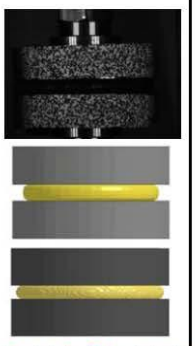

Drop tests (low/Medium strain rate)

Other areas of interest

- Penetration injury

Generation of wound tract in human neck

Effect of wearing collar

Summary

- Dstl are working with ICL (Dr Spyros Masouros) and MPS (Dr Oliver Flanagan) with respect to the study of lower limb injury caused within blast-loaded vehicles
- Numerical models of vehicles, seating, hybrids and humans are being developed to predict levels of human injury (representative experiments have also been generated for the purposes of model validation)
- A rudimentary quick running code "VIP" has also been developed
- Other numerical models (involving similar considerations) have been generated to scrutinise penetration injury


Workshop on Numerical Analysis of Human and Surrogate Response to Accelerative Loading, Aberdeen, MD, Jan. 7~9, 2014
PREVENTION THROUGH BIOMECHANICS
INJURY
Optimal Design of a Novel Energy Absorbing Material to Mitigate the Blast Effect on the Lower Extremities
Feng Zhu and King H. Yang
Bioengineering Center
Wayne State University
Detroit, Michigan
WAYNE STATE UNIVERSITY
COLLEGE OF ENGINEERING
Bioengineering Center
Impact Biomechanics from Head to Toe Since 1939

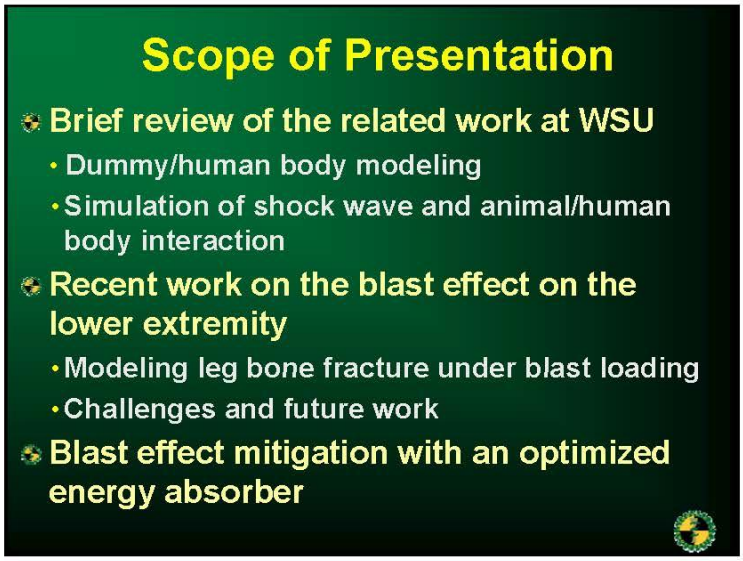
Scope of Presentation
Brief review of the related work at WSU
Dummy/human body modeling
Simulation of shock wave and animal/human body interaction
Recent work on the blast effect on the lower extremity
Modeling leg bone fracture under blast loading
Challenges and future work
Blast effect mitigation with an optimized energy absorber

Related Work at WSU

Dummy models

912892

Mathematical Modeling of the Hybrid III Dummy Chest with Chest Foam

David Lasry
Engineering Systems International
France

King H. Yang
Department of Mechanical Engrg.
Bioengineering Center
Wayne State University

Rainer Hoffmann
Engineering Systems International
Germany

Hong Pan
Bioengineering Center
Wayne State University

922526

Finite Element Modeling of Hybrid III Head-Neck Complex

King H. Yang and Jialiang Le
Wayne State Univ.

Related Work at WSU (cont'd)

Human body models

SAE TECHNICAL PAPER SERIES 983157

Development of a Finite Element Model of the Human Neck

King H. Yang, Fuchun Zhu, Feng Luan, Longmao Zhao and Paul C. Begeman
Wayne State Univ.

Neck

SAE TECHNICAL PAPER SERIES 99SC11

Foot and Ankle Finite Element Modeling Using CT-Scan Data

Philippe Beillas and François Lavaste
Laboratoire de Biomécanique, ENSAM Paris

Dimitri Nicolopoulos and Kambiz Kayvantash
Mécalog SA / Radioss Consulting Corp.

King H. Yang
Bioengineering Center, Wayne State University

Stephane Robin
Laboratoire d'Accidentologie et Biomécanique

Foot/ankle

SAE TECHNICAL PAPER SERIES 2001-22-0007

Development of a Computer Model to Predict Aortic Rupture Due to Impact Loading

Chirag S. Shah, King H. Yang, Warren Hardy, H. Kevin Wang and Albert I. King
Bioengineering Center, Wayne State Univ.

Aorta

SAE TECHNICAL PAPER SERIES 2001-22-0004

Development of a Finite Element Model of the Human Abdomen

Jong B. Lee and King H. Yang
Bioengineering Center, Wayne State Univ.

Abdomen

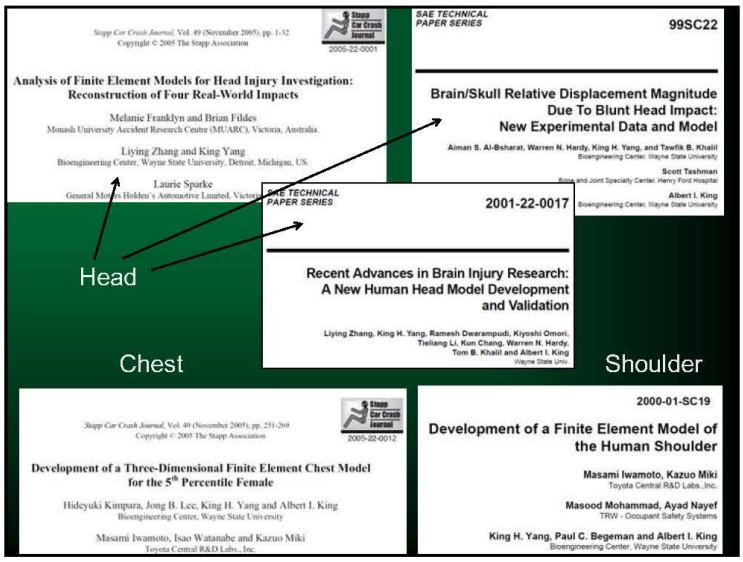
Stapp Car Crash Journal, Vol. 49 (November 2005), pp. 1-32
Copyright © 2005 The Stapp Association
2005-22-0001
Analysis of Finite Element Models for Head Injury Investigation: Reconstruction of Four Real-World Impacts
Melanie Franklyn and Brian Fildes
Monash University Accident Research Centre (MUARC), Victoria, Australia.
Liying Zhang and King Yang
Bioengineering Center, Wayne State University, Detroit, Michigan, US.
Laurie Sparke
SAE TECHNICAL PAPER SERIES
99SC22
Brain/Skull Relative Displacement Magnitude Due To Blunt Head Impact: New Experimental Data and Model
Aiman S. Al-Bsharat, Warren N. Hardy, King H. Yang, and Tawfik B. Khalil
Bioengineering Center, Wayne State University
Scott Tashman
Albert I. King
Bioengineering Center, Wayne State University
SAE TECHNICAL PAPER SERIES
2001-22-0017
Recent Advances in Brain Injury Research: A New Human Head Model Development and Validation
Liying Zhang, King H. Yang, Ramesh Dwarampudi, Kiyoshi Omori, Tieliang Li, Kun Chang, Warren N. Hardy, Tom B. Khalil and Albert I. King
Wayne State Univ.
Head
Chest
Shoulder
Stapp Car Crash Journal, Vol. 49 (November 2005), pp. 251-269
Copyright © 2005 The Stapp Association
2005-22-0012
Development of a Three-Dimensional Finite Element Chest Model for the 5th Percentile Female
Hideyuki Kimpara, Jong B. Lee, King H. Yang and Albert I. King
Bioengineering Center, Wayne State University
Masami Iwamoto, Isao Watanabe and Kazuo Miki
Toyota Central R&D Labs., Inc.
2000-01-SC19
Development of a Finite Element Model of the Human Shoulder
Masami Iwamoto, Kazuo Miki
Toyota Central R&D Labs.,Inc.
Masood Mohammad, Ayad Nayef
TRW - Occupant Safety Systems
King H. Yang, Paul C. Begeman and Albert I. King
Bioengineering Center, Wayne State University

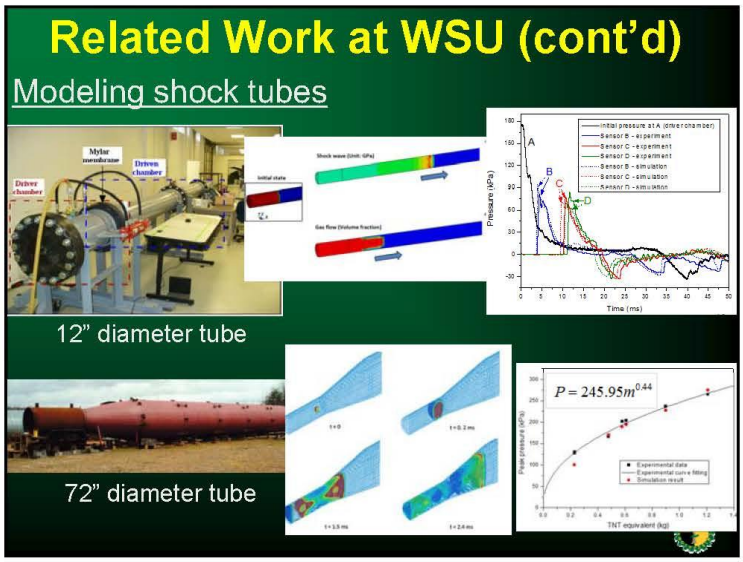
Related Work at WSU (cont'd)
Modeling shock tubes
Mylar membrane
Driven chamber
Driver chamber
12" diameter tube
72" diameter tube
Pressure (kPa)
Time (ms)
$P = 245.95m^{0.44}$
TNT equivalent (kg)

Related Work at WSU (cont'd)

Modeling blast wave/head interaction

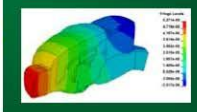

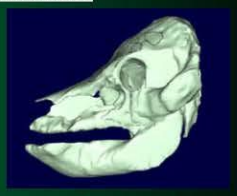

Rat head

Pig head

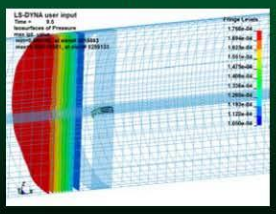

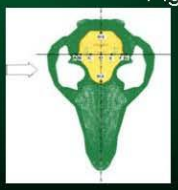

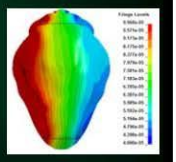

Blast Related Publications

Biomech Model Mechanobiol (2012) 11:341–353
DOI 10.1007/s10237-011-0314-2

ORIGINAL PAPER

Using a gel/plastic surrogate to study the biomechanical response of the head under air shock loading: a combined experimental and numerical investigation

Feng Zhu · Christina Wagner · Alessandra Dal Cengio Leonardi · Xin Jin · Pamela VandeVord · Clifford Chou · King H. Yang · Albert I. King

Physical surrogate

INTERNATIONAL JOURNAL FOR NUMERICAL METHODS IN BIOMEDICAL ENGINEERING
Int. J. Numer. Meth. Biomed. Engng. 2013; 29:392–407
Published online 29 September 2012 in Wiley Online Library (wileyonlinelibrary.com). DOI: 10.1002/cnm.2518

Pig head

Biomechanical responses of a pig head under blast loading: a computational simulation

Feng Zhu*,†, Paul Skelton, Cliff C. Chou, Haojie Mao, King H. Yang and Albert I. King

Bioengineering Center, Wayne State University, 818 W. Hancock, Detroit, MI 48201, USA

Stapp Car Crash Journal, Vol. 54 (November 2010), pp. 211-225
Copyright © 2010 The Stapp Association

2010-22-0011

Development of an FE Model of the Rat Head Subjected to Air Shock Loading

Feng Zhu, Haojie Mao, Alessandra Dal Cengio Leonardi, Christina Wagner, Clifford Chou, Xin Jin, Cynthia Bir, Pamela VandeVord, King H. Yang, and Albert I. King
Bioengineering Center, Wayne State University, Detroit, MI 48201, USA

Rat head

Blast Related Publications (cont'd)

Int. J. Nonlinear Sci. Numer. Simul., Vol. 13 (2012), pp. 25–29 Copyright © 2012 De Gruyter DOI 10.1515/IJNSNS.2011.095

Numerical Simulation of a Shock Tube for Bio-dynamics Study

Feng Zhu,[1,*] Cliff C. Chou,[1] King H. Yang[1] and Zhihua Wang[2]

[1] Bioengineering Center, Wayne State University, Detroit, USA
[2] Institute of Applied Mechanics, Taiyuan University of Technology, Taiyuan, China

Shock tube

Journal of Mechanics in Medicine and Biology
Vol. 13, No. 4 (2013) 1350065 (16 pages)
© World Scientific Publishing Company
DOI: 10.1142/S0219519413500656

SOME CONSIDERATIONS ON THE THRESHOLD AND INTER-SPECIES SCALING LAW FOR PRIMARY BLAST-INDUCED TRAUMATIC BRAIN INJURY: A SEMI-ANALYTICAL APPROACH

FENG ZHU*, CLIFF C. CHOU, KING H. YANG and ALBERT I. KING
*Bioengineering Center, Wayne State University, Detroit, MI 48201, USA
*fengzhou@gmail.com

Injury threshold & scaling law

Original Article

Numerical simulations of the occupant head response in an infantry vehicle under blunt impact and blast loading conditions

SAGE

Gopinath Sevagan[1], Feng Zhu[1], Binhui Jiang[1,2] and King H Yang[1]

Military vehicle occupant

Commercialization

The shock tube and animal head numerical models have been integrated into Inventium™, a blast simulation module, developed by Engineering Technology Association Inc. (ETA, Troy, MI). The software has been available for purchase since January 2012.

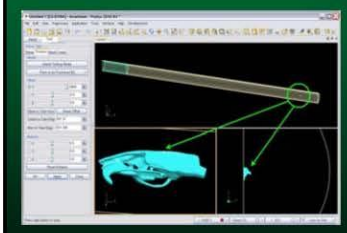

10

Blast Effect on the Lower Extremity

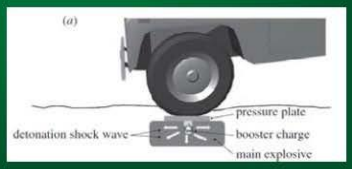

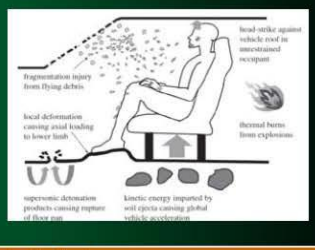

Blast injury	Mechanism	Clinical effects
Primary	Blast shock wave	Traumatic amputation; soft tissue deformation and fracture
Secondary	Flying fragments	Penetrating wounds
Tertiary	Vehicle acceleration; Floor pan deformation	Axial leading to lower limb, pelvis and spinal injuries
Quaternary	Thermal injuries	Burns

Recent Work on the Cadavers

WSU landmine simulator

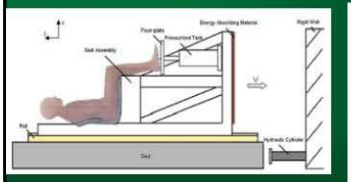

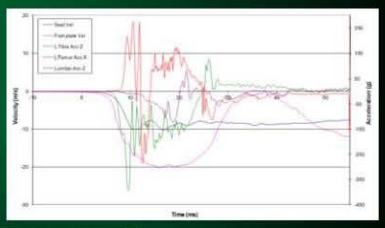

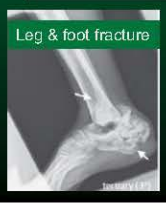

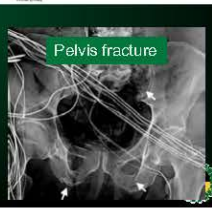

WSU Human Model (WSUHM)

Total number of elements: 354,603; Average mesh size: 3 mm

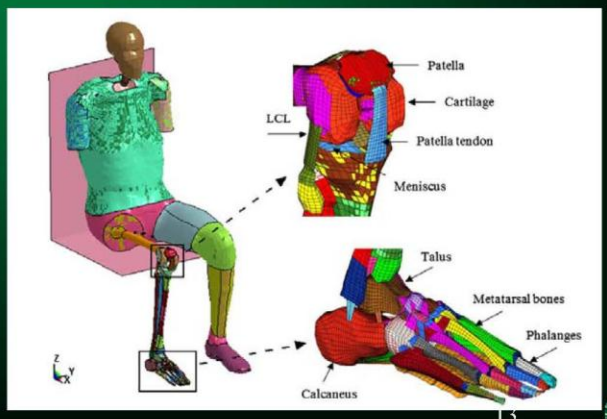

13

Rate – Dependent Behavior of Leg Bones – Material Properties Calibration

McElhaney (1966): Bovine femur

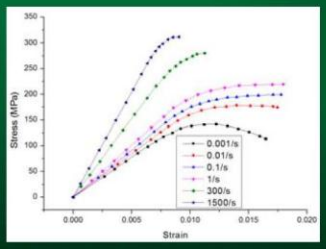

Flow stresses at 0.8% strain VS strain rate

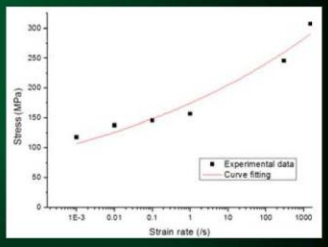

Constitutive model

$$\sigma_Y^d(\varepsilon_{eff}^p, \dot{\varepsilon}_{eff}^p) = \underbrace{(\sigma_Y^s + E_{tan}\varepsilon_{eff}^p)}_{\text{Strain hardening}}\underbrace{(1+\left(\frac{\dot{\varepsilon}_{eff}^p}{C}\right)^{\frac{1}{P}})}_{\text{Strain rate}}$$

Calibrated material constants

σ_Y (MPa)	E_{tan} (MPa)	C (/s)	P
118	1400	177.6	4.6

7

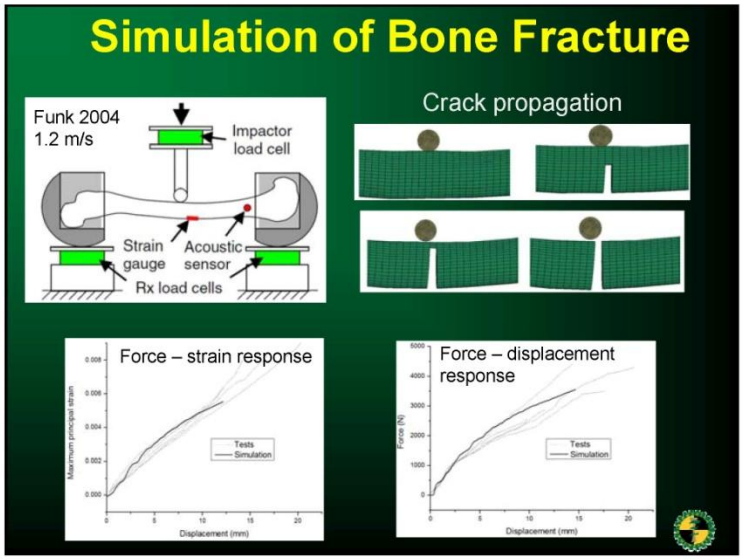
Simulation of Bone Fracture
Funk 2004
1.2 m/s
Impactor
load cell
Strain
gauge
Acoustic
sensor
Rx load cells
Crack propagation
Force – strain response
Force – displacement
response
Tests
Simulation
Displacement (mm)

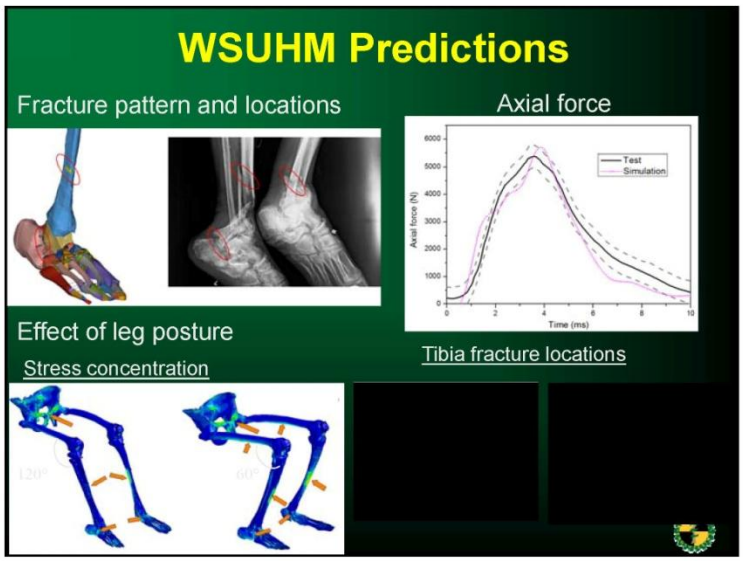
WSUHM Predictions
Fracture pattern and locations
Axial force
Test
Simulation
Time (ms)
Effect of leg posture
Stress concentration
Tibia fracture locations

Injury Threshold

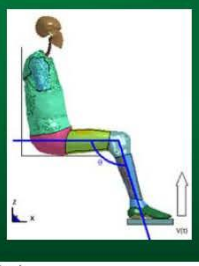

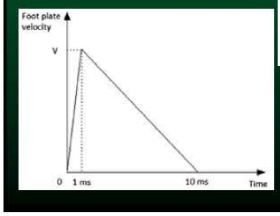

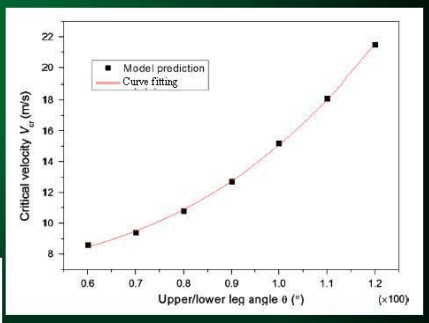

$$V_{cr} = 8.3\left(\frac{\theta}{100}\right)^{3.2} + 6.8$$

where V_{cr} is in m/s and θ is in degree

Current Issues/Future Work

- Unavailability of injury data in the real world
- Lack of material properties of human bones, muscle, skin and tendons at high strain rates
- It is imperative to compare the performances of different material laws (particularly the failure models) in the bone fracture prediction

Newly Purchased Split Hopkinson Pressure Bar System (with Temperature Effect)

Temperature effect
High temperature – Infra-red heater
Low temperature – Liquid Nitrogen freezer

Pressure: up to 1 MPa
Material: Steel and Aluminum alloy
Diameter: 14 mm and 25 mm
Length: 200, 300, 400 and 600 mm (Striker bar)
1500 and 2400 mm (Incident bar)
2000 and 1200 mm (Transmission bar)

A Novel Energy Absorber - SKYDEX® Material

- Base material: grey thermoplastic polyurethane
- Each layer has an array of twin-hemisphere
- The cells are chemically bonded together

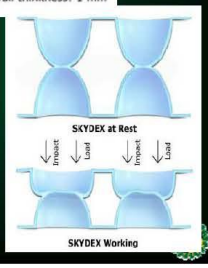

Application of SKYDEX® Material in Blast Protection

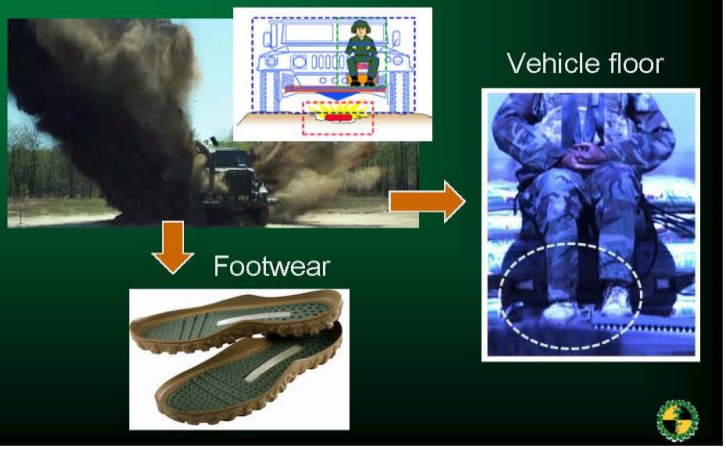

Modeling of Microstructures

Constitutive equation of the base material

$$\sigma_Y^d(\varepsilon_{eff}^p, \dot{\varepsilon}_{eff}^p) = \sigma_Y(1 + E_{\tan}\varepsilon_{eff}^p) + \sigma_Y\left(\frac{\dot{\varepsilon}_{eff}^p}{C}\right)^{\frac{1}{P}}$$

with σ_Y and σ_Y^d being quasi-static yield strength and dynamic flow stress, respectively. ε_{eff}^p and $\dot{\varepsilon}_{eff}^p$ are effective plastic strain and effective plastic strain rate, respectively. $E_{\tan}$ is tangent modulus describing strain hardening effect. P and C are two strain rate related parameters.

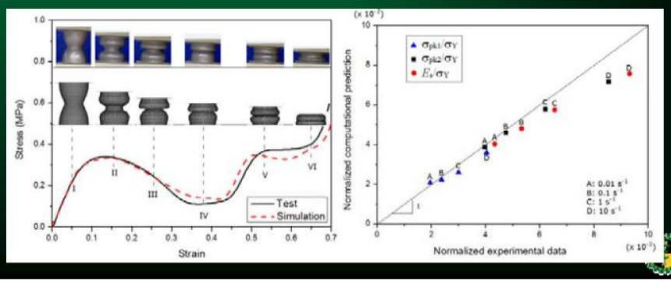

Optimal Design of Microstructure

Parameterization of the microstructure

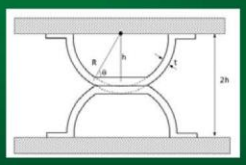

Relative density

$$\bar{\rho} = \frac{\pi t(2Rh + R^2 - h^2)}{4R^2 h} = \frac{\pi}{4} \cdot \frac{t}{R}\left(2 + \frac{1}{\sin\theta} - \sin\theta\right)$$

Deformation modes (Mode I is preferred)

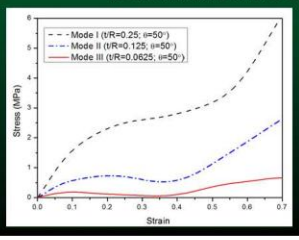

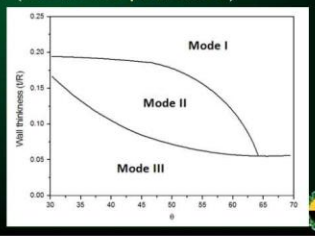

Optimal Design of Microstructure (cont'd)

Optimization objective

$$\begin{cases} \text{Find} & \theta, \quad t/R \\ \text{make} & \bar{U}_m(\theta, \quad t/R) -> \max \\ s.t. & \bar{\sigma}_{pk} < 0.19 \\ & 30^\circ \le \theta \le 70^\circ \\ & 0.20 \le t/R \le 0.28 \end{cases}$$

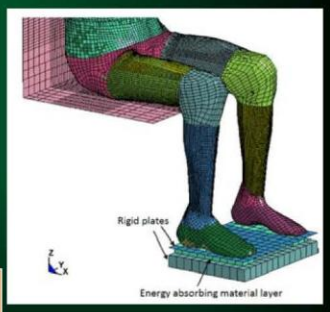

No-optimized vs. optimized microstructures

Optimized?	Critical velocity causing tibia fracture (m/s)
No	15.2
Yes	18.7

Multiple Layered Structures

Uniformed multiple layers

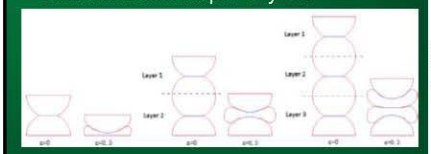

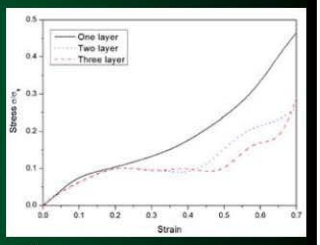

Graded multiple layers –
(various wall thickness in different layers)

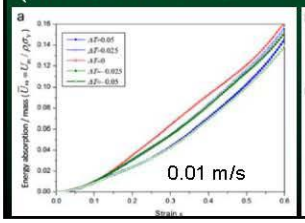

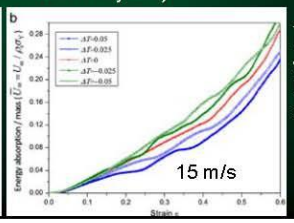

ΔT:
Difference in wall thickness between two adjacent layers

Related Publications

Crushing behavior of SKYDEX® material

Feng Zhu, Binhui Jiang, King H. Yang, Dong Ruan, Mike S. Boczek, and Rabih Tannous

Composite Structures

Computational modeling of the crushing behavior of SKYDEX® material using homogenized material laws

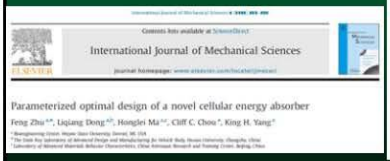

International Journal of Mechanical Sciences

Parameterized optimal design of a novel cellular energy absorber

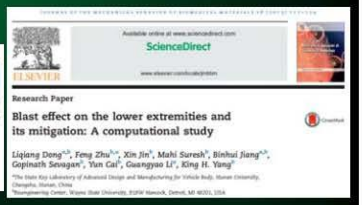

ScienceDirect

Research Paper

Blast effect on the lower extremities and its mitigation: A computational study

Optimal Design of a Novel Energy Absorbing Material to Mitigate the Blast Effect on the Lower Extremities

Feng Zhu and King H. Yang

ef9520@wayne.edu
aa0007@wayne.edu
Bioengineering Center
Wayne State University
Detroit, Michigan

U.S. Army Research, Development and Engineering Command

Constitutive Model and Parameter Sensitivity in Predicting Lower Leg Response for Underbody Blast Events

ARL

Workshop on Numerical Analysis of Human and Surrogate Response to Accelerative Loading
Jan 7-9, 2014

TECHNOLOGY DRIVEN. WARFIGHTER FOCUSED.

Megan Lynch[1] and Adam Sokolow PhD[1,2]

[1]U.S. Army Research Laboratory, Aberdeen Proving Ground, MD
[2]Oak Ridge Institute for Science and Technology, Aberdeen, MD

APPROVED FOR PUBLIC RELEASE - DISTRIBUTION UNLIMITED

APPROVED FOR PUBLIC RELEASE - DISTRIBUTION UNLIMITED

Background

ARL

Vehicle Occupant During Underbody Blast Event

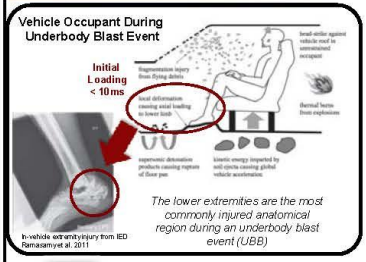

The lower extremities are the most commonly injured anatomical region during an underbody blast event (UBB)

- Goal: To capture the human response to underbody blast using finite element modeling
- Understand > Predict > Prevent injury
- Focus is on the lower extremities

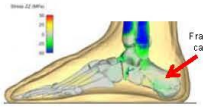

ARL Lower Leg Model 2012

- Previous work modeling the lower leg obtained qualitative agreement with experiments
- Model run with a single set of material models, parameters, and used a stress-based failure criterion
- To refine and build confidence in this model, "what if" questions need to be answered

TECHNOLOGY DRIVEN. WARFIGHTER FOCUSED.

APPROVED FOR PUBLIC RELEASE - DISTRIBUTION UNLIMITED

Background cont'd

- How does one describe a human being mathematically? Complex, multi-scale problem
- State variables are often used to predict injury at the continuum-level, which are highly dependent upon the constitutive models and material parameters used
- A subset of material models, parameters, and failure criteria has been identified from the literature to describe bone and flesh/ soft tissues
  - Plan to explore this extraordinarily large phase space and beyond
  - Develop data corridor to capture relevant cadaveric data, accounting for limited biological variability

Constitutive Models and Material Parameters from the Literature

Bone

		Cortical	Trabecular
Elastic-Plastic / Elastic	Density	1680-2000 kg/m^3	654-1100 kg/m^3
	Youngs Modulus	15-19 GPa	145-900 MPa
	Poissons Ratio	0.3-0.35	0.3-0.45
	Yield Strength	114-165 MPa	1.2-9.3 MPa
	Tangent Modulus	0.7-6.4 GPa	n/a
	Failure Stress	124-175 MPa	5.3-30.6 MPa
	Failure Strain	1.6-2.2 %	12.2-13.4 %
	⋮		

Flesh

Viscoelastic / Hyperelastic / Elastic	Density	1000-1300 kg/m^3
	Bulk Modulus	2.5-333 MPa
	Poissons Ratio	0.42-0.49
	C_1	-
	C_2	-
	⋮	
	S_1, S_2	-
	T_1, T_2	-
	⋮	

APPROVED FOR PUBLIC RELEASE - DISTRIBUTION UNLIMITED

Current Study

Bone

		Cortical	Trabecular
Elastic-Plastic / Elastic	Density	1850 kg/m^3	654-1100 kg/m^3
	Youngs Modulus	15-19 GPa	145-900 MPa
	Poissons Ratio	0.3	0.3-0.45
	Yield Strength	114-165 MPa	1.2-9.3 MPa
	Tangent Modulus	0.7-6.4 GPa	n/a
	Failure Stress	124-175 MPa	5.3-30.6 MPa
	Failure Strain	1.6-2.2 %	12.2-13.4 %
	⋮		

Flesh

Viscoelastic / Hyperelastic / Elastic	Density	1000 kg/m^3
	Bulk Modulus	2.5-333 MPa
	Poissons Ratio	0.42-0.49
	C_1	-
	C_2	-
	⋮	
	S_1, S_2	-
	T_1, T_2	-
	⋮	

- A range of material models and parameters have been found in the literature to describe bone and flesh/ soft tissues
- Various failure criteria for finite elements have been found as well
- Trabecular bone properties exhibit the greatest min/max range (*highly location dependent)
- A rather large phase space exists for just these three materials (cortical bone, trabecular bone, flesh)
- The current study uses the elastic material model for both bone and flesh with high/low properties as shown (totaling 64 combinations)
- A select few combinations will be highlighted in this talk

TECHNOLOGY DRIVEN. WARFIGHTER FOCUSED.
APPROVED FOR PUBLIC RELEASE - DISTRIBUTION UNLIMITED

Model Geometry

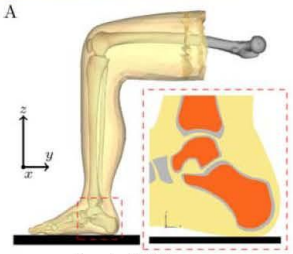

Figure A – Model Geometry.

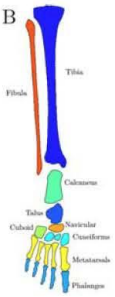

Figure B – Bone Map.

- Single leg model (right-side only) with the ankle and knee flexed at 90 degrees
- Geometry meshed with 500k tetrahedral elements
- Four material/ main geometry components: Cortical bone, trabecular bone, flesh, foot plate
  - Exploded ankle view shows layout
  - Flesh is a homogenization of soft tissues
- 2D bone layout ("bone map") for the lower leg
  - All bones constructed entirely of solid elements; hindfoot and long bones have trabecular component

Applied Loading

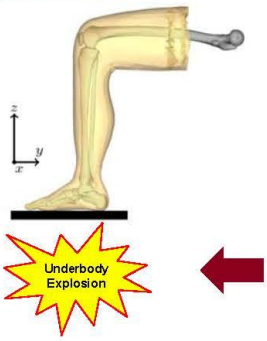

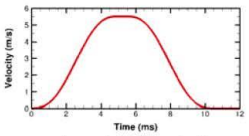

Figure – Applied Velocity Profile.

- Bottom of the foot in direct contact with a steel plate
- Velocity condition applied to plate in the upward z-direction to replicate underbody blast loading
  - The magnitude and temporal characteristics of this velocity condition are representative of an underbody blast event

Preliminary Results

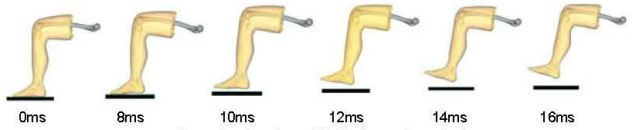

Figure – Time Series Images of Leg Displacement During Simulation.

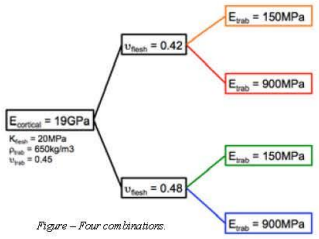

Figure – Four combinations.

- Four combinations will be discussed
  - Poissons ratio of the flesh and Youngs modulus of trabecular bone are investigated
- Stress in the cortical bone is used as a metric
  - Stress vs. time at various probe locations in the leg
  - Max stress on the whole-bone level

APPROVED FOR PUBLIC RELEASE - DISTRIBUTION UNLIMITED

Calcaneus

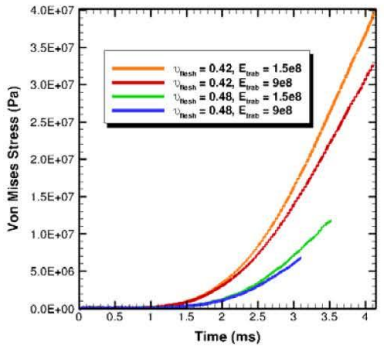

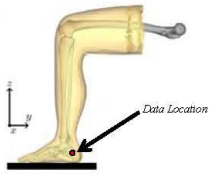

- Von Mises stress is calculated in the cortical layer of the lateral calcaneus
- Stress is affected by both the flesh and trabecular properties
  - Poissons ratio of flesh seems to have a larger effect than the Youngs modulus of trabecular bone (orange & red curves vs. green & blue curves)

TECHNOLOGY DRIVEN. WARFIGHTER FOCUSED.
APPROVED FOR PUBLIC RELEASE - DISTRIBUTION UNLIMITED

Distal Tibia

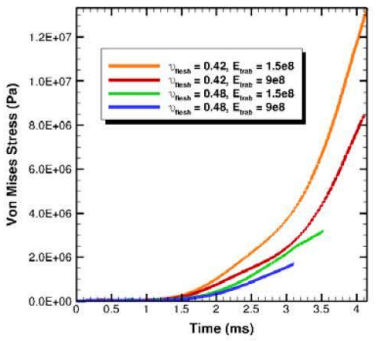

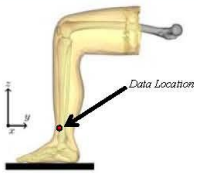

- Von Mises stress is calculated in the cortical layer of the anterior distal tibia
- The Poissons ratio of flesh does not seem to have as large of an effect here as seen in the calcaneus
  - Mesh effects?
  - Proximity to the ankle joint?

APPROVED FOR PUBLIC RELEASE - DISTRIBUTION UNLIMITED

Proximal Tibia

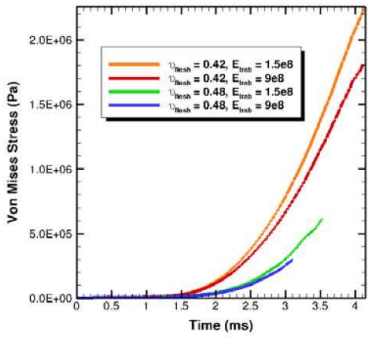

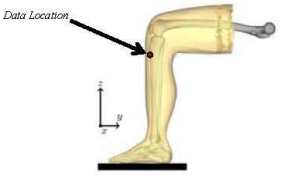

- Von Mises stress is calculated in the cortical layer of the anterior proximal tibia
- More similar response to the calcaneus in that the Poissons ratio of flesh shows a larger effect than the Youngs modulus of trabecular bone

TECHNOLOGY DRIVEN. WARFIGHTER FOCUSED.
APPROVED FOR PUBLIC RELEASE - DISTRIBUTION UNLIMITED

C337

Preliminary Conclusions

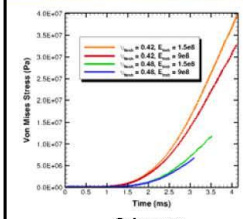

Calcaneus

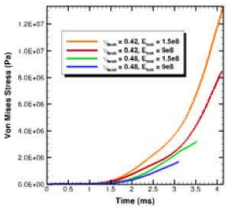

Distal tibia

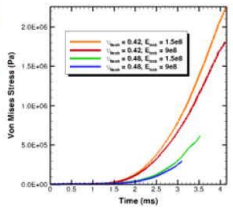

Proximal tibia

- Additional probe locations may be needed to attain more conclusive results
- All 64 combinations of the elastic case must be interpreted
- Data corridor is starting to form, which could be used to account for limited biological variability in experiments

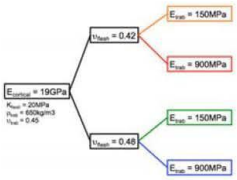

APPROVED FOR PUBLIC RELEASE - DISTRIBUTION UNLIMITED

Whole Bone Results

υ_{flesh} = 0.42, E_{trab} = 150MPa

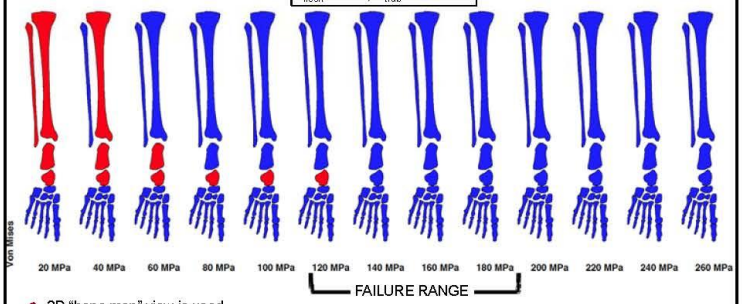

- 2D "bone map" view is used
  - A red bone indicates that at least one element in the cortical layer of that bone has reached/ exceeded the indicated Von Mises stress during the simulation
  - A blue bone indicates that no elements have reached the indicated Von Mises stress
  - This can illustrate the relative fracture risk of bones for a given failure criterion
- The talus experiences the highest stress and appears to be at the highest risk of fracture, followed by the calcaneus, tibia, and fibula

TECHNOLOGY DRIVEN. WARFIGHTER FOCUSED.
APPROVED FOR PUBLIC RELEASE - DISTRIBUTION UNLIMITED

Whole Bone Results cont'd

υ_{flesh} = 0.42, E_{trab} = 900MPa

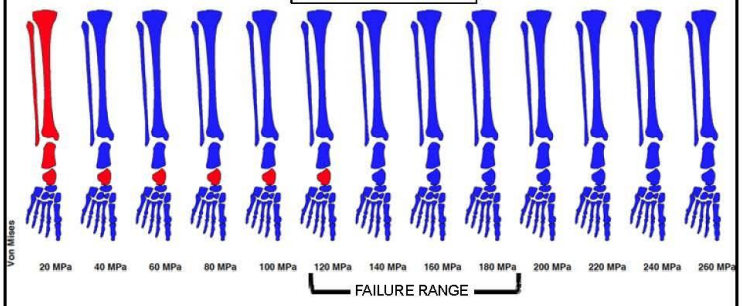

- The talus experiences the highest stress and appears to be at the highest risk of fracture
- Comparatively, the stress in the calcaneus, tibia, and fibula is much lower than the talus
  - This is in contrast to the previous υ_{flesh} = 0.42 case, where the calcaneus and tibia experienced stresses up to 60 and 40MPa, respectively

APPROVED FOR PUBLIC RELEASE - DISTRIBUTION UNLIMITED

Whole Bone Results cont'd

υ_{flesh} = 0.48, E_{trab} = 150MPa

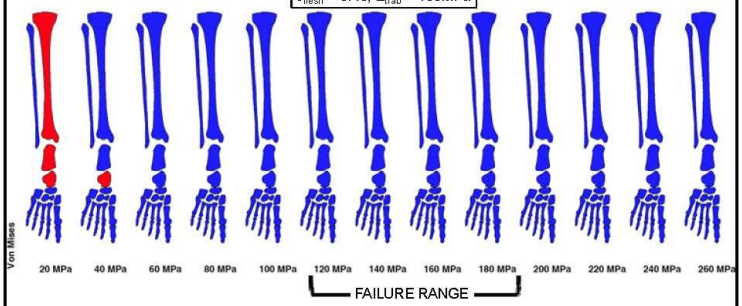

- The talus experiences the highest stress, though it is well below the failure range
- A longer simulation time is needed to support further conclusions/ a comparison with υ_{flesh} = 0.42 cases

TECHNOLOGY DRIVEN. WARFIGHTER FOCUSED.
APPROVED FOR PUBLIC RELEASE - DISTRIBUTION UNLIMITED

C339

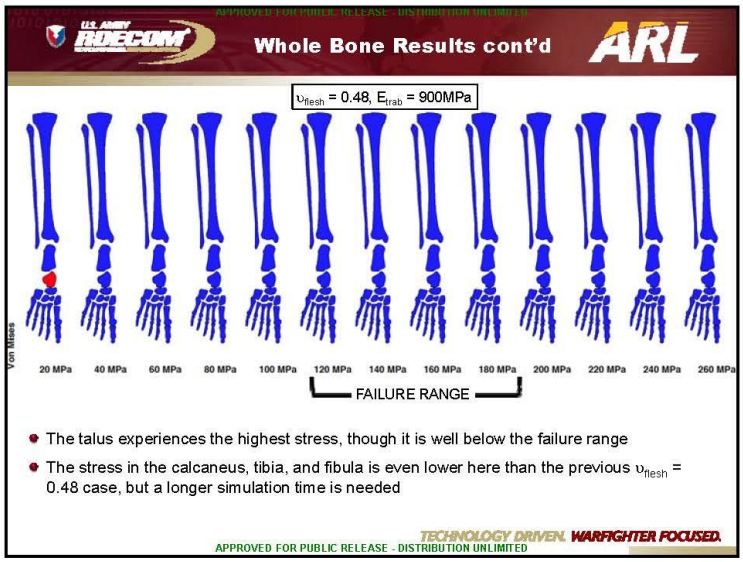
APPROVED FOR PUBLIC RELEASE - DISTRIBUTION UNLIMITED
Whole Bone Results cont'd
ARL
υ_{flesh} = 0.48, E_{trab} = 900MPa
Von Mises
20 MPa
40 MPa
60 MPa
80 MPa
100 MPa
120 MPa
140 MPa
160 MPa
180 MPa
200 MPa
220 MPa
240 MPa
260 MPa
FAILURE RANGE
The talus experiences the highest stress, though it is well below the failure range
The stress in the calcaneus, tibia, and fibula is even lower here than the previous υ_{flesh} = 0.48 case, but a longer simulation time is needed
TECHNOLOGY DRIVEN. WARFIGHTER FOCUSED.
APPROVED FOR PUBLIC RELEASE - DISTRIBUTION UNLIMITED

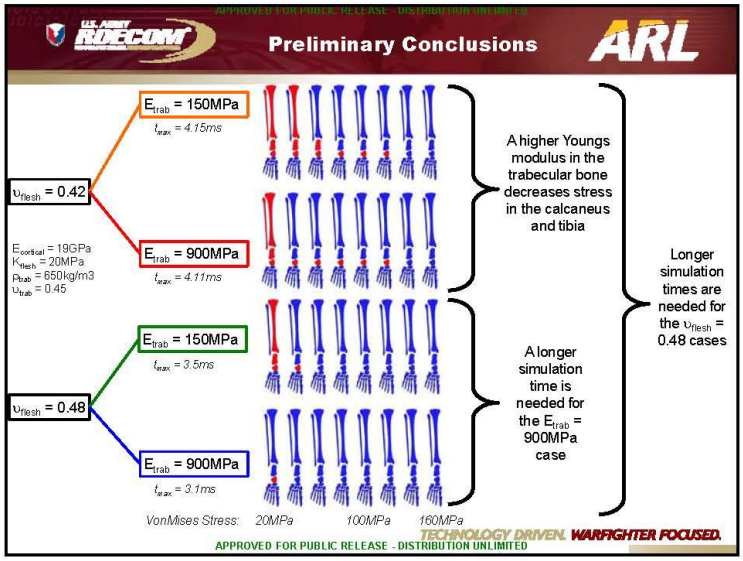
APPROVED FOR PUBLIC RELEASE - DISTRIBUTION UNLIMITED
Preliminary Conclusions
ARL
υ_{flesh} = 0.42
E_{trab} = 150MPa
t_{max} = 4.15ms
E_{trab} = 900MPa
t_{max} = 4.11ms
$E_{cortical}$ = 19GPa
K_{flesh} = 20MPa
ρ_{trab} = 650kg/m3
υ_{trab} = 0.45
υ_{flesh} = 0.48
E_{trab} = 150MPa
t_{max} = 3.5ms
E_{trab} = 900MPa
t_{max} = 3.1ms
VonMises Stress: 20MPa 100MPa 160MPa
A higher Youngs modulus in the trabecular bone decreases stress in the calcaneus and tibia
A longer simulation time is needed for the E_{trab} = 900MPa case
Longer simulation times are needed for the υ_{flesh} = 0.48 cases
TECHNOLOGY DRIVEN. WARFIGHTER FOCUSED.
APPROVED FOR PUBLIC RELEASE - DISTRIBUTION UNLIMITED

Future Work

- Finish data analysis on the elastic study
- Continue parametric study to include additional material models/ parameters and failure criteria for bone and flesh
- Identify model sensitivities relevant to tissue failure
- Study different lower extremity meshes to identify additional sensitivities (i.e. geometry, mesh refinement, etc.)
- Compare probe location results to experimental data (falls within calculated data corridor?)

Bone

		Cortical	Trabecular
Elastic-Plastic Elastic	Density	1680-2000 kg/m^3	654-1100 kg/m^3
	Youngs Modulus	15-19 GPa	145-900 MPa
	Poissons Ratio	0.3-0.35	0.3-0.45
	Yield Strength	114-165 MPa	1.2-9.3 MPa
	Tangent Modulus	0.7-6.4 GPa	n/a
	Failure Stress	124-175 MPa	5.3-30.6 MPa
	Failure Strain	1.6-2.2 %	12.2-13.4 %
	⋮		

Flesh

Viscoelastic Hyperelastic Elastic	Density	1000-1300 kg/m^3
	Bulk Modulus	2.5-333 MPa
	Poissons Ratio	0.42-0.49
	C_1	-
	C_2	-
	⋮	
	S_1, S_2	-
	T_1, T_2	-
	⋮	

TECHNOLOGY DRIVEN. WARFIGHTER FOCUSED.

APPROVED FOR PUBLIC RELEASE - DISTRIBUTION UNLIMITED

Questions?

Thank you!

TECHNOLOGY DRIVEN. WARFIGHTER FOCUSED.
APPROVED FOR PUBLIC RELEASE - DISTRIBUTION UNLIMITED

C341

References

Iwamoto, M.; Miki, K.; Tanaka, E. Ankle skeletal injury predictions using anisotropic inelastic constitutive model of cortical bone taking into account damage evolution.. *Stapp car crash journal* **2005**, *49* 133.

Bandak, F.; Tannous, R.; Toridis, T. On the development of an osseo-ligamentous finite element model of the human ankle joint. *International journal of solids and structures* **2001**, *38* (10) 1681–1697.

Dong, L.; Zhu, F.; Jin, X.; Suresh, M.; Jiang, B.; Sevagan, G.; Cai, Y.; Li, G.; Yang, K. H. Blast effect on the lower extremities and its mitigation: A computational study. *Journal of the mechanical behavior of biomedical materials* **2013**, *28* 111–124.

Shin, J.; Yue, N.; Untaroiu, C. D. A finite element model of the foot and ankle for automotive impact applications. *Annals of biomedical engineering* **2012**, *40* (12) 2519–2531.

Untaroiu, C.; Darvish, K.; Crandall, J.; Deng, B.; Wang, J.-T. A finite element model of the lower limb for simulating pedestrian impacts.. *Stapp car crash journal* **2005**, *49* 157.

Schuster, P. J.; Chou, C. C.; Prasad, P.; Jayaraman, G. Development and validation of a pedestrian lower limb non-linear 3-d finite element model.. *Stapp car crash journal* **2000**, *44* 315.

Currey, J. D. *Bones: structure and mechanics*; Princeton University Press: 2002.

APPROVED FOR PUBLIC RELEASE - DISTRIBUTION UNLIMITED

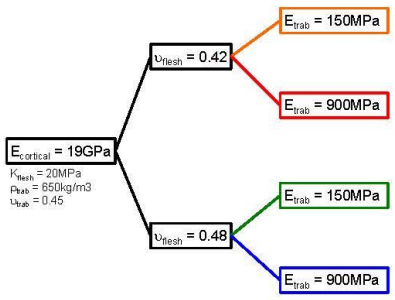

TECHNOLOGY DRIVEN. WARFIGHTER FOCUSED.
APPROVED FOR PUBLIC RELEASE - DISTRIBUTION UNLIMITED

Workshop on Numerical Analysis of Human and Surrogate Response to Accelerative Loading
Aberdeen Proving Ground, MD
January 7-9, 2014

Coupled Eulerian and Lagrangian Approaches for Dynamic Injury Analysis

Timothy Harrigan, Robert Armiger, Catherine Carneal, Travis Nissley, JiangYue Zhang, Andrew Merkle

BIOMECHANICS AND INJURY MITIGATION SYSTEMS

The Johns Hopkins University
APPLIED PHYSICS LABORATORY

Introduction

- Effective modeling of human body during impact scenarios requires numerical stability under large deformation
- Soft tissue is nearly incompressible (high bulk modulus & low shear modulus)
- Complex contact conditions exist within soft-tissue, interstitial, and skeletal anatomy

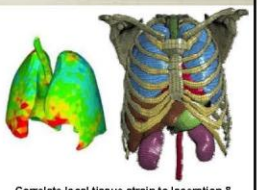

Correlate local tissue strain to laceration & local stress/pressure to contusion

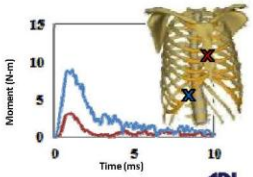

2

Coupled methods are well established

Lagrangian FEA

- Material element: Elements define a mass of material
- Momentum conserved in each element
- Information available
  - Histories (yield, failure, damage)
  - Organ-level forces and moments
  - Stresses and section forces (from nodal point loads)
  - Stiffness (incremental)

Easy to Implement Damage Models

Eulerian FEA

- Spatial element: Elements are fixed in space
- Mass conserved in each element (advection)
  - Internal state variables transferred with the material (stresses, yield/ damage states)
  - Shear stress/strain as well as pressure
  - Not limited to fluids
  - LS-Dyna, CTH

Numerically Stable under Large Strain and Deformations

- **Interaction via constraint conditions in commercial codes**

3

APL

Coupled Lagrangian-Eulerian Methods: Rationale

- **Model large deformation and strain**
  - Lagrangian: Strain based damage assessment (organs, skeletal)
  - Eulerian: Large strain (Interstitial tissue, fluids)
- **Parametric mesh development**
  - Postural changes
  - Range of anthropometries
- **Model internal pressure effects along with inter-organ contact forces**
- **Simplifies contact definitions**

Complex geometries for Lagrangian meshing

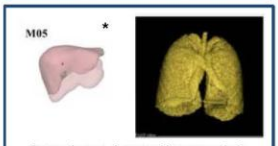

Organ shapes change with posture (left) and population size (right)

- **Critical Challenges to Address:**
  - New coupling parameters must be understood (penalty parameters)
  - Implementation of strain failure criteria in Eulerian (advected) parts

4

* Ann Adv Automot Med, "Abdominal Organ Location, Morphology, and Rib Coverage for the 5th, 50th, and 95th Percentile Males and Females in the Supine and Seated Posture using Multi-Modality Imaging," Sept 2013

APL

Study Objectives

- **Develop and verify mixed Lagrangian and Eulerian finite element methods for injury assessment in human models under military-relevant loading environments (accelerative, blunt, ballistic)**
  - Evaluate numerical stability/artifacts
  - Evaluate ability to model relevant physical effects
    - High strain damage assessments
    - Pressure transmission

5 APL

Accelerative Loading to Lower Extremity
Numerical Stability

- **High rate bending simulated for simplified model of bone in thigh**
- **Initially good Lagrangian elements become badly deformed**
  - Numerical results in flesh elements unreliable
  - Common challenge for all soft tissue structures

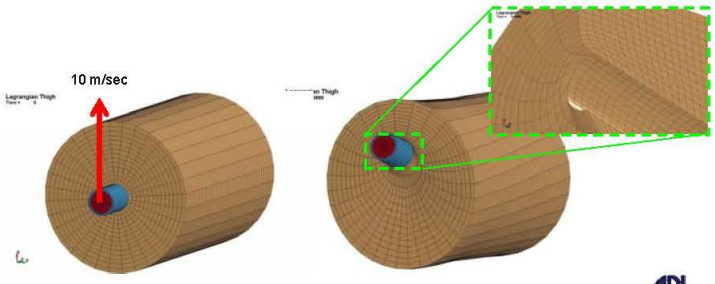

6 APL

Accelerative Loading to Lower Extremity
Numerical Stability

- **Incorporating Lagrangian bone in Eulerian flesh preserves bone response for injury prediction, while improving soft-tissue stability**

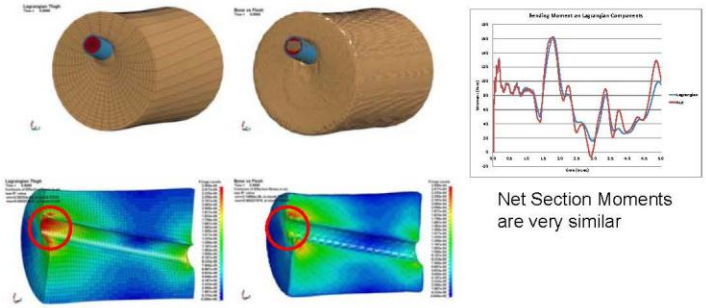

Net Section Moments are very similar

Soft tissue stress estimates differ where Lagrangian elements are skewed

7

APL

Accelerative Loading to Lower Extremity
Numerical Stability

- **Incorporating Lagrangian bone in Eulerian flesh preserves bone response for injury prediction, while improving soft-tissue stability**
- **To model accelerative loading due to structures:**
  - Add Lagrangian skin over the flesh,
  - Couple the skin to the Eulerian material
  - Use standard Lagrangian contact for structural interaction

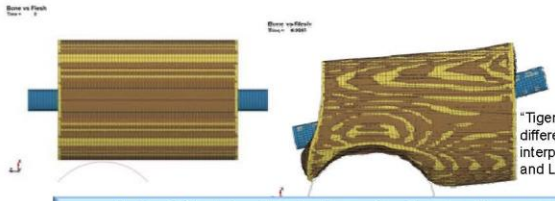

"Tiger stripes" Show the difference between the interpolated Eulerian Surface and Lagrangian skin

Method fits into standard accelerative loading models

8

APL

Blast Loading to Thoracic Organs
Numerical Stability

- **Lagrangian hexahedral human liver integrated into Eulerian flesh mesh**
  - Vacuum under liver
  - Penalty-based coupling
- **ConWep input for C4 Explosive**
  - Air also Eulerian
  - Initial 1 Atm pressure

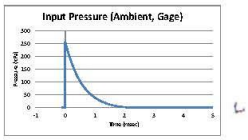

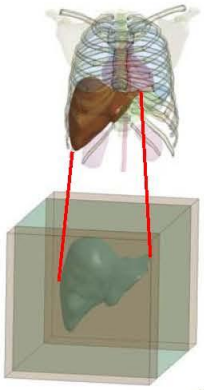

9

APL

Blast Loading to Thoracic Organs
Numerical Stability

- **Flesh Properties**
  - High Bulk Modulus (2 GPa)
  - Low Shear modulus (28 kPa)
- **Prone to mild Checkerboarding**
- **Local Interface Stress Artifacts**
  - Turn off Nodal Averaging to observe

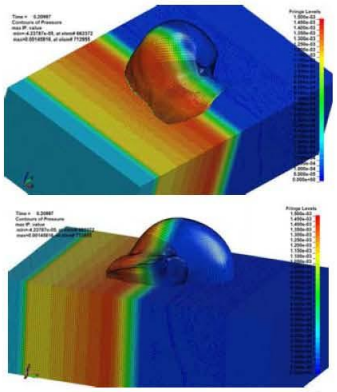

10

APL

Blast Loading to Thoracic Organs
Numerical Stability

Non-averaged element data

Nodal Averaging can add artifacts and obscure checkerboarding

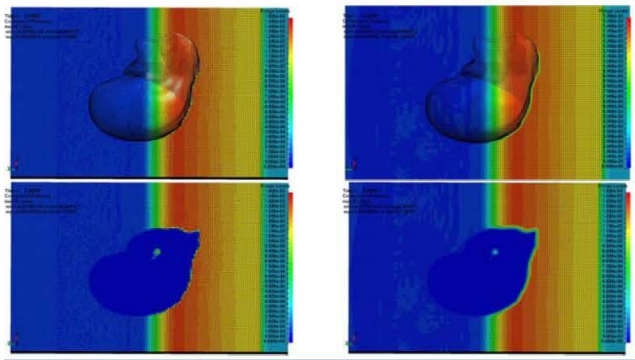

11

APL

Blast Loading to Thoracic Organs
Numerical interface artifacts are localized

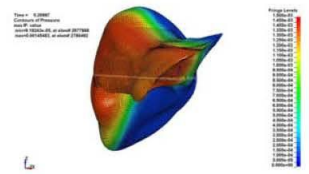

- Low-amplitude variations near surfaces

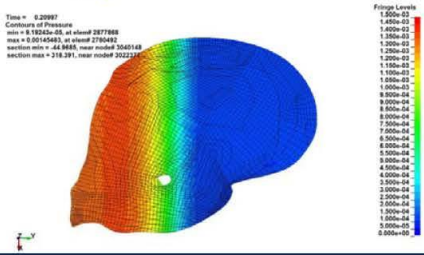

12

APL

Blast Loading to Thoracic Organs
Mesh refinement affects interfaces

- **Lagrangian Liver Mesh**

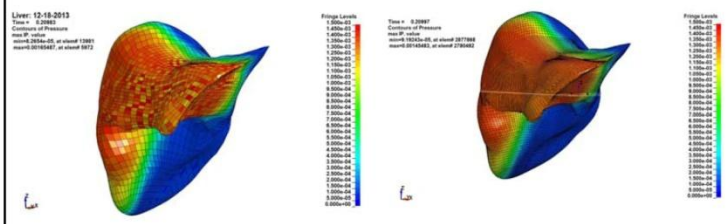

13

APL

Blast Loading to Thoracic Organs
Numerical Stability

Nodal point averaging turned off

14

APL

Blast Loading to Organ

Pressure Transmission: Effect of Material Properties

- **Bulk Modulus decreased (sound speed from 1480 m/s to 1000 m/s): Slower propagation in liver**

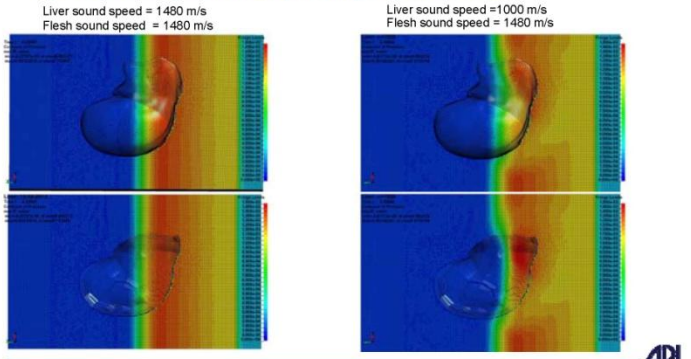

15

APL

Blunt Impact to Thoracic Organ

- **Spherical Projectile Hitting Flesh (10 m/s), Liver embedded in flesh: Strain transfer to Lagrangian Organ**

16

APL

Ballistic Injury to Thoracic Organ
Strain Tracking

- **Ballistic impact to Lagrangian mesh causes instability**
  - Assess strain estimation in an Eulerian mesh
- **Simulated penetrating impact near liver to investigate ability to calculate strain in Eulerian models**
  - Flesh is Eulerian in all cases → facilitates simulation of projectile penetration
  - Liver modeling
    - Lagrangian solid elements
    - Eulerian with tracer point definition
- **Penetration characteristics:**
  - 64gr RCC with initial velocity 400 m/s
  - Passing underneath liver (~3 cm)

64gr RCC with initial velocity 400 m/s passing underneath liver (~3 cm)

17

APL

Ballistic Injury to Thoracic Organ
Strain estimates in Eulerian regions

- **Specialized numerical approach using tracer particles implemented to track strain in Eulerian liver mesh**
- **Similar strain results show validity of approach for strain-based injury assessment in Eulerian models**

Strain equations

$$\varepsilon_{xx} = \frac{\partial u}{\partial x} + \frac{1}{2}\left[\left(\frac{\partial u}{\partial x}\right)^2 + \left(\frac{\partial v}{\partial x}\right)^2 + \left(\frac{\partial w}{\partial x}\right)^2\right]$$

$$\varepsilon_{yy} = \frac{\partial v}{\partial y} + \frac{1}{2}\left[\left(\frac{\partial u}{\partial y}\right)^2 + \left(\frac{\partial v}{\partial y}\right)^2 + \left(\frac{\partial w}{\partial y}\right)^2\right]$$

$$\varepsilon_{zz} = \frac{\partial w}{\partial z} + \frac{1}{2}\left[\left(\frac{\partial u}{\partial z}\right)^2 + \left(\frac{\partial v}{\partial z}\right)^2 + \left(\frac{\partial w}{\partial z}\right)^2\right]$$

$$\gamma_{xy} = 2 * \left[\frac{\partial u}{\partial v} + \frac{\partial v}{\partial x} + \frac{\partial u}{\partial x}\frac{\partial u}{\partial v} + \frac{\partial v}{\partial x}\frac{\partial v}{\partial v} + \frac{\partial w}{\partial x}\right]$$

$$\gamma_{xz} = 2 * \left[\frac{\partial u}{\partial z} + \frac{\partial w}{\partial x} + \frac{\partial u}{\partial x}\frac{\partial u}{\partial z} + \frac{\partial v}{\partial x}\frac{\partial v}{\partial z} + \frac{\partial w}{\partial x}\right]$$

$$\gamma_{yz} = 2 * \left[\frac{\partial v}{\partial z} + \frac{\partial w}{\partial v} + \frac{\partial u}{\partial v}\frac{\partial u}{\partial z} + \frac{\partial v}{\partial v}\frac{\partial v}{\partial z} + \frac{\partial w}{\partial v}\right]$$

*Non-linear terms not currently implemented

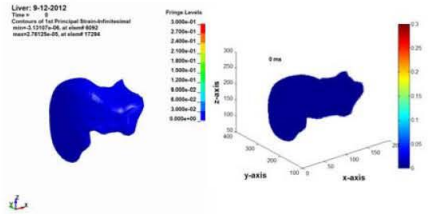

Lagrangian strain *ALE tracer point strain*

18

APL

Mixed Lagrangian – Eulerian Methods
Summary

- **Addresses modeling of high-rate events**
  - Blast/shock wave loading
  - High rate blunt/accelerative loading
  - Soft tissue modeling requirements
- **Advantages**
  - Mesh for interstitial tissue accommodates Lagrangian Parts
    - Vary mesh density
    - Simulate postural changes
    - Simulate locally high strains that would crash Lagrangian models
  - Pressure transmission across Eulerian-Lagrangian interface is modelled well
  - Can simulate shock impingement in fully coupled manner
- **Challenges**
  - Computational cost
  - Controlling numerical artifacts (assessing them)
  - Making results insensitive to internal coupling parameters

APL
19

Mixed Lagrangian – Eulerian Methods
Future Needs

- **Numerical requirements:**
  - Assessing large-scale model requirements
  - Scalability for large computing systems
  - Mesh sensitivity for nearly incompressible damage or plasticity
- **Modeling Specific Physical effects**
  - Thin fluid films
  - Cavitation/phase change
- **Experimental validation**
  - Pressure transmission
  - Blunt impact

APL
20

C352

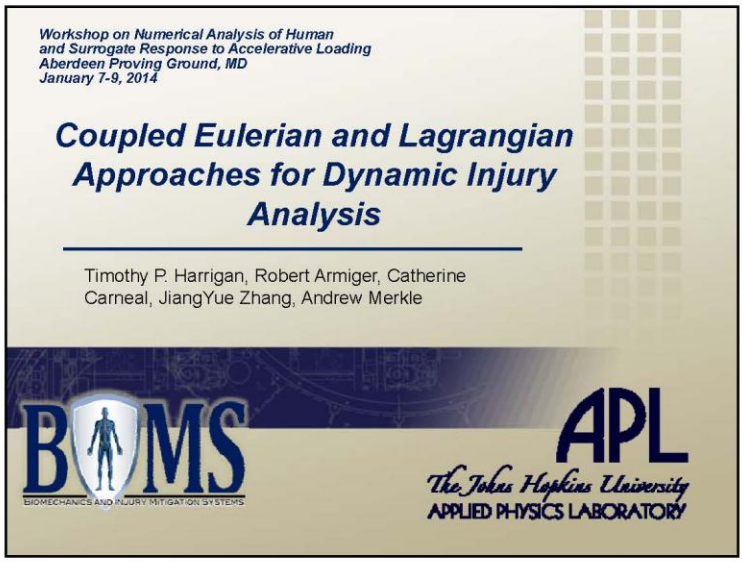
Workshop on Numerical Analysis of Human
and Surrogate Response to Accelerative Loading
Aberdeen Proving Ground, MD
January 7-9, 2014
Coupled Eulerian and Lagrangian Approaches for Dynamic Injury Analysis
Timothy P. Harrigan, Robert Armiger, Catherine Carneal, JiangYue Zhang, Andrew Merkle
BIOMECHANICS AND INJURY MITIGATION SYSTEMS
APL
The Johns Hopkins University
APPLIED PHYSICS LABORATORY


CORVID
TECHNOLOGIES
145 Overhill Drive · Mooresville, NC 28117 · 704.799.6944 · www.corvidtechnologies.com
Crew Response in Full System HFCP
Allen D. Shirley
Cameron Bell
Kevin Lister
Kim Meeks
January 9, 2014
DISTRIBUTION A: Approved for public release.
ashirley@corvidtec.com
UNCLASSIFIED

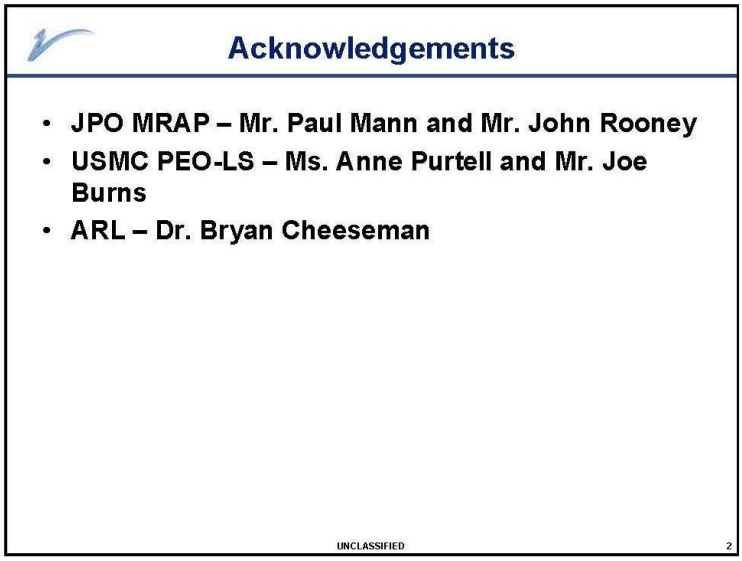
Acknowledgements
• JPO MRAP – Mr. Paul Mann and Mr. John Rooney
• USMC PEO-LS – Ms. Anne Purtell and Mr. Joe Burns
• ARL – Dr. Bryan Cheeseman
UNCLASSIFIED
2

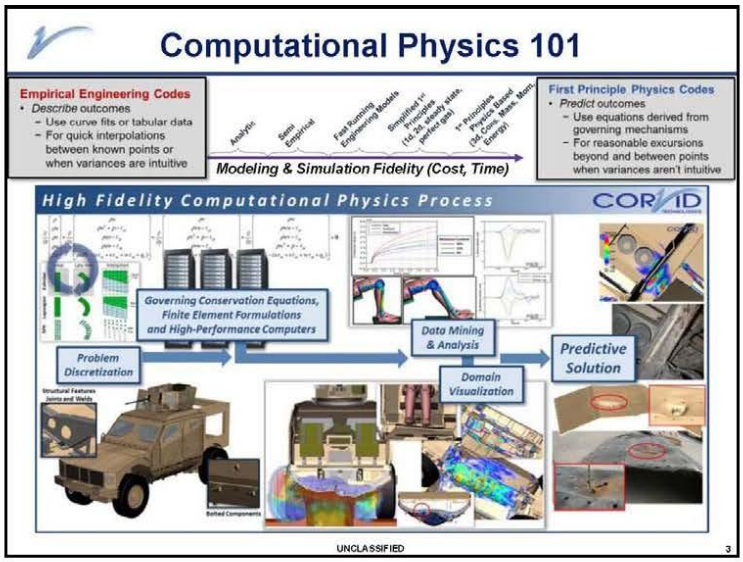
Computational Physics 101
Empirical Engineering Codes
• Describe outcomes
– Use curve fits or tabular data
– For quick interpolations between known points or when variances are intuitive
Analytic
Data Empirical
Fast Running Engineering Models
Simplified 1st Principles (1d, 2d, steady state, perfect gas)
1st Principles Physics Based (3d, Conti, Mom, Mom, Energy)
Modeling & Simulation Fidelity (Cost, Time)
First Principle Physics Codes
• Predict outcomes
– Use equations derived from governing mechanisms
– For reasonable excursions beyond and between points when variances aren't intuitive
High Fidelity Computational Physics Process
CORVID
Governing Conservation Equations, Finite Element Formulations and High-Performance Computers
Problem Discretization
Data Mining & Analysis
Domain Visualization
Predictive Solution
UNCLASSIFIED
3

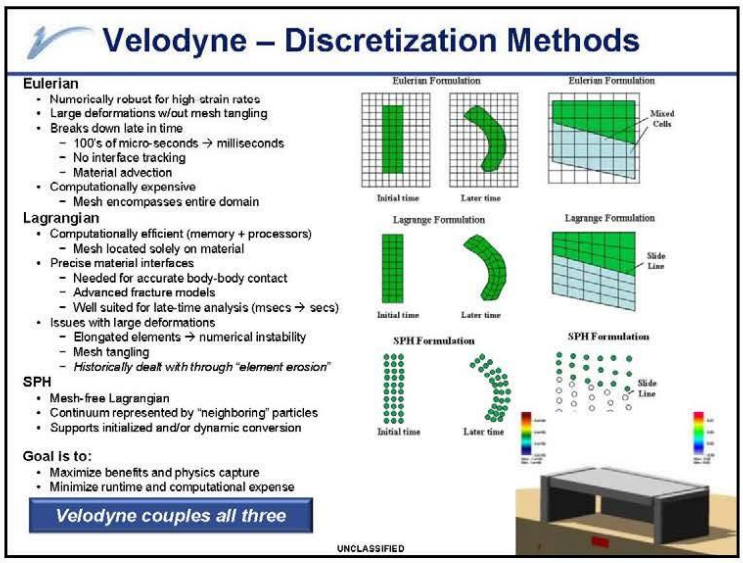
Velodyne – Discretization Methods
Eulerian
• Numerically robust for high strain rates
• Large deformations w/out mesh tangling
• Breaks down late in time
– 100's of micro-seconds → milliseconds
– No interface tracking
– Material advection
• Computationally expensive
– Mesh encompasses entire domain
Lagrangian
• Computationally efficient (memory + processors)
– Mesh located solely on material
• Precise material interfaces
– Needed for accurate body-body contact
– Advanced fracture models
– Well suited for late-time analysis (msecs → secs)
• Issues with large deformations
– Elongated elements → numerical instability
– Mesh tangling
– Historically dealt with through "element erosion"
SPH
• Mesh-free Lagrangian
• Continuum represented by "neighboring" particles
• Supports initialized and/or dynamic conversion
Goal is to:
• Maximize benefits and physics capture
• Minimize runtime and computational expense
Velodyne couples all three
Eulerian Formulation
Initial time
Later time
Eulerian Formulation
Mixed Cells
Lagrange Formulation
Initial time
Later time
Lagrange Formulation
Slide Line
SPH Formulation
Initial time
Later time
SPH Formulation
Slide Line
UNCLASSIFIED

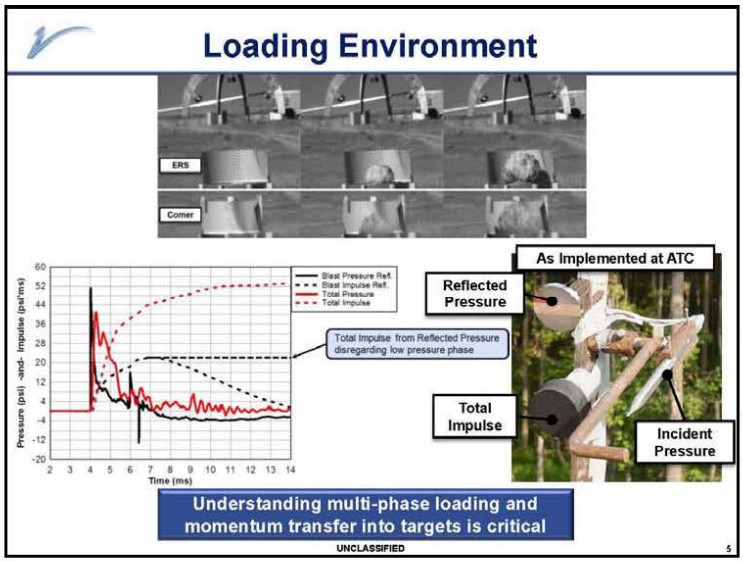
Loading Environment
ERS
Corner
Blast Pressure Ref.
Blast Impulse Ref.
Total Pressure
Total Impulse
Pressure (psi) -and- Impulse (psi*ms)
Time (ms)
Total Impulse from Reflected Pressure disregarding low pressure phase
As Implemented at ATC
Reflected Pressure
Total Impulse
Incident Pressure
Understanding multi-phase loading and momentum transfer into targets is critical
UNCLASSIFIED
5

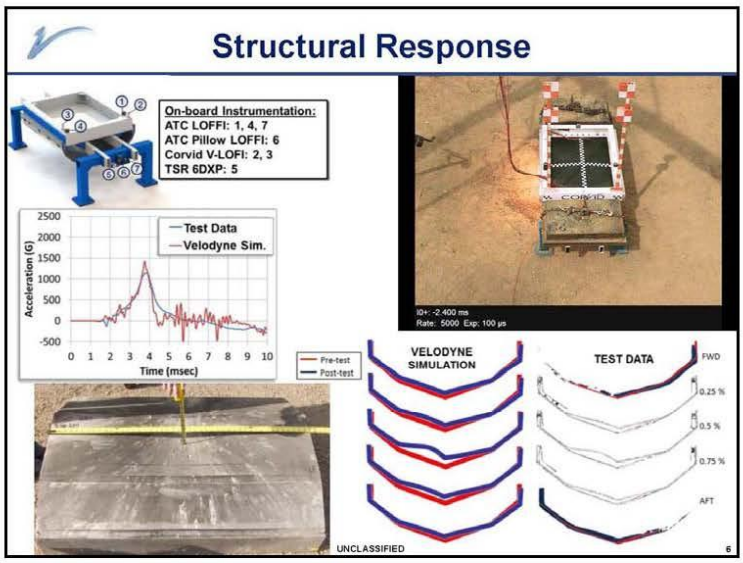
Structural Response
On-board Instrumentation:
ATC LOFFI: 1, 4, 7
ATC Pillow LOFFI: 6
Corvid V-LOFI: 2, 3
TSR 6DXP: 5
Test Data
Velodyne Sim.
Acceleration (G)
Time (msec)
Pre-test
Post-test
VELODYNE SIMULATION
TEST DATA
FWD
0.25 %
0.5 %
0.75 %
AFT
UNCLASSIFIED
6

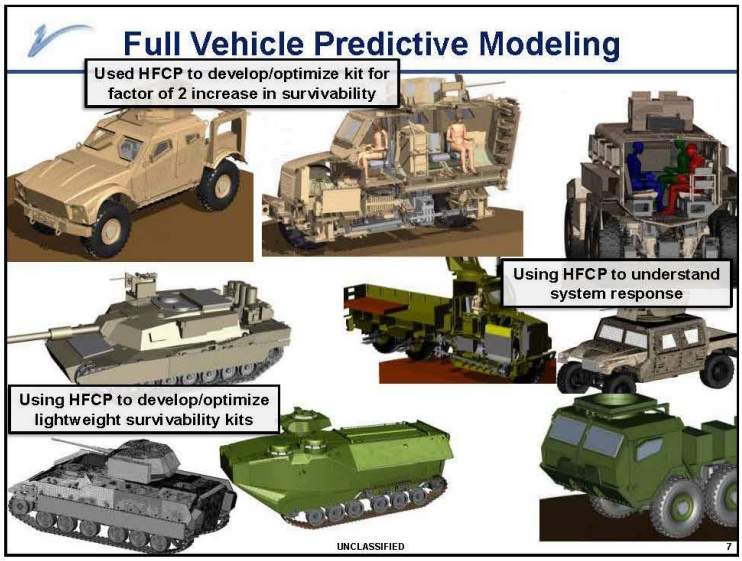
Full Vehicle Predictive Modeling
Used HFCP to develop/optimize kit for factor of 2 increase in survivability
Using HFCP to understand system response
Using HFCP to develop/optimize lightweight survivability kits
UNCLASSIFIED
7

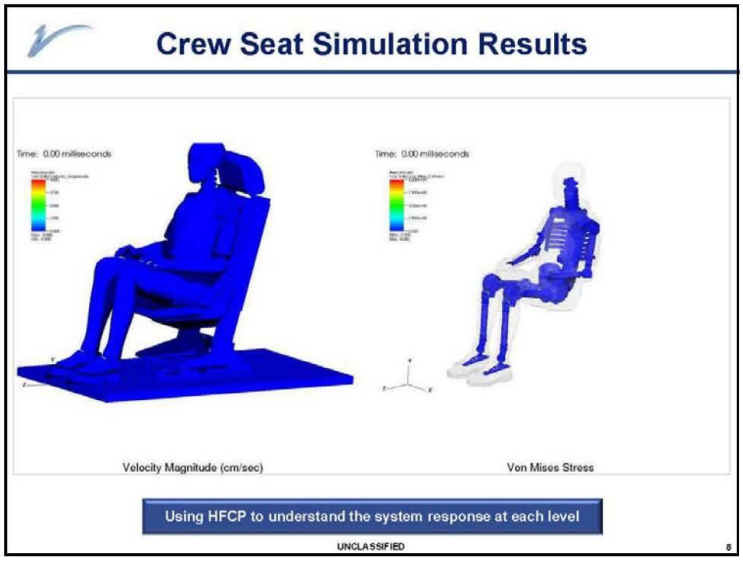
Crew Seat Simulation Results
Time: 0.00 milliseconds
Time: 0.00 milliseconds
Velocity Magnitude (cm/sec)
Von Mises Stress
Using HFCP to understand the system response at each level
UNCLASSIFIED

Blast Injury Modeling Approaches

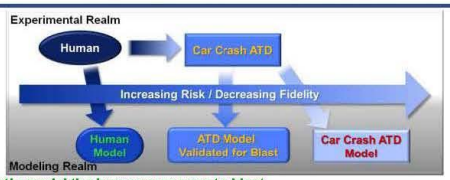

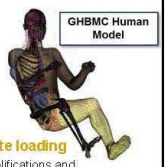

Ideal Case: Directly model the human response to blast

- Valid comparison to theater events and cadaver testing based on *limited* set of simplifications and assumptions
  - High rate loading response of tissue and bone materials
  - Fidelity focused on areas of concern to Blast Induced Injury criteria

Intermediate Case: Validate H350 ATD model specifically for its response to high-rate loading

- Valid for comparisons to DT and LFT&E event data using H350 ATD's; Based on *practical* set of simplifications and assumptions. Validate with appropriate data:
  - CSBES and Drop tower data available; may need additional data
  - Uses fully elastic/plastic and rate dependent materials

Highest Risk Case: Employing a fast running automotive crash simulation based model of the H350 is not valid

- Validated only for ATD response to 30 mph frontal impact car crash
- Based on *overwhelming* set of simplifications and assumptions:
  - **Rigid and linear elastic material** assumptions highly questionable
  - Beam, shell, and tet element simplifications not valid for plasticity
  - Joint simplification not valid for ankle, knee, and pelvis load paths

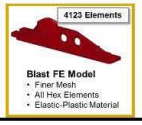

UNCLASSIFIED 9

Corvid HIII ATD FE Model

- **Corvid Teamed with Humanetics**
  - International leader in ATD manufacturing
  - Leveraging accurate CAD data (not existing FEA model)
- **Improved Model Fidelity to Capture Blast Response**
  - Using fully plastically deformable components
  - Efforts concentrated between foot and pelvis for seat and floor performance evaluations
  - Total element increase from ~128k to ~500k (≈4x)
- **HFCP Model Highlights**
  - Explicit representation of all joint functionality
  - Explicit modeling of load cells and accelerometers
  - Capable of capturing deformation/failure seen in testing

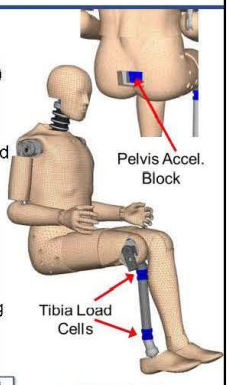

Car crash FE model assumes rigid material

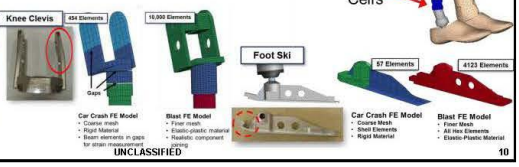

UNCLASSIFIED 10

High Rate Material Characterization

- High rate material testing of the ATD and boot "soft" materials for Corvid is complete
  - **ATD:** Ensolite foam, Butyl rubber, PVC rubber, White PU foam
  - **Boot:** Brown PU foam, Vulcanized rubber
- Split Hopkinson Pressure Bar (SHPB) data received from Purdue University

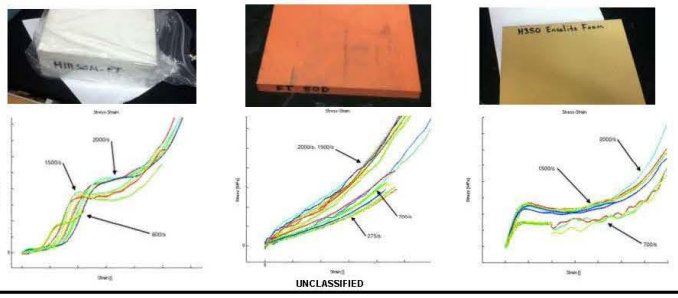

UNCLASSIFIED 11

Material Model Fitting

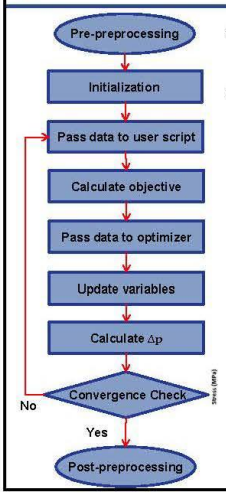

- Material model parameter fitting through an optimization routine
- The following materials have been parameterized to-date (on-going process)
  - PVC rubber (Skin)
  - Ensolite (Foam Heel Pad)
  - Vulcanized Rubber (Boot Outsole)

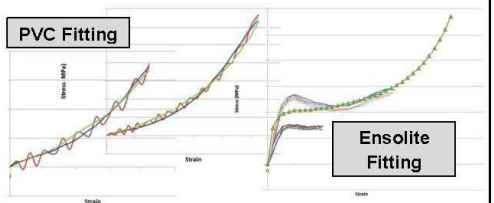

UNCLASSIFIED 12

Validation Results

- Axial loading and impulse error comparisons:
  - original "baseline" material models
  - new SHPB based material models

Simulation	Axial Loading (Error)	Impulse (Error)
Baseline Material Models	13.4%	42.9%
SHPB Based Material Models	3.4%	18.3%

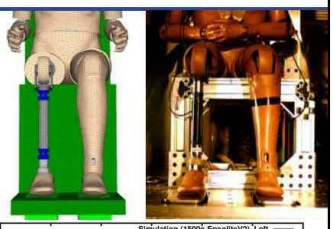

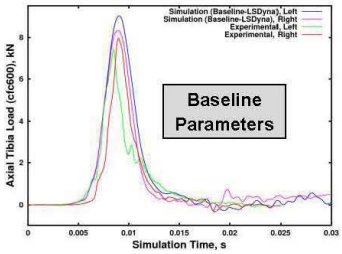

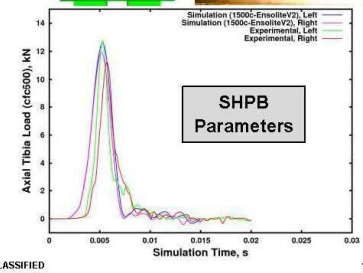

UNCLASSIFIED 13

4.2 WIAMAN Test Rig Simulation BLUF

Progress to date:

1) Received CAD, data, and test photos
2) Completed test rig meshing & ATD placement
3) Analyzed data
   a) Set-up first test simulation (MS 8: 90°/120°, No PPE)
   b) Multiple iterations to understand effects of test structure on crew response
   c) Output focus determined (tibia and lumbar forces, pelvis accelerations)
   d) Cross-compare with similar test events

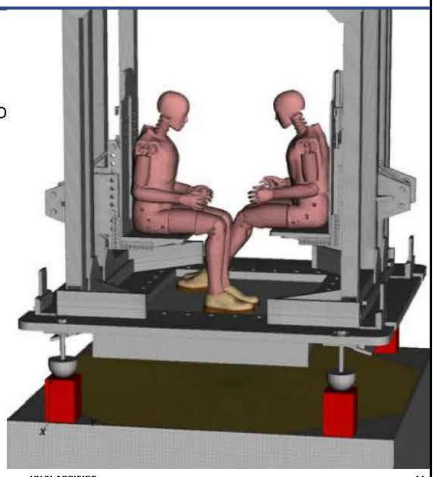

UNCLASSIFIED 14

Animations

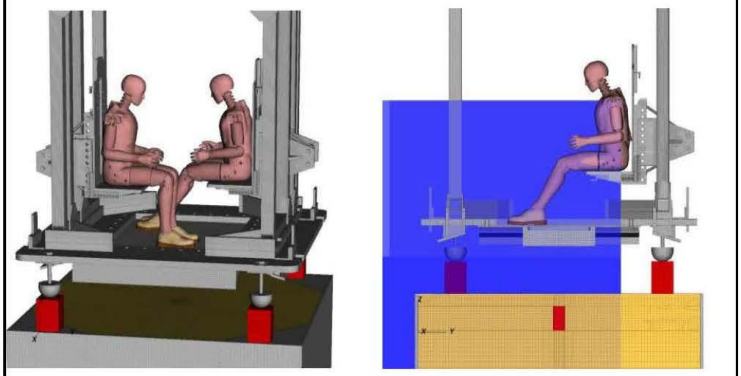

Initial simulations showing structure and ATD response

UNCLASSIFIED 15

Tibia Forces

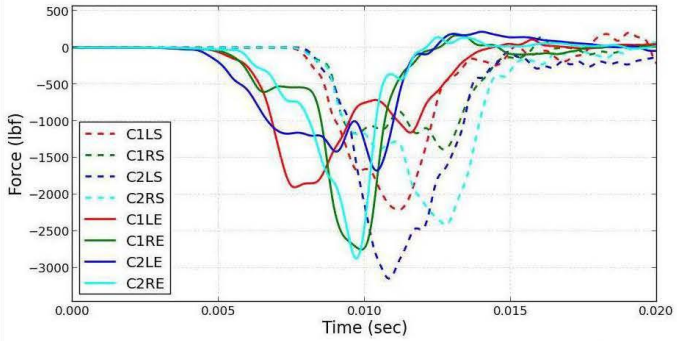

Setup needs to be configured correctly to see better correlation, but timing and magnitude reasonable for a "sanity check"

UNCLASSIFIED 16

Human Blast Injury Modeling (CAVEMAN)

- **Proposed path forward:**
  - Obtain CAD built from scans of representative 50th male
  - Thorough validation of biofidelic representation of segmented body regions
    - Use of anthropometric databases for verification and validation of CAD data
  - Develop high fidelity meshed model from CAD
  - Gather existing material characterization data and fill gaps
  - Validate against segment and full body experimental data
  - Compare the ATD and human response to blast loading
  - Start with 50th percentile male to assess value to DoD; 95th male and 5th female to follow
- **Challenges:**
  - Limited availability of corroborated / agreed upon high rate material characterization data
  - Theater data difficult for validation / comparison
    → limited initial condition data
- **Leverage-able projects:**
  - Academic Research through DoD Lab Partnerships
  - WIAMAN project investigating PMHS injury and generating good model validation type data

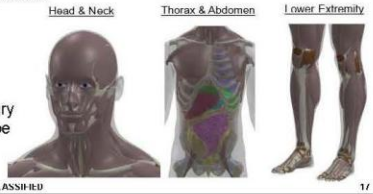

UNCLASSIFIED 17

50th Percentile CAD

- Average human male solid geometry constructed from scan data (MRI, CT, Ultrasound, …)
- Comparison to DOD 50th percentile standards:
  - DOD-HDBK-743A
    - 4.8% average measurement error (74% within one standard deviation)
  - ANSUR
    - 4.6% average measurement error (70% within one standard deviation)
  - ANSUR II
    - 4.2% average measurement error (74% within one standard deviation)
- Includes:
  - Skeletal, muscular, vascular, and nervous systems in addition to connective tissue and internal organs

UNCLASSIFIED 18

Discretization

- Preliminary tetrahedral mesh of entire human body (skeletal, muscular, connective and organs) has been completed
- Estimated final element count: ~3 to 4 million
  - Skeletal: ~1 to 1.5 million
  - Musclar: ~1.5 to 2 million
  - Connective Tissue: ~0.5 million
- Explicit representation of all joint functionality
- Transition towards complete hex mesh has begun starting with the muscular system in the leg

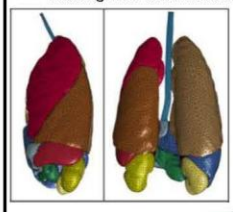

Preliminary mesh of the skeletal and musculature systems, primary organs (skin not shown), and connective tissue

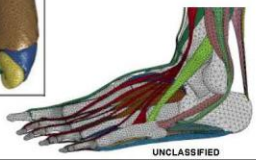

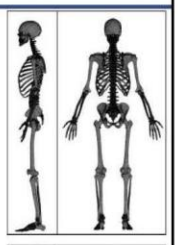

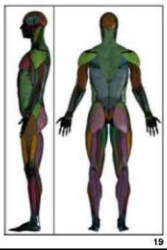

UNCLASSIFIED 19

High Stain Rate Material Models

- Literature review to determine state of high strain rate modeling of biological materials
- Focus on strain rates seen in BII (up to ~3000/s)
- Develop constitutive models base on high strain rate test data
- Perform high rate testing on cadaveric tissue to fill in gaps in the literature

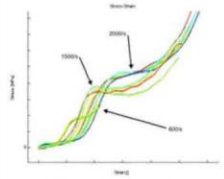

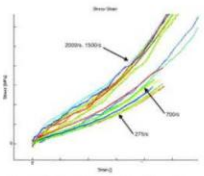

Examples of material response for high strain rate testing of soft viscoelastic materials

High strain rate data from literature review for constitutive material definitions in CAVEMAN 1.0

	Tissue Type	Species
Skeletal	Bone (Cancellous)	Human
	Bone (Cortical)	Bovine
	Cartilage	Porcine
Muscular	Muscle	Porcine
	Ligament	Human
	Tendon	Bovine
Organs	Heart	Human
	Stomach	Human
	Liver	Human
	Lung	Human
	Kidney	Bovine
	Spleen	Porcine
	Pancreas	----------
	Bladder	----------
	Small Intestine	----------
	Large Intestine	----------
	Gallbladder	----------
	Skin	Porcine
	Fat	Porcine

- High strain rate human data exists
- High strain rate animal data exists
- No high strain rate data available

UNCLASSIFIED 20

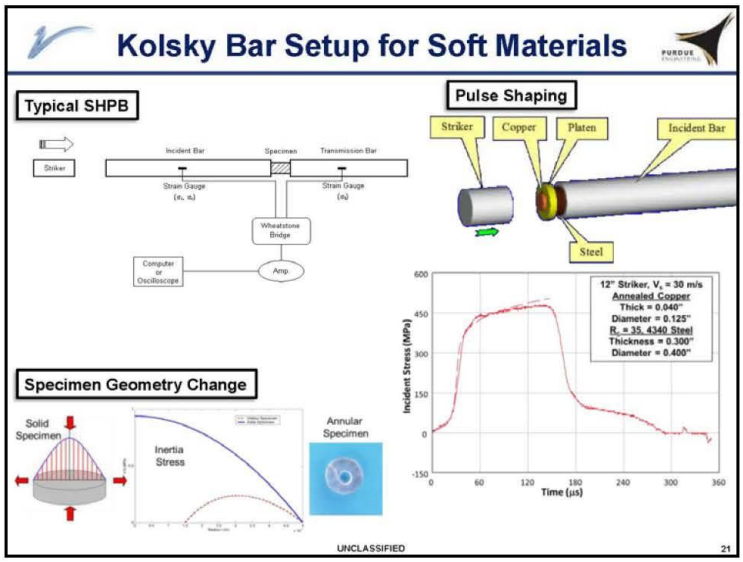
Kolsky Bar Setup for Soft Materials
Typical SHPB
Striker
Incident Bar
Specimen
Transmission Bar
Strain Gauge
Strain Gauge
Wheatstone Bridge
Computer or Oscilloscope
Amp
Pulse Shaping
Striker
Copper
Platen
Incident Bar
Steel
12" Striker, V = 30 m/s
Annealed Copper
Thick = 0.040"
Diameter = 0.125"
R. = 35. 4340 Steel
Thickness = 0.300"
Diameter = 0.400"
Incident Stress (MPa)
Time (μs)
Specimen Geometry Change
Solid Specimen
Inertia Stress
Annular Specimen
UNCLASSIFIED
21

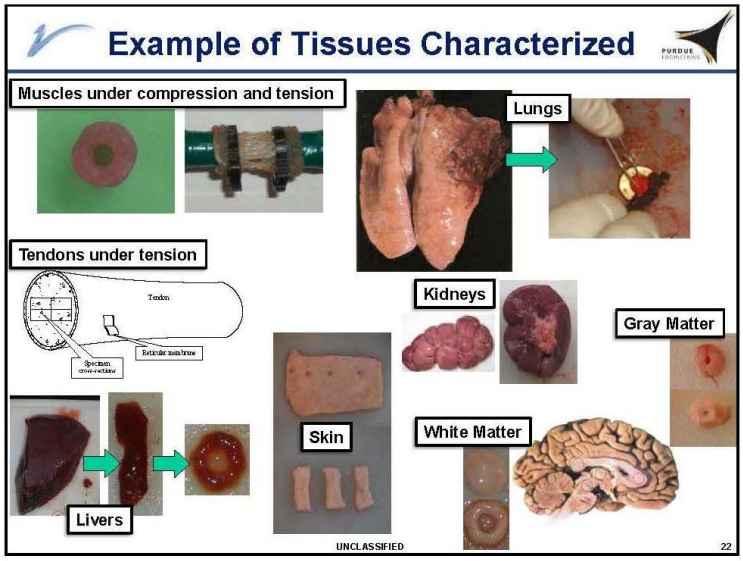
Example of Tissues Characterized
Muscles under compression and tension
Lungs
Tendons under tension
Tendon
Reticular membrane
Specimen cross-section
Kidneys
Gray Matter
Skin
White Matter
Livers
UNCLASSIFIED
22

Strain-Rate Effects
(Along Fiber Direction)

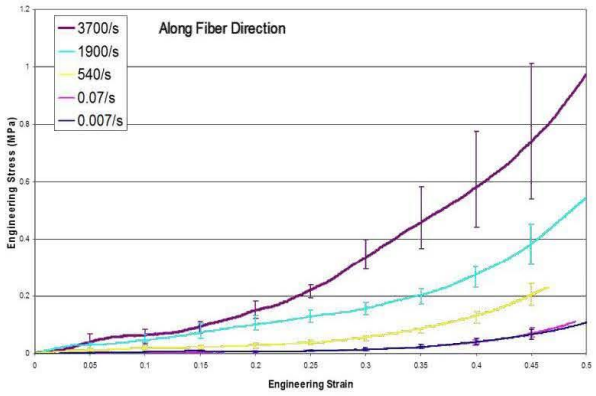

UNCLASSIFIED 23

Summary

- **Vehicle IED Survivability System-level Modeling**
  - **Use HFCP coupled with ample computational resources to gain insight into critical details**
  - **Represent physics of multi-phase IED loading**
  - **Resolve structural details down to millimeter length scales**
  - **Include injury mitigation technology explicitly rather than empirical representation developed for single axis test**
- **Crew Response Modeling**
  - **Began with Anthropomorphic Test Device currently used**
    - Expanded material characterization to higher rates
    - Validate against multiple experimental data sets
    - Used to support system development and testing
  - **Current effort to develop high fidelity human model**
    - For use in full system modeling in conjunction with ATD model
    - Understand system effects as tested and as used in theater

UNCLASSIFIED 24

U.S. ARMY TANK AUTOMOTIVE RESEARCH, DEVELOPMENT AND ENGINEERING CENTER (TARDEC)

Evaluating the effectiveness of various blast load descriptors as occupant injury predictors for underbody blast events

Workshop on Numerical Analysis of Human and Surrogate Response to Accelerative Loading
Army Research Laboratory (ARL)
Aberdeen, MD
Jan 7-9, 2014

Jai Ramalingam
Ravi Thyagarajan
Kumar Kulkarni
TARDEC/Analytics

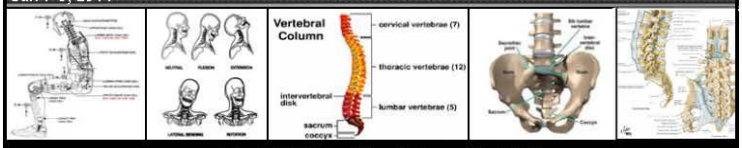

Introduction

- It is a well known fact that underbody blasts have become one of the most widespread reasons for warfighter casualties in recent wars.
- Spinal injuries to occupants have particularly increased in theater from these roadside blast incidents, followed by tibia and lower leg injuries.
- The most common occupant injuries in these extremely short duration events arise out of the very high vertical acceleration of vehicle due to its close proximity to hot high pressure gases from the blast.
- It is of considerable interest to developers of military vehicles to assess occupant injury risk due to blast loading in the early phase of the design process.

Blast pulse and occupant injury

A typical blast loading pulse is triangular in shape and can be characterized by its peak acceleration (G_{peak}) or change in velocity (Δv) with or without considering the duration of the pulse (T).

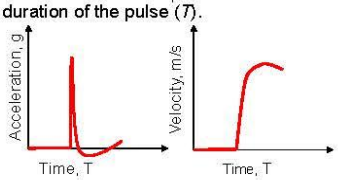

Occupant injury risk is proportional to;

1. Peak acceleration, G_{peak} in g's
2. Time duration of the pulse, T in ms
3. Rate of onset of acceleration, $\dot{G}$ in g/ms
4. Change in velocity, Δv, in m/s
5. Direction of loading
6. etc.

It has been shown before that there is no single input parameter which can be used to effectively assess occupant injury. However, the design community often use peak acceleration, G_{peak} or Δv to determine the severity of any given pulse.

Earlier efforts to more adequately characterize the blast loading pulses include defining dependent variables such as Effective-g (slope of the velocity profile), and Specific Power ($G_{peak} \times \Delta v$) with some success when compared against a few of the injury criteria.

Objectives

1. To determine If a single blast loading parameter is sufficient to adequately identify the occupant injury for the *duration of typical blast events (0-20ms).*
2. Effect of pulse "shape" on the occupant injuries
3. To create look-up tables/response surfaces for the different injury responses
   - for both stroking and non-stroking seat systems.

Preferred response relationship

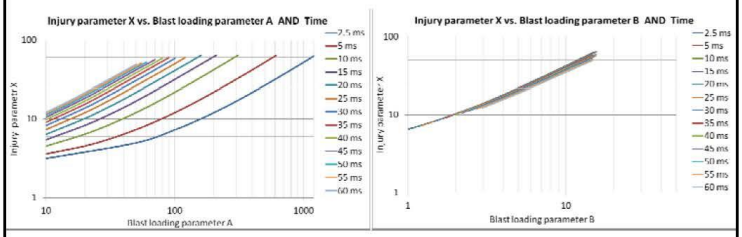

For the two notional plots above showing the same injury response shown against two different blast loading parameters (A and B including duration of the pulse T), the plot on the right (and hence that blast loading parameter) is preferred for the following reasons;

1. Less sensitive to change in pulse duration
2. Easier to establish a simple 2d relationship

Vertical drop tower test and simulation

Vertical drop tower test fixture

MADYMO Dynamic simulation model including Q-version of Hybrid III ATD

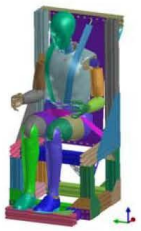

LSDYNA model with FTSS v7.1.6 finite element dummy

C368

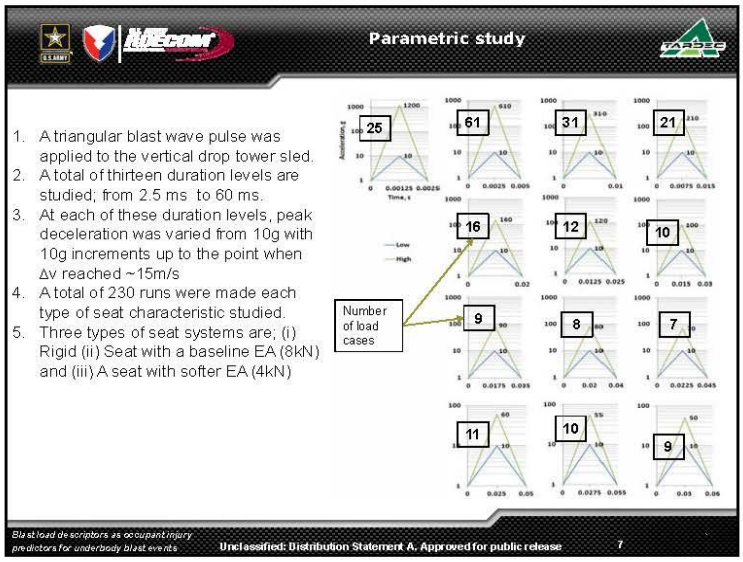
Parametric study
1. A triangular blast wave pulse was applied to the vertical drop tower sled.
2. A total of thirteen duration levels are studied; from 2.5 ms to 60 ms.
3. At each of these duration levels, peak deceleration was varied from 10g with 10g increments up to the point when Δv reached ~15m/s
4. A total of 230 runs were made each type of seat characteristic studied.
5. Three types of seat systems are; (i) Rigid (ii) Seat with a baseline EA (8kN) and (iii) A seat with softer EA (4kN)
Number of load cases
25
61
31
21
16
12
10
9
8
7
11
10
9
Low
High
Blast load descriptors as occupant injury predictors for underbody blast events
Unclassified: Distribution Statement A. Approved for public release
7

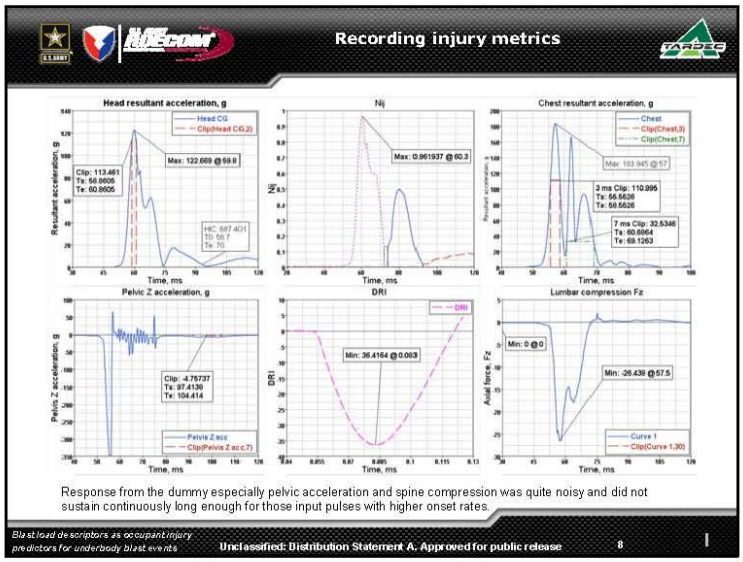
Recording injury metrics
Head resultant acceleration, g
Nij
Chest resultant acceleration, g
Pelvic Z acceleration, g
DRI
Lumbar compression Fz
Time, ms
Response from the dummy especially pelvic acceleration and spine compression was quite noisy and did not sustain continuously long enough for those input pulses with higher onset rates.
Blast load descriptors as occupant injury predictors for underbody blast events
Unclassified: Distribution Statement A. Approved for public release
8

Blast loading parameters

- For each injury criterion the data is plotted against derived input quantities, viz.,

1. effective-g[1,3], defined as the slope of the integral of the velocity trace;

$$G_{eff} = \frac{1}{T}\int_0^T adt = \frac{V_f - V_0}{T}$$

2. Specific power[2], defined as;

$$S = G_{peak} \times \Delta V$$

3. **ΔV, defined as;**

$$\Delta V = \int_0^T adt = V_f - V_0$$

Definition of Effective-g[1,3]

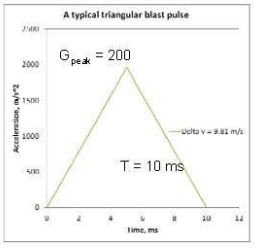

ΔV = 9.81 m/s

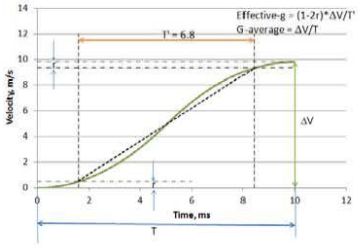

When, r = 5%;

Effective-g = 0.9* ΔV/T' = 132
G-average = ΔV/T = 100

$$G_{eff} = G_{Peak}\left(\frac{1+\sqrt{2r}}{2}\right) \qquad (0 \le r \le 0.5)$$

For triangular pulses used in this parametric study, the ratio of G_{eff} to G_{peak} is 0.6581 when r=0.05

C370

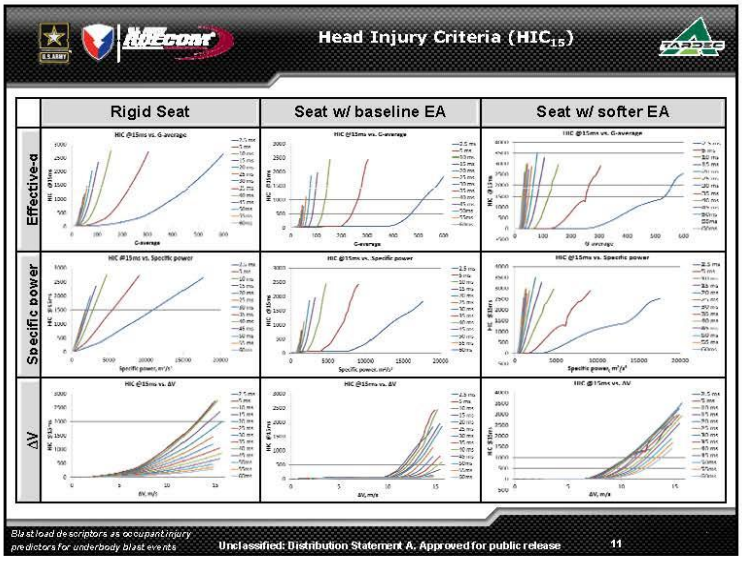
Head Injury Criteria (HIC15)
Rigid Seat
Seat w/ baseline EA
Seat w/ softer EA
Effective-q
Specific power
ΔV
Blast load descriptors as occupant injury predictors for underbody blast events
Unclassified: Distribution Statement A. Approved for public release
11

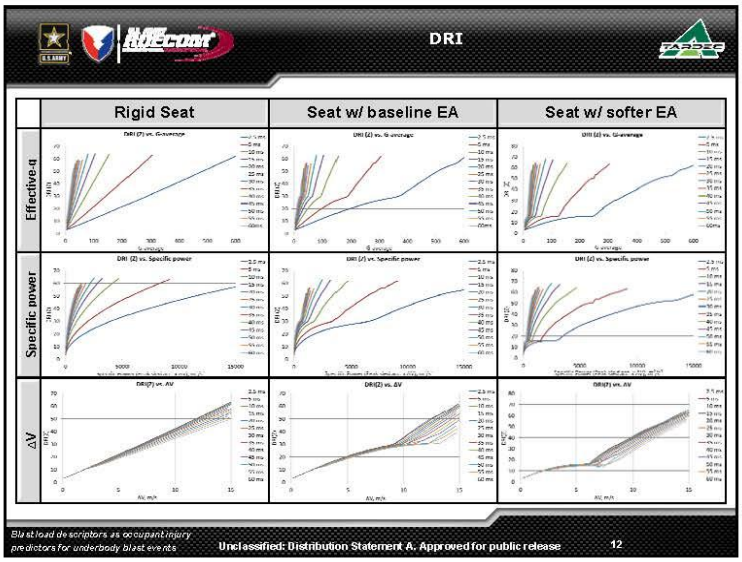
DRI
Rigid Seat
Seat w/ baseline EA
Seat w/ softer EA
Effective-q
Specific power
ΔV
Blast load descriptors as occupant injury predictors for underbody blast events
Unclassified: Distribution Statement A. Approved for public release
12

6

Observations and analysis

- None of the primary input pulse parameters considered in this study, by itself, is an indicator of occupant injury.
- One reason could be that our range of time duration of input pulses which ranged from 2.5 ms to 60 ms is too broad.
- Among the three loading parameters under consideration, Δv by itself, has the potential to be a single good indicator in the typical blast loading range of 0-20ms.
- For a wider range of *T*, any of these primary parameters in combination with the pulse duration can be used to estimate occupant injury.

Analysis of pulse duration < 20ms

- Trend lines were drawn by grouping data points based on time duration of pulses, e.g., 0-10ms, 11-20ms and 21-60ms
- Correlation coefficients (r_c) are computed and tabulated for every injury criterion against the three variables (G-average, Sp. Power and ΔV)

$$r_c = \frac{\sum(x-\bar{x})(y-\bar{y})}{\sqrt{\sum(x-\bar{x})^2 \sum(y-\bar{y})^2}}$$

where, x and y are injury criterion and input variable respectively

C372

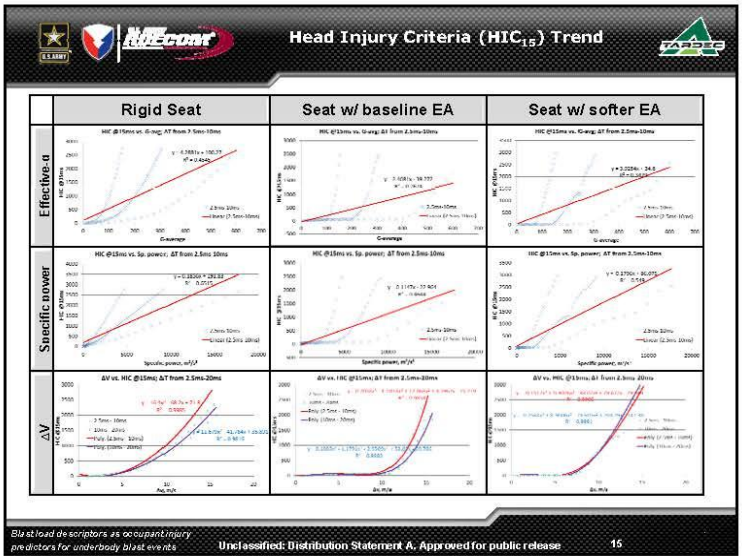
Head Injury Criteria (HIC15) Trend
Rigid Seat
Seat w/ baseline EA
Seat w/ softer EA
Effective-a
Specific power
ΔV
Blast load descriptors as occupant injury predictors for underbody blast events
Unclassified: Distribution Statement A. Approved for public release
15

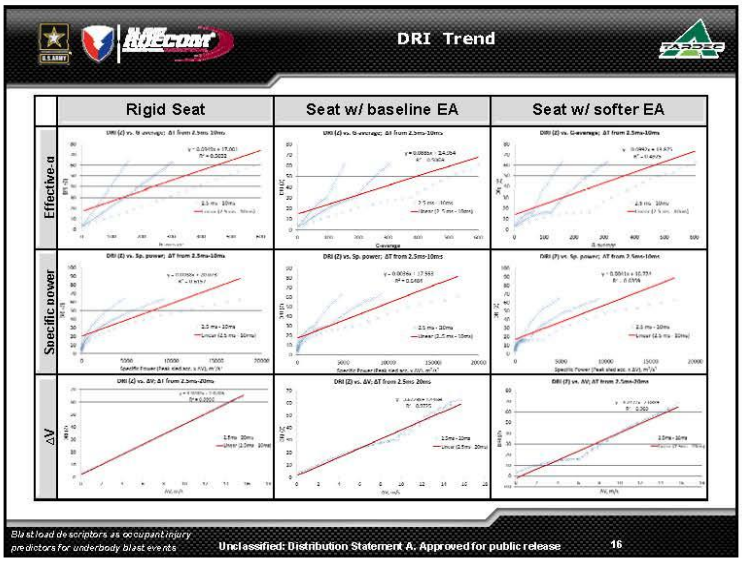
DRI Trend
Rigid Seat
Seat w/ baseline EA
Seat w/ softer EA
Effective-a
Specific power
ΔV
Blast load descriptors as occupant injury predictors for underbody blast events
Unclassified: Distribution Statement A. Approved for public release
16

Correlation coeff. (T = 0-10ms)

		Correlation Coefficients T from 0-10ms								
		G-average			Specific power			ΔV		
		Rigid	EA1	EA2	Rigid	EA1	EA2	Rigid	EA1	EA2
1	HIC @15ms	0.67	0.52	0.59	0.81	0.74	0.74	0.94	0.74	0.89
2	Head resultant acceleration @2ms	0.73	0.63	0.65	0.79	0.77	0.77	1.00	0.85	0.96
3	Head resultant acclelaration @0ms	0.73	0.62	0.66	0.78	0.78	0.78	1.00	0.85	0.96
4	Neck injury criteria, N_{ij}	0.71	0.61	0.65	0.79	0.77	0.77	1.00	0.84	0.95
5	Chest resultant acceleration @3ms	0.74	0.63	0.62	0.78	0.74	0.74	0.99	0.87	0.94
6	Chest resultant acceleration @7ms	0.65	0.57	0.73	0.72	0.80	0.80	0.96	0.83	0.95
7	Lumbar spine compression @30ms	0.59	-0.42	0.19	0.53	0.40	0.40	0.77	-0.65	0.30
8	Lumbar spine compression @0ms	-0.75	-0.66	-0.68	-0.80	-0.81	-0.81	-1.00	-0.88	-0.96
9	Pelvis vertical acceleration @7ms	0.46	0.23	0.13	0.63	0.08	0.08	0.74	0.58	0.22
10	DRI (Z)	0.71	0.71	0.70	0.78	0.80	0.80	1.00	0.99	0.99

	0.5 < r < 0.75
	0.75 < r < 0.9
	r > 0.9

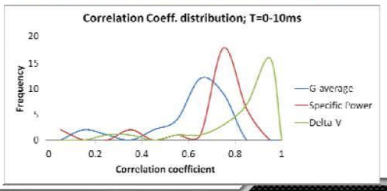

Analysis and Observations

Probability of achieving r > 0.8			
	0-10 ms	10 - 20 ms	20 - 60ms
G-Avg	0.00	0.80	0.60
Sp. Pwr	0.20	0.83	0.77
Delta V	0.77	0.83	0.63

For rigid seat only

Probability of achieving r > 0.8			
	0-10 ms	10 - 20 ms	20 - 60ms
G-Avg	0.00	0.90	0.90
Sp. Pwr	0.20	0.90	0.90
Delta V	0.80	0.90	0.80

- Among the three loading parameters under consideration, Δv by itself, is a single good indicator in the typical blast loading range of 0-20ms.
- A metamodel is constructed using the results from the parametric study to generate 3d response surfaces for the ten upper body injuries.
- An injury lookup table is constructed based on this parametric study using linear/quadratic regression equations.

C374

Physical Test data - summary

#	Test	Date	Peak acc., g	ΔV, m/s	0.05% ΔV, m/s	0.95% ΔV, m/s	0.05% T, ms	0.95%T, ms	T, ms	G-avg	Eff-g	Lumbar spine		Pelvic Z acc., g		DRI
												Peak	30 ms clip	Peak	7 ms clip	
1	5ms-3mps	2/17/2011	93.87	3.09	0.154	2.9353	0.632	4.659	4.43	63	70	1504.1	311.5	67.73	15.41	11.85
2	5ms-3mps-repeat	2/18/2011	87.10	2.93	0.146	2.7790	0.729	4.861	4.55	60	65	1244.7	180.9	54.38	19.97	10.45
3	5ms-4mps	2/17/2011	139.48	4.26	0.213	4.0516	0.686	4.446	4.14	87	104	2221.4	312.8	131.91	12.91	16.07
4	5ms-6mps	2/18/2011	189.00	5.52	0.276	5.2453	0.519	4.134	3.98	113	140	2730.5	205.2	189.24	8.14	19.7
5	5ms-6msp-repeat	2/18/2011	201.69	5.88	0.294	5.5883	0.548	4.162	3.98	120	149	2965.1	234.1	204.14	5.48	20.7
6	5ms-7mps	2/18/2011	237.72	6.87	0.343	6.5228	0.545	4.132	3.95	140	176	3688.4	214.9	260.74	5.81	24.29
7	20ms-3mps	2/17/2011	27.79	2.35	0.117	2.2310	0.663	10.592	10.92	48	22	1345.9	325.8	39.72	23.77	11.45
8	20ms-4mps	2/17/2011	47.80	3.81	0.191	3.6198	1.110	10.878	10.74	78	36	1935.7	374.8	74.27	25.23	16.27
9	20ms-5mps	2/17/2011	68.07	4.82	0.241	4.5764	1.275	10.262	9.89	98	49	2580.3	375.2	113.24	22.6	19.92
10	20ms-5mps-repeat	2/17/2011	65.60	4.75	0.238	4.5172	1.317	10.503	10.10	97	47	2607.1	402.1	110.3	20.44	19.68
11	5ms-10in	NA	74.25	2.78	0.139	2.6403	0.411	5.953	6.10	57	46	1466.7	200.1	91.61	4.41	10.65
12	5ms-19in	NA	112.04	3.73	0.186	3.5397	0.391	5.721	5.86	76	64	2096.3	200.2	138.97	4.74	14.52
13	5ms-30in	NA	156.53	4.90	0.245	4.6537	0.384	5.726	5.88	100	84	3015.4	171.9	187.05	5.17	18.63
14	20ms-10in	NA	**30.71**	3.13	0.157	2.9753	10.116	20.154	11.04	64	29	1310.7	188.1	**30.71**	19.84	9.62
15	20ms-19in	NA	**92.47**	4.21	0.210	3.9969	9.663	17.917	9.08	86	47	1893.5	211.5	**92.47**	15.31	15.08
16	20ms-30in	NA	**92.47**	4.21	0.210	3.9969	9.663	17.917	9.08	86	47	2844.4	187.4	**92.47**	15.31	14.96

	Peak Acc., g	ΔV, m/s	T, ms
Minimum	28	2.3	3.95
Maximum	238	6.9	11.04
Mean	111	4.2	6.83

Blast load descriptors as occupant injury predictors for underbody blast events

Unclassified: Distribution Statement A. Approved for public release 19

Physical Test data

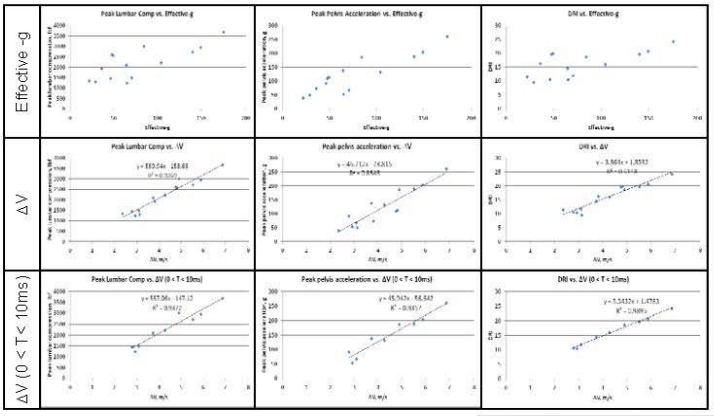

Blast load descriptors as occupant injury predictors for underbody blast events

Unclassified: Distribution Statement A. Approved for public release 20

C375

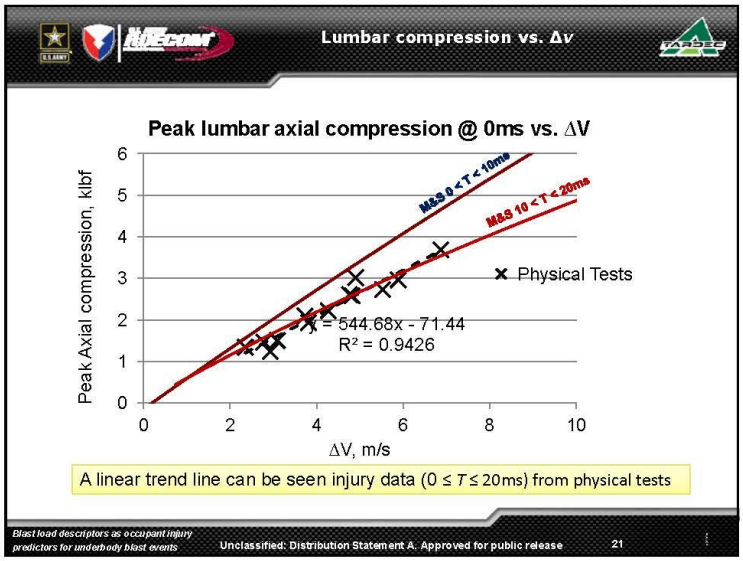
Lumbar compression vs. Δv
Peak lumbar axial compression @ 0ms vs. ΔV
Peak Axial compression, klbf
ΔV, m/s
M&S 0 < T < 10ms
M&S 10 < T < 20ms
Physical Tests
y = 544.68x - 71.44
R² = 0.9426
A linear trend line can be seen injury data (0 ≤ T ≤ 20ms) from physical tests
Blast load descriptors as occupant injury predictors for underbody blast events
Unclassified: Distribution Statement A. Approved for public release
21

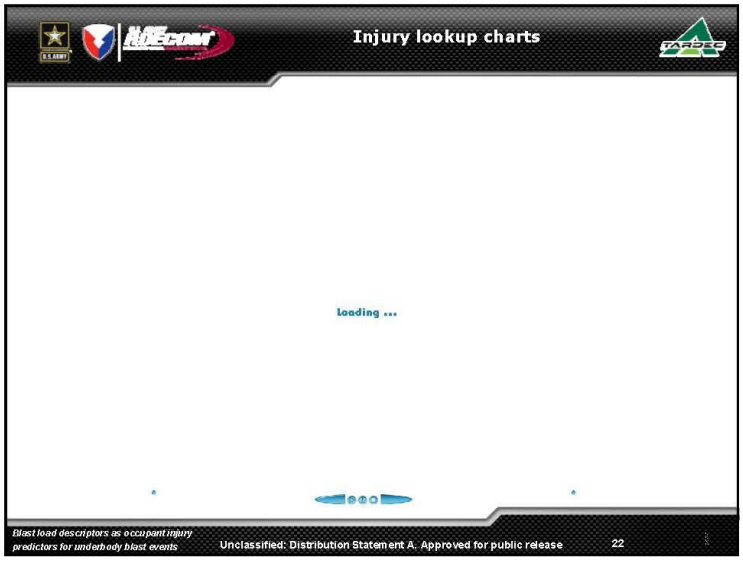
Injury lookup charts
loading ...
Blast load descriptors as occupant injury predictors for underbody blast events
Unclassified: Distribution Statement A. Approved for public release
22


Injury lookup tool
loading ...
Blast load descriptors as occupant injury predictors for underbody blast events
Unclassified: Distribution Statement A. Approved for public release
23

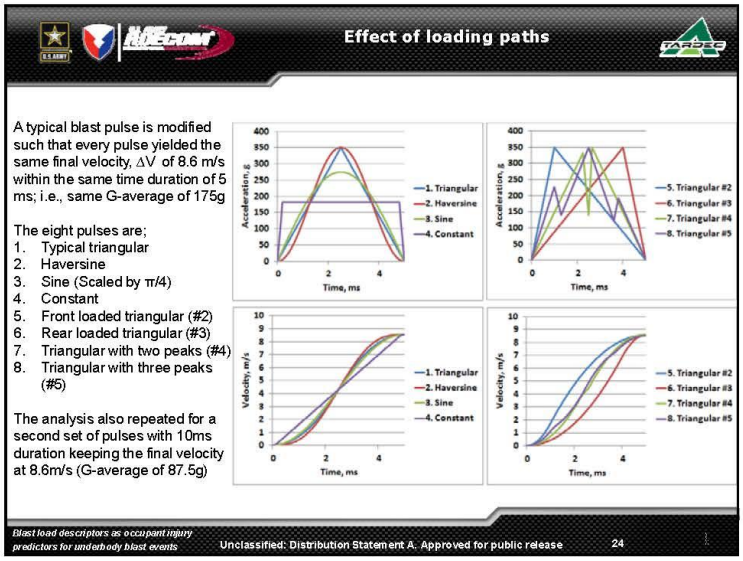
Effect of loading paths
A typical blast pulse is modified such that every pulse yielded the same final velocity, ΔV of 8.6 m/s within the same time duration of 5 ms; i.e., same G-average of 175g
The eight pulses are;
1. Typical triangular
2. Haversine
3. Sine (Scaled by π/4)
4. Constant
5. Front loaded triangular (#2)
6. Rear loaded triangular (#3)
7. Triangular with two peaks (#4)
8. Triangular with three peaks (#5)
The analysis also repeated for a second set of pulses with 10ms duration keeping the final velocity at 8.6m/s (G-average of 87.5g)
Acceleration, g
Velocity, m/s
Time, ms
1. Triangular
2. Haversine
3. Sine
4. Constant
5. Triangular #2
6. Triangular #3
7. Triangular #4
8. Triangular #5
Blast load descriptors as occupant injury predictors for underbody blast events
Unclassified: Distribution Statement A. Approved for public release
24

Effect of loading paths (T = 5ms)

T = 5ms

#	Pulse type	Peak, Dec., g	Durat-ion, ms	Rate of onset, g/ms	ΔV, m/s	Sp. Pwr	Eff. G	G-avg	HEAD Resultant acceleration, g @ 2ms	HEAD Resultant acceleration, g @ 0ms	HEAD HIC @ 15 ms	NECK N_{ij} CFC 1000	CHEST Resultant acceleration, g @ 3ms	CHEST Resultant acceleration, g @ 7ms	PELVIS Z-Accele-ration, g @ 7ms	PELVIS DRI (z), g	LUMBAR SPINE Axial compression, kN @30ms	LUMBAR SPINE Axial compression, kN @0ms
1	Triangular	350	5	140	8.6	3004	218	175	113.4	122.7	687	0.96	111.2	33.9	-4.9	36.4	0.0	-26.5
2	Haversine	350	5	140	8.6	3003	235	175	113.6	122.9	689	0.96	111.7	34.9	-4.8	36.4	0.0	-26.5
3	Sine	275	5	110	8.6	2360	210	175	113.2	122.5	679	0.96	110.7	32.6	-4.8	36.2	0.0	-26.4
4	Constant	182	5	NA	8.6	1562	181	175	112.5	121.5	673	0.96	109.1	30.5	-4.9	36.3	0.0	-26.3
5	Triangular #2	350	5	140	8.6	3004	212	175	113.8	123.1	689	0.97	111.3	33.8	-4.9	36.4	0.0	-26.5
6	Triangular #3	350	5	140	8.6	3004	212	175	112.9	122.1	683	0.96	110.6	32.7	-4.9	36.4	0.0	-26.4
7	Triangular #4	350	5	140	8.6	3004	217	175	114.0	123.4	701	0.97	111.7	33.8	-5.0	36.6	0.0	-26.6
8	Triangular #5	350	5	140	8.6	3004	205	175	112.9	122.1	673	0.96	110.3	33.0	-4.9	36.2	0.0	-26.3

Including "Constant" type pulse

Mean, μ =	8.6	2743	211.2	175.0	113.3	122.5	684.3	1.0	110.8	33.2	-4.9	36.4	0.0	-26.4
Standard deviation, σ =	0.0	528	15.1	0.0	0.5	0.6	9.4	0.0	0.9	1.3	0.1	0.1	0.0	0.1
Coefficient of variation, C_v (%)	0%	19%	7%	0%	0%	1%	1%	0%	1%	4%	1%	0%	0%	0%

Excluding "Constant" type pulse

Mean, μ =	8.6	2912.0	215.4	175.0	113.4	122.7	685.9	1.0	111.1	33.5	-4.9	36.4	0.0	-26.5
Standard deviation, σ =	0.0	243.6	9.8	0.0	0.4	0.5	8.9	0.0	0.5	0.8	0.1	0.1	0.0	0.1
Coefficient of variation, C_v (%)	0%	8%	5%	0%	0%	0%	1%	1%	0%	2%	1%	0%	0%	0%

No path dependency of loading is observed

Conclusions

- There is no single blast loading parameter from an input pulse which can be used to fully determine the occupant injury risk from a blast loading over a wide range of pulse durations (0-60ms).
- Correlation coefficients distribution for Δv especially in the 0-10ms range is narrower and closer to 1 than those for Specific Power and Effective-g.
- Among the different blast pulse parameters considered in this study, Δv is the best single indicator for estimating injury criteria, for typical blast pulse duration ranges.
- Two different approaches to estimate occupant injuries as a function of Blast duration, Δv, and Seat characteristics have been employed using the results from this parametric study, namely:
  - **Injury lookup tables using linear/quadratic regression equations**
  - **Meta-model based Response surface methodology**
- Other:
  - **For any given Δv and T (0-10ms), the shape of the pulse and its peak value has no significant effect on the injury criteria (excluding the constant type)**
  - **Trends in the test data strongly support M&S findings of this study.**

Disclaimer

Reference herein to any specific commercial company, product, process, or service by trade name, trademark, manufacturer, or otherwise does not necessarily constitute or imply its endorsement, recommendation, or favoring by the United States Government or the Dept. of the Army (DoA). The opinions of the authors expressed herein do not necessarily state or reflect those of the United States Government or the DoD, and shall not be used for advertising or product endorsement purposes.

Acknowledgements

The authors would like to thank the Underbody Blast Modeling/Methodology (UBM) program managed by ARL/SLAD and ATEC, for the provided funding which made this project possible. This material is based on R&D work supported by the U.S. Army TACOM Life Cycle Command under Contract No. W56HZV-08-C-0236, through a subcontract with Mississippi State University (MSU), and was performed for the Simulation Based Reliability and Safety (SimBRS) research program. Any opinions, finding and conclusions or recommendations in this paper are those of the author(s) and do not necessarily reflect the views of the U.S. Army TACOM Life Cycle Command.

The authors are also most grateful to Mr. Sudhakar Arepally for his reviews of this work, and for patiently providing insight to his earlier research on Effective-G [13], which served as the precursor for this project.

BACKUP SLIDES

Effective-g comparisons

For triangular shaped pulses studied;

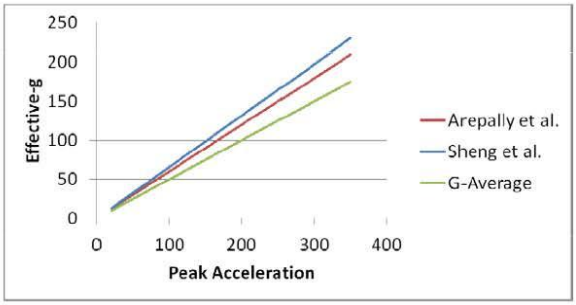

G_{eff} (Arepally et. al.) $= 0.6 * G_{peak}$
G_{eff} (Sheng et. al.) $= 0.6581 * G_{peak}$ (when r=0.05)
$G_{avg} = 0.5 * G_{peak}$

C380

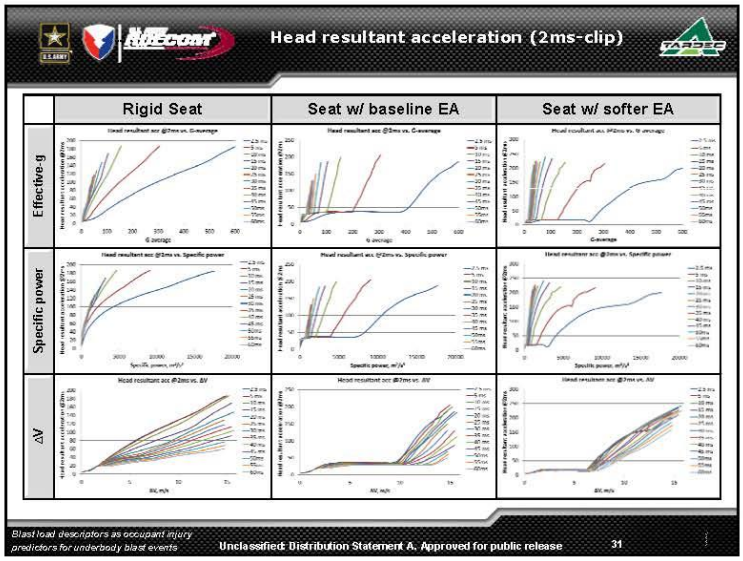
Head resultant acceleration (2ms-clip)
Rigid Seat
Seat w/ baseline EA
Seat w/ softer EA
Effective-g
Specific power
ΔV
Blast load descriptors as occupant injury predictors for underbody blast events
Unclassified: Distribution Statement A. Approved for public release
31

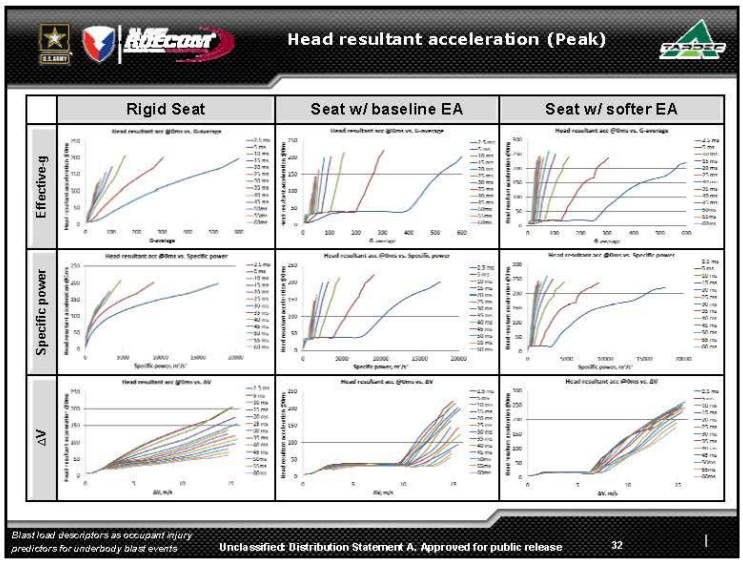
Head resultant acceleration (Peak)
Rigid Seat
Seat w/ baseline EA
Seat w/ softer EA
Effective-g
Specific power
ΔV
Blast load descriptors as occupant injury predictors for underbody blast events
Unclassified: Distribution Statement A. Approved for public release
32

C381

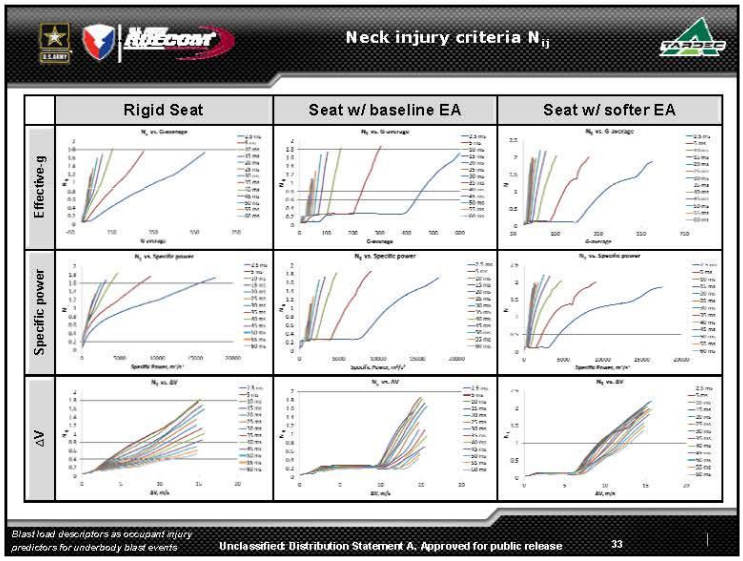
Neck injury criteria N_{ij}
Rigid Seat
Seat w/ baseline EA
Seat w/ softer EA
Effective-g
Specific power
ΔV
Blast load descriptors as occupant injury predictors for underbody blast events
Unclassified: Distribution Statement A. Approved for public release
33

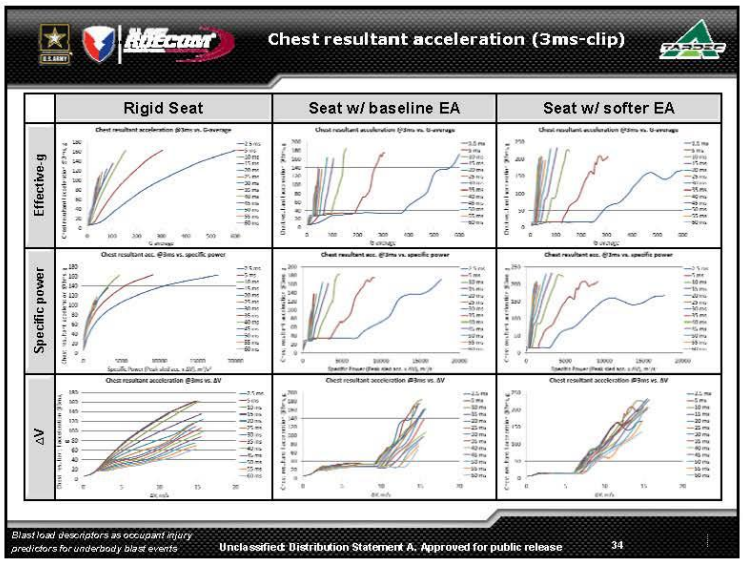
Chest resultant acceleration (3ms-clip)
Rigid Seat
Seat w/ baseline EA
Seat w/ softer EA
Effective-g
Specific power
ΔV
Blast load descriptors as occupant injury predictors for underbody blast events
Unclassified: Distribution Statement A. Approved for public release
34

C382

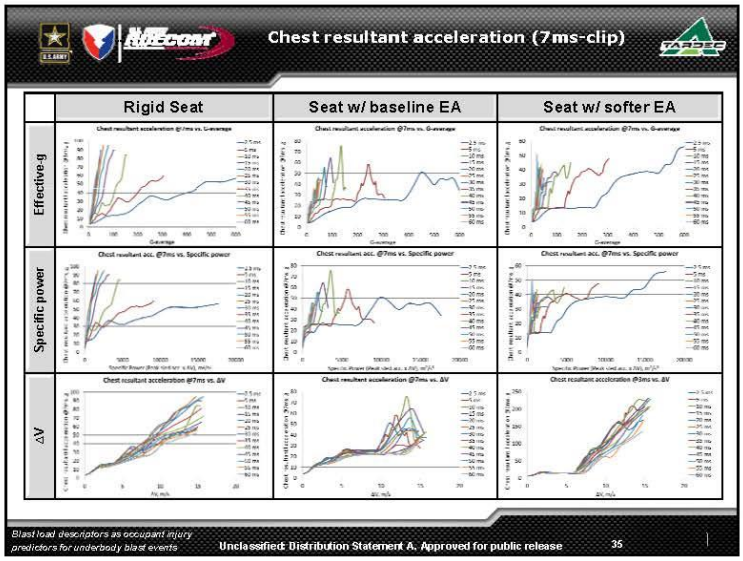
Chest resultant acceleration (7ms-clip)
Rigid Seat
Seat w/ baseline EA
Seat w/ softer EA
Effective-g
Specific power
ΔV
Blast load descriptors as occupant injury predictors for underbody blast events
Unclassified: Distribution Statement A. Approved for public release
35

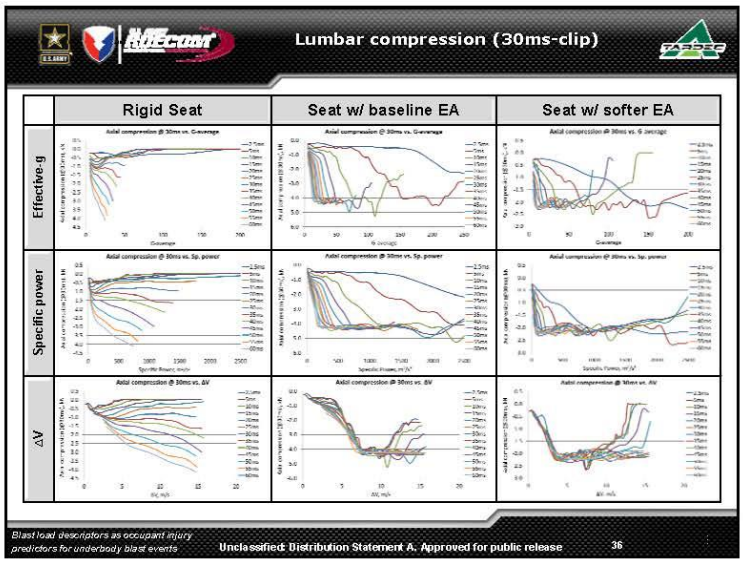
Lumbar compression (30ms-clip)
Rigid Seat
Seat w/ baseline EA
Seat w/ softer EA
Effective-g
Specific power
ΔV
Blast load descriptors as occupant injury predictors for underbody blast events
Unclassified: Distribution Statement A. Approved for public release
36

C383

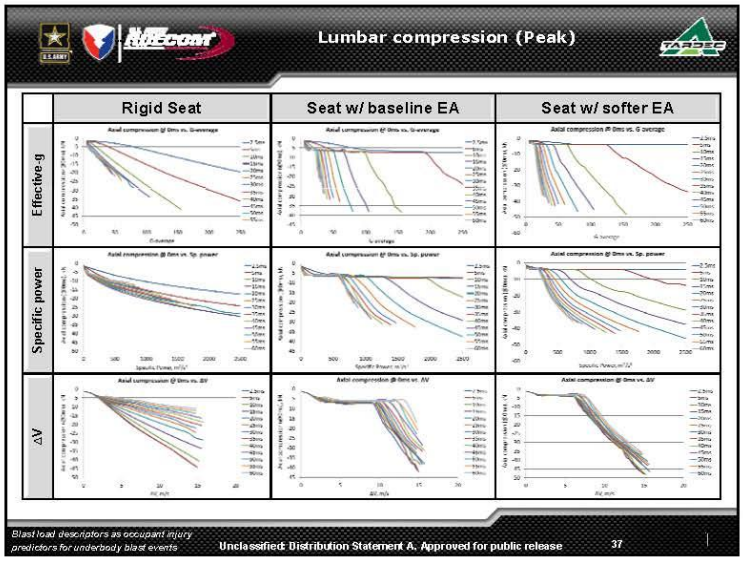
Lumbar compression (Peak)
Rigid Seat
Seat w/ baseline EA
Seat w/ softer EA
Effective-g
Specific power
ΔV
Blast load descriptors as occupant injury predictors for underbody blast events
Unclassified: Distribution Statement A. Approved for public release
37

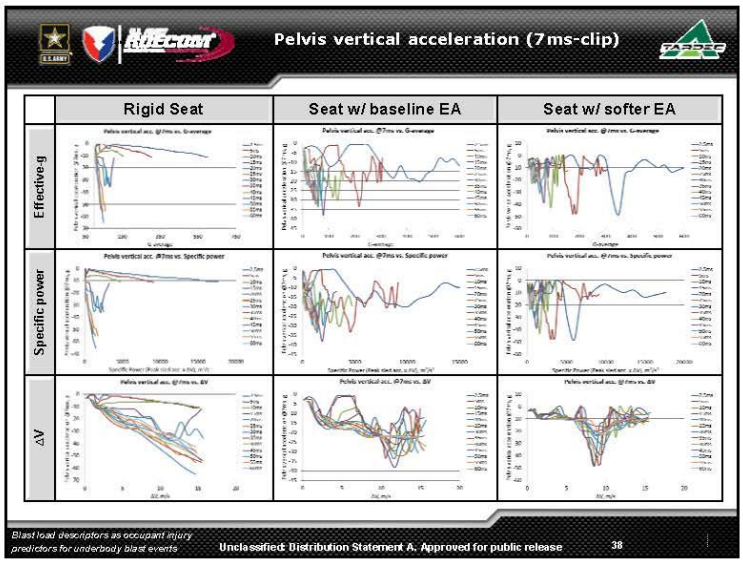
Pelvis vertical acceleration (7ms-clip)
Rigid Seat
Seat w/ baseline EA
Seat w/ softer EA
Effective-g
Specific power
ΔV
Blast load descriptors as occupant injury predictors for underbody blast events
Unclassified: Distribution Statement A. Approved for public release
38

C384

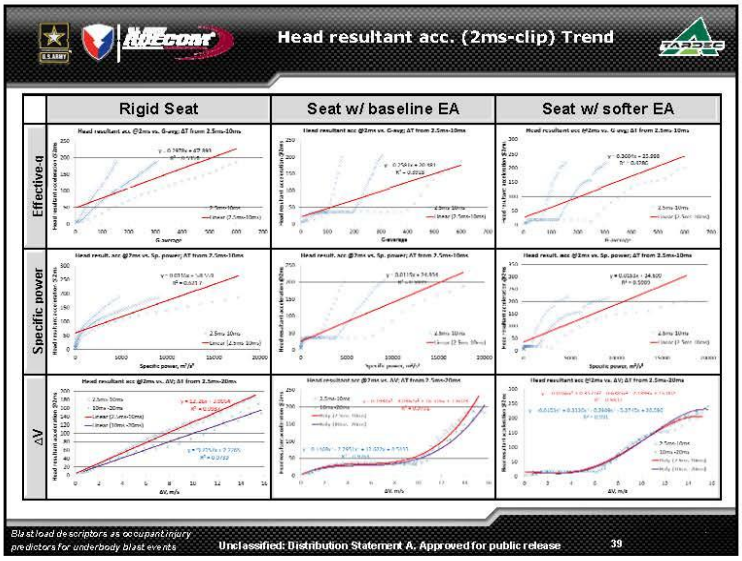
Head resultant acc. (2ms-clip) Trend
Rigid Seat
Seat w/ baseline EA
Seat w/ softer EA
Effective a
Specific power
ΔV
Blast load descriptors as occupant injury predictors for underbody blast events
Unclassified: Distribution Statement A. Approved for public release
39

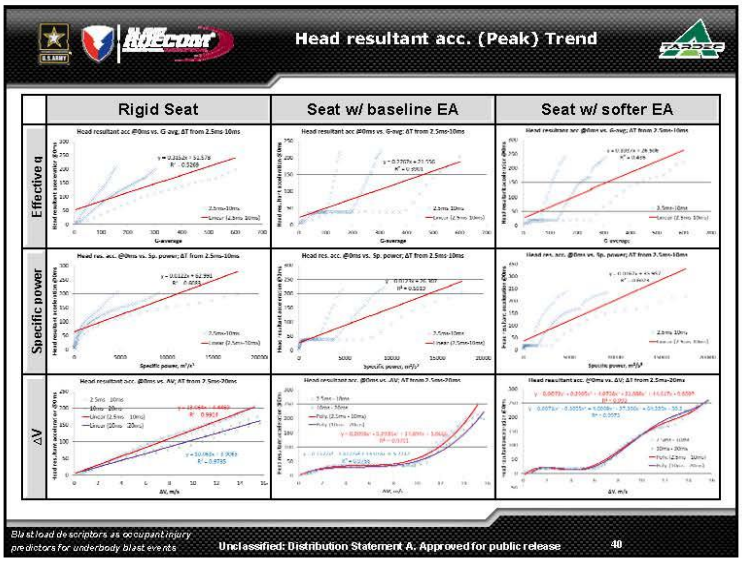
Head resultant acc. (Peak) Trend
Rigid Seat
Seat w/ baseline EA
Seat w/ softer EA
Effective a
Specific power
ΔV
Blast load descriptors as occupant injury predictors for underbody blast events
Unclassified: Distribution Statement A. Approved for public release
40

C385

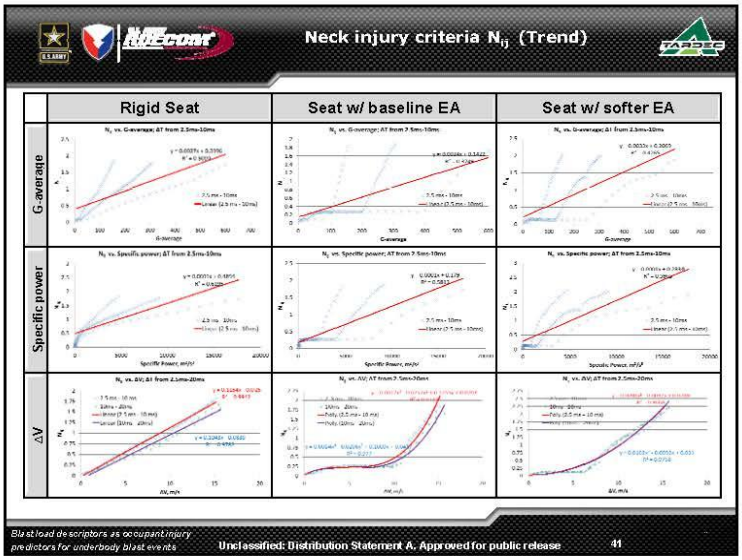
Neck injury criteria N_{ij} (Trend)
Rigid Seat
Seat w/ baseline EA
Seat w/ softer EA
G-average
Specific power
ΔV
Blast load descriptors as occupant injury predictors for underbody blast events
Unclassified: Distribution Statement A. Approved for public release
41

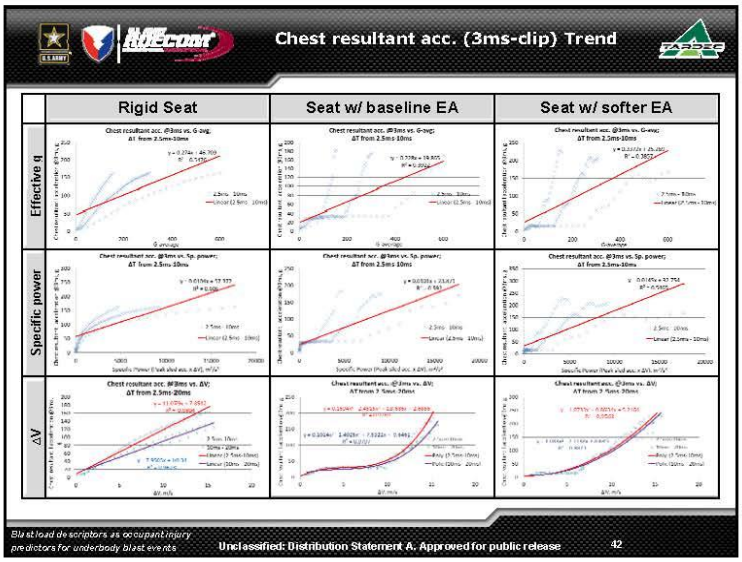
Chest resultant acc. (3ms-clip) Trend
Rigid Seat
Seat w/ baseline EA
Seat w/ softer EA
Effective q
Specific power
ΔV
Blast load descriptors as occupant injury predictors for underbody blast events
Unclassified: Distribution Statement A. Approved for public release
42

C386

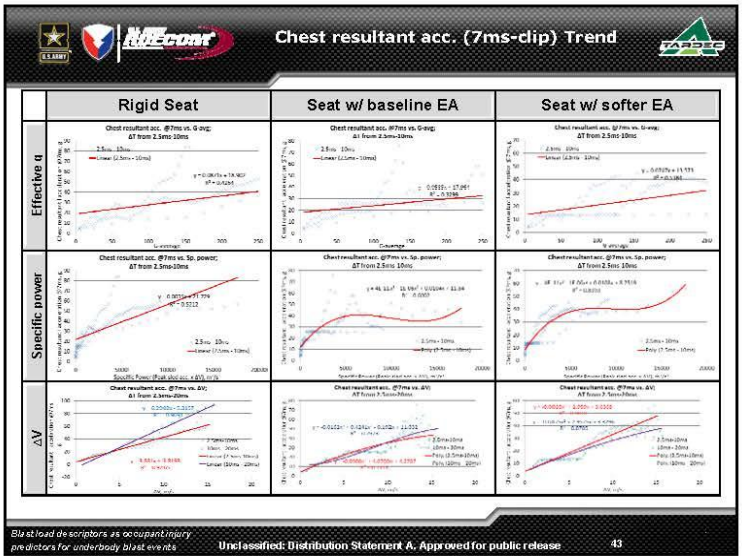
Chest resultant acc. (7ms-clip) Trend
Rigid Seat
Seat w/ baseline EA
Seat w/ softer EA
Effective q
Specific power
ΔV
Blast load descriptors as occupant injury predictors for underbody blast events
Unclassified: Distribution Statement A. Approved for public release
43

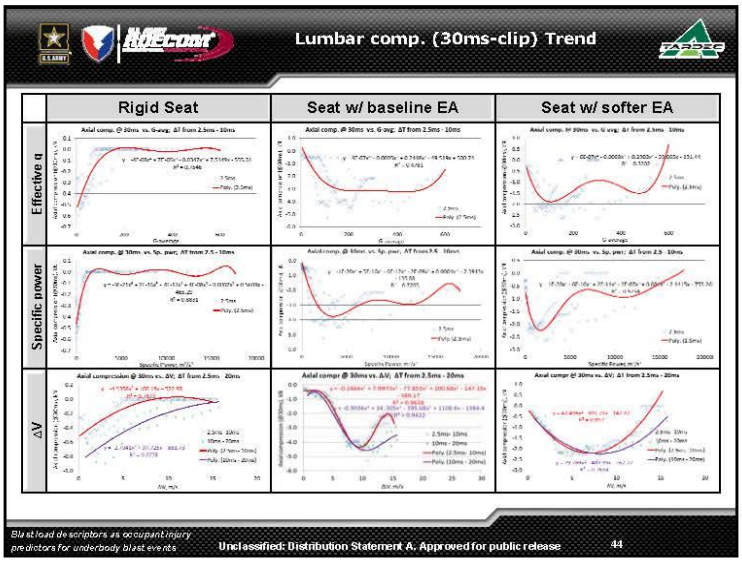
Lumbar comp. (30ms-clip) Trend
Rigid Seat
Seat w/ baseline EA
Seat w/ softer EA
Effective q
Specific power
ΔV
Blast load descriptors as occupant injury predictors for underbody blast events
Unclassified: Distribution Statement A. Approved for public release
44

C387

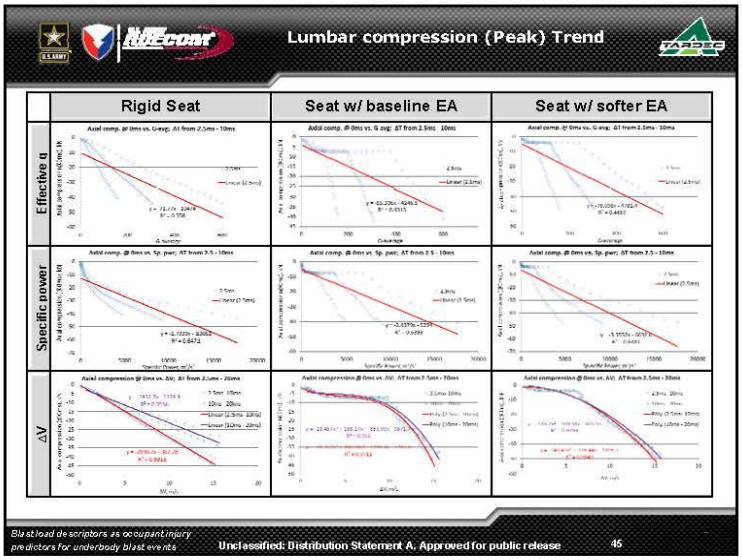
Lumbar compression (Peak) Trend
Rigid Seat
Seat w/ baseline EA
Seat w/ softer EA
Effective q
Specific power
ΔV
Blast load descriptors as occupant injury predictors for underbody blast events
Unclassified: Distribution Statement A. Approved for public release
45

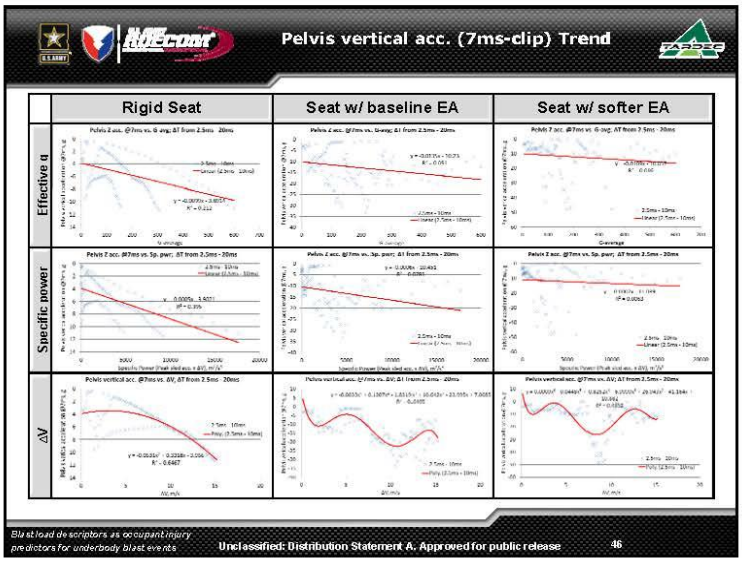
Pelvis vertical acc. (7ms-clip) Trend
Rigid Seat
Seat w/ baseline EA
Seat w/ softer EA
Effective q
Specific power
ΔV
Blast load descriptors as occupant injury predictors for underbody blast events
Unclassified: Distribution Statement A. Approved for public release
46

Correlation coeff. (T = 10-20ms)

		Correlation Coefficients								
		T from 10-20ms								
		G-average			Specific power			ΔV		
		Rigid	EA1	EA2	Rigid	EA1	EA2	Rigid	EA1	EA2
1	HIC @15ms	0.94	0.73	0.86	0.99	0.85	0.95	0.95	0.75	0.90
2	Head resultant acceleration @2ms	0.98	0.83	0.92	0.98	0.92	0.96	0.99	0.85	0.96
3	Head resultant acclelaration @0ms	0.99	0.82	0.92	0.97	0.92	0.96	0.99	0.85	0.96
4	Neck injury criteria, N_{ij}	0.97	0.81	0.92	0.98	0.92	0.97	0.99	0.84	0.96
5	Chest resultant acceleration @3ms	0.99	0.84	0.92	0.94	0.93	0.98	0.98	0.87	0.96
6	Chest resultant acceleration @7ms	0.94	0.90	0.95	0.96	0.89	0.91	0.98	0.89	0.93
7	Lumbar spine compression @30ms	0.92	-0.77	0.09	0.84	-0.66	0.29	0.86	-0.82	0.04
8	Lumbar spine compression @0ms	-0.99	-0.84	-0.92	-0.96	-0.94	-0.97	-0.98	-0.88	-0.96
9	Pelvis vertical acceleration @7ms	-0.67	-0.55	-0.04	-0.62	-0.47	0.10	-0.76	-0.56	-0.06
10	DRI (Z)	0.96	0.95	0.94	0.96	0.97	0.97	1.00	0.98	0.98

	0.5 < r < 0.75
	0.75 < r < 0.9
	r > 0.9

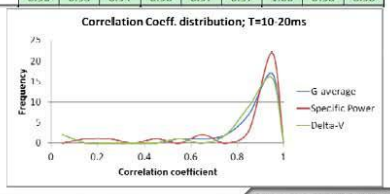

Correlation coeff. (T = 20-60ms)

		Correlation Coefficients								
		T from 20-60ms								
		G-average			Specific power			ΔV		
		Rigid	EA1	EA2	Rigid	EA1	EA2	Rigid	EA1	EA2
1	HIC @15ms	0.96	0.69	0.82	0.98	0.77	0.93	0.77	0.53	0.82
2	Head resultant acceleration @2ms	0.98	0.79	0.88	0.98	0.88	0.96	0.86	0.68	0.92
3	Head resultant acclelaration @0ms	0.98	0.79	0.87	0.98	0.88	0.96	0.85	0.68	0.92
4	Neck injury criteria, N_{ij}	0.98	0.79	0.88	0.99	0.88	0.96	0.84	0.69	0.92
5	Chest resultant acceleration @3ms	0.97	0.80	0.86	0.98	0.90	0.95	0.88	0.74	0.92
6	Chest resultant acceleration @7ms	0.96	0.90	0.69	0.98	0.93	0.76	0.92	0.85	0.89
7	Lumbar spine compression @30ms	0.16	-0.69	-0.28	0.00	-0.67	-0.21	-0.41	0.86	-0.40
8	Lumbar spine compression @0ms	-0.99	-0.79	-0.84	-0.96	-0.89	-0.93	-0.84	-0.74	-0.95
9	Pelvis vertical acceleration @7ms	-0.91	-0.69	-0.08	-0.94	-0.70	0.02	-0.94	-0.79	-0.15
10	DRI (Z)	0.89	0.90	0.86	0.93	0.95	0.94	0.99	0.95	0.96

	0.5 < r < 0.75
	0.75 < r < 0.9
	r > 0.9

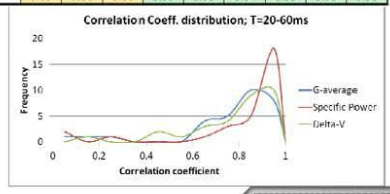

Lumbar compression vs. Effective-g

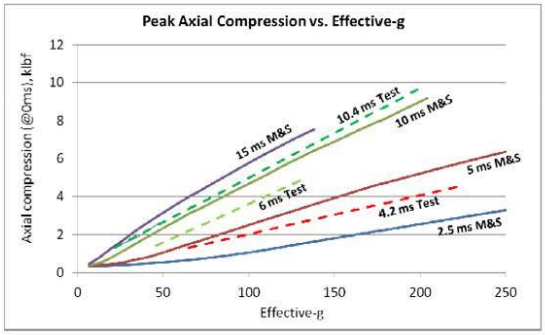

Lumbar compression from physical tests also do not show a good relationship with Effective-g. Dependence on T can be observed. Good correlation with M&S data can also be seen.

Pulses with same Δv

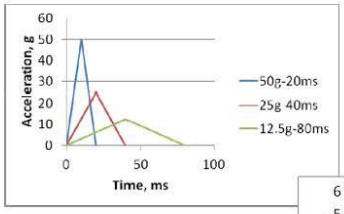

Three same three pulses with a constant Δv of 4.9m/s and a duration of 20, 40 and 80ms taken from Ref 1 (Fig 14).

Effective-g for these pulses are 26.6, 13.3 and 6.65 g.

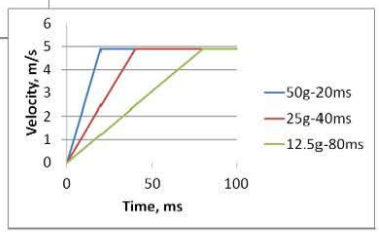

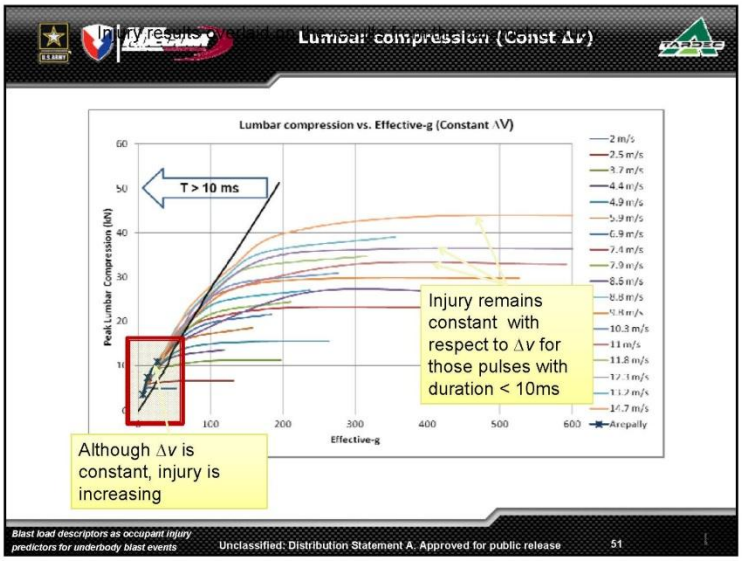
Injury requires overland propagation
Lumbar compression (Const Δv)
Lumbar compression vs. Effective-g (Constant ΔV)
Peak Lumbar Compression (kN)
Effective-g
T > 10 ms
Injury remains constant with respect to Δv for those pulses with duration < 10ms
Although Δv is constant, injury is increasing
Blast load descriptors as occupant injury predictors for underbody blast events
Unclassified: Distribution Statement A. Approved for public release
51

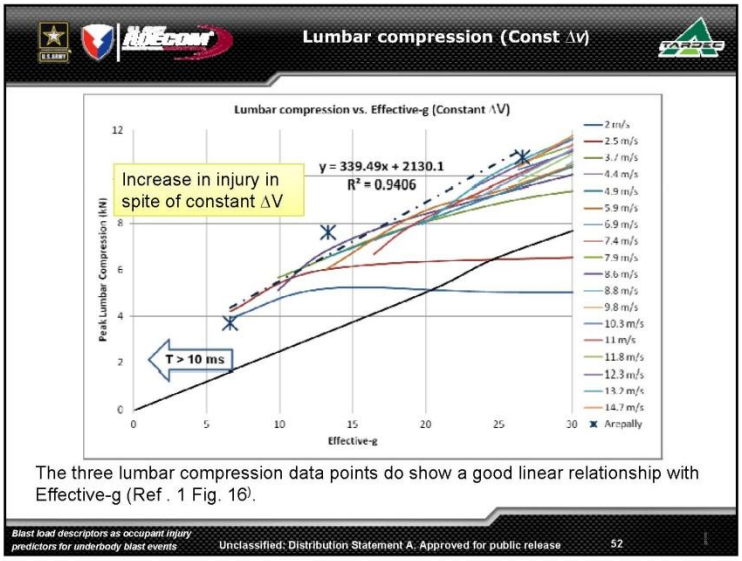
Lumbar compression (Const Δv)
Lumbar compression vs. Effective-g (Constant ΔV)
Peak Lumbar Compression (kN)
Effective-g
y = 339.49x + 2130.1
R² = 0.9406
Increase in injury in spite of constant ΔV
T > 10 ms
The three lumbar compression data points do show a good linear relationship with Effective-g (Ref . 1 Fig. 16).
Blast load descriptors as occupant injury predictors for underbody blast events
Unclassified: Distribution Statement A. Approved for public release
52

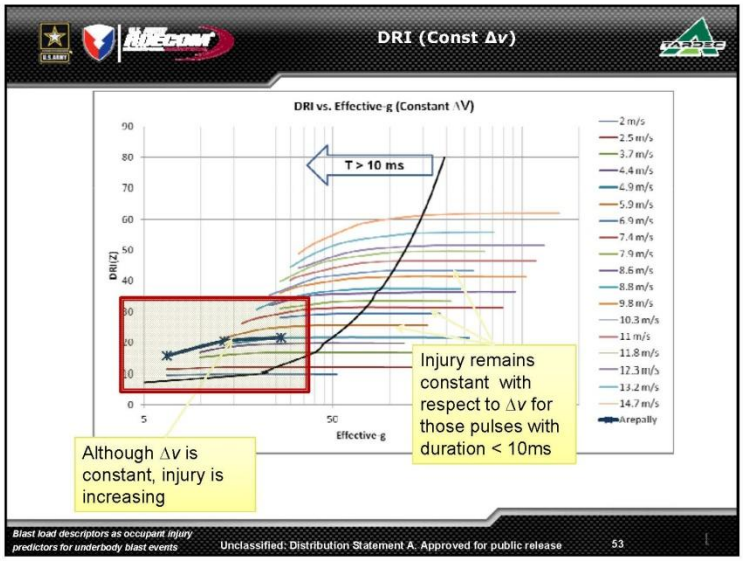
DRI (Const Δv)
DRI vs. Effective-g (Constant ΔV)
T > 10 ms
DRI(Z)
Effective g
2 m/s
2.5 m/s
3.7 m/s
4.4 m/s
4.9 m/s
5.9 m/s
6.9 m/s
7.4 m/s
7.9 m/s
8.6 m/s
8.8 m/s
9.8 m/s
10.3 m/s
11 m/s
11.8 m/s
12.3 m/s
13.2 m/s
14.7 m/s
Arepally
Although Δv is constant, injury is increasing
Injury remains constant with respect to Δv for those pulses with duration < 10ms
Blast load descriptors as occupant injury predictors for underbody blast events
Unclassified: Distribution Statement A. Approved for public release
53

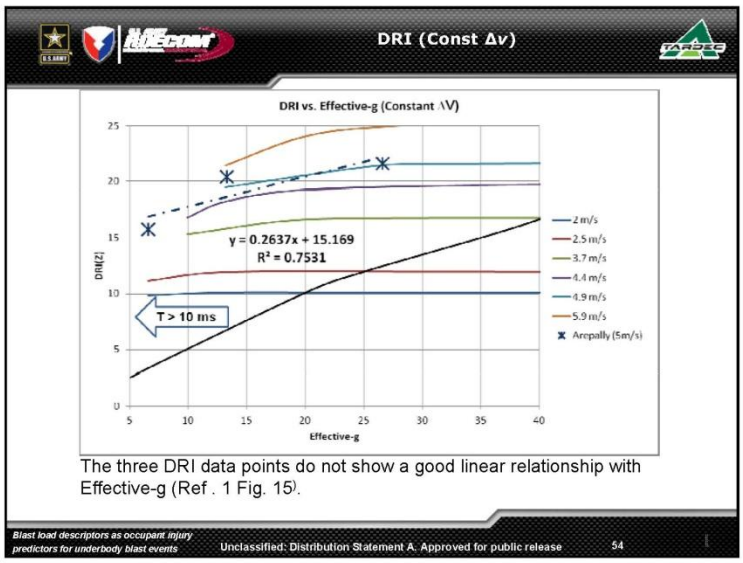
DRI (Const Δv)
DRI vs. Effective-g (Constant ΔV)
y = 0.2637x + 15.169
R² = 0.7531
T > 10 ms
DRI(Z)
Effective-g
2 m/s
2.5 m/s
3.7 m/s
4.4 m/s
4.9 m/s
5.9 m/s
Arepally (5m/s)
The three DRI data points do not show a good linear relationship with Effective-g (Ref . 1 Fig. 15).
Blast load descriptors as occupant injury predictors for underbody blast events
Unclassified: Distribution Statement A. Approved for public release
54

Pulses with same Effective-g

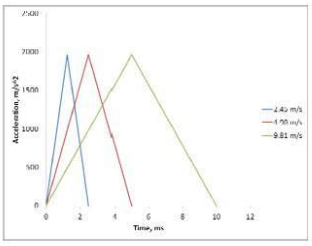

Three pulses are chosen such that peak acceleration for each is 200g and the duration of the pulses are 2.5, 5 and 10ms. Δv for these pulses are 2.45, 4.9 and 9.81 m/s. Effective-g for these pulses are all equal to 132 g.

Pulses with same Effective-g

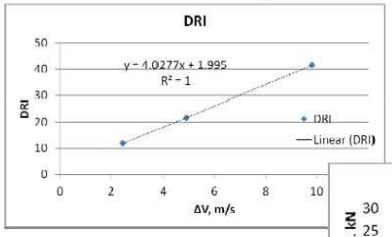

The three example pulses have the same effective-g of 132 but the injuries are not the same.

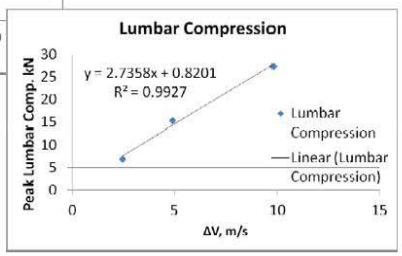

However, both these injuries demonstrate a linear relationship with Δv.

Pulses with same Effective-g

Injury results overlaid on the results from the parametric study

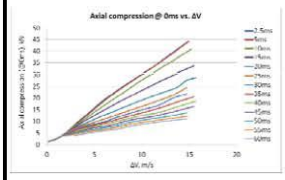

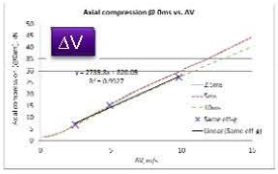

A linear relationship between injury and Δv

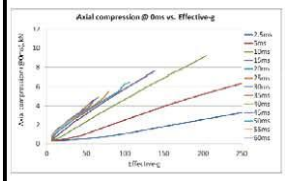

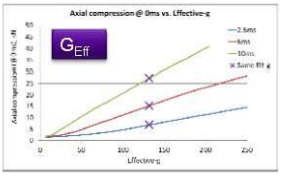

Occupant injury dependence on T is observed as reported in Ref #3.

Effect of loading paths (T = 10ms)

T = 10ms

Pulse iterations									HEAD			NECK	CHEST		PELVIS		LUMBAR SPINE	
									Resultant acceleration, g		HIC	N_{ij}	Resultant acceleration, g		Z-Acceleration, g	DRI (z), g	Axial compression, kN	
#	Pulse type	Peak, Dec., g	Duration, ms	Rate of onset, g/ms	ΔV, m/s	Sp. Pwr	Eff. G	G-avg	@ 2ms	@ 0ms	@ 15 ms	CFC 1000	@ 3ms	@ 7ms	@ 7ms		@30ms	@0ms
1	Triangular	175	10	35	8.6	1502	109	88	103.8	111.4	628	0.88	101.0	27.8	-5.9	36.4	0.0	-23.9
2	Haversine	175	10	35	8.6	1502	118	88	107.1	115.0	649	0.91	103.4	28.0	-5.5	36.4	0.0	-24.9
3	Sine	138	10	28	8.6	1180	105	88	101.7	109.1	621	0.86	99.3	29.9	-6.2	36.3	0.0	-24.1
4	Constant	91	10	NA	8.6	781	91	88	90.8	98.2	582	0.78	93.3	45.1	-20.0	36.4	0.0	-22.1
5	Triangular #2	175	10	35	8.6	1502	106	88	102.6	110.1	622	0.87	100.9	31.7	-4.8	36.4	0.0	-24.3
6	Triangular #3	175	10	35	8.6	1502	106	88	101.8	109.1	626	0.87	98.1	28.5	-8.5	36.5	0.0	-23.9
7	Triangular #4	175	10	35	8.6	1502	108	88	103.6	111.1	638	0.88	100.9	28.6	-6.0	36.7	0.0	-24.2
8	Triangular #5	175	10	35	8.6	1502	103	88	100.9	108.4	610	0.86	98.9	30.0	-6.0	36.2	0.0	-23.9
Including "Constant" type pulse																		
	Mean, μ =	8.6	1372	105.6	87.5	101.5	109.1	621.9	0.9	99.5	31.2	-7.9	36.4	0.0	-23.9			
	Standard deviation, σ =	0.0	264	7.6	0.0	4.7	4.8	19.8	0.0	3.0	5.8	5.0	0.1	0.0	0.8			
	Coefficient of variation, C_v (%)	0%	19%	7%	0%	5%	4%	3%	4%	3%	18%	64%	0%	0%	3%			
Excluding "Constant" type pulse																		
	Mean, μ =	8.6	1456.0	107.7	87.5	103.1	110.6	627.6	0.9	100.4	29.2	-6.1	36.4	0.0	-24.2			
	Standard deviation, σ =	0.0	121.8	4.9	0.0	2.1	2.2	12.5	0.0	1.8	1.4	1.1	0.2	0.0	0.4			
	Coefficient of variation, C_v (%)	0%	8%	5%	0%	2%	2%	2%	2%	2%	5%	19%	0%	0%	1%			

No path dependency of loading is observed on most of the injuries except pelvic clip values

C394

Effect of loading paths (T = 40ms)

T = 40ms

Pulse iterations									HEAD			NECK	CHEST		PELVIS		LUMBAR	
									Resultant acceleration, g		HIC	N_{ij}	Resultant acceleration, g		Z-Acceleration, g	DRI (z), g	Axial compression, kN	
#	Pulse type	Peak, Dec., g	Duration, ms	Rate of onset, g/ms	ΔV, m/s	Sp. Pwr	Eff. G	G-avg	@ 2ms	@ 0ms	@ 15 ms	CFC 1000	@ 3ms	@ 7ms	@ 7ms		@30ms	@0ms
1	Triangular	44	40	2	8.6	376	27	22	54.6	55.4	223	0.46	47.4	42.0	-31.6	33.7	-1.3	-11.4
2	Haversine	44	40	2	8.6	375	29	22	62.2	63.7	274	0.53	50.0	49.2	-31.2	34.4	-1.0	-12.7
3	Sine	34	40	2	8.6	295	26	22	50.7	51.2	190	0.42	44.9	42.2	-28.0	33.3	-1.6	-10.7
4	Constant	23	40	NA	8.6	195	23	22	39.4	40.0	100	0.30	35.9	34.4	-25.0	31.4	-3.5	-8.5
5	Triangular #2	44	40	2	8.6	376	27	22	52.7	54.0	221	0.45	49.3	41.0	-24.7	33.3	-1.5	-11.5
6	Triangular #3	44	40	2	8.6	376	27	22	50.6	51.0	172	0.42	45.2	44.9	-30.9	33.3	-1.5	-10.1
7	Triangular #4	44	40	2	8.6	376	27	22	53.6	54.3	212	0.45	46.1	44.1	-31.3	33.8	-1.4	-11.2
8	Triangular #5	44	40	2	8.6	376	26	22	52.4	53.6	183	0.43	40.9	39.8	-30.8	33.1	-1.7	-10.8
Including "Constant" type pulse																		
	Mean, μ =	8.6	343	26.4	21.9	52.0	52.9	196.9	0.4	45.0	42.2	-29.2	33.3	-1.7	-10.9			
	Standard deviation, σ =	0.0	66	1.9	0.0	6.3	6.5	50.3	0.1	4.6	4.3	2.9	0.9	0.8	1.2			
	Coefficient of variation, C_v (%)	0%	19%	7%	0%	12%	12%	26%	15%	10%	10%	10%	3%	45%	11%			
Excluding "Constant" type pulse																		
	Mean, μ =	8.6	364.0	26.9	21.9	53.8	54.7	210.7	0.5	46.3	43.3	-29.8	33.6	-1.4	-11.2			
	Standard deviation, σ =	0.0	30.5	1.2	0.0	4.0	4.3	34.1	0.0	3.1	3.1	2.5	0.4	0.2	0.8			
	Coefficient of variation, C_v (%)	0%	8%	5%	0%	7%	8%	16%	8%	7%	7%	9%	1%	16%	7%			

No path dependency of loading is observed except lumbar clip values and HIC_{15}

References

1. "*Application of mathematical modeling in potentially survivable blast threats in military vehicles*" - Sudhakar Arepally, Dr. David Gorsich, Karrie Hope, Stephen Gentner and Kari Dortleff - 26th Army Science Conference, 1-4 December 2008, Orlando, Florida, United States
2. "*Response of dummies to high onset rate G_z loading on sled*" – Nagarajan Rangarajan, Jason Moore, Paul Gromowski, James Rinaldi, Narayan Yoganandan, Frank Pintar, Dennis Mariman and B Joseph McEntire –
3. "*Crew Injury Risk Assessment – Effective g vs. Delta V*" – James Sheng and Sudhakar Arepally – Undated TARDEC Brief

Neck Response of a Finite Element Human Body Model During a Simulated Rotary-Wing Aircraft Impact

Nicholas A. White, Kerry Danelson, F. Scott Gayzik, Joel D. Stitzel

ARL Workshop on Numerical Analysis of Human and Surrogate Response to Accelerative Loading

January 9, 2014

Center for Injury Biomechanics

Wake Forest School of Medicine

Virginia Tech COLLEGE of ENGINEERING

How can we study neck response during a dynamic impact???

ATD

Pro: Load cells

Cons: Biofidelity

Cadaver

Forman, 2006

Pro: Biofidelity

Cons: No direct way to measure neck loads

2

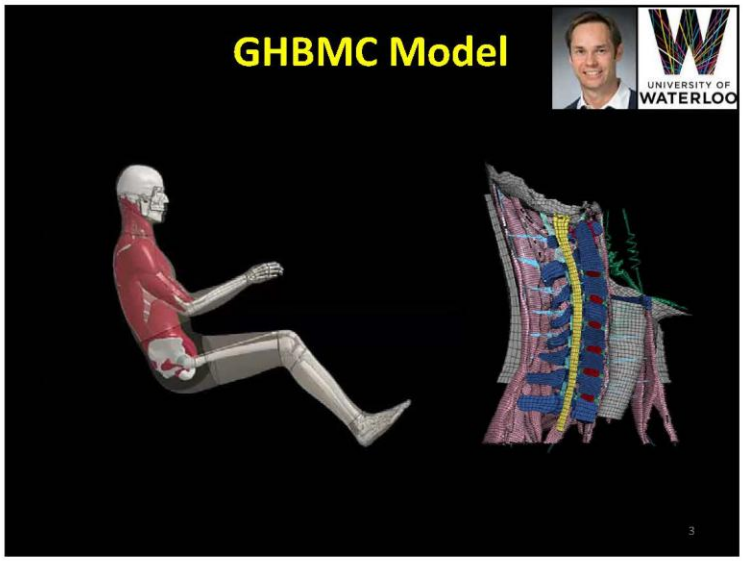
GHBMC Model
UNIVERSITY OF WATERLOO
3

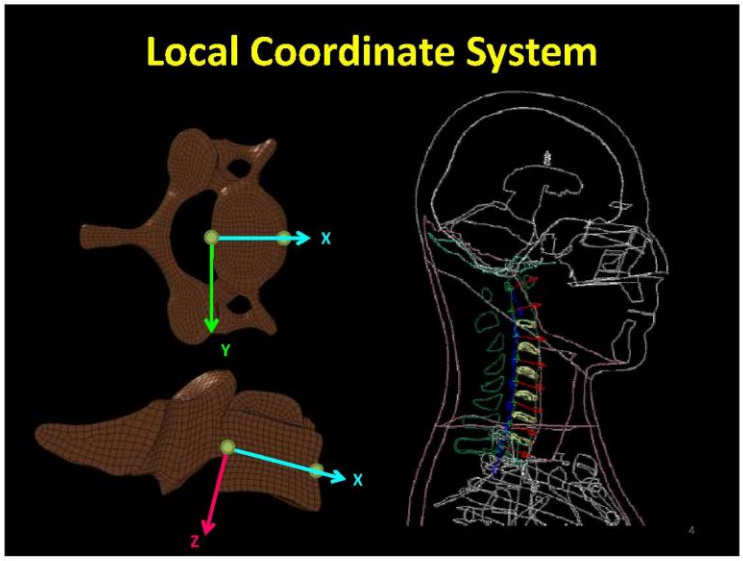
Local Coordinate System
X
Y
X
Z
4

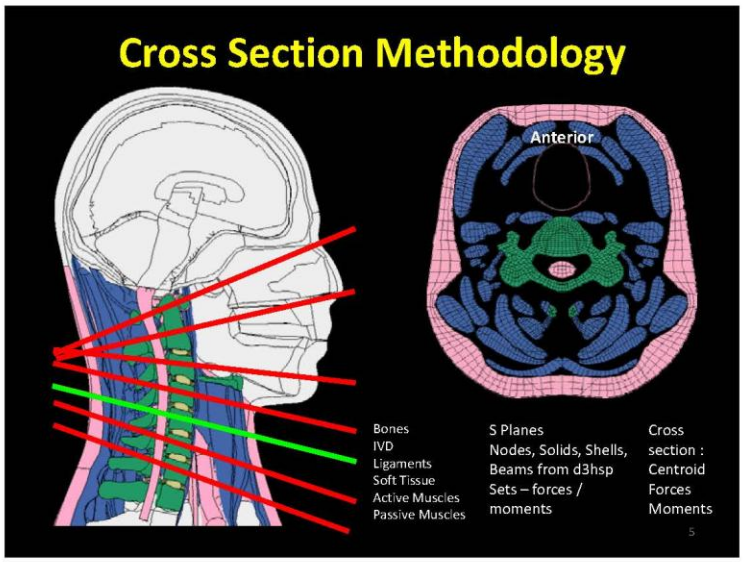
Cross Section Methodology
Anterior
Bones
IVD
Ligaments
Soft Tissue
Active Muscles
Passive Muscles
S Planes
Nodes, Solids, Shells, Beams from d3hsp
Sets – forces / moments
Cross section : Centroid
Forces
Moments
5

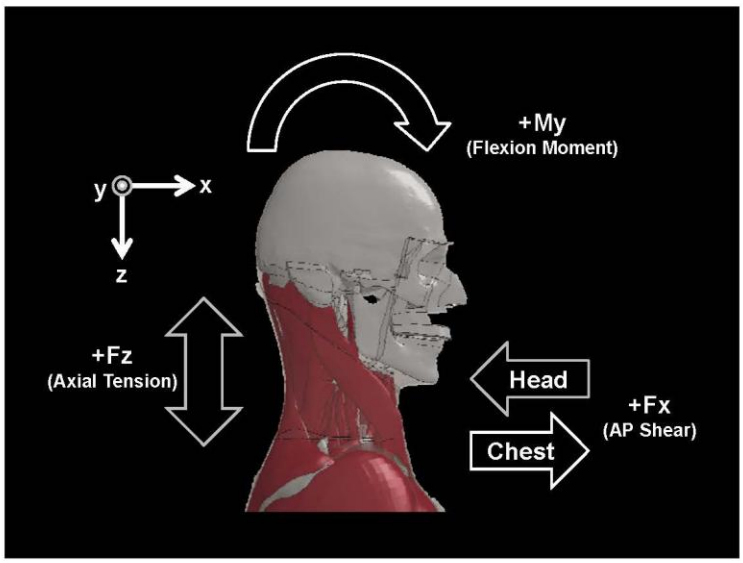
+My
(Flexion Moment)
y
x
z
+Fz
(Axial Tension)
Head
Chest
+Fx
(AP Shear)

Intervertebral Discs and Facets

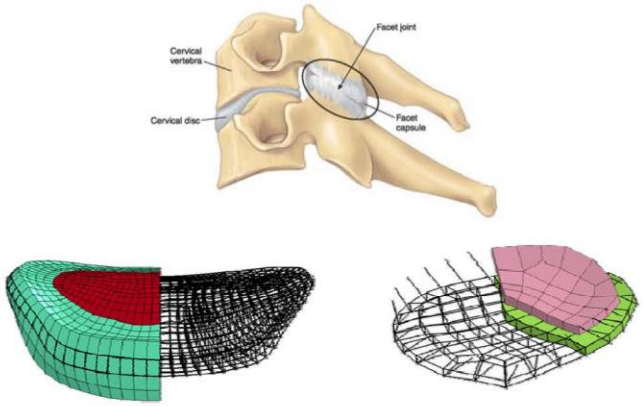

7

Frontal Impact (48 kph)

30 mph
15 g

8

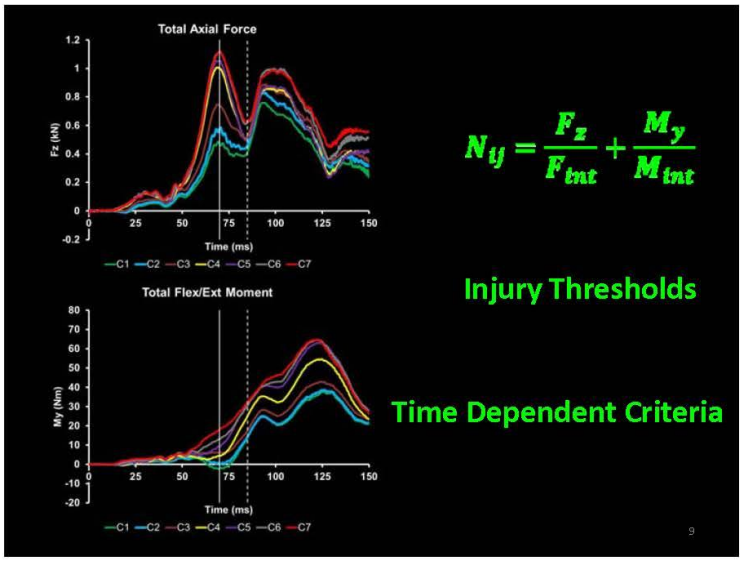
Total Axial Force
Fz (kN)
Time (ms)
C1 C2 C3 C4 C5 C6 C7
Total Flex/Ext Moment
My (Nm)
Time (ms)
C1 C2 C3 C4 C5 C6 C7
$N_{ij} = \frac{F_z}{F_{int}} + \frac{M_y}{M_{int}}$
Injury Thresholds
Time Dependent Criteria
9


10

ATD Sled Test

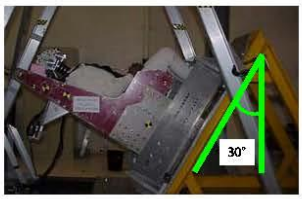

Paskoff, 2004

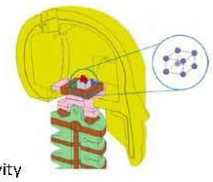

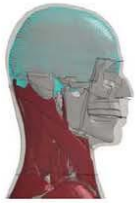

7.62 m/s
16 g
70 ms gravity
40 lb belt

11

Sled Pulse

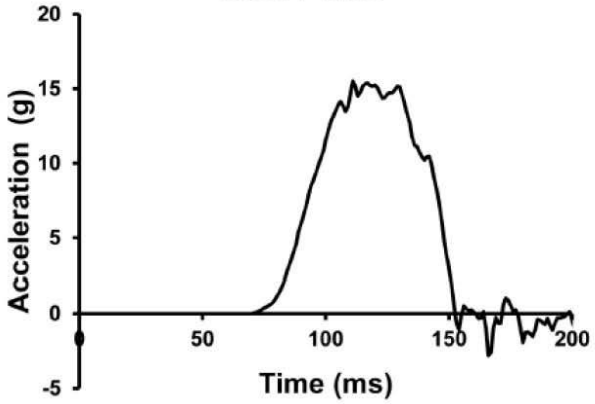

Quantitative Analysis

- CORA: CORrelation and Analysis
- Objective comparison between benchmark and simulation time histories
  - Corridor Rating (narrow/wide corridor)
  - Cross-correlation Rating (phase shift, size, shape)
- Rating
  - 0 (no correlation)
  - 1 (perfect correlation)

13

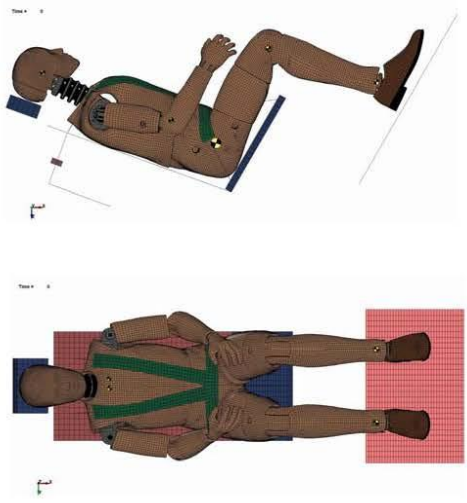

14

Head and Chest Response

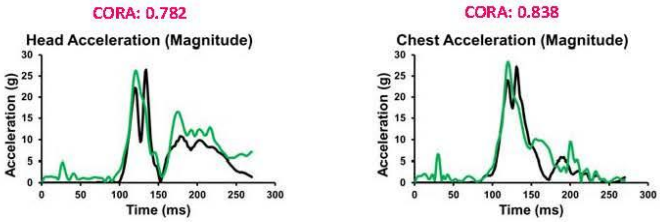

Exp (530) ATD (exp)

Neck Response

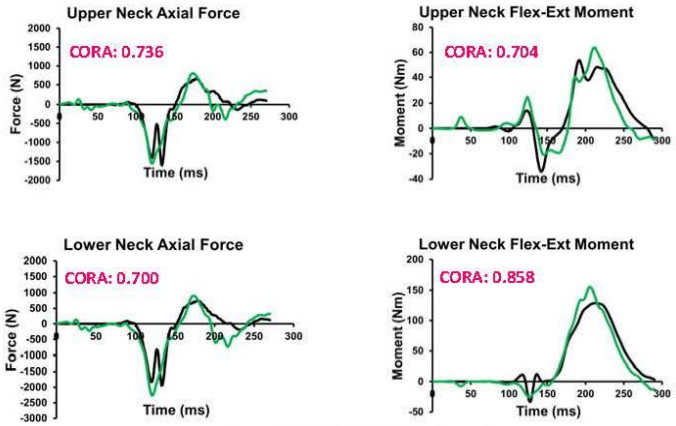

Exp (530) ATD (exp)

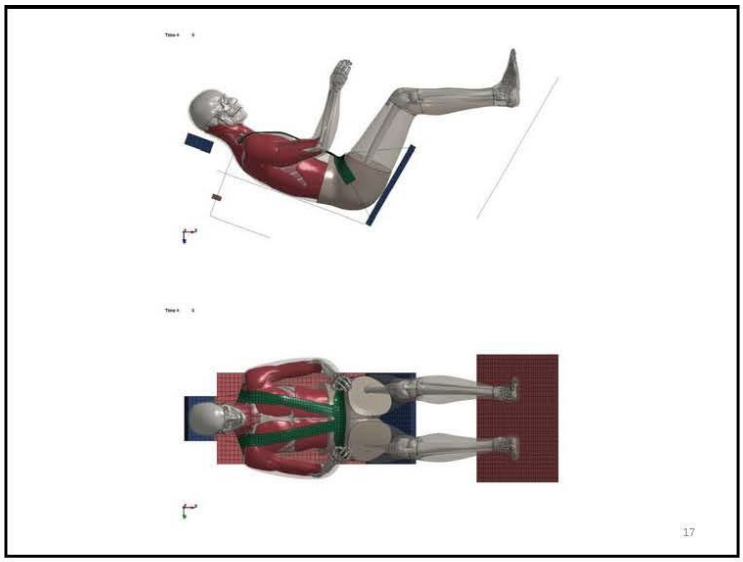
17

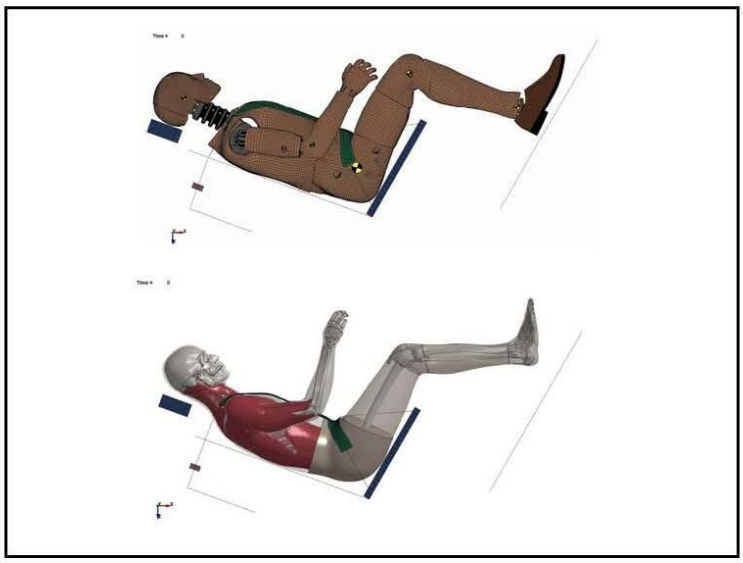

Head and Chest Response

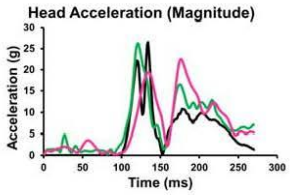

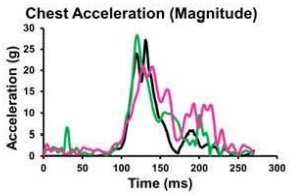

Exp (530) ATD (exp) GHBMC

Neck Response

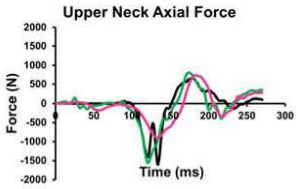

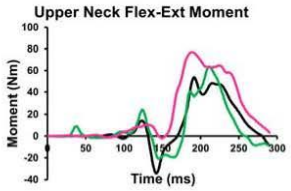

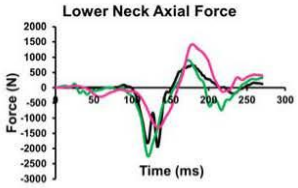

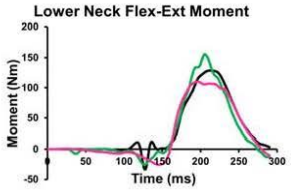

Exp (530) ATD (exp) GHBMC


Motion about C7 CG
Time = 0
21

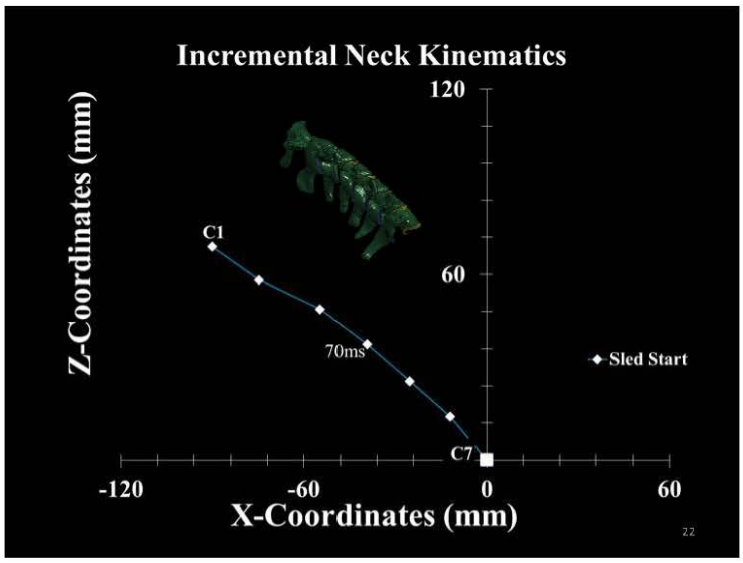
Incremental Neck Kinematics
120
60
Z-Coordinates (mm)
C1
70ms
Sled Start
C7
-120
-60
0
60
X-Coordinates (mm)
22

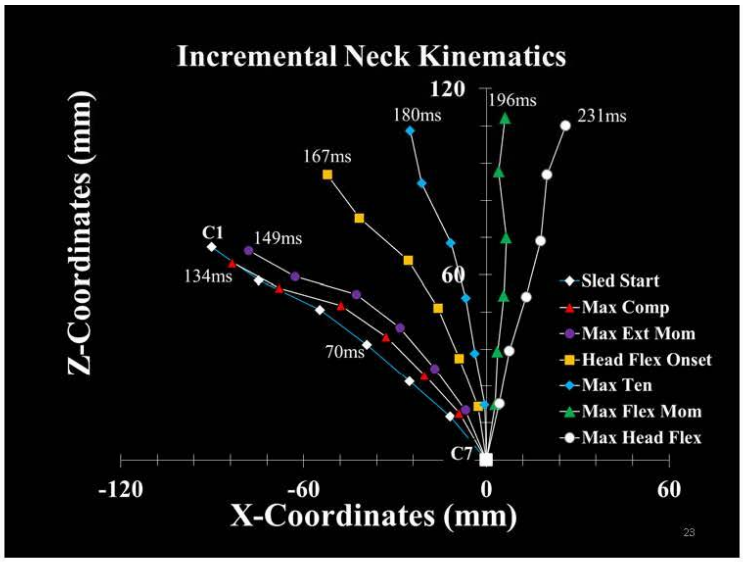
Incremental Neck Kinematics
Z-Coordinates (mm)
120
60
-120
-60
0
60
X-Coordinates (mm)
C1
C7
134ms
149ms
167ms
180ms
196ms
231ms
70ms
Sled Start
Max Comp
Max Ext Mom
Head Flex Onset
Max Ten
Max Flex Mom
Max Head Flex
23

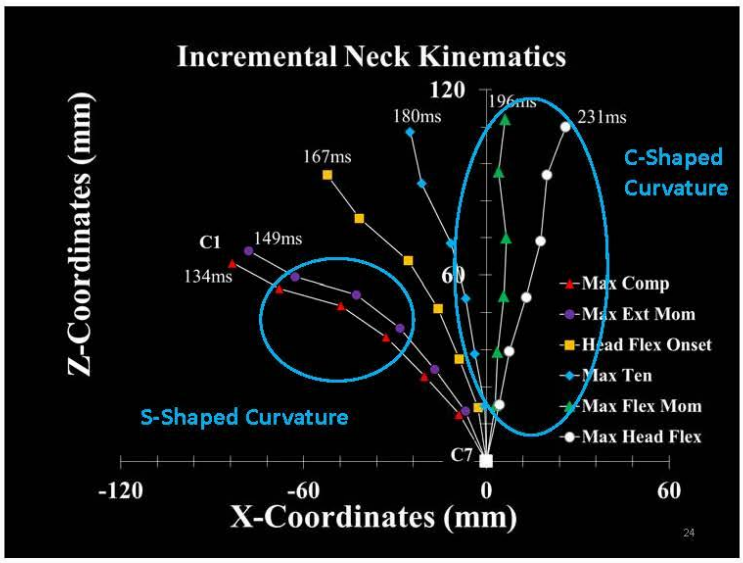
Incremental Neck Kinematics
Z-Coordinates (mm)
120
60
-120
-60
0
60
X-Coordinates (mm)
C1
C7
134ms
149ms
167ms
180ms
196ms
231ms
C-Shaped Curvature
S-Shaped Curvature
Max Comp
Max Ext Mom
Head Flex Onset
Max Ten
Max Flex Mom
Max Head Flex
24

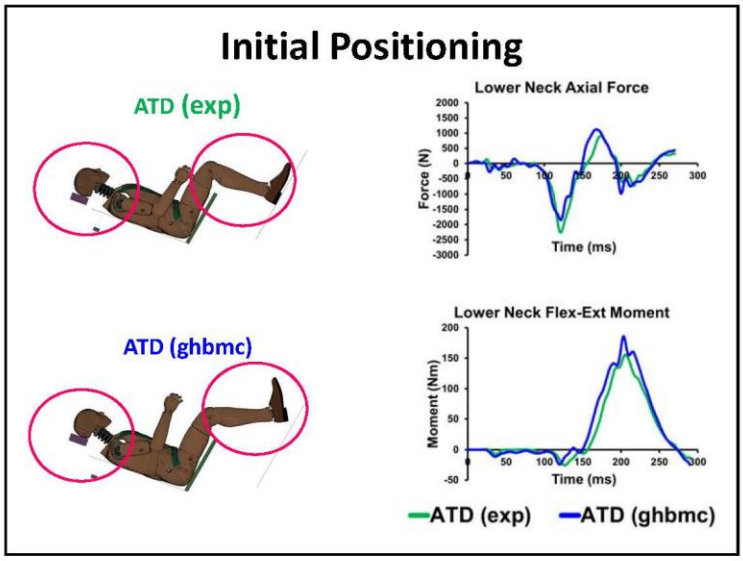
Initial Positioning
ATD (exp)
ATD (ghbmc)
Lower Neck Axial Force
Force (N)
Time (ms)
Lower Neck Flex-Ext Moment
Moment (Nm)
Time (ms)
ATD (exp)
ATD (ghbmc)

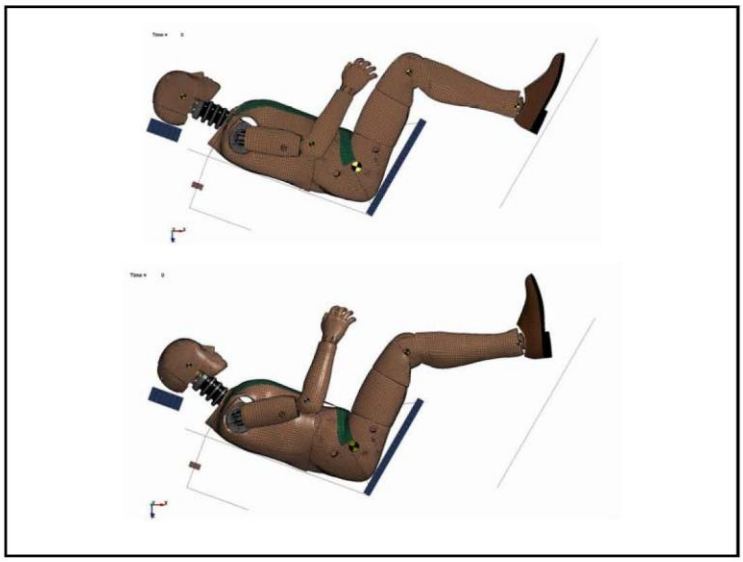

Future Work

- Experimental Work
  - Dynamic testing of cadaver cervical spine with CTDRs
  - Full body cadaver tests, high-speed biplane x-ray
  - Pressure transducers, pressure mat system, accelerometers
- Computational Work
  - Effects of muscle activation
  - Loading of posterior ligaments
  - Different impact scenarios

27

Publications

- Title: Cross-Section Neck Response of a Total Human Body FE Model during Simulated Frontal and Side Automobile Impacts
  - Journal: Computer Methods in Biomechanics and Biomedical Engineering (published)
- Title : Head and Neck Response of a Finite Element Anthropomorphic Test Device and Human Body Model during a Simulated Rotary-Wing Aircraft Impact
  - Journal: The Journal of Biomechanical Engineering (under review)

28


Acknowledgements
• Funding: United States Army Aeromedical Research and Materiel Command
• FE Model: Global Human Body Models Consortium
• CTDRs: Medtronic and Synthes Spine
• Computations: WFU DEAC Cluster
• Experiment Consult: Glenn Paskoff
GHBMC
Global Human Body Models Consortium
Distributed Environment for Academic Computing
29

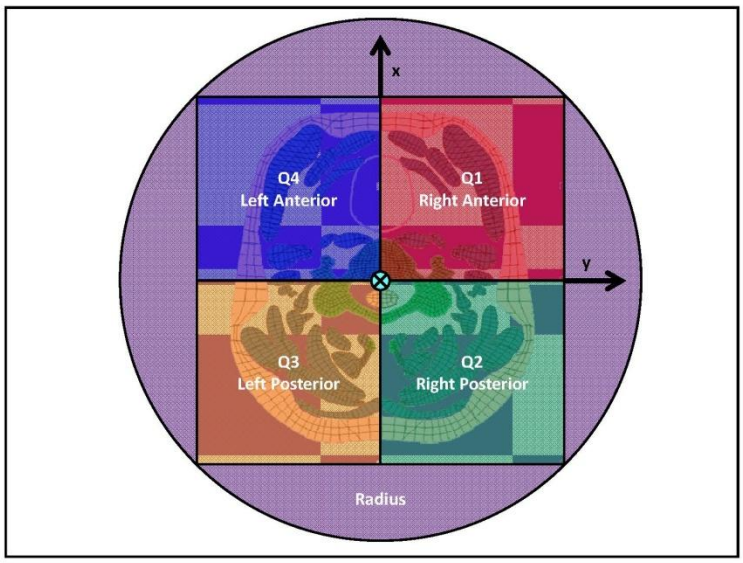
x
y
Q4
Left Anterior
Q1
Right Anterior
Q3
Left Posterior
Q2
Right Posterior
Radius

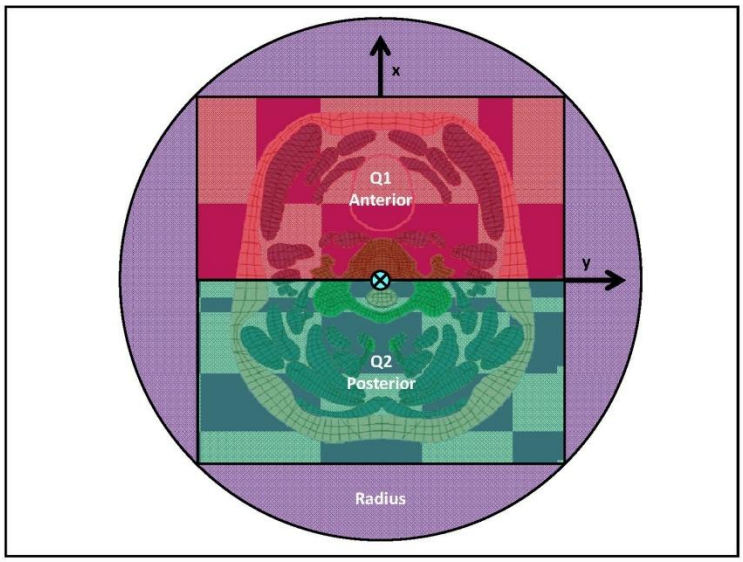
x
Q1
Anterior
y
Q2
Posterior
Radius

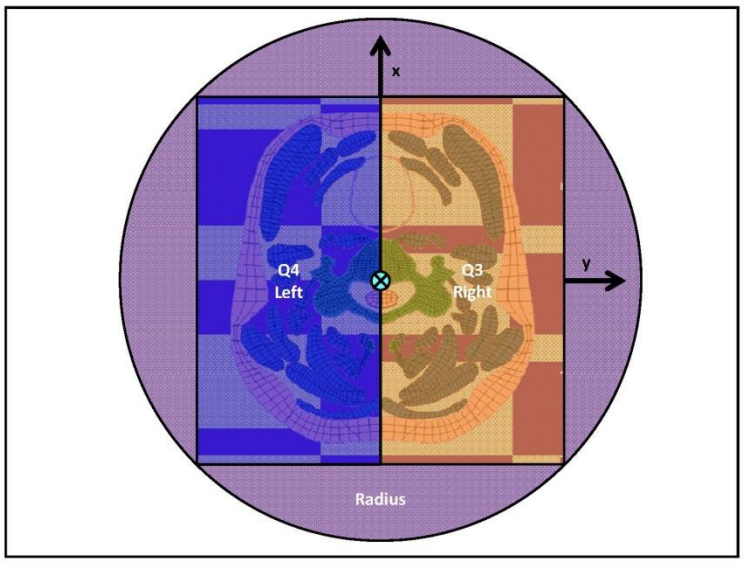
x
Q4
Left
Q3
Right
y
Radius

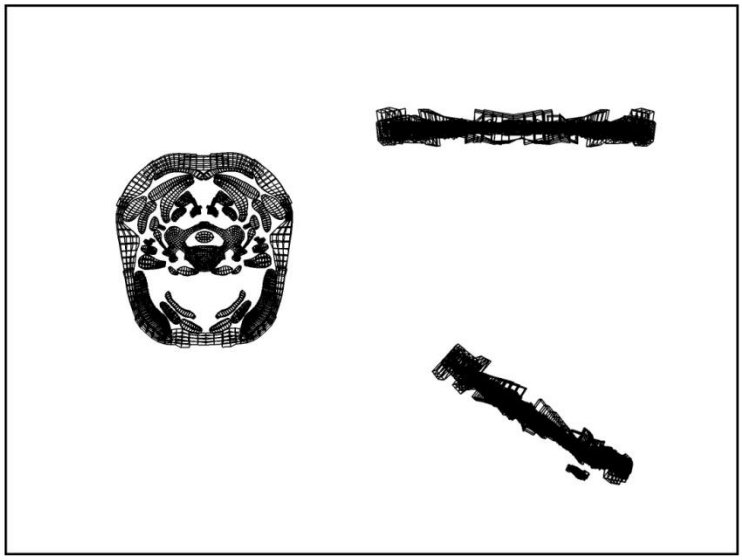

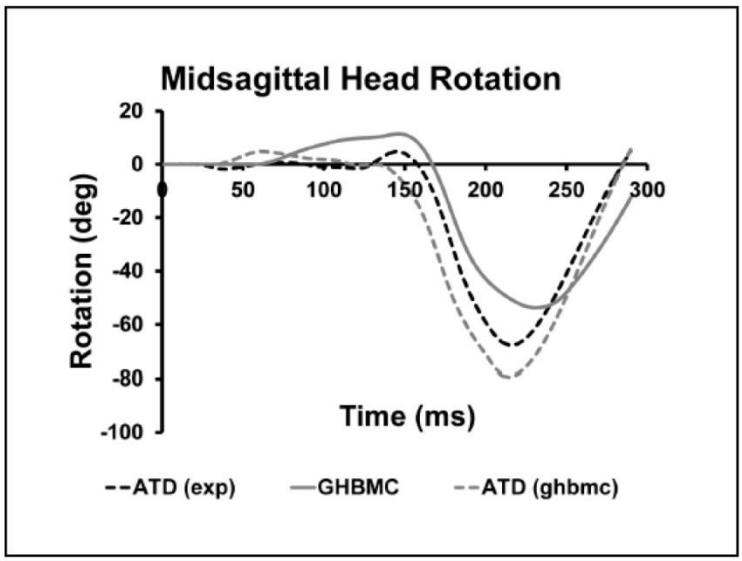
Midsagittal Head Rotation
Rotation (deg)
20
0
-20
-40
-60
-80
-100
50
100
150
200
250
300
Time (ms)
ATD (exp)
GHBMC
ATD (ghbmc)

Bass CR, Donnellan L, Salzar R, Lucas S, Folk R, Davis M, Rafaels K, Planchak C, Meyerhoff K, Ziemba A, Akkerman M A New Neck Injury Criterion in Combined Vertical/Frontal Crashes with Head Supported Mass. In: International Research Council on Biomechanics of Injury, Madrid, Spain, 2006.
Bass CR, Salzar R, Donnellan L, Lucas H (2004) Injury Risk from HSM Loading (HM 2,3,4,5 Series). Report HEADMA052.
Boitnott RL, Jackson KE, Fasanella EL, Kellas S Full-Scale Crash Test of the Sikorsky Advanced Composite Airframe Program Helicopter. In: Proceedings of the American Helicopter Society Forum 56, Virginia Beach, VA, 2000.
Burrows L, Lane R, McElhaney J (1978) CH-47 Crash Test (T-40) Structural, Cargo Restraint, and Airscrew Inflatable Restraint Experiments. USAMTL-TR-78-22.
Coltman JW (1983) Design and test criteria for increased energy-absorbing seat effectiveness. USAAVRADCOM-TR-82-D-42.
Coltman JW, Van Ingen C, Selker F (1988) Crash Resistant Crewseat Limit Load Optimization through Dynamic Testing with Cadavers. USAAVSCOM TR-85-D-11.
Cromlish JD, Mazza LT Bell ACAP Full-Scale Aircraft Crash Test and KRASH Correlation. In: Proceedings of the 44th Annual Forum of the American Helicopter Society, Washington, D.C., 1988.
DeWit JA, Cronin DS (2012) Cervical spine segment finite element model for traumatic injury prediction. Journal of the mechanical behavior of biomedical materials 10:138-150. doi:10.1016/j.jmbbm.2012.02.015
Dorris J (2001) Chopper: A History of American Military Helicopter Operations from WWII to the War on Terror. The Berkley Publishing Group, New York, NY.
Fasanella EL, Carden HC, Boitnott RL, Hayduk RJ (2002) A Review of the Analytical Simulation of Aircraft Crash Dynamics. NASA Technical Memorandum (TM) 102595.
Fasanella EL, Jackson KE (2002) Best Practices for Crash Modeling and Simulation. ARL-TR-2849.
Fice JB, Cronin DS (2012) Investigation of whiplash injuries in the upper cervical spine using a detailed neck model. Journal of biomechanics 45 (9):1068-1102. doi:10.1016/j.jbiomech.2011.01.016
Fice JB, Cronin DS, Panzer MB (2011) Cervical spine model to predict capsular ligament response in rear impact. Annals of biomedical engineering 39 (8): 2152-2162. doi:10.1007/s10439-011-0315-4
Foster J, Kortge J, Wolanin M (1977) Hybrid III-A Biomechanically-Based Crash Test Dummy. SAE Technical Paper 770938
Gayzik FS, Moreno DP, Danelson KA, McNally C, Klinich KD, Stitzel JD (2012a) External landmark, body surface, and volume data of a mid-sized male in seated and standing postures. Annals of biomedical engineering 40 (9): 2159-2032. doi:10.1007/s10439-012-0546-z
Gayzik FS, Moreno DP, Geer CP, Wuertzer SD, Martin RS, Stitzel JD (2011) Development of a full body CAD dataset for computational modeling: a multi-modality approach. Annals of biomedical engineering 39 (10):2568-2583. doi:10.1007/s10439-011-0359-5
Gayzik FS, Moreno DP, Vavalle NA, Rhyne AC, Stitzel JD Development of a Full Human Body Finite Element Model for Blunt Injury Prediction Utilizing a Multi-Modality Medical Imaging Protocol. In: 12th International LS-DYNA User Conference, Dearborn, MI, 2012b.
Gebicke MR, Farrell BS (1986) Military Personnel: Actions Needed to Better Define Pilot Requirements and Promote Retention. B-213375.
Gehre C, Gades H, Wernicke P Objective rating of Signals using Test and Simulation Responses. In: 21st International Technical Conference on the Enhanced Safety of Vehicles, Stuttgart, Germany, 2009.
Gehre C, Stahlschmidt S Assessment of Dummy Models by using Objective Rating Methods. In: 22nd International Technical Conference on the Enhanced Safety of Vehicles, Washington, DC, 2011.
Haley Jr. JL, McEntire BJ (1984) CH-53E Pilot Display Unit (PDU) Simulated Crash Tests. USAARL Report No. 85-10.
Haley Jr. JL, Palmer RW (1984) Evaluation of a Retrofit CH-53E Pilot's Seat to Prevent Back Injury. USAARL Report No. 85-9.
Heyes AR, Vavalle NA, Moreno DP, Stitzel JD, Gayzik FS (2013) Validation of Simulated Chestband Data in Frontal and Lateral Loading using a Human Body Finite Element Model. Traffic Injury Prevention. doi:10.1080/15389588.2013.799278
Humanetics (2013a) Hybrid III 50th Dummy DYNA Model Technical Report, Release Version 8.0.
Humanetics (2013b) Hybrid III 50th Dummy LS-DYNA Model, Pre-Simulation Positioning, Version 8.0.
Humanetics (2013c) User's Guide for the Hybrid III 50th Percentile Male Dummy LS-DYNA Model Version 8.0.
Jackson K, Fuchs Y, Kellas S (2006) Overview of the National Aeronautics and Space Administration Subsonic Rotary Wing Aeronautics Research Program in Rotorcraft Crashworthiness. Journal of Aerospace Engineering 22 (3):229-239. doi:doi:10.1061/(ASCE)0893-1321(2009)22:3(229)
Jackson KE, Boitnott RL, Fasanella EL, Jones LE, Lyle KH A History of Full-Scale Aircraft and Rotorcraft Crash Testing and Simulation at NASA Langley Research Center. In: Fourth Triennial International Fire and Cabin Safety Research Conference, 2004.
Jackson KE, Fasanella EL, Boitnott RL, McEntire BJ, Lewis A (2002) Occupant Responses in a Full-Scale Crash Test of the Sikorsky ACAP Helicopter. NASA/TM-2002-211733 (ARL-TR-2735).
Jackson KE, Fasanella EL, Lyle KH Crash Certification by Analysis – Are We There Yet? In: American Helicopter Society 62nd Annual Forum, Phoenix, AZ, 2006.
Mattucci SF, Moulton JA, Chandrashekar N, Cronin DS (2012) Strain rate dependent properties of younger human cervical spine ligaments. Journal of the mechanical behavior of biomedical materials 10:216-226. doi:10.1016/j.jmbbm.2012.02.004
Mertz HJ, Irwin AL, Prasad P (2003) Biomechanical and scaling bases for frontal and side impact injury assessment reference values. Stapp car crash journal 47:155-188.
National Highway Traffic Safety Administration (2008) Title 49 Code of Federal Regulations (CFR) Part 571 Section 208, Occupant Crash Protection.
Nichols JP Overview of Ejection Neck Injury Criteria. In: Forty Fourth Annual SAFE Association Symposium, 2006.
Paskoff GR (2006) Cervical Injury Risk Resulting From Rotary Wing Impact: Assessment of Injury Based Upon Aviator Size, Helmet Mass Properties and Impact Severity. NAWCADPAX/RTR-2006/86.
Paskoff GR, Shewchuk T Influence of Added Head Mass Properties on Head/Neck Loads During Standard Helicopter Impact Conditions. In: Forty Second Annual SAFE Association Symposium, Salt Lake City, Utah, 2004. SAFE Association, pp 20-40.
Patwardekl JC, Blair JA, Schoenfeld AJ, Lehman RA, Hsu JR, Skeletal Trauma Research TC (2012) Multiple associated injuries are common with spine fractures during war. The spine journal : official journal of the North American Spine Society 12 (9):791-797. doi:10.1016/j.spinee.2011.10.003
Pellettiere J, Moorcroft D, Oliveira G Anthropomorphic Test Dummy Lumbar Load Variation. In: 22nd Enhanced Safety of Vehicles Conference, Washington, DC, 2011.
Perschbacher JF, Clarke C, Furnas K, Carnell B (1988) Advanced Composite Airframe Program (ACAP) Militarization Test and Evaluation (MT&E) Volume V- Airframe Drop Test. USAATCOM TR 88-D-22E.
Putnam JB, Ontario CO Investigation of Human Kinematics and Risk of Injury during a Vertical Impact using Dummy and Human Finite Element Models. In: The Ohio State University's 9th Annual Injury Biomechanics Symposium, Columbus, OH, 2013.
Shannon SG, Albano JP, Mason KT, Licina JR (1998) Head injury risk in US Army rotary-wing mishaps: Changes since 1980. USAARL Report No. 98-13.
Shipley CT, 1/7 Full-Scale Crash Testing of a CH-47D Helicopter. In: Proceedings of the 32nd VFS/CAL Forum of the American Helicopter Society, Washington, D.C., May 1976.
Smith KF (1988) Full-Scale Crash Test (T-41) of the YAH-63 Attack Helicopter. USAAVSCOM TR 88-D-2.
Society of Automotive Engineers (2007) SAE J211/1 - Instrumentation for Impact Test-Part 1-Electronic Instrumentation.
Stitzel JD (2011) Global Human Body Models Consortium, LLC. Male 50th Percentile (M50) Occupant Model Manual.
Thomson DT, Clarke CW (1989) Advanced Composite Airframe Program (ACAP) Militarization Test and Evaluation (MT&E) Volume I- Landing Gear Drop Test. USAAVSCOM TR-88-D-22A.
Thunert C (2013) ICSRA Release 3.6 User's Manual. Graz, Austria
U.S. Army (2013) U.S. Army Fact Files: Aircraft. Accessed July 15 2013
U.S. Army Combat Readiness/Safety Center (2013) U.S. Army Accident Information Aviation Accident Statistics - Year End, 01 October Through 30 September. Accessed 10 July 2013
Vavalle NA, Jelen B, Stitzel JD, Gayzik FS (2013a) Analysis of objective rating methods for full body finite element model comparison to PMHS tests. Traffic Injury Prevention 14 (supplement 1):S87-S94.
Vavalle NA, Moreno DP, Rhyne AC, Stitzel JD, Gayzik FS (2013b) Lateral impact validation of a geometrically accurate full body finite element model for blunt injury prediction. Annals of biomedical engineering 41 (3):497-512. doi:10.1007/s10439-012-0684-3
White NA, Moreno DP, Gayzik FS, Stitzel JD (2013) Cross-Sectional Neck Response of a Total Human Body FE Model during Simulated Frontal and Side Automobile Impacts. Computer methods in biomechanics and biomedical engineering (Epub 9 Aug)
Zimmerman ST, Merritt AM, Patrol Aircraft Crash Survival Design Guide, Volume 1- Design Criteria and Checklists

Imperial College London

THE ROYAL BRITISH LEGION CENTRE FOR BLAST INJURY STUDIES AT IMPERIAL COLLEGE LONDON

FE model of the MIL-Lx with combat boot

Nic Newell and Spyros Masouros
The Royal British Legion Centre for Blast Injury Studies,
Department of Bioengineering,
Imperial College London, UK

Workshop on Numerical Analysis of Human and Surrogate Response to Accelerative Loading,
Aberdeen Proving Ground,
January 7-9, 2014

Introduction - ATDs

Hybrid-III

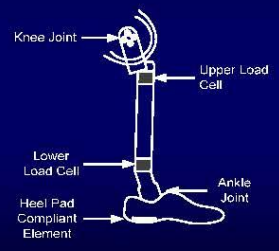

MIL-Lx

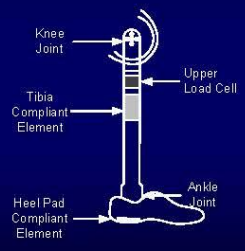

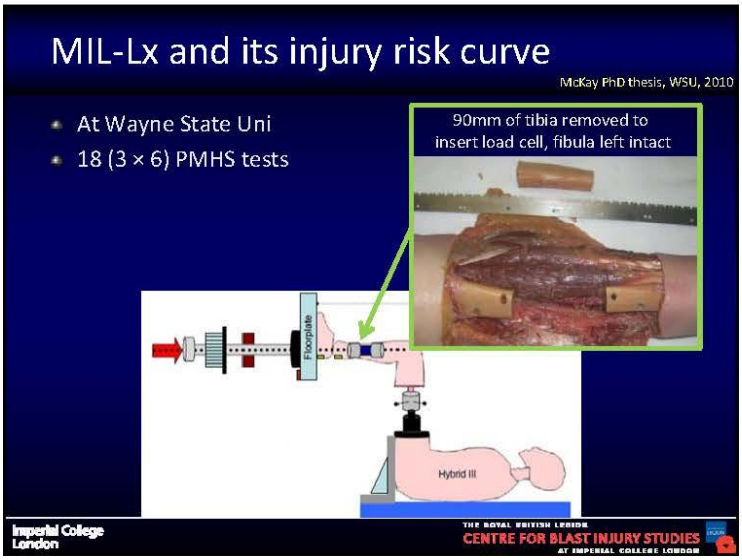
MIL-Lx and its injury risk curve
McKay PhD thesis, WSU, 2010
At Wayne State Uni
18 (3 × 6) PMHS tests
90mm of tibia removed to insert load cell, fibula left intact
Floorplate
Hybrid III
Imperial College London
THE ROYAL BRITISH LEGION
CENTRE FOR BLAST INJURY STUDIES
AT IMPERIAL COLLEGE LONDON

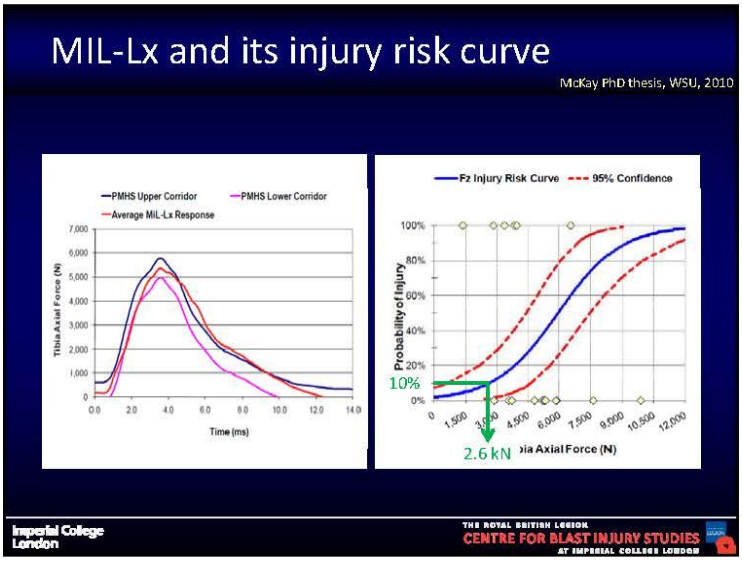
MIL-Lx and its injury risk curve
McKay PhD thesis, WSU, 2010
PMHS Upper Corridor
PMHS Lower Corridor
Average MiL-Lx Response
Tibia Axial Force (N)
Time (ms)
Fz Injury Risk Curve
95% Confidence
Probability of Injury
10%
2.6 kN
Imperial College London
THE ROYAL BRITISH LEGION
CENTRE FOR BLAST INJURY STUDIES
AT IMPERIAL COLLEGE LONDON

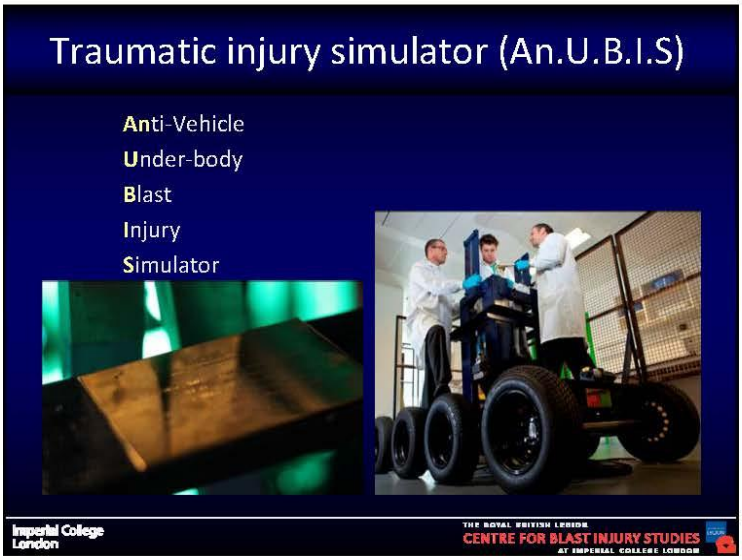
Traumatic injury simulator (An.U.B.I.S)
Anti-Vehicle
Under-body
Blast
Injury
Simulator
Imperial College London
THE ROYAL BRITISH LEGION
CENTRE FOR BLAST INJURY STUDIES
AT IMPERIAL COLLEGE LONDON

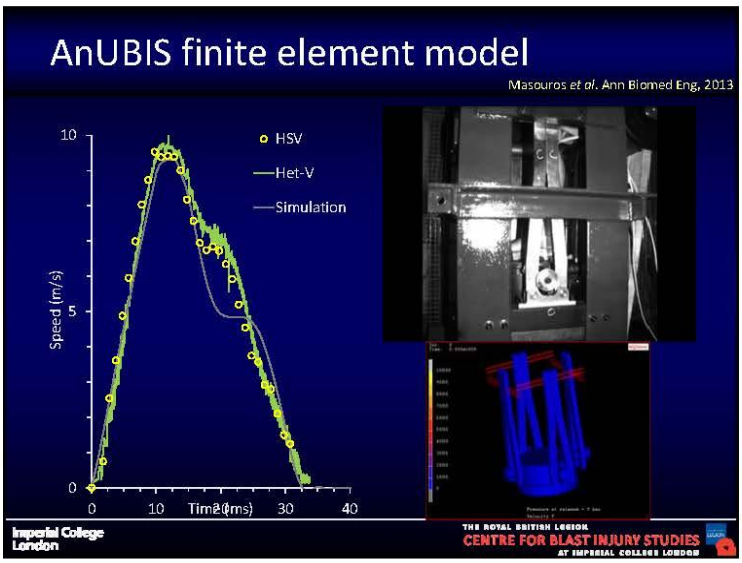
AnUBIS finite element model
Masouros et al. Ann Biomed Eng, 2013
HSV
Het-V
Simulation
Speed (m/s)
Time (ms)
0
5
10
0
10
20
30
40
Imperial College London
THE ROYAL BRITISH LEGION
CENTRE FOR BLAST INJURY STUDIES
AT IMPERIAL COLLEGE LONDON

Cadaver *vs.* H-III *vs.* MIL-Lx

Newell *et al.* 2012, IRCOBI Conference

- MIL-Lx is more biofidelic[1,2,3]

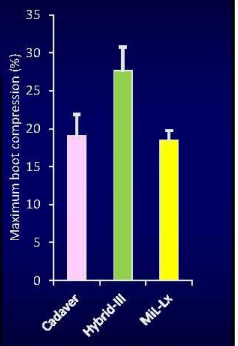

[1]McKay & Bir, 2009, Stapp Car Crash J
[2]Pandelani *et al.* 2010, CSIR Conference
[3]Newell *et al.* 2012, IRCOBI Conference

Imperial College London

THE ROYAL BRITISH LEGION CENTRE FOR BLAST INJURY STUDIES AT IMPERIAL COLLEGE LONDON

Aim – an FE model of the MIL-Lx

- If we believe that the MIL-Lx is biofidelic for axial loads then let's develop a simple FE model.
- Objectives
  - quick assessment of injury risk
  - in multiple loading modes
  - of multiple (albeit simple) designs of mitigation

Imperial College London

THE ROYAL BRITISH LEGION CENTRE FOR BLAST INJURY STUDIES AT IMPERIAL COLLEGE LONDON

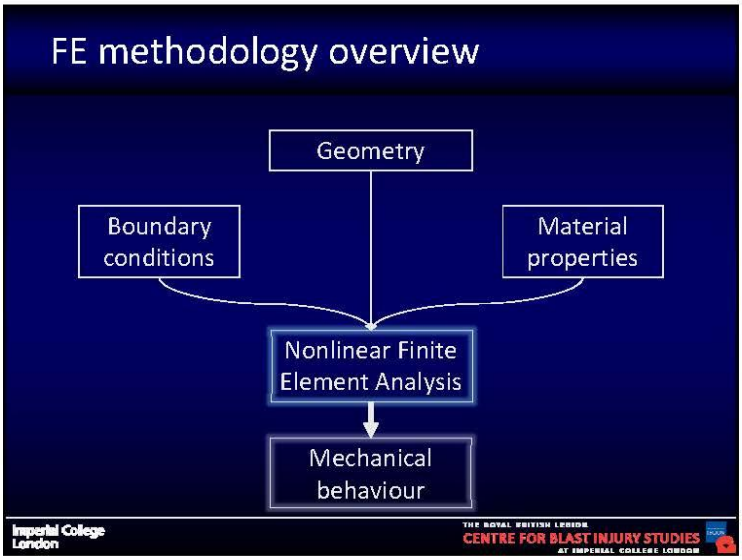
FE methodology overview
Geometry
Boundary conditions
Material properties
Nonlinear Finite Element Analysis
Mechanical behaviour
Imperial College London
THE ROYAL BRITISH LEGION
CENTRE FOR BLAST INJURY STUDIES
AT IMPERIAL COLLEGE LONDON

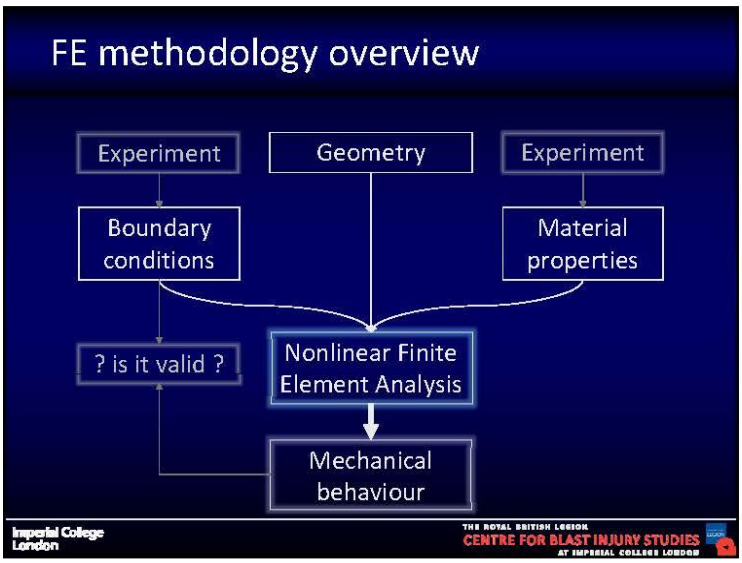
FE methodology overview
Experiment
Geometry
Experiment
Boundary conditions
Material properties
? is it valid ?
Nonlinear Finite Element Analysis
Mechanical behaviour
Imperial College London
THE ROYAL BRITISH LEGION
CENTRE FOR BLAST INJURY STUDIES
AT IMPERIAL COLLEGE LONDON

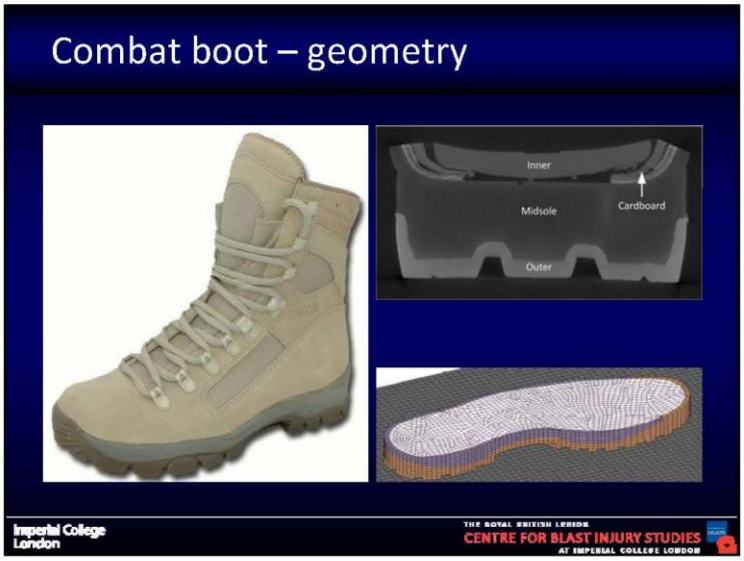
Combat boot – geometry
Inner
Midsole
Cardboard
Outer
Imperial College London
THE ROYAL BRITISH LEGION
CENTRE FOR BLAST INJURY STUDIES
AT IMPERIAL COLLEGE LONDON

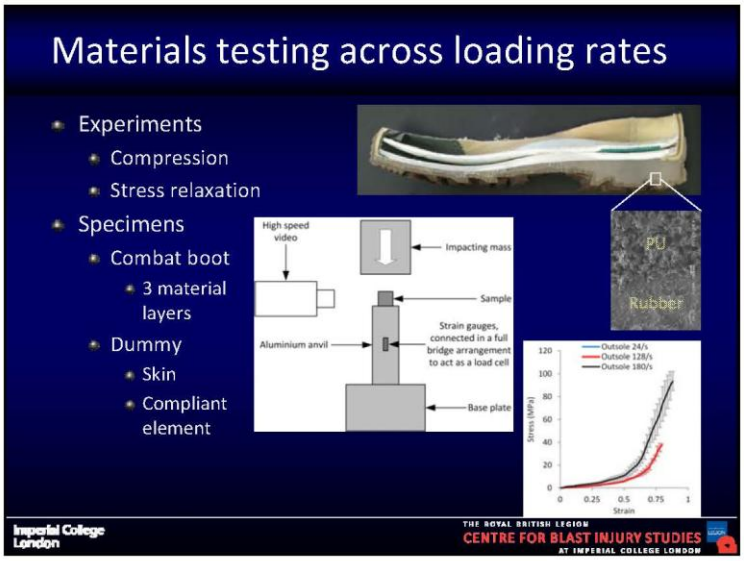
Materials testing across loading rates
Experiments
Compression
Stress relaxation
Specimens
Combat boot
3 material layers
Dummy
Skin
Compliant element
High speed video
Impacting mass
Sample
Aluminium anvil
Strain gauges, connected in a full bridge arrangement to act as a load cell
Base plate
PU
Rubber
Outsole 24/s
Outsole 128/s
Outsole 180/s
Stress (MPa)
Strain
Imperial College London
THE ROYAL BRITISH LEGION
CENTRE FOR BLAST INJURY STUDIES
AT IMPERIAL COLLEGE LONDON

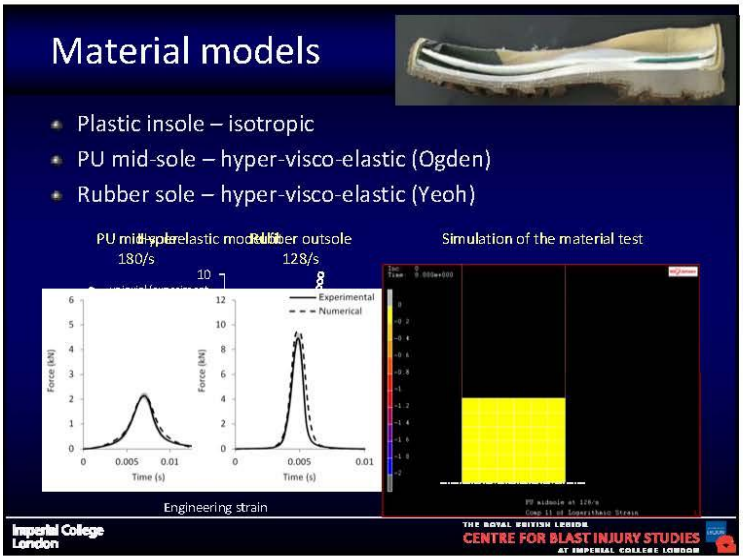
Material models
Plastic insole – isotropic
PU mid-sole – hyper-visco-elastic (Ogden)
Rubber sole – hyper-visco-elastic (Yeoh)
PU mid-sole hyper-elastic model
180/s
Rubber outsole
128/s
Simulation of the material test
Experimental
Numerical
Force (kN)
Time (s)
Engineering strain
Imperial College London
THE ROYAL BRITISH LEGION
CENTRE FOR BLAST INJURY STUDIES
AT IMPERIAL COLLEGE LONDON

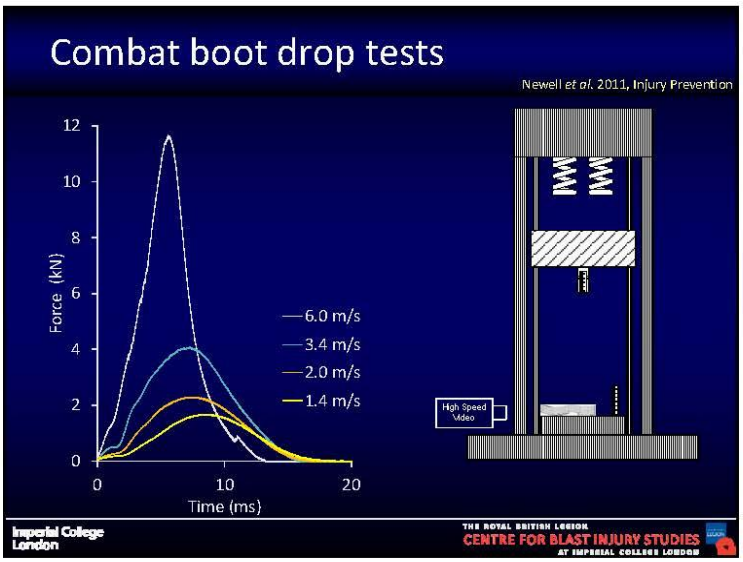
Combat boot drop tests
Newell et al. 2011, Injury Prevention
Force (kN)
Time (ms)
6.0 m/s
3.4 m/s
2.0 m/s
1.4 m/s
High Speed Video
Imperial College London
THE ROYAL BRITISH LEGION
CENTRE FOR BLAST INJURY STUDIES
AT IMPERIAL COLLEGE LONDON

Validation – Drop tests

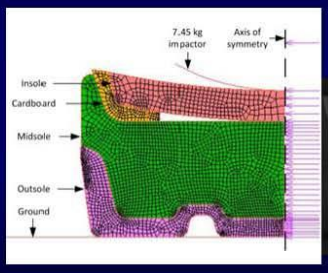

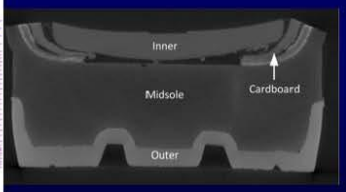

Imperial College London

THE ROYAL BRITISH LEGION CENTRE FOR BLAST INJURY STUDIES AT IMPERIAL COLLEGE LONDON

Validation – Drop tests

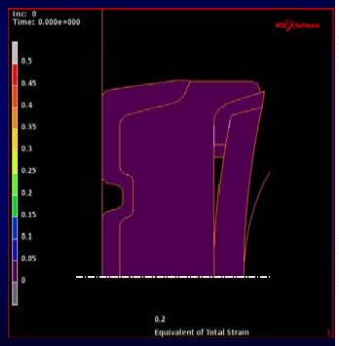

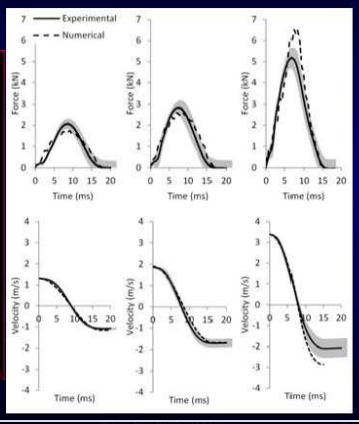

Imperial College London

THE ROYAL BRITISH LEGION CENTRE FOR BLAST INJURY STUDIES AT IMPERIAL COLLEGE LONDON

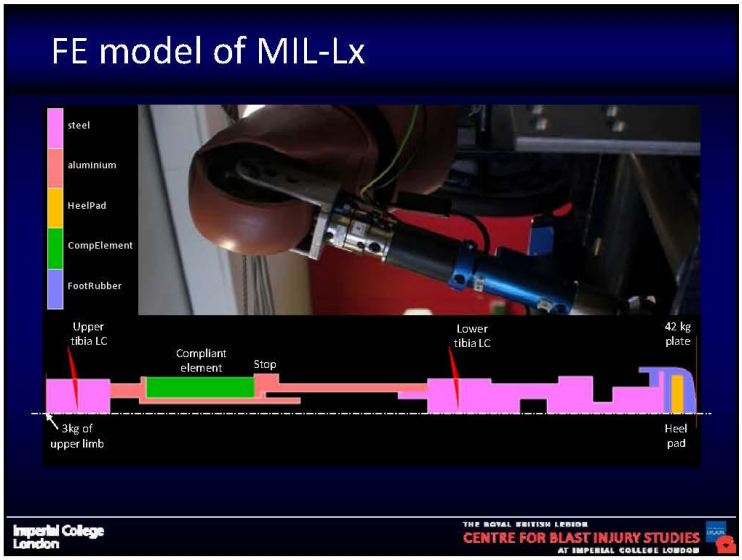
FE model of MIL-Lx
steel
aluminium
HeelPad
CompElement
FootRubber
Upper tibia LC
Compliant element
Stop
Lower tibia LC
42 kg plate
3kg of upper limb
Heel pad
Imperial College London
THE ROYAL BRITISH LEGION
CENTRE FOR BLAST INJURY STUDIES
AT IMPERIAL COLLEGE LONDON

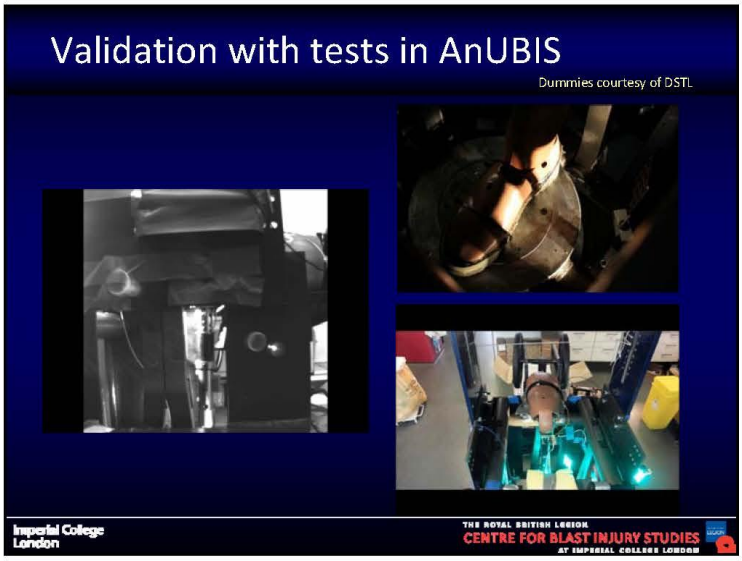
Validation with tests in AnUBIS
Dummies courtesy of DSTL
Imperial College London
THE ROYAL BRITISH LEGION
CENTRE FOR BLAST INJURY STUDIES
AT IMPERIAL COLLEGE LONDON

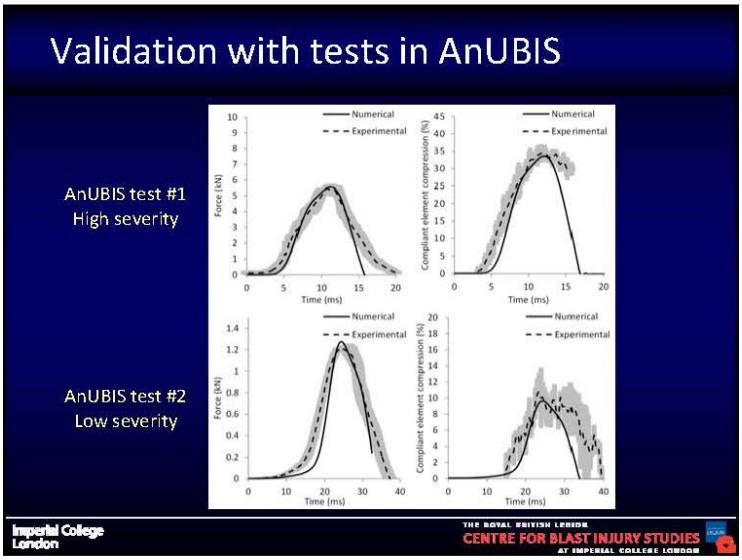
Validation with tests in AnUBIS
AnUBIS test #1
High severity
AnUBIS test #2
Low severity
Numerical
Experimental
Force (kN)
Compliant element compression (%)
Time (ms)
Imperial College London
THE ROYAL BRITISH LEGION
CENTRE FOR BLAST INJURY STUDIES
AT IMPERIAL COLLEGE LONDON

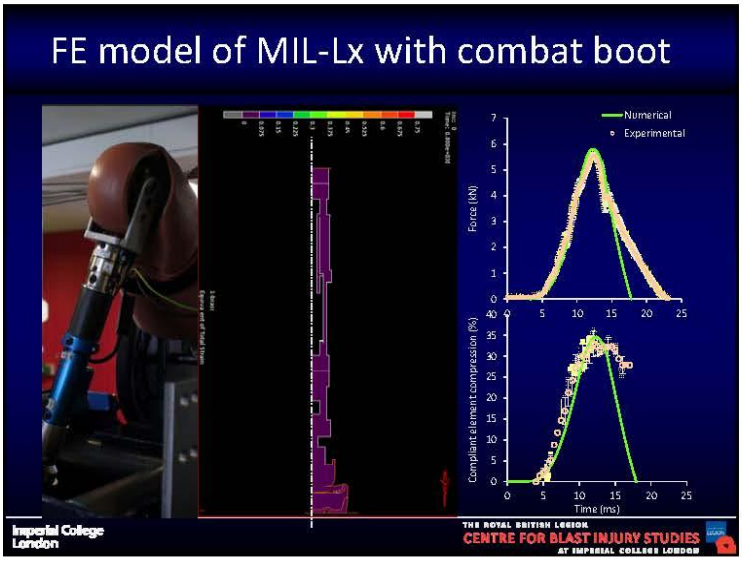
FE model of MIL-Lx with combat boot
Numerical
Experimental
Force (kN)
Compliant element compression (%)
Time (ms)
Imperial College London
THE ROYAL BRITISH LEGION
CENTRE FOR BLAST INJURY STUDIES
AT IMPERIAL COLLEGE LONDON

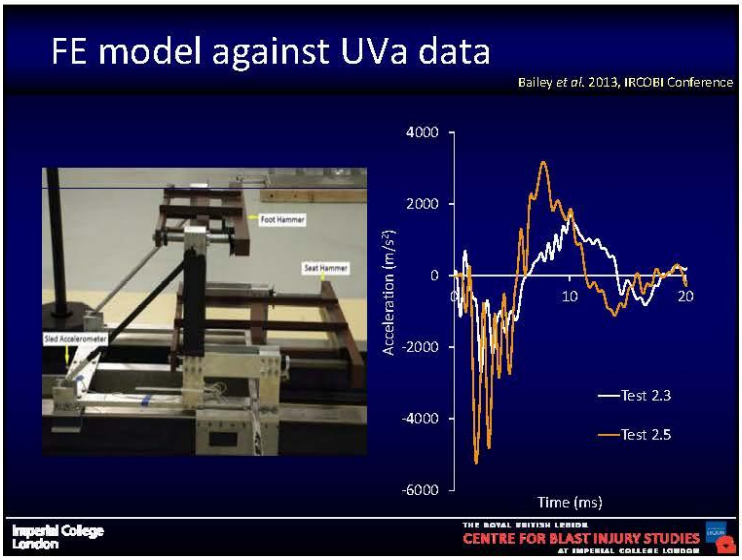
FE model against UVa data
Bailey et al. 2013, IRCOBI Conference
Foot Hammer
Seat Hammer
Sled Accelerometer
Acceleration (m/s²)
4000
2000
0
-2000
-4000
-6000
0
10
20
Test 2.3
Test 2.5
Time (ms)
Imperial College London
THE ROYAL BRITISH LEGION
CENTRE FOR BLAST INJURY STUDIES
AT IMPERIAL COLLEGE LONDON

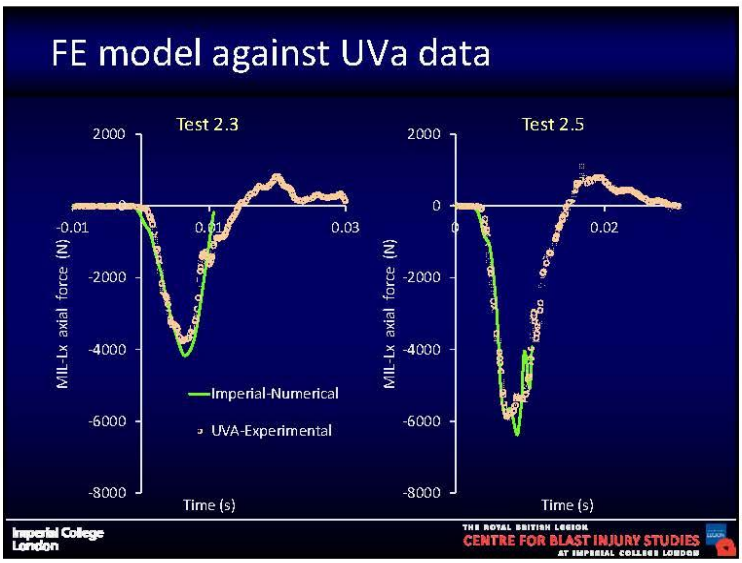
FE model against UVa data
Test 2.3
Test 2.5
MIL-Lx axial force (N)
2000
0
-2000
-4000
-6000
-8000
-0.01
0.01
0.03
0
0.02
Imperial-Numerical
UVA-Experimental
Time (s)
Imperial College London
THE ROYAL BRITISH LEGION
CENTRE FOR BLAST INJURY STUDIES
AT IMPERIAL COLLEGE LONDON

Sensitivity of the model to inputs

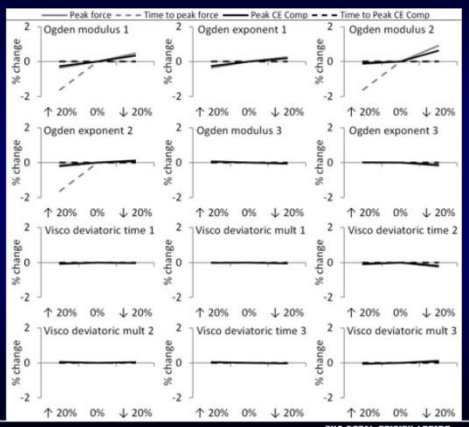

Imperial College London

THE ROYAL BRITISH LEGION CENTRE FOR BLAST INJURY STUDIES AT IMPERIAL COLLEGE LONDON

Sensitivity of the model to inputs

	Peak force		Peak compliant element compression	
Material / Boundary condition / Initial condition	Most sensitive property	Change (%)	Most sensitive property	Change (%)
Aluminium	Mass density	0.81	Mass density	1.27
Steel	Mass density	6.82	Mass density	6.17
Compliant element	Visco time 1	20.47	Visco time 1	20.68
Foot rubber	C30	0.63	C30	0.47
Heel pad	C10	1.01	C10	0.71
Insole	Young's modulus	0.50	Young's modulus	0.36
Midsole	Foam modulus 2	4.33	Foam modulus 1	6.89
Outsole	Ogden modulus 2	0.90	Ogden modulus 2	0.62
Cardboard	Mass density	0.21	Mass density	0.15
Mass of plate		0.12		0.09
Proximal leg mass		16.88		10.38
Plate displacement		17.94		13.80

Imperial College London

THE ROYAL BRITISH LEGION CENTRE FOR BLAST INJURY STUDIES AT IMPERIAL COLLEGE LONDON

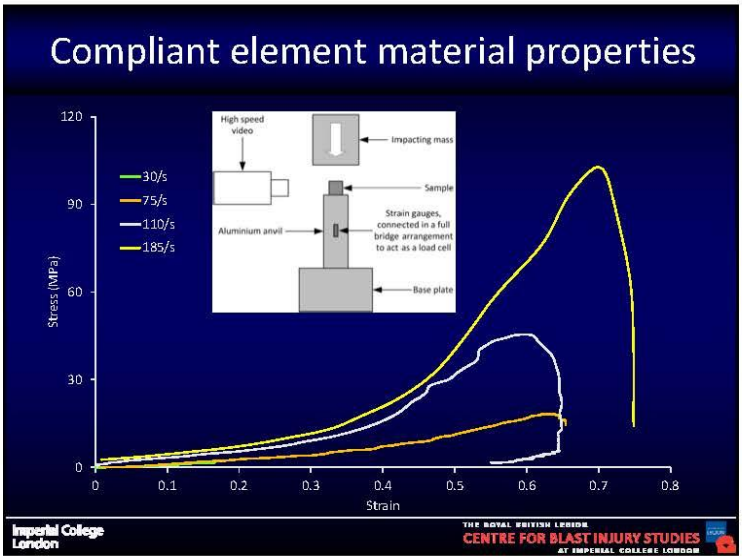
Compliant element material properties
120
90
60
30
0
Stress (MPa)
30/s
75/s
110/s
185/s
High speed video
Impacting mass
Sample
Aluminium anvil
Strain gauges, connected in a full bridge arrangement to act as a load cell
Base plate
0
0.1
0.2
0.3
0.4
0.5
0.6
0.7
0.8
Strain
Imperial College London
THE ROYAL BRITISH LEGION
CENTRE FOR BLAST INJURY STUDIES
AT IMPERIAL COLLEGE LONDON

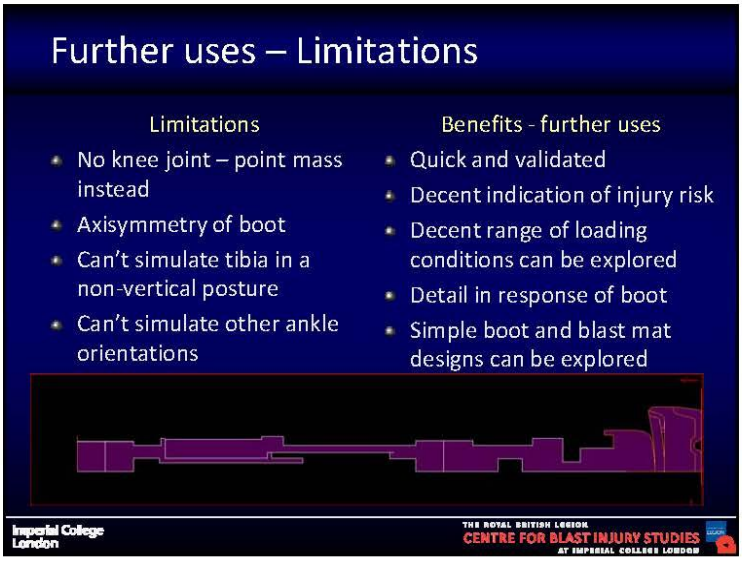
Further uses – Limitations
Limitations
No knee joint – point mass instead
Axisymmetry of boot
Can't simulate tibia in a non-vertical posture
Can't simulate other ankle orientations
Benefits - further uses
Quick and validated
Decent indication of injury risk
Decent range of loading conditions can be explored
Detail in response of boot
Simple boot and blast mat designs can be explored
Imperial College London
THE ROYAL BRITISH LEGION
CENTRE FOR BLAST INJURY STUDIES
AT IMPERIAL COLLEGE LONDON


Imperial College London
THE ROYAL BRITISH LEGION
CENTRE FOR BLAST INJURY STUDIES
AT IMPERIAL COLLEGE LONDON
FE model of the MIL-Lx with combat boot
Nic Newell and Spyros Masouros
The Royal British Legion Centre for Blast Injury Studies,
Department of Bioengineering,
Imperial College London, UK
s.masouros@imperial.ac.uk
www.imperial.ac.uk/traumabiomechanics
www.imperial.ac.uk/blastinjurystudies

Rubber Material Modeling Methodology for FE Dummy Development

Hyunsok Pang, Ph.D
Byeong Sam Kim, Ph.D

HUMANETICS

Contents

HUMANETICS

Introduction

- Crash Dummy Materials – Rubber, Foam, Damping, Plastic, Metal
- Critical Body Parts – Neck, Thorax Ribs, Lumbar Spine, Skin,
- Rubber - the most important & widely used material in Crash Dummies.
- MAT_077_O (Ogden Rubber) for Rubber Material Modeling
- Ogden Parameters & Prony Series Parameters for MAT_077_O
- Material Test Matrix for MAT_077_O

HUMANETICS

Introduction (Cont'd)

- Ogden Parameters based on Strain Energy Curves w/ Uniaxial Compression & Tension Test Data
- Effect of Poisson Ratio on Ogden Parameters
- Ogden Parameters based on Stress Curves w/ Uniaxial Compression & Tension Test Data
- Ogden Parameters from Stress Curves w/ Uniaxial Compression & Tension + Planar Tension + Equi-biaxial Tension Test Data

HUMANETICS

Introduction (Cont'd)

- Prony Series Parameters from Short Term Compression Relaxation Test
- Coupon simulations – Compression 0.01 /s, Compression relaxation (20% strain), Tension 0.01 /s, Tension 0.1 /s, Tension 1 /s, Tension 10 /s, Tension 100 /s

HUMANETICS

MAT_077_O (Ogden Rubber)

TITLE								
Rubber								
MID	RO	PR	N	NV	G	SIGF	REF	CONST
5	1.19E-6	0.4984	0	0			---	6
MU1	MU2	MU3	MU4	MU5	MU6	MU7	MU8	
-1.21E-5	-3.23E-5	0.0001814	0.0005796	0.0009076	0.0003867	0.0002516	7.8E-6	
ALPHA1	ALPHA2	ALPHA3	ALPHA4	ALPHA5	ALPHA6	ALPHA7	ALPHA8	
-3.8069	-0.04	0.9784	0.9551	1.7752	1.0143	0.1649	1.0151	
GI	BETAI							
0.0007614	0.008							
0.0008273	0.1082							
0.0004976	0.0021							
0.0004776	0.0982							
1.7E-6	10.9877							
5.83E-5	0.0822							

RO : Mass Density
PR : Poisson Ratio
MUi : the ith shear modulus
ALPHAi : the ith exponent
GI : the ith shear relaxation modulus of Prony Series
BETAI : the ith decay constant of Prony Series

HUMANETICS

Material Test Matrix for MAT_077_O

Material Test Matrix for Ogden Rubber

Compression	Tension	Planar Tension	Biaxial Tension	Short Term Compression Relaxation	Volumetric Compression
0.01 /s	0.01 /s	0.01 /s	0.01 /s	20% strain, 10 ms rampup	0.01 /s
0.1 /s	0.1 /s				
1 /s	1 /s				
10 /s	10 /s				
100 /s	100 /s				
		Required test conditions			

HUMANETICS

Compression Test Setup

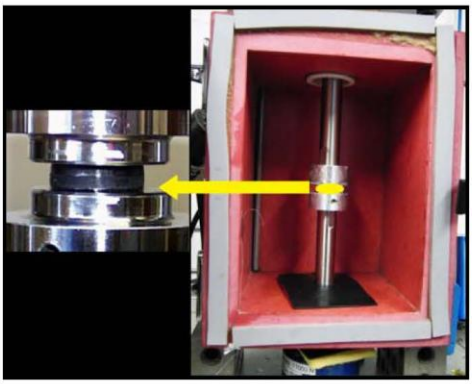

HUMANETICS

Tension Test Setup

HUMANETICS

Pure Shear / Planar Tension Test Setup

HUMANETICS

Equi-Biaxial Tension Test Setup

HUMANETICS

Strain Energy-Based Ogden Model

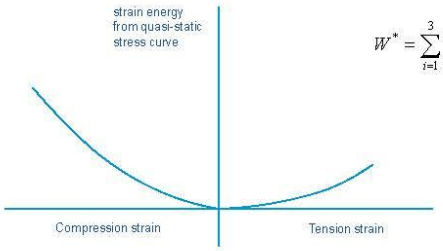

$$W^* = \sum_{i=1}^{3}\sum_{j=1}^{n}\frac{\mu_j}{\alpha_j}(\lambda_i^{*\alpha_j} - 1) + \frac{K}{2}(J-1)^2$$

$$J = \lambda_1\lambda_2\lambda_3 = \frac{V}{V_0}$$

$$\lambda_i^* = J^{-1/3}\lambda_i$$

$$\frac{\Delta V}{V_0} = \left(1 + \frac{\Delta L}{L_0}\right)^{1-2\nu} - 1$$

$$\mu_1, \mu_2, \ldots, \mu_n, \alpha_1, \alpha_2, \ldots, \alpha_n$$

To be determined

HUMANETICS

Rubber Strain Energy Curve Fitting – Poisson Ratio 0.499

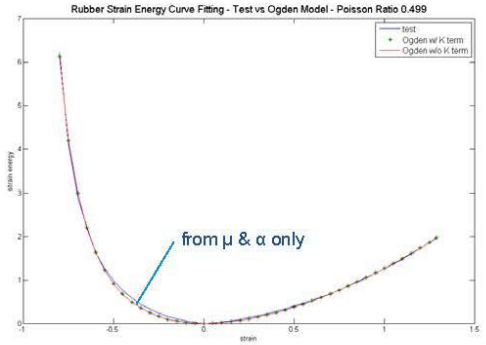

HUMANETICS
Innovative Solutions

Rubber Strain Energy Curve Fitting – Poisson Ratio 0.495

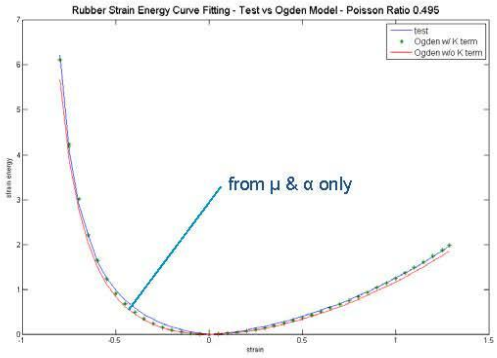

HUMANETICS
Innovative Solutions

Rubber Strain Energy Curve Fitting – Poisson Ratio 0.49

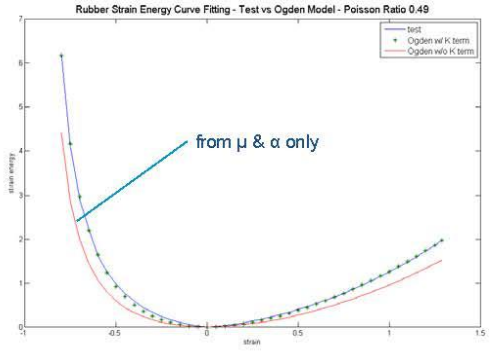

HUMANETICS

Stress-Based Ogden Model

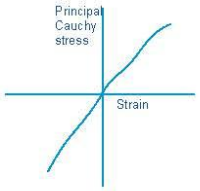

Quasi-static true stress-strain test curve

$$\sigma_i = \frac{1}{\lambda_j \lambda_k}\frac{\partial w}{\partial \lambda_i} = \sum_{j=1}^{n}\frac{\mu_j}{J}\left[\lambda_i^{*\alpha_j} - \sum_{k=1}^{3}\frac{\lambda_k^{*\alpha_j}}{3}\right] + K(J-1)$$

$$\mu_1, \mu_2, \ldots, \mu_n, \alpha_1, \alpha_2, \ldots, \alpha_n$$

To be determined

Uniaxial test – Principal Stretches

$$\sigma_1 = \frac{1}{\lambda_2 \lambda_3}\frac{\partial w}{\partial \lambda_1} = \frac{2}{3}\sum_{j=1}^{n}\frac{\mu_j}{J}\left[\lambda_1^{*\alpha_j} - \lambda_2^{*\alpha_j}\right] + K(J-1)$$

$\lambda_1 = l/L_0 = 1+\varepsilon_{eng}$ $\quad \lambda_2 = \lambda_3 = \sqrt{\frac{J}{\lambda_1}}$ $\quad \lambda_i^* = \lambda_i / J^{1/3}$

HUMANETICS

Rubber Uniaxial Stress Curve Fitting w/ J=1

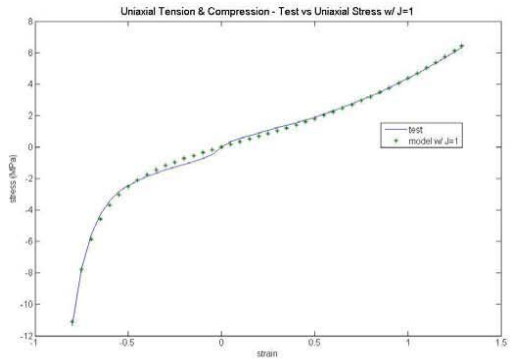

HUMANETICS

Rubber Uniaxial Stress Curve Fitting – Poisson Ratio 0.499

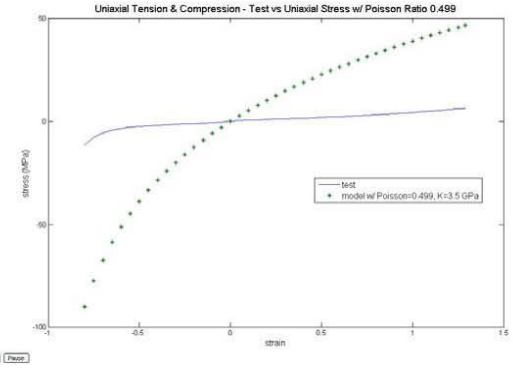

HUMANETICS

Engineering Stress Equation in terms of Stretch (J=1)

Uniaxial Tension & Compression $\lambda_1 = \lambda,\ \lambda_2 = \lambda_3 = \lambda^{-\frac{1}{2}}$

Pure Shear or Planar Tension $\lambda_1 = \lambda, \lambda_2 = 1, \lambda_3 = \lambda^{-1}$

Equibiaxial Tension $\lambda_1 = \lambda_2 = \lambda, \lambda_3 = \lambda^{-2}$

Engineering Stress $$\sigma = \sum_{n=1}^{N} \mu_n [\lambda^{-1+\alpha_n} - \lambda^{-1+C\alpha_n}]$$

where

$C = -1/2$	*uniaxial tension or compression*
-1	*pure shear or planar tension*
-2	*equibiaxial tension*

HUMANETICS

Rubber Uniaxial Stress Curve Fitting w/ J=1

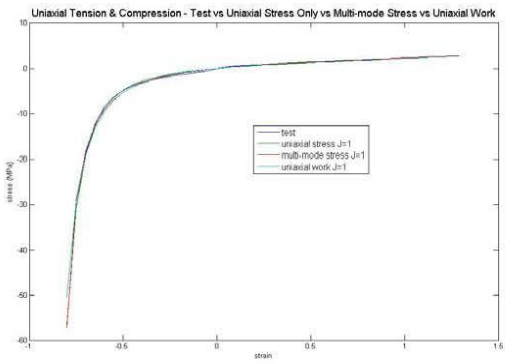

HUMANETICS

Rubber Equibiaxial Tension Stress Curve Fitting w/ J=1

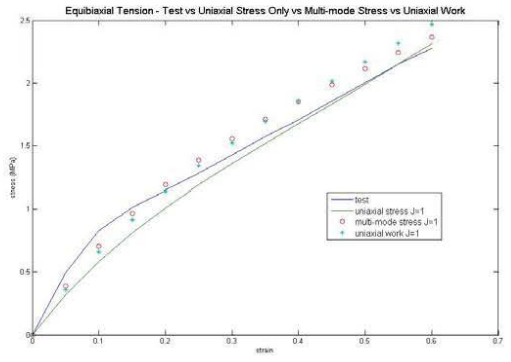

HUMANETICS
Innovative Solutions

Rubber Planar Tension Stress Curve Fitting w/ J=1

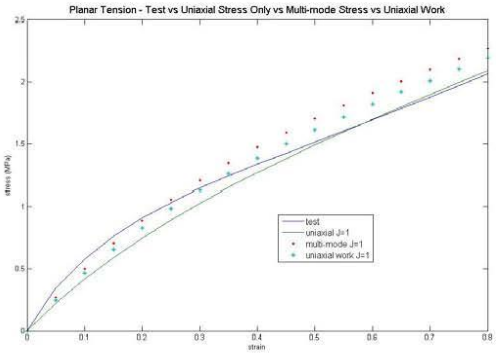

HUMANETICS
Innovative Solutions

Stress Relaxation – Prony Series Parameters

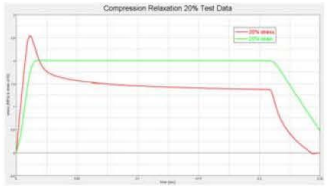

Rate effects are taken into account through linear viscoelasticity by a convolution integral of the form:

$$\sigma_{ij} = \int_0^t g_{ijkl}(t-\tau)\frac{\partial E_{kl}}{\partial \tau}\,d\tau$$

This stress is added to the stress tensor determined from the strain energy functional.

If we wish to include only simple rate effects, the relaxation function is represented by six terms from the Prony series:

$$g(t) = \alpha_0 + \sum_{n=1}^{N} \alpha_n e^{-\beta_n}$$

given by,

$$g(t) = \sum_{i=1}^{n} G_i e^{-\beta_i}$$

HUMANETICS

Stress Equation – Stress Relaxation

$$\sigma_{11} = \sum_{n=1}^{N} \frac{\mu_n}{J}[\lambda_1^{*\alpha_n} - \frac{1}{3}(\lambda_1^{*\alpha_n} + \lambda_2^{*\alpha_n} + \lambda_3^{*\alpha_n})] + K(J-1)$$

$$+ 2(1+\nu)\int_0^t \sum_{i=1}^{n} G_i e^{-\beta_i(t-\tau)} \frac{\partial e_{11}}{\partial \tau}\,d\tau$$

To be determined

$$G_1, G_2, \ldots, G_n, \beta_1, \beta_2, \ldots, \beta_n$$

HUMANETICS

Relaxation Test Data Curve

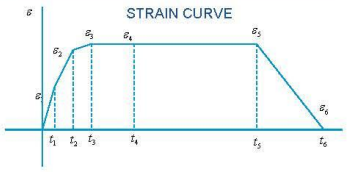

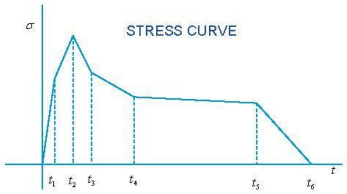

$$\sigma_P = \int_0^t G(t-\tau)\frac{\partial \varepsilon}{\partial \tau}d\tau = \int_0^t \sum_{i=1}^{M} G_i e^{-\beta_i(t-\tau)}\frac{\partial \varepsilon}{\partial \tau}d\tau$$

$0 \le t \le t_1 \quad \alpha = \frac{\varepsilon_1}{t_1} = \alpha_1$

$t_1 \le t \le t_2 \quad \alpha = \frac{\varepsilon_2 - \varepsilon_1}{t_2 - t_1} = \alpha_2$

$t_2 \le t \le t_3 \quad \alpha = \frac{\varepsilon_3 - \varepsilon_2}{t_3 - t_2} = \alpha_3$

$t_3 \le t \le t_4 \quad \alpha = \frac{\varepsilon_4 - \varepsilon_3}{t_4 - t_3} = \alpha_4$

$t_3 \le t \le t_4 \quad \alpha = \frac{\varepsilon_5 - \varepsilon_4}{t_5 - t_4} = \alpha_5$

$t_6 \le t \le t_5 \quad \alpha = \frac{\varepsilon_6 - \varepsilon_5}{t_6 - t_5} = \alpha_6$

HUMANETICS

Stress Relaxation Equations w/ Prony Series

$0 \le t \le t_1$

$$\sigma_P(t) = \int_0^t [\sum_{i=1}^{N} G_i e^{-\beta_i(t-\tau)}]\alpha_1 d\tau$$

$t_1 \le t \le t_2$

$$\sigma_P(t) = \int_0^{t_1} [\sum_{i=1}^{N} G_i e^{-\beta_i(t-\tau)}]\alpha_1 d\tau + \int_{t_1}^{t} [\sum_{i=1}^{N} G_i e^{-\beta_i(t-\tau)}]\alpha_2 d\tau$$

$t_2 \le t \le t_3$

$$\sigma_P(t) = \int_0^{t_1} [\sum_{i=1}^{N} G_i e^{-\beta_i(t-\tau)}]\alpha_1 d\tau + \int_{t_1}^{t_2} [\sum_{i=1}^{N} G_i e^{-\beta_i(t-\tau)}]\alpha_2 d\tau + \int_{t_2}^{t} [\sum_{i=1}^{N} G_i e^{-\beta_i(t-\tau)}]\alpha_3 d\tau$$

$t_3 \le t \le t_4$

$$\sigma_P(t) = \int_0^{t_1} [\sum_{i=1}^{N} G_i e^{-\beta_i(t-\tau)}]\alpha_1 d\tau + \int_{t_1}^{t_2} [\sum_{i=1}^{N} G_i e^{-\beta_i(t-\tau)}]\alpha_2 d\tau + \int_{t_2}^{t_3} [\sum_{i=1}^{N} G_i e^{-\beta_i(t-\tau)}]\alpha_3 d\tau + \int_{t_3}^{t} [\sum_{i=1}^{N} G_i e^{-\beta_i(t-\tau)}]\alpha_4 d\tau$$

$t_4 \le t \le t_5$

$$\sigma_P(t) = \int_0^{t_1} [\sum_{i=1}^{N} G_i e^{-\beta_i(t-\tau)}]\alpha_1 d\tau + \int_{t_1}^{t_2} [\sum_{i=1}^{N} G_i e^{-\beta_i(t-\tau)}]\alpha_2 d\tau + \int_{t_2}^{t_3} [\sum_{i=1}^{N} G_i e^{-\beta_i(t-\tau)}]\alpha_3 d\tau + \int_{t_3}^{t_4} [\sum_{i=1}^{N} G_i e^{-\beta_i(t-\tau)}]\alpha_4 d\tau + \int_{t_4}^{t} [\sum_{i=1}^{N} G_i e^{-\beta_i(t-\tau)}]\alpha_5 d\tau$$

$t_5 \le t \le t_6$

$$\sigma_P(t) = \int_0^{t_1} [\sum_{i=1}^{N} G_i e^{-\beta_i(t-\tau)}]\alpha_1 d\tau + \int_{t_1}^{t_2} [\sum_{i=1}^{N} G_i e^{-\beta_i(t-\tau)}]\alpha_2 d\tau + \int_{t_2}^{t_3} [\sum_{i=1}^{N} G_i e^{-\beta_i(t-\tau)}]\alpha_3 d\tau + \int_{t_3}^{t_4} [\sum_{i=1}^{N} G_i e^{-\beta_i(t-\tau)}]\alpha_4 d\tau + \int_{t_4}^{t_5} [\sum_{i=1}^{N} G_i e^{-\beta_i(t-\tau)}]\alpha_5 d\tau + \int_{t_5}^{t} [\sum_{i=1}^{N} G_i e^{-\beta_i(t-\tau)}]\alpha_6 d\tau$$

HUMANETICS

Stress Relaxation Curve Fitting w/ Ogden+Prony Series (J=1)

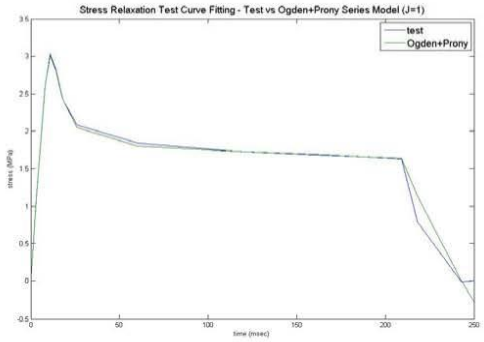

HUMANETICS

Stress Relaxation Curve Fitting w/ Ogden+Prony Series (Poisson Ratio 0.499)

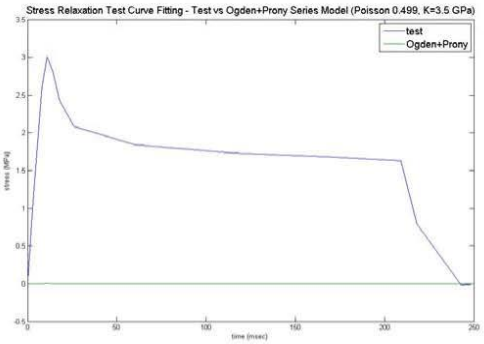

HUMANETICS

Stress Relaxation Curve Fitting w/ Prony Series Only

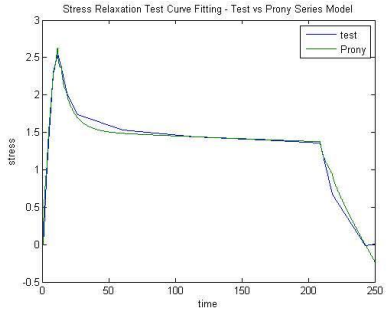

HUMANETICS

Stress Relaxation Curve Fitting in Excel – Direct Integration (Convolution Integral)

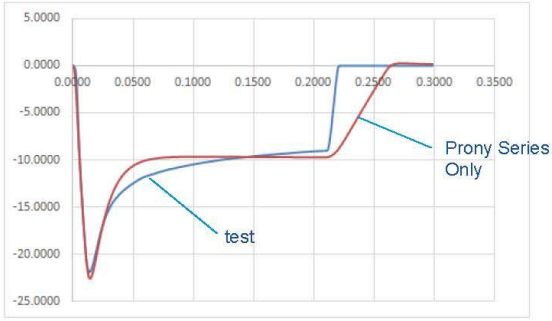

HUMANETICS

Compression Coupon Simulation Model

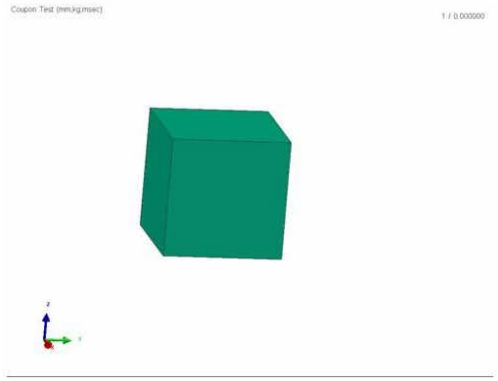

HUMANETICS

Tension Coupon Simulation Model

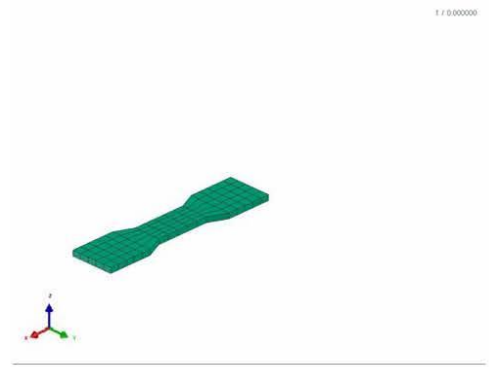

HUMANETICS

Rubber Compression Coupon Simulation – 0.01 /s

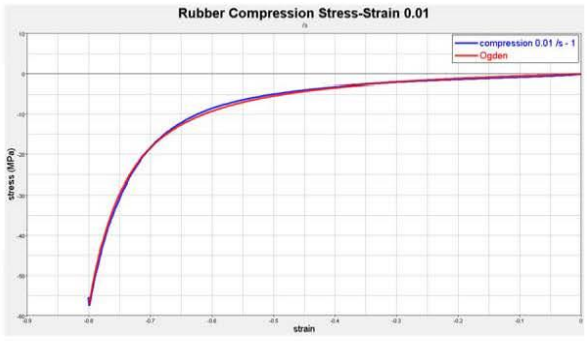

HUMANETICS

Rubber Compression Relaxation Coupon Simulation – 20% Strain

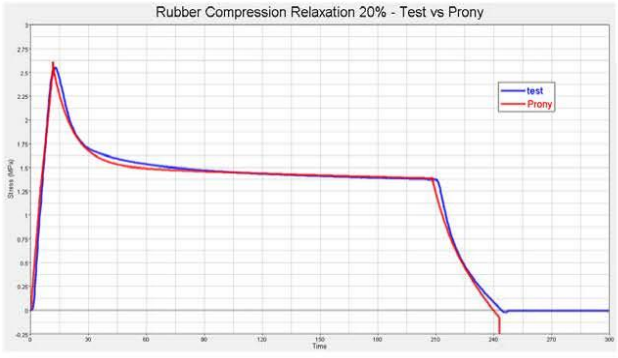

HUMANETICS

Rubber Tension Coupon Simulation – 0.01 /s

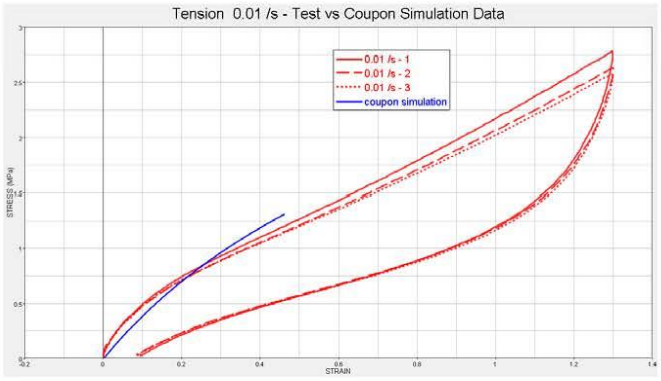

HUMANETICS
Innovative Solutions

Rubber Tension Coupon Simulation – 0.1 /s

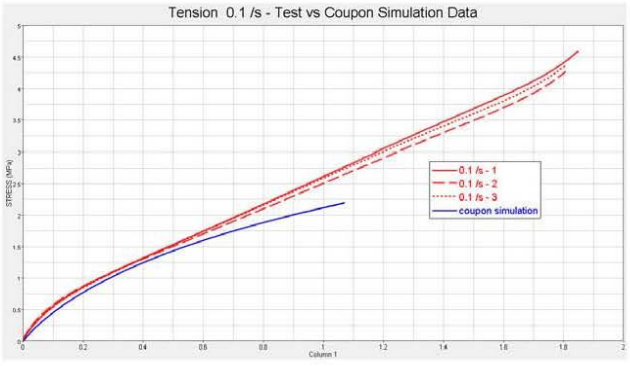

HUMANETICS
Innovative Solutions

Rubber Tension Coupon Simulation – 1 /s

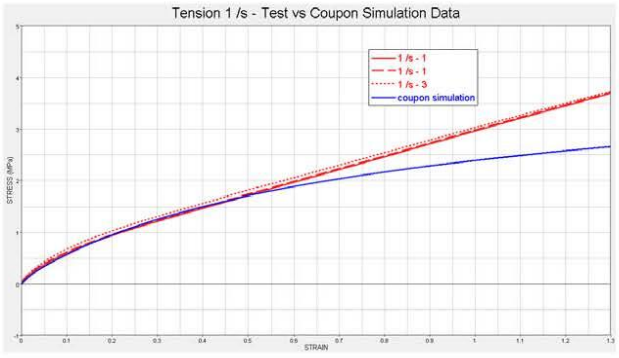

HUMANETICS
Innovative Solutions

Rubber Tension Coupon Simulation – 10 /s

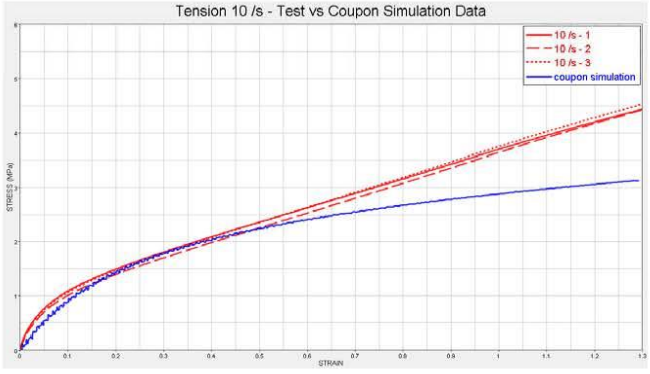

HUMANETICS
Innovative Solutions

Rubber Tension Coupon Simulation – 100 /s

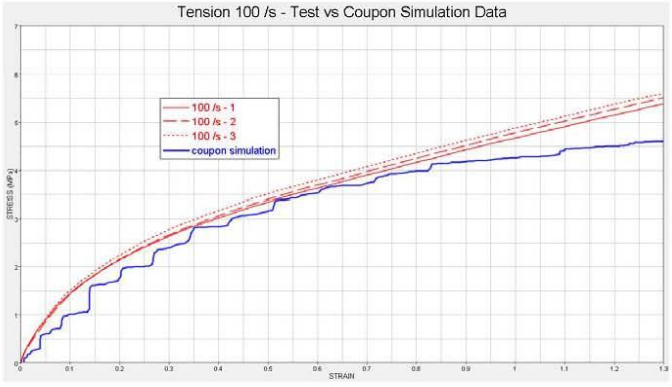

HUMANETICS

Discussions & Conclusions

- Poisson ratio plays an important role in obtaining Ogden parameters μ & α from strain energy curve fitting.
- Stress curve fitting for Ogden parameters μ & α does not converge even with the Poisson ratio 0.499. Only with J=1, stress curve fitting converges.
- With J=1, Ogden parameters μ & α from strain energy equation, uniaxial stress equation and multi-mode stress equations create similar stress-strain curve fitting to test data curve.
- For dynamic stress relaxation curve fitting to obtain G_i & β_i , J=1 should be assumed if the quasi-static term is considered in the stress equation. If not, curve fitting for G_i & β_i , does not converge even with the Poisson ratio 0.499.

HUMANETICS

Discussions & Conclusions (cont'd)

- To consider the Poisson ratio in obtaining the Prony series parameters $G_i \& \beta_i$, the quasi-static term should be dropped from dynamic stress equation in curve fitting.
- The Prony series parameters $G_i \& \beta_i$ are directly obtained from the compression stress relaxation test curve fitting.
- In the compression relaxation coupon simulation, initial curve fitting parameters $G_i \& \beta_i$ do not make good matching over relaxation range. Therefore, the relaxation portion in the test data should be modified by scaling down the relaxation region, based on experience. Then curve fitting needs to be done with the modified relaxation test curve.

HUMANETICS

Discussions & Conclusions (cont'd)

- For coupon simulation, started with compression 0.01 /s. One or two times, Poisson ratio or K values may be tuned to obtain μ & α, which means curve fitting again with compression-tension 0.01 /s test curve.
- Then, relaxation coupon simulation is done with the μ & α and $G_i \& \beta_i$ parameters. If the simulation result is reasonable, continue with tension strain rate 0.01 /s, 0.1 /s, 1 /s, 10 /s and 100 /s cases.
- For coupon simulation tension 0.01 /s, simulation can not be done up to 130% strain due to instability.
- For coupon simulation tension 0.1 /s, simulation can not be done up to 130% strain due to instability.
- For coupon simulation tension 1 /s, simulation can be done up to 130% strain without instability.
- For coupon simulation tension 10 /s, simulation can be done up to 130% strain without instability.
- For coupon simulation tension 100 /s, simulation can be done up to 130% strain with some instability due to vibration issues seen in kinematics.

HUMANETICS

Discussions & Conclusions (cont'd)

- In all coupon simulations, it could be observed that rate effects were reflected with G_i & β_i and simulation curves are close to test curves up to around 50% strain.
- To resolve instability in tension 0.01 /s, 0.1 /s and 100 /s, parameters can be tuned by doing curve fitting again with different Poisson ratio and K values. Also, meshing and coupon geometry can be considered for modification to prevent from instability.

- Through this study, a practical method for Ogden rubber model has been developed.
- Strain rate effect could be realized with Prony series parameters from curve fitting in coupon simulations.
- The minimum required material testing conditions were determined for Ogden rubber material model.

HUMANETICS

PUBLIC RELEASE-DISTRIBUTION UNLIMITED

US ARMY RDECOM U.S. Army Research, Development and Engineering Command

Effect of Strain Rate on the Compressive Response of ATD Neck and Foot Rubber Under Different Loading Sequences

ARL

TECHNOLOGY DRIVEN. WARFIGHTER FOCUSED.

Brett Sanborn and Tusit Weerasooriya

Workshop on Numerical Analysis of Human and Surrogate Response to Accelerative Loading
January 2013

PUBLIC RELEASE-DISTRIBUTION UNLIMITED

US ARMY RDECOM PUBLIC RELEASE-DISTRIBUTION UNLIMITED ARL

Background

- Anthropomorphic test dummies (ATD's) used in automotive and aircraft industries as test devices
- First ATD's used in 1949
  - "Sierra Sam" used to test ejection seats
- ATD's used in automobile tests in 1972
  - Hybrid II (HII) developed by General Motors
  - Evolved into the Hybrid III (HIII) in 1976
- Different rubbers are used on the HIII to simulate different parts of the human body
- New goal is to develop a new dummy for use in blast testing

http://www.secretsdeclassified.af.mil/shared/media/photodb/photos/570101-F-7892W-007.jpg

TECHNOLOGY DRIVEN. WARFIGHTER FOCUSED.

PUBLIC RELEASE-DISTRIBUTION UNLIMITED

PUBLIC RELEASE-DISTRIBUTION UNLIMITED

Motivation

- Experiments are needed to develop constitutive models used in simulation
- Accelerative loadings seen in blast occur at high loading rates
- Accurate simulation requires experiments that are conducted at these relevant loading rates

Current work: Evaluate **Neck** and **Foot** rubber from Humanetics HIII 50th percentile male dummy at different loading rates and sequences

TECHNOLOGY DRIVEN. WARFIGHTER FOCUSED. 3

PUBLIC RELEASE-DISTRIBUTION UNLIMITED

PUBLIC RELEASE-DISTRIBUTION UNLIMITED

Materials

Neck and Foot rubber sheets of the same type used in the HIII dummy

Neck Rubber:
- Butyl Rubber
- Durometer: 70-80

Foot Rubber:
- Vinyl Rubber
- Durometer: 37.3 ±0.9

Heel Pad Rubber:
- Durometer: 27.3 ±0.6

Skin (vinyl) Rubber:
- Durometer: 58.5 ± 0.6

Tibia Rubber:
- Durometer: 69.3 ± 0.6

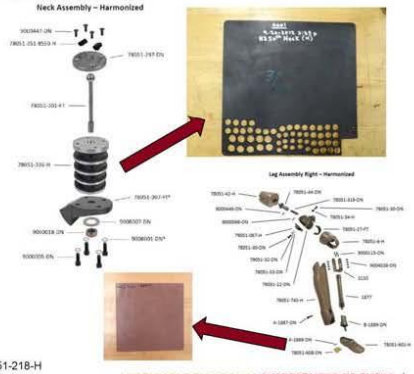

Hybrid III 50th Male Dummy Parts Catalogue. 78051-218-H
Humanetics. FMVSS208, 49CFR Part 572, Subpart E

TECHNOLOGY DRIVEN. WARFIGHTER FOCUSED. 4

PUBLIC RELEASE-DISTRIBUTION UNLIMITED

Experiments

Experiments conducted on both Neck and Foot Rubbers

- Uniaxial Compression
  - Quasi-static
  - Intermediate
  - High-rate
- Stress Relaxation
  - Load at constant strain rate and hold for a predetermined time
- Compression Dynamic Mechanical Analysis (DMA)
  - Isothermal frequency sweeps at different mean strain and strain amplitudes
  - Storage and Loss moduli as a function of frequency
- Tensile DMA
  - Temperature sweeps at constant frequency
  - Storage and Loss moduli as a function of temperature as well as glass transition temperature

Number of Experiments

Strain Rate [1/s]	Uniaxial Compression	Stress Relaxation	Compression DMA	Tensile DMA
0.001	5	5	5 (isothermal frequency sweep)	5 (temperature sweep)
1	5	5		
500	5			
1100-1300	5			
1200-2200	5			

Experimental Setups

- Quasi-static and Intermediate Rates
  - Bose Electroforce Testbench
- Compression DMA (BOSE)
  - Frequency Sweep DMA capability – up to 200 Hz
- Tensile DMA (DMA Q800)
- Compression Kolsky Bar/split Hopkinson pressure bar

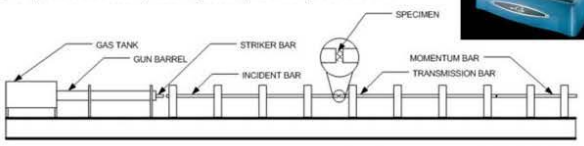

PUBLIC RELEASE-DISTRIBUTION UNLIMITED

Radial Inertia

- Inertia in the radial direction is a concern when testing soft materials such as rubber using at high strain rates using the Kolsky Bar
- Extra stress due to radial inertia is measured in the axial direction
- For soft materials with low stiffness such as rubber, the extra stress can overshadow the intrinsic material response
- Estimate of radial inertia induced stress is provided by Warren and Forrestal:

$$\sigma_i = \frac{3\rho_s r^2}{16(1-\varepsilon_x)^3}\dot{\varepsilon}_x^{\,2} + \frac{\rho_s r^2}{8(1-\varepsilon_x)^2}\ddot{\varepsilon}_x$$

  - Dependent on density, radius, strain rate (squared term), and especially maximum strain (cubed term)
- For **Neck** (ρ = 1250 kg/m^3, ε_x = 0.58, $\varepsilon_{x\ dot}$ = 2300 s^{-1} and r = 4) and **Foot** (ρ = 1150 kg/m^3, ε_x = 0.41, $\varepsilon_{x\ dot}$ = 2200 s^{-1} and r = 5)
- **Neck** σ_i = **0.270 MPa** => Actual response = **100 MPa** (0.27%)
- **Foot** σ_i = **0.127 MPa** => Actual response = **8 MPa** (1.6%)
- Foot rubber is at the lower end of what is an acceptable level of radial inertia stress

Ignore Inertia Stress

Warren, T.L., Forrestal, M.J. Comments on the effect of radial inertia in the Kolsky bar test for an incompressible material. Experimental Mechanics, 2010.

PUBLIC RELEASE-DISTRIBUTION UNLIMITED

PUBLIC RELEASE-DISTRIBUTION UNLIMITED

Results

- Pulse shaping used to achieve constant strain rate

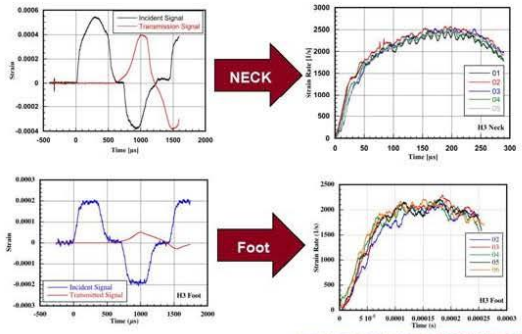

PUBLIC RELEASE-DISTRIBUTION UNLIMITED

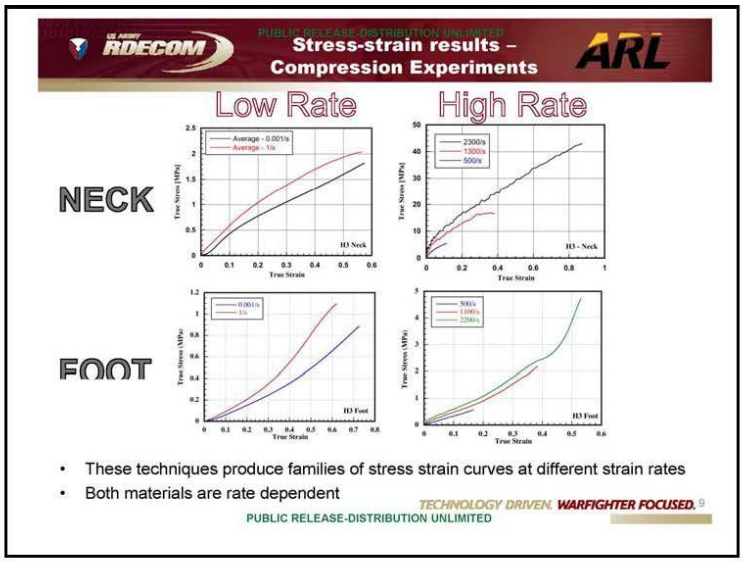
PUBLIC RELEASE-DISTRIBUTION UNLIMITED
RDECOM
Stress-strain results – Compression Experiments
ARL
Low Rate
High Rate
NECK
FOOT
Average - 0.001/s
Average - 1/s
2300/s
1300/s
500/s
H3 Neck
H3 - Neck
H3 Foot
True Stress [MPa]
True Strain
• These techniques produce families of stress strain curves at different strain rates
• Both materials are rate dependent
TECHNOLOGY DRIVEN. WARFIGHTER FOCUSED. 9
PUBLIC RELEASE-DISTRIBUTION UNLIMITED

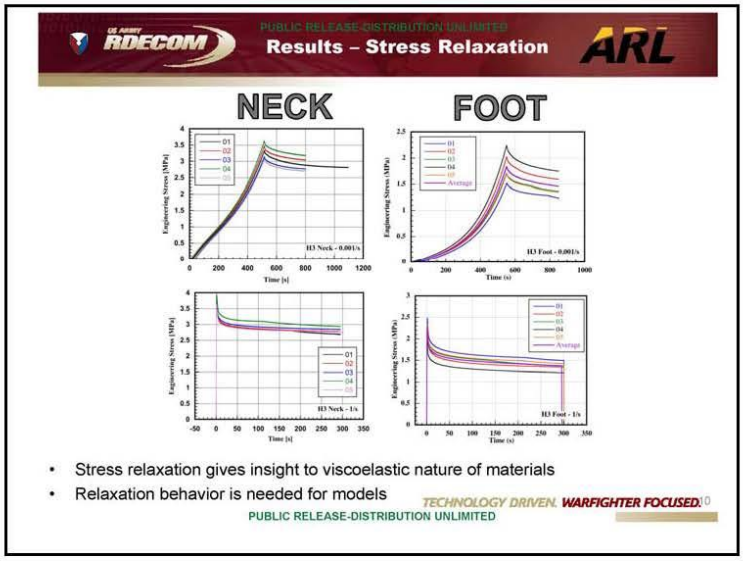
PUBLIC RELEASE-DISTRIBUTION UNLIMITED
RDECOM
Results – Stress Relaxation
ARL
NECK
FOOT
H3 Neck - 0.001/s
H3 Foot - 0.001/s
H3 Neck - 1/s
H3 Foot - 1/s
Engineering Stress [MPa]
Time [s]
Average
• Stress relaxation gives insight to viscoelastic nature of materials
• Relaxation behavior is needed for models
TECHNOLOGY DRIVEN. WARFIGHTER FOCUSED. 10
PUBLIC RELEASE-DISTRIBUTION UNLIMITED

PUBLIC RELEASE-DISTRIBUTION UNLIMITED

DMA Results

- Compression DMA results from isothermal frequency sweep
- Tensile DMA results provide glass transition temperature and storage and loss modulus
- These data are used when calibrating numerical models

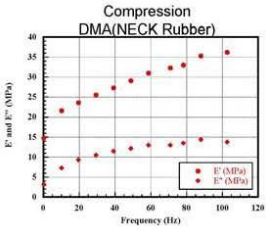

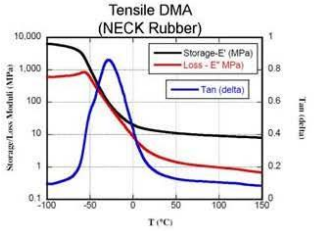

PUBLIC RELEASE-DISTRIBUTION UNLIMITED

PUBLIC RELEASE-DISTRIBUTION UNLIMITED

Bergstrom Boyce (BB) Model for Neck Rubber

- Two-part hyperelastic model
  - A: Equilibrium response with hyperelastic element
  - B: Time-dependent response with hyperelastic element in series

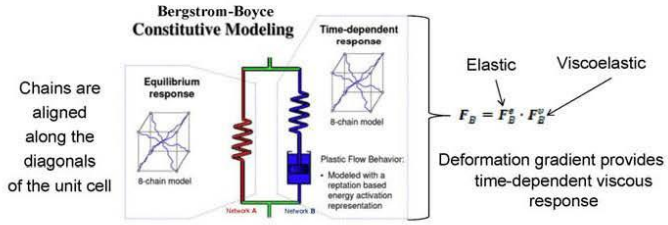

J. S. Bergstrom and M. C. Boyce. Constitutive modeling of the large strain time-dependent behavior of elastomers. J. Mech. Phys. Solids, 46:931–954, 1998.

PUBLIC RELEASE-DISTRIBUTION UNLIMITED

Determine Model Parameters

- For the uniaxial loading experiments, the Cauchy stress is defined as:

$$\sigma = \sigma_A + \sigma_B$$

- Where σ_A and σ_B are

$$\sigma_A = \frac{\mu}{\bar{\lambda}} \frac{\mathcal{L}^{-1}\left(\bar{\lambda}/\lambda_L\right)}{\mathcal{L}^{-1}\left(1/\lambda_L\right)}\left[F^2 - \frac{1}{F}\right] \qquad \sigma_B = \frac{s\mu}{\bar{\lambda}_B^v} \frac{\mathcal{L}^{-1}\left(\bar{\lambda}_B^v/\lambda_L\right)}{\mathcal{L}^{-1}\left(1/\lambda_L\right)}\left[(F_B^e)^2 - \frac{1}{F_B^e}\right]$$

Parameters:

s – shear modulus of network B compared to A

μ – shear modulus

λ_L – limiting chain stretch

$\mathcal{L}(x) = \coth(x) - 1/x$ (Langevin function)

$$\mathcal{L}^{-1}(x) \approx \begin{cases} 1.31446\tan(1.58986x) + 0.91209x, & \text{if } |x| < 0.84136 \\ 1/(sign(x) - x, & \text{If } 0.84136 \le |x| < 1 \end{cases}$$

Strain-Stretch:

$$\bar{\lambda} = \sqrt{\frac{1}{3}\left[(F)^2 + \frac{2}{F}\right]} \qquad \bar{\lambda}_B^v = \sqrt{\frac{1}{3}\left[(F_B^e)^2 + \frac{2}{F_B^e}\right]}$$

Viscous Flow

Rate equation for viscous flow in B

Where: $\dot{\gamma}_B^v = \dot{\gamma}_0(\overline{\lambda_B^v} - 1 + \xi)^C \left[R\left(\frac{2|\sigma_B|}{3\tau_{base}} - \hat{\tau}_{cut}\right)\right]^m$

$$\overline{\lambda_B^v} = \sqrt{\frac{1}{3}\left[(F_B^v)^2 + \frac{2}{F_B^v}\right]}$$

Deformation gradient becomes:

$$\dot{F}_B^v = \dot{\gamma}_B^v \ \text{sign}[\sigma_B] F_B^v$$

And:

$\dot{\gamma}_0 = 1/s$ - constant for dimensional consistency

$R(x) = (x + |x|)/2$ – ramp function

$\hat{\tau}_{cut}$ - cut off stress where no flow occurs

ξ - strain adjustment factor

C - strain exponent

τ_{base} - flow resistance

m - stress exponent

Parameters to optimize using experimental results

Optimization Results

- 1 s^{-1}, 500^{-1}, 1300^{-1}, 2300^{-1} (High Rate biased) model with DMA vibratory response

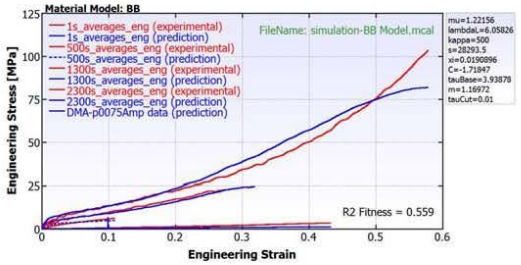

Optimization Results

- 0.001 s^{-1}, 1 s^{-1}, 500 s^{-1} High Rate biased model with DMA vibratory response

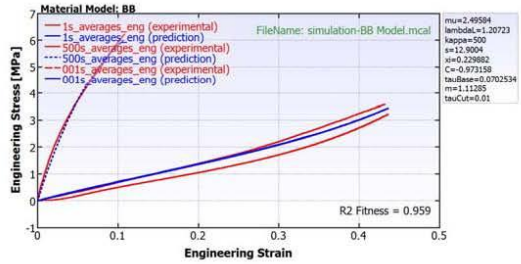

Parameters for different cases

Model constants for **Neck** rubber using BB model for different loading rate scenarios:

Model Parameter Description	CASE	A1 Impact-rates	B1 Blast-Rates	C1 Auto-Rates	A2 Impact-Rates (+Cyclic)	B2 Blast-Rates (+Cyclic)	C2 Auto-Rates (+Cyclic)
	Model Constants	2300, 1300, 500, 1/s	500, 1, 0.001/s	1, 0.001/s	2300, 1300, 500, 1/s, {E', E''}-freq	500, 1, 0.001/s, {E', E''}-freq	1, 0.001/s {E', E''}-freq
Shear modulus of network A (MPa)	μ	1.22156	2.49584	2.17583	1.22156	2.17881	2.17583
Locking stretch	λ_L	6.05826	1.20723	1.18675	6.05826	1.15367	1.18675
Bulk Modulus (MPa)	κ	500	500	500	500	500	500
Stiffness of Network B relative to A	s	28293.5	12.9004	7.21539	28293.5	9.5676	7.21683
Strain adjustment factor	ξ	0.01909	0.229882	0.317087	0.01909	0.337517	0.317087
Strain exponent	c	-1.71847	-0.97316	-1.01733	-1.71847	-0.95967	-1.01733
Flow resistance (MPa)	τ_{base}	3.93878	0.070253	0.296996	3.93878	0.693538	0.296996
Stress exponent	m	1.16972	1.11285	1.51296	1.16972	1.26362	1.51296
Normalized cut-off stress for flow	$\bar{\tau}^*_{cut}$	0.01	0.01	0.005	0.01	0.01	0.005
R^2 for goodness of fit		0.699	0.959	0.966	0.559	0.712	0.652

Model constants will be obtained for the foot rubber using a similar approach but may require use of a different model

Summary

- Conducted a variety of experiments on HIII neck and foot rubber including quasi-static, intermediate, and high rate compression. Stress relaxation and DMA experiments were also carried out
- The rubber materials were rate dependent and the mechanical response was not overshadowed by radial inertia from the experimental technique
- Model constants were generated for the Neck rubber that predict stress-strain behavior similar to the experimental results
- Current models in LSDYNA do not accurately represent the experimental results

UNCLASSIFIED

U.S. Army Research, Development and Engineering Command

Inertial Effects in Compression and Torsional Kolsky Bar Tests on Soft and Nearly Incompressible Materials

TECHNOLOGY DRIVEN. WARFIGHTER FOCUSED.

Adam Sokolow, John Fitzpatrick, and Mike Scheidler

Inertial Effects in Compression and Torsional Kolsky Bar Tests on Soft and Nearly Incompressible Materials
U.S. Army Research Laboratory
13 Dec 2013

UNCLASSIFIED

UNCLASSIFIED

Motivation

Humans in Extreme Environments

1. To adequately simulate the response of the human body to blast, impact and accelerative loadings, the constitutive response of its tissues must be understood.
2. Soft tissues of the body are typically:
   - viscoelastic
   - non-linear
   - Shear moduli (~1 - 500 kPa)
   - Nearly incompressible (Bulk moduli ~ water , 2.3 GPa)
3. Most of the strain-rate dependence of soft tissues is exhibited by the shear stress (as opposed to the pressure). As we show, the shear stress can be quite difficult to measure in high-rate (~ 1000/s) tests.

Kolsky Bar

- Used with great success to characterize the high strain-rate response of metals and stiff polymers.
- Recently has been used in an attempt to characterize the response of soft tissues and tissue simulants.

UNCLASSIFIED TECHNOLOGY DRIVEN. WARFIGHTER FOCUSED.

Compression Kolsky Bar Split Hopkinson Pressure Bar

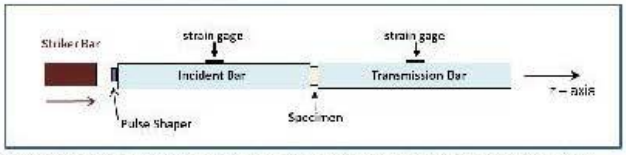

Standard test technique for measuring strain-rate sensitivity of the specimen in a *state of (uniform) uniaxial stress* at moderate-to-large strains.

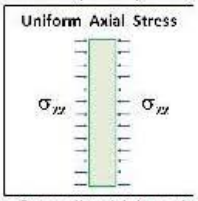

Uniaxial Stress State

Components of stress tensor σ:

$\sigma_{22} > 0$ (positive in compression)

$$\sigma_{rr} = \sigma_{\theta\theta} = 0 \qquad \sigma_{r\theta} = \sigma_{rz} = \sigma_{\theta z} = 0$$

Conventional data analysis depends on these conditions!

Issues for Sufficiently Soft Specimens and Sufficiently High Strain-Rates

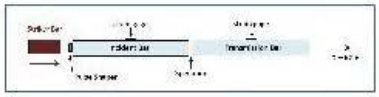

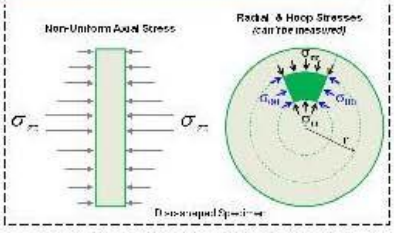

- Because of the presence of radial and hoop stresses, can't extract the deviatoric stress tensor $\boldsymbol{s}$ from the measured (average) axial stress σ_{22}.
- Need $\boldsymbol{s}$ for constitutive models. The components of $\boldsymbol{s}$ are the shear stresses, which contain most of the rate-dependent, viscoelastic response.

Consequences of Radial Inertia of the Specimen

UNCLASSIFIED

Analytical Inertial Estimate

Measured Axial Stress — Axial Component of Deviatoric (shear) Stress — Pressure — Radial Stress — Hoop Stress

$$\sigma_{zz} = s_{zz} + p \qquad p = \frac{1}{3}\left(\sigma_{zz} + \sigma_{rr} + \sigma_{\theta\theta}\right)$$

$$\sigma_{zz} = \frac{3}{2} s_{zz} + \frac{1}{2}\left(\sigma_{rr} + \sigma_{\theta\theta}\right)$$

$$s_{zz} = \frac{2}{3}\left(\sigma_{zz} - \sigma_{rr}\right) \text{ and } s_{rr} = s_{\theta\theta} = -\frac{1}{2} s_{zz} \text{ if } \sigma_{rr} = \sigma_{\theta\theta}$$

Constitutive theoretical

Valid (approximately) for isotropic solid (i.e., disc-shaped) specimens

Analytical inertial estimate for σ_{rr} (based on radial momentum balance) in terms of measured axial strain ε_z and its rates:

$$\sigma_{rr} = \frac{\rho_0 (R_0)^2}{16}\left[\frac{2\ddot{\varepsilon}_z}{(1-\varepsilon_z)^2} + \frac{3(\dot{\varepsilon}_z)^2}{(1-\varepsilon_z)^3}\right]$$

The measured axial stress and this inertial estimate for radial stress yield the components of deviatoric stress (i.e., shear stresses) in the specimen

UNCLASSIFIED

TECHNOLOGY DRIVEN. WARFIGHTER FOCUSED.

UNCLASSIFIED

Analytical Inertial Estimate

Measured Axial Stress — Axial Component of Deviatoric (shear) Stress — Pressure — Radial Stress — Hoop Stress

$$\sigma_{zz} = s_{zz} + p \qquad p = \frac{1}{3}\left(\sigma_{zz} + \sigma_{rr} + \sigma_{\theta\theta}\right)$$

$$\sigma_{zz} = \frac{3}{2} s_{zz} + \frac{1}{2}\left(\sigma_{rr} + \sigma_{\theta\theta}\right)$$

$$s_{zz} = \frac{2}{3}\left(\sigma_{zz} - \sigma_{rr}\right) \text{ and } s_{rr} = s_{\theta\theta} = -\frac{1}{2} s_{zz} \text{ if } \sigma_{rr} = \sigma_{\theta\theta}$$

Constitutive theoretical

Valid (approximately) for isotropic solid (i.e., disc-shaped) specimens

Analytical inertial estimate for σ_{rr} (based on radial momentum balance) in terms of measured axial strain ε_z and its rates:

$$\sigma_{rr} = \frac{\rho_0 (R_0)^2}{16}\left[\frac{2\ddot{\varepsilon}_z}{(1-\varepsilon_z)^2} + \frac{3(\dot{\varepsilon}_z)^2}{(1-\varepsilon_z)^3}\right]$$

The measured axial stress and this inertial estimate for radial stress yield the components of deviatoric stress (i.e., shear stresses) in the specimen

UNCLASSIFIED

TECHNOLOGY DRIVEN. WARFIGHTER FOCUSED.

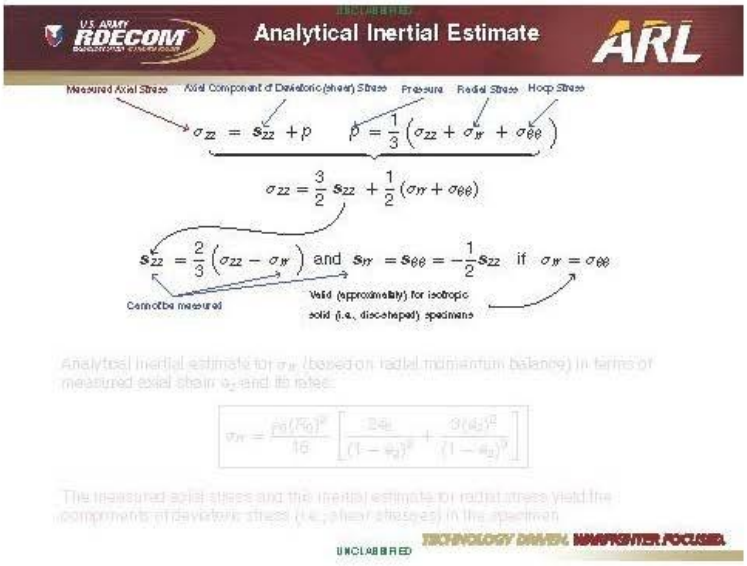
UNCLASSIFIED
U.S. ARMY RDECOM
Analytical Inertial Estimate
ARL
Measured Axial Stress
Axial Component of Deviatoric (shear) Stress
Pressure
Radial Stress
Hoop Stress
$\sigma_{zz} = s_{zz} + p \qquad p = \frac{1}{3}\left(\sigma_{zz} + \sigma_{rr} + \sigma_{\theta\theta}\right)$
$\sigma_{zz} = \frac{3}{2} s_{zz} + \frac{1}{2}\left(\sigma_{rr} + \sigma_{\theta\theta}\right)$
$s_{zz} = \frac{2}{3}\left(\sigma_{zz} - \sigma_{rr}\right)$ and $s_{rr} = s_{\theta\theta} = -\frac{1}{2} s_{zz}$ if $\sigma_{rr} = \sigma_{\theta\theta}$
Cannot be measured
Valid (approximately) for isotropic solid (i.e., disc-shaped) specimens
Analytical inertial estimate for σ_{rr} (based on radial momentum balance) in terms of measured axial strain ϵ_z and its rates:
$\sigma_{rr} = \frac{\rho_0 (R_0)^2}{16}\left[\frac{2\ddot{\epsilon}_z}{(1-\epsilon_z)^2} + \frac{3(\dot{\epsilon}_z)^2}{(1-\epsilon_z)^3}\right]$
The measured axial stress and this inertial estimate for radial stress yield the components of deviatoric stress (i.e., shear stresses) in the specimen.
UNCLASSIFIED
TECHNOLOGY DRIVEN. WARFIGHTER FOCUSED.

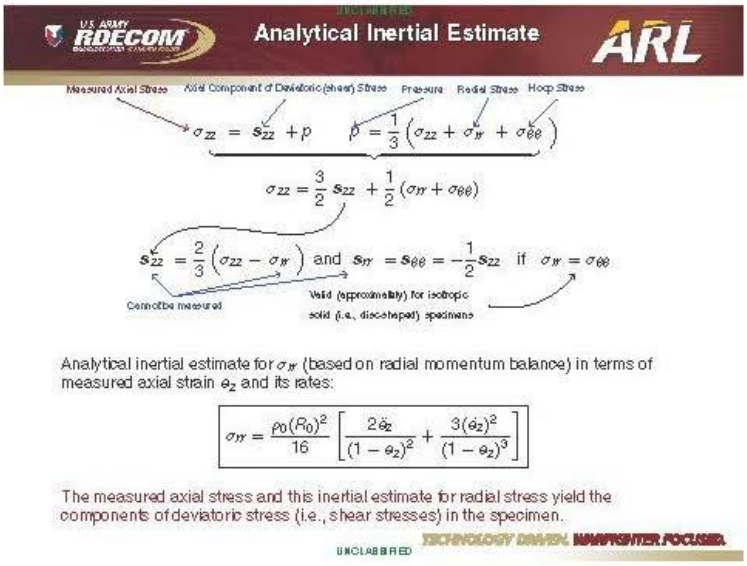
UNCLASSIFIED
U.S. ARMY RDECOM
Analytical Inertial Estimate
ARL
Measured Axial Stress
Axial Component of Deviatoric (shear) Stress
Pressure
Radial Stress
Hoop Stress
$\sigma_{zz} = s_{zz} + p \qquad p = \frac{1}{3}\left(\sigma_{zz} + \sigma_{rr} + \sigma_{\theta\theta}\right)$
$\sigma_{zz} = \frac{3}{2} s_{zz} + \frac{1}{2}\left(\sigma_{rr} + \sigma_{\theta\theta}\right)$
$s_{zz} = \frac{2}{3}\left(\sigma_{zz} - \sigma_{rr}\right)$ and $s_{rr} = s_{\theta\theta} = -\frac{1}{2} s_{zz}$ if $\sigma_{rr} = \sigma_{\theta\theta}$
Cannot be measured
Valid (approximately) for isotropic solid (i.e., disc-shaped) specimens
Analytical inertial estimate for σ_{rr} (based on radial momentum balance) in terms of measured axial strain ϵ_z and its rates:
$\sigma_{rr} = \frac{\rho_0 (R_0)^2}{16}\left[\frac{2\ddot{\epsilon}_z}{(1-\epsilon_z)^2} + \frac{3(\dot{\epsilon}_z)^2}{(1-\epsilon_z)^3}\right]$
The measured axial stress and this inertial estimate for radial stress yield the components of deviatoric stress (i.e., shear stresses) in the specimen.
UNCLASSIFIED
TECHNOLOGY DRIVEN. WARFIGHTER FOCUSED.

UNCLASSIFIED

How Do We Know When This Works?

Note: We cannot check against experimental data because the stress components we are estimating cannot be measured — that's the reason for the estimates in the first place!

We compare our estimates for the radial, hoop, and deviatoric stress components against numerical simulations of the Kolsky bar test, since simulations provide the full stress state.
This has been done for a range of:

- specimen constitutive models
- material parameters
- specimen geometries
- peak strain-rates
- strain-rate histories (i.e., loading pulse shapes)

Example on the next two slides.

UNCLASSIFIED

Example of Comparison with Simulations

Nonlinear Viscoelastic Model Used in These Simulations
(approximate stiffness of Brain Tissue)

Stress relaxation function $G(t)$ decreases from an *instantaneous shear modulus* of 31 kPa to an *equilibrium shear modulus* of 2 kPa

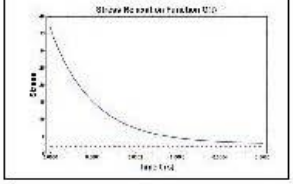

This is a tough case because specimen is very soft!

Comparison of simulation data (symbols) with our estimates (solid curves) for the axial component of deviatoric stress, s_{zz}, for three strain-rates.

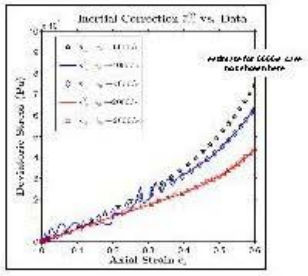

Note: the conventional data analysis would yield values for s_{zz} more than an order of magnitude higher and hence way off the page!

UNCLASSIFIED

Example of Comparison with Simulations

Comparison of simulation data (symbols) with our estimates (solid curves) for the axial component of deviatoric stress, S_{zz}, for three strain-rates.

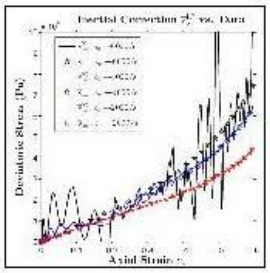

Conclusions

For a specimen as soft as *brain tissue*, our approach:

- Works well for strain-rates of 2000/s or lower.
- At 4000/s, works only for strains > 0.3.
- Does not work at all for a strain-rate of 6000/s.

Torsional Kolsky Bar Tests

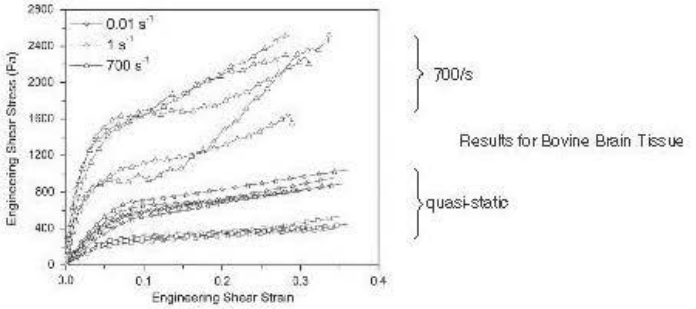

X. Nie, B. Sanborn, T. Weerasooriya, W. Chen, High-rate bulk and shear responses of bovine brain tissue. IJIE 2013

Torsional Kolsky Bar

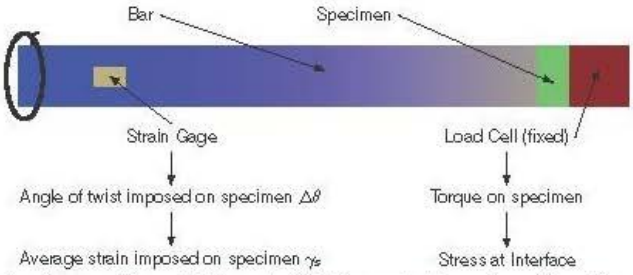

If uniform conditions exist, the angle of twist imposed on the specimen (inferred from the strain gage) yields the average strain within the specimen. In conjunction with stress response measured at the Load Cell a stress-strain curve can be deduced.

Specimen Travel Time

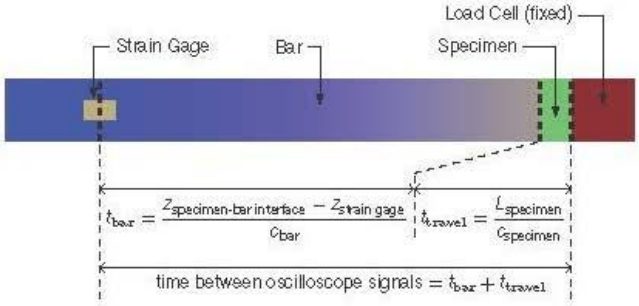

$t_{bar} \approx 500\ \mu s$
t_{travel} for stiff specimens (or compression tests) $\approx \mu s$ (negligible)
t_{travel} for soft specimens ≈ 200—$600\ \mu s$

Wave propagation within the specimen is important to consider for soft specimens!

Simulations

Loading Conditions

- maximum (average) strain-rate of 700/s
- maximum (average) strain of 0.3
- pulse duration of 680 μs
- rise time of 250 μs

Simulation I:

- μ = 800 kPa, ($\approx$ 100 x brain tissue)
- $c \approx 0.03$ mm/μs
- L = 1.7 mm
- travel time $\approx$ 60 μs

Simulation II:

- μ = 8 kPa, ($\approx$ brain tissue)
- $c \approx 0.003$ mm/μs
- L = 1.7 mm
- travel time $\approx$ 600 μs

Note: shear wave speed in Aluminum or Steel is $\approx$ 3 mm/μs.

Average Imposed Loading

Average Strain-Rate History $\dot{\gamma}_s$

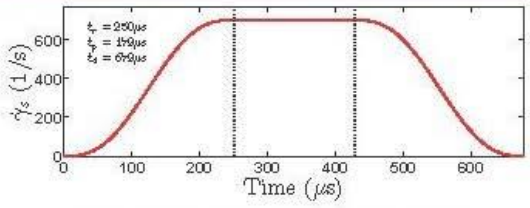

Average Strain History

$$\gamma_s = -\frac{\bar{R}}{L}\Delta\theta(0,t)$$

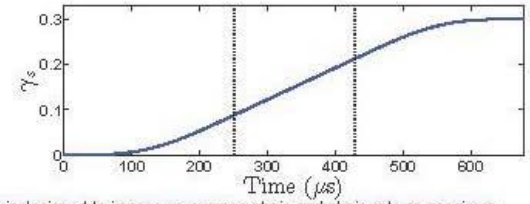

Loading condition is designed to impose an average strain and strain-rate on specimen

1D Simulations Linear Elastic

Simulation I
$\mu = 800$ kPa

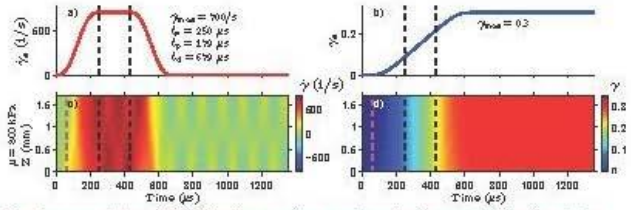

For shear modulus of 800 kPa, the specimen reaches "uniform conditions" so that a traditional Kolsky bar analysis could be applied.

Stress vs. Strain Curve

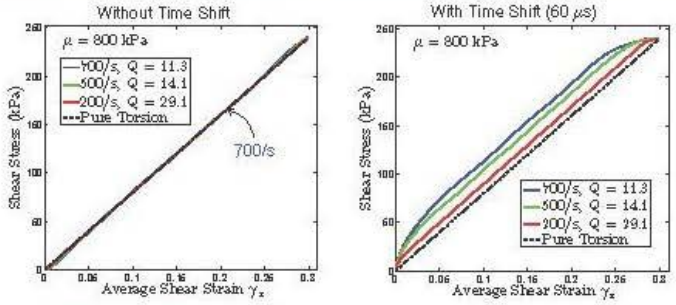

- Without time shift is valid data
- With a time shift (≈ 60 μs) introduces apparent "rate-effects"

1D Simulations Linear Elastic

Simulation II
$\mu = 8$ kPa

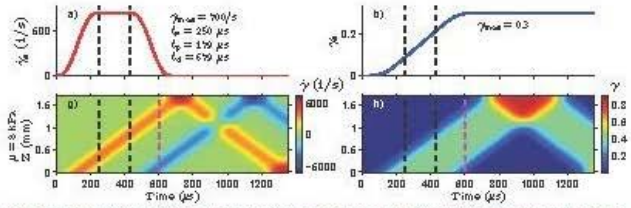

For shear modulus of 8 kPa, the specimen never reaches "uniform conditions" so that a traditional Kolsky bar analysis cannot be applied.

Stress vs. Strain Curve

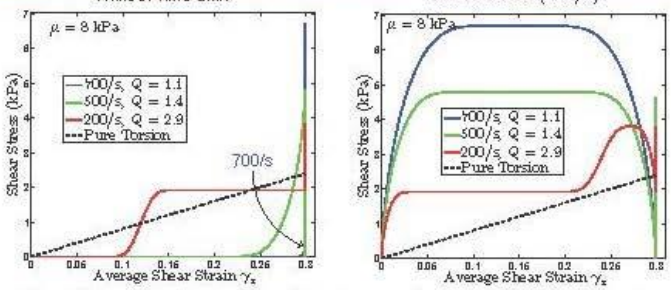

Time shift is equal to the travel time of the shear wave from one end of the specimen to the other

- Without a time shift is meaningless — no stress at finite strain, multiple stresses at fixed strain.
- Using a time shift (≈ 600 μs) introduces erroneous "rate-effects"
- Strain is multiplied on reflection at the load cell.

1D Dynamic Simulations

Conclusions

- The stress history at the load cell should never be time-shifted to synchronize it with the history of the average strain in order to produce a "stress-strain curve".
- Other Kolsky bar tests such as double-lap shear or circular shearing will have similar issues with dynamic equilibrium.
- Travel time of the loading wave can be on the order of loading pulse duration, in which case there is insufficient time for ring-up to dynamic equilibrium. For the torsional Kolsky bar tests on bovine brain tissue at a strain-rate of "700/s" that were reported in Nie et al 2013, the specimen could not have been in dynamic equilibrium, contrary to statements made in that paper.
- Both the solid and annular specimens have non-zero hoop and axial stresses that increase with strain. These normal stresses should not be considered a nuisance, but rather an important feature of the material. Axial stress can and should be measured.

Issues and Future Direction

Issues/Open Questions

- How can we characterize the high strain-rate response of soft tissues?
- Could multiple test results be used to deduce the constitutive relationship, i.e., using the compression Kolsky bar test results with the inertial corrections for solid specimens, the complete strain-gage and load cell time histories in the torsional Kolsky bar, along with axial stresses measured in quasistatic torsion tests?

Questions?

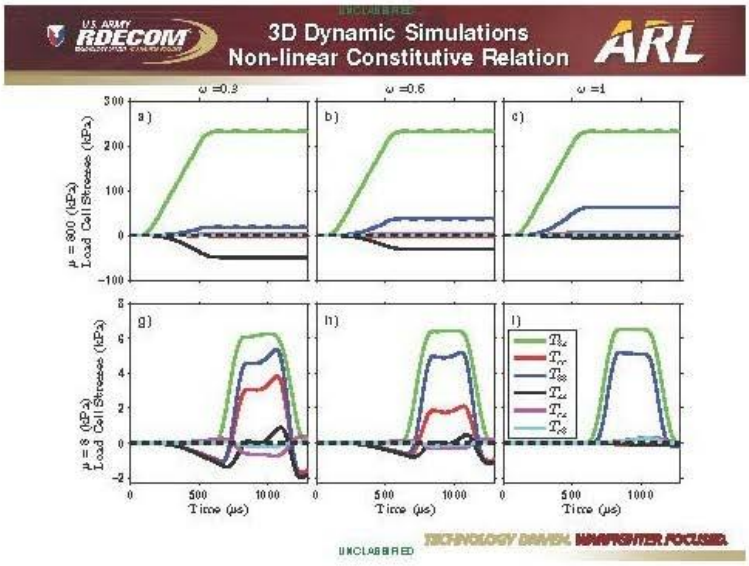
3D Dynamic Simulations
Non-linear Constitutive Relation
ω =0.3
ω =0.6
ω =1
a)
b)
c)
g)
h)
i)
μ = 800 (kPa)
Load Cell Stresses (kPa)
μ = 8 (kPa)
Load Cell Stresses (kPa)
Time (μs)
UNCLASSIFIED

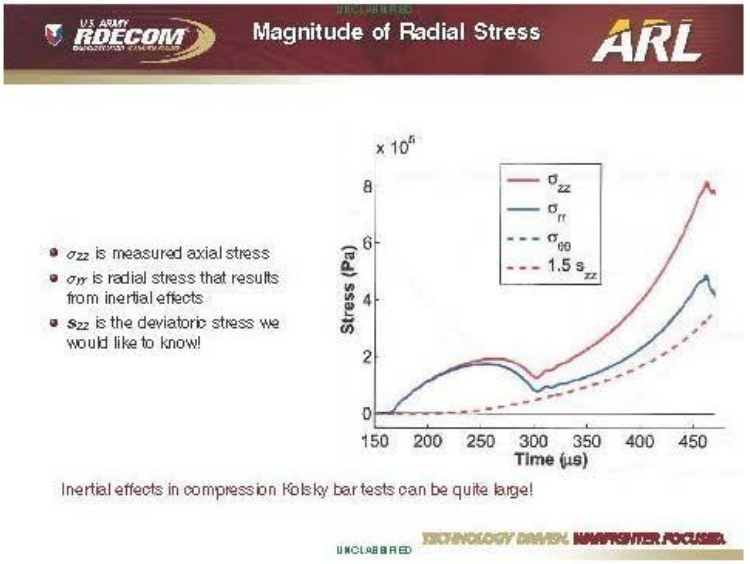
Magnitude of Radial Stress
σzz is measured axial stress
σrr is radial stress that results from inertial effects
szz is the deviatoric stress we would like to know!
x 10^6
Stress (Pa)
Time (μs)
1.5 szz
Inertial effects in compression Kolsky bar tests can be quite large!
UNCLASSIFIED

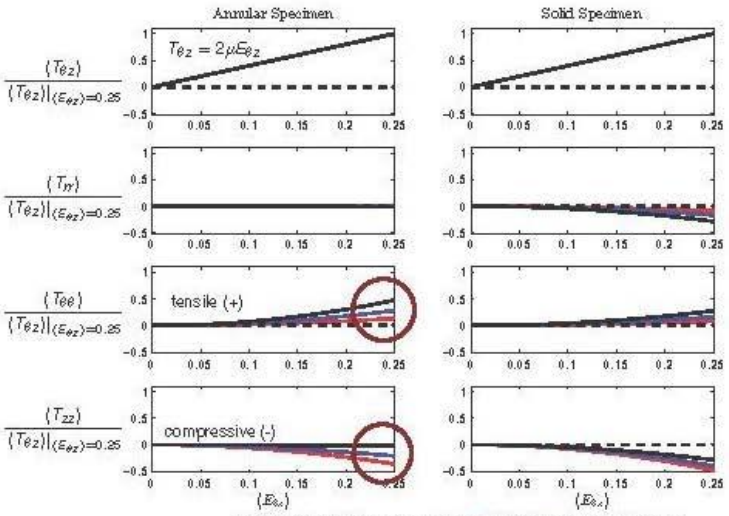

3D Quasi-static Sims: $\omega = 0.3$ (red), 0.6 (blue), and 1.0 (black)

$\langle\ \rangle$ denotes volume average

INTENTIONALLY LEFT BLANK.

Appendix D. Slide Overview

This appendix appears in its original form, without editorial change.


UNCLASSIFIED
U.S. Army Research, Development and Engineering Command
Workshop on Numerical Analysis of Human and Surrogate Response to Accelerative Loading
ARL
TECHNOLOGY DRIVEN. WARFIGHTER FOCUSED.
Ravi Thyagarajan and Mike Tegtmeyer
TARDEC and U.S. Army Research Laboratory
09 January 2014
UNCLASSIFIED

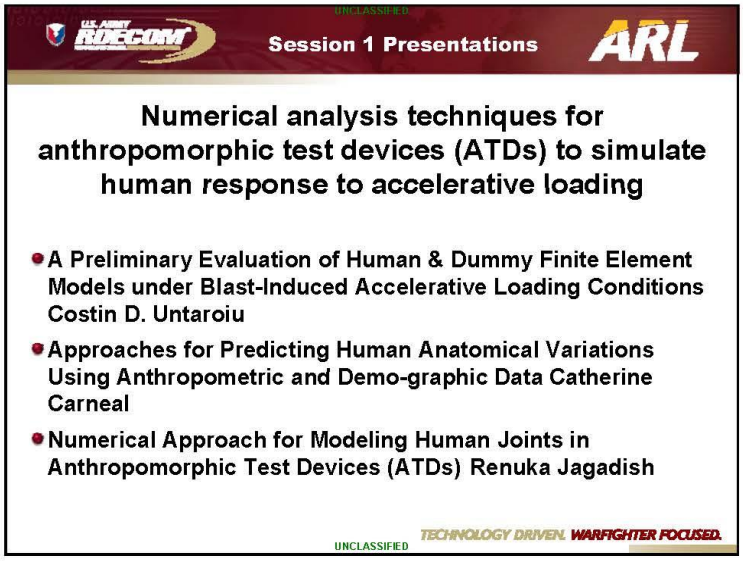
UNCLASSIFIED
Session 1 Presentations
ARL
Numerical analysis techniques for anthropomorphic test devices (ATDs) to simulate human response to accelerative loading
A Preliminary Evaluation of Human & Dummy Finite Element Models under Blast-Induced Accelerative Loading Conditions Costin D. Untaroiu
Approaches for Predicting Human Anatomical Variations Using Anthropometric and Demo-graphic Data Catherine Carneal
Numerical Approach for Modeling Human Joints in Anthropomorphic Test Devices (ATDs) Renuka Jagadish
TECHNOLOGY DRIVEN. WARFIGHTER FOCUSED.
UNCLASSIFIED

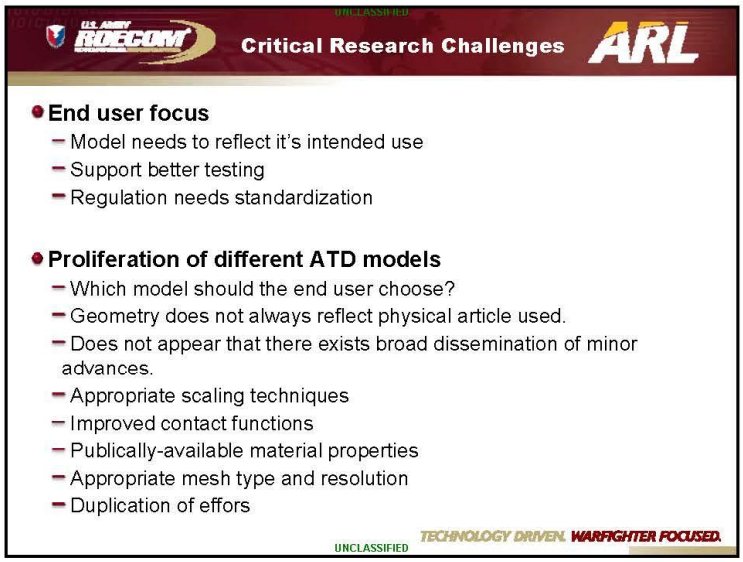
UNCLASSIFIED
Critical Research Challenges
ARL
End user focus
Model needs to reflect it's intended use
Support better testing
Regulation needs standardization
Proliferation of different ATD models
Which model should the end user choose?
Geometry does not always reflect physical article used.
Does not appear that there exists broad dissemination of minor advances.
Appropriate scaling techniques
Improved contact functions
Publically-available material properties
Appropriate mesh type and resolution
Duplication of effors
UNCLASSIFIED
TECHNOLOGY DRIVEN. WARFIGHTER FOCUSED.

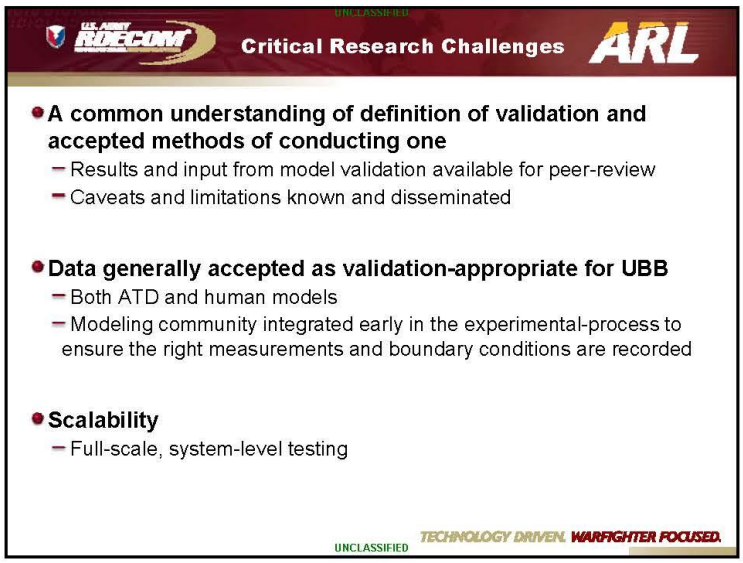
UNCLASSIFIED
Critical Research Challenges
ARL
A common understanding of definition of validation and accepted methods of conducting one
Results and input from model validation available for peer-review
Caveats and limitations known and disseminated
Data generally accepted as validation-appropriate for UBB
Both ATD and human models
Modeling community integrated early in the experimental-process to ensure the right measurements and boundary conditions are recorded
Scalability
Full-scale, system-level testing
UNCLASSIFIED
TECHNOLOGY DRIVEN. WARFIGHTER FOCUSED.

UNCLASSIFIED

Challenges not Being Addressed by the Research Community

- **Inclusion of personal protective and support equipment**
  - All end-user application will include a fully encumbered Soldier
  - Soldiers are not all equipped the same
- **Posture, posture, posture**
  - Vehicle refresh lag – we will have our current vehicles for a long time
  - Validated models need to be useful for near and medium-term occupant postures
  - Articulation of ATD and human models into military-relevant postures is *required*.
- **A common understanding of the UBB loading environment**
  - Definition of "High Rate"
  - Loading is not uniform

UNCLASSIFIED TECHNOLOGY DRIVEN. WARFIGHTER FOCUSED.

UNCLASSIFIED

Challenges not Being Addressed by the Research Community

- **Common anthropometry definition**
  - WIAMan?
- **Are we sensitive in the right places?**
  - Testing (and by extension, modeling) is intended to enhance protection systems
- **Kinetics and kinematics**
  - Entrapment
  - Belts and safety-systems
- **Bridge between accurate ATD and human response**
  - Regulation is ATD. Occupant protection is human.

UNCLASSIFIED TECHNOLOGY DRIVEN. WARFIGHTER FOCUSED.


UNCLASSIFIED
U.S. Army Research, Development and Engineering Command
Multi-scale Modeling Techniques for Human Tissue Response
Session Two
ARL
TECHNOLOGY DRIVEN. WARFIGHTER FOCUSED.
Dan Nicolella (SWRI) and Sikhanda Satapathy (ARL)
07 January 2014
UNCLASSIFIED

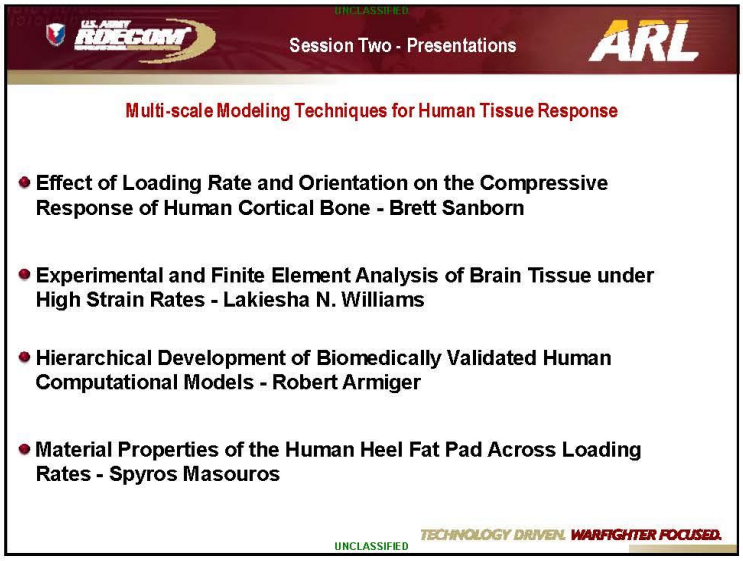
UNCLASSIFIED
Session Two - Presentations
ARL
Multi-scale Modeling Techniques for Human Tissue Response
Effect of Loading Rate and Orientation on the Compressive Response of Human Cortical Bone - Brett Sanborn
Experimental and Finite Element Analysis of Brain Tissue under High Strain Rates - Lakiesha N. Williams
Hierarchical Development of Biomedically Validated Human Computational Models - Robert Armiger
Material Properties of the Human Heel Fat Pad Across Loading Rates - Spyros Masouros
TECHNOLOGY DRIVEN. WARFIGHTER FOCUSED.
UNCLASSIFIED

UNCLASSIFIED

Session Two - Critical Research Challenges

- **Model validation**
  - Model calibration vs. model validation
  - Quantitative model validation
    - Standard quantitative validation metrics
    - Hierarchical approach
- **Incorporating biological variability in M&S and validation**
  - anatomy
  - Material properties
- **Develop experiments explicitly for model validation**
  - Coordination between modelers and experimentalists
- **High rate material properties**
- **Microstructural/tissue anisotropy**
  - Do we have the correct material models
- **Appropriate number of specimens**
  - Capture the variability in biological systems

UNCLASSIFIED TECHNOLOGY DRIVEN. WARFIGHTER FOCUSED.

UNCLASSIFIED

Session Two - Challenges not Being Addressed by the Research Community

- **Material failure**
- **Post failure behavior**
- **Availability/Consolidation of experimental data**
  - Model development
  - Model V&V
- **Develop model validation strategies/metrics**
- **Provide community with adjudicated model validation data sets**
- **Sensitivity analyses**

UNCLASSIFIED TECHNOLOGY DRIVEN. WARFIGHTER FOCUSED.

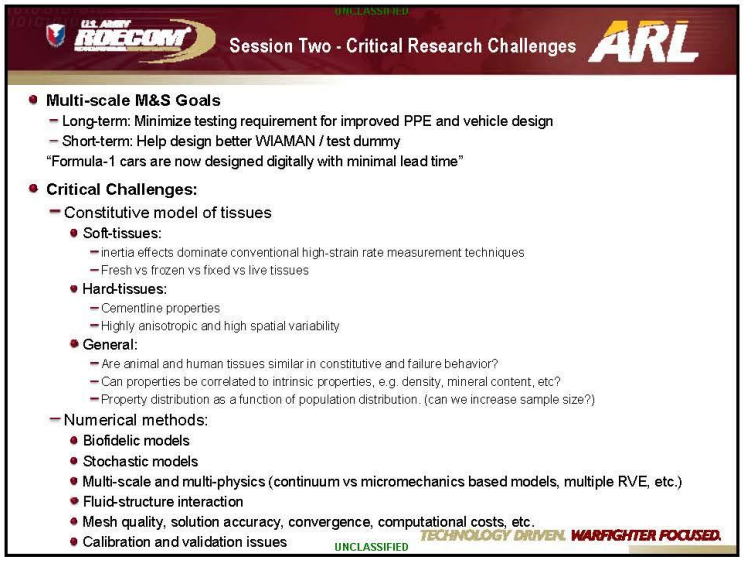
UNCLASSIFIED
Session Two - Critical Research Challenges
ARL
Multi-scale M&S Goals
Long-term: Minimize testing requirement for improved PPE and vehicle design
Short-term: Help design better WIAMAN / test dummy
"Formula-1 cars are now designed digitally with minimal lead time"
Critical Challenges:
Constitutive model of tissues
Soft-tissues:
inertia effects dominate conventional high-strain rate measurement techniques
Fresh vs frozen vs fixed vs live tissues
Hard-tissues:
Cementline properties
Highly anisotropic and high spatial variability
General:
Are animal and human tissues similar in constitutive and failure behavior?
Can properties be correlated to intrinsic properties, e.g. density, mineral content, etc?
Property distribution as a function of population distribution. (can we increase sample size?)
Numerical methods:
Biofidelic models
Stochastic models
Multi-scale and multi-physics (continuum vs micromechanics based models, multiple RVE, etc.)
Fluid-structure interaction
Mesh quality, solution accuracy, convergence, computational costs, etc.
Calibration and validation issues
UNCLASSIFIED
TECHNOLOGY DRIVEN. WARFIGHTER FOCUSED.

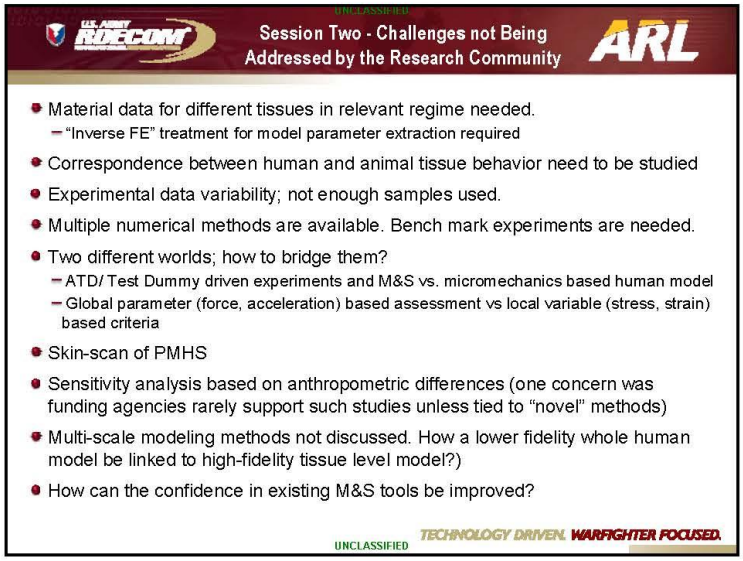
UNCLASSIFIED
Session Two - Challenges not Being Addressed by the Research Community
ARL
Material data for different tissues in relevant regime needed.
"Inverse FE" treatment for model parameter extraction required
Correspondence between human and animal tissue behavior need to be studied
Experimental data variability; not enough samples used.
Multiple numerical methods are available. Bench mark experiments are needed.
Two different worlds; how to bridge them?
ATD/ Test Dummy driven experiments and M&S vs. micromechanics based human model
Global parameter (force, acceleration) based assessment vs local variable (stress, strain) based criteria
Skin-scan of PMHS
Sensitivity analysis based on anthropometric differences (one concern was funding agencies rarely support such studies unless tied to "novel" methods)
Multi-scale modeling methods not discussed. How a lower fidelity whole human model be linked to high-fidelity tissue level model?)
How can the confidence in existing M&S tools be improved?
UNCLASSIFIED
TECHNOLOGY DRIVEN. WARFIGHTER FOCUSED.

Session Three - Presentations

Numerical Methods to Simulate the Response of Human Tissue and Bone to High-Rate Loading

- Comparing the Use of Dynamic Response Index (DRI) and Lumbar Load as Relevant Spinal Injury Metrics - Ravi Thyagarajan
- Developing and Empirical Model to Estimate Tibia Injury – Joseph O'Bruba
- Towards A Micromechanics-Based Simulation of Calcaneus Fracture and Fragmentation Due to Impact loading - Reuben H. Kraft
- Pelvis Response Effects on Whole Body Under-Body Blast Simulations - Adam Golman
- Numerical Methods for Large-Scale Simulation of Tissue and Tissue Simulant Response to Blast, Model Validation and Limitations – Raul Radovitzky

Session Three - Critical Research Challenges (being addressed and not)

- Dynamic Response Index (DRI) as indication of Lumbar spinal injury is inappropriate. Need to develop:
  - Injury severity based scaled (not 0 or 1) injury assessment tool.
    - May be similar to AIS scales but more understanding and quantitative, preferable related to short term return to duty and long term quality of life
    - Can account for different failure modes (e.g., disc burst vs. wedge failure).
    - Based on observed dynamic injury mechanisms at different scales.
    - Effects of loading rate and duration?
- For empirical injury model development, a worst-case scenario needs to be identified, although the subsequently designed vehicle or protective gears may be over designed for most cases.
  - Effects of bending?
  - Non-vertical tibia position?

Session Three - Critical Research Challenges (being addressed and not)

- Failure criteria at micromechanis scales or meso scales are needed to identify injury or failure initiation and early-stage propagation
  - Effects of viscos fluid passing through permeable cell walls at high rates?
- Surrogates' response to blast loading needs to be validated by cadaver response.
  - Biofidelity?
  - Will cadaver skin be punctured through?
  - Can the degrees of freedom at a joint mimic human joints?
  - Effects of boots in shock isolation?
  - Effects of existing damage?
  - Effects of PPE?
- Data for tissue response to high-rate loading highly scattered.
  - Need high fidelity characterization methods to generate input data and validation cases

Session Three - Critical Research Challenges (being addressed and not)

- Experimental programs communicate with simulation programs in planning tasks.
- Research findings need to be disseminated to vehicle designers.
  - It is much more efficient when blast protection features are integrated with vehicle structure at design stage.
  - Retro-fit blast protection packages are much less effective

Session Three - Challenges not Being Addressed by the Research Community

- Loading scenarios by (potential) available protection systems
- Injury mechanism development based on injury data registered in theatre (actual data missing ?)

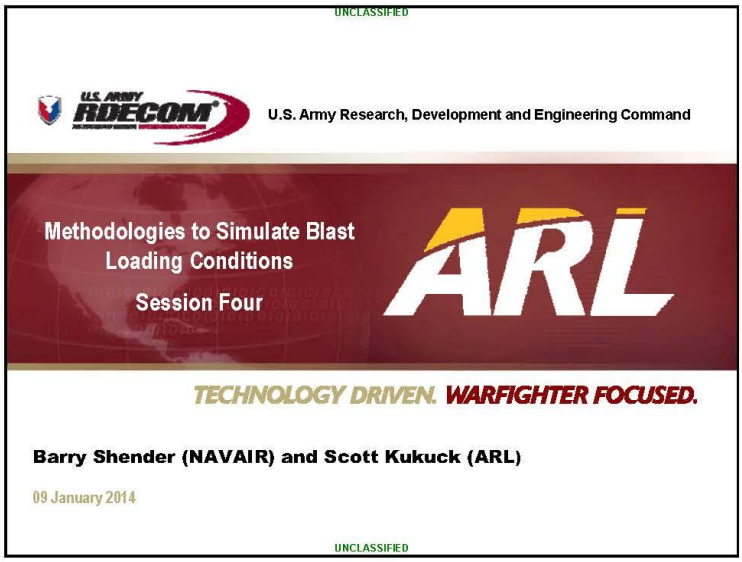
UNCLASSIFIED
U.S. Army Research, Development and Engineering Command
Methodologies to Simulate Blast Loading Conditions
Session Four
ARL
TECHNOLOGY DRIVEN. WARFIGHTER FOCUSED.
Barry Shender (NAVAIR) and Scott Kukuck (ARL)
09 January 2014
UNCLASSIFIED


UNCLASSIFIED
Session Four – Presentations
ARL
Methodologies to Simulate Blast Loading Conditions
Development and Validation of the WSU Human Body Model - Alan Goertz
Adapting Automotive-Based Finite Element Models of Lower Extremity for High-Rate Impact Simulation of Occupants Subject to Under-Vehicle Blasts - Robert Salzar
Current Research and Development Activities of the Full Body Model Center of Expertise of the Global Human Body Models Consortium Project - Scott Gayzik
Modeling the Human Head and Neck: Sensitivity and Response - Dale Bass
Effects of Posture, Torso Borne Mass and Seat Energy Absorbing Characteristic on Pelvis and Lumbar Spine Injury During Under Body Blast Event Using a Hierarchically Validated Finite Element Model - Andrew Merkle
Human Body Model Injury Analysis in Real-World Crash Simulations - Kerry Danelson
Numerical Modelling Undertaken at Dstl (UK) Concerning Vehicle Floor Plate Impact of Surrogates and Anatomical Human Entities Due to Under-Body Mine Loading - Daniel Pope
Optimal Design of a Novel Energy Absorbing Material to Mitigate the Blast Effect on the Lower Extremities - King Yong
TECHNOLOGY DRIVEN. WARFIGHTER FOCUSED.
UNCLASSIFIED

UNCLASSIFIED

Session Four - Summary Observations and Research Challenges (1)

- **The Verification / Validation Question**
  - What is validation ? The definition varies. Validation outside of the context is meaningless.
  - Validation should be quantitative, not merely a visual match. r^2 is not sufficient. Metrics and methods should be identified.
  - Validation must be accompanied by an explanation of how it was performed and what limitations / caveats are. It is as important to identify where NOT valid and where valid and where to stop believing.
  - Can we develop a standard for validation ? (method, metrics, data, etc)
  - Hierarchical model development
  - Occupant / Surrogate must interact with environment, so don't forget models for vehicle, seating, restraints, PPE
- **What constitutes valid scaling ?**

UNCLASSIFIED TECHNOLOGY DRIVEN. WARFIGHTER FOCUSED.

UNCLASSIFIED

Session Four - Summary Observations and Research Challenges (2)

- **Variability**
  - Accounting for unknowns; physiology; muscle activation; structure
- **What's important to model & what's not ?**
  - Sensitivity analysis and focus on what's important based on requirements not on inclusion of the n^{th} detail
- **What are the ultimate goals of the program ?**
  - What do we want from the modeling? If, for example, it's a design tool then it needs to be driven by operational requirements (persistent, common injuries – don't focus on unsurvivable injuries)
  - Ultimately, we want to develop modes of mitigation (technology or behavior)
  - Prioritize investments based on the goal
    - The goal is NOT a manikin. We are building a manikin, but it is protection for the HUMAN occupant

UNCLASSIFIED TECHNOLOGY DRIVEN. WARFIGHTER FOCUSED.

UNCLASSIFIED

Session Four - Summary Observations and Research Challenges (3)

- **Modeling Issues**
  - Model requirements inform test requirements, not vice-versa
  - If the underlying component characteristics and behaviors are correct, then the model can be used for future threats
  - The 50th percentile of what ? What about the rest of the population ? What about sensitivities across the population ?
  - Posture and motion must not be neglected
  - Input parameter variability with distributions (working to probablistic?)
  - Resolution (fidelity) should be based on operational requirement
  - Post-failure behavior and cascading responses
  - Muscular responses
  - Automotive may be good starting point, but require modification for blast
  - Clearly define operationally relevant injuries – informs experimentalist requirements for modeling

UNCLASSIFIED TECHNOLOGY DRIVEN. WARFIGHTER FOCUSED.

UNCLASSIFIED

Session Four – References (1)

Oreskes N, Shrader-Frechette K, Belitz K; 'Verification, Validation and Confirmation of Numerical Models in Eart Sciences' *Science* **263**, pp. 641-646 (1994).

Henninger HB, Reese SP, Anderson AE & Weiss JA; 'Validation of computational models in biomechanics' *Proc IMechE* **224** *Part H: J Engineering in Medicine*, pp. 801-812 (2010).

Anderson AE, Ellis BJ & Weiss JA; 'Verification, validation and sensitivity studies in computational biomechanics' *Computer Methods in Biomechanics and Biomedical Engineering* **10**, pp. 171-184 (2007).

ASME V&V 10-2006; *Guide for Verification and Validation in Computational Solid Mechanics*.

ASME V&V 20-2009; *Standard for Verification and Validation in Computational Fluid Dynamics and Heat Transfer*.

UNCLASSIFIED TECHNOLOGY DRIVEN. WARFIGHTER FOCUSED.

Session Four – References (2)

Francis, Eliason, Thacker, Paskoff, Shender and Nicolella; 'Implementation & Validation of probablistic models of the anterior longitudinal ligament and posterior longitudinal ligament of the cervical spine' *Computer Methods in Biomechanics and Biomedical Engineering* (2012).

Nicolella, Francis, Bonivtch, Thacker, Paskoff, Shender; 'Development, verification and validation of a parametric cervical spine injury prediction model' AIAA SDM Conference **6**, pp. 3977-3985 (2006).

Thacker, Francis, Nicolella; 'Model Validation and Uncertainty Quantification Applied to Cervical Spine Injury Assessment' *NATO Computational Uncertainty in Military Vehicle Design*, pp. 22-1-26-30 (2007).


UNCLASSIFIED
U.S. Army Research, Development and Engineering Command
Numerical Analysis Methodologies for Human Body Subject to High Rate Loading
Session Five
ARL
TECHNOLOGY DRIVEN. WARFIGHTER FOCUSED.
Spyros Masouros, Imperial College, and Sarah Hug (ARL)
09 January 2014
UNCLASSIFIED


UNCLASSIFIED
Session Five - Presentations
ARL
Numerical Analysis Methodologies for Human Body Subject to High Rate Loading
Constitutive Model and Parameter Sensitivity in Predicting Lower Leg Response for Underbody Blast Events - Megan Lynch
Coupled Eulerian and Lagrangian Approaches for Dynamic Injury Analysis - Timothy P. Harrigan
Crew Response in Full System HFCP - Allen Shirley
Evaluating the Effectiveness of Various Blast Loading Descriptors as Occupant Injury Predictors for Underbody Blast Events - Jai Ramalingam
Neck Response of a Finite Element Human Body Model During a Simulated Rotary-Wing Aircraft Impact - Joel Stitzel
TECHNOLOGY DRIVEN. WARFIGHTER FOCUSED.
UNCLASSIFIED

UNCLASSIFIED

Session Five - Critical Research Challenges

- **Applicability of available human and H3 models to UBB**
- **Applicability of some injury criteria (eg DRIz, HIC) – consensus that they are not good enough for UBB.**
- **Requirement (Y/N?) for Eulerian / ALE models to look at injury to human organs.**
- **Muscle inputs to lower and cervical spine in UBB?**
- **Material properties / constitutive models of relevant human tissue at appropriate rates**
- **The 'WIAMan' FE model**
  - is it required (seems that the consensus is yes)
  - Where do we start from (is the global human model an appropriate starting point?)
  - What strategy do we take to get there

UNCLASSIFIED

Session Five - Challenges not Being Addressed by the Research Community

- **The 'WIAMan' FE model**
  - is it required (seems that the consensus is yes)
  - Where do we start from (is the global human model an appropriate starting point?)
  - What strategy do we take to get there
- **Sensitivity of human FE models to input parameters on appropriate outputs**
  - which of the material parameters are actually important and so which ones do we need to capture as accurately as we can.


UNCLASSIFIED
U.S. Army Research, Development and Engineering Command
Numerical Methods for Analysis of ATD Materials (Including Soft Materials) Undergoing High-Rate Loading
Session Six
ARL
TECHNOLOGY DRIVEN. WARFIGHTER FOCUSED.
Tusit Weerasooriya (ARL) and Joel Stitzel (Wake Forest)
09 January 2014
UNCLASSIFIED

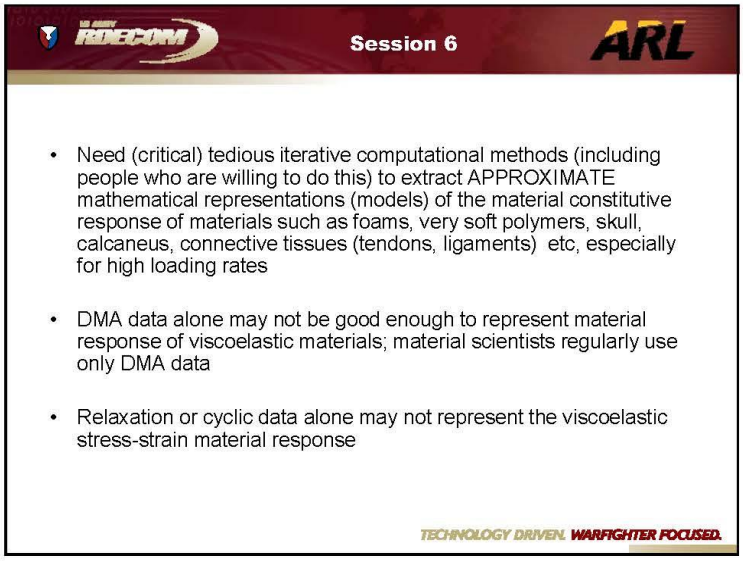
Session 6
ARL
• Need (critical) tedious iterative computational methods (including people who are willing to do this) to extract APPROXIMATE mathematical representations (models) of the material constitutive response of materials such as foams, very soft polymers, skull, calcaneus, connective tissues (tendons, ligaments) etc, especially for high loading rates
• DMA data alone may not be good enough to represent material response of viscoelastic materials; material scientists regularly use only DMA data
• Relaxation or cyclic data alone may not represent the viscoelastic stress-strain material response
TECHNOLOGY DRIVEN. WARFIGHTER FOCUSED.

Session 6

- All tissues are anisotropic or not uniform – need to start thinking about designing, characterizing and modeling methods for new surrogate materials that actually mimic real hard, connective and soft tissues to capture real human response
- It is almost impossible to extract specimens (uniform with needed sizes) from all the components of the human for experimental characterization; need to think different – how do we extract APPROXIMATE material response models from these possible human samples (small structures) with a combined computational/experimental hybrid approach
- LSDYNA (widely used) could have an easy user interface to incorporate new material models or variations of existing models (without going through the code company)

TECHNOLOGY DRIVEN. WARFIGHTER FOCUSED.

Session 6

- It is almost IMPOSSIBLE to tune any of the material model concepts (including state of the art) to all possible experimental data types – so focus on the application specific material behavior experiments
- Need to understand the change in response (and hence the change in const response) of the ATD after repeated use
- Fracture of bones: we may need to develop new replaceable components (with novel designed-materials tuned to bone fracture response) in future Gen Xs to capture actual fracture response of bones
- Experiments should have enough tissue samples to extract variability and future models should have variability built in to them? A tough task….

TECHNOLOGY DRIVEN. WARFIGHTER FOCUSED.

Appendix E. List of Attendees

This appendix appears in its original form, without editorial change.

List of Attendees

Name	Title	Organization
Walter Andrefsky	Test Officer	ATC
Robert Armiger	Asst Group Supervisor	JHU/APL
Patrick Baker	Director WMRD	U.S. Army Research Laboratory
Craig Barker	Mechanical Engineer	ARL/SLAD
Dale Bass		
Brian Benesch		
Bob Bocchieri	Principal Engineer	ARA
Ronald Bowers		ARL/SLAD
Alex Breuer		
Catherine Carneal	Asst Program Manager	JHU/APL
Bryan Cheeseman	Mechanical Engineer	US Army Research Laboratory
Mostafiz Chowdhury	Engineer	ARL, RDRL-DW
Raquel Ciappi	Mechanical Engineer	SURVICE Engineering/ARL SLAD
Sarah Coard	Biologist	ARL/SLAD
Randy Coates	Supervisory Physical Scientist	ARL, RDRL-DW
Maribeth Cohey	Physiologist	ARL/SLAD
Joseph Cordell		DSTL
Brian Corner		NSRDEC Warfighter Directorate
Mark Couch	Research Staff Member	Institute for Defense Analyses
Christopher Coward	Mechanical Engineer	SLAD
Joshua Crone	Mechanical Engineer	ARL (CISD)

Chris Cummins		ARL-WMRD Blast Protection Branch
Brock Cunningham	Lead Analyst	Booz Allen Hamilton, contract support to HQMC CD&I, CDD, FMID
Jerry Czarnecki	Research Staff Member	Institute for Defense Analyses
Kerry Danielson		
Thomas Digliani	Mechanical Engineer	ARL/WMRD
Ashley Eidsmore	SMART Student	ARL/SMART Student
Ian Elgy		dstl
Rebecca Fielding	Graduate Student	Penn State University
Craig Foster	Engineer	TARDEC
Adam Fournier	Bio-Mechanical Engineer	ATC
Patricia Frounfelker	Biomedical Engineer	ARL, RDRL-DW
F. Scott Gayzik	Assistant Professor	Wake Forest University School of Medicine
Neil Gniazdowski		
Alan Goertz		
Adam Golman	Biomechanical Engineer	JHU/APL
David Grove	Computer Scientist	ARL/CISD/CSD/SSB
Allan Gunnarsson	Mechanical Engineer	ARL
Raj Gupta	Dep Director	USAMRMC-DoD Blast Injury Research PCO
Carolyn Hampton	Postdoctoral Associate	Virginia Tech
Warren Hardy	Associate Professor/Director	VT-WFU Center for Injury Biomechanics

Timothy Harrigan	Biomechanical Engineer	JHU/APL
Krista Harris	Mechanical Engineer	NSWC Carderock
Janice Hester	Research Staff Member	Institute for Defense Analyses
Dixie Hisley	General Engineer	ARL/SLAD
James Hoffman	Engineer	ARL, RDRL-DW
Terry Holdren	Mathematical Statistician	ARL, RDRL-DW
Christopher Hoppel	Chief, Soldier Protection Sciences Branch	ARL
Douglas Howle	Mechanical Engineer	ARL/SLAD
Yolin Huang		WMRD/ARL
Renuka Jagadish	CAE Engineer	Humanetics Innovative Solutions, Inc.
Vincent Jakubowski	Systems Engineer	PM-Allied Tactical Vehicles
Aaron Kahn		
Matthew Kaufman	General Engineer	U.S. Army Research Lab, Survivability/Lethality Analysis Dir, Ballistic Vulnerability/Lethality Div
Dean Kleissas	Engineer	Johns Hopkins University Applied Physics Laboratory
Stephanie Koch	Physical Scientist	OSD, DOT&E
Reuben Kraft		
Scott Kukuck		
Kumar Kulkarni	Sr. Technical Specialist	ESI-US Inc. on-site at TARDEC
Bruce LaMattina	Director of Federal Research Relations and Research Professor in Mechanical and Aerospace Engineering	Rutgers University
Ronald Lehman		
Jaclyn Lerg	Product Integrator	PM Bradley

Kevin Lister	Senior Analyst	CORVID Technologies
Megan Lynch	Mechanical Engineer	U.S. Army Research Laboratory
David Lyon	Chief Protection Division	U.S. Army Research Laboratory
Mike Maffeo		NSRDEC Warfighter Directorate
Patrick Maloney	President/CEO PM13 Consulting	PM13 Consulting
Spyridon Masouros	Dr.	Imperial College London
Lydia Mattern	Test Officer	US Army Aberdeen Test Center
Jason McDonald	Senior Scientist	Bowhead Science and Technology LLC
Kimberly Meeks	Program Manager	CORVID Technologies
Andrew Merkle		
Andrew Merkle	Program Manager	The Johns Hopkins University Applied Physics Laboratory
William Mermagen		
Brian Minch	Engineer	ARL, RDRL-DW
Daniel Nicolella		
Joseph O'Bruba	Engineer	ARL/SLAD (SURVICE Contractor)
Paul Palmer	Director of Business Development (Active Protections Systems)	TenCate
Hyunsok Pang	CAE Chief Engineer	Humanetics Innovative Solutions, Inc
Matthew Panzer	Research Scientist	UVA
Joseph Park	Engineer	SURVICE Engineering / USMC MRAP
Mathieu Philippens		
Frank Pintar	Professor	Medical College of Wisconsin
Daniel Pope		DSTL
David Powell	Mechanical Engineer	ARL
Emelia Probasco	Johns Hopkins University - Applied Physics Lab	

Andrzej Przekwas	CTO	CFD Research Corp
Anne Purtell	Survivability Lead	Auto Cell, PEO-Land Systems
Jacob Putnam Raul Radovitzky	Graduate Research Assistant	Virginia Tech
Jaisankar Ramalingam	Mechanical Engineer	TARDEC
Mark Rapo	Engineer	L-3 Applied Technologies, Inc
Tyler Rooks	General Engineer	U.S. Army Aeromedical Research Laboratory
Daniel Rusin	Staff Engineer	RDECOM HQ
Thomas Russell	Director ARL	U.S. Army Research Laboratory
Grace Sadia	Physiologist	ARL/SLAD
Erick Sagebiel	Chief Survivability Engineer (Active Systems)	TenCate
Masayuki Sakamoto	ESEP Research Engineer	Survivability Research Section, Ballistic Research Division, Ground Systems Research Center Technical Research and Development Japan Institute, Japan Ministry of Defense
Robert Salzar	Principal Scientist	UVA
Brett Sanborn		ARL/ORISE
Sikhanda Satapathy		
Richard Sayre		
Mike Scheidler		WMRD/ARL
Shane Schumacher	Mechanical Engineer	Sandia National Laboratories
Welling Scott	Mechanical Engineer / Team Leader (a)	ARL / SLAD
Allen Shirley	Program Manager	CORVID Technologies
Kevin Silas	Associate Engineer	SURVICE Engineering
Darnell Slaughter	Research Assistant	Penn State University

Stephanie Snead	Chief, Warfighter Survivability Branch	ARL/SLAD
Adam Sokolow	ORISE Postdoctoral Fellow	ARL
Dominik Soyka	Engineer	ARL, RDRL-DW
Robert Spink	Biomedical Engineer	WIAMan PMO, ARL
Joel Stitzel	Professor and Chair, Biomedical Engineering Associate Head, VT-WFU	Wake Forest Baptist Health
Christopher Taggart		DSTL
Rabih Tannous	President	AASA Inc.
Michael Tegtmeyer	Computer Scientist	ARL, RDRL-DW
Steven Thompson	Computer Systems Analyst Principle	ARL, Lockheed Martin
Ravi Thyagarajan	Senior Technical Specialist, Analytics	TARDEC/Analytics
Benjamin Turner	Research Staff Member	Institute for Defense Analyses
Jerome Tzeng	Mechanical Engineer	ARL
Costin Untaroiu		
Vincent Volpe	Research Staff Member	Institute for Defense Analyses
Liming Voo	Project Manager	Johns Hopkins University Applied Physics Laboratory
James Walbert	Adjunct Research Staff	Institute for Defense Analyses
Kerry Walzl		Institute for Defense Analyses
Kate Weaver	Mathematician	ARL
Paul Weber	Research Staff Member	Institute for Defense Analyses

Tusit Weerasooriya	Mechanical Engineer	ARL
Lakiesha Williams	Assistant Professor	Mississippi State University
King Yang	Professor and Director	Wayne State University
Narayan Yoganandan	Professor	Medical College of Wisconsin
Jonathan Young	Engineer III	L-3 Applied Technologies, Inc
Timothy Zhang	Senior Scientist	ARL
Kimberly Ziegler	Biomedical Engineer	ARL

1 (PDF) DEFENSE TECHNICAL INFORMATION CTR DTIC OCA

2 (PDF) DIRECTOR US ARMY RESEARCH LAB RDRL CIO LL IMAL HRA MAIL & RECORDS MGMT

1 (PDF) GOVT PRINTG OFC A MALHOTRA

1 (PDF) UNIV OF PITTSBURGH DEPT OF ORTHOPEDIC SURGERY P ALEXANDER

4 (PDF) DEFNS RSRCH & DEV CANADA VALCARTIER A BOUAMOUL L MARTINEAU D NANDLALL K WILLIAMS

1 (PDF) DEFNS RSRCH & DEV CANADA TORONTO C BURRELL TORONTO

6 (PDF) NATICK SOLDIER RSRCH DEV & ENGRG CTR M CARBONI M CODEGA P CUNNIFF J FITEK D LEE J WARD

3 (PDF) US ARMY AEROMEDICAL RSRCH LAB V CHANCEY B MCENTYRE D WISE

1 (PDF) UNIV OF NEBRASKA N CHANDRA

8 (PDF) DEFNS SCIENCE & TECHLGY LAB I ELGY A HEPPER S HOLDEN R LIVESEY M NEALE D POPE A SEDMAN C TAGGART

1 (PDF) ATC A FOURNIER

1 (PDF) CFD RSRCH CORP A PRZEKWAS

2 (PDF) SOUTHWEST RSRCH INST MECHL ENGRG DIV W L FRANCIS D NICOLELLA

2 (PDF) WAKE FOREST UNIV CTR FOR INJURY BIOMECHANICS F S GAYZIK J STITZEL

1 (PDF) US ARMED FORCES MEDICAL EXAMINER SYS J GETZ

3 (PDF) MRMC DOD BLAST INJURY RSRCH PROG COORDINATING OFC R GUPTA M LEGGIERI R SHOGE

2 (PDF) ENERGETICS TECHLGY CTR R KAVETSKY E MORITZ

1 (PDF) PENNSYLVANIA STATE UNIV R KRAFT

3 (PDF) MRMC JTAPIC PRGM OFC F LEBEDA W LEI J USCILOWICZ

1 (PDF) UNIV OF PENNSYLVANIA DEPT OF BIOENGINEERING D MEANEY

2 (PDF) THE JOHNS HOPKINS UNIV DEPT OF MECHL ENGRG T NGUYEN K RAMESH

2 (PDF) MASSACHUSETTS INST OF TECHLGY INST FOR SOLDIER NANOTECHNOLOGIES R RADOVITZKY S SOCRATE

1 (PDF) UNIFORMED SERVICES UNIV OF THE HEALTH SCIENCES
P RAPP

1 (PDF) TARDEC
R SCHERER

1 (PDF) UNIV OF PITTSBURGH
W SCHNEIDER

1 (PDF) SANDIA NATL LAB
S SCHUMACHER

1 (PDF) NAVAL AIR WARFARE CTR AIRCRAFT DIV
B SHENDER

1 (PDF) BAE SYSTEMS
R TANNOUS

1 (PDF) MISSISSIPPI STATE UNIV
L WILLIAMS

1 (PDF) WALTER REED NATL MILITARY MEDICAL CTR
E WRIGHT

4 (PDF) JOHNS HOPKINS UNIV APPLIED PHYSICS LAB
R ARMIGER
C CARNEAL
T HARRIGAN
E PROBASCO

1 (PDF) ARA
R BOCCHIERI

3 (PDF) NSRDEC WARFIGHTER DIRCTRT
J CORDELL
B CORNER
M MAFFEO

1 (PDF) WAKE FOREST UNIV
K DANIELSON

8 (PDF) INST FOR DEFNS ANALYSES
M COUCH
J CZARNECKI
J HESTER
B W TURNER
V VOLPE
J N WALBERT
K WALZL
P WEBER

1 (PDF) BOOZ ALLEN HAMILTON
B CUNNINGHAM

1 (PDF) PENN STATE UNIV
R FIELDING

1 (PDF) USAMRMC DOD BLAST INJURY RESEARCH PCO
R GUPTA

1 (PDF) VIRGINIA TECH
C HAMPTON

1 (PDF) VT WFU CTR FOR INJURY BIOMECHANICS
W N HARDY

1 (PDF) NSWC CARDEROCK
K HARRIS

1 (PDF) HUMANETICS INNOVATIVE SOLUTIONS INC.
R JAGADISH

1 (PDF) PM ALLIED TACTICAL VEHICLES
V JAKUBOWSKI

3 (PDF) JOHNS HOPKINS UNIV APPLIED PHYSICS LAB
D KLEISSAS
A MERKLE
L VOO

1 (PDF) OSD DOT & E
S KOCH

1 (PDF) PENN STATE UNIV
R KRAFT

1 (PDF) RDTA RS ESI US INC TARDEC
K B KULKARNI

1 (PDF) RUTGERS UNIV
B LAMATTINA

1 (PDF) J LERG
PM BRADLEY

1 (PDF) CORVID TECHNOLOGIES
K LISTER

1 (PDF) PM13 CONSULTING
P MALONEY

1 (PDF) CORVID TECHNOLOGIES
K S MEEKS

1 (PDF) SOUTHWEST RSCH INST
D NICOLELLA

1 (PDF) ARL SLAD SURVICE CONTRACTOR
J OBRUBA

2 (PDF) TENCATE
P PALMER
E SAGEBIEL

1 (PDF) HUMANETICS INNOVATIVE SOLUTIONS INC
H PANG

2 (PDF) UVA
M B PANZER
R SALZAR

1 (PDF) SURVICE ENGRG USMC MRAP
J PARK

1 (PDF) MEDICAL COLLEGE OF WISCONSIN
F A PINTAR

1 (PDF) CFD RSRCH CORP
A PRZEKWAS

1 (PDF) AUTO CELL PEO LAND SYS
A PURTELL

1 (PDF) VIRGINIA TECH
J PUTNAM

1 (PDF) TARDEC
J RAMALINGAM

2 (PDF) L-3 APPLIED TECHNOLOGIES INC
M RAPO
J YOUNG

1 (PDF) US ARMY AEROMEDICAL RSRCH LAB
T ROOKS

1 (PDF) CORVID TECHNOLOGIES
A SHIRLEY

1 (PDF) SURVICE ENGRG
K SILAS

1 (PDF) PENN STATE UNIV
D SLAUGHTER

1 (PDF) WAKE FOREST BAPTIST HEALTH
J STITZEL

1 (PDF) AASA INC
R TANNOUS

1 (PDF) ARL LOCKHEED MARTIN
S R THOMPSON

1 (PDF) TARDEC ANALYTICS
R THYAGARAJAN

1 (PDF) VIRGINIA TECH
C UNTAROIU

1 (PDF) MISSISSIPPI STATE UNIV
L N WILLIAMS

1 (PDF) WAYNE STATE UNIV
K H YANG

1 (PDF) MEDICAL COLLEGE OF WISCONSIN
N YOGANANDAN

1 (PDF) SANDIA NATL LAB
S SCHUMACHER

1 (PDF) IMPERIAL COLLEGE LONDON
DEPT OF BIOENGINEERING
S MASOUROS

3 (PDF) DSTL
J CORDELL
D POPE
C TAGGART

1 (PDF) DSTL
I ELGY

1 (PDF) SURVIVABILITY RSRCH SECTION
BALLISTIC RSRCH DIV GROUND SYS RSRCH CTR TECH RSRCH & DEV JAPAN INSTITUTE
JAPAN MINISTRY OF DEFNS
M SAKAMOTO

2 (PDF) US ARMY ABERDEEN TEST CTR
W ANDREFSKY
L MATTERN

1 (PDF) ARL SMART STUDENT
A EIDSMORE

1 (PDF) RDECOM HQ
AMSRD PE
D RUSIN

1 (PDF) WIAMAN PMO
R SPINK

100 (PDF) DIR USARL
RDRL CIH C
J CRONE
B HENZ
M VINDIOLA
RDRL D
T RUSSELL
RDRL DP
R COATES
P FROUNFELKER
R SPINK
M TEGTMEYER
RDRL DW
M CHOWDHURY
J HOFFMAN
T HOLDREN
B MINCH
D SOYKA
M B TEGTMEYER
RDRL HR
P FRANASZCZUK
RDRL HRS C
S GORDON
W HAIRSTON
B LANCE
J MCARDLE
K MCDOWELL
K OIE
A PASSARO
M PETERSON
J VETTEL
RDRL ROP L
F GREGORY
RDRL SL
S COARD
RDRL SLB D
D M HISLEY
RDRL SLB E
C BARKER
D BASS
B BENESCH
R CIAPPI
M COHEY
C COWARD
DB HOWLE
M B KAUFMAN
G SADIA
K WEAVER
S WELLING
RDRL SLB S
R BOWERS
RDRL SLB W
D BOOTHE
A BREUER
N EBERIUS
P GILLICH
C KENNEDY
A KULAGA
M MENTZER
E MERMAGEN
S SNEAD
RDRL WM
P BAKER
S KARNA
RDRL WML C
L PIEHLER
RDRL WML H
B SCHUSTER
RDRL WMM A
J TZENG
RDRL WMM B
B CHEESEMAN
B LOVE
RDRL WMM G
T PIEHLER
N ZANDER
RDRL WMP
D LYON
S SCHOENFELD
RDRL WMP B
W EVANS
A DAGRO
A DWIVEDI
A C GUNNARSSON
C HOPPEL
Y HUANG
M LYNCH
J MCDONALD
P MCKEE
D POWELL
B SANBORN
S SATAPATHY
M SCHEIDLER
A SOKOLOW
C WEAVER
T WEERASOORIYA
S WOZNIAK
T ZHANG
K ZIEGLER
RDRL WMP C
S BILYK
T BJERKE
D CASEM
J CLAYTON
D DANDEKAR
M GREENFIELD
B LEAVY
M RAFTENBERG
RDRL WMP D

R DONEY
J RUNYEON
RDRL WMP E
P SWOBODA
RDRL WMP F
C CUMMINS
E FIORAVANTE
A FRYDMAN
A GOERTZ
N GNIAZDOWSKI
R GUPTA
R KARGUS
RDRL WMP G
N ELDREDGE
R BANTON
T DIGLIANI
S KUKUCK

INTENTIONALLY LEFT BLANK.